

# Overview on quantum entanglement

Collection of papers

J. Ladvánszky, Ericsson Hungary

06.29.2019

## Content

<b>1. Preface.....</b>	<b>3</b>
<b>2. Definition of entanglement.....</b>	<b>5</b>
<b>3. Description of entanglement .....</b>	<b>17</b>
<b>4. Observation and measurement of entanglement .....</b>	<b>138</b>
<b>5. Generation of entanglement .....</b>	<b>212</b>
<b>6. Influence on entanglement.....</b>	<b>245</b>
<b>7. Death and revival of entanglement.....</b>	<b>259</b>
<b>8. Effect of noise on entanglement .....</b>	<b>313</b>
<b>9. Exploiting entanglement.....</b>	<b>341</b>
<b>10. Explanation of entanglement.....</b>	<b>521</b>

# 1. Preface

This work is a collection of papers on quantum entanglement. It is intended as a glimpse for the younger colleagues of the author at Ericsson Hungary. Our intention was to introduce as many features as possible, within a readable extent. Our selection criteria are very wide, the work spans the gap from university lecture through research paper to magazine article. Our goal is to illustrate that the topic is very interesting and it covers several unsolved problems. It can be a good basis for research.

During preparation, I received a criticism that I did not add my opinion. This is intentional. The purpose is to obtain the reader as much freedom as possible, without influencing him/her in any directions. But in case the reader wants to have my opinion, my private email is:

Ladvanszky55@t-online.hu

A big thank is due to Dr. E. Simonyi for his help in formatting the text.

This research was supported by the National Research Development and Innovation Office of Hungary within the Quantum Technology National Excellence Program (Project No. 2017-1.2.1-NKP-2017-00001).

## 2. Definition of entanglement

**Abstract:** Entanglement is a correlation between the same physical property of different particles of the same kind.

**Keywords:** History, concept, non-locality and entanglement, quantum-mechanical framework, applications, naturally entangled systems

WIKIPEDIA

# Quantum entanglement

**Quantum entanglement** is a physical phenomenon which occurs when pairs or groups of particles are generated, interact, or share physical proximity in ways such that the quantum state of each particle cannot be described independently of the state of the other(s), even when the particles are separated by a large distance—instead, a quantum state must be described for the system as a whole.

**Measurements** of physical properties such as **position**, **momentum**, **spin**, and **polarization**, performed on entangled particles are found to be **correlated**. For example, if a pair of particles is generated in such a way that their total spin is known to be zero, and one particle is found to have clockwise spin on a certain axis, the spin of the other particle, measured on the same axis, will be found to be counterclockwise, as is to be expected due to their entanglement. However, this behavior gives rise to **paradoxical effects**: any measurement of a property of a particle can be seen as acting on that particle (e.g., by collapsing a number of **superposed states**) and will change the original quantum property by some unknown amount; and in the case of entangled particles, such a measurement will be on the entangled system as a whole. It thus appears that one particle of an entangled pair "knows" what measurement has been performed on the other, and with what outcome, even though there is no known means for such information to be communicated between the particles, which at the time of measurement may be separated by arbitrarily large distances.

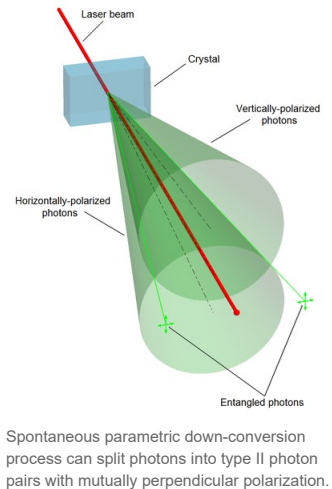
Such phenomena were the subject of a 1935 paper by Albert Einstein, Boris Podolsky, and Nathan Rosen,<sup>[1]</sup> and several papers by Erwin Schrödinger shortly thereafter,<sup>[2][3]</sup> describing what came to be known as the **EPR paradox**. Einstein and others considered such behavior to be impossible, as it violated the **local realist** view of causality (Einstein referring to it as "spooky action at a distance")<sup>[4]</sup> and argued that the accepted formulation of **quantum mechanics** must therefore be incomplete. Later, however, the counterintuitive predictions of quantum mechanics were verified experimentally<sup>[5]</sup> in tests where the polarization or spin of entangled particles were measured at separate locations, statistically violating Bell's inequality, demonstrating that the classical conception of "local realism" cannot be correct.

In earlier tests it couldn't be absolutely ruled out that the test result at one point (or which test was being performed) could have been **subtly transmitted** to the remote point, affecting the outcome at the second location.<sup>[6]</sup> However so-called "loophole-free" Bell tests have been performed in which the locations were separated such that communications at the speed of light would have taken longer—in one case 10,000 times longer—than the interval between the measurements.<sup>[7][8]</sup> Since **faster-than-light** signaling is impossible according to the **special theory of relativity**, any doubts about entanglement due to such a loophole have thereby been quashed.

According to **some interpretations of quantum mechanics**, the effect of one measurement occurs instantly. Other interpretations which don't recognize **wavefunction collapse**, dispute that there is any "effect" at all. After all, if the separation between two events is **spacelike**, then observers in different **inertial frames** will disagree about the order of events. Joe will see that the detection at point **A** occurred first, and could not have been caused by the measurement at point **B**, while Mary (moving at a different velocity) will be certain that the measurement at point **B** occurred first and could not have been caused by the **A** measurement. Of course both Joe and Mary are correct: there is no demonstrable cause and effect. However all interpretations agree that entanglement produces **correlation** between the measurements, and that the **mutual information** between the entangled particles can be exploited, but that any **transmission** of information at faster-than-light speeds is impossible.<sup>[9][10]</sup>

In May 2018, researchers performed **Bell test experiments** in which further "loopholes" were closed.<sup>[11][12]</sup>

Entanglement is considered fundamental to quantum mechanics, even though it wasn't recognized in the beginning. Quantum entanglement has been demonstrated experimentally with **photons**,<sup>[13][14]</sup> **neutrinos**,<sup>[15]</sup> **electrons**,<sup>[16]</sup> **molecules** as large as **buckyballs**,<sup>[20][21]</sup> and even small diamonds.<sup>[22][23]</sup> The utilization of entanglement in **communication** and **computation** is a very active area of research.



Spontaneous parametric down-conversion process can split photons into type II photon pairs with mutually perpendicular polarization.

## Contents

### History

#### Concept

- Meaning of entanglement
- Paradox
- Hidden variables theory
- Violations of Bell's inequality
- Other types of experiments
- Mystery of time
- Source for the arrow of time

#### Non-locality and entanglement

#### Quantum mechanical framework

- Pure states
- Ensembles
- Reduced density matrices
- Two applications that use them
- Entropy
  - Definition
  - As a measure of entanglement
- Entanglement measures
- Quantum field theory

#### Applications

- Entangled states
- Methods of creating entanglement
- Testing a system for entanglement

#### Naturally entangled systems

#### Photosynthesis

#### See also

#### References

#### Further reading

## External links

## History

The counterintuitive predictions of quantum mechanics about strongly correlated systems were first discussed by [Albert Einstein](#) in 1935, in a joint paper with [Boris Podolsky](#) and [Nathan Rosen](#).<sup>[1]</sup> In this study, the three formulated the [EPR paradox](#), a [thought experiment](#) that attempted to show that [quantum mechanical theory](#) was [incomplete](#). They wrote: "We are thus forced to conclude that the quantum-mechanical description of physical reality given by wave functions is not complete."<sup>[1]</sup>

However, the three scientists did not coin the word [entanglement](#), nor did they generalize the special properties of the state they considered. Following the EPR paper, [Erwin Schrödinger](#) wrote a letter to Einstein in [German](#) in which he used the word *Verschränkung* (translated by himself as [entanglement](#)) "to describe the correlations between two particles that interact and then separate, as in the EPR experiment."<sup>[24]</sup>

Schrödinger shortly thereafter published a seminal paper defining and discussing the notion of "entanglement." In the paper he recognized the importance of the concept, and stated:<sup>[2]</sup> "I would not call [entanglement] one but rather *the* characteristic trait of [quantum mechanics](#), the one that enforces its entire departure from [classical](#) lines of thought."

Like Einstein, Schrödinger was dissatisfied with the concept of entanglement, because it seemed to violate the speed limit on the transmission of information implicit in the [theory of relativity](#).<sup>[25]</sup> Einstein later famously derided entanglement as "*spukhafte Fernwirkung*"<sup>[26]</sup> or "spooky action at a distance."

The EPR paper generated significant interest among physicists and inspired much discussion about the foundations of quantum mechanics (perhaps most famously Bohm's [interpretation](#) of quantum mechanics), but produced relatively little other published work. So, despite the interest, the weak point in EPR's argument was not discovered until 1964, when [John Stewart Bell](#) proved that one of their key assumptions, the [principle of locality](#), which underlies the kind of hidden variables interpretation hoped for by EPR, was mathematically inconsistent with the predictions of quantum theory.

Specifically, Bell demonstrated an upper limit, seen in [Bell's inequality](#), regarding the strength of correlations that can be produced in any theory obeying [local realism](#), and he showed that quantum theory predicts violations of this limit for certain entangled systems.<sup>[27]</sup> His inequality is experimentally testable, and there have been numerous [relevant experiments](#), starting with the pioneering work of [Stuart Freedman](#) and [John Clauser](#) in 1972<sup>[28]</sup> and [Alain Aspect](#)'s experiments in 1982,<sup>[29]</sup> all of which have shown agreement with quantum mechanics rather than the principle of local realism.

Until recently each had left open at least one loophole by which it was possible to question the validity of the results. However, in 2015 an experiment was performed that simultaneously closed both the detection and locality loopholes, and was heralded as "loophole-free"; this experiment ruled out a large class of local realism theories with certainty.<sup>[30]</sup> Alain Aspect notes that the setting-independence loophole, which he refers to as "far-fetched" yet a "residual loophole" that "cannot be ignored" has yet to be closed, and the free-will, or superdeterminism, loophole is unclosable, saying "no experiment, as ideal as it is, can be said to be totally loophole-free."<sup>[31]</sup>

A minority opinion holds that although quantum mechanics is correct, there is no superluminal instantaneous action-at-a-distance between entangled particles once the particles are separated.<sup>[32][33][34][35]</sup>

Bell's work raised the possibility of using these super-strong correlations as a resource for communication. It led to the discovery of [quantum key distribution](#) protocols, most famously [BB84](#) by [Charles H. Bennett](#) and [Gilles Brassard](#)<sup>[36]</sup> and [E91](#) by [Artur Ekert](#).<sup>[37]</sup> Although BB84 does not use entanglement, Ekert's protocol uses the violation of a Bell's inequality as a proof of security.

## Concept

### Meaning of entanglement

An entangled system is defined to be one whose [quantum state](#) cannot be factored as a product of states of its local constituents; that is to say, they are not individual particles but are an inseparable whole. In entanglement, one constituent cannot be fully described without considering the other(s). Note that the state of a composite system is always expressible as a [sum](#), or [superposition](#), of products of states of local constituents; it is entangled if this sum necessarily has more than one term.

[Quantum systems](#) can become entangled through various types of interactions. For some ways in which entanglement may be achieved for experimental purposes, see the section below on [methods](#). Entanglement is broken when the entangled particles [decohere](#) through interaction with the environment; for example, when a measurement is made.<sup>[38]</sup>

As an example of entanglement: a [subatomic particle decays](#) into an entangled pair of other particles. The decay events obey the various [conservation laws](#), and as a result, the measurement outcomes of one daughter particle must be highly correlated with the measurement outcomes of the other daughter particle (so that the total momenta, angular momenta, energy, and so forth remains roughly the same before and after this process). For instance, a spin-zero particle could decay into a pair of spin-½ particles. Since the total spin before and after this decay must be zero (conservation of angular momentum), whenever the first particle is measured to be [spin up](#) on some axis, the other, when measured on the same axis, is always found to be [spin down](#). (This is called the [spin anti-correlated](#) case; and if the prior probabilities for measuring each spin are equal, the pair is said to be in the [singlet state](#).)

The special property of entanglement can be better observed if we separate the said two particles. Let's put one of them in the White House in Washington and the other in Buckingham Palace (think about this as a thought experiment, not an actual one). Now, if we measure a particular characteristic of one of these particles (say, for example, spin), get a result, and then measure the other particle using the same criterion (spin along the same axis), we find that the result of the measurement of the second particle will match (in a complementary sense) the result of the measurement of the first particle, in that they will be opposite in their values.

The above result may or may not be perceived as surprising. A classical system would display the same property, and a [hidden variable theory](#) (see below) would certainly be required to do so, based on conservation of angular momentum in classical and quantum mechanics alike. The difference is that a classical system has definite values for all the observables all along, while the quantum system does not. In a sense to be discussed below, the quantum system considered here seems to [acquire](#) a probability distribution for the outcome of a measurement of the spin along *any* axis of the *other* particle upon measurement of the *first* particle. This probability distribution is in general *different* from what it would be *without* measurement of the first particle. This may certainly be perceived as surprising in the case of spatially separated entangled particles.

### Paradox

The paradox is that a measurement made on either of the particles apparently collapses the state of the entire entangled system—and does so instantaneously, before any information about the measurement result could have been communicated to the other particle (assuming that information cannot travel [faster than light](#)) and hence assured the "proper" outcome of the measurement of the other part of the entangled pair. In the [Copenhagen interpretation](#), the result of a spin measurement on one of the particles is a collapse

## EINSTEIN ATTACKS QUANTUM THEORY

**Scientist and Two Colleagues Find It Is Not 'Complete' Even Though 'Correct.'**

### SEE FULLER ONE POSSIBLE

**Believe a Whole Description of 'the Physical Reality' Can Be Provided Eventually.**

Article headline regarding the EPR paper, in the May 4, 1935 issue of *The New York Times*.

into a state in which each particle has a definite spin (either up or down) along the axis of measurement. The outcome is taken to be random, with each possibility having a probability of 50%. However, if both spins are measured along the same axis, they are found to be anti-correlated. This means that the random outcome of the measurement made on one particle seems to have been transmitted to the other, so that it can make the "right choice" when it too is measured.<sup>[39]</sup>

The distance and timing of the measurements can be chosen so as to make the interval between the two measurements spacelike, hence, any causal effect connecting the events would have to travel faster than light. According to the principles of special relativity, it is not possible for any information to travel between two such measuring events. It is not even possible to say which of the measurements came first. For two spacelike separated events  $x_1$  and  $x_2$  there are inertial frames in which  $x_1$  is first and others in which  $x_2$  is first. Therefore, the correlation between the two measurements cannot be explained as one measurement determining the other: different observers would disagree about the role of cause and effect.

### **Hidden variables theory**

A possible resolution to the paradox is to assume that quantum theory is incomplete, and the result of measurements depends on predetermined "hidden variables".<sup>[40]</sup> The state of the particles being measured contains some hidden variables, whose values effectively determine, right from the moment of separation, what the outcomes of the spin measurements are going to be. This would mean that each particle carries all the required information with it, and nothing needs to be transmitted from one particle to the other at the time of measurement. Einstein and others (see the previous section) originally believed this was the only way out of the paradox, and the accepted quantum mechanical description (with a random measurement outcome) must be incomplete. (In fact similar paradoxes can arise even without entanglement: the position of a single particle is spread out over space, and two widely separated detectors attempting to detect the particle in two different places must instantaneously attain appropriate correlation, so that they do not *both* detect the particle.)

### **Violations of Bell's inequality**

The hidden variables theory fails, however, when we consider measurements of the spin of entangled particles along different axes (for example, along any of three axes that make angles of 120 degrees). If a large number of pairs of such measurements are made (on a large number of pairs of entangled particles), then statistically, if the local realist or hidden variables view were correct, the results would always satisfy Bell's inequality. A number of experiments have shown in practice that Bell's inequality is not satisfied. However, prior to 2015, all of these had loophole problems that were considered the most important by the community of physicists.<sup>[41][42]</sup> When measurements of the entangled particles are made in moving relativistic reference frames, in which each measurement (in its own relativistic time frame) occurs before the other, the measurement results remain correlated.<sup>[43][44]</sup>

The fundamental issue about measuring spin along different axes is that these measurements cannot have definite values at the same time—they are incompatible in the sense that these measurements' maximum simultaneous precision is constrained by the uncertainty principle. This is contrary to what is found in classical physics, where any number of properties can be measured simultaneously with arbitrary accuracy. It has been proven mathematically that compatible measurements cannot show Bell-inequality-violating correlations,<sup>[45]</sup> and thus entanglement is a fundamentally non-classical phenomenon.

### **Other types of experiments**

In experiments in 2012 and 2013, polarization correlation was created between photons that never coexisted in time.<sup>[46][47]</sup> The authors claimed that this result was achieved by entanglement swapping between two pairs of entangled photons *after* measuring the polarization of one photon of the early pair, and that it proves that quantum non-locality applies not only to space but also to time.

In three independent experiments in 2013 it was shown that classically-communicated separable quantum states can be used to carry entangled states.<sup>[48]</sup> The first loophole-free Bell test was held in TU Delft in 2015 confirming the violation of Bell inequality.<sup>[49]</sup>

In August 2014, Brazilian researcher Gabriela Barreto Lemos and team were able to "take pictures" of objects using photons that had not interacted with the subjects, but were entangled with photons that did interact with such objects. Lemos, from the University of Vienna, is confident that this new quantum imaging technique could find application where low light imaging is imperative, in fields like biological or medical imaging.<sup>[50]</sup>

### **Mystery of time**

There have been suggestions to look at the concept of time as an emergent phenomenon that is a side effect of quantum entanglement.<sup>[51][52]</sup> In other words, time is an entanglement phenomenon, which places all equal clock readings (of correctly prepared clocks, or of any objects usable as clocks) into the same history. This was first fully theorized by Don Page and William Wootters in 1983.<sup>[53]</sup> The Wheeler–DeWitt equation that combines general relativity and quantum mechanics – by leaving out time altogether – was introduced in the 1960s and it was taken up again in 1983, when the theorists Don Page and William Wootters made a solution based on the quantum phenomenon of entanglement. Page and Wootters argued that entanglement can be used to measure time.<sup>[54]</sup>

In 2013, at the Istituto Nazionale di Ricerca Metrologica (INRIM) in Turin, Italy, researchers performed the first experimental test of Page and Wootters' ideas. Their result has been interpreted to confirm that time is an emergent phenomenon for internal observers but absent for external observers of the universe just as the Wheeler-DeWitt equation predicts.<sup>[54]</sup>

## Source for the arrow of time

Physicist Seth Lloyd says that quantum uncertainty gives rise to entanglement, the putative source of the arrow of time. According to Lloyd; "The arrow of time is an arrow of increasing correlations."<sup>[55]</sup> The approach to entanglement would be from the perspective of the causal arrow of time, with the assumption that the cause of the measurement of one particle determines the effect of the result of the other particle's measurement.

## Non-locality and entanglement

In the media and popular science, quantum non-locality is often portrayed as being equivalent to entanglement. While it is true that a pure bipartite quantum state must be entangled in order for it to produce non-local correlations, there exist entangled states that do not produce such correlations, and there exist non-entangled (separable) quantum states that present some non-local behaviour. A well-known example of the first case is the Werner state that is entangled for certain values of  $p_{sym}$ , but can always be described using local hidden variables.<sup>[56]</sup> In short, entanglement of a two-party state is necessary but not sufficient for that state to be non-local. Moreover, it was shown that, for arbitrary numbers of particles, there exist states that are genuinely entangled but admits a fully local strategy. It is important to recognize that entanglement is more commonly viewed as an algebraic concept, noted for being a precedent to non-locality as well as to quantum teleportation and to superdense coding, whereas non-locality is defined according to experimental statistics and is much more involved with the foundations and interpretations of quantum mechanics.

## Quantum mechanical framework

The following subsections are for those with a good working knowledge of the formal, mathematical description of quantum mechanics, including familiarity with the formalism and theoretical framework developed in the articles: bra–ket notation and mathematical formulation of quantum mechanics.

### Pure states

Consider two noninteracting systems  $A$  and  $B$ , with respective Hilbert spaces  $H_A$  and  $H_B$ . The Hilbert space of the composite system is the tensor product

$$H_A \otimes H_B.$$

If the first system is in state  $|\psi\rangle_A$  and the second in state  $|\phi\rangle_B$ , the state of the composite system is

$$|\psi\rangle_A \otimes |\phi\rangle_B.$$

States of the composite system that can be represented in this form are called separable states, or product states.

Not all states are separable states (and thus product states). Fix a basis  $\{|i\rangle_A\}$  for  $H_A$  and a basis  $\{|j\rangle_B\}$  for  $H_B$ . The most general state in  $H_A \otimes H_B$  is of the form

$$|\psi\rangle_{AB} = \sum_{i,j} c_{ij} |i\rangle_A \otimes |j\rangle_B.$$

This state is separable if there exist vectors  $[c_i^A], [c_j^B]$  so that  $c_{ij}=c_i^A c_j^B$ , yielding  $|\psi\rangle_A=\sum_i c_i^A |i\rangle_A$  and  $|\phi\rangle_B=\sum_j c_j^B |j\rangle_B$ . It is inseparable if for any vectors  $[c_i^A], [c_j^B]$  at least for one pair of coordinates  $c_i^A, c_j^B$  we have  $c_{ij}\neq c_i^A c_j^B$ . If a state is inseparable, it is called an entangled state.

For example, given two basis vectors  $\{|0\rangle_A, |1\rangle_A\}$  of  $H_A$  and two basis vectors  $\{|0\rangle_B, |1\rangle_B\}$  of  $H_B$ , the following is an entangled state:

$$\frac{1}{\sqrt{2}} (|0\rangle_A \otimes |1\rangle_B - |1\rangle_A \otimes |0\rangle_B).$$

If the composite system is in this state, it is impossible to attribute to either system  $A$  or system  $B$  a definite pure state. Another way to say this is that while the von Neumann entropy of the whole state is zero (as it is for any pure state), the entropy of the subsystems is greater than zero. In this sense, the systems are "entangled". This has specific empirical ramifications for interferometry.<sup>[57]</sup> It is worthwhile to note that the above example is one of four Bell states, which are (maximally) entangled pure states (pure states of the  $H_A \otimes H_B$  space, but which cannot be separated into pure states of each  $H_A$  and  $H_B$ ).

Now suppose Alice is an observer for system  $A$ , and Bob is an observer for system  $B$ . If in the entangled state given above Alice makes a measurement in the  $\{|0\rangle, |1\rangle\}$  eigenbasis of  $A$ , there are two possible outcomes, occurring with equal probability:<sup>[58]</sup>

1. Alice measures 0, and the state of the system collapses to  $|0\rangle_A |1\rangle_B$ .
2. Alice measures 1, and the state of the system collapses to  $|1\rangle_A |0\rangle_B$ .

If the former occurs, then any subsequent measurement performed by Bob, in the same basis, will always return 1. If the latter occurs, (Alice measures 1) then Bob's measurement will return 0 with certainty. Thus, system  $B$  has been altered by Alice performing a local measurement on system  $A$ . This remains true even if the systems  $A$  and  $B$  are spatially separated. This is the foundation of the EPR paradox.

The outcome of Alice's measurement is random. Alice cannot decide which state to collapse the composite system into, and therefore cannot transmit information to Bob by acting on her system. Causality is thus preserved, in this particular scheme. For the general argument, see no-communication theorem.

### Ensembles

As mentioned above, a state of a quantum system is given by a unit vector in a Hilbert space. More generally, if one has less information about the system, then one calls it an ensemble and describes it by a density matrix, which is a positive-semidefinite matrix, or a trace class when the state space is infinite-dimensional, and has trace 1. Again, by the spectral theorem, such a matrix takes the general form:

$$\rho = \sum_i w_i |\alpha_i\rangle \langle \alpha_i|,$$

where the  $w_i$  are positive-valued probabilities (they sum up to 1), the vectors  $\alpha_i$  are unit vectors, and in the infinite-dimensional case, we would take the closure of such states in the trace norm. We can interpret  $\rho$  as representing an ensemble where  $w_i$  is the proportion of the ensemble whose states are  $|\alpha_i\rangle$ . When a mixed state has rank 1, it therefore describes a pure ensemble. When there is less than total information about the state of a quantum system we need density matrices to represent the state.

Experimentally, a mixed ensemble might be realized as follows. Consider a "black box" apparatus that spits electrons towards an observer. The electrons' Hilbert spaces are identical. The apparatus might produce electrons that are all in the same state; in this case, the electrons received by the observer are then a pure ensemble. However, the apparatus could produce electrons in different states. For example, it could produce two populations of electrons: one with state  $|z+\rangle$  with spins aligned in the positive z direction, and the other with state  $|y-\rangle$  with spins aligned in the negative y direction. Generally, this is a mixed ensemble, as there can be any number of populations, each corresponding to a different state.

Following the definition above, for a bipartite composite system, mixed states are just density matrices on  $H_A \otimes H_B$ . That is, it has the general form

$$\rho = \sum_i w_i \left[ \sum_j \bar{c}_{ij} (|\alpha_{ij}\rangle \otimes |\beta_{ij}\rangle) \right] \otimes \left[ \sum_k c_{ik} (\langle \alpha_{ik}| \otimes \langle \beta_{ik}|) \right]$$

where the  $w_i$  are positively valued probabilities,  $\sum_j |c_{ij}|^2 = 1$ , and the vectors are unit vectors. This is self-adjoint and positive and has trace 1.

Extending the definition of separability from the pure case, we say that a mixed state is separable if it can be written as<sup>[59]:131–132</sup>

$$\rho = \sum_i w_i \rho_i^A \otimes \rho_i^B,$$

where the  $w_i$  are positively valued probabilities and the  $\rho_i^A$ 's and  $\rho_i^B$ 's are themselves mixed states (density operators) on the subsystems A and B respectively. In other words, a state is separable if it is a probability distribution over uncorrelated states, or product states. By writing the density matrices as sums of pure ensembles and expanding, we may assume without loss of generality that  $\rho_i^A$  and  $\rho_i^B$  are themselves pure ensembles. A state is then said to be *entangled* if it is not separable.

In general, finding out whether or not a mixed state is entangled is considered difficult. The general bipartite case has been shown to be NP-hard.<sup>[60]</sup> For the  $2 \times 2$  and  $2 \times 3$  cases, a necessary and sufficient criterion for separability is given by the famous Positive Partial Transpose (PPT) condition.<sup>[61]</sup>

## Reduced density matrices

The idea of a reduced density matrix was introduced by Paul Dirac in 1930.<sup>[62]</sup> Consider as above systems A and B each with a Hilbert space  $H_A$ ,  $H_B$ . Let the state of the composite system be

$$|\Psi\rangle \in H_A \otimes H_B.$$

As indicated above, in general there is no way to associate a pure state to the component system A. However, it still is possible to associate a density matrix. Let

$$\rho_T = |\Psi\rangle \langle \Psi|.$$

which is the projection operator onto this state. The state of A is the partial trace of  $\rho_T$  over the basis of system B:

$$\rho_A \stackrel{\text{def}}{=} \sum_j \langle j|_B (|\Psi\rangle \langle \Psi|) |j\rangle_B = \text{Tr}_B \rho_T.$$

$\rho_A$  is sometimes called the reduced density matrix of  $\rho$  on subsystem A. Colloquially, we "trace out" system B to obtain the reduced density matrix on A.

For example, the reduced density matrix of A for the entangled state

$$\frac{1}{\sqrt{2}} (|0\rangle_A \otimes |1\rangle_B - |1\rangle_A \otimes |0\rangle_B),$$

discussed above is

$$\rho_A = \frac{1}{2} (|0\rangle_A \langle 0|_A + |1\rangle_A \langle 1|_A)$$

This demonstrates that, as expected, the reduced density matrix for an entangled pure ensemble is a mixed ensemble. Also not surprisingly, the density matrix of A for the pure product state  $|\psi\rangle_A \otimes |\phi\rangle_B$  discussed above is

$$\rho_A = |\psi\rangle_A \langle \psi|_A.$$

In general, a bipartite pure state  $\rho$  is entangled if and only if its reduced states are mixed rather than pure.

## Two applications that use them

Reduced density matrices were explicitly calculated in different spin chains with unique ground state. An example is the one-dimensional AKLT spin chain.<sup>[63]</sup> the ground state can be divided into a block and an environment. The reduced density matrix of the block is proportional to a projector to a degenerate ground state of another Hamiltonian.

The reduced density matrix also was evaluated for XY spin chains, where it has full rank. It was proved that in the thermodynamic limit, the spectrum of the reduced density matrix of a large block of spins is an exact geometric sequence<sup>[64]</sup> in this case.

## Entropy

In this section, the entropy of a mixed state is discussed as well as how it can be viewed as a measure of quantum entanglement.

### Definition

In classical information theory  $H$ , the Shannon entropy, is associated to a probability distribution  $p_1, \dots, p_n$ , in the following way.<sup>[65]</sup>

$$H(p_1, \dots, p_n) = - \sum_i p_i \log_2 p_i.$$

Since a mixed state  $\rho$  is a probability distribution over an ensemble, this leads naturally to the definition of the von Neumann entropy:

$$S(\rho) = -\text{Tr}(\rho \log_2 \rho).$$

In general, one uses the Borel functional calculus to calculate a non-polynomial function such as  $\log_2(\rho)$ . If the nonnegative operator  $\rho$  acts on a finite-dimensional Hilbert space and has eigenvalues  $\lambda_1, \dots, \lambda_n$ ,  $\log_2(\rho)$  turns out to be nothing more than the operator with the same eigenvectors, but the eigenvalues  $\log_2(\lambda_1), \dots, \log_2(\lambda_n)$ . The Shannon entropy is then:

$$S(\rho) = -\text{Tr}(\rho \log_2 \rho) = -\sum_i \lambda_i \log_2 \lambda_i.$$

Since an event of probability 0 should not contribute to the entropy, and given that

$$\lim_{p \rightarrow 0} p \log p = 0,$$

the convention  $0 \log(0) = 0$  is adopted. This extends to the infinite-dimensional case as well: if  $\rho$  has spectral resolution

$$\rho = \int \lambda dP_\lambda,$$

assume the same convention when calculating

$$\rho \log_2 \rho = \int \lambda \log_2 \lambda dP_\lambda.$$

As in statistical mechanics, the more uncertainty (number of microstates) the system should possess, the larger the entropy. For example, the entropy of any pure state is zero, which is unsurprising since there is no uncertainty about a system in a pure state. The entropy of any of the two subsystems of the entangled state discussed above is  $\log(2)$  (which can be shown to be the maximum entropy for  $2 \times 2$  mixed states).

#### As a measure of entanglement

Entropy provides one tool that can be used to quantify entanglement, although other entanglement measures exist.<sup>[66]</sup> If the overall system is pure, the entropy of one subsystem can be used to measure its degree of entanglement with the other subsystems.

For bipartite pure states, the von Neumann entropy of reduced states is the unique measure of entanglement in the sense that it is the only function on the family of states that satisfies certain axioms required of an entanglement measure.

It is a classical result that the Shannon entropy achieves its maximum at, and only at, the uniform probability distribution  $\{1/n, \dots, 1/n\}$ . Therefore, a bipartite pure state  $\rho \in H_A \otimes H_B$  is said to be a **maximally entangled state** if the reduced state of  $\rho$  is the diagonal matrix

$$\begin{bmatrix} \frac{1}{n} & & \\ & \ddots & \\ & & \frac{1}{n} \end{bmatrix}.$$

For mixed states, the reduced von Neumann entropy is not the only reasonable entanglement measure.

As an aside, the information-theoretic definition is closely related to entropy in the sense of statistical mechanics (comparing the two definitions, we note that, in the present context, it is customary to set the Boltzmann constant  $k = 1$ ). For example, by properties of the Borel functional calculus, we see that for any unitary operator  $U$ ,

$$S(\rho) = S(U\rho U^*).$$

Indeed, without this property, the von Neumann entropy would not be well-defined.

In particular,  $U$  could be the time evolution operator of the system, i.e.,

$$U(t) = \exp\left(\frac{-iHt}{\hbar}\right),$$

where  $H$  is the Hamiltonian of the system. Here the entropy is unchanged.

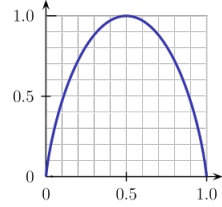
The reversibility of a process is associated with the resulting entropy change, i.e., a process is reversible if, and only if, it leaves the entropy of the system invariant. Therefore, the march of the arrow of time towards thermodynamic equilibrium is simply the growing spread of quantum entanglement.<sup>[67]</sup> This provides a connection between quantum information theory and thermodynamics.

Rényi entropy also can be used as a measure of entanglement.

#### Entanglement measures

Entanglement measures quantify the amount of entanglement in a (often viewed as a bipartite) quantum state. As aforementioned, entanglement entropy is the standard measure of entanglement for pure states (but no longer a measure of entanglement for mixed states). For mixed states, there are some entanglement measures in the literature<sup>[68]</sup> and no single one is standard.

- Entanglement cost
- Distillable entanglement
- Entanglement of formation
- Relative entropy of entanglement
- Squashed entanglement
- Logarithmic negativity



The plot of von Neumann entropy Vs Eigenvalue for a bipartite 2-level pure state. When the eigenvalue has value .5, von Neumann entropy is at a maximum, corresponding to maximum entanglement.

Most (but not all) of these entanglement measures reduce for pure states to entanglement entropy, and are difficult ([NP-hard](#)) to compute.<sup>[68]</sup>

## Quantum field theory

The [Reeh-Schlieder theorem](#) of [quantum field theory](#) is sometimes seen as an analogue of quantum entanglement.

## Applications

---

Entanglement has many applications in [quantum information theory](#). With the aid of entanglement, otherwise impossible tasks may be achieved.

Among the best-known applications of entanglement are [superdense coding](#) and [quantum teleportation](#).<sup>[69]</sup>

Most researchers believe that entanglement is necessary to realize [quantum computing](#) (although this is disputed by some).<sup>[70]</sup>

Entanglement is used in some protocols of [quantum cryptography](#).<sup>[71][72]</sup> This is because the "shared noise" of entanglement makes for an excellent [one-time pad](#). Moreover, since measurement of either member of an entangled pair destroys the entanglement they share, entanglement-based quantum cryptography allows the sender and receiver to more easily detect the presence of an interceptor.

In [interferometry](#), entanglement is necessary for surpassing the [standard quantum limit](#) and achieving the [Heisenberg limit](#).<sup>[73]</sup>

## Entangled states

There are several canonical entangled states that appear often in theory and experiments.

For two [qubits](#), the [Bell states](#) are

$$\begin{aligned} |\Phi^\pm\rangle &= \frac{1}{\sqrt{2}}(|0\rangle_A \otimes |0\rangle_B \pm |1\rangle_A \otimes |1\rangle_B) \\ |\Psi^\pm\rangle &= \frac{1}{\sqrt{2}}(|0\rangle_A \otimes |1\rangle_B \pm |1\rangle_A \otimes |0\rangle_B). \end{aligned}$$

These four pure states are all maximally entangled (according to the [entropy of entanglement](#)) and form an [orthonormal basis](#) ([linear algebra](#)) of the Hilbert space of the two qubits. They play a fundamental role in [Bell's theorem](#).

For M>2 qubits, the [GHZ state](#) is

$$|\text{GHZ}\rangle = \frac{|0\rangle^{\otimes M} + |1\rangle^{\otimes M}}{\sqrt{2}},$$

which reduces to the Bell state  $|\Phi^+\rangle$  for  $M = 2$ . The traditional GHZ state was defined for  $M = 3$ . GHZ states are occasionally extended to [qudits](#), i.e., systems of  $d$  rather than 2 dimensions.

Also for M>2 qubits, there are [spin squeezed states](#).<sup>[74]</sup> Spin squeezed states are a class of [squeezed coherent states](#) satisfying certain restrictions on the uncertainty of spin measurements, and are necessarily entangled.<sup>[75]</sup> Spin squeezed states are good candidates for enhancing precision measurements using quantum entanglement.<sup>[76]</sup>

For two [bosonic](#) modes, a [NOON state](#) is

$$|\psi_{\text{NOON}}\rangle = \frac{|N\rangle_a |0\rangle_b + |0\rangle_a |N\rangle_b}{\sqrt{2}},$$

This is like a Bell state  $|\Phi^+\rangle$  except the basis kets 0 and 1 have been replaced with "the  $N$  photons are in one mode" and "the  $N$  photons are in the other mode".

Finally, there also exist [twin Fock states](#) for bosonic modes, which can be created by feeding a [Fock state](#) into two arms leading to a beam splitter. They are the sum of multiple of NOON states, and can be used to achieve the Heisenberg limit.<sup>[77]</sup>

For the appropriately chosen measure of entanglement, Bell, GHZ, and NOON states are maximally entangled while spin squeezed and twin Fock states are only partially entangled. The partially entangled states are generally easier to prepare experimentally.

## Methods of creating entanglement

Entanglement is usually created by direct interactions between subatomic particles. These interactions can take numerous forms. One of the most commonly used methods is [spontaneous parametric down-conversion](#) to generate a pair of photons entangled in polarisation.<sup>[78]</sup> Other methods include the use of a [fiber coupler](#) to confine and mix photons, photons emitted from decay cascade of the bi-exciton in a [quantum dot](#),<sup>[79]</sup> the use of the [Hong–Ou–Mandel effect](#), etc., In the earliest tests of Bell's theorem, the entangled particles were generated using [atomic cascades](#).

It is also possible to create entanglement between quantum systems that never directly interacted, through the use of [entanglement swapping](#). Two independently-prepared, identical particles may also be entangled if their wave functions merely spatially overlap, at least partially.<sup>[80]</sup>

## Testing a system for entanglement

Systems which contain no entanglement are said to be separable. For 2-Qubit and Qubit-Qutrit systems ( $2 \times 2$  and  $2 \times 3$  respectively) the simple [Peres–Horodecki criterion](#) provides both a necessary and a sufficient criterion for separability, and thus for detecting entanglement. However, for the general case, the criterion is merely a sufficient one for separability, as the problem becomes [NP-hard](#).<sup>[81][82]</sup> A numerical approach to the problem is suggested by [Jon Magne Leinaas](#), [Jan Myrheim](#) and [Eirik Ovrum](#) in their paper "Geometrical aspects of entanglement".<sup>[83]</sup> Leinaas et al. offer a numerical approach, iteratively refining an estimated separable state towards the target state to be tested, and checking if the target state can indeed be reached. An implementation of the algorithm (including a built-in Peres-Horodecki criterion testing) is brought in the "StateSeparator" web-app.

In 2016 China launched the world's first quantum communications satellite.<sup>[84]</sup> The \$100m [Quantum Experiments at Space Scale](#) (QUESS) mission was launched on Aug 16, 2016, from the Jiuquan Satellite Launch Center in northern China at 01:40 local time.

For the next two years, the craft – nicknamed "Micius" after the ancient Chinese philosopher – will demonstrate the feasibility of quantum communication between Earth and space, and test quantum entanglement over unprecedented distances.

In the June 16, 2017, issue of *Science*, Yin et al. report setting a new quantum entanglement distance record of 1203 km, demonstrating the survival of a 2-photon pair and a violation of a Bell inequality, reaching a CHSH valuation of  $2.37 \pm 0.09$ , under strict Einstein locality conditions, from the Micius satellite to bases in Lijian, Yunnan and Delingha, Quinhai, increasing the efficiency of transmission over prior fiberoptic experiments by an order of magnitude.<sup>[85]</sup>

## Naturally entangled systems

The electron shell of multi-electron atoms always consists of entangled electrons. The correct ionization energy can be calculated only by consideration of electron entanglement.<sup>[86]</sup>

## Photosynthesis

It has been suggested that in the process of photosynthesis, entanglement is involved in the transfer of energy between light-harvesting complexes and photosynthetic reaction centers where the kinetic energy is harvested in the form of chemical energy. Without such a process, the efficient conversion of optical energy into chemical energy cannot be explained. Using femtosecond spectroscopy, the coherence of entanglement in the Fenna-Matthews-Olson complex was measured over hundreds of femtoseconds (a relatively long time in this regard) providing support to this theory.<sup>[87][88]</sup>

## See also

- CNOT gate
- Concurrence (quantum computing)
- Einstein's thought experiments
- Entanglement distillation
- Entanglement witness
- Faster-than-light communication
- Ghirardi–Rimini–Weber theory
- Multipartite entanglement
- Normally distributed and uncorrelated does not imply independent
- Observer effect (physics)
- Quantum coherence
- Quantum discord
- Quantum phase transition
- Quantum computing
- Quantum pseudo-telepathy
- Quantum teleportation
- Retrocausality
- Separable state
- Squashed entanglement
- Ward's probability amplitude
- Wheeler–Feynman absorber theory

## References

1. Einstein A, Podolsky B, Rosen N; Podolsky; Rosen (1935). "Can Quantum-Mechanical Description of Physical Reality Be Considered Complete?" (<http://cds.cern.ch/record/1060284/files/PhysRev.48.696.pdf>) (PDF). *Phys. Rev.* **47** (10): 777–780. Bibcode:1935PhRv...47..777E. doi:10.1103/PhysRev.47.777 (<https://doi.org/10.1103/2FPhysRev.47.777>).
2. Schrödinger E (1935). "Discussion of probability relations between separated systems". *Mathematical Proceedings of the Cambridge Philosophical Society*. **31** (4): 555–563. Bibcode:1935PCPS...31..555S. (<http://adsabs.harvard.edu/abs/1935PCPS...31..555S>). doi:10.1017/S0305004100013554 (<https://doi.org/10.1017%2FS0305004100013554>).
3. Schrödinger E (1936). "Probability relations between separated systems". *Mathematical Proceedings of the Cambridge Philosophical Society*. **32** (3): 446–452. Bibcode:1936PCPS...32..446S. (<http://adsabs.harvard.edu/abs/1936PCPS...32..446S>). doi:10.1017/S0305004100019137 (<https://doi.org/10.1017%2FS0305004100019137>).
4. Physicist John Bell depicts the Einstein camp in this debate in his article entitled "Bertmann's socks and the nature of reality", p. 143 of *Speakable and unspeakable in quantum mechanics*: "For EPR that would be an unthinkable 'spooky action at a distance'. To avoid such action at a distance they have to attribute, to the space-time regions in question, real properties in advance of observation, correlated properties, which predetermine the outcomes of these particular observations. Since these real properties, fixed in advance of observation, are not contained in quantum formalism, that formalism for EPR is incomplete. It may be correct, as far as it goes, but the usual quantum formalism cannot be the whole story." And again on p. 144 Bell says: "Einstein had no difficulty accepting that affairs in different places could be correlated. What he could not accept was that an intervention at one place could influence, immediately, affairs at the other." Downloaded 5 July 2011 from Bell, J. S. (1987). *Speakable and Unspeakable in Quantum Mechanics* (<https://web.archive.org/web/20150412044550/http://philosophyfaculty.ucsd.edu/faculty/BellJohnS1981Spe.pdf>) (PDF). CERN. ISBN 0521334950. Archived from the original (<http://philosophyfaculty.ucsd.edu/faculty/wuthrich/GSSPP09/Files/BellJohnS1981Spe.pdf>) on 12 April 2015. Retrieved 14 June 2014.
5. "75 years of entanglement – Science News" ([http://www.sciencenews.org/view/feature/id/65093/title/75\\_years\\_of\\_entanglement](http://www.sciencenews.org/view/feature/id/65093/title/75_years_of_entanglement)). Retrieved 13 October 2014.
6. Francis, Matthew. *Quantum entanglement shows that reality can't be local* (<https://arstechnica.com/science/2012/10/quantum-entanglement-shows-that-reality-can-t-be-local/>). *Ars Technica*, 30 October 2012
7. Matson, John (13 August 2012). "Quantum teleportation achieved over record distances". *Nature News*. doi:10.1038/nature.2012.11163 (<https://doi.org/10.1038%2Fnature.2012.11163>).
8. "Bounding the speed of 'spooky action at a distance'". *Physical Review Letters*. **110**: 260407. 2013. arXiv:1303.0614 (<https://arxiv.org/abs/1303.0614>). Bibcode:2013PhRvL.110z0407Y (<http://adsabs.harvard.edu/abs/2013PhRvL.110z0407Y>). doi:10.1103/PhysRevLett.110.260407 (<https://doi.org/10.1103%2FPhysRevLett.110.260407>).
9. Roger Penrose, *The Road to Reality: A Complete Guide to the Laws of the Universe*, London, 2004, p. 603.
10. Griffiths, David J. (2004). *Introduction to Quantum Mechanics* (2nd ed.), Prentice Hall, ISBN 0-13-111892-7
11. The BIG Bell Test Collaboration (9 May 2018). "Challenging local realism with human choices" (*Nature*. **557**: 212–216. doi:10.1038/s41586-018-0085-3 (<https://doi.org/10.1038%2Fs41586-018-0085-3>).
12. Mandelbaum, Ryan F. (11 May 2018). "100,000 Video Game Players Helped Scientists Prove Einstein Wrong" (<https://gizmodo.com/100-000-video-game-players-helped-scientists-prove-eins-1825935176>). *Gizmodo*. Retrieved 12 May 2018.
13. Kwiat, PG; Mattle, K; Weinfurter, H; Zeilinger, A; Sergienko, AV; Shih, Y (1995). "New High-Intensity Source of Polarization-Entangled Photon Pairs". *Physical Review Letters*. **75**: 4337–4341. Bibcode:1995PhRvL..75.4337K (<http://adsabs.harvard.edu/abs/1995PhRvL..75.4337K>). doi:10.1103/PhysRevLett.75.4337 (<https://doi.org/10.1103%2FPhysRevLett.75.4337>). PMID 10059884 (<https://www.ncbi.nlm.nih.gov/pubmed/10059884>).
14. Zhao, Z; Chen, YA; Zhang, AN; Yang, T; Briegel, HJ; Pan, JW (July 2004). "Experimental demonstration of five-photon entanglement and open-destination teleportation" (<http://www.nature.com/nature/journal/v430/n6995/full/nature02643.html>). *Nature*. **430**: 54–58. arXiv:quant-ph/0402096 (<https://arxiv.org/abs/quant-ph/0402096>). Bibcode:2004Natur.430...54Z (<http://adsabs.harvard.edu/abs/2004Natur.430...54Z>). doi:10.1038/nature02643 (<https://doi.org/10.1038%2Fnature02643>). PMID 15229594 (<https://www.ncbi.nlm.nih.gov/pubmed/15229594>).
15. Lu, Chao-Yang (2007). "Experimental entanglement of six photons in graph states" (<http://www.nature.com/nphys/journal/v3/n2/full/nphys507.html>). *Nature Physics*. **3**: 91–95. arXiv:quant-ph/0609130 (<https://arxiv.org/abs/quant-ph/0609130>). Bibcode:2007NatPh...3...91L (<http://adsabs.harvard.edu/abs/2007NatPh...3...91L>). doi:10.1038/nphys507 (<https://doi.org/10.1038%2Fnphys507>).
16. Yao, Xing-Can (2012). "Observation of eight-photon entanglement" (<http://www.nature.com/nphoton/journal/v6/n4/full/nphoton.2011.354.html>). *Nature Photonics*. **6**: 225–228. arXiv:1105.6318 (<https://arxiv.org/abs/1105.6318>). Bibcode:2012NaPho...6..225Y (<http://adsabs.harvard.edu/abs/2012NaPho...6..225Y>). doi:10.1038/nphoton.2011.354 (<https://doi.org/10.1038%2Fnphoton.2011.354>).
17. J. A. Formaggio, D. I. Kaiser, M. M. Mursky, and T. E. Weiss (2016), "Violation of the Leggett-Garg inequality in neutrino oscillations". *Phys. Rev. Lett.* Accepted 23 June 2016. <https://journals.aps.org/prl/accepted/6f072Y00C3318d41f5739ec7f83a9acf1ad67b002>

18. Hensen, B.; et al. (21 October 2015). "Loophole-free Bell inequality violation using electron spins separated by 1.3 kilometres". *Nature*. **526**: 682–686. arXiv:1508.05949 (<https://arxiv.org/abs/1508.05949>). Bibcode:2015Natur.526..682H. doi:10.1038/nature15759 (<https://doi.org/10.1038/nature15759>). PMID 26503041 (<https://www.ncbi.nlm.nih.gov/pubmed/26503041>). Retrieved 21 October 2015. See also free online access version ([https://www.nature.com/articles/nature15759.epdf?referrer\\_access\\_token=1QB20mTNTZW6nExi0D79RgN0AjWeI9jnR3ZoTvPfU6MAlltuikCZOJrG8QbdRRghlecFwmixLbQpWuw1dtaib4Le5DQOG3u\\_aXHU85x1JEhOc](https://www.nature.com/articles/nature15759.epdf?referrer_access_token=1QB20mTNTZW6nExi0D79RgN0AjWeI9jnR3ZoTvPfU6MAlltuikCZOJrG8QbdRRghlecFwmixLbQpWuw1dtaib4Le5DQOG3u_aXHU85x1JEhOc))
19. Markoff, Jack (21 October 2015). "Sorry, Einstein. Quantum Study Suggests 'Spooky Action' Is Real" (<https://www.nytimes.com/2015/10/22/science/quantum-theory-experiment-said-to-prove-spooky-interactions.html>). *The New York Times*. Retrieved 21 October 2015.
20. Arndt, M; Nairz, O; Vos-Andreae, J; Keller, C; van der Zouw, G; Zeilinger, A (14 October 1999). "Wave-particle duality of C<sub>60</sub> molecules". *Nature*. **401**: 680–682. Bibcode:1999Natur.401..680A. doi:10.1038/44348 (<https://doi.org/10.1038%2F44348>). PMID 18494170 (<https://www.ncbi.nlm.nih.gov/pubmed/18494170>). (subscription required)
21. Olaf Nairz, Markus Arndt, and Anton Zeilinger, "Quantum interference experiments with large molecules", American Journal of Physics, 71 (April 2003) 319–325.
22. Lee, K. C.; Sprague, M. R.; Sussman, B. J.; Nunn, J.; Langford, N. K.; Jin, X.- M.; Champion, T.; Michelberger, P.; Reim, K. F.; England, D.; Jaksch, D.; Walmsley, I. A. (2 December 2011). "Entangling macroscopic diamonds at room temperature" (<http://www.sciencemag.org/content/334/6060/1253.full>). *Science*. **334** (6060): 1253–1256. Bibcode:2011Sci...334.1253L. doi:10.1126/science.1211914 (<https://doi.org/10.1126%2Fscience.1211914>). PMID 22144620 (<https://www.ncbi.nlm.nih.gov/pubmed/22144620>). Lay summary (<https://www.newscientist.com/article/dn21235-entangled-diamonds-blur-quantumclassical-divide.html>).
23. sciencemag.org (<http://www.sciencemag.org/content/334/6060/1253/suppl/DC1>), supplementary materials
24. Kumar, M., *Quantum*, Icon Books, 2009, p. 313.
25. Alisa Bokulich, Gregg Jaeger, *Philosophy of Quantum Information and Entanglement*, Cambridge University Press, 2010, xv.
26. Letter from Einstein to Max Born, 3 March 1947; *The Born-Einstein Letters; Correspondence between Albert Einstein and Max and Hedwig Born from 1916 to 1955*, Walker, New York, 1971. (cited in M. P. Hobson; et al., *Quantum Entanglement and Communication Complexity* (1998), pp. 1/13, CiteSeerX 10.1.20.8324 (<https://citeseerx.ist.psu.edu/viewdoc/summary?doi=10.1.20.8324>))
27. J. S. Bell (1964). "On the Einstein-Podolsky-Rosen paradox". *Physics*.
28. Freedman, Stuart J.; Clauser, John F. (1972). "Experimental Test of Local Hidden-Variable Theories". *Physical Review Letters*. **28** (14): 938–941. Bibcode:1972PhRvL..28..938F. doi:10.1103/PhysRevLett.28.938 (<https://doi.org/10.1103%2FPhysRevLett.28.938>).
29. A. Aspect; P. Grangier & G. Roger (1982). "Experimental Realization of Einstein-Podolsky-Rosen-Bohm Gedankenexperiment: A New Violation of Bell's Inequalities". *Physical Review Letters*. **49** (2): 91–94. Bibcode:1982PhRvL..49...91A. doi:10.1103/PhysRevLett.49.91 (<https://doi.org/10.1103%2FPhysRevLett.49.91>).
30. Hanson, Ronald (2015). "Loophole-free Bell inequality violation using electron spins separated by 1.3 kilometres". *Nature*. **526**: 682–686. arXiv:1508.05949 (<https://arxiv.org/abs/1508.05949>). Bibcode:2015Natur.526..682H. doi:10.1038/nature15759 (<https://doi.org/10.1038%2Fnature15759>). PMID 26503041 (<https://www.ncbi.nlm.nih.gov/pubmed/26503041>).
31. <https://physics.aps.org/articles/v8/123>
32. <http://www.worldscientific.com/doi/abs/10.1142/S0217979206034078>
33. <https://arxiv.org/ftp/quant-ph/papers/0404/0404011.pdf>
34. <http://physicsessays.org/browse-journal-2/product/47-3-dean-l-mamas-an-intrinsic-quantum-state-interpretation-of-quantum-mechanics.html>
35. Khrennikov, Andrei (2016). "After Bell". *Fortschritte der Physik*. **65**: 1600044. doi:10.1002/prop.201600044 (<https://doi.org/10.1002%2Fprop.201600044>).
36. C. H. Bennett and G. Brassard. "Quantum cryptography: Public key distribution and coin tossing". In *Proceedings of IEEE International Conference on Computers, Systems and Signal Processing*, volume 175, page 8. New York, 1984. <http://researcher.watson.ibm.com/researcher/files/us-bennet/BB84highest.pdf>
37. Ekert, A.K. (1991). "Quantum cryptography based on Bell's theorem". *Phys. Rev. Lett.* **APL**. **67** (6): 661–663. Bibcode:1991PhRvL..67..661E. doi:10.1103/PhysRevLett.67.661 (<https://doi.org/10.1103%2FPhysRevLett.67.661>). ISSN 0031-9007 (<https://www.worldcat.org/issn/0031-9007>). PMID 10044956 (<https://www.ncbi.nlm.nih.gov/pubmed/10044956>). (Subscription required ([help](#))).
38. Asher Peres, *Quantum Theory, Concepts and Methods*, Kluwer, 1993; ISBN 0-7923-2549-4 p. 115.
39. Rupert W., Anderson (28 March 2015). *The Cosmic Compendium: Interstellar Travel* (<https://books.google.com/books?id=JxaucQAQBAJ&pg=PA100&lpg=PA100&dq=The+outcome+is+taken+to+be+random+correlated.+This+means+that+the+random+outcome+of+the+measurement+made+or+correlated.%20This%20means%20that%20the%20random%20outcome%20of%20the+First+ed.+The+Cosmic+Compendium.+p.+100>). The Cosmic Compendium. p. 100. ISBN 9781329022027.
40. magazine, Elizabeth Gibney, Nature. "Cosmic Test Bolsters Einstein's "Spooky Action at a Distance"" (<https://www.scientificamerican.com/article/cosmic-test-bolsters-einstein-s-diamonds-spooky-action-at-a-distance/>). *WT.mc\_id=SA\_FPHYS\_NEWS*, *Scientific American*. Retrieved 2017-02-04.
41. I. Gerhardt; Q. Liu; A. Lamas-Linares; J. Skaar; V. Scarani; V. Makarov; C. Kurtsiefer (2011). "Experimentally faking the violation of Bell's inequalities". *Phys. Rev. Lett.* **107** (17): 170404. arXiv:1106.3224 (<https://arxiv.org/abs/1106.3224>). Bibcode:2011PhRvL.107q0404G. doi:10.1103/PhysRevLett.107.170404 (<https://doi.org/10.1103%2FPhysRevLett.107.170404>). PMID 22107491 (<https://www.ncbi.nlm.nih.gov/pubmed/22107491>)
42. Santos, E (2004). "The failure to perform a loophole-free test of Bell's Inequality supports local realism". *Foundations of Physics*. **34**: 1643–1673. Bibcode:2004FoPh..34.1643S. doi:10.1007/s10701-004-1308-z (<https://doi.org/10.1007%2Fsp10701-004-1308-z>).
43. H. Zbinden; et al. (2001). "Experimental test of nonlocal quantum correlations in relativistic configurations". *Phys. Rev. A*. **63** (2): 22111. arXiv:quant-ph/0007009 (<https://arxiv.org/abs/quant-ph/0007009>). Bibcode:2001PhRvA..63b2111Z. doi:10.1103/PhysRevA.63.022111 (<https://doi.org/10.1103%2FPhysRevA.63.022111>)
44. Some of the history of both referenced Zbinden, et al. experiments is provided in Gilder, L., *The Age of Entanglement*, Vintage Books, 2008, pp. 321–324.
45. Cirel'son, B. S. (1980). "Quantum generalizations of Bell's inequality". *Letters in Mathematical Physics*. **4** (2): 93–100. Bibcode:1980LMPa...4...93C. doi:10.1007/BF00417500 (<https://doi.org/10.1007%2FBF00417500>).
46. Xiao-song Ma, Stefan Zoller, Johannes Kofler, Rupert Ursin, Thomas Jennewein, Časlav Brukner & Anton Zeilinger; Zoller; Kofler; Ursin; Jennewein; Brukner; Zeilinger (26 April 2012). "Experimental delayed-choice entanglement swapping". *Nature Physics*. **8** (6): 480–485. arXiv:1203.4834 (<https://arxiv.org/abs/1203.4834>). Bibcode:2012NatPh...8..480M. doi:10.1038/nphys2294 (<https://doi.org/10.1038%2Fnphys2294>).
47. Megidish, E.; Halevy, A.; Shacham, T.; Dvir, T.; Dovrat, L.; Eisenberg, H. S. (2013). "Entanglement Swapping between Photons that have Never Coexisted". *Physical Review Letters*. **110** (21): 210403. arXiv:1209.4191 (<https://arxiv.org/abs/1209.4191>). Bibcode:2013PhRvL.110u0403M. doi:10.1103/physrevlett.110.210403 (<https://doi.org/10.1103%2Fphysrevlett.110.210403>). PMID 23745845 (<https://www.ncbi.nlm.nih.gov/pubmed/23745845>).
48. "Classical carrier could create entanglement" (<http://physicsworld.com/cws/article/news/2013/dec/11/classical-carrier-could-create-entanglement>). physicsworld.com. Retrieved 2014-06-14.
49. <http://hansonlab.tudelft.nl/loophole-free-bell-test/>
50. "Entangled photons make a picture from a paradox" (<http://www.nature.com/news/entangled-photons-make-a-picture-from-a-paradox-1.15781>). *Nature News & Comment*. Retrieved 13 October 2014.
51. Moreva, Ekaterina (2014). "Time from quantum entanglement: an experimental illustration". *Physical Review A*. **89**. arXiv:1310.4691 (<https://arxiv.org/abs/1310.4691>). Bibcode:2014PhRvA..89e2122M. doi:10.1103/PhysRevA.89.052122 (<https://doi.org/10.1103%2FPhysRevA.89.052122>).
52. "Entangled toy universe shows time may be an illusion" ([https://www.newscientist.com/article/dn24473-entangled-toy-universe-shows-time-may-be-an-illusion.html#.U8\\_ApSSx2A](https://www.newscientist.com/article/dn24473-entangled-toy-universe-shows-time-may-be-an-illusion.html#.U8_ApSSx2A)). Retrieved 13 October 2014.
53. David Deutsch, The Beginning of infinity. Page 299
54. "Quantum Experiment Shows How Time 'Emerges' from Entanglement" (<https://medium.com/the-physics-arciv-blog/quantum-experiment-shows-how-time-emerges-from-entanglement-d5d3dc850933>). Medium. Retrieved 13 October 2014.
55. "New Quantum Theory Could Explain the Flow of Time" (<https://www.wired.com/2014/04/quantum-theory-flow-time/>). WIRED. Retrieved 13 October 2014.
56. Werner, R.F. (1989). "Quantum States with Einstein-Podolsky-Rosen correlations admitting a hidden-variable model". *Physical Review A*. **40** (8): 4277–4281. Bibcode:1989PhRvA..40.4277W. doi:10.1103/PhysRevA.40.4277 (<https://doi.org/10.1103%2FPhysRevA.40.4277>). PMID 9902666 (<https://www.ncbi.nlm.nih.gov/pubmed/9902666>).
57. Jaeger G, Shimony A, Vaidman L; Shimony; Vaidman (1995). "Two Interferometric Complementarities". *Phys. Rev.* **51** (1): 54–67. Bibcode:1995PhRvA..51...54J. doi:10.1103/PhysRevA.51.54J (<https://doi.org/10.1103%2FPhysRevA.51.54J>).

58. Nielsen, Michael A.; Chuang, Isaac L. (2000). *Quantum Computation and Quantum Information*. Cambridge University Press, pp. 112–113. ISBN 0-521-63503-9.
59. Laloe, Franck (2012). *Do We Really Understand Quantum Mechanics*, Cambridge University Press, arXiv:quant-ph/0209123 (<https://arxiv.org/abs/quant-ph/0209123>). Bibcode:2002quant.ph..9123L (<http://adsabs.harvard.edu/abs/2002quant.ph..9123L>). ISBN 978-1-107-02501-1.
60. Gurvits L (2003). "Classical deterministic complexity of Edmonds' Problem and quantum entanglement". *Proceedings of the thirty-fifth annual ACM symposium on Theory of computing*: 10. arXiv:quant-ph/0303055 (<https://arxiv.org/abs/quant-ph/0303055>) doi:10.1145/780542.780545 (<https://doi.org/10.1145%2F780542.780545>). ISBN 1-58113-674-9.
61. Horodecki M, Horodecki P, Horodecki R; Horodecki; Horodecki (1996). "Separability of mixed states: necessary and sufficient conditions". *Physics Letters A*. 223: 210. arXiv:quant-ph/9605038 (<https://arxiv.org/abs/quant-ph/9605038>). Bibcode:1996PhLA..223...1H (<http://adsabs.harvard.edu/abs/1996PhLA..223...1H>). doi:10.1016/S0375-9601(96)00706-2 (<https://doi.org/10.1016%2FS0375-9601%2896%2900706-2>).
62. Dirac, P. A. M. (2008). "Note on Exchange Phenomena in the Thomas Atom". *Mathematical Proceedings of the Cambridge Philosophical Society*. 26 (3): 376. Bibcode:1930PCPS...26..376D (<http://adsabs.harvard.edu/abs/1930PCPS...26..376D>). doi:10.1017/S0305004100016108 (<https://doi.org/10.1017%2FS0305004100016108>).
63. Fan, H.; Korepin V; Roychowdhury V (26 November 2004). "Entanglement in a Valence-Bond Solid State". *Physical Review Letters*. 93 (22): 227203. arXiv:quant-ph/0406067 (<https://arxiv.org/abs/quant-ph/0406067>). Bibcode:2004PhRvL..93v7203F (<http://adsabs.harvard.edu/abs/2004PhRvL..93v7203F>). doi:10.1103/PhysRevLett.93.227203 (<https://doi.org/10.1103%2FPhysRevLett.93.227203>). PMID 15601113 (<https://www.ncbi.nlm.nih.gov/pubmed/15601113>).
64. Franchini, F.; Its, A. R.; Korepin, V. E.; Takhtajan, L. A. (2010). "Spectrum of the density matrix of a large block of spins of the XY model in one dimension". *Quantum Information Processing*. 10 (3): 325–341. arXiv:1002.2931 (<https://arxiv.org/abs/1002.2931>) doi:10.1007/s11128-010-0197-7 (<https://doi.org/10.1007%2Fs11128-010-0197-7>).
65. Cerf, Nicolas J.; Cleve, Richard. "Information-theoretic interpretation of quantum error-correcting codes" (<http://authors.library.caltech.edu/5516/1/CERpra97b.pdf#page=10>) (PDF).
66. Plenio; Virmani (2007). "An introduction to entanglement measures". *Quant. Inf. Comp.* 1: 1–51. arXiv:quant-ph/0504163 (<https://arxiv.org/abs/quant-ph/0504163>). Bibcode:2005quant.ph..4163P (<http://adsabs.harvard.edu/abs/2005quant.ph..4163P>).
67. Wolchover, Natalie (25 April 2014). "New Quantum Theory Could Explain the Flow of Time" (<https://www.wired.com/2014/04/quantum-theory-flow-time/>). www.wired.com. Quanta Magazine. Retrieved 27 April 2014.
68. Huang, Yichen (21 March 2014). "Computing quantum discord is NP-complete" (<http://iopscience.iop.org/1367-2630/16/3/033027/article>). *New Journal of Physics*. 16 (3): 033027. arXiv:1305.5941 (<https://arxiv.org/abs/1305.5941>). Bibcode:2014NJPh..16c3027H (<http://adsabs.harvard.edu/abs/2014NJPh..16c3027H>). doi:10.1088/1367-2630/16/3/033027 (<https://doi.org/10.1088%2F1367-2630%2F16%2F3%2F033027>).
69. Bouwmeester, Dik; Pan, Jian-Wei; Mattle, Klaus; Eibl, Manfred; Weinfurter, Harald & Zeilinger, Anton (1997). "Experimental Quantum Teleportation" (<http://qudev.ethz.ch/content/courses/QSIT06/pdfs/Bouwmeester97.pdf>) (PDF). *Nature*. 390 (6660): 575–579. Bibcode:1997Natur.390..575B (<http://adsabs.harvard.edu/abs/1997Natur.390..575B>). doi:10.1038/2F37539 (<https://doi.org/10.1038%2F37539>).
70. Richard Jozsa; Noah Linden (2002). "On the role of entanglement in quantum computational speed-up". *Proceedings of the Royal Society A: Mathematical, Physical and Engineering Sciences*. 459 (2036): 2011–2032. arXiv:quant-ph/0201143 (<https://arxiv.org/abs/quant-ph/0201143>). Bibcode:2003RSPSA.459.2011J (<http://adsabs.harvard.edu/abs/2003RSPSA.459.2011J>). doi:10.1098/rspa.2002.1097 (<https://doi.org/10.1098%2Frspa.2002.1097>).
71. Ekert, Artur K. (1991). "Quantum cryptography based on Bell's theorem". *Physical Review Letters*. 67 (6): 661–663. Bibcode:1991PhRvL..67..661E (<http://adsabs.harvard.edu/abs/1991PhRvL..67..661E>). doi:10.1103/PhysRevLett.67.661 (<https://doi.org/10.1103%2FPhysRevLett.67.661>). PMID 10044956 (<https://www.ncbi.nlm.nih.gov/pubmed/10044956>).
72. Karol Horodecki; Michal Horodecki; Paweł Horodecki; Ryszard Horodecki; Marcin Pawłowski; Mohamed Bourennane (2010). "Contextuality offers device-independent security". arXiv:1006.0468 (<https://arxiv.org/abs/1006.0468>) (<https://arxiv.org/archive/quant-ph/>).
73. Pezze, Luca & Smerzi, Augusto (2009). "Entanglement, Nonlinear Dynamics, and the Heisenberg Limit" (<http://link.aps.org/doi/10.1103/PhysRevLett.102.100401>) (PDF). *Phys. Rev. Lett.* 102 (10): 100401. arXiv:0711.4840 (<https://arxiv.org/abs/0711.4840>). Bibcode:2009PhRvL.102j0401P (<http://adsabs.harvard.edu/abs/2009PhRvL.102j0401P>). doi:10.1103/PhysRevLett.102.100401 (<https://doi.org/10.1103%2FPhysRevLett.102.100401>). PMID 19392092 (<https://www.ncbi.nlm.nih.gov/pubmed/19392092>).
74. Database error – Qwiki ([http://qwiki.stanford.edu/index.php/Spin\\_Squeezed\\_State](http://qwiki.stanford.edu/index.php/Spin_Squeezed_State)) Archived ([https://web.archive.org/web/20120821011018/http://qwiki.stanford.edu/index.php/Spin\\_Squeezed\\_State](https://web.archive.org/web/20120821011018/http://qwiki.stanford.edu/index.php/Spin_Squeezed_State)) 21 August 2012 at the Wayback Machine.
75. Kitagawa, Masahiro; Ueda, Masahito (1993). "Squeezed Spin States" ([http://pra.aps.org/abstract/PRA/v47/i6/p5138\\_1](http://pra.aps.org/abstract/PRA/v47/i6/p5138_1)). *Phys. Rev. A*. 47: 5138–5143. Bibcode:1993PhRvA..47.5138K (<http://adsabs.harvard.edu/abs/1993PhRvA..47.5138K>). doi:10.1103/physreva.47.5138 (<https://doi.org/10.1103%2Fphysreva.47.5138>).
76. Wineland, D. J.; Bollinger, J. J.; Itano, W. M.; Moore, F. L.; Heinzen, D. J. (1992). "Spin squeezing and reduced quantum noise in spectroscopy". *Phys. Rev. A*. 46: R6797–R6800. Bibcode:1992PhRvA..46.6797W (<http://adsabs.harvard.edu/abs/1992PhRvA..46.6797W>). doi:10.1103/PhysRevA.46.R6797 (<https://doi.org/10.1103%2FPhysRevA.46.R6797>).
77. "Phys. Rev. Lett." 71, 1355 (1993): Interferometric detection of optical phase shifts at the Heisenberg limit" ([http://prl.aps.org/abstract/PRL/v71/i9/p1355\\_1](http://prl.aps.org/abstract/PRL/v71/i9/p1355_1)). *Physical Review Letters*. Retrieved 13 October 2014.
78. Horodecki R, Horodecki P, Horodecki M, Horodecki K; Horodecki; Horodecki (2007). "Quantum entanglement". *Rev. Mod. Phys.* 81 (2): 865–942. arXiv:quant-ph/0702225 (<https://arxiv.org/abs/quant-ph/0702225>). Bibcode:2009RvMP...81..865H (<http://adsabs.harvard.edu/abs/2009RvMP...81..865H>). doi:10.1103/RevModPhys.81.865 (<https://doi.org/10.1103%2FRevModPhys.81.865>).
79. Akopian, N. (2006). "Entangled Photon Pairs from Semiconductor Quantum Dots" (<https://doi.org/10.1103/PhysRevLett.96.130501>). *Phys. Rev. Lett.* 96: 130501. arXiv:quant-ph/0509060 (<https://arxiv.org/abs/quant-ph/0509060>). Bibcode:2006PhRvL..96b0501D (<http://adsabs.harvard.edu/abs/2006PhRvL..96b0501D>). doi:10.1103/PhysRevLett.96.020501 (<https://doi.org/10.1103%2FPhysRevLett.96.020501>) – via APS.
80. Rosario Lo Franco and Giuseppe Compagno, "Indistinguishability of Elementary Systems as a Resource for Quantum Information Processing", *Phys. Rev. Lett.* 120, 240403, 14 June 2018.
81. Gurvits, L., Classical deterministic complexity of Edmonds' problem and quantum entanglement, in Proceedings of the 35th ACM Symposium on Theory of Computing, ACM Press, New York, 2003.
82. Sevag Gharibian, Strong NP-Hardness of the Quantum Separability Problem, Quantum Information and Computation, Vol. 10, No. 3&4, pp. 343–360, 2010. arXiv:0810.4507.
83. "Geometrical aspects of entanglement", *Physical Review A* 74, 012313 (2006)
84. <http://physicsworld.com/cws/article/news/2016/aug/16/china-launches-world-s-first-quantum-science-satellite>
85. Science 16 Jun 2017: Vol. 356, Issue 6343, pp. 1140-1144 DOI: 10.1126/science.aan3211
86. Frank Jensen: *Introduction to Computational Chemistry*. Wiley, 2007, ISBN 978-0-470-01187-4.
87. Berkeley Lab Press Release: *Untangling the Quantum Entanglement Behind Photosynthesis: Berkeley scientists shine new light on green plant secrets*. (<http://newscenter.lbl.gov/feature-stories/2010/05/10/untangling-quantum-entanglement/>)
88. Mohan Sarovar, Akihito Ishizaki, Graham R. Fleming, K. Birgitta Whaley: *Quantum entanglement in photosynthetic light harvesting complexes*. arXiv:0905.3787

## Further reading

- Bengtsson I; Życzkowski K (2006). "Geometry of Quantum States". *An Introduction to Quantum Entanglement*. Cambridge: Cambridge University Press. second, revised edition (2017) (<http://chaos.if.uj.edu.pl/~karol/geometry.htm>)
- Cramer, JG (2015). *The Quantum Handshake: Entanglement, Nonlocality and Transactions*. Springer Verlag. ISBN 978-3-319-24642-0.
- Gühne, O.; Tóth, G. (2009). "Entanglement detection". *Physics Reports*. 474: 1–75. arXiv:0811.2803 (<https://arxiv.org/abs/0811.2803>). Bibcode:2009PhR...474....1G (<http://adsabs.harvard.edu/abs/2009PhR...474....1G>). doi:10.1016/j.physrep.2009.02.004 (<https://doi.org/10.1016%2Fj.physrep.2009.02.004>).
- Horodecki R, Horodecki P, Horodecki M, Horodecki K; Horodecki; Horodecki; Horodecki (2009). "Quantum entanglement". *Rev. Mod. Phys.* 81 (2): 865–942. arXiv:quant-ph/0702225 (<https://arxiv.org/abs/quant-ph/0702225>). Bibcode:2009RvMP...81..865H (<http://adsabs.harvard.edu/abs/2009RvMP...81..865H>). doi:10.1103/RevModPhys.81.865 (<https://doi.org/10.1103%2FRevModPhys.81.865>).
- Jaeger G (2009). *Entanglement, Information, and the Interpretation of Quantum Mechanics*. Heidelberg: Springer. ISBN 978-3-540-92127-1.

- Plenio MB, Virmani S; Virmani (2007). "An introduction to entanglement measures". *Quant. Inf. Comp.* 1 (7): 151. arXiv:quant-ph/0504163 (<https://arxiv.org/abs/quant-ph/0504163>) Bibcode:2005quant.ph..4163P (<http://adsabs.harvard.edu/abs/2005quant.ph..4163P>).
- Shadbolt PJ, Verde MR, Peruzzo A, Politi A, Laing A, Lobino M, Matthews JCF, Thompson MG, O'Brien JL; Verde; Peruzzo; Politi; Laing; Lobino; Matthews; Thompson; O'Brien (2012). "Generating, manipulating and measuring entanglement and mixture with a reconfigurable photonic circuit". *Nature Photonics*. 6: 45–59. arXiv:1108.3309 (<https://arxiv.org/abs/1108.3309>) Bibcode:2012NaPho...6...45S (<http://adsabs.harvard.edu/abs/2012NaPho...6...45S>). doi:10.1038/nphoton.2011.283 (<https://doi.org/10.1038%2Fnphoton.2011.283>).
- Steward EG (2008). *Quantum Mechanics: Its Early Development and the Road to Entanglement*. Imperial College Press. ISBN 978-1-86094-978-4.
- Vedral, V. (2002). "The role of relative entropy in quantum information theory". *Reviews of Modern Physics*. 74: 197–234. arXiv:quant-ph/0102094 (<https://arxiv.org/abs/quant-ph/0102094>) Bibcode:2002RvMP...74..197V (<http://adsabs.harvard.edu/abs/2002RvMP...74..197V>). doi:10.1103/RevModPhys.74.197 (<https://doi.org/10.1103%2FRevModPhys.74.197>).

## External links

---

- The original EPR paper ([http://prola.aps.org/abstract/PR/v47/i10/p777\\_1](http://prola.aps.org/abstract/PR/v47/i10/p777_1))
  - Quantum Entanglement at Stanford Encyclopedia of Philosophy (<http://plato.stanford.edu/entries/qt-entangle/>)
  - How to entangle photons experimentally (subscription required) (<http://physicsworldarchive.iop.org/index.cfm?action=summary&doc=11%2F3%2Fphwv11i3a29%40pwa-xml&q=1>)
  - A creative interpretation of Quantum Entanglement (<https://web.archive.org/web/20110220045318/http://www.physicaltv.com.au/DanceFilmEntanglementTheoryrichardJamesAllenkarenPearlmangaryHayesmixedRealityLiveActions>)
  - Albert's chest: entanglement for lay persons ([http://www.science20.com/hammock\\_physicist/einstein\\_got\\_it\\_wrong\\_can\\_you\\_do\\_better-85544](http://www.science20.com/hammock_physicist/einstein_got_it_wrong_can_you_do_better-85544))
  - How Quantum Entanglement Works (<https://web.archive.org/web/20080402000326/http://davidjarvis.ca/entanglement/>)
  - Explanatory video by Scientific American magazine (<https://www.youtube.com/watch?v=xM3GOXacizw>)
  - Hanson Lab – Loophole-free Bell test 'Spooky action at a distance', no cheating. (<http://hansonlab.tudelft.nl/loophole-free-bell-test/>)
  - Two Diamonds Linked by Strange Quantum Entanglement (<https://news.yahoo.com/two-diamonds-linked-strange-quantum-entanglement-190805281.html>)
  - Entanglement experiment with photon pairs – interactive (<http://www.didaktik.physik.uni-erlangen.de/quantumlab/english/index.html>)
  - Multiple entanglement and quantum repeating (<http://www.physorg.com/news63037231.html>)
  - Quantum Entanglement and Bell's Theorem at MathPages (<http://www.mathpages.com/home/kmath521/kmath521.htm>)
  - Audio – Cain/Gay (2009) Astronomy Cast (<http://www.astronomycast.com/physics/ep-140-entanglement/>) Entanglement
  - Recorded research seminars at Imperial College relating to quantum entanglement (<http://www.imperial.ac.uk/quantuminformation>)
  - Quantum Entanglement and Decoherence: 3rd International Conference on Quantum Information (ICQI) (<http://www.osa.org/meetings/topicalmeetings/ICQI/default.aspx>)
  - Ion trapping quantum information processing (<http://www.npl.co.uk/server.php?show=ConWebDoc.433>)
  - IEEE Spectrum On-line: *The trap technique* (<http://www.spectrum.ieee.org/aug07/5378/1>)
  - Was Einstein Wrong?: A Quantum Threat to Special Relativity (<http://www.sciam.com/article.cfm?id=was-einstein-wrong-about-relativity>)
  - Citizenium: Entanglement ([http://en.citizenium.org/wiki/Entanglement\\_\(physics\)](http://en.citizenium.org/wiki/Entanglement_(physics)))
  - Spooky Actions At A Distance?: Oppenheimer Lecture, Prof. David Mermin (Cornell University) Univ. California, Berkeley, 2008. Non-mathematical popular lecture on YouTube, posted Mar 2008 (<https://www.youtube.com/watch?v=ta09WXiUqcQ>)
  - "StateSeparator" web-app (<http://physics.technion.ac.il/statesseparator/>)
- 

Retrieved from "[https://en.wikipedia.org/w/index.php?title=Quantum\\_entanglement&oldid=846509975](https://en.wikipedia.org/w/index.php?title=Quantum_entanglement&oldid=846509975)"

### 3. Description of entanglement

**Abstract:** Mathematical description is obtained using bra-ket notation.

**Keywords:** Bra-ket notation

## **Entanglement: from its mathematical description to its experimental observation**

Daniel Cavalcanti Santos

Director: Antonio Acín Dal Maschio  
Tutor: José Ignacio Latorre

Tesis presentada para optar al grado de doctor por el programa de física avanzada del Departament d'Estructura i Constituents de la Matèria de la Universitat de Barcelona.  
Bienio: 2006/2007.  
Barcelona, May, 2008.



# Acknowledgments

Of course it will be difficult to put everybody i should thank in this acknowledgment. So let me say THANKS for everybody who helped me to get here, in BCN, defending this PhD thesis. Uff....now I didn't miss anybody! But ok...let me make some specially thank some people who helped me a lot during all these years .

I must start by thanking Toni, first of all for being a friend. We always had a good time together, in ICFO, having dinners, beers, playing football, .... But of course i have to say that he is also a really good supervisor: relaxed enough for *making light work* (hmmm?!!!!), but at the same time always pushing me with a lot of good ideas. Ah, and i can't forget to thank him for the hitchhiking during the flats change!

The second person i must thank is Flavia. Leaving one year far away was not easy, but i am sure it was as easy as possible!!! Thanks for coming, for waking up with me everyday (this is not easy, hm?!!!), for making "mousse de chocolate" (apesar de me pôr pra bater clara em neve ;)), for listen to me talking about entanglement, ...for so many things that it is impossible to put all of them here. Thanks thanks thanks thanks....smacechhhh!!!!

A BIG thanks for my family. Um beij ao pra vovô Dêa, vovô Émis, Mamãe Malina e pro Fulustrico The support they always gave me is amazing.

A special thank for Terra for being so open-minded and letting me scape to BCN!

I also must say that I am very luck to work in this group. Nothing is better than working besides friends! I have been learning so many things with Maf, Artur, Stefano, Ale, Miguel, Joonwoo, Giuseppe, and Leandro! Thank you guys! But specially, thanks: Ale, for saving me in Pisa. Man, i will never forget your face, at 4am, saying "él doctor dijo que tendrás que operar ahora mismo!!!" Que putada! Maf, for all the good time we had together (quanta festa heim!!!). Brigadão! Miguel and Stefano for the good emails (please, keep thinking that a good joke is better than a PRL).

Let me also thank Simone Montangero for the help in Pisa. I think he doesn't know, but his friend appeared in a crucial moment!!!

I am very thankful for all my collaborators: Terra, Leandro (Ciolletti), Marcelo França, Fernando, Zé Jr, Zé Pai, Xubaca, Franklin, Leandro (Aolita), Planet, Alejo, Luiz, Vlatko, Christian, Monken, Pablo, Olavo, Sebastião, Toni, Ale Ferraro, and Artur.

2

Finally, before start talking about entanglement many thanks also for...

...Carlos (for being noisy) and Irene (for being noiseless).

...Leandro, Planet, Ale, and Sol for bikes and bikes.

...Clara for correcting my spanish.

...Banasque Center for Sciences for organizing the best conference ever.

...A. Buchleitner's group for the very nice week in Freiburg.

...C. Monken and Mario Sergio for pushing me to come to BCN.

...the good weather of BCN.

THANK YOU ALL!

# Abstract

Entanglement is the main quantum property that makes quantum information protocols more powerful than any classical counterpart. Moreover, understanding entanglement allows a better comprehension of physical phenomena in the fields of condensed matter, statistical physics, and quantum optics among others.

The open questions on entanglement range from fundamental to practical issues. How to characterize the entanglement of quantum systems? What is entanglement useful for? What is the relation between entanglement and other physical phenomena? These are some open questions we are faced with nowadays.

This thesis contains several original results in this field. Some of the addressed questions rely on the mathematical description of entanglement while others on its description in some physical systems. More specifically,

- (i) it will be shown a relation between two quantifiers of entanglement, the *generalized robustness* and the *geometric measure of entanglement*;
- (ii) the entanglement of superpositions will be generalized to the multi-partite case and to several entanglement quantifiers;
- (iii) a recently proposed Bell inequality for continuous-variable (CV) systems will be used to extend, for the CV scenario, the Peres' conjecture that bound entangled states admit a description in terms of hidden variables.
- (iv) a proposal to probe the geometry of the set of separable states will be made. This approach is able to find singularities in the border of this set, and those are reflected in the entanglement properties of condensed matter, atomic, and photonic systems. An experiment involving entangled photons coming from parametric down conversion will be described to illustrate the theoretical results;
- (v) the decay of entanglement of generalized  $N$ -particle GHZ states interacting with independent reservoirs will be investigated. Scaling laws for the decay of entanglement and for its finite-time extinction (sudden death) are derived for different types of reservoirs. The latter is found to increase with the number of particles. However, entanglement becomes arbitrarily small, and therefore useless as a resource, much before it completely disappears, around a time which is inversely proportional to the number of particles. The decay of multi-particle GHZ states will be shown to generate bound entangled states;

(vi) and finally, the entanglement properties of particles in a non-interacting Fermi gas are studied. Since there is no interaction among the particles, this entanglement comes solely from the statistical properties of the particles. It will be shown how the way we detect the particles changes their entanglement properties. Additionally a realistic proposal to convert identical particle entanglement of fermions in a quantum well into useful photonic entanglement will be given.

# List of Publications

1. *Scaling Laws for the decay of multiqubit entanglement.*  
 L. Aolita, R. Chaves, D. Cavalcanti, A. Acín, and L. Davidovich.  
 Physical Review Letters **100**, 080501 (2008).
2. *Thermal bound entanglement in macroscopic systems and area law.*  
 A. Ferraro, D. Cavalcanti, A. García-Saez, and A. Acín.  
 Physical Review Letters **100**, 080502 (2008).
3. *Area laws and entanglement distillability of thermal states.*  
 D. Cavalcanti, A. Ferraro, A. García-Saez, and A. Acín.  
 Proceedings of the “Entanglement and Many-body Systems” Conference, Pisa May 2008.
4. *Distillable entanglement and area laws in spin and harmonic-oscillator systems.*  
 D. Cavalcanti, A. Ferraro, A. García-Saez, and A. Acín.  
 Submitted to Physical Review A (2008) - preprint available as arXiv:0705.3762.
5. *Geometrically induced singular behavior of entanglement.*  
 D. Cavalcanti, P.L. Saldanha, O. Cosme, F.G.S.L. Brandão, C.H. Monken,  
 S. Pádua, M. F. Santos, and M. O. Terra Cunha.  
 Submitted to Physical Review Letters (2008) - preprint available as  
 arXiv:0709.0301.
6. *Non-locality and Partial Transposition for Continuous-Variable Systems.*  
 A. Salles, D. Cavalcanti and A. Acín.  
 Submitted to Physical Review Letters (2008) - preprint available as  
 arXiv:0804.4703.
7. *Multipartite entanglement of superpositions.*  
 D. Cavalcanti, M. O. Terra Cunha, and A. Acín.  
 Physical Review A **76**, 042329 (2007).
8. *Useful entanglement from the Pauli principle.*  
 D. Cavalcanti, L. M. Moreira, F. M. Matinaga, M.O. Terra Cunha, and  
 M.F. Santos.  
 Phys. Rev. B **76**, 113304 (2007).

9. *Connecting the generalized robustness and the geometric measure of entanglement.*  
D. Cavalcanti.  
Physical Review A **73**, 044302 (2006).
10. *Estimating entanglement of unknown states.*  
D. Cavalcanti and M. O. Terra Cunha.  
Applied Physics Letters **89**, 084102 (2006).
11. *Entanglement versus energy in the entanglement transfer problem.*  
D. Cavalcanti, J. G. Oliveira Jr, J. G. Peixoto de Faria, M.O. Terra Cunha, and M.F. Santos.  
Physical Review A **74**, 042328, (2006).
12. *Entanglement quantifiers, entanglement crossover, and phase transitions.*  
D. Cavalcanti, F.G.S.L. Brandão, and M.O. Terra Cunha.  
New Journal of Physics **8**, 260 (2006).
13. *Are all maximally entangled states pure?*  
D. Cavalcanti, F.G.S.L. Brandão, and M.O. Terra Cunha.  
Physical Review A **72**, 040303(R) (2005).
14. *Increasing identical particle entanglement by fuzzy measurements.*  
D. Cavalcanti, M.F. Santos, M. O. Terra Cunha, C. Lunkes, and V. Vedral.  
Physical Review A **72**, 062307 (2005).
15. *Tomographic characterization of three-qubit pure states using only two-qubit detectors.*  
D. Cavalcanti, L.M. Cioletti, and M.O. Terra Cunha.  
Physical Review A **71**, 034301 (2005).

# Contents

<b>Acknowledgments</b>	<b>1</b>
<b>Abstract</b>	<b>3</b>
<b>List of Publications</b>	<b>5</b>
<b>1 Introduction</b>	<b>11</b>
1.1 Motivation . . . . .	12
1.2 Contributions . . . . .	14
1.3 Overview . . . . .	17
<b>2 Background</b>	<b>19</b>
2.1 What is entanglement? . . . . .	19
2.2 How to detect entanglement? . . . . .	21
2.3 How to quantify entanglement? . . . . .	24
<b>3 Connecting the Geometric Measure and the Generalized Robustness of Entanglement</b>	<b>31</b>
3.1 Relating $R_g$ and $E_{GME}$ to entanglement witnesses. . . . .	31
3.2 $E_{GME}$ as a lower bound for $R_g$ . . . . .	32
3.3 Examples . . . . .	33
3.4 Concluding remarks . . . . .	35
<b>4 Multipartite entanglement of superpositions</b>	<b>37</b>
4.1 Dealing with the witnessed entanglement . . . . .	37
4.2 Are these relations tight? . . . . .	39
4.3 Concluding remarks . . . . .	41
<b>5 Non-locality and partial transposition for continuous variable systems</b>	<b>43</b>
5.1 The CFRD inequality . . . . .	45
5.2 SV criterion . . . . .	46

5.3	Nonlocality implies NPT . . . . .	47
5.4	Non-orthogonal quadratures . . . . .	49
5.5	Relevance of the CFRD inequality . . . . .	50
5.6	Concuding remarks . . . . .	51
<b>6</b>	<b>Geometrically induced singular behavior of entanglement</b>	<b>53</b>
6.1	The random robustness as a geometric microscope . . . . .	54
6.2	Where do these singularities appear? . . . . .	56
6.2.1	Entanglement swapping . . . . .	56
6.2.2	Bit-flip noisy channel . . . . .	56
6.2.3	Spin systems . . . . .	58
6.3	Concluding remarks . . . . .	58
<b>7</b>	<b>Scaling laws for the decay of multiqubit entanglement</b>	<b>63</b>
7.1	Decoherence models . . . . .	64
7.1.1	Generalized Amplitude Damping Channel . . . . .	65
7.1.2	Depolarizing Channel . . . . .	65
7.1.3	Phase Damping Channel . . . . .	66
7.2	Entanglement sudden death . . . . .	66
7.3	The environment as a creator of bound entanglement . . . . .	69
7.4	Does the time of ESD really matter for large N? . . . . .	69
7.5	Concluding remarks . . . . .	71
<b>8</b>	<b>Identical particle entanglement in Fermionic systems</b>	<b>73</b>
8.1	Non-interacting Fermi gas . . . . .	74
8.1.1	Perfect detection . . . . .	74
8.1.2	Imperfect detection . . . . .	76
8.2	Useful entanglement from the Pauli principle . . . . .	78
8.2.1	Selection rules . . . . .	79
8.2.2	From fermions to photons . . . . .	80
8.2.3	Some imperfections . . . . .	82
8.3	Concluding remarks . . . . .	84
<b>9</b>	<b>Conclusions and Perspectives</b>	<b>87</b>
<b>A</b>	<b>Multipartite entanglement</b>	<b>89</b>
<b>B</b>	<b><math>R_R^k</math> as a detector of singularities in <math>S_k</math></b>	<b>91</b>
<b>C</b>	<b>Experimental Setup</b>	<b>93</b>

<i>CONTENTS</i>	9
<b>D Full separability of GHZ states under the Amplitude Damping Channel</b>	<b>95</b>
<b>E Resumen</b>	<b>97</b>
E.1 Introducción a la teoría del entrelazamiento . . . . .	100
E.1.1 Definiciones . . . . .	100
E.1.2 Detectando el entrelazamiento . . . . .	101
E.1.3 Cuantificando el entrelazamiento . . . . .	102
E.2 Contribuciones . . . . .	103



# Chapter 1

## Introduction

Quantum Mechanics was born as a framework to describe physical phenomena at the atomic level. Amazingly successful, this theory was rapidly applied to a lot of scenarios such as atomic emission, particle scattering, and radiation-matter interaction [ER85, FLS65].

The first strong criticism to quantum theory came with the Einstein, Podolsky and Rosen's (EPR) paper “Can quantum-mechanical description of the physical reality be considered complete?” [EPR35]. These authors recognized that, although quantum theory could catch many physical effects, it allowed weird predictions such as instantaneous actions at distance. In the essence of the EPR argument was the use of what is nowadays called an *entangled* state. Motivated by EPR, Schödinger was the one who first discussed the fact that some composite quantum systems can be better understood if we look at them as a whole, instead of addressing their parts separately [Sch35].

Many years passed until J. Bell put all this discussion in more solid grounds. Accepting the notion of local realism adopted by EPR, Bell developed his famous inequality involving statistics of measurements on composite quantum systems [Bel87]. From that point on, the local realism debate could go to the labs. Some time later the first experimental tests of Bell inequalities started to appear [FC72, FT76, AGG81, ADG82] and confirm the non-local aspect of quantum mechanics. As unentangled states (also called separable states) can never violate a Bell inequality, the experimental violation of Bell inequalities can be seen as the first observation of entanglement [Ter00].

Up to the 90's the debate on separability was played mostly in a fundamental level, relying in the grounds of Quantum Mechanics. It was only with the appearance of the first tasks on Quantum Communication and Quantum Computation that the term “entanglement” got the status of “the resource” capable of providing us advantageous methods over classical information pro-

cessing [NC00, BEZ00]. In 1991, it was described a Cryptographic protocol entirely based on entanglement [Eke91]. However, at that time, the community already knew that without entanglement the same goal could be reached [BB84, BBD92]. Perhaps the turning point on the theory of entanglement was the discovery of Quantum Teleportation [BBC+93]. At that moment it became completely clear the role of entanglement in practical tasks.

From that point on entanglement theory took its own road, being recognized as a discipline itself inside Quantum Information. Among the main goals of entanglement theory are the development of a mathematical framework able to describe this issue, the search for applications of entanglement, the study of the role it plays in natural physical phenomena, and, coming back to fundamental problems, its importance in the foundations of Quantum Mechanics. Nowadays the literature on entanglement is amazingly big. The purpose of this thesis is not to give the reader a survey on this topic, but, instead, to contribute to the knowledge of this field. More appropriate reviews on entanglement are found in Refs. [HHHH07, AFOV07, PV05, Bru02, Ter02, PV98, Ver02, Eis01, EP03].

## 1.1 Motivation

As commented before the open questions in this field range from the mathematical description to practical applications. Among all these facets of entanglement I will try to give here a small flavor of those which motivated me more during my PhD.

Although the mathematical definition of entanglement is relatively simple, the task of deciding if a general state is entangled is incredibly difficult [Ter02, HHHH07]<sup>1</sup>. Developing techniques to attack this problem is one of the major goals of entanglement theory. A step further of “just” knowing whether a state is entangled is to know how much entangled it is. Following this vein, entanglement quantifiers are a set of rules one applies to a quantum state in order to estimate its amount of entanglement [PV98]. Behind the initial attempts to quantify entanglement was the idea of quantifying how useful a quantum state is to perform some task [BBP+96, BDSW96]. This is a very promising way of defining entanglement quantifiers, but it certainly depends on the task one is dealing with. A more axiomatic road is just to define a set of properties an entanglement quantifier must satisfy, without wondering whether the quantifier itself carries a physical meaning [Vid00, VPRK97]. Finally, another approach frequently followed is to quan-

---

<sup>1</sup>In technical terms it is said that the problem of determining if a general state is entangled is NP-hard [Gur03].

tify entanglement using geometric ideas. We can organize quantum states in mathematical sets, and define distances on these sets. The amount of entanglement of a given state can be quantified, in this way, by the distance between this state and the set of unentangled states [VPRK97, VP98]. The number of proposed entanglement quantifiers is huge, and understanding the properties of each quantifier and the information they bring is an important branch of entanglement theory. In this sense, getting relations among the existing quantifiers could help us to get a better understanding on how to order quantum states in terms of their entanglement content.

With the development of entanglement theory it started to be possible to connect this issue to other fields of physics. For instance, the study of entanglement in realistic models has allowed us to get a deeper understanding of several phenomena in condensed matter, atomic and photonic systems [RMH01, LBMW03, KWN+07, AFOV07]. Practical questions concern which kinds of interactions allow the production of entanglement, how it behaves under specific unitary evolution and how is entanglement affected by the presence of noisy environments.

Following the last point, it is essential to understand how entanglement behaves in realistic situations where unavoidable errors in the preparation of states and unwanted interactions during the post-processing are present. Many studies linking entanglement and decoherence have appeared so far [Dio03, DH04, YE04, YE06, YE07, SMDZ07, Ter07, AJ07], but some fundamental questions are still to be answered. One of them concerns the behavior of multiparticle entanglement under decoherence processes [SK02, CMB04, DB04, HDB05]. From a theoretical point of view, understanding this problem would give us a better understanding on the appearance of classicality when increasing the system's size. From a practical point of view, this issue is crucial since the speed-up gained when using quantum-mechanical systems, instead of classical ones, for information processing is specially relevant in the limit of large systems.

Finally, most of the theory of entanglement was constructed in the scenario of distinguishable particles. In this case one identifies (labels) the subsystems and then defines what is a local, or individual, operation. When dealing with identical particles the idea of entanglement becomes much subtler: in an identical particle scenario labeling the subsystems makes no sense anymore and then talking about local operations is misleading. Another problem concerning identical particles is that entanglement “comes for free” in this case. Two fermions in the same location get spin entangled (in a singlet state) just because they obey the fermionic statistics. It is then not clear, and actually controversial, how to describe this kind of quantum correlations, if they are useful for quantum information processing, or even if

we should call them “entanglement” [ESBL04, GM04] .

## 1.2 Contributions

Let me briefly comment on some of the ideas that I, together with collaborators, developed to get a better understanding of entanglement.

### Geometric Measure vs. the Robustness of Entanglement.

As already commented, many are the entanglement quantifiers proposed up to now. Finding relations between them can help us to classify them, and get a better understanding on the information they give us. I have found a relation between two standard quantifiers, the Geometric Measure ( $E_{GME}$ ) and the Generalized Robustness of Entanglement ( $R_g$ ). While the first has a clear geometrical meaning as a distance between an entangled states and the set of separable states, the latter was proposed as a measure of how much noise a state can tolerate before it loses its entanglement.

It follows from their definition that  $R_g$  is always larger than or equal to  $E_{GME}$ . I will show a better lower bound to  $R_g$  based only on the purity of the quantum state and its maximal overlap to a separable state. As we will see it is possible to express this lower bound in terms of  $E_{GME}$ . I will finally identify cases where this bound is tight.

### Multipartite entanglement of superpositions.

Given two pure states  $|\Psi\rangle$  and  $|\Phi\rangle$ , how is the entanglement of the superposition state  $a|\Psi\rangle+b|\Phi\rangle$  related to the entanglement of the constituents  $|\Psi\rangle$  and  $|\Phi\rangle$ ? This question was first addressed by Linden, Popescu and Smolin, who gave upper bounds to the entanglement of the superposed state in terms of the entanglement of the former states [LPS06].

M. Terra Cunha, A. Acín and I have considered a possible generalization of the Linden, Popescu and Smolin’s result to the multipartite scenario: an upper bound to the multipartite entanglement of a superposition was given in terms of the entanglement of the superposed states and the superposition coefficients. We have proven that this bound is tight for a class of states composed by an arbitrary number of qubits. Our results also extend the entanglement of superpositions to a large family of quantifiers which includes the negativity, the robustness of entanglement, and the best separable approximation measure.

### Bound entanglement and Bell violation in a continuous-variable scenario.

Guided by the similarities between the processes of entanglement distillation [BDSW96] and revealing hidden non-locality [Pop95, Per96a], A. Peres conjectured that all undistillable states<sup>2</sup> satisfy Bell inequalities. This conjecture has been confirmed only in the scenario where  $N$  individuals apply just two measurement settings of binary outcomes.

Recently a new Bell inequality has appeared which can be applied to unbounded operators, i.e. it works in a continuous-variable scenario [CFRD07]. Using this new Bell inequality we will see that it is possible to extend Peres conjecture to the CV scenario, and prove that all states having a positive partial transposition satisfy this inequality<sup>3</sup>. These results were found in collaboration with A. Salles and A. Acín.

### Shining light on the geometry of entanglement.

The set of quantum states is convex and closed: convex combinations of quantum states are also quantum states. The set of separable states forms a subset, which is again convex and closed. Apart from these features that follow directly from the definition of quantum and separable states [BZ06], subtler questions arise when considering these states. How to characterize the shape or the volume of these sets and to determine whether they have any influence on directly measurable quantities are some of these queries.

In collaboration with M. Terra Cunha, M. F. Santos, F. Brandão, P. Lima, O. Cosme, S. Pádua, and C. Monken I proposed a method to investigate the shape of the set of separable states through an entanglement quantifier called *random robustness of entanglement*. This quantifier serves as a “microscope” to probe the boundary of the set of separable states. Moreover this investigation can be done experimentally, what allows to get information on the shape of the set of different entangled states in real experiments. We implemented this method in a photonic experiment and found singularities in the shape of the separable states in the two-qubit case. As a consequence, singularities appear in the quantum correlations a system presents. I will also show that this phenomenon appears naturally in physical processes like the entanglement transfer problem, spin systems under varying magnetic fields, and decoherence processes.

---

<sup>2</sup>The concept of entanglement distillation will be discussed later.

<sup>3</sup>All states having positive partial transposition are undistillable [HHH98], while the opposite is not known.

### Multipartite Entanglement vs. Decoherence.

In the real world we never have a pure quantum state. Due to unavoidable errors in the preparation of states or noise in their postprocessing we always deal with mixed states. Entanglement is very fragile to these noisy processes and this is certainly the main obstacle to real applications on Quantum Communication and Computation. On the other hand, the phenomenon of coherence loss, or decoherence, is in the core of the quantum-classical transition [Zur03]. So, understanding how quantum systems behave under the presence of noise is a fascinating challenge both from a practical and a fundamental perspective.

With L. Aolita, R. Chaves, L. Davidovich, and A. Acín, I have addressed this point and investigated the decay of entanglement of a representative family of states, namely unbalanced GHZ states consisting of an arbitrary number of particles. Different types of reservoirs interacting independently with each subsystem were considered and scaling laws for the decay of entanglement and for its finite-time extinction were found. The latter increases with the number of particles. However, entanglement becomes arbitrarily small, and therefore useless as a resource, much before it completely disappears, around a time which is inversely proportional to the number of particles. It was also shown that the decay of multi-particle GHZ states can generate bound entangled states.

### Is identical-particle entanglement useful?

Suppose a gas of non-interacting fermions at zero temperature. If we pick up two fermions from this gas, are they spin-entangled? I have studied this question together with M. F. Santos, M. Terra Cunha, C. Lunkes, and V. Vedral, and showed that its answer depends not only on the distance between the particles but also on the way (the detector) we pick them. We first considered an ideal measurement apparatus and defined operators that detect the symmetry of the spatial and spin part of the density matrix as a function of particle distance. Then, moving to realistic devices that can only detect the position of the particle to within a certain spread, it was surprisingly found that the entanglement between particles increases with the broadening of detection.

In this context we also considered the problem of using this identical particle entanglement. For this aim, L. Malard and F. Matinaga joined us to report on a scheme to extract entanglement from semiconductor quantum wells. Two independent photons excite non-interacting electrons in the semiconductor. As the electrons relax to the bottom of the conduction band,

the Pauli exclusion principle forces the appearance of quantum correlations between them. I will show that, after the electron-hole recombination, this correlation is transferred to the emitted photons as entanglement in polarization, which can be further used for quantum information tasks. We can then conclude that *identical particle entanglement is indeed useful for quantum information processing!*

## 1.3 Overview

I will start this thesis by reviewing the existing ideas needed to the derivation of the thesis' results. They consist on basic concepts on entanglement theory and are given here for the sake of completeness. In the remaining chapters I will expose some of the original results I developed during my PhD.

The next three chapters are more related to the mathematical formalism of entanglement theory: chapter 2 shows a connection between two entanglement quantifiers, chapter 3 discusses the problem of the entanglement of superpositions, and chapter 4 focuses on the relation between entanglement and violation of Bell inequalities. Chapter 5 deals with a mathematical problem as well, the geometry of entanglement, but also aims at finding consequences of it in physical phenomena. A photonic experiment was implemented to illustrate our achievements on this subject.

The following chapters are related to the characterization of entanglement in specific physical processes. Chapter 6 describes how the entanglement of an important family of multiparticle system changes in the presence of noise. Chapter 7 discusses the entanglement properties of degenerate Fermi gases and how the way we observe this system influences the entanglement we detect. Moreover I consider an exemplary system, a semiconductor quantum well, to show that the Pauli principle can be used to create useful entanglement. Finally I will draw some conclusions in the last chapter and point out future directions that could be followed towards a better understanding of entanglement.



# Chapter 2

## Background

In this chapter I will briefly review the concepts used in the development of the ideas presented in the next chapters. The goal is not to give a broad overview on each of the addressed topic. Thus, many important results on entanglement will be skipped here. The purpose of this chapter is to provide the reader a self-contained text and also of finding some useful references. Those who are already familiar with entanglement theory can skip this part of the thesis. More complete reviews on entanglement can be found in Refs. [HHHH07, AFQV07, PV05, Bru02, Ter02, PV98, Ver02, Eis01, EP03].

### 2.1 What is entanglement?

Quantum states are described by semi-definite positive operators of unity trace acting on a Hilbert space  $\mathcal{H}$  known as the state space. Thus, an operator  $\rho \in \mathcal{B}(\mathcal{H})$  (the Hilbert space of operators acting on  $\mathcal{H}$ ) representing a quantum states satisfies:

1.  $\rho \geq 0$ ;
2.  $\text{Tr}(\rho) = 1$ .

Such operators are called density matrices or density operators. Any density operator can be written (non-uniquely) through convex combinations of one-dimensional projectors, that is,

$$\rho = \sum_i p_i |\psi_i\rangle \langle \psi_i|, \quad (2.1)$$

such that

$$\sum_i p_i = 1 \quad \text{and} \quad p_i \geq 0. \quad (2.2)$$

A special case of representation (2.1) is when  $p_i = 1$  for some  $i$ , so we can describe a quantum state by a unidimensional projector, *i.e.*:

$$\rho = |\psi_i\rangle \langle \psi_i|. \quad (2.3)$$

In this case,  $\rho$  is called a pure state. Pure states are the extreme points of the set of quantum states and then represent those systems from which we have the most complete information.

System composed by many parts  $A, B, \dots$ , and  $N$  are also represented by density operators, but now acting on a vectorial space  $\mathcal{H}$  with a tensorial structure:

$$\mathcal{H} = \mathcal{H}_A \otimes \mathcal{H}_B \otimes \dots \otimes \mathcal{H}_N, \quad (2.4)$$

where  $\mathcal{H}_A, \mathcal{H}_B, \dots$ , and  $\mathcal{H}_N$  are the state spaces for each part.

The notion of entanglement appears in these composite spaces. Let me first present the definition of entanglement and separability for bipartite systems, and then move on to the idea of multipartite entanglement.

**Definition 1 - Bipartite separability:** *Bipartite separable states are those which can be written as a convex combination of tensor products of density matrices, i.e.:  $\rho \in \mathcal{B}(\mathcal{H}_A \otimes \mathcal{H}_B)$  is separable if*

$$\rho = \sum_i p_i \rho_i^A \otimes \rho_i^B, \quad (2.5)$$

where  $\{p_i\}$  is a probability distribution. Alternatively, states that cannot be written in this form are called entangled.

An example of an entangled state is  $|\Phi_+\rangle = (|00\rangle + |11\rangle)/\sqrt{2}$ .

In the case of bipartite systems we need just to make a distinction between separable and entangled states. When multiple parts are involved it may happen that a state contains entanglement among some parts which, at the same time, are separated from others. An example is the state

$$\frac{(|00\rangle + |11\rangle)}{\sqrt{2}} \otimes \frac{(|00\rangle + |11\rangle)}{\sqrt{2}}, \quad (2.6)$$

which contains entanglement between the first two and between the last two subsystems, but not between these two subgroups. In this context, different ways of entangling multiple parts emerge. We are then led to the notion of  $k$ -separability [DCT99, DC00, ABLS01]:

**Definition 2 -  $k$ -separability:** *A quantum state is called  $k$ -separable if it can be written as a convex combination of states which are product of  $k$  tensor factors (as a generalization of (2.5)).*

The state (E.6) is just an example of a 2-separable (or biseparable) states. A more detailed description of multipartite entanglement is presented in Appendix A.

## 2.2 How to detect entanglement?

Given a general quantum state  $\rho$ , how to determine if it is entangled? In principle one could think of checking whether  $\rho$  can be written as (2.5). However, as  $\rho$  can be represented in infinitely many convex combinations, the task of finding if one of these forms reads like (2.5) is amazingly difficult [Gur03, Ter02, HHHH07]. We must then find other methods to check separability. Following this reasoning several *entanglement criteria* have been developed in the last years [Ter02], but up to now there is no definitive test for separability and it is unlikely to exist in general. In what follows I will present some criteria that will be used along the text.

### Bell Inequalities

Suppose an experimental scenario where two physicists, usually called Alice and Bob, in two space separated locations are given a particle each produced by a common source. Alice and Bob choose some measurement settings to perform on their particles. For instance, Alice chooses to perform measurements using two different devices (settings),  $A_1$  and  $A_2$ , each one delivering a possible set of outcomes labeled by  $a_1$  and  $a_2$  respectively. Equivalently Bob chooses  $B_1$  and  $B_2$ , with possible outcomes  $b_1$  and  $b_2$ . The basic objects Alice and Bob might compute are their joint probabilities obtained from the experiments. For example,

$$P(a_2 = 1, b_1 = -1 | A_2, B_1) \quad (2.7)$$

is the probability of Alice getting outcome 1 when measuring her system with apparatus  $A_2$  and Bob getting  $-1$  when measuring  $B_1$ .

The main problem concerning non-locality consists in asking whether the measured joint probabilities are compatible with local-realistic theories. In other words, whether the measurement data can be explained under the assumption that Alice's outcomes are completely independent of Bob's setup (locality) and that the measured properties have preexisting values, independent of their observation (realism) [WW01b, Gis07].

Bell has shown that some quantum states do not admit such local-realistic interpretation (also called a *local-hidden-variable (LHV) model*) [Bel87]. This was done through the derivation of inequalities (Bell inequalities) involving

the measured probabilities, which turn out to be satisfied by joint probabilities admitting an LHV model. As the statistics obtained by measuring separable states always admit an LHV model, the violation of Bell inequalities also indicates entanglement [Ter00, WW01b].

The first conclusive experimental demonstrations of Bell violations started to appear in the 80's [AGG81, ADG82], much before entanglement was recognized as an important resource<sup>1</sup>. Nowadays, Bell type experiments have become a routine, and are performed sometimes just as an experimental calibration. It must be stressed that some entangled states do not violate Bell inequalities [Wer89, TA06, APB+07].

### Schmidt decomposition.

Any bipartite pure state  $|\psi\rangle \in \mathcal{H}_A \otimes \mathcal{H}_B$  can be written as

$$|\psi\rangle = \sum_i^m \lambda_i |i\rangle_A |i\rangle_B, \quad (2.8)$$

where  $m = \min[\dim(\mathcal{H}_A), \dim(\mathcal{H}_B)]$ ,  $\{|i\rangle_A\}$  ( $\{|i\rangle_B\}$ ) is an orthonormal basis for  $\mathcal{H}_A$  ( $\mathcal{H}_B$ ), and  $\lambda_i > 0$  [Sch07, EK95, NC00]. The decomposition (2.8) is called the *Schmidt decomposition*, and the coefficients  $\lambda_i$  are called the *Schmidt coefficients* of  $|\psi\rangle$ .

If  $|\psi\rangle$  has only one non zero Schmidt coefficient, it is clearly separable, and if it has more than one Schmidt coefficient it is entangled. In this way the Schmidt decomposition completely characterizes separability for *bipartite pure* states.

### Peres-Horodecki criterion.

Although the Schmidt decomposition is a very powerful and useful entanglement criterion, it can be applied only to pure states. The first entanglement criterion for mixed states was proposed by A. Peres and uses the notion of partial transposition [Per96b].

Writing a bipartite state  $\rho_{AB}$  in a product basis  $\{|ij\rangle\}$ , *i.e.*:

$$\rho_{AB} = \sum_{ij,kl} \lambda_{ij,kl} |ij\rangle \langle kl|, \quad (2.9)$$

---

<sup>1</sup>All the experimental violations of Bell inequalities up to now suffered from some loop-hole problem [Gis07]. Hence, although all of them indicate the non-local nature of quantum mechanics no definitive proof has appeared so far.

## 2.2. HOW TO DETECT ENTANGLEMENT?

23

where  $\lambda_{ij,kl}$  are the matrix elements of  $\rho_{AB}$  in this basis, the partial trasposition of  $\rho_{AB}$  is defined as:

$$\rho_{AB}^{T_B} = \sum_{ij,kl} \lambda_{ij,kl} |il\rangle \langle kj|. \quad (2.10)$$

It is possible to see that if  $\rho_{AB}$  is separable  $\rho_{AB}^{T_B}$  is a positive operator. We can then state: *If  $\rho_{AB}^{T_B}$  has a negative eigenvalue,  $\rho_{AB}$  is entangled* (Peres criterion).

Although Peres conjectured that his criterion was able to detect any bipartite entangled state this was proven to be the case only for systems of dimensions smaller than 6. For higher dimensions there exist entangled states with positive partial transposition [Hor97, HHH96, HHH98].

### Entanglement Witnesses.

It follows directly from definition 2 that  $k$ -separable states form a convex set,  $\mathcal{S}_k$ : convex combinations of  $k$ -separable states are also  $k$ -separable. The task of determining if a quantum state  $\rho$  is  $k$ -separable can be reinterpreted as determining if  $\rho$  is inside the convex set  $\mathcal{S}_k$ . It follows from the Hanh-Banach theorem that any point outside a convex set, can be separated from this set by a hyperplane (see fig. 4.14) [BV04]. This geometrical fact can be used in the separability problem by stating that *for any entangled state  $\rho$  there exists some Hermitian operator  $W^k$  such that*

$$(i) \text{ Tr}(W^k \rho) < 0,$$

and

$$(ii) \text{ Tr}(W^k \sigma) \geq 0 \quad \forall \sigma \in \mathcal{S}_k$$

[HHH96]. We call  $W^k$  a  *$k$ -entanglement witness* for the state  $\rho$ .

Entanglement witnesses are the theoretical solution for separability. However, given a general state it is not easy to find a witness detecting it. Numerical methods to find witnesses have been proposed [BV04a, BV04b, DPS04], but they are usually inefficient for high dimensional systems.

Entanglement witnesses were also shown to be able to quantify [Bra05] or at least to estimate the amount of entanglement a state has (see next Section) [CT06, EBA07, GRW07]. Finally, as  $W^k$  is a Hermitian operator it can, in principle, be measured, and then entanglement can be experimentally verified (see *e.g.*: Refs. [BEK+04, BMN+03, AJK+05, HHR+05, KST+07]). Moreover, Bell inequalities can be seen as examples of entanglement witnesses [Ter02, HGBL05].

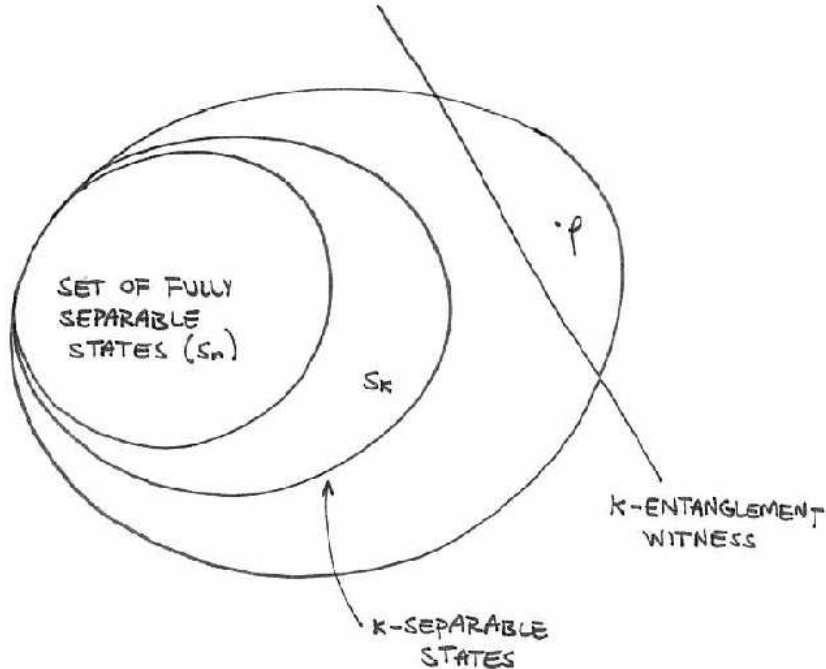


Figure 2.1: Geometric representation of  $k$ -entanglement witnesses.

## 2.3 How to quantify entanglement?

With the advent of Quantum Information Theory entanglement started to be seen as a resource. Then it became fundamental to know how much of this resource is available in each state. Let me start with an example. The state  $|\Phi_+\rangle = (|00\rangle + |11\rangle)/\sqrt{2}$  can be used to perform perfect teleportation of a one-qubit state [BBC+93]. As a convention we can say that  $|\Phi_+\rangle$  has 1 *ebit* of entanglement, and define it as the basic unity of this resource. What happens if we use another quantum state for teleportation?

Several measures of entanglement have been proposed so far [PV05]. Different approaches to get entanglement quantifiers were considered, most of them based on the following ideas:

1. *Convertibility of states*: The state  $|\psi\rangle$  is said to be more entangled than  $|\phi\rangle$  if we can transform  $|\psi\rangle$  into  $|\phi\rangle$  deterministically using just local operations and classical communication (LOCC). This way of ordering states comes naturally from the fact that entanglement cannot be created by LOCC, since it is a purely non-local resource. One of the problems with this approach is that very little is known about conversion of mixed states [Jan02, LMD08]. Furthermore, even in the

pure-state case, some states are not convertible [JP99].

2. *Usefulness:* A state  $|\psi\rangle$  is more entangled than  $|\phi\rangle$  if it supersedes  $|\phi\rangle$  in realizing some task. As one can see, this way of quantifying entanglement is highly dependent on the considered task. Hence given two states the first can be better than the second for some task, but worse for others.
3. *Geometric approach:* The amount of entanglement of a quantum state is given by the distance between this state and the set of separable states. Again, this approach does not depend only on the states themselves, but also on the chosen distance measure.

Examples of quantifiers following these ideas can be found in Refs. [PV05, HHHH07]. In what follows I am going to present the quantifiers I will use along this thesis.

### Distillable entanglement

Keeping in mind that  $|\Phi_+\rangle$  is in general the optimal state to perform quantum information tasks, one can think on the following problem. Suppose two separated observers, Alice and Bob, would like to perform one of these tasks but do not share  $|\Phi_+\rangle$  states. Instead, they are supplied with as many mixed states  $\rho_{AB}$  as they want<sup>2</sup>. Can they use their states  $\rho_{AB}$  to establish  $|\Phi^+\rangle$  states between them by LOCC? What is the cost of this transformation?

The *distillable entanglement* answers these questions and determines how many  $|\Phi^+\rangle$  pairs can be extracted (or distilled) out of  $n$  pairs of the state  $\rho_{AB}$  using LOCC, in the limit of  $n \rightarrow \infty$ . In mathematical words the distillable entanglement of  $\rho_{AB}$  is given by

$$E_D(\rho_{AB}) = \sup_{\Lambda_{LOCC}} \lim_{n \rightarrow \infty} \frac{m}{n}, \quad (2.11)$$

where  $m$  is the number of  $|\Phi^+\rangle$  pairs that can be extracted by applying LOCC strategies  $\Lambda_{LOCC}$  on  $\rho_{AB}^{\otimes n}$ .

The main difficulty of the distillable entanglement is the optimization over all possible LOCC protocols it contains. This makes this quantifier extremely hard to compute in general.

Another curious feature of distillation is the fact that not every entangled state is distillable [HHH98]. For some states there is no LOCC protocol

---

<sup>2</sup>This scenario is the typical one in real tasks, where errors typically decrease the purity of the state one deals with.

able to get maximally entangled states out of them, even if many copies are available<sup>3</sup>. These undistillable states are called bound entangled states.

### Negativity

In the previous section we saw that if a state  $\rho_{AB}$  has a negative partial transposition, it is entangled. The *negativity* ( $N(\rho_{AB})$ ) makes use of this fact and quantifies entanglement as the sum of the absolute values of the negative eigenvalues of  $\rho^{T_B}$  [LK00, VW02], *i.e.*:

$$N(\rho_{AB}) = \sum_{\lambda_i < 0} |\lambda_i|, \quad (2.12)$$

being  $\lambda_i$  the eigenvalues of  $\rho_{AB}^{T_B}$ .

The main advantage of  $N(\rho_{AB})$  is that it is an operational quantifier and can be easily calculated for any bipartite state. However, as already commented, the Peres criterion is not able to detect all entangled states. Consequently the negativity of some *entangled* states is null. It was interestingly shown that those entangled states with null negativity are undistillable [HHH98].

### Robustness of Entanglement

The *robustness of entanglement* of a  $k$ -partite state  $\rho$  is a natural quantifier of how much noise  $\rho$  admits before it becomes  $k$ -separable [HN03, VT99]. Suppose we would like to have a  $k$ -partite state  $\rho$  but due to errors we end up having the noisy state  $\frac{\rho+s\pi}{1+s}$ , where  $\pi$  is another quantum state and  $s$  is a positive number. How much noise  $\pi$  the state  $\rho$  tolerates before getting  $k$ -separable? The *relative robustness* ( $R^k(\rho||\pi)$ ) aims at quantifying that, and is mathematically defined as

$$R^k(\rho||\pi) = \min s \text{ such that } \sigma = \frac{\rho + s\pi}{1+s} \text{ is } k\text{-separable.} \quad (2.13)$$

It might happen that for some particular choices of  $\pi$ ,  $\sigma$  is never  $k$ -separable. In this thesis I will be more concerned with two related quantities. The first is called the *random robustness* ( $R_R^k$ ) and represents the robustness of the state  $\rho$  with respect to the most mixed state  $I/D$ , where  $I$  is the  $D \times D$  identity matrix, *i.e.*:

$$R_R^k(\rho) = \min s \text{ such that } \sigma = \frac{\rho + sI/D}{1+s} \text{ is } k\text{-separable.} \quad (2.14)$$

---

<sup>3</sup>In the special case of 2 qubits all states are distillable [HHH97].

## 2.3. HOW TO QUANTIFY ENTANGLEMENT?

27

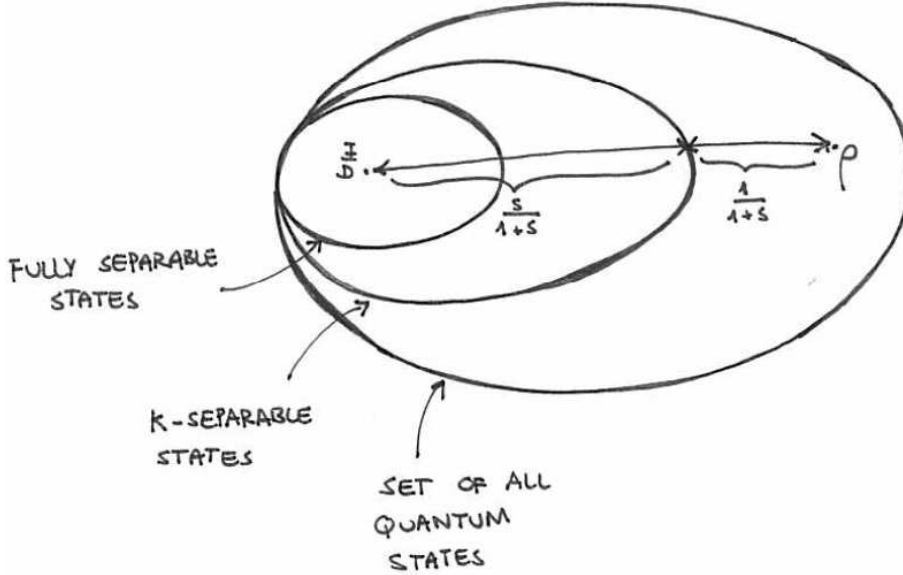


Figure 2.2: **Geometrical interpretation of  $R_R^k$**  - The straight line represents the convex combination  $\frac{\rho+sI/D}{1+s}$ .  $R_R^k(\rho)$  is given by the value of  $s$  such that this combination becomes  $k$ -separable.

As the state  $I/D$  is always interior to the set of  $n$ -separable states (*i.e.*: the fully separable states)[ZHSL98], the minimization in (2.14) is well defined.

Another useful quantity is the *generalized robustness of entanglement* ( $R_g^k(\rho)$ ) which is the minimization of the relative robustness over all possible states  $\pi$  [Ste03], *i.e.*:

$$R_g^k(\rho) = \min_{\pi} R^k(\rho||\pi). \quad (2.15)$$

Apart from the direct operational meaning in terms of resistance to noise, the robustness of entanglement have other interesting features. First it can quantify any kind of multipartite entanglement. Furthermore the robustness also has a clear geometric interpretation. The state  $\sigma$  can be seen as a convex combination of the state  $\rho$  and the noisy state  $\pi$ . The robustness of entanglement gives the point where this convex combination crosses the border of the set of  $k$ -separable states (see Fig. 2.3).

### Geometric Measure of Entanglement

The geometric measure of entanglement  $E_{GME}^k(\psi)$  quantifies entanglement through the minimum angle between a state  $|\psi\rangle$  and a  $k$ -separable

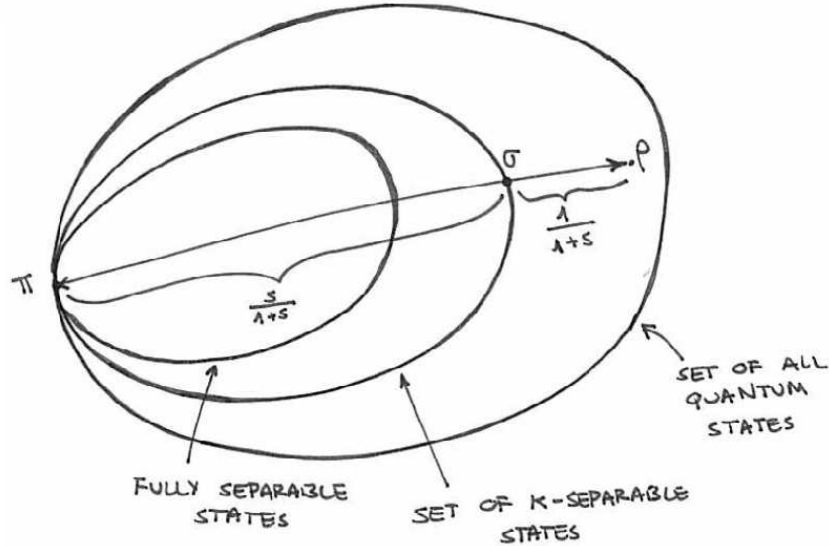


Figure 2.3: **Geometrical interpretation of  $R_g^k$**  - The straight line represents the convex combination  $\frac{\rho+s\pi}{1+s}$ . We see that for a given state  $\pi$  and a value of  $s$  this combination becomes  $k$ -separable.  $R_g^k(\rho)$  is defined as the minimum  $s$ , considering all possible states  $\pi$ .

state  $|\phi\rangle$  [BL01, WG03], i.e.:

$$E_{GME}^k(\psi) = 1 - \Lambda_k^2(\psi), \quad (2.16)$$

where

$$\Lambda_k^2(\psi) = \max_{\phi \in S^k} |\langle \phi | \psi \rangle|^2. \quad (2.17)$$

Thus  $E_{GME}^k$  is also able to quantify multipartite entanglement.

For mixed states,  $E_{GME}^k$  uses the so-called convex-roof construction:

$$E_{GME}^k(\rho) = \min_{\{p_i, |\psi_i\rangle\}} \sum_i p_i E_{GME}^k(\psi_i), \quad (2.18)$$

where  $\{p_i, |\psi_i\rangle\}$  are possible ensemble realizations of  $\rho$ .

### Witnessed Entanglement

The *witnessed entanglement* ( $E_W^k(\rho)$ ) uses the notion of  $k$ -entanglement witnesses to quantify entanglement [Bra05]. We have seen that, given a  $k$ -entanglement witness  $W^k$ ,  $\text{Tr}(W^k \rho) < 0$  is an indicator of entanglement in the state  $\rho$ .  $E_W^k$  uses the value of this trace as a quantifier:

$$E_W^k(\rho) = \max\{0, -\min_{W^k \in \mathcal{M}} \text{Tr}(W^k \rho)\}, \quad (2.19)$$

## 2.3. HOW TO QUANTIFY ENTANGLEMENT?

29

where  $\mathcal{M}$  is a restricted set of  $k$ -entanglement witnesses which guarantees that the above minimization is well defined.

Again this entanglement quantifier can deal with different kinds of multipartite entanglement since we can choose the set  $\mathcal{M}$  as being the set of witnesses with respect to  $k$ -separable states. Moreover, as entanglement witnesses are linked to experimental observables, in principle,  $E_W^k$  can be experimentally determined, or at least estimated [CT06, EBA07]. The main problem in the definition of  $E_W^k$  is the minimization process it involves.

Finally, several entanglement quantifiers can be written as (2.19) by adjusting the set  $\mathcal{M}$  [Bra05]. Among these quantifiers are the concurrence [Woo98], the negativity [VW02], the robustness of entanglement [VT99, HN03, Ste03], and the best separable approximation [LS98, KL01]. For instance, the generalized robustness of entanglement corresponds to the choice  $\mathcal{M} = \{W^k \mid W^k \leq I\}$  and for the random robustness  $\mathcal{M} = \{W^k \mid \text{Tr}(W^k) = D\}$ .



# Chapter 3

## Connecting the Geometric Measure and the Generalized Robustness of Entanglement

The purpose of this chapter is to point out a connection between two well discussed entanglement quantifiers, the generalized robustness ( $R_g^k$ ) [Ste03] and the geometric measure of entanglement ( $E_{GME}^k$ ) [BL01, WG03]. The relation between these quantifiers is not straightforward, since they rely on distinct interpretations (see Chapter 1).

### 3.1 Relating $R_g$ and $E_{GME}$ to entanglement witnesses.

As we will see, the connection of these two quantifiers will be made through the fact that both can be related to the notion of  $k$ -entanglement witnesses. This relation is shown in what follows.

One can always construct a  $k$ -entanglement witnesses  $W^k$ , for a pure state  $|\psi\rangle$  with  $k$ -entanglement, of the type [WG03]

$$W^k = \lambda^2 - |\psi\rangle\langle\psi|, \quad (3.1)$$

$\lambda \in \mathbb{R}$ . As this operator must have a positive mean value for every  $k$ -separable state, the relation

$$1 \geq \lambda^2 \geq \max_{|\phi\rangle \in S_k} \|\langle\phi|\psi\rangle\|^2 \equiv \Lambda_k^2 \quad (3.2)$$

must hold. The optimal witness of the form (3.1),  $W_{opt}^k$ , is the one for which

$\lambda = \Lambda_k^2$ . Thus we can write

$$W_{opt}^k = \Lambda_k^2 - |\psi\rangle\langle\psi|. \quad (3.3)$$

In a different fashion, we have seen that the robustness of entanglement of a state  $\rho$  quantifies how robust the entanglement of  $\rho$  is under the presence of noise. As well as the geometric measure,  $R_g^k$  is intimately connected to the notion of entanglement witnesses, and can be expressed as (2.19) by choosing  $\mathcal{M}$  as the set of  $k$ -entanglement witness satisfying  $W^k \leq I$  [Bra05].

### 3.2 $E_{GME}$ as a lower bound for $R_g$

As the witness (3.3) satisfies the condition  $W^k \leq I$  we can attest the following: for pure states  $|\psi\rangle$ ,

$$R_g^k(\psi) \geq E_{GME}^k(\psi). \quad (3.4)$$

Some points concerning the inequality (3.4) must be stressed. First, it is a relation valid for all kinds of multipartite entanglement. Moreover this relation is strict whenever the witness (3.3) is a solution of the minimization problem in (2.19). Finally, one could argue that the relation (3.4) may be, in fact, a consequence of standard results from matrix analysis relating different distance measures between operators (as commented, both  $R_g^k$  and  $E_{GME}^k$  are related to such distances). It must be clear that  $R_g^k(\psi)$  is not simply the distance between  $\psi$  and its closest state  $\sigma \in S_k$ . One should keep in mind that this function also depends on the reference state  $\pi$ <sup>1</sup> (recall Figure 2.3). This makes the closest  $k$ -separable state usually different for  $R_g^k$  and  $E_{GME}^k$ .

In fact, it is possible to give a tighter relation between  $R_g^k$  and  $E_{GME}^k$ . I am going to need the following result for this aim:

**Lemma 1** *For every state  $\rho$ ,*

$$R_g^k(\rho) \geq \frac{\text{Tr}(\rho^2)}{\max_{\sigma \in S_k} \text{Tr}(\rho\sigma)} - 1. \quad (3.5)$$

**Proof.** Suppose a  $k$ -entanglement witness of the form  $W = \lambda I - \rho$ . The fact that  $\text{Tr}(W\sigma) \geq 0 \forall \sigma \in S_k$  implies that

$$\text{Tr}[(\lambda I - \rho)\sigma] = \lambda - \text{Tr}(\rho\sigma) \geq 0. \quad (3.6)$$

It is now easy to see that  $\max_{\sigma \in S_k} \text{Tr}(\rho\sigma)$  is equal to the minimum value of  $\lambda$  ( $\lambda_{min}$ ), i.e.:  $\lambda_{min} = \max_{\sigma \in S_k} \text{Tr}(\rho\sigma)$ .

---

<sup>1</sup>Besides that there is a minimization among all possible states  $\pi$ .

### 3.3. EXAMPLES

33

Note that

$$W' = \frac{W}{\lambda_{\min}} = I - \frac{\rho}{\lambda_{\min}} < I. \quad (3.7)$$

So we can write  $R_g^k(\rho) \geq -\text{Tr}(W'\rho)$ , from which follows the required result.

□

The lower bound on  $R_g^k$  expressed by (3.5) can be easily interpreted:  $\text{Tr}\rho^2$  measures the purity of  $\rho$ , and  $\text{Tr}(\rho\sigma)$  is the Hilbert-Schmidt scalar product between  $\rho$  and  $\sigma$ . It is expected that the more mixed  $\rho$  is, the lower the value of  $\text{Tr}\rho^2$ , and the state becomes less entangled. Similarly, the larger  $\max_{\sigma \in S_k} \text{Tr}(\rho\sigma)$ , the closer to the set  $S_k$   $\rho$  gets, and the system will show less entanglement.

Note that in the special case of pure states the relations  $\text{Tr}(\rho^2) = 1$  and  $\max_{\sigma \in S_k(H)} \text{Tr}(\rho\sigma) = \Lambda_k^2(\rho)$  hold and therefore we have the general relation

$$R_g^k(\psi) \geq \frac{1}{\Lambda_k^2(\psi)} - 1. \quad (3.8)$$

We can finally arrive at the relation we were looking for:

$$R_g^k(\psi) \geq \frac{E_{GME}^k}{1 - E_{GME}^k}. \quad (3.9)$$

It is interesting that two entanglement quantifiers with different geometric interpretations are actually related. Moreover relation (3.5) allows an analytic lower bound to the generalized robustness for all states whenever  $\Lambda_k^2(\rho)$  can be analytically computed. This is the case, for example, of completely symmetric states, Werner states, and isotropic states [WG03, WEGM04].<sup>2</sup>

## 3.3 Examples

For bipartite pure states all the quantities considered so far can be analytically computed. In this case, the generalized robustness is given by

$$R_g^k(\psi) = (\sum_i \lambda_i)^2 - 1, \quad (3.10)$$

being  $\{\lambda_i\}$  the spectrum of Schmidt of  $|\psi\rangle$  [Ste03]. In this context it can be noted that  $\Lambda_k$  is given by the modulus of the highest Schmidt coefficient of

---

<sup>2</sup>We can furthermore see from (3.8) that  $\log_2(1+R_g^k) \geq -2\log_2 \Lambda_k$ . The left-hand side of this expression is the logarithmic robustness of entanglement ( $LR_g^k$ ), another entanglement quantifier with interesting features [Bra05]. Curiously, this is exactly the same lower bound expressed to the relative entropy of entanglement in Ref. [WEGM04].

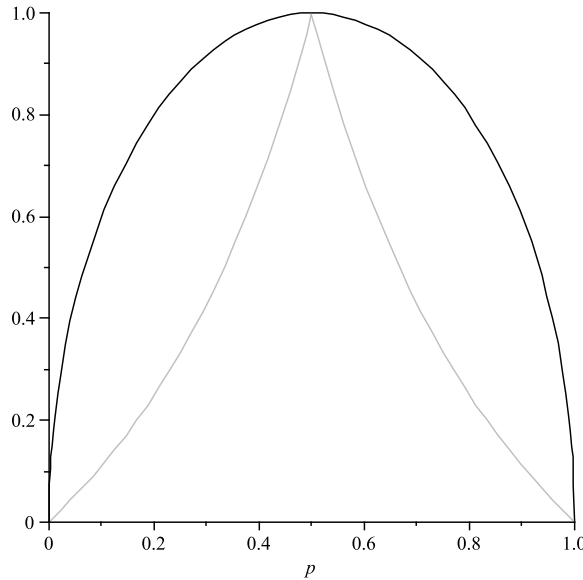


Figure 3.1: Generalized Robustness of Entanglement (black) and its lower bound given in Eq. (3.9) (grey) for the state (3.11).

$|\psi\rangle$  [WG03]. To visualize and compare these entanglement measures I have calculated the generalized robustness, and the lower bound expressed in (3.9) for the state

$$|\psi(p)\rangle = \sqrt{p}|00\rangle + \sqrt{1-p}|11\rangle. \quad (3.11)$$

The plots are available in figure 3.1.

As the presented relations between  $R_g^k$  and  $E_{GME}^k$  are also valid for multipartite entanglement it is useful to illustrate the results in this context. Consider for instance the completely symmetric states defined as:

$$|S(n, k)\rangle = \sqrt{\frac{k!(n-k)!}{n!}} S \left| \underbrace{000\dots 0}_k \underbrace{11\dots 1}_{n-k} \right\rangle, \quad (3.12)$$

where  $S$  is the total symmetrization operator. Wei and Goldbart showed an analytical expression to  $E_{GME}^n(|S(n, k)\rangle)$  (*i.e.*: the geometric measure of  $|S(n, k)\rangle$  with relation to the completely separable states) [WG03]. Additionally, in this case it was shown that the bound (3.9) is saturated [HMM+08]. It allows us to compute analytically the generalized robustness for the states (3.12) and compare it with the geometric measure. As an illustration, some examples are shown in Table 3.1.

	$ S(2, 1)\rangle$	$ S(3, 2)\rangle$	$ S(4, 3)\rangle$	$ S(4, 2)\rangle$
$E_{GME}^n$	0.5	0.55	0.58	0.625
$R_g^n$	1	1.25	1.36	1.65

Table 3.1: A comparison among multipartite entanglement of some states (3.12), given by geometric measure of entanglement ( $E_{GME}^n$ ) - see Ref. [WG03] - and the robustness of entanglement ( $R_g^n$ ) - see Ref. [HMM+08].

### 3.4 Concluding remarks

In brief, I have shown some relations between the geometric measure of entanglement and the generalized robustness of entanglement. A lower bound to  $R_g^k$  with a natural interpretation was derived in terms of  $E_{GME}^k$ . Examples were given to illustrate the results.

Since many entanglement quantifiers exist it is important to understand their relation and this, I believe, should be a major goal in the theory of entanglement.



## Chapter 4

# Multipartite entanglement of superpositions

Given the pure states  $|\Psi\rangle$  and  $|\Phi\rangle$  on a bipartite system, how is the entanglement of the superposition state

$$|\Gamma\rangle = a|\Psi\rangle + b|\Phi\rangle, \quad (4.1)$$

related to the entanglement of the constituents  $|\Psi\rangle$  and  $|\Phi\rangle$  and to the coefficients  $a$  and  $b$ ? In a recent work [LPS06], Linden, Popescu and Smolin have raised this question which was shown to exhibit a rich answer in terms of nontrivial inequalities relating these quantities. In order to quantify the entanglement, these authors used the *distillable entanglement*<sup>1</sup>. However other entanglement quantifiers can also be used and, in fact, distinct bounds for the entanglement of a superposition can be found depending on this choice [YYS07, OF07].

In this Chapter I will discuss the route A. Acín, M. Terra Cunha and I took to generalize the ideas raised in [LPS06] to the multipartite scenario.

### 4.1 Dealing with the witnessed entanglement

I will deal with the previously discussed family of quantifiers expressed by the *witnessed entanglement* (see (2.19)) [Bra05]. For an entangled pure

---

<sup>1</sup>In the case of bipartite pure states the distillable entanglement can be analytically calculated by means of the Von Neuman entropy of the reduced state [BBP+96].

state  $\rho = |\psi\rangle\langle\psi|$ , the witnessed entanglement can be expressed as<sup>2</sup>

$$E_W^k(\psi) = -\langle\psi|W_{\psi_{opt}}^k|\psi\rangle, \quad (4.2)$$

being  $W_{\psi_{opt}}^k$  an optimal witness for the state  $|\psi\rangle$  (*i.e.*: a witness satisfying the minimization problem in (2.19)). This simplified way of writing  $E_W^k$  will be particularly useful in our constructions. Let me recall that several entanglement quantifiers can be expressed as  $E_W^k$ , and then the present results will be valid for all those quantifiers.

The main scope of this work is to obtain an upper bound to the witnessed entanglement of the state (4.1) based on the entanglement of the superposed states  $|\Psi\rangle$  and  $|\Phi\rangle$  and the coefficients appearing in the superposition. In what follows, I will first derive an inequality relating these quantities and then prove its tightness. The witnessed entanglement of  $|\Gamma\rangle$  can be written as

$$\begin{aligned} E_W^k(\Gamma) &= \max\{0, -\min_{W^k \in \mathcal{M}} \langle\Gamma|W^k|\Gamma\rangle\} \\ &= \max\{0, -\min_{W^k \in \mathcal{M}} [|a|^2 \langle\Psi|W^k|\Psi\rangle + |b|^2 \langle\Phi|W^k|\Phi\rangle \\ &\quad + 2\text{Re}(a^*b \langle\Psi|W^k|\Phi\rangle)]\}, \end{aligned} \quad (4.3)$$

an expression that resembles the usual interference pattern originated by superpositions. For finite dimension the minimization problem is solved using the so-called optimal entanglement witness  $W_{opt}$  (inside the set  $\mathcal{M}$  which defines the quantifier). So we can write

$$\begin{aligned} E_W^k(\Gamma) &= \max\{0, -|a|^2 \langle\Psi|W_{\Gamma_{opt}}^k|\Psi\rangle - |b|^2 \langle\Phi|W_{\Gamma_{opt}}^k|\Phi\rangle \\ &\quad - 2\text{Re}(a^*b \langle\Psi|W_{\Gamma_{opt}}^k|\Phi\rangle)\}. \end{aligned} \quad (4.4)$$

Again,  $W_{\Gamma_{opt}}^k$  denotes a witness that is optimal for the state  $|\Gamma\rangle$ . Different states usually have different optimal entanglement witnesses. We are naturally led to the inequality

$$\begin{aligned} E_W^k(\Gamma) &\leq \max\{0, -|a|^2 \langle\Psi|W_{\Psi_{opt}}^k|\Psi\rangle\} + \max\{0, -|b|^2 \langle\Phi|W_{\Phi_{opt}}^k|\Phi\rangle\} \\ &\quad + \max\{0, -2\text{Re}(a^*b \langle\Psi|W_{\Gamma_{opt}}^k|\Phi\rangle)\} \\ &= |a|^2 E_W^k(\Psi) + |b|^2 E_W^k(\Phi) + 2 \max\{0, -\text{Re}(a^*b \langle\Psi|W_{\Gamma_{opt}}^k|\Phi\rangle)\}, \end{aligned} \quad (4.5)$$

---

<sup>2</sup>I suppose  $|\psi\rangle$  to have the kind of entanglement which  $W_{\psi_{opt}}^k$  is constructed to witness. Remember that in the multipartite case a state can show different kinds of entanglement, and possibly the set  $\mathcal{M}$  is tailored to witness one kind of entanglement, while  $|\psi\rangle$  can show only other kinds of entanglement.

where I have also made use of the inequality  $\max\{0, a + b\} \leq \max\{0, a\} + \max\{0, b\}$ . Attention must now be payed to the interference term. The Cauchy-Schwarz inequality implies

$$E_W^k(\Gamma) \leq |a|^2 E_W^k(\Psi) + |b|^2 E_W^k(\Phi) + 2|a||b| \|W_{\Gamma_{opt}}^k\|. \quad (4.6)$$

Note that the normalization of the involved kets was used and I take the norm of an operator as its maximal singular value. Expression (4.6) relates the entanglement of  $|\Gamma\rangle$  to the entanglement of each one of the superposed states (and the coefficients of the superposition) but also depends on the form of the optimal entanglement witness  $W_{opt}^\Gamma$ . This dependence on the optimal entanglement witness is expected as the restrictions in  $W_{opt}^\Gamma$  imply the features of the entanglement quantifier we are dealing with.

At this point it is worth asking if inequality (4.6) can be saturated. Considering the negativity as a quantifier we can compute  $W_{opt}^\Gamma$  analytically. For a given state  $\rho$ , it is given by the partial transposition of the projector onto the subspace of negative eigenvalues of  $\rho^{T_A}$ , where  $\rho^{T_A}$  denotes the partial transposition of  $\rho$  [LKCH00]. It is now easy to see that for the two-qubit states  $|\Phi\rangle = |00\rangle$  and  $|\Psi\rangle = |11\rangle$ , the inequality (4.6) becomes an equality.

In the previous examples I used the fact that the optimal witness  $W_{opt}^k$  is known. Let me now remove this strong assumption. It was shown in Ref. [Bra05] that the choice of  $\mathcal{M}$  (in Eq. (2.19)) being the set of  $k$ -entanglement witnesses satisfying  $-nI \leq W^k \leq mI$ , where  $m, n \geq 0$ , defines proper entanglement quantifiers. Setting  $\gamma = \max(m, n)$  we have

$$E_W^k(\Gamma) \leq |a|^2 E_W^k(\Psi) + |b|^2 E_W^k(\Phi) + 2\gamma|a||b|. \quad (4.7)$$

## 4.2 Are these relations tight?

As the main goal here is to work in the multipartite case it would be interesting to find examples of multipartite states for which relation (4.7) is saturated. The main barrier to be overcome in this case is the fact that it is not known, in general, how to compute multipartite entanglement quantifiers. Nevertheless I will show a way of calculating the generalized robustness of entanglement for GHZ-like states and use this information to prove the tightness of inequality (4.7) regardless the number of particles involved.

As discussed in chapter 2, the generalized robustness of entanglement admits two representations. The first, given in eq. (2.15), establishes how much noise we can mix to a state before it gets separable. The second express  $R_g^k$  as a witnessed entanglement  $E_W^k(\rho)$  when  $\mathcal{M}$  is the set of witness

operators satisfying  $W^k \leq I$ . I will make use of both definitions to show that for the  $N$ -qubit family of states

$$|GHZ_N(\phi)\rangle = \frac{|0^{\otimes N}\rangle + e^{i\phi}|1^{\otimes N}\rangle}{\sqrt{2}}, \quad (4.8)$$

the inequality (4.7) is saturated. Clearly if one chooses an arbitrary state  $\pi$  such that the state  $\sigma(\rho, \pi, s)$  is separable for some value of  $s$ , this number  $s$  gives an upper bound for the value of  $R_g^k(\rho)$ . On the other hand, taking an arbitrary  $k$ -entanglement witness  $W^k$  for the state  $\rho$  satisfying the condition  $W^k < I$ ,  $-\text{Tr}(W^k \rho)$  gives a lower bound to  $R_g^k(\rho)$  according to (2.19). I will now establish lower and upper bounds for  $R_g^k(GHZ_N(\phi))$  that turn out to be equal, getting the exact value of this quantity and also the value of  $\gamma$  needed for the bound (4.7).

*Upper bound.* Consider, in the definition of  $R_g^k$  given by Eq. (2.15),

$$\rho = |GHZ_N(\phi)\rangle \langle GHZ_N(\phi)| \quad (4.9)$$

and

$$\pi = |GHZ_N(\phi)_\perp\rangle \langle GHZ_N(\phi)_\perp|, \quad (4.10)$$

where

$$|GHZ_N(\phi)_\perp\rangle = \frac{|0^{\otimes N}\rangle - e^{i\phi}|1^{\otimes N}\rangle}{\sqrt{2}}. \quad (4.11)$$

Using the Peres criterion [Per96b, HHH96] we see that

$$\sigma = \frac{\rho + s\pi}{1+s} \quad (4.12)$$

has positive partial transposition(according to any bipartition) only for  $s = 1$ . Moreover, for this point it can be directly verified that  $\sigma$  is also  $N$ -separable. So we get

$$R_g^N(GHZ_N(\phi)) \leq 1. \quad (4.13)$$

*Lower bound.* The following operator is a genuine  $N$ -entanglement witness for the state  $|GHZ_N(\phi)\rangle$  [WG03, CT06]:

$$W^N = I - 2|GHZ_N(\phi)\rangle \langle GHZ_N(\phi)|, \quad (4.14)$$

which clearly satisfies the condition  $W^N < I$ . Hence, definition (2.19) leads to

$$-\text{Tr}(W^N |GHZ_N(\phi)\rangle \langle GHZ_N(\phi)|) = 1 \leq R_g(GHZ_N(\phi)). \quad (4.15)$$

As the upper bound (4.13) and lower bound (4.15) coincide we have that  $R_g^N(GHZ_N(\phi)) = 1$ , and can also conclude that the witness (4.14) satisfies the minimization problem in (2.19). It then allows us to extract the value  $\gamma = 1$ .

Putting all these facts together we conclude that the inequality (4.7) saturates for the class of states (4.8).

### 4.3 Concluding remarks

I have shown that the notion of *entanglement of superpositions* can be extended to the multipartite scenario. An inequality relating the entanglement of two quantum states to the entanglement of the state constructed through their superposition was found. This inequality was proven to be tight for a family of  $N$ -qubit states and a choice of entanglement quantifier. Moreover a large class of entanglement quantifiers, with both operational and geometrical meanings, was put in this context.

It is also worth noting that the inequalities derived here can be extended to the case where more than two states are superposed [XXH]. Future research could include the study of other examples of states and quantifiers.



## Chapter 5

# Non-locality and partial transposition for continuous variable systems

Since the early stages of Quantum Mechanics the question whether nature is non-local is the subject of much debate. After J. Bell's derivation of experimentally testable conditions [Bel87] - known as Bell inequalities - a huge amount of experimental tests of non-locality were developed, but no one could definitively answer this question so far. All of the performed experiments suffered from loop-holes problem coming usually from low-efficient detection or non space-like separated measurements [Gis07]. An alternative for these problems is to use quadrature measurements of the electromagnetic field since photons can be easily distributed among distant locations and can be efficiently measured by homodyning techniques [GFC+04, GFC05].

There has been little work done so far on Bell inequalities for continuous variable (CV) systems<sup>1</sup>, and most of the proposals used some kind of measurement discretization (also termed *binning*). Only recently a Bell inequality dealing with unbounded operators came up. Cavalcanti, Foster, Reid and Drummond (CFRD) introduced a multipartite Bell inequality where each part measures two field quadratures [CFRD07]. Unfortunately the only violation the authors could find consists on using a ten-mode system, which makes this test extremely difficult from an experimental point of view.

During most of the history of quantum mechanics, the concepts of entan-

---

<sup>1</sup>There exist several works studying the violation of “standard” Bell inequalities, that is, with a finite number of outcomes, in CV systems (*e.g.*: [BW99, Mun99, WHG+03, WHG+03, GFC+04, GFC05]. Here, I refer to inequalities with a continuous variable flavour, in the sense of an arbitrary number of outcomes. An example of this type of inequalities could be the entropic inequality given by N. J. Cerf and C. Adami [CA97].

lement and non-locality were considered as a single feature of the theory. It was only with the recent advent of quantum information science that the relation between these concepts started to be considered in depth. On the one hand, we know that entanglement is necessary for a state to be nonlocal<sup>2</sup>. But, on the other hand, some entangled states admit a local-hidden-variable (LHV) model [Wer89, TA06, APB+07]. The situation is even richer due to the fact that there exist other meaningful scenarios where sequences of measurements [Pop95, Gis96] or the use of ancillary systems [Per96a, MLD08] allow detecting hidden non-locality. More in general, the relation between these concepts is still not fully understood. Clarifying this relation is highly desirable, for it would lead us to ultimately grasp the very essence of quantum correlations.

One way to tackle this problem is by studying the relation between non-locality and other concepts regularly related to entanglement, such as partial transposition. Let me recall some ideas about the partial transposition discussed in Chapter 2. The positivity of the partial transposition (PPT) represents a necessary condition for a state to be separable [Per96b]. Indeed, partial transposition is just the simplest example of positive maps, linear maps that are useful for the detection of mixed-state entanglement [HHH96]. A second fundamental result on the connection between partial transposition and entanglement was to notice that all PPT states are non-distillable [HHH98]. In other words, if an entangled state is PPT, it is impossible to extract pure-state entanglement out of it by local operations assisted by classical communication (LOCC), even if the parties are allowed to perform operations on many copies of the state. Guided by the similarities between the processes of entanglement distillation [BDSW96] and extraction of hidden non-locality, Peres conjectured [Per99] that any state having a positive partial transposition should admit an LHV model. Equivalently, any state violating a Bell inequality should have a negative partial transposition (NPT).

Proving Peres' conjecture in full generality represents one of the open challenges in quantum information theory. The proof of this conjecture has been achieved for some particular cases up to now: labeling the nonlocality scenario as is customary by the numbers  $(n, m, o)$ , meaning that  $n$  parties can choose among  $m$  measurement settings of  $o$  outcomes each, the most general proof obtained so far was for correlation functions Bell inequalities in the  $(n, 2, 2)$  case [WW01a]<sup>3</sup>. Increasing the number of settings per part or the number of outcomes per setting are the natural extensions of this result.

---

<sup>2</sup>Remember the discussion about non-locality and Bell inequalities made in chapter 2.

<sup>3</sup>A related, and perhaps more physical question is whether the violation of a Bell inequality implies entanglement distillability. This connection has also been proven in the  $(n, 2, 2)$  scenario for correlation Bell inequalities [ASW02, Aci02, Mas06].

Here I will follow the last approach and show that the CFRD inequality with two arbitrary quadrature measurements in each site is not violated for PPT states. To the best of my knowledge, this is the first result on the connection between Bell violation and partial transposition for CV systems, which corresponds to the  $(n, 2, o)$  with  $o \rightarrow \infty$  scenario.

In this chapter I will start by introducing the CFRD inequality for arbitrary quadratures and proving that any state violating the inequality must necessarily be NPT. The key point in the demonstration is the Shchukin and Vogel (SV) NPT criterion [SV05, SV06, MP06], which will be briefly described. I then proceed to show that no two-mode quantum state can violate the generalized CFRD inequality. The present finding were reached with A. Salles and A. Acín.

## 5.1 The CFRD inequality

In Ref. [CFRD07], the authors present a general Bell inequality for CV systems. They use the fact that the variance of any function of random variables must necessarily be positive. Thus, by choosing functions of local observables one can get discrepancies between the quantum and the classical predictions just using the fact that in the quantum case these observables are given by Hermitian operators (usually satisfying non-trivial commutation relations), while in an LHV scenario the observables are just numbers, given a priori by the hidden variables (and obviously commute with each other). Interestingly, this idea can lead to strong Bell inequalities as it is the case of the Mermin, Ardehali, Belinskii and Klyshko (MABK) inequality [Mer90, Ard92, BK93]. More importantly for the present discussion, the CFRD approach works for unbounded observables as well, leading to Bell inequalities for continuous variable systems.

Consider a complex function  $C_n$  of local real observables  $\{X_k, Y_k\}$ , where  $k$  labels the different parties, defined as:

$$C_n = \tilde{X}_n + i\tilde{Y}_n = \prod_{k=1}^n (X_k + iY_k), \quad (5.1)$$

Applying the positivity of the variance of both its real ( $\tilde{X}_n$ ) and imaginary ( $\tilde{Y}_n$ ) part, and assuming LHV (*i.e.*: setting commutators to zero) we obtain [CFRD07]:

$$\langle \tilde{X}_n \rangle^2 + \langle \tilde{Y}_n \rangle^2 \leq \left\langle \prod_{k=1}^n (X_k^2 + Y_k^2) \right\rangle. \quad (5.2)$$

This inequality must be satisfied by LHV models for any set of observables  $\{X_k, Y_k\}$ , regardless of their spectrum.

If we now choose for each site orthogonal quadratures defined in terms of the annihilation (creation) operators  $\hat{a}_k$  ( $\hat{a}_k^\dagger$ ) as:

$$\begin{aligned}\hat{X}_k &= \hat{a}_k e^{-i\theta_k} + \hat{a}_k^\dagger e^{i\theta_k}, \\ \hat{Y}_k &= \hat{a}_k e^{-i(\theta_k+s_k\pi/2)} + \hat{a}_k^\dagger e^{i(\theta_k+s_k\pi/2)},\end{aligned}\quad (5.3)$$

where  $s_k \in \{-1, 1\}$ , and denote  $\hat{A}_k(1) = \hat{a}_k$  and  $\hat{A}_k(-1) = \hat{a}_k^\dagger$ , inequality (5.2) becomes:

$$\left\langle \prod_{k=1}^n \hat{A}_k(s_k) \right\rangle^2 \leq \left\langle \prod_{k=1}^n \left( \hat{a}_k^\dagger \hat{a}_k + \frac{1}{2} \right) \right\rangle. \quad (5.4)$$

I will be first concerned with this family of inequalities, parameterized by the choice of the  $s_k$ . Note that the inequality is independent of the choice of relative phases  $\theta_k$ .

In Ref. [CFRD07] it was shown that the GHZ-like state

$$|GHZ_n\rangle = \frac{1}{2}(|0\rangle^{\otimes n/2} |1\rangle^{\otimes n/2} + |0\rangle^{\otimes n/2} |1\rangle^{\otimes n/2})$$

violates the inequality (5.4) with the choice  $s_k = 1$  for  $1 \leq k \leq n/2$  and  $s_k = -1$  for  $n/2 + 1 \leq k \leq n$ , whenever  $n \geq 10$ . Moreover it was also shown that this violation grows exponentially with the number of subsystems.

As we will see all states violating the inequality (5.4) must be NPT according to some bipartition. In order to prove this fact I will need to recall the Shchukin and Vogel's (SV) NPT criterion [SV05, SV06, MP06].

## 5.2 SV criterion

A necessary and sufficient condition for the positivity of the partial transpose of a CV state, given in terms of matrices of moments, was introduced and further generalized to the multipartite case in Refs.[SV05, SV06, MP06]. When dealing with many parties, one must analyze the positivity of the partial transposition for a given bipartition of the system. I will say that a state is PPT when it is PPT according to *all* bipartitions. Let me briefly introduce the SV criterion for the multipartite scenario.

For each bipartition of the system, which I will label by the set of parties that is chosen to be transposed  $I$ , a matrix of moments  $M^I$  is constructed. The elements of this matrix are given by:

$$M_{st}^I = \left\langle \prod_{i \in I} \hat{a}_i^{\dagger q_i} \hat{a}_i^{p_i} \hat{a}_i^{\dagger k_i} \hat{a}_i^{l_i} \prod_{i \in \bar{I}} \hat{a}_i^{\dagger l_i} \hat{a}_i^{k_i} \hat{a}_i^{\dagger p_i} \hat{a}_i^{q_i} \right\rangle, \quad (5.5)$$

where  $\mathbf{k} = (k_1, \dots, k_n)$  and  $\mathbf{l} = (l_1, \dots, l_n)$  correspond to row index  $s$ , and  $\mathbf{p} = (p_1, \dots, p_n)$  and  $\mathbf{q} = (q_1, \dots, q_n)$  correspond to column index  $t$ , with some prescribed ordering that is not relevant for the present purposes (see [SV05, SV06] for details); and  $\bar{I}$  denotes the complement of  $I$ , that is, those parties that are *not* transposed. I stress that, for fixed row and column indices, the ordering of the operators entering the corresponding matrix element will depend on the bipartition  $I$ .

Shchukin and Vogel's criterion says that, for a state to be PPT according to bipartition  $I$ , all principal minors of  $M^I$  should be nonnegative<sup>4</sup>. For the state to be PPT according to *all* bipartitions, all principal minors of *all* matrices  $M^I$  must be nonnegative, for all nontrivial bipartitions  $I$ . By nontrivial bipartitions it is meant the exclusion of the bipartition labeled by  $I = \emptyset$ , as well as that labeled by  $I = \mathcal{N}$ , the entire set, both corresponding to no transposition at all. In these cases, the criterion speaks about the positivity of the state itself, instead of its partial transposition.

### 5.3 Nonlocality implies NPT

I am now in the position of proving that any state violating the CFRD quadrature inequality (5.4) is necessarily NPT. As a sake of simplicity I will first consider the case of orthogonal quadratures. Then, in the next section, I will move to the most general case of arbitrary measurement directions. I begin by expanding the products in the RHS of inequality (5.4) as follows:

$$\begin{aligned} \left\langle \prod_k \left( \hat{N}_k + \frac{1}{2} \right) \right\rangle &= \frac{1}{2^n} + \frac{1}{2^{n-1}} \sum_{i_1=1}^n \left\langle \hat{N}_{i_1} \right\rangle + \frac{1}{2^{n-2}} \sum_{i_1=1}^n \sum_{i_2>i_1}^n \left\langle \hat{N}_{i_1} \hat{N}_{i_2} \right\rangle + \dots \\ &\dots + \frac{1}{2} \sum_{i_1=1}^n \sum_{i_2>i_1}^n \dots \sum_{i_{n-1}>i_{n-2}}^n \left\langle \hat{N}_{i_1} \hat{N}_{i_2} \dots \hat{N}_{i_{n-1}} \right\rangle + \left\langle \hat{N}_1 \hat{N}_2 \dots \hat{N}_n \right\rangle, \end{aligned} \tag{5.6}$$

where the number operators defined as  $\hat{N}_k \equiv \hat{a}_k^\dagger \hat{a}_k$  were used. Take all but the last term on the RHS of eq. (5.6) and call their sum  $S^2$ , so that:

$$\left\langle \prod_k \left( \hat{N}_k + \frac{1}{2} \right) \right\rangle = S^2 + \left\langle \prod_k \hat{N}_k \right\rangle. \tag{5.7}$$

---

<sup>4</sup>The principal minors of a matrix  $M^I$  are the determinants of the submatrices obtained by picking out some rows and columns of  $M^I$ , while guaranteeing that whenever we choose to pick row  $j$ , we also pick the corresponding *column*  $j$ .

Note that  $S^2$  is a nonnegative quantity, since it is given by a sum of expectation values of products of number operators, which are always nonnegative. The inequality (5.4) can now be rewritten as follows:

$$\left\langle \prod_k \hat{N}_k \right\rangle - \left\langle \prod_k \hat{A}_k(s_k) \right\rangle \left\langle \prod_k \hat{A}_k(-s_k) \right\rangle \geq -S^2, \quad (5.8)$$

where I used the fact that  $\hat{A}_k^\dagger(s_k) = \hat{A}_k(-s_k)$ .

The key point in the proof is to realize that, for any choice of the parameters  $s_k$ , the left-hand side (LHS) of eq. (5.8) is just one of the principal minors of  $M^I$ , provided we choose the bipartition  $I$  appropriately. The principal minor we should look at is:

$$D^I = \begin{vmatrix} 1 & \left\langle \prod_k \hat{A}_k(s_k) \right\rangle \\ \left\langle \prod_k \hat{A}_k(-s_k) \right\rangle & \eta_I \end{vmatrix}, \quad (5.9)$$

where  $\eta_I$  depends on the bipartition  $I$ , and which we want to take the form  $\eta_I = \left\langle \prod_k \hat{N}_k \right\rangle$ .

Looking at the elements of the matrix of moments  $M^I$  given by eq. (5.5), we note that the indices labeling the diagonal element that has one creation operator  $\hat{a}_k^\dagger$  and one annihilation operator  $\hat{a}_k$  in normal order are  $l_k = 1$ ,  $k_k = 0$ ,  $p_k = 0$  and  $q_k = 1$ . The corresponding upper right element is in turn labeled, for the  $k$  part, by  $l_k = 0$ ,  $k_k = 0$ ,  $p_k = 0$  and  $q_k = 1$ . If we have the choice of setting  $s_k = -1$  we want this to correspond to a creation operator  $\hat{a}_k^\dagger$  appearing in this position, which means that our bipartition must be such that  $I$  includes site  $k$ . Conversely, if we have, for a different  $k$ ,  $s_k = 1$ , site  $k$  should *not* be in  $I$ .

Hence, if we choose the bipartition as that labeled by  $I$  including all sites with setting  $s_k = -1$ , we get  $\eta_I = \left\langle \prod_k \hat{N}_k \right\rangle$ , and thus:

$$D^I = \left\langle \prod_k \hat{N}_k \right\rangle - \left\langle \prod_k \hat{A}_k(s_k) \right\rangle \left\langle \prod_k \hat{A}_k(-s_k) \right\rangle. \quad (5.10)$$

It follows that a violation of inequality (5.8) implies that  $D^I < 0$ , and the violating state must be NPT according to bipartition  $I$ , or simply NPT, which concludes the proof.

Note that if all  $s_k$  are equal to either 1 or  $-1$ , this corresponds respectively to  $I = \emptyset$  or  $I = \mathcal{N}$ , meaning no transposition at all. As I have mentioned before, in this case the positivity of the minors speaks no longer of the positivity of the partial transpose of the state but of the positivity of the state

itself. A violation for this choice of parameters, thus, would mean that the state is not positive semidefinite, which is not physical.

## 5.4 Non-orthogonal quadratures

I now extend the previous result to the case in which two distinct, arbitrary quadratures are measured in each site. These quadratures are defined as:

$$\begin{aligned}\hat{X}'_k &= \hat{X}_k = \hat{a}_k e^{-i\theta_k} + \hat{a}_k^\dagger e^{i\theta_k}, \\ \hat{Y}'_k &= \hat{a}_k e^{-i(\theta_k + \delta_k + s'_k \pi/2)} + \hat{a}_k^\dagger e^{i(\theta_k + \delta_k + s'_k \pi/2)},\end{aligned}\quad (5.11)$$

where again  $s'_k \in \{-1, 1\}$  and  $-\pi/2 < \delta_k < \pi/2$  quantifies the departure from orthogonality. With these parameters all possible angle choices are covered, noting that  $\delta_k = -\pi/2, \pi/2$  corresponds to measuring only a single quadrature.

Instead of writing the new inequality as before in terms of the  $\hat{a}_k$  and  $\hat{a}_k^\dagger$  operators, I define new operators  $\hat{b}_k$  and  $\hat{b}_k^\dagger$  as:

$$\hat{b}_k = \frac{(\hat{X}'_k + e^{is_k \pi/2} \hat{Y}'_k) e^{i\theta_k}}{2}, \quad \hat{b}_k^\dagger = \frac{(\hat{X}'_k + e^{-is_k \pi/2} \hat{Y}'_k) e^{-i\theta_k}}{2}, \quad (5.12)$$

for  $s'_k = \pm 1$ , such that:

$$\begin{aligned}\hat{X}'_k &= \hat{b}_k e^{-i\theta_k} + \hat{b}_k^\dagger e^{i\theta_k}, \\ \hat{Y}'_k &= \hat{b}_k e^{-i(\theta_k + s'_k \pi/2)} + \hat{b}_k^\dagger e^{i(\theta_k + s'_k \pi/2)},\end{aligned}\quad (5.13)$$

thus mimicking the relation (5.3) between the orthogonal quadratures  $\hat{X}_k$  and  $\hat{Y}_k$  and the operators  $\hat{a}_k$  and  $\hat{a}_k^\dagger$ . Computing the commutation relations for these new operators, we arrive at  $[\hat{b}_k, \hat{b}_k^\dagger] = \cos \delta_k$ , independently of the  $s'_k$ .

Noting that equation (5.13) has exactly the same form as (5.3), and taking into account that the commutators are neglected in deriving the inequalities, we can write the CFRD inequality (5.2) for the *non-orthogonal* quadratures  $\hat{X}'_k$  and  $\hat{Y}'_k$  in terms of the  $\hat{b}_k$  and  $\hat{b}_k^\dagger$  operators as:

$$\left\langle \prod_k \hat{B}_k(s_k) \right\rangle^2 \leq \left\langle \prod_k \left( \hat{b}_k^\dagger \hat{b}_k + \frac{1}{2} \right) \right\rangle, \quad (5.14)$$

where now  $\hat{B}_k(1) = \hat{b}_k$  and  $\hat{B}_k(-1) = \hat{b}_k^\dagger$ .

Despite having reached an inequality identical in form to (5.4), I am yet not entitled to make any statements about the state being PPT or not, since inequality (5.14) is given in terms of operators with different commutation relations. Let me then proceed with a further definition:

$$\hat{c}_k = \frac{1}{\sqrt{\cos \delta_k}} \hat{b}_k, \quad \hat{c}_k^\dagger = \frac{1}{\sqrt{\cos \delta_k}} \hat{b}_k^\dagger, \quad (5.15)$$

recalling that  $-\pi/2 < \delta_k < \pi/2$  and hence  $\cos \delta_k > 0$ . These new operators satisfy the standard commutation relations  $[\hat{c}_k, \hat{c}_k^\dagger] = 1$ .

Rewriting inequality (5.14) in terms of  $\hat{c}_k$  and  $\hat{c}_k^\dagger$ , we get:

$$\left| \left\langle \prod_k \sqrt{\cos \delta_k} \hat{C}_k(s_k) \right\rangle \right|^2 \leq \left\langle \prod_k \left( \cos \delta_k \hat{c}_k^\dagger \hat{c}_k + \frac{1}{2} \right) \right\rangle, \quad (5.16)$$

once more with  $\hat{C}_k(1) = \hat{c}_k$  and  $\hat{C}_k(-1) = \hat{c}_k^\dagger$ . Expanding the RHS as before, we can rewrite the inequality as:

$$\left\langle \prod_k \hat{N}'_k \right\rangle - \left\langle \prod_k \hat{C}_k(s'_k) \right\rangle \left\langle \prod_k \hat{C}_k(-s'_k) \right\rangle \geq -S'^2, \quad (5.17)$$

where now  $\hat{N}'_k \equiv \hat{c}_k^\dagger \hat{c}_k$  and

$$\begin{aligned} S'^2 &= \frac{1}{\prod_{k=1}^n \cos \delta_k} \left( \frac{1}{2^n} + \frac{1}{2^{n-1}} \sum_{i_1=1}^n \cos \delta_{i_1} \left\langle \hat{N}_{i_1} \right\rangle \right. \\ &\quad + \frac{1}{2^{n-2}} \sum_{i_1=1}^n \sum_{i_2>i_1}^n \cos \delta_{i_1} \cos \delta_{i_2} \left\langle \hat{N}_{i_1} \hat{N}_{i_2} \right\rangle + \dots \\ &\quad \dots + \frac{1}{2} \sum_{i_1=1}^n \sum_{i_2>i_1}^n \dots \sum_{i_{n-1}>i_{n-2}}^n \cos \delta_{i_1} \cos \delta_{i_2} \dots \cos \delta_{i_{n-1}} \\ &\quad \left. \left\langle \hat{N}_{i_1} \hat{N}_{i_2} \dots \hat{N}_{i_{n-1}} \right\rangle \right) > 0. \end{aligned} \quad (5.18)$$

Applying the same reasoning as before allows to generalize the result for the case of two arbitrary quadratures per site.

## 5.5 Relevance of the CFRD inequality

In this section I will show that, in the case of two parties, the CFRD inequality is never violated for measurements on two quadratures per site.

Thus, in spite of its elegance and conceptual beauty, at present there is no feasible scheme<sup>5</sup> producing a violation of the CFRD inequality. This remains as an interesting open question.

Let me start by considering systems of two parties with measurements on arbitrary quadratures. Applying the positivity of the variance for the real and imaginary parts of  $C_2$  (see (5.1)) without neglecting the terms containing commutators we get:

$$\underbrace{\langle \tilde{X}_2 \rangle^2 + \langle \tilde{Y}_2 \rangle^2 - \left\langle \prod_{k=1}^2 (X_k^2 + Y_k^2) \right\rangle}_{\beta_2} \leq -\langle [X_1, Y_1][X_2, Y_2] \rangle \quad (5.19)$$

The Bell inequality (5.2) follows by setting the right-hand side (RHS) of this inequality to zero, and we are left with  $\beta_2 \leq 0$ , since for LHV models all commutators are null. So, in order to have a violation we need to find a state such that  $\beta_2 > 0$ . I am going to show that this never happens with the choice (5.11).

Choosing (5.11) the RHS of (5.19) becomes  $4s_1 s_2 \cos \delta_1 \cos \delta_2$ , so we have  $\beta_2 \leq 4s_1 s_2 \cos \delta_1 \cos \delta_2$ . If the parameters are chosen to be different, *i.e.*:  $s_1 = -s_2 = 1$  (or equivalently  $s_1 = -s_2 = -1$ ), we have that  $\beta_2 \leq -4 \cos \delta_1 \cos \delta_2 < 0$  for all quantum states, and then there is no violation in this case. As we have previously shown for arbitrary  $n$ , no violation can take place for the case in which the parameters are equal,  $s_1 = s_2$ .

## 5.6 Concuding remarks

The results presented here have consequences both from a fundamental and a practical point of view. First the Peres' conjecture was extended to a scenario involving measurements with an arbitrary number of outcomes. This gives more support for the belief that the impossibility of distilling entanglement is intimately linked to the existence of a local hidden model for a given state. Second, CV Bell inequalities suitable for practical tests are very desired due to the high control attained in CV photonic experiments. However we have discarded the possibility of using these inequalities for testing two mode non-locality. Moreover, out of the family of multipartite inequalities, we also discarded those for which all  $s_k$  equal, showing that no quantum

---

<sup>5</sup>A feasible scheme could, for instance, consist of (i) a state of a small number of modes whose preparation requires a few non-Gaussian operations and (ii) homodyne measurements.

state can violate them. A future research could involve the study of CV Bell inequalities involving more measurements per site [SV08].

# Chapter 6

## Geometrically induced singular behavior of entanglement

A geometrical structure follows directly from the definition of quantum states: the mathematical set of quantum states is convex and closed. Moreover, since convex combinations of separable states are also separable, these states form a convex set interior to the set of all quantum states. Apart from these direct facts, subtler questions concerning the geometry of quantum states may arise [BZ06]. In this chapter I will focus on the following problems: what is the shape of such sets? Are the boundary of these sets smooth? Do they present singularities? Apart from these abstract questions I will discuss a more physical query: Is there any consequence of the geometry of quantum states in physical phenomena?

Entanglement is tightly linked to geometry [BZ06]. For instance, many of the recent attempts to quantify quantum correlations are based on the definition of some distance between entangled states and the set of classically correlated states [PV05]. The main goal here is to develop a general approach to investigate the effects of geometry on entanglement. I will show that the non-trivial shape of the boundary of the separable states' set - which is shown to exhibit singularities - induces singular behaviour of entanglement in several physical processes, ranging from state transfer dynamics to spin-chain-ground-state properties [RVF+04, RVF+05, OPM06]. An experiment with linear optics was implemented to simulate this effect and verify the theoretical predictions.

The results covered in this chapter were developed in collaboration with P.L. Saldanha, O. Cosme, F.G.S.L. Brandão, C.H. Monken, S. Pádua, M. F. Santos, and M. O. Terra Cunha.

## 6.1 The random robustness as a geometric microscope

A geometric way to quantify entanglement is to see how far - using some definition of distance on the state space - an entangled state is from the set of  $k$ -separable states  $S_k$ . This has been carried over for a variety of notions of distance, generating different measures of entanglement [HHHH07, PV05]. As seen in Chapter 2, one of these geometric quantifiers is the random robustness,  $R_R$  (2.14). The physical motivation behind its definition is clear:  $\sigma$  represents a mixture of  $\rho$  with the random state  $\pi = I/D$ , and  $R_R(\rho)$  quantifies how much of this noise must be added to  $\rho$  in order to obtain a  $k$ -separable state. The main result of this section is to show that  $R_R^k$  can be used to investigate the shape of the boundary of  $S_k$ ,  $\partial S_k$ .

Take an entangled state depending smoothly on one parameter  $q$  and compute  $R_R^k$  as a function of  $q$ . The one-parameter density matrices  $\rho(q)$  can be seen as a curve in the set of quantum states as shown in Fig. 6.1. Singularities at  $\partial S_k$  will show up as singularities in  $R_R^k(\rho(q))$ , as if we were probing the geometry of  $S_k$  with a “microscope”. This statement is general for any finite dimension and will be formalized by the contrapositive:

**Proposition 1** *If  $\partial S_k$  is non-singular, then  $R_R^k(\rho(q))$  is also non-singular.*

A formal proof of this result can be found in Appendix B. Let me insist on the interpretation: Proposition 1 means that any singularity in  $R_R^k$  for a well chosen path  $\rho(q)$  reflects singularities in  $\partial S_k$ .

From this point on, I will specialize on the situation for two qubits, which is related to the performed experiment described here. I will come back to higher dimensional systems in the final remarks. For two-qubit systems, Ref. [BV06] shows that the Random Robustness is proportional to the Negativity ( $N(\rho)$ ). It turns out that, in this particular case, an optimal entanglement witness  $W_{opt}$  satisfying (2.19) is proportional to the partial transposition of the projector onto the eigenspace of the negative eigenvalue of  $\rho^{T_B}$ <sup>1</sup> [LKCH00]. Using this fact we can conclude that for every two-qubit entangled state  $\rho$  [BV06],

$$2N(\rho) = R_R(\rho) = - \min_{W \in \mathcal{W}} \text{Tr}(W\rho), \quad (6.1)$$

where  $\mathcal{M}$  is the set of entanglement witnesses  $W$  with  $\text{Tr}W = 4$ .

---

<sup>1</sup>Remember that  $\rho^{T_B}$  denotes the partial transposition of  $\rho$ .

## 6.1. THE RANDOM ROBUSTNESS AS A GEOMETRIC MICROSCOPE 55

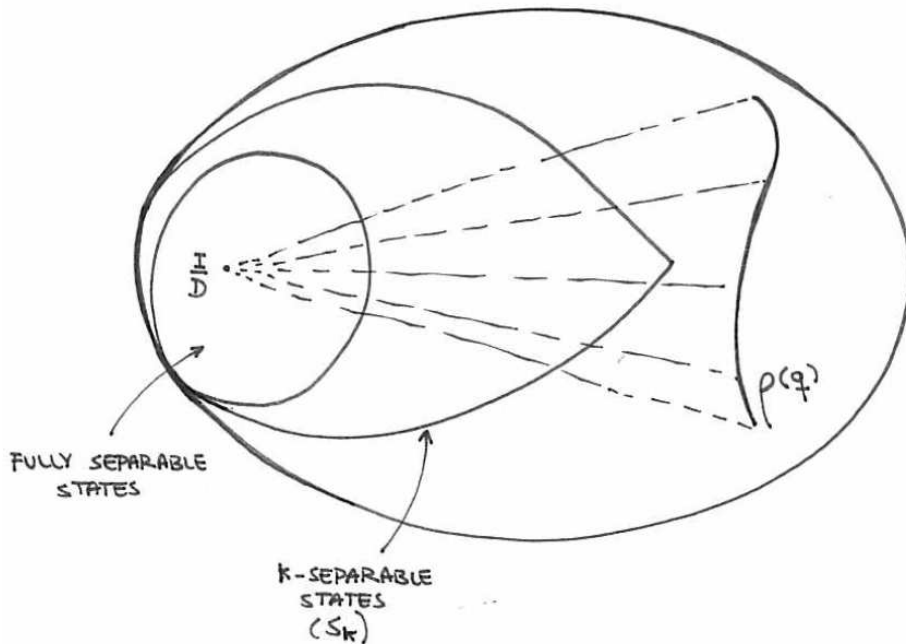


Figure 6.1: **Probing**  $\partial S$ . The curved line represents the path  $\rho(q)$  followed by  $\rho$  when parameter  $q$  is changed. For each value of  $q$ ,  $R_R$  is measured (dotted lines). It is worth noting that  $S_k$  can present singular points in its shape and to remember that the “true” picture is much subtler, given the large dimensionality of the state space, even in the simplest two-qubit case [BZ06].

## 6.2 Where do these singularities appear?

At this point we might ask some natural questions. Is there in fact any singularity in the shape of  $S_k$ ? In the affirmative case, does this singularity appear in any physical setup? I proceed to answer positively both questions by showing physical processes where a singularity in  $\partial S_2$  is revealed by monitoring the entanglement of a given two-qubit system.

### 6.2.1 Entanglement swapping

First, let me consider a general system of four qubits  $a$ ,  $b$ ,  $A$ , and  $B$ , subject to the following Hamiltonian [COP+03]:

$$H = H^{aA} + H^{bB}, \quad (6.2)$$

where

$$H^{aA} = \frac{\omega}{2}\sigma_z^a + \frac{\omega}{2}\sigma_z^A + \frac{g}{2}(\sigma_-^a\sigma_+^A + \sigma_+^a\sigma_-^A), \quad (6.3)$$

and an equivalent for  $H^{bB}$ . Here  $\sigma_+ = (\sigma_x + i\sigma_y)/2$  and  $\sigma_- = (\sigma_x - i\sigma_y)/2$ , where  $\sigma_x$ ,  $\sigma_y$  and  $\sigma_z$  are the usual Pauli matrices. This scenario can be realized in systems like cavity QED [RMH01] and trapped ions [LBMW03]. Set the initial state to be  $|\psi(t=0)\rangle = |\Phi_+\rangle_{ab} \otimes |\Psi_+\rangle_{AB}$ , where qubits  $ab$  are in the Bell state  $|\Phi_+\rangle = (|00\rangle + |11\rangle)/\sqrt{2}$  and qubits  $AB$  are in the orthogonal Bell state  $|\Psi_+\rangle = (|01\rangle + |10\rangle)/\sqrt{2}$ . Hamiltonian (6.2) induces a swapping process which leads (in the interaction picture) to the following temporal evolution for the subsystem  $AB$ , obtained by tracing out the subsystem  $ab$ :

$$\rho_{AB}(t) = q |\Psi_+\rangle \langle \Psi_+| + (1 - q) |\Phi_+\rangle \langle \Phi_+, \quad (6.4)$$

where  $q = \cos^2(gt)$ . For this state the negativity reads

$$N(\rho_{AB}(t)) = \frac{1}{2} \max \{1 - 2q, 2q - 1\} = \frac{|1 - 2q|}{2}. \quad (6.5)$$

This function presents a singularity for  $q = 0.5$  ( $gt = n\pi/4$ , with  $n$  odd) signaling then a singularity at  $\partial S_2$ .

### 6.2.2 Bit-flip noisy channel

Another physical process which also produces the family of states (6.4) is the following simple quantum communication task: Alice prepares a Bell state  $|\Phi_+\rangle$  and sends one qubit to Bob through a quantum channel; if this

## 6.2. WHERE DO THESE SINGULARITIES APPEAR?

57

channel has a probability  $q$  of introducing a bit flip, and  $1 - q$  of no error at all, the state (6.4) is the output of the process<sup>2</sup>.

To illustrate the dynamics given by Eq. (6.4), an all-optical experiment which reproduces the noisy channel described above was performed. The experimental setup is illustrated in Fig. 6.2. In the experiment, twin photons maximally entangled in polarization are generated in a non-linear crystal [KMW+05] and sent to an unbalanced Michelson interferometer. The experiment works as follows: a two-photon  $|\Psi_+\rangle$  state is produced. While one of the photons is sent directly to the detection stage the other goes to the (unbalanced) interferometer. One of the arms of this interferometer does not change the polarization of the photon, and if the photon went through this path the two photons would be detected in  $|\Psi_+\rangle$ . However if the photon went through the other path its polarization would be rotated in such a way that the final two-photon state would become  $|\Phi_+\rangle$ . A tomographic characterization of the photonic states corresponding to these two extremal points was then performed. The reconstructed density matrices are displayed in Fig. 6.3. These two possibilities are then incoherently recombined, thus allowing the preparation of state (6.4). Each preparation yields a different value for  $q$  with the corresponding optimal witness given by

$$W_{opt} = \begin{cases} I - 2|\Phi_+\rangle\langle\Phi_+|, & \text{for } 0 \leq q \leq 1/2, \\ I - 2|\Psi_+\rangle\langle\Psi_+|, & \text{for } 1/2 \leq q \leq 1. \end{cases} \quad (6.6)$$

For the family of generated states these two observables are the only candidates of optimal entanglement witnesses. In a more general situation, if less is known about the prepared state, much more candidate witnesses should be measured. The results are displayed in Fig. 6.4. The blue curve in the figure shows the witnessed negativity measurement and its edge indicates the existence of singularities at  $\partial S$ . This experimental result shows the abrupt change in the optimal witness at the value  $q = \frac{1}{2}$ , which heralds the singularity in  $\partial S$ . As a proof of principle, each operator  $W$  is measured for the whole range of  $q$ , which yields the points below zero in Fig. 6.4. Note that the singularity occurs exactly for  $R_R = 0$  ( $q = 1/2$ ). According to the present geometrical interpretation, this means the path followed by the parameterized state  $\rho(q)$  touches the border of  $S$ <sup>3</sup>.

---

<sup>2</sup>The simplest way of drawing the complete line represented by Eq. (6.4) is to consider three different initial conditions: from  $|\Phi_+\rangle$  one obtains  $q \in [0, 1/2]$ , from  $|\Psi_+\rangle$ ,  $q \in (1/2, 1]$ , and  $q = 1/2$  is a fixed point of this dynamical system.

<sup>3</sup>This result must not be a surprise, since it is well known that in the tetrahedron generated by the Bell states (which we access in our experiment) the separable states form a inscribed octahedron [HH96].

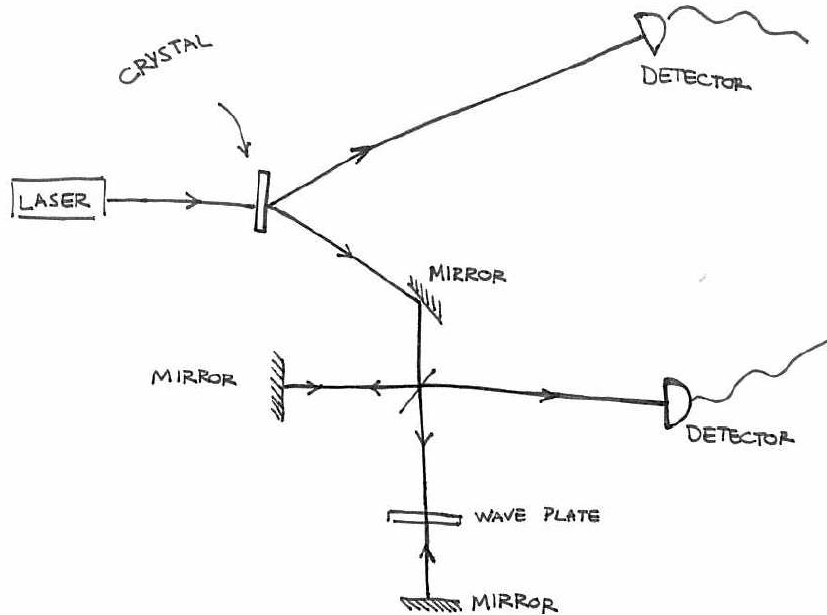


Figure 6.2: Experimental setup.

### 6.2.3 Spin systems

The geometrical properties of entanglement discussed here give new insight into singularities found recently in the entanglement of condensed matter systems. Striking examples, dealing with entanglement properties of certain spin- $\frac{1}{2}$  models subjected to a transverse magnetic field  $h$ , are described in Refs. [RVF+04, RVF+05, OPM06]. In these works, the two-qubit reduced state shows a singularity in entanglement for a particular field value  $h_f$  far from the critical field of the respective model. As correlation functions, ground-state energy, and even reduced density matrices are all smooth at  $h_f$ , there was no clear origin for these singularities. Our results offer an explanation by interpreting the non-analyticities exhibited by entanglement as a consequence of geometric singularities at  $\partial S$ <sup>4</sup>.

## 6.3 Concluding remarks

As previously mentioned,  $R_R^k$  can be used to probe  $\partial S_k$  in any finite dimensional system. For example, a previous work showed a singular behavior

---

<sup>4</sup>Although the results of Refs. [RVF+04, RVF+05, OPM06] were obtained in terms of the concurrence, a completely analogous result holds for the negativity as well.

## 6.3. CONCLUDING REMARKS

59

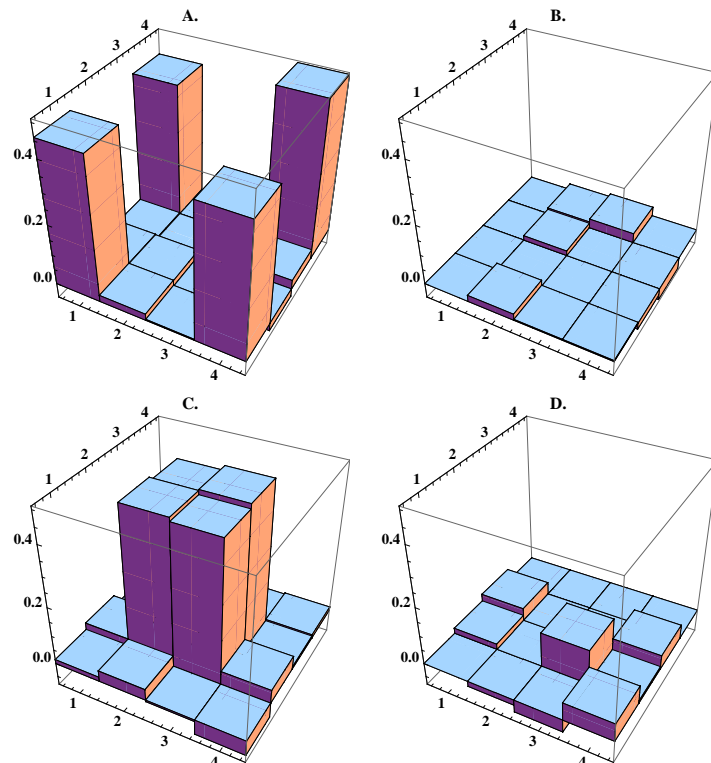


Figure 6.3: The reconstructed density matrices corresponding (ideally) to the states  $|\Phi_+\rangle$  (A. real and B. imaginary parts) and  $|\Psi_+\rangle$  (C. real and D. imaginary parts). The attained fidelity for these states are, respectively,  $F_{\Phi_+} \equiv \langle \Phi_+ | \rho | \Phi_+ \rangle \approx (92 \pm 3)\%$  and  $F_{\Psi_+} \equiv \langle \Psi_+ | \rho | \Psi_+ \rangle \approx (96 \pm 3)\%$ .

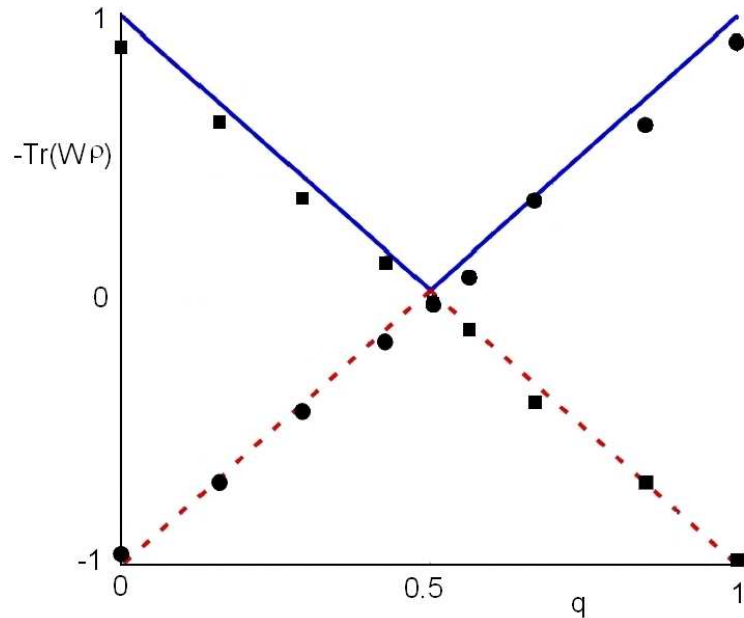


Figure 6.4: Measurement of the mean value of both operators described in (6.6) for the full range  $0 \leq q \leq 1$ . Each  $W$  is expanded as a linear combination of products of local operators which are then measured independently. The blue continuous line corresponds to the theoretical value of  $N(\rho(q))$  for the state  $\rho(q) = q|\Psi_+\rangle\langle\Psi_+| + (1-q)|\Phi_+\rangle\langle\Phi_+|$ . Note that each  $W$  only witnesses entanglement for a restricted range of  $q$  values as predicted by the theory. The local singularity of  $\partial S$  is evidenced by the abrupt change of optimal  $W$ . Experimental errors are within the dots' sizes.

## 6.3. CONCLUDING REMARKS

61

of  $R_R$  in three qubits systems [BV06]. Within the scope of the present discussion, we can interpret it as originated by a singularity at the border of the respective separable set. Note, however, that in this case, due to the higher dimensionality of the system, the singularity at  $\partial S$  occurs in the interior of the set of density matrices (not at its border), with  $R_R$  showing a singularity at a positive value.

To sum up, I have presented a method for probing the shape of the set of separable states. Singularities in this set were found and connected to non-analytical behavior of entanglement in different physical systems. It is an interesting open question to find physical implications of such singularities.



## Chapter 7

# Scaling laws for the decay of multiqubit entanglement

Entanglement has been identified as a key resource for many potential practical applications, such as quantum computation, quantum teleportation and quantum cryptography [NC00]. Being it a resource, it is of fundamental importance to study the entanglement properties of quantum states in realistic situations, where the system unavoidably loses its coherence due to interactions with the environment.

In the simplest case of two qubits a peculiar dynamical feature of entangled states has been found: even when the constituent parts of an entangled state decay asymptotically in time, entanglement may disappear at a finite time [SK02, CMB04, DB04, Dio03, Dio03, DH04, YE04, YE06, YE07, SMDZ07, Ter07, YE07, AJ07, AMH+07]. The phenomenon of finite-time disentanglement, also known as entanglement sudden death (ESD) [AMH+07, YE04, AJ07, YE07], illustrates the fact that the global behavior of an entangled system, under the effect of local environments, may be markedly different from the individual and local behavior of its constituents.

Since the advantages of using quantum-mechanical systems to information and communication tasks is only apparent in the case of large-scale information processing, it is fundamental to understand the scaling properties of disentanglement for multiparticle systems. Important steps in this direction were given in Refs. [SK02, CMB04, DB04]. In particular, it was shown in Ref. [SK02] that (i) balanced GHZ states,  $|\Psi\rangle = (|0\rangle^{\otimes N} + |1\rangle^{\otimes N})/\sqrt{2}$ , subject to the action of individual depolarization [NC00], undergo ESD, (ii) that the last bipartitions to loose entanglement are the most-balanced ones, and (iii) that the time at which such entanglement disappears grows with the number  $N$  of particles in the system. Soon afterwards it was shown in Ref. [DB04] that the first bipartitions to loose entanglement are the least-

balanced ones (one particle vs. the others), the time at which this happens decreasing with  $N$ . A natural question arises from these considerations: is the time for which entanglement vanishes a truly physically-relevant quantity to assess the robustness of multi-particle entanglement?

In this chapter I will describe the achievements I have made together with L. Aolita, R. Chaves, L. Davidovich and A. Acín on this subject. We have shown that, for an important family of genuine-multipartite entangled states, the answer for the last question is no. For several kinds of decoherence, we derived analytical expressions for the time of disappearance of bipartite entanglement, which in several instances is found to increase with  $N$ . However, the time at which bipartite entanglement becomes arbitrarily small decreases with the number of particles, independently of ESD. This implies that for multi-particle systems, the amount of entanglement can become too small for any practical application long before it vanishes. In addition, for some specific cases, we were able to characterize not only bipartite entanglement but also to attest full separability of the states. As a byproduct we showed that in several cases the action of the environment can naturally lead to bound entangled states [HHH98], in the sense that, for a period of time, it is not possible to extract pure-state entanglement from the system through local operations and classical communication, even though the state is still entangled.

The exemplary states we analyzed the robustness of multipartite entanglement are generalized GHZ states:

$$|\Psi_0\rangle = \alpha|0\rangle^{\otimes N} + \beta|1\rangle^{\otimes N}, \quad (7.1)$$

with  $\alpha$  and  $\beta \in \mathbb{C}$  such that  $|\alpha|^2 + |\beta|^2 = 1$ . Therefore, the present results also constitute a generalization of those of Refs. [SK02, DB04]. Although the generalized GHZ states represent just a restricted class of states, the study of their entanglement properties is important in its own right: these can be seen as simple models of the Schrödinger-cat state [Sch35], they are crucial for communication problems [BVK98, HBB99, DP99], and such states have been experimentally produced in atomic [LKS+05] and photonic systems [LZG+07] of up to six particles.

## 7.1 Decoherence models

The following three paradigmatic types of noisy channels were studied: depolarization, dephasing, and a thermal bath at arbitrary temperature (generalized amplitude-damping channel). Consider  $N$  qubits of ground state  $|0\rangle$

and excited state  $|1\rangle$  without mutual interaction, each one individually coupled to its own noisy environment. The dynamics of the  $i$ th qubit,  $1 \leq i \leq N$ , is governed by a master equation that gives rise to a completely positive trace-preserving map (or channel)  $\mathcal{E}_i$  describing the evolution as  $\rho_i = \mathcal{E}_i \rho_{0i}$ , where  $\rho_{0i}$  and  $\rho_i$  are, respectively, the initial and evolved reduced states of the  $i$ th subsystem [NC00].

### 7.1.1 Generalized Amplitude Damping Channel

The generalized amplitude damping (GAD) channel is given, in the Born-Markov approximation, via its Kraus representation by [NC00, YE07]

$$\mathcal{E}_i^{\text{GAD}} \rho_i = E_0 \rho_i E_0^\dagger + E_1 \rho_i E_1^\dagger + E_2 \rho_i E_2^\dagger + E_3 \rho_i E_3^\dagger; \quad (7.2)$$

with

$$E_0 \equiv \sqrt{\frac{\bar{n}+1}{2\bar{n}+1}} (|0\rangle\langle 0| + \sqrt{1-p} |1\rangle\langle 1|),$$

$$E_1 \equiv \sqrt{\frac{\bar{n}+1}{2\bar{n}+1} p} |0\rangle\langle 1|,$$

$$E_2 \equiv \sqrt{\frac{\bar{n}}{2\bar{n}+1}} (\sqrt{1-p} |0\rangle\langle 0| + |1\rangle\langle 1|)$$

and

$$E_3 \equiv \sqrt{\frac{\bar{n}}{2\bar{n}+1} p} |1\rangle\langle 0|$$

being its Kraus operators. Here  $\bar{n}$  is the mean number of excitations in the bath,  $p \equiv p(t) \equiv 1 - e^{-\frac{1}{2}\gamma(2\bar{n}+1)t}$  is the probability of the qubit exchanging a quantum with the bath at time  $t$ , and  $\gamma$  is the zero-temperature dissipation rate. Channel (7.2) is a generalization to finite temperature of the purely dissipative amplitude damping channel (AD), which is obtainen from (7.2) in the zero- temperature limit  $\bar{n} = 0$ . On the other hand, the purely diffusive case is obtained from (7.2) in the composite limit  $\bar{n} \rightarrow \infty$ ,  $\gamma \rightarrow 0$ , and  $\bar{n}\gamma = \Gamma$ , where  $\Gamma$  is the diffusion constant.

### 7.1.2 Depolarizing Channel

The depolarizing channel (D) describes the situation in which the  $i$ th qubit remains untouched with probability  $1 - p$ , or is depolarized (white noise)—meaning that its state is taken to the maximally mixed state—with probability  $p$ . It can be expressed as

$$\mathcal{E}_i^{\text{D}} \rho_i = (1 - p)\rho_i + (p)I/2, \quad (7.3)$$

where  $I$  is the identity operator.

### 7.1.3 Phase Damping Channel

Finally, the phase damping channel (PD) - also called dephasing - represents the situation in which there is loss of quantum coherence with probability  $p$ , but without any energy exchange. It is defined as

$$\mathcal{E}_i^{\text{PD}} \rho_i = (1-p)\rho_i + p(|0\rangle\langle 0| |\rho_i| 0\rangle\langle 0|) + |1\rangle\langle 1| |\rho_i| 1\rangle\langle 1|). \quad (7.4)$$

The parameter  $p$  in channels (7.2), (7.3) and (7.4) is a convenient parametrization of time:  $p = 0$  refers to the initial time 0 and  $p = 1$  refers to the asymptotic  $t \rightarrow \infty$  limit.

The density matrix corresponding to the initial state,

$$\begin{aligned} \rho_0 &\equiv |\Psi_0\rangle\langle\Psi_0| \\ &= \alpha|^2(|0\rangle\langle 0|)^{\otimes N} + |\beta|^2(|1\rangle\langle 1|)^{\otimes N} + \alpha\beta^*(|0\rangle\langle 1|)^{\otimes N} + \alpha^*\beta(|1\rangle\langle 0|)^{\otimes N}, \end{aligned} \quad (7.5)$$

evolves in time into a mixed state  $\rho$  given simply by the composition of all  $N$  individual maps:  $\rho \equiv \mathcal{E}_1\mathcal{E}_2 \dots \mathcal{E}_N\rho_0$ , where, in what follows,  $\mathcal{E}_i$  will either be given by Eqs. (7.2), (7.3) or (7.4).

## 7.2 Entanglement sudden death

Here I will use the negativity as a quantifier of entanglement [VW02]. As commented in chapter 2, the negativity fails to quantify entanglement of some entangled states (those ones with positive partial transposition) in dimensions higher than six [Per96b, HHH96]. However, for the states considered here, the task of calculating the negativity reduces to a four-dimensional problem. So, in the considered cases, the negativity brings all the relevant information about the separability in bipartitions of the states, i.e., null negativity means separability in the corresponding partition.

Application of channel (7.2) to every qubit multiplies the off-diagonal elements of  $\rho_0$  by the factor  $(1-p)^{N/2}$ , whereas application of channels (7.3) or (7.4), by the factor  $(1-p)^N$ . The diagonal terms  $(|0\rangle\langle 0|)^{\otimes N}$  and  $(|1\rangle\langle 1|)^{\otimes N}$  in turn give rise to new diagonal terms of the form  $(|0\rangle\langle 0|)^{\otimes N-k} \otimes (|1\rangle\langle 1|)^{\otimes k}$ , for  $1 \leq k < N$ , and all permutations thereof, with coefficients  $\lambda_k$  given below. In what follows I present the main results concerning the entanglement behavior of these states.

### Generalized amplitude-damping channel

Consider a bipartition  $k : N - k$  of the quantum state. For channel (7.2), the coefficients  $\lambda_k^{\text{GAD}}$  are given by

$$\lambda_k^{\text{GAD}} \equiv |\alpha|^2 x^{N-k} y^k + |\beta|^2 w^{N-k} z^k, \quad (7.6)$$

with

$$0 \leq x \equiv \frac{-p\bar{n}}{2\bar{n}+1} + 1, y \equiv \frac{p\bar{n}}{2\bar{n}+1}, w \equiv \frac{p(\bar{n}+1)}{2\bar{n}+1} \text{ and } z \equiv \frac{-p(\bar{n}+1)}{2\bar{n}+1} + 1 \leq 1.$$

From them, the minimal eigenvalue of the states' partial transposition,  $\Lambda_k^{\text{GAD}}(p)$ , is immediately obtained for the GAD channel<sup>1</sup>:

$$\Lambda_k^{\text{GAD}}(p) \equiv \delta_k - \sqrt{\delta_k^2 - \Delta_k}, \quad (7.7)$$

where

$$\delta_k = \frac{[\lambda_k^{\text{GAD}}(p) + \lambda_{N-k}^{\text{GAD}}(p)]}{2} \quad (7.8)$$

and

$$\Delta_k = \lambda_k^{\text{GAD}}(p)\lambda_{N-k}^{\text{GAD}}(p) - |\alpha\beta|^2(1-p)^N. \quad (7.9)$$

One can see that

$$|\Lambda_1^{\text{GAD}}(p)| \leq |\Lambda_2^{\text{GAD}}(p)| \leq \dots \leq |\Lambda_{\frac{N}{2}}^{\text{GAD}}(p)|, \quad (7.10)$$

for  $N$  even, and

$$|\Lambda_1^{\text{GAD}}(p)| \leq |\Lambda_2^{\text{GAD}}(p)| \leq \dots \leq |\Lambda_{\frac{N-1}{2}}^{\text{GAD}}(p)|, \quad (7.11)$$

for  $N$  odd.

For arbitrary temperature, the condition for disappearance of bipartite entanglement,  $\Lambda_k^{\text{GAD}}(p) = 0$ , is a polynomial equation of degree  $2N$ . In the purely dissipative case  $\bar{n} = 0$ , a simple analytical solution yields the corresponding critical probability for the amplitude-decay channel,  $p_c^{\text{AD}}$  (with  $\beta \neq 0$ ):

$$p_c^{\text{AD}}(k) = \min\{1, |\alpha/\beta|^{2/N}\}. \quad (7.12)$$

For  $|\alpha| < |\beta|$  this is always smaller than 1, meaning that bipartite entanglement disappears before the steady state is asymptotically reached. Thus,

---

<sup>1</sup>Since the analyzed states are permutationally invariant,  $\Lambda_k^{\text{GAD}}$  will correspond to the minimum eigenvalue of the state's partial transposition according to all possible  $k : N - k$  partitions. This is also true for the other channels.

(7.12) is the direct generalization to the multiqubit case of the ESD condition of Refs. [YE04, AMH+07] for two qubits subject to amplitude damping. A remarkable feature about Eq. (7.12) is that it displays no dependence on the number of qubits  $k$  of the sub-partition. The negativities corresponding to bipartitions composed of different numbers of qubits all vanish at the same time, even though they follow different evolutions. In Appendix D, I will prove that at this point the state is fully separable.

For arbitrary temperature, it is enough to consider the case  $k = N/2$ , as the entanglement corresponding to the most balanced bipartitions is the last one to disappear (I take  $N$  even from now on just for simplicity). The condition  $\Lambda_{N/2}^{\text{GAD}}(p) = 0$  reduces to a polynomial equation of degree  $N$ , which for the purely diffusive case yields:

$$p_c^{\text{Diff}}(N/2) = 1 + 2|\alpha\beta|^{2/N} - \sqrt{1 + 4|\alpha\beta|^{4/N}}. \quad (7.13)$$

### Depolarizing channel

Moving to the case of the depolarizing channel the negativity associated to the most-balanced bipartition again is always higher than the others, while the one corresponding to the least-balanced partition is the smallest one. The critical probability for the disappearance of entanglement in the  $N/2 : N/2$  partition is given by:

$$p_c^{\text{D}}(N/2) = 1 - (1 + 4|\alpha\beta|^{2/N})^{-1/2}. \quad (7.14)$$

Note that (7.13) and (7.14) always lead to ESD, for  $\alpha\beta \neq 0$ .

### Phase damping channel

Finally, for the phase damping channel, whereas the off-diagonal terms of the density matrix evolve as mentioned before, all the diagonal ones remain the same, with  $\lambda_k^{\text{PD}} \equiv 0$  for  $1 \leq k \leq N - 1$ . In this case,

$$\Lambda_k^{\text{PD}}(p) \equiv -|\alpha\beta|(1 - p)^N. \quad (7.15)$$

This expression is independent of  $k$ , and therefore of the bipartition, and for any  $\alpha, \beta \neq 0$  it vanishes only for  $p = 1$ , i.e., only in the asymptotic time limit, when the state is completely separable: *generalized GHZ states, subject to dephasing, never experience ESD*.

### 7.3. THE ENVIRONMENT AS A CREATOR OF BOUND ENTANGLEMENT 69

## 7.3 The environment as a creator of bound entanglement

Some effort has been recently done in order to understand whether bound entangled (i.e. undistillable) states naturally arise from natural physical processes [PFA07, TKGB07, FCGA08]. In this context, it has been found that different many-body models present thermal bound entangled states [PFA07, TKGB07, FCGA08]. In this section I will show, in a conceptually different approach, that bound entanglement can also appear in dynamical processes, namely decoherence.

For all channels here considered, the property

$$|\Lambda_1(p)| \leq |\Lambda_2(p)| \leq \dots \leq |\Lambda_{\frac{N}{2}}(p)| \quad (7.16)$$

holds. Therefore, when  $|\Lambda_1(p)| = 0$ , there may still be entanglement in the global state for some time afterwards, as detected by other partitions. When this happens, the state, even though entangled, is separable according to every  $1 : N - 1$  partition, and then no entanglement can be distilled by (single-particle) local operations.

An example of this is shown in Fig. 7.3, where the negativity for partitions  $1 : N - 1$  and  $N/2 : N/2$  is plotted versus  $p$ , for  $N = 4$  and  $\alpha = 1/\sqrt{2} = \beta$ , for channel D. After the  $1 : 3$  negativity vanishes, the  $2 : 2$  negativity remains positive until  $p = p_c^D(2)$  given by Eq. (7.14). Between these two values of  $p$ , the state is bound entangled since it is not separable but no entanglement can be extracted from it locally. Therefore, the environment itself is a natural generator of bound entanglement. Of course, this is not the case for channels AD and PD, since for the former the state is fully separable at  $p_c^{AD}(k)$  (see Eq. (7.12) and Appendix D) while the latter never induces ESD.

## 7.4 Does the time of ESD really matter for large N?

Inspection of critical probabilities (7.12), (7.13) and (7.14) shows that in all three cases the ESD time grows with  $N$ . This might be interpreted as the state's entanglement becoming more robust when the system's size increases. However, what really matters is not that the initial entanglement does not disappear but that a significant fraction of it remains, either to be directly used, or to be distilled without an excessively large overhead in resources. The idea is clearly illustrated in Fig. 7.4, where the negativity corresponding to the most-balanced partitions is plotted versus  $p$  for different values of  $N$ .

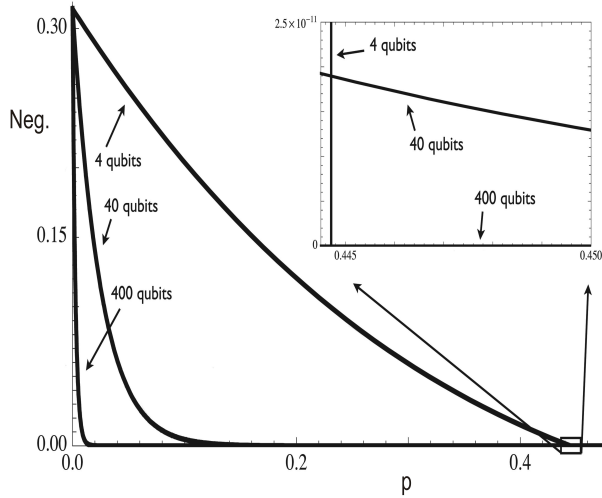


Figure 7.1: Negativity as a function of  $p$  for a balanced,  $\alpha = 1/\sqrt{2} = \beta$ , four-qubit GHZ state and independent depolarizing channels. A similar behavior is observed with channel GAD with  $\bar{n} \neq 0$ , but the effect is not so marked (the smaller  $\bar{n}$ , the weaker the effect).

Even though the ESD time increases with  $N$ , the time at which entanglement becomes arbitrarily small decreases with it. The channel used in Fig. 7.4 is the depolarizing channel, nevertheless the behavior is absolutely general, as discussed in the following.

For an arbitrarily small real  $\epsilon > 0$ , and all states for which  $|\alpha\beta| \neq 0$ , the critical probability  $p_\epsilon$  at which  $\Lambda_{N/2}(p_\epsilon) = \epsilon\Lambda_{N/2}(0)$ , becomes inversely proportional to  $N$  in the limit of large  $N$ . For channel (7.2), this is shown by setting  $k = N/2$  in  $\Lambda_{N/2}^{\text{GAD}}(p)$ , which simplifies to

$$\Lambda_{N/2}^{\text{GAD}}(p) = -|\alpha\beta|(1-p)^{N/2} + |\alpha|^2 x^{N/2} y^{N/2} + |\beta|^2 w^{N/2} z^{N/2}. \quad (7.17)$$

For any mean bath excitation  $\bar{n}$ ,  $x^{N/2}$  and  $z^{N/2}$  are at most of the same order of magnitude as  $(1-p)^{N/2}$ , whereas  $y^{N/2}$  and  $w^{N/2}$  are much smaller than one. Therefore, for all states such that  $|\alpha\beta| \neq 0$  we can neglect the last two terms and approximate  $\Lambda_{N/2}^{\text{GAD}}(p) \approx -|\alpha\beta|^2(1-p)^{N/2}$ . Set now

$$\Lambda_{N/2}^{\text{GAD}}(p_\epsilon) = \epsilon\Lambda_{N/2}^{\text{GAD}}(0) \Rightarrow \epsilon = (1-p_\epsilon)^{N/2} \Rightarrow \log(\epsilon) = \frac{N}{2} \log(1-p_\epsilon). \quad (7.18)$$

Since  $p_\epsilon \ll p_c^{\text{GAD}}(N/2) \leq 1$ , we can approximate the logarithm on the right-hand side of the last equality by its Taylor expansion up to first order in  $p_\epsilon$

and write  $\log(\epsilon) = -\frac{N}{2}p_\epsilon$ , implying that

$$p_\epsilon^{\text{GAD}} \approx -(2/N)\log(\epsilon). \quad (7.19)$$

Similar reasonings, applied to channels (7.3) and (7.4), lead to

$$p_\epsilon^{\text{D,PD}}(t) \approx -(1/N)\log(\epsilon). \quad (7.20)$$

Eqs. (7.19) and (7.20) assess the robustness of the state's entanglement better than the ESD time. Much before ESD, negativity becomes arbitrarily small. The same behavior is observed for all studied channels, and all coefficients  $\alpha$ ,  $\beta \neq 0$ , despite the fact that for some cases, like for instance for channel (7.4), no ESD is observed. The presence of  $\log \epsilon$  in the above expression shows that our result is quite insensitive to the actual value of  $\epsilon \ll 1$ .

## 7.5 Concluding remarks

In this chapter I have probed the robustness of the entanglement of unbalanced GHZ states of arbitrary number of particles subject to independent environments. The states possess in general longer entanglement sudden death time, the more particles in the system, but the time at which such entanglement becomes arbitrarily small is inversely proportional to the number of constituent particles. The latter time characterizes better the robustness of the state's entanglement than the time at which ESD itself occurs. In several cases the action of the environment can naturally lead to bound entangled states. An open question still remains on how other genuinely multipartite entangled states, such as W-type or graph states, behave. Our results suggest that maintaining a significant amount of multiqubit entanglement in macroscopic systems might be an even harder task than believed so far.

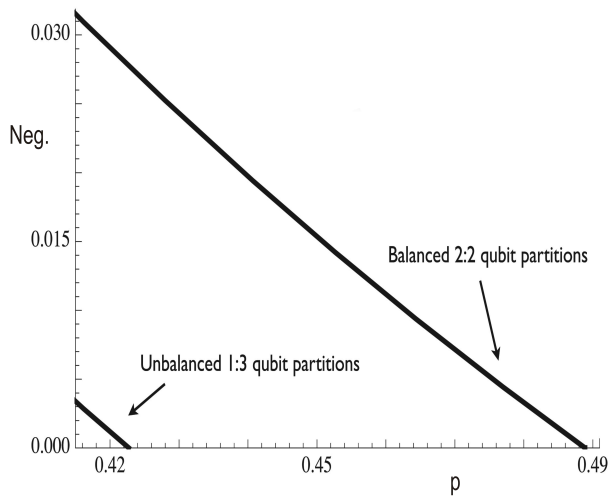


Figure 7.2: Negativity versus  $p$  for  $N = 4, 40$  and  $400$ , for the depolarizing channel and for the most balanced partitions. In this graphic  $\alpha = 1/3$  and  $\beta = \sqrt{8}/3$ , but the same behavior is displayed for all other parameters and maps. The inset shows a magnification of the region in which  $|\Lambda_2^D(p)|$  vanishes. Even though  $|\Lambda_{40}^D(p)|$  and  $|\Lambda_{400}^D(p)|$  cross the latter and vanish much later, they become orders of magnitude smaller than their initial value long before reaching the crossing point.

## Chapter 8

# Identical particle entanglement in Fermionic systems

Quantum correlations can naturally appear due to the indistinguishable character of quantum systems. For example, the state of a pair of identical fermions is always antisymmetric, hence naturally entangled. This entanglement comes from the indistinguishability of the fermions and can manifest itself in one or more degrees of freedom, depending, for example, on the spatial shape of the wave function [Ved03]. However, there is an interesting ongoing debate on the possibility of using this strictly spin-statistical entanglement to perform quantum information tasks [ESBL04, GM04].

Usually, when talking about entanglement, one tends to ignore the role of the measurement apparatus, always considering ideal situations. However, there is no such a thing as an ideal detector, and the detector bandwidth affects the measurement of entanglement. Furthermore, in the particular case of identical particles, it is still not clear how the symmetry of detection in external degrees of freedom affects the entanglement of the internal ones.

In this Chapter I will discuss the quantum correlations that naturally arises in a non-interacting Fermi gas at zero temperature. In particular, I will analyze how the measurement of external degrees of freedom can affect the entanglement in internal degrees of freedom in this system. Then, I will discuss how imperfect detections affect the observation of entanglement in the fermionic gas.

A second step consists on proposing a scheme to extract entanglement created solely by the Pauli exclusion principle. In this scheme two independent photons excite non-interacting electrons in a semiconductor quantum well. As the electrons relax to the bottom of the conduction band, the Pauli exclusion principle forces quantum correlations between their spins. It will be shown that after the electron-hole recombination this correlation is

transferred to the emitted photons as entanglement in polarization, which can subsequently be used for quantum information tasks. This proposal is quite unorthodox in the sense that decoherence, usually viewed as an enemy of entanglement, actually plays an important role in the extraction of this identical particle entanglement.

The results contained in this chapter are due to collaborations with M. F. Santos, M. O. Terra Cunha, L. Malard, F. Matinaga, C. Lunkes, and V. Vedral.

## 8.1 Non-interacting Fermi gas

The symmetrization principle establishes that the quantum state of two identical particles must be symmetrized or anti-symmetrized according to the particles species. However, in practice no physicist seems to care about the existence of other particles that do not take part of the system under study. In his book, A. Peres analyzes this question and concludes that “ (...)it is hardly conceivable that observable properties of the particles in our laboratory are affected by the possible existence on the Moon of another particle of the same species(...)”. However, until recently there was no formal study concerning this belief. In what follows I will describe some steps towards the understanding of correlations arising due to the Pauli principle.

### 8.1.1 Perfect detection

Suppose we pick up two fermion from a non-interacting Fermi gas at zero temperature, one at position  $r$  and the other at  $r'$ . What is the spin entanglement between them? Vedral showed that the amount of entanglement between these particles decreases with increasing distance between them [Ved03]. He also showed that there is a limit below which any two fermions extracted from the gas are certainly entangled. In particular, if both fermions are extracted at the same position, then the Pauli exclusion principle forces their spin to be maximally entangled in a typical antisymmetric Bell state. In what follows I am going to briefly review these results and then present a clearer and more complete explanation to this behavior through the analysis of the symmetry of the position detection.

The spin density matrix of these selected particles can be defined by

$$\rho_{ss',tt'} = \langle \Phi_0 | \Psi_{t'}^\dagger(r') \Psi_t^\dagger(r) \Psi_{s'}(r') \Psi_s(r) | \Phi_0 \rangle, \quad (8.1)$$

where  $|\phi_0\rangle$  is the ground state of the Fermi gas,

$$|\phi_0\rangle = \Pi_{s,p} b_s^\dagger(p) |0\rangle, \quad (8.2)$$

## 8.1. NON-INTERACTING FERMI GAS

75

and the detection operator at position  $r$  and spin  $s$  is given by,

$$\Psi_s^\dagger(r) = \int_0^{p_f} \frac{d^3 p}{(2\pi)^3} e^{-ipr} b_s^\dagger(p). \quad (8.3)$$

this integral is taken over the Fermi sphere with radio  $p_f$  (the Fermi's momentum). The matrix elements (8.1) are second order correlation functions, which correspond to measuring these two fermions at positions  $r$  and  $r'$ .

The upper limit for guaranteed entanglement can be calculated applying the Peres-Horodecki criterion [Per96b] to the state (8.1). The following condition for the existence of entanglement holds:  $f^2 > \frac{1}{2}$ , where  $f(r - r') = 3j_1(k_F|r - r'|)/(k_F|r - r'|)$ ,  $|r - r'|$  is the distance between the fermions,  $k_F = p_f/\hbar$  and  $j_1$  is a spherical Bessel function. This condition establishes a region  $0 \leq |r - r'| < r_e$ , where  $r_e$  is the solution of  $f^2 = 1/2$ , for which the fermions are found to be entangled.

In order to get an interpretation of this result let me arrive at his result in a different way. Define new detection operators:

$$\Pi_{ss'}^+(r, r') \equiv \frac{(\Psi_s(r)\Psi_{s'}(r') + \Psi_{s'}(r)\Psi_s(r'))}{\sqrt{2}}, \quad (8.4a)$$

$$\Pi_{ss'}^-(r, r') \equiv \frac{(\Psi_s(r)\Psi_{s'}(r') - \Psi_{s'}(r)\Psi_s(r'))}{\sqrt{2}}. \quad (8.4b)$$

The operator  $\Pi_{ss'}^+(\Pi_{ss'}^-)$ , detects the antisymmetric (symmetric) spatial part and the symmetric (antisymmetric) spin part of fermion wavefunction.

In terms of these new operators, Eq.(8.1) becomes:

$$\rho_{ss',tt'} = \frac{1}{2} \langle \Phi_0 | [\Pi_{tt'}^{+\dagger}(r, r') + \Pi_{tt'}^{-\dagger}(r, r')] [\Pi_{ss'}^+(r, r') + \Pi_{ss'}^-(r, r')] | \Phi_0 \rangle \quad (8.5)$$

Note that written in this way, the two-fermion density matrix is the sum of four different terms, two of which contain only symmetric and antisymmetric spin detectors. The other two are the crossing terms, which vanish due to the exclusion principle (spin and position of two fermions cannot be both symmetric or antisymmetric). The remaining terms are:

$$\rho_{sym} = \frac{1}{2} \langle \Phi_0 | \Pi_{tt'}^{+\dagger}(r, r') \Pi_{ss'}^+(r, r') | \Phi_0 \rangle, \quad (8.6a)$$

$$\rho_{asym} = \frac{1}{2} \langle \Phi_0 | \Pi_{tt'}^{-\dagger}(r, r') \Pi_{ss'}^-(r, r') | \Phi_0 \rangle. \quad (8.6b)$$

Here  $\rho_{sym}$  takes into consideration only the symmetric spin function (therefore, it is related to the detection of the antisymmetric part of the spatial wavefunction) while  $\rho_{asym}$  contains only the antisymmetric spin function

(therefore related to the detection of the symmetric part of the spatial wavefunction). The density matrix can be rewritten as:

$$\begin{aligned}\rho &= \rho_{asym} + \rho_{sym} \\ &= \int \int dp dp' \frac{1}{2} \left\{ (1 + e^{i(p-p')(r-r')}) \begin{pmatrix} 1 & -1 \\ -1 & 1 \end{pmatrix} \right. \\ &\quad \left. + (1 - e^{i(p-p')(r-r')}) \begin{pmatrix} 2 & & \\ & 1 & 1 \\ & 1 & 1 \\ & & 2 \end{pmatrix} \right\}. \quad (8.7)\end{aligned}$$

First, note that, as expected, for  $r = r'$ , the antisymmetric spatial function goes to zero, and the spin wavefunction has to be antisymmetric (first term in Eq.(8.7)). For  $r - r' \neq 0$  both parts contribute. Note, however, that the symmetric spin density matrix can be viewed as an equal weight mixture of the three triplet components, and has no entanglement at all<sup>1</sup>. The spin state in Eq.(8.7) represents a convex combination of singlet state and the equal mixture of triplet states. It will have entanglement iff the fraction of singlet is sufficiently larger than the fraction of triplets. In the limit  $r - r' \gg 1/k_F$ , as the integrals on Eq.(8.7) are performed over momenta below the (momentum equivalent of) Fermi surface the momentum dependent terms oscillate too fast, and average to zero. Therefore, the spin density matrix becomes just the identity ( $\delta_{ts}\delta_{t's'}$ ). This behavior can be seen as a smooth transition from a quantum statistics (Fermi-Dirac) to a classical one (Maxwell-Boltzmann).

### 8.1.2 Imperfect detection

An interesting question arises when considering non-punctual (non-ideal) position detections, i.e. more realistic apparatus that detect the position of those fermions with some incertitude. Instead of Eq.(8.3), the detection operator should be written as the general field operator:

$$\Psi_s(r) = \int \int e^{ipr''} D(r - r'') b_s(p) dr'' dp. \quad (8.8)$$

The perfect position measurement situation is the particular case of Eq.(8.8) corresponding to  $D(r - r'') = \delta(r - r'')$ . However, if  $D(r - r'')$  has some

---

<sup>1</sup>This again can be seen from the Peres-Horodecki criterion.

position uncertainty, like, for example, if it is described by a gaussian with spread  $\sigma$ ,

$$D(r - r'') = \frac{1}{\sqrt{2\pi}\sigma} e^{\frac{-|r-r''|^2}{2\sigma^2}}, \quad (8.9)$$

then, the field operators become

$$\Psi_s(r) = \frac{1}{\sqrt{2\pi}\sigma} \int \int e^{ipr''} e^{\frac{-|r-r''|^2}{2\sigma^2}} b_s(p) dr'' dp. \quad (8.10)$$

These operators, when substituted back in Eq.(8.1), give:

$$\rho_{ss',tt'} = \delta_{st}\delta_{s't'}f(d,\sigma) + \delta_{st'}\delta_{s't}g(d,\sigma), \quad (8.11a)$$

with  $d = |r - r'|$ ,

$$f(d,\sigma) = \left( \frac{\text{erf}(\sigma p_f)}{\sigma} \right)^2, \quad (8.11b)$$

$$g(d,\sigma) = \frac{e^{\frac{-d^2}{2\sigma^2}}}{\sigma^2} |\text{erf}(\sigma p_f - \frac{id}{2\sigma}) - \text{erf}(-\frac{id}{2\sigma})|^2, \quad (8.11c)$$

where  $\text{erf}(x)$  is the “error function”, defined via:

$$\text{erf}(x) \equiv \frac{2}{\sqrt{\pi}} \int_0^x e^{-t^2} dt. \quad (8.11d)$$

In order to make clearer the behavior of entanglement in relation to changes in  $d$  and  $\sigma$  we can compute the negativity of the state  $\rho(d,\sigma,p_f)$ :

$$N(\rho) = \max\{0, -\frac{f - 2g}{4f - 2g}\} \quad (8.12)$$

This function is plotted in Fig. 8.1 for some values of  $\sigma$ .

Note that, for imperfect position detection, the entanglement decreases as the detectors become apart from each other, but increases if the spread in the detection becomes larger. The fact that inaccuracy in the detection increases entanglement may seem surprising at first sight. However it has to be noted that as our knowledge in position gets worst, our knowledge in momentum gets better. In the limit of infinite spread, both detectors become perfect momentum detectors (centered at  $p = 0$ , see Eq.(8.9)), which means again that their spin wavefunction should be totally antisymmetrized, hence they are found in the antisymmetric Bell state. It is important to stress that Eq.(8.8) describes a coherent combination of localized field operators instead of a statistical average of them. That is the reason for the infinite spread limit be a momentum-localized detector instead of just a vague “there is a particle somewhere”.

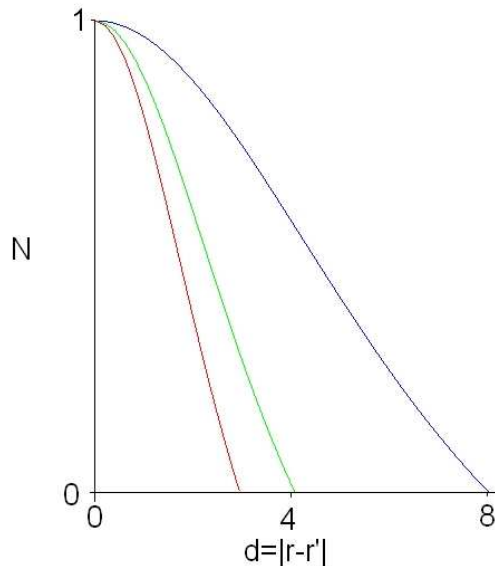


Figure 8.1:  $N(\rho)$  vs.  $d$  for  $p_f = 1$  and  $\sigma = 1$  (red),  $\sigma = 2$  (green) and  $\sigma = 4$  (blue).

## 8.2 Useful entanglement from the Pauli principle

In this section I would like to make the previous discussion less abstract and propose a way of observing this fermionic entanglement in a realistic system.

Consider that one excites a semi-conductor from its electronic ground state by exactly promoting two electrons to the conduction band. These two electrons will be described by some quantum state with momentum and spin distribution. Due to phonon scattering, no matter the initial polarization, in a short time scale the spin state will be essentially random (supposing no energy difference between the possible polarizations). With the condition that relaxation time ( $\tau_D$ ) is much shorter than recombination time ( $\tau_{eh}$ ), the electronic momentum distribution will tend to the bottom of the band. In fact, the quantum state will tend to the “ground state” of the band, which can be viewed as null momentum spin singlet, due to the Pauli principle. By the same time, but in a statistically independent way, electrons in the valence band also relax, with the net effect of promoting the holes to the top of the band. Also supposing that the relaxation time of the holes is much shorter than recombination time, there will be a singlet of holes in the top of

## 8.2. USEFUL ENTANGLEMENT FROM THE PAULI PRINCIPLE 79

the valence band. In this scheme, quantum correlations were created by the Pauli principle through relaxation. The remaining question is whether these correlations can be used to implement some quantum protocol.

Continuing with the argument, let me assume a selection rule for the radiative decay: electrons with spin  $+1/2$  ( $-1/2$ ) can only decay emitting photons circularly polarized to the right (left) (Fig. ??B). After both electrons have decayed we will therefore obtain two photons in a polarization entangled state, which can be used for different quantum information protocols. I emphasize that this state is only obtained due to the existence of fermionic entanglement between the electrons.

The idea described in the previous paragraphs can indeed be implemented in solid state physics. Two independent photons coming from single photon sources are used to create two electron-hole pairs of different  $k$ 's and spins in a semiconductor quantum well. The system rapidly relax to the bottom of the conduction band. The electrons then emit photons recombining with the holes in the valence band. For the argument presented before to hold, conduction and valence bands relaxation processes have to be much faster than the recombination time, which is the case in semiconductors (typically  $\tau_D \sim 10^{-12} s$  and  $\tau_{eh} \sim 10^{-9} s$  [Fat05]). Note that the emitted photons will be entangled in polarization no matter in which direction they are emitted. However, in order to enhance the spontaneous recombination process and to give a preferred direction for the emission (also enhancing the probability of detection), the semiconductor can be placed inside an optical cavity [Yam91, WNIA92, BMYI91]. After escaping the cavity, these photons can be used for quantum information.

### 8.2.1 Selection rules

Take semiconductors of the group III-V [YC96] for which the conduction (valence) band has orbital angular momentum  $L = 0$  ( $L = 1$ ). The valence band has two branches corresponding to heavy-holes ( $J_z = \pm 3/2$ ) and light-holes ( $J_z = \pm 1/2$ ) which are degenerate at  $k = 0$  for bulk semiconductors. But in a semiconductor quantum well this degeneracy is lifted off due to the confinement in one of the directions. Each new valence band still has the usual free-particle dispersion relation ( $E \propto k^2$ ) around the energy gap, but the gap itself is smaller for the heavy-hole electrons. Therefore, by shining light of the proper frequency, it is possible to selectively excite electrons from the heavy-hole band without ever touching the light-hole ones (see Fig. 8.2). The electrons are excited by dipolar interaction, which means that there will be a selection rule that couples each eigenstate in the heavy-hole band to a partner in the conduction band, depending only on the photon polarization

(see Fig. 8.3).

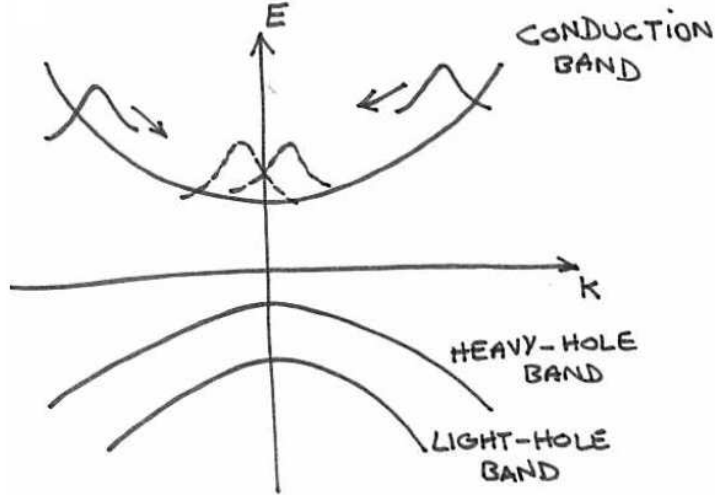


Figure 8.2: **Band structure for the semiconductor quantum well -**  
For each value of  $k$  there can exist just two electrons according to the Pauli principle.

### 8.2.2 From fermions to photons

Let me now treat in some details what was described above. Suppose we have a semiconductor quantum well with exactly two excitations with well defined momentum  $k$  above the ground state (full valence band). Consider the creation operator of two particles (electron + hole):

$$\Psi_s^\dagger(k) = e_s^\dagger(k) h_s^\dagger(-k), \quad (8.13)$$

where  $e_s^\dagger(k)$  (resp.  $h_s^\dagger(k)$ ) creates an electron (hole) in the conduction (valence) band with logical spin  $s$  and momentum  $k$ . The spin notation is utilized to emphasize correlation in the creation process, and the following correspondence between the real spins with the logical basis is implied through the text:

	$ 0\rangle$	$ 1\rangle$
electrons	$-1/2$	$1/2$
holes	$-3/2$	$3/2$

The spin state I am going to analyze can be described by a spin density operator for the electrons and holes determined (up to normalization) by the

## 8.2. USEFUL ENTANGLEMENT FROM THE PAULI PRINCIPLE 81

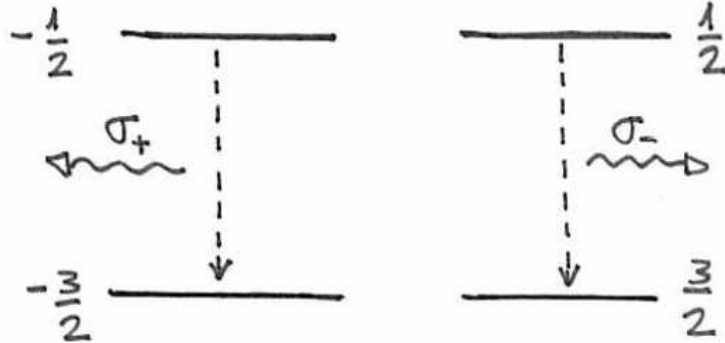


Figure 8.3: **Selection rules** - The following transitions are considered:  
 $J_z = -\frac{3}{2} \leftrightarrow J_z = -\frac{1}{2}$  through an emission/absorption of a  $\sigma_+$  photon, and  
 $J_z = \frac{3}{2} \leftrightarrow J_z = \frac{1}{2}$  through an emission/absorption of a  $\sigma_-$  photon.

correlation function [Ved03, DDW06]:

$$\begin{aligned} \rho_{rr'ss'} &= \langle \Phi_0 | \Psi_r(k) \Psi_{r'}(k) \Psi_s^\dagger(k) \Psi_{s'}^\dagger(k) | \Phi_0 \rangle \quad (8.14) \\ &= \left\langle \phi_0^{(e)} \right| e_r(k) e_{r'}(k) e_s^\dagger(k) e_{s'}^\dagger(k) \left| \phi_0^{(e)} \right\rangle \\ &\times \left\langle \phi_0^{(h)} \right| h_r(-k) h_{r'}(-k) h_s^\dagger(-k) h_{s'}^\dagger(-k) \left| \phi_0^{(h)} \right\rangle, \end{aligned}$$

where  $\left| \phi_0^{(e)} \right\rangle$  ( $\left| \phi_0^{(h)} \right\rangle$ ) denotes the electron (hole) initial state (vacuum) and  $|\Phi_0\rangle$  is their tensor product. As the operators obey fermionic anti-commutation rules

$$[e_s^\dagger(k), e_{s'}(k')]_+ = \delta_{ss'} \delta(k - k') \quad (8.15)$$

(the same for  $h_s(k)$ ), we have

$$\rho_{rr'ss'} = (\delta_{rs'} \delta_{r's} - \delta_{rs} \delta_{r's'})^2. \quad (8.16)$$

Note that I have used a shortened label to represent the matrix elements (8.14). In the electron-hole-electron-hole ordering, this operator is a density matrix representing the (unnormalized) state

$$|\psi\rangle = \left| -\frac{1}{2}, -\frac{3}{2}; +\frac{1}{2}, +\frac{3}{2} \right\rangle + \left| +\frac{1}{2}, +\frac{3}{2}; -\frac{1}{2}, -\frac{3}{2} \right\rangle. \quad (8.17)$$

In order to enhance the emission process, and also to have control over the emitted photons, the sample can be placed within an optical cavity in resonance with the transitions we are interested in [Yam91, WNIA92, BMYI91].

By the selection rules described above, the emitted photons state is

$$|\sigma_-\sigma_+\rangle + |\sigma_+\sigma_-\rangle, \quad (8.18)$$

which is a maximally entangled Bell state. Note that it is essential that the electrons have the same momentum for the creation of a maximally entangled pair of photons.

We are interested in creating entangled photons from independent ones, and that is where decoherence plays an important role. Independent photons create electrons of different  $k$ 's. However, the incoherent energy losses to the network phonons end up dragging those electrons to the conduction-band ground state (similarly the holes), where both of them have the same  $k = 0$  momentum! Taking into consideration the selectivity of the decay process, the photons will indeed be emitted in the Bell state of Eq. (8.18).

### 8.2.3 Some imperfections

The scenario that was discussed up to now is pretty much idealized. It is important to stress, however, that one very robust point in favor of this proposal is its independency on the specific model of decoherence used. Whenever the imposed conditions on the time scales are fulfilled, the state of the system before recombination will be very close to the one here described. And so the state of the emitted photons.

One possible way to mimic the effects of the imperfection in this approach is to consider a broadening in the momentum distribution, and also an imperfect coincidence of the momenta. This can be taken into account by modifying Eq. (8.13) to

$$\Psi_{ss}^\dagger(k) = \iint f(k_j - k) f(\tilde{k}_j - \tilde{k}) e_s^\dagger(k_j) h_s^\dagger(\tilde{k}_j) dk_j d\tilde{k}_j. \quad (8.19)$$

This operator creates an electron with spin  $s$  and momentum distribution given by the function  $f(k_j - k)$ , and a hole with spin  $s$  and momentum distribution given by  $f(\tilde{k}_j - \tilde{k})$ . Later I will associate  $k = -\tilde{k}$ <sup>2</sup>. With this operator, Eq. (8.14) can be rewritten as

---

<sup>2</sup>This association reflects the fact that an electron moving to a certain direction is equivalent to a hole moving to the opposite way.

## 8.2. USEFUL ENTANGLEMENT FROM THE PAULI PRINCIPLE 83

$$\begin{aligned}
\rho_{rr'ss'} &= \int f^*(k_0 - k) f^*(k_1 - k') f(k_2 - k) f(k_3 - k') \\
&\quad \left\langle \phi_0^{(e)} \middle| e_r(k_0) e_{r'}(k_1) e_s^\dagger(k_2) e_{s'}^\dagger(k_3) \right| \phi_0^{(e)} \right\rangle dk_0 \dots dk_3 \\
&\times \int f^*(\tilde{k}_0 - \tilde{k}) f^*(\tilde{k}_1 - \tilde{k}') f(\tilde{k}_2 - \tilde{k}) f(\tilde{k}_3 - \tilde{k}') \\
&\quad \left\langle \phi_0^{(h)} \middle| h_r(\tilde{k}_0) h_{r'}(\tilde{k}_1) h_s^\dagger(\tilde{k}_2) h_{s'}^\dagger(\tilde{k}_3) \right| \phi_0^{(h)} \right\rangle d\tilde{k}_0 \dots d\tilde{k}_3.
\end{aligned} \tag{8.20}$$

Anti-commutation rules (8.15) imply that the only non-null matrix elements are:

$$\begin{aligned}
\rho_{0000} &= \rho_{1111} \\
&= (L(k, k') - M(k, k'))(\tilde{L}(\tilde{k}, \tilde{k}') - \tilde{M}(\tilde{k}, \tilde{k}')),
\end{aligned} \tag{8.21a}$$

$$\rho_{0101} = \rho_{1010} = L(k, k')\tilde{L}(\tilde{k}, \tilde{k}'), \tag{8.21b}$$

$$\rho_{0110} = \rho_{1001} = M(k, k')\tilde{M}(\tilde{k}, \tilde{k}'), \tag{8.21c}$$

where

$$L(k, k') = \int dk_0 dk_1 |f(k_0 - k)|^2 |f(k_1 - k')|^2, \tag{8.22a}$$

$$M(k, k') = \int dk_0 dk_1 f^*(k_0 - k) f^*(k_1 - k') f(k_1 - k) f(k_0 - k'), \tag{8.22b}$$

with similar expressions for  $\tilde{L}(\tilde{k}, \tilde{k}')$  and  $\tilde{M}(\tilde{k}, \tilde{k}')$  by changing  $k \mapsto \tilde{k}$  and  $k' \mapsto \tilde{k}'$ .

The emitted photons (non-normalized) polarization state will thus be:

$$\rho = \begin{pmatrix} (L - M)(\tilde{L} - \tilde{M}) & & & \\ & L\tilde{L} & M\tilde{M} & \\ & M\tilde{M} & L\tilde{L} & \\ & & & (L - M)(\tilde{L} - \tilde{M}) \end{pmatrix}, \tag{8.23}$$

where I leave blank the null entries. Note that when  $k = k'$  and  $\tilde{k} = \tilde{k}'$  hold,  $L = M$  and  $\tilde{L} = \tilde{M}$ , giving a maximally entangled photonic state. Notice the generality of this result: state (8.23) is written in terms of arbitrary momentum distributions of the electrons before the decaying process. For illustration, a chart of the entanglement between the two photons (characterized by the negativity) versus the difference in momentum distribution of

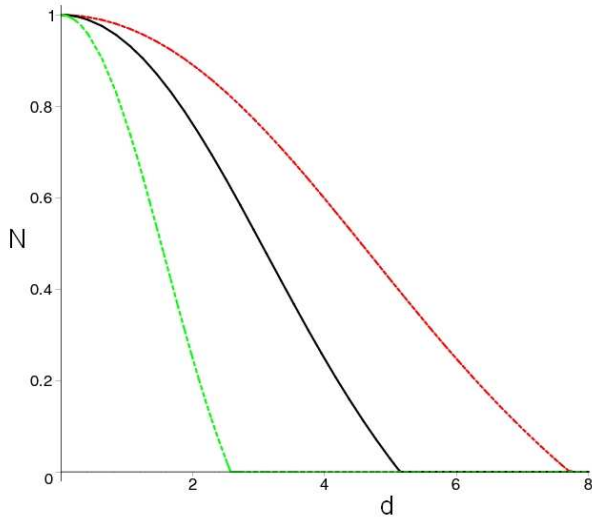


Figure 8.4: Photonic entanglement (negativity) versus  $d = |k - k'|$ . Green-dotted line:  $\delta = 2$ , black-solid line:  $\delta = 4$ , red-dashed curve:  $\delta = 6$ , where  $\delta$  is a measure of the width of the momentum distribution, assumed the same for electrons and holes (see Eq. (8.24)). We see that the greater the spread in the momentum, the higher the entanglement between the photons. This is due to the fact that wider momentum distributions blur the difference in  $k$ 's, so that once again it is impossible to distinguish the electrons by momentum.

the decaying electrons is displayed in Fig. 8.4. I have chosen a Lorentzian distribution of spread  $\delta$  centered in  $k$  ( $k'$ ) for the momentum distributions, *i.e.*:

$$f(k_j - k) = \frac{\delta}{\pi[(k_j - k)^2 + \delta^2]}. \quad (8.24)$$

### 8.3 Concluding remarks

In conclusion it was shown that the measurement apparatus plays a central role in the entanglement of identical particles. The fact that entanglement increases because of broadening in detection can sound weird at first. However it is important to say that the detections discussed here are done in a coherent way (as in most of real cases).

Concerning the semiconductor proposal, I stress once again that the origin of the entanglement lies in the fermionic nature of the electrons. This gives

## 8.3. CONCLUDING REMARKS

85

a decisive positive answer to the question whether identical-particle entanglement is useful for quantum information purposes. Specifically, identical-particle entanglement can in fact be extracted and converted to usual entanglement, and one important ingredient in this convertibility is the use of more than one degree of freedom.

Finally, I would like to emphasize the role played by the coupling to the environment in the discussed scheme. Usually, decoherence is seen as the road from quantum to classical, implying information loss and entropy creation, which makes it a plague for quantum information tasks. However, a very special situation occurs when decoherence is dictated by a null temperature heat reservoir: after a transient time, the system asymptotically approaches its ground state. Whenever the ground state is nondegenerate, the result of null temperature decoherence is a pure state. When the system in question is composed, decoherence leads to statistical mixture, which tends to wash out entanglement. However, if, at zero temperature, the nondegenerate ground state is also entangled, decoherence can actually create entangled states! That is a central part of the proposed scheme: here, decoherence plays the crucial role of washing out the distinguishable origin of the input photons, allowing the extraction of entanglement from the Pauli principle.

Let me finish this chapter with a more practical issue. Ideally, the described setup could be viewed as a practical entangling machine, where the input is a two photon unentangled state and the output an entangled state. Moreover, this machine would work on demand, *i.e.*: whenever we input two independent photons we receive back two entangled photons.



# Chapter 9

## Conclusions and Perspectives

Understanding entanglement is one of the biggest challenges physicists are faced with. A lot of effort has been employed to get a complete theory of this resource, and also to apply it in real tasks. There are still many questions involving entanglement, and some of them were not even cited in this thesis. The experimental production and use of entanglement in different systems and scales, the computational hardness of classically simulating quantum effects, and the link between entanglement and quantum phase transitions are just few examples of these questions. All these points make entanglement characterization one of the most interdisciplinary branches of Physics.

In this thesis I have presented some results on the characterization of entanglement I could address during the last years. Although the present contribution represents just few steps on entanglement theory, I hope they can help to give a better understanding and to motivate future research on this field. I would like to finish this text by raising some future research that could follow the presented ideas.

I have shown a connection between two entanglement quantifiers, the generalized robustness of entanglement ( $R_g$ ) and the geometric measure ( $E_{GME}$ ). This was made through a lower bound to  $R_g$  based on  $E_{GME}$ . It would be interesting to find additional examples where this bound is tight and to seek for the geometrical explanation of this fact. Furthermore whenever we have a way of calculating one of these measures, this gives a bound for the other. This might be useful because these quantities have also operational appeals [HMM+05, Bra07]. Seeking for relations among other entanglement quantifiers is also desirable as it can lead us to a better understanding on the different forms of entanglement quantification.

Chapter 4 presented improvements on two big dilemmas concerning entanglement and non-locality. The first is the Peres' conjecture that undistillable states never violate a Bell inequality. I have shown a partial proof of

this conjecture for the CFRD inequality by showing that all violating states are NPT. A complementary result would be to prove that all violating states are distillable. Further generalizations could consider other Bell inequalities, including those ones involving many measurement settings per site. On the other hand, finding a bound entangled state which violates a Bell inequality would disprove Peres' conjecture<sup>1</sup>. The second big issue on this theme is to find appropriate tests to prove non-locality, *i.e.*: loop-hole free experiments. Quadratures of the electromagnetic field is a promising degree of freedom where this tests could be proposed. First, photons can be distributed over long distances using optical fibers or even in free-space. Second, quadrature measurements attain incredibly high efficiencies through homodyning.

Concerning the study of the geometry of entanglement I hope the presented method for investigating the boundary features of separable sets can give us a better idea on the mathematical description of quantum states. It is interesting that singularities in these sets appear in physical phenomena. An open question consists in looking for physical consequences of these singularities (if any).

Many are the open questions on the entanglement properties of decohered states. First, a whole line of research consists in the study of the quantum-classical transition, and entanglement certainly plays a major role in this arena. Furthermore, as said before, it is crucial to understand the degradation of entanglement in real protocols since it is a valuable resource. In this sense further studies should include other multipartite states (*e.g.*: W, cluster, and CV states) and other decoherence models. In the end the big query is whether scalable quantum computation is possible.

Finally, the entanglement properties of many body systems is among the hottest lines of research nowadays. The Fermi gas is a first approximation for many systems and it is then important to understand the features of this model. Moreover, we could propose a realistic system where the discussed effects could be seen. In my opinion, an implementation of this scheme, if feasible, would be interesting not only from a fundamental but also from a practical point of view.

---

<sup>1</sup>Here I mean bound entangled among all the partitions.

# Appendix A

## Multipartite entanglement

In this chapter I will discuss in more details the different kinds of multipartite entanglement.

When several parts are involved we can have different notions of entanglement, depending on the partition we apply to this state [DC00, DCT99, ABLS01, EG06]. For example, in a tripartite scenario, some states can be written as

$$\rho^{ABC} = \rho^{AB} \otimes \rho^C, \quad (\text{A.1})$$

where  $\rho^{AB}$  is an entangled state. This state is separable according to the partition  $AB|C$  and can be built by joint operations on particles  $A$  and  $B$  and independent single operations on  $C$ . Hence it is said that such a  $\rho^{ABC}$  has no tripartite entanglement.

We could go further in the classification of entanglement and define convex combinations of states like (A.1), *i.e.*:

$$\rho = \sum_i p_i \rho_i^{AB} \otimes \rho_i^C + q_i \rho_i^A \otimes \rho_i^{BC} + r_i \rho_i^{AC} \otimes \rho_i^B, \quad (\text{A.2})$$

with  $p_i, q_i, r_i \geq 0$  and  $\sum_i p_i + q_i + r_i = 1$ . To build these states we again do not need to perform joint operations on the three particles, but instead can use just (classically) correlated two-particle operations. Because of that fact, states (A.2) do not have *genuine* tripartite entanglement. However some of them do have entanglement among the three particles, since they cannot be written as (A.1) for example. This classification can be extended for states composed by more than three parties straightforwardly.

Note that each one of these sets is convex. Fully separable states form a subset of the set of biseparable states like (A.1), which by the other hand is a subset of the set of states like (A.2), and so on. We thus have a hierarchy of entangled states, and we can see the set of quantum states as composed having an onion-like structure (see Fig.A.1).

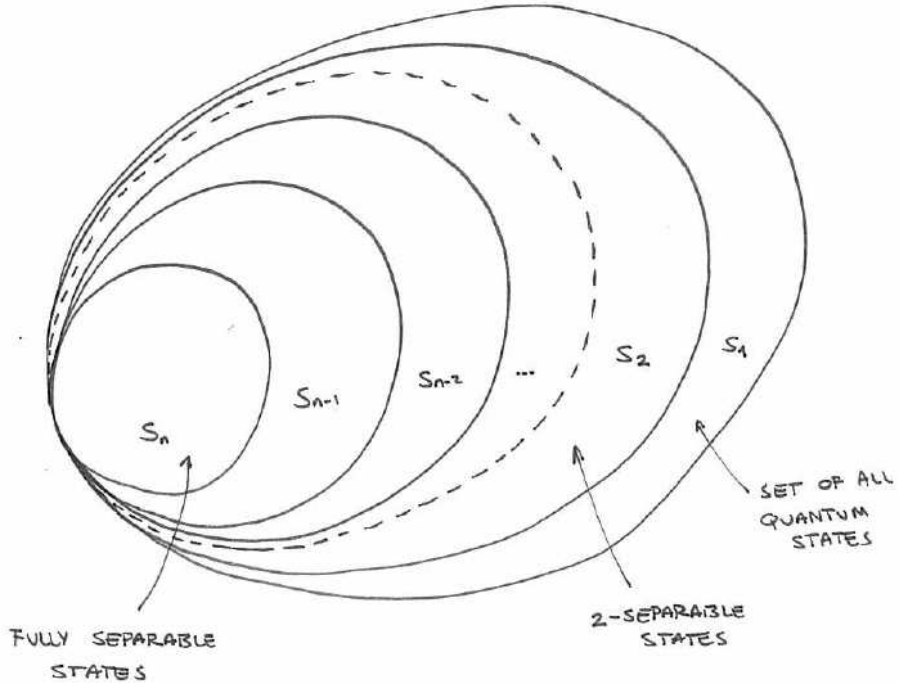


Figure A.1: State space structure.

As commented in Chapter 1, when talking about multipartite entanglement we can define different kinds of separability. Suppose a state  $\rho$  can be written as a convex combination of states which are product of  $k$  tensor factors. The state  $\rho$  is then said to be a  $k$ -separable state. One should note that in a system of  $n$  parts,  $n$ -separability means that none of the subsystems share quantum correlations with the others. Besides, every state is trivially 1-separable. The set of  $k$ -separable states will be denoted by  $S_k$ . It is clear that  $S_n \subset S_{n-1} \subset \dots \subset S_1 = D$ , where  $D$  denotes the set of density operators.

## Appendix B

# $R_R^k$ as a detector of singularities in $S_k$

In this Appendix we aim to prove Proposition 1, in Chapter 6. This can be done in a more general way through the following result:

**Proposition 2** *Let  $D$  be a closed, convex set. Let  $S \subset D$  also be closed and convex, with  $\pi$  a point in the interior of  $S$ . If  $\partial S$  is a  $C^m$  manifold and the states  $\rho(q)$  describe a  $C^m$  curve in  $D$  with no points in the interior of  $S$  and obeying the condition that the tangent vector  $\rho'(q)$  is never parallel to  $\pi - \rho(q)$ , then  $R_R(\rho(q))$  is also a  $C^m$  function.*

One must remember that a manifold is called  $C^m$  if it can be parameterized by functions with continuous derivatives up to order  $m$  [?]. The reader can change  $C^m$  by smooth, in the usual sense of  $C^\infty$ , with almost no loss (actually, we use smooth throughout this Letter in the less precise sense of “as regular as necessary”). Other topological remarks before the proof: the fact that  $S$  has interior points implies that  $S$  and  $D$  have the same dimensionality (since there is an open ball of  $D$  contained in  $S$ ), and the proof will use the notion of (topological) cone, which simply means the union of all segments from a given point  $V$  to each point of a given set  $A$ : this is called the cone of  $A$  with vertex  $V$ .

**Proof:** The geometrical situation leads to the cone, given by  $(p, q) \mapsto p\pi + (1-p)\rho(q)$ ,  $p \in [0, 1]$ . The condition on the tangent vector (together with the fact that  $\pi$  is interior to  $S$ , while  $\rho(q)$  has no point in this interior) is sufficient for this cone to be  $C^m$ , except at the vertex  $\pi$ , at least locally in  $q$ .

As  $S$  is bounded and convex, and  $\pi$  is in its interior, every straight line from  $\pi$  crosses  $\partial S$  exactly once. As  $\rho(q)$  has no point in the interior of  $S$ , this crossing always happens for  $0 \leq p < 1$ . Denote this crossing value by

92

 $R_R^k$  as a detector...

$p_c(q)$ . The curve  $q \mapsto p_c(q)\pi + (1 - p_c(q))\rho(q)$  is  $C^m$ , implying  $p_c$  is a  $C^m$  function of  $q$ .

The random robustness is given by  $R_R(\rho(q)) = \frac{p_c}{1-p_c}$ . As  $p_c < 1$ , we also obtain that  $R_R$  is a  $C^m$  function of  $q$ .  $\square$

## Appendix C

# Experimental Setup

In this appendix it will be shown the details of the setup used in the experiment described in Chapter 6.

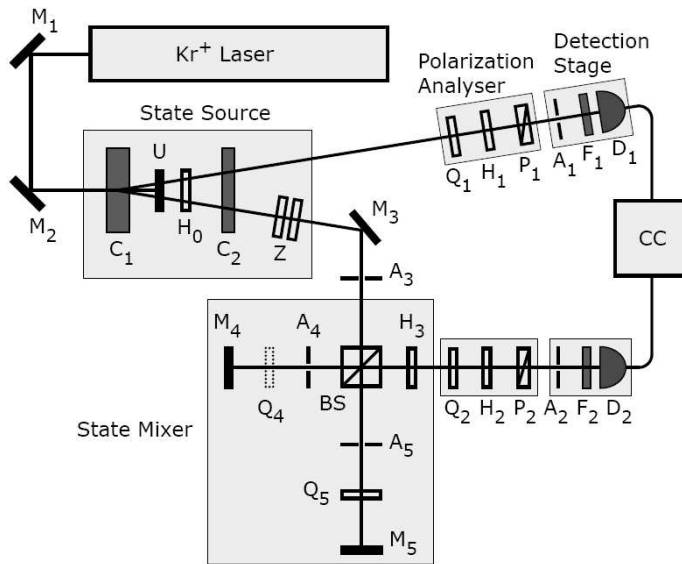


Figure C.1: Experimental setup.

The state source is composed by a 2mm-thick BBO ( $\beta\text{-BaB}_2\text{O}_4$ ) nonlinear crystal ( $C_1$ ) pumped by a cw krypton laser operating at 413nm, generating photon pairs at 826nm by type II spontaneous parametric down-conversion. Crystal  $C_1$  is cut and oriented to generate either one of the polarization entangled Bell states  $|\Psi_-\rangle$  or  $|\Psi_+\rangle$ . Walk-off and phase compensation is provided by the half-wave plate  $H_0$  followed by a 1mm-thick BBO crystal ( $C_2$ ) [KMW+05], together with two 1mm-thick crystalline quartz plates ( $Z$ )

inserted in one of the down-converted photon paths. The unconverted laser beam transmitted by crystal  $C_1$  is discarded by means of a dichroic mirror (U). The detection stages are composed by photon counting diode modules  $D_1$  and  $D_2$ , preceded by 8nm FWHM interference filters  $F_1$  and  $F_2$  centered at 825nm, and by circular apertures  $A_1$  of 1.6mm $\emptyset$  and  $A_2$  of 3.0mm  $\emptyset$ . Single and coincidence counts with 5ns resolving time are registered by a computer controlled electronic module (CC). Polarization analyzers are composed by quarter-wave plates  $Q_1$  and  $Q_2$ , half-wave plates  $H_1$  and  $H_2$ , followed by polarizing cubes  $P_1$  and  $P_2$ . The State Source produces state  $|\Psi_-\rangle$ . For each pair, the photon emerging in the upper path goes straight to the polarization analyzer and to the detection stage 1. The lower path photon is directed by mirror  $M_3$  through the circular aperture  $A_3$  into the state mixer (an unbalanced Michelson interferometer), composed by the beam splitter BS, mirrors  $M_4$  and  $M_5$ , quarter-wave plates  $Q_4$  and  $Q_5$ , variable circular apertures  $A_4$  and  $A_5$ , and by the half-wave plate  $H_3$ , whose purpose is to compensate for an unwanted slight polarization rotation caused by the beam splitter. The quarter-wave plate  $Q_4$  is switched off which means that if the lower photon follows path labeled 4, there is no change to its polarization and the half-wave plate  $H_3$  changes the state to  $|\Psi_+\rangle$ . On the other hand, if the lower photon follows path labeled 5,  $Q_5$  is oriented with the fast axis at 45° in order to flip its polarization. The path length difference, 130mm, is much larger than the coherence length of the down-converted fields, ensuring an incoherent recombination at BS. The pair detected by CC is in state  $q|\Psi_+\rangle\langle\Psi_+| + (1 - q)|\Phi_+\rangle\langle\Phi_+|$  where  $q$  is defined by the relative sizes of apertures  $A_4$  and  $A_5$ .

## Appendix D

# Full separability of GHZ states under the Amplitude Damping Channel

Here we prove that the amplitude damping channel leads the state (7.1) to a fully separable state when all of its bipartite entanglements vanish.

*Proof:* First of all note that the evolved density matrix can be written as  $\rho = |\alpha|^2(|0\rangle\langle 0|)^{\otimes N} + \rho_s$ , where  $\rho_s$  is an unnormalized state. The goal is to show that  $\rho_s$  is fully separable. This will be done by defining a fully separable state  $\sigma$  and showing a *local* measurement protocol, a local POVM [?], which transforms  $\sigma$  into  $\rho_s$  with certain probability. Because only local operations are applied we will conclude that  $\rho_s$ , and then  $\rho$ , must be fully separable.

The (unnormalized) state  $\sigma$  is defined as  $\sigma = \beta^2(1-p)^N\{I + (|0\rangle\langle 1|)^{\otimes N} + (|1\rangle\langle 0|)^{\otimes N}\}$ , being  $I$  the  $2^N \times 2^N$  identity matrix. State  $\sigma$  is GHZ-diagonal (see def. in Ref. [DC00]) and all of its negativities are null. Hence, by the Dür-Cirac-Tarrach criterion [DCT99],  $\sigma$  is fully separable. Consider, for each qubit  $i$ , the local POVM  $\{A_m^{(i)}\}_{m=1}^2$  with elements  $A_1^{(i)} = \delta(\sqrt{\frac{p}{1-p}}|0\rangle\langle 0| + |1\rangle\langle 1|)$ , where  $\delta$  is such that  $A_1^{(i)\dagger} A_1^{(i)} \leq I$ , and  $A_2^{(i)\dagger} A_2^{(i)} = I - A_1^{(i)\dagger} A_1^{(i)}$ . One can see that by applying this POVM for every qubit of state  $\sigma$ , when the measurement outcome is  $m = 1$  (corresponding to  $A_1$ ) for all the qubits, the final state is nothing but  $\rho_s$ .  $\square$



# Appendix E

## Resumen

La mecánica cuántica fue concebida como una teoría capaz de describir los fenómenos físicos a nivel atómico. Rápidamente fue aplicada en otros casos como el estudio de la dispersión de las partículas y de la interacción entre la luz y la materia.

La primera crítica importante a la teoría cuántica fue hecha por Einstein, Podolski y Rosen (EPR) en su artículo titulado "Can quantum-mechanical description of physical reality be considered complete?" [EPR35]. Estos autores resaltan que a pesar de que la teoría cuántica acierta al describir correctamente muchos fenómenos físicos, también permite hacer predicciones extrañas como la acción instantánea entre objetos distantes. En el fondo, el argumento expuesto por EPR estaba basado en la posibilidad de tener un estado entrelazado. Basándose en las críticas de EPR, Schrödinger llamó la atención sobre el hecho de que algunos estados cuánticos pueden ser mejor entendidos cuando son investigados como un todo y no a través de cada uno de sus subsistemas [Sch35].

Muchos años después J. Bell puso esta discusión en un ámbito más firme. Aceptando la idea de realismo local introducida por EPR, Bell desarrolló sus famosas desigualdades incluyendo estadísticas de medidas hechas en sistemas compuestos [Bel87]. A partir de entonces la discusión acerca de la no-localidad de la mecánica cuántica podía ser hecha a un nivel experimental. Unos años después los primeros resultados experimentales usando las desigualdades de Bell fueron reportados [FC72, FT76, AGG81, ADG82] y dieron fuerza a la creencia de la no-localidad de la mecánica cuántica. Dado estados que no son entrelazados nunca podrían violar una desigualdad de Bell, estas pruebas pueden ser vistas como las primeras observaciones experimentales de entrelazamiento.

Hasta los años 90, la discusión acerca del entrelazamiento se hizo a un nivel más fundamental, el de los pilares mismos de la teoría cuántica. Fue

después de las primeras propuestas de protocolos de información cuántica, que el término "entrelazamiento" pasó a tener una connotación de "recurso", capaz de proporcionar ventajas sobre las maneras clásicas de procesar información [NC00, BEZ00]. En 1991, un protocolo de criptografía totalmente basado en el entrelazamiento fue propuesto [Eke91]. Para entonces ya se sabía que el entrelazamiento no era algo necesario para garantizar la seguridad de la comunicación [BB84, BBD92]. Quizás fue el descubrimiento de la teleportación cuántica el cambio mas grande en la teoría del entrelazamiento [BBC+93]. Desde entonces quedó clara la importancia de este recurso para aplicaciones prácticas.

A partir de ese momento la teoría del entrelazamiento empezó su propio camino y ganó el status de disciplina independiente. Entre los objetivos principales de la teoría del entrelazamiento están el desarrollo de un formalismo matemático que pueda describir este recurso, la búsqueda de sus aplicaciones, la investigación de la conexión del entrelazamiento con otros fenómenos físicos y, volviendo a aspectos más fundamentales, la importancia del entrelazamiento para los fundamentos de la mecánica cuántica. Actualmente la literatura acerca del entrelazamiento es enorme. El objetivo de esa tesis no es proporcionar una revisión en este tema, pero contribuir con resultados originales. Revisiones acerca del entrelazamiento pueden ser encontradas en las referencias [HHHH07, AFOV07, PV05, Bru02, Ter02, PV98, Ver02, Eis01, EP03]. Las cuestiones abiertas acerca del entrelazamiento van desde su descripción matemática hasta su utilización. Entre todos esos aspectos, en esta tesis yo abordé aquéllos que más me motivaron durante mi doctorado.

A pesar de que la definición matemática del entrelazamiento es sencilla, el problema de determinar si un estado cuántico general está entrelazado o no es muy difícil [Ter02, HHHH07]. Una de las ramas más importantes de la teoría del entrelazamiento se centra en encontrar técnicas que sean capaces de resolver este problema. El paso siguiente, después de determinar si un estado está entrelazado, sería determinar la cantidad de entrelazamiento presente en el sistema [PV98]. Para esto se usan los cuantificadores de entrelazamiento, un conjunto de reglas que se puede aplicar a un estado cuántico para decidir su contenido de entrelazamiento. Una de las primeras maneras de cuantificar el entrelazamiento fue determinar la capacidad de cada estado en realizar tareas de información cuántica [BBP+96, BDSW96]. Esta forma de abordar el problema, a pesar de ser muy productiva depende profundamente de cada tarea en cuestión. Una manera más abstracta de tratar este problema consiste en determinar un conjunto de reglas que un cuantificador de entrelazamiento debe seguir, sin preocuparse por su significado físico [Vid00, VPRK97]. Finalmente, podemos también utilizar conceptos geométricos para cuantificar el entrelazamiento. Podemos organizar los esta-

dos cuánticos en conjuntos matemáticos y definir distancias entre ellos. La cantidad de entrelazamiento en un estado puede ser definida de esa manera como la distancia entre ese estado y en conjunto de estados no entrelazados [VPRK97, VP98].

Actualmente el número de cuantificadores de entrelazamiento es muy grande, así que entender sus propiedades y la información que contienen son los objetivos más importantes de la teoría del entrelazamiento. En este sentido, encontrar relaciones entre cuantificadores podría darnos un conocimiento mejor acerca de cómo ordenar los estados cuánticos con relación al contenido de entrelazamiento.

Con el desarrollo de la teoría del entrelazamiento ese tema empezó a estar conectado con otros campos de la física. El estudio del entrelazamiento en modelos realistas nos permite obtener un conocimiento más adecuado de varios fenómenos físicos en sistemas de materia condensada, óptica y física atómica [RMH01, LBMW03, KWN+07, AFOV07]. En ese sentido se han generado importantes cuestiones prácticas como ¿cuál es el tipo de interacción capaz de producir entrelazamiento? ¿Cómo el entrelazamiento cambia en procesos dinámicos ideales? o ¿cómo se comporta en presencia de pérdidas?.

Con relación a esta última pregunta, es fundamental entender como el entrelazamiento cambia en situaciones reales donde siempre ocurren errores en la preparación de los estados o en su procesamiento. Varios estudios conectando entrelazamiento y decoherencia han aparecido en los últimos años [Dio03, DH04, YE04, YE06, YE07, SMDZ07, Ter07, AJ07], pero muchas cuestiones fundamentales necesitan respuesta todavía. Una de ellas consiste en entender el comportamiento de estados de muchas partes durante procesos de decoherencia [SK02, CMB04, DB04, HDB05]. Desde un punto de vista teórico ese problema podría darnos un entendimiento mejor acerca de la transición clásico-cuántica. Desde un punto práctico, esa cuestión es crucial pues las ventajas de utilizar sistemas cuánticos para procesar la información son considerables sobre todo en el límite del procesamiento de sistemas de muchas partículas.

Finalmente, la teoría del entrelazamiento está casi toda construida para partícula distinguibles. Es decir, en el caso en el que podemos identificar (etiquetar) los subsistemas y definir operaciones individuales o locales con precisión. Cuando tratamos con partículas idénticas el concepto de entrelazamiento se torna más sutil pues la definición de operaciones locales se torna vaga. Otro problema es que, en ese escenario, el entrelazamiento surge gratuitamente. Por ejemplo, dos fermiones que están en el mismo sitio se entrelazan (en un estado singlete) sólamente por el hecho de seguir la estadística fermiónica. Así, no está claro cómo describir ese tipo de correla-

ciones cuánticas, o si son útiles para el procesamiento de información, o incluso si deberíamos llamarlas entrelazamiento.

## E.1 Introducción a la teoría del entrelazamiento

### E.1.1 Definiciones

Los estados cuánticos son descritos por operadores positivos de traza unitaria actuando en un espacio vectorial  $\mathcal{H}$  llamado el espacio de estados. Así un operador  $\rho \in \mathcal{B}(\mathcal{H})$  que representa un estado cuántico satisface:

1.  $\rho \geq 0$ ;
2.  $\text{Tr}(\rho) = 1$ .

Estos operadores son llamados operadores de densidad. Cualquier operador de densidad puede ser escrito (de manera no única) como una combinación convexa de proyectores unidimensionales:

$$\rho = \sum_i p_i |\psi_i\rangle \langle \psi_i|, \quad (\text{E.1})$$

donde

$$\sum_i p_i = 1 \text{ and } p_i \geq 0. \quad (\text{E.2})$$

Un caso especial de la representación (E.1) es cuando  $p_i = 1$  para algún  $i$ , en este caso podemos escribir el estado como un solo proyector unidimensional, *i.e.:*

$$\rho = |\psi_i\rangle \langle \psi_i|. \quad (\text{E.3})$$

En ese caso,  $\rho$  es llamado estado puro. Estados puros son los puntos extremos del conjunto de estados cuánticos y representan aquellos sistemas acerca de los cuales tenemos la máxima información posible.

Si un sistema cuántico está compuesto por varias partes  $A, B, \dots, N$  también lo representamos por un operador de densidad, pero ahora definido en un espacio vectorial  $\mathcal{H}$  dotado de una estructura tensorial:

$$\mathcal{H} = \mathcal{H}_A \otimes \mathcal{H}_B \otimes \dots \otimes \mathcal{H}_N, \quad (\text{E.4})$$

donde  $\mathcal{H}_A, \mathcal{H}_B, \dots, \mathcal{H}_N$ , representan los espacios de estados para cada parte.

La noción de entrelazamiento aparece en esos espacios compuestos. En seguida presentaré la definición de entrelazamiento para sistemas de dos partes para después generalizar para sistemas de muchas partes.

## E.1. INTRODUCCIÓN A LA TEORÍA DEL ENTRELAZAMIENTO 101

**Definición - Separabilidad de estados bipartidos:** Estados bipartidos entrelazados son aquellos que no pueden ser escritos como una combinación convexa de productos de operadores de densidad. Dicho de otra forma,  $\rho \in \mathcal{B}(\mathcal{H}_A \otimes \mathcal{H}_B)$  es entrelazado si y sólo si

$$\rho \neq \sum_i p_i \rho_i^A \otimes \rho_i^B, \quad (\text{E.5})$$

donde  $\{p_i\}$  es una distribución de probabilidades. Los estados que pueden ser escritos como (E.5) son llamados estados separables.

Un ejemplo de un estado entrelazado es  $|\Phi_+\rangle = (|00\rangle + |11\rangle)/\sqrt{2}$ .

En el caso de sistemas de dos partes tenemos solo que diferenciar estados entrelazados de estados separables. Cuando hay muchas partes, un estado puede tener entrelazamiento solamente entre algunas de las partes. Un ejemplo es el estado

$$\frac{(|00\rangle + |11\rangle)}{\sqrt{2}} \otimes \frac{(|00\rangle + |11\rangle)}{\sqrt{2}}. \quad (\text{E.6})$$

Este tipo de estados posee entrelazamiento entre las dos primeras partículas y también entre las dos últimas, mientras que no hay entrelazamiento entre esos dos bloques de partículas. En ese contexto surgen maneras distintas de entrelazar un sistema. Tenemos entonces que definir la  $k$ -separabilidad [DCT99, DC00, ABLS01]:

**Definition 3 -  $k$ -separabilidad:** Un estado cuántico es llamado  $k$ -separable si puede ser escrito como una combinación convexa de estados que son un producto de  $k$  factores.

### E.1.2 Detectando el entrelazamiento

Dado un estado general  $\rho$ , ¿cómo podemos determinar si está entrelazado? Inicialmente podríamos intentar escribir  $\rho$  como en (E.5). Pero, como  $\rho$  admite infinitas representaciones por combinaciones convexas, la tarea de buscar, entre todas las representaciones, si alguna es equivalente a (E.5) se torna impracticable. Claramente tenemos que desarrollar métodos más eficaces para detectar el entrelazamiento. Siguiendo esa idea varios criterios de entrelazamientos fueron propuestos en los últimos años [Ter02]. Desgraciadamente no hay una prueba definitiva para comprobar la separabilidad de estados generales.

Entre los criterios de entrelazamiento más utilizados están:

- Desigualdades de Bell [Bel87, Ter00, WW01b, Gis07].

- La decomposición de Schmidt [Sch07, EK95, NC00].
- El criterio de Peres-Horodecki [Per96b, HHH96]
- El criterio de Nielsen y Kempe [NK01].
- Testigos de entrelazamiento [HHH96, Ter00].

Más criterios de entrelazamiento pueden ser encontrados en [HHHH07].

### E.1.3 Cuantificando el entrelazamiento

Como el entrelazamiento empezó a ser tratado como un recurso, se tornó fundamental cuantificar este recurso para cada estado. Empezamos con un ejemplo. El estado  $|\Phi_+\rangle = (|00\rangle + |11\rangle)/\sqrt{2}$  puede ser usado para teleportar el estado de un qubit [BBC+93]. De esa manera decimos que  $|\Phi_+\rangle$  tiene 1 ebit de entrelazamiento, y definimos esa cantidad como la unidad básica de entrelazamiento. Pero ¿qué pasa si usamos otro estado para la teleportación?

Muchos cuantificadores de entrelazamiento fueron propuestos en los últimos años. Además hay distintas formas de abordar el problema de la cuantificación de entrelazamiento, siendo las más frecuentes basadas en las siguientes ideas:

- *Utilidad del estado*: El estado  $|\psi\rangle$  tiene más entrelazamiento que  $|\phi\rangle$ , si realiza de manera más adecuada alguna tarea. A pesar de que esta forma de abordar el problema sea la más aplicada, depende dramáticamente de cada tarea elegida. Así que a veces un estado es mejor para una tarea, pero peor para otras.
- *Conversión entre estados*: El estado  $|\psi\rangle$  tiene más entrelazamiento que  $|\phi\rangle$  si podemos convertir  $|\psi\rangle$  en  $|\phi\rangle$  a través de operaciones locales y comunicación clásica (LOCC<sup>1</sup>). Esa definición es natural pues no es posible crear entrelazamiento por operaciones LOCC. El problema con esa idea es que se conoce muy poco acerca de conversión de estados mezcla [Jan02, LMD08]. Además, en el caso de estados puros, algunos estados no son convertibles [JP99].
- *Enfoque geométrico*: La cantidad de entrelazamiento de un estado es dada por la distancia (en el espacio de estados) entre él y su estado separable más cercano. Nuevamente esta definición depende no solo de los estados cuánticos pero también de la medida de distancia utilizada.

---

<sup>1</sup>Del inglés *local operations and classical communication*.

Ejemplos de cuantificadores de entrelazamiento pueden ser encontrados en [PV05, HHHH07].

## E.2 Contribuciones

En esa sección comentaré las ideas acerca del entrelazamiento que pude proponer junto con algunos colaboradores.

### La medida Geométrica y la Robustez del Entrelazamiento

Como he dicho anteriormente hay muchos cuantificadores de entrelazamiento. Encontrar relaciones entre ellos puede ayudarnos a clasificarlos y a entender mejor la información que ellos contienen. Se estableció relaciones entre dos cuantificadores frecuentemente utilizados, la Medida Geométrica ( $E_{GME}$ <sup>2</sup>) y la Robustez Generalizada del Entrelazamiento ( $R_g$ <sup>3</sup>). El primero posee una interpretación geométrica clara: es la distancia entre el estado y su estado separable más cercano. El último fue inicialmente propuesto como una medida de la cantidad de ruido que un estado puede tolerar hasta que se vuelva separable.

Se puede ver que  $R_g$  es siempre más grande que  $E_{GME}$ . Un límite inferior para  $R_g$  más preciso está basado en la pureza del estado cuántico y su producto escalar máximo con un estado separable. Además, en el caso de estados puros, ese límite puede ser expresado en términos de  $E_{GME}$ . Finalmente es posible identificar casos donde ese límite es estricto.

### El entrelazamiento de superposiciones

Supongamos dos estados puros,  $|\Psi\rangle$  y  $|\Phi\rangle$ . ¿Existe una relación entre el entrelazamiento de la superposición  $a|\Psi\rangle + b|\Phi\rangle$  y el entrelazamiento de sus constituyentes  $|\Psi\rangle$  y  $|\Phi\rangle$ ? Esta cuestión fue recientemente estudiada por Linden, Popescu y Smolin en el caso de sistemas de dos partes. Ellos pudieron mostrar límites superiores para el entrelazamiento de una superposición en términos del entrelazamiento de sus componentes [LPS06].

M. Terra Cunha, A. Acín y yo consideramos una posible generalización del resultado de Linden, Popescu y Smolin para sistemas de muchas partes. Nosotros encontramos límites para el entrelazamiento de superposiciones de estados de muchas partes basados sólo en el entrelazamiento de los estados formadores. Se demostró que el límite es estricto para una familia de estados

---

<sup>2</sup>Del inglés *Geometric Measure of Entanglement*.

<sup>3</sup>Del inglés *Generalized Robustness of Entanglement*.

compuestos por un número arbitrario de qubits. Además nuestros resultados también se extienden a un conjunto amplio de cuantificadores de entrelazamiento, incluyendo la *negatividad*, la *robustez del entrelazamiento* y la *medida de la mejor aproximación separable*.

### **Entrelazamiento PPT y violación de desigualdades de Bell para variables continuas**

Inspirado por las similitudes entre los procesos de destilación del entrelazamiento [BDSW96] y la detección de la no-localidad escondida [Pop95, Per96a], A. Peres conjeturó que todos los estados no distilables admiten una descripción a través de modelos realistas locales. O sea, esos estados no violan desigualdades de Bell. Esa conjetura fue demostrada apenas en el caso donde dos medidas individuales binarias son aplicadas a un sistema de N partes.

Recientemente una nueva desigualdad de Bell para variables continuas utilizando operadores no-acotados fue propuesta [CFRD07]. Utilizando esa desigualdad A. Salles, A. Acín y yo pudimos extender la conjetura de Peres para el caso continuo y probar que todos los estados con una transposición parcial positiva satisfacen la desigualdad.

### **Clarificando la geometría del entrelazamiento**

El conjunto de los estados cuánticos es cerrado y convexo: combinaciones convexas de estados cuánticos son estados cuánticos. El conjunto de los estados separables es un subconjunto, que también es cerrado y convexo. Además de esas características que son consecuencias directas de la definición de estados cuánticos y estados separables, otras preguntas surgen de ese análisis. ¿Cómo es la forma de esos conjuntos? ¿Cuál es su volumen? ¿Cómo caracterizar esas cantidades? ¿Están estas cantidades directamente relacionadas con fenómenos físicos?

En una colaboración con M. Terra Cunha, M. F. Santos, F. Brandão, P. Lima, O. Cosme, S. Pádua, y C. Monken, propusimos un método para investigar la forma del conjunto de estados separables. Para ello utilizamos un cuantificador de entrelazamiento llamado *robustez aleatoria del entrelazamiento*. Ese cuantificador puede ser usado como un microscopio para investigar la frontera del conjunto de estados separables. Además, como esta investigación puede ser hecha a un nivel experimental, llevamos a cabo un experimento con fotones entrelazados para ilustrar nuestras predicciones teóricas. Singularidades en el conjunto de estados separables para dos qubits fueron encontradas. Esas singularidades aparecen naturalmente en fenómenos como

la transferencia de entrelazamiento en sistemas de spines sujetos a campos magnéticos variables y en procesos de decoherencia.

### Entrelazamiento de muchas partículas y decoherencia

En el mundo real no es posible generar un estado cuántico puro. Debido a errores en la preparación de los estados y ruido en su dinámica siempre tratamos con estados mezcla. El entrelazamiento es muy sensible a esos procesos ruidosos y esa es seguramente la principal dificultad para la implementación real de protocolos de información cuántica. Además el fenómeno de decoherencia está en la esencia de la transición entre el mundo cuántico y el clásico [Zur03]. En este sentido, entender como los estados cuánticos se comportan en presencia de ruido es importante no solamente desde un punto de vista práctico sino también fundamental.

Junto con L. Aolita, R. Chaves, L. Davidovich y A. Acín, estudiamos el decaimiento del entrelazamiento de una familia importante de estados cuánticos, los estados GHZ compuestos por un número arbitrario de qubits. Varias fuentes de decoherencia interactuando independientemente con cada partícula fueron consideradas y leyes de escala para el decaimiento del entrelazamiento y para su tiempo de desaparición fueron obtenidas. Ese tiempo crece con el tamaño del sistema. Sin embargo el entrelazamiento se vuelve arbitrariamente pequeño mucho antes de desaparecer, en un tiempo que escala inversamente con el número de subsistemas. Además, nosotros mostramos que el decaimiento de estados GHZ puede llevar a estados de entrelazamiento confinado <sup>4</sup>.

### Entrelazamiento de partículas idénticas

Supongamos un gas de fermiones que no interactúan a temperatura cero. ¿Si tomamos dos de esos fermiones, estos están entrelazados? Junto con M. França, M. Terra Cunha, C. Lunkes y V. Vedral, hemos demostrado que la respuesta a esa pregunta depende no sólo de la posición de esas partículas, pero también de la manera (el detector) con que las escogemos. Primero consideramos un medidor ideal para las partículas y definimos operadores de medida que detectan la simetría de la parte espacial y la parte de espín del estado como una función de la distancia entre las partículas. Moviendo los a un escenario más realista consideramos aparatos que miden la posición de las partículas con una cierta imprecisión. Inesperadamente obtenemos que el entrelazamiento de los fermiones puede crecer con la imprecisión de la medida.

---

<sup>4</sup>Del inglés *bound entanglement*.

En ese mismo contexto, también consideramos el problema de utilizar ese entrelazamiento de partículas idénticas. En ese problema L. Malard y F. Matinaga se han unido a nuestro trabajo y con ellos hemos propuesto un esquema que permite la extracción de entrelazamiento desde pozos cuánticos semiconductores. Dos fotones independientes excitan dos electrones que no interactúan en el semiconductor. Cuando los electrones se relajan moviéndose hacia el fondo de la banda de conducción, el Príncipio de Pauli fuerza correlaciones entre ellos. Después de que esos electrones decaen hacia la banda de valencia, esa correlación es transferida a los fotones, que pueden ser entonces utilizados para el procesamiento de información. Concluimos entonces que el entrelazamiento de partículas idénticas puede ser útil!

# Bibliography

- [Aci02] A. Acín, *Distillability, Bell Inequalities, and Multiparticle Bound Entanglement*, Phys. Rev. Lett. **88**, 027901 (2002).
- [ASW02] A. Acín, V. Scarani, and M. M. Wolf, *Bell's inequalities and distillability in N-quantum-bit systems* , Phys. Rev. A **66**, 042323 (2002).
- [ABLS01] A. Acín, D. Bruss, M. Lewenstein, and A. Sanpera, *Classification of mixed three-qubit states*, Phys. Rev. Lett. **87**, 040401 (2001).
- [Ard92] M. Ardehali, *Bell inequalities with a magnitude of violation that grows exponentially with the number of particles* , Phys. Rev. A **46**, 5375 (1992).
- [AFOV07] L. Amico, R. Fazio, A. Osterloh, and V. Vedral, *Entanglement in many-body systems*, quant-ph/0703044 (2007).
- [AGG81] A. Aspect, P. Grangier, and G. Roger, *Experimental Tests of Realistic Local Theories via Bell's Theorem*, Phys. Rev. Lett. **47**, 460 (1981).
- [ADG82] A. Aspect, J. Dalibard, and G. Roger, *Experimental Test of Bell's Inequalities Using Time- Varying Analyzers*, Phys. Rev. Lett. **49**, 1804 (1982).
- [AJK+05] J.B. Altepeter, E.R. Jeffrey, P.G. Kwiat, S. Tanzilli, N. Gisin and A. Acín, *Experimental methods for detecting entanglement*, Phys. Rev. Lett. **95**, 033601 (2005).
- [AJ07] A. Al-Qasimi, D. F. V. James, *Sudden death of entanglement at finite temperature*, Phys. Rev. A **77**, 012117 (2008).
- [AMH+07] M. P. Almeida, F. de Melo, M. Hor-Meyll, A. Salles, S. P. Walborn, P. H. Souto Ribeiro, and L. Davidovich, *Environment-induced sudden death of entanglement*, Science **316**, 579 (2007).

- [APB+07] M. L. Almeida, S. Pironio, J. Barrett, G. Tóth, and A. Acín, *Noise Robustness of the Nonlocality of Entangled Quantum States*, Phys. Rev. Lett. **99**, 040403 (2007).
- [Bel87] J.S. Bell, *Speakable and unspeakable in quantum mechanics*, Cambridge Univesity Press (1987).
- [Bru02] D. Bruß, *Characterizing entanglement*, J. Math. Phys. **43**, 4237 (2002).
- [BK93] A. V. Belinskii and D. N. Klyshko, *Interference of light and Bell's theorem*, Phys. Usp. **36**, 653 (1993).
- [BB84] C. H. Bennett and G. Brassard, *Quantum cryptography: Public key distribution and coin tossing*, Proceedings of IEEE International Conference on Computers, Systems and Signal Processing, p.175 (1984).
- [BBD92] C. H. Bennett, G. Brassard, and N. David Mermin, *Quantum cryptography without Bell's theorem*, Phys. Rev. Lett. **68**, 557 (1992).
- [BBC+93] C.H. Bennett, G. Brassard, C. Crépeau, R. Jozsa, A. Peres e W. K. Wootters, *Teleporting an unknown quantum state via dual classical and EPR channels*, Phys. Rev. Lett. **70**, 1895 (1993).
- [BBP+96] C.H. Bennett, G. Brassard, S. Popescu, B. Schumacher, J.A. Smolin, and W.K. Wootters, *Purification of noisy entanglement and faithful teleportation via noisy channels*, Phys. Rev. Lett. **76**, 722 (1996).
- [BDSW96] C.H. Bennett, D.P. DiVincenzo, J.A. Smolin and W.K. Wootters, *Mixed-state entanglement and quantum error correction*, Phys. Rev. A **54**, 3824 (1996).
- [BEK+04] M. Bourennane, M. Eibl, C. Kurtsiefer, S. Gaertner, H. Weinfurter, O. Gühne, P. Hyllus, D. Bruß, M. Lewenstein, and A. Sanpera, *Experimental detection of multipartite entanglement using witness operators*, Phys. Rev. Lett. **92**, 087902 (2004).
- [BEZ00] D. Bouwmeester, A. Ekert, and A. Zeilinger, *The physics of quantum information*, Springer Verlag (2000).
- [BL01] H. Barnum and N. Linden, *Monotones and invariants for multi-particle quantum states*, J. Phys. A: Math. Gen. **34**, 6787 (2001).

## BIBLIOGRAPHY

## 109

- [BMN+03] M. Barbieri, F. De Martini, G. Di Nepi, P. Mataloni, G.M. D'Ariano and C. Macchiavello, *Detection of Entanglement with Polarized Photons: Experimental Realization of an Entanglement Witness*, Phys. Rev. Lett. **91**, 227901 (2003).
- [BMYI91] G. Björk, S. Machida, Y. Yamamoto, and K. Igeta, *Modification of spontaneous emission rate in planar dielectric microcavity structures*, Phys. Rev. A **44**, 669 (1991).
- [BV04a] F.G.S.L. Brandão and R.O. Vianna, *Separable Multipartite Mixed States: Operational Asymptotically Necessary and Sufficient Conditions*, Phys. Rev. Lett. **93**, 220503 (2004).
- [BV04b] F.G.S.L. Brandão and R.O. Vianna, *Robust semidefinite programming approach to the separability problem*, Phys. Rev. A **70**, 062309 (2004).
- [Bra05] F.G.S.L. Brandão, *Quantifying entanglement by witness operators*, Phys. Rev. A **72**, 022310 (2005).
- [BV06] F. G. S. L. Brandão and R. O. Vianna, *Witnessed entanglement*, Int. J. Quant. Inf. **4**, 331 (2006).
- [Bra07] F. G. S. L. Brandão, *Entanglement activation and the robustness of quantum correlations* Phys. Rev. A **76**, 030301 (2007).
- [BV04] S. Boyd and L. Vandenberghe, *Convex Optimization*, Cambridge University Press (2004).
- [BVK98] S. Bose, V. Vedral, and P. L. Knight, *Multiparticle generalization of entanglement swapping*, Phys. Rev. A **57**, 822 (1998).
- [BW99] K. Banaszek and K. Wódkiewicz, *Testing quantum nonlocality in phase space* Phys. Rev. Lett. **82**, 2009 (1999).
- [BZ06] I. Bengtsson and K. Życzkowski, *Geometry of Quantum States: An Introduction to Quantum Entanglement*, Cambridge University Press (2006).
- [CA97] N. Cerf and C. Adami, *Entropic Bell inequalities*, Phys. Rev. A **55**, 3371 (1997).
- [CFRD07] E. G. Cavalcanti, C. J. Foster, M. D. Reid, and P. D. Drummond, *Bell Inequalities for Continuous-Variable Correlations*, Phys. Rev. Lett. **99**, 210405 (2007).

- [CMB04] A. R. R. Carvalho, F. Mintert, and A. Buchleitner, *Decoherence and multipartite entanglement*, Phys. Rev. Lett. **93**, 230501 (2004).
- [COP+03] D. Cavalcanti, J. G. Oliveira Jr, J. G. Peixoto de Faria, M. O. Terra Cunha, and M. F. Santos, *Entanglement versus energy in the entanglement transfer problem*, Phys. Rev. A **74**, 042328 (2006).
- [CT06] D. Cavalcanti and M. O. Terra Cunha, *Estimating entanglement of unknown states*, Appl. Phys. Lett. **89**, 084102 (2006).
- [Dio03] L. Diósi, *Irrversible Quantum Dynamics*, Springer (2003).
- [DB04] W. Dür and H.-J Briegel, *Stability of macroscopic entanglement under decoherence*, Phys. Rev. Lett. **92**, 180403 (2004).
- [DC00] W. Dür and J.I. Cirac, *Classification of multiqubit mixed states: Separability and distillability properties*, Phys. Rev. A **61**, 042314 (2000).
- [DCT99] W. Dür, J.I. Cirac, and R. Tarrach, *Separability and Distillability of Multiparticle Quantum Systems*, Phys. Rev. Lett. **83**, 3562 (1999).
- [DDW06] M. R. Dowling, A. C. Doherty, and H. M. Wiseman, *Entanglement of indistinguishable particles in condensed-matter physics*, Phys. Rev. A **73**, 052323 (2006).
- [DHR02] M.J. Donald, M. Horodecki e O. Rudolph, *The uniqueness theorem for entanglement measures*, J. Math. Phys. **43**, 4252 (2002).
- [DH04] P. J. Dodd and P. J. Halliwell, *Disentanglement and decoherence by open system dynamics*, Phys. Rev. A **69**, 052105 (2004).
- [DP99] E. D'Hondt and P. Panangaden, *The Computational Power of the W and GHZ states*, Quantum Inf. and Comp. **6**, 173 (2005).
- [DPS04] A. C. Doherty, P. A. Parrilo, and F. M. Spedalieri, *Complete family of separability criteria*, Phys. Rev. A **69**, 022308 (2004).
- [Eis01] J. Eisert, *Entanglement in quantum information theory*, PhD thesis, University of Potsdam (2001), quant-ph/0610253.
- [EP03] J. Eisert and M.B. Plenio, *Introduction to the basics of entanglement theory in continuous-variable systems*, Int. J. Quant. Inf. **1**, 479 (2003).
- [EG06] J. Eisert and D. Gross, *Multiparticle entanglement*, Lectures on quantum information (VCH, Weinheim, 2006); arXiv:quant-ph/0505149.

- [EBA07] J. Eisert, F.G.S.L. Brando, and K.M.R. Audenaert, *Quantitative entanglement witnesses*, New J. Phys. **9**, 46 (2007).
- [Eke91] A. K. Ekert, *Quantum cryptography based on Bell's theorem*, Phys. Rev. Lett. **67**, 661 (1991).
- [EK95] A. Ekert and P. Knight, *Entangled quantum systems and the Schmidt decomposition*, Am. J. Phys. **63**, 415 (1995).
- [ESBL04] K. Eckert, J. Schliemann, D. Bruss, and M. Lewenstein, *Quantum correlations in systems of indistinguishable particles*, Annals of Physics **299**, 88 (2002).
- [EPR35] A. Einstein, B. Podolsky, and N. Rosen, *Can quantum-mechanical description of physical reality be considered complete?*, Phys. Rev. **47**, 777 (1935).
- [ER85] R. Eisberg and R. Resnick, *Quantum Physics of Atoms, Molecules, Solids, Nuclei, and Particles*, (John Wiley and Sons, 1985).
- [Fat05] D. Fattal, *Single Photons for Quantum Information Processing*, PhD Thesis, Univ. of Stanford (2005).
- [FC72] S. J. Freedman and J. F. Clauser, *Experimental Test of Local Hidden-Variable Theories*, Phys. Rev. Lett. **28**, 938 (1972).
- [FCGA08] A. Ferraro, D. Cavalcanti, A. García-Saez, and A. Acín, *Thermal bound entanglement in macroscopic systems and area law*, Phys. Rev. Lett. **100**, 080502 (2008).
- [FLS65] R. Feynman, R. Leighton and M. sands, *The Feynman Lectures on Physics*, (Pearson Addison Wesley, 1965).
- [FT76] E. S. Fry and R. C. Thompson, *Experimental Test of Local Hidden-Variable Theories* Phys. Rev. Lett. **37**, 465 (1976).
- [Gis96] N. Gisin, *Hidden quantum nonlocality revealed by local filters*, Phys. Lett. A **210**, 151 (1996).
- [Gis07] N. Gisin, *Bell inequalities: many questions, a few answers*, arXiv:quant-ph/0702021v2 (2007).
- [Gur03] L. Gurvits, *Classical deterministic complexity of Edmonds' Problem and quantum entanglement*, Proceedings of the 35th ACM Symposium on the Theory of Computing, pp. 10 – 19, ACM Press (2003).

- [GFC+04] R. García-Patrón, J. Fiurásék, N. J. Cerf, J. Wenger, R. Tualle-Bouri and Ph. Grangier, *Proposal for a Loophole-Free Bell Test Using Homodyne Detection*, Phys. Rev. Lett. **93**, 130409 (2004);
- [GFC05] R. García-Patrón, J. Fiurásék, N. J. Cerf, *Loophole-free test of quantum nonlocality using high-efficiency homodyne detectors*, Phys. Rev. A **71**, 022105 (2005).
- [GM04] G. Ghirardi and L. Marinatto, *General criterion for the entanglement of two indistinguishable particles*, Phys. Rev. A **70**, 012109 (2004).
- [GRW07] O. Gühne, M. Reimpell, and R.F. Werner, *Estimating entanglement measures in experiments*, Phys. Rev. Lett. **98**, 110502 (2007).
- [HBB99] M. Hillery, V. Bužek, and A. Berthiaume, *Quantum secret sharing* Phys. Rev. A **59**, 1829 (1999).
- [HDB05] M. Hein, W. Dür, H.-J. Briegel, *Entanglement properties of multi-partite entangled states under the influence of decoherence*, Phys. Rev. A **71**, 032350 (2005).
- [HGBL05] P. Hyllus, O. Gühne, D. Bruss, and M. Lewenstein, *Relations between Entanglement Witnesses and Bell Inequalities* Phys. Rev. A **72**, 012321 (2005).
- [Hor97] P. Horodecki, *Separability criterion and inseparable mixed states with positive partial transposition*, Phys. Lett. A **232**, 333 (1997).
- [HH96] R. Horodecki and M. Horodecki, *Information-theoretic aspects of inseparability of mixed states*, Phys. Rev. A **54**, 1838 (1996).
- [HHH96] M. Horodecki, P. Horodecki, and R. Horodecki, *Separability of mixed states: necessary and sufficient conditions*, Phys. Lett. A **223**, 1-8 (1996).
- [HHH97] M. Horodecki, P. Horodecki, and R. Horodecki, *Inseparable Two Spin-1/2 Density Matrices Can Be Distilled to a Singlet Form*, Phys. Rev. Lett. **78**, 574 (1997).
- [HHHH07] R. Horodecki, P. Horodecki, M. Horodecki, and K. Horodecki, *Quantum Entanglement*, quant-ph/0702225v2 (2007).

- [HHH98] M. Horodecki, P. Horodecki, and R. Horodecki, *Mixed-state entanglement and distillation: is there a “bound” entanglement in nature?*, Phys. Rev. Lett. **80**, 5239 (1998).
- [HHR+05] H. Häffner, W. Hänsel, C.F. Roos, J. Benhelm, D. Chek-al-kar, M. Chwalla, T. Körber, U.D. Rapol, M. Riebe, P.O. Schmidt, C. Becher, O. Gühne, W. Dür, and R. Blatt, *Scalable multiparticle entanglement of trapped ions*, Nature **438**, 643 (2005).
- [HMM+05] M. Hayashi, D. Markham, M. Murao, M. Owari, and S. Virmani, *Bounds on Multipartite Entangled Orthogonal State Discrimination Using Local Operations and Classical Communication*, Phys. Rev. Lett. **96**, 040501 (2005).
- [HMM+08] M. Hayashi, D. Markham, M. Murao, M. Owari, and S. Virmani, *Entanglement of multiparty-stabilizer, symmetric, and antisymmetric states*, Phys. Rev. A **77**, 012104 (2008).
- [HN03] A.W. Harrow and M.A. Nielsen, *Robustness of quantum gates in the presence of noise*, Phys. Rev. A **68**, 012308 (2003).
- [Jan02] E. Jané, *Purification of two-qubit mixed states*, Quant. Inf. Comp. **2**, 348 (2002).
- [JP99] D. Jonathan and M.B. Plenio, *Entanglement-assisted local manipulation of pure quantum states*, Phys. Rev. Lett. **83**, 3566 (1999).
- [KMW+05] P. G. Kwiat, K. Mattle, H. Weinfurter, A. Zeilinger, A. V. Sergienko and Y. Shih, *New high-intensive source of polarization-entangled photon pairs*, Phys. Rev. Lett. **75**, 4337 (1995).
- [KL01] S. Karnaś and M. Lewenstein, *Separable approximations of density matrices of composite quantum systems*, J. Phys. A **34**, 318 (2001).
- [KST+07] N. Kiesel, C. Schmid, G. Tóth, E. Solano, and H. Weinfurter, *Experimental Observation of Four-Photon Entangled Dicke State with High Fidelity*, Phys. Rev. Lett. **98**, 063604 (2007).
- [KWN+07] P. Kok, W. J. Munro, K. Nemoto, T. C. Ralph, J. P. Dowling, and G. J. Milburn, *Linear optical quantum computing with photonic qubits* Rev. Mod. Phys. **79**, 135 (2007).
- [LBMW03] D. Leibfried, R. Blatt, C. Monroe, and D. Wineland, *Quantum dynamics of single trapped ions*, Rev. Mod. Phys. **75**, 281 (2003).

- [LKS+05] D. Leibfried, E. Knill, S. Seidelin, J. Britton, R. B. Blakestad, J. Chiaverini, D. B. Hume, W. M. Itano, J. D. Jost, C. Langer, R. Ozeri, R. Reichle and D. J. Wineland, *Creation of a six-atom 'Schrödinger cat' state*, Nature **438**, 639 (2005).
- [LK00] J. Lee and M. S. Kim, *Entanglement Teleportation via Werner States* Phys. Rev. Lett. **84**, 4236 (2000).
- [LKCH00] M. Lewenstein, B. Kraus, J. I. Cirac, and P. Horodecki, *Optimization of entanglement witnesses*, Phys. Rev. A **62**, 052310 (2000).
- [LMD08] Y-C. Liang, L. Masanes, and A. C. Doherty, *Convertibility between two-qubit states using stochastic local quantum operations assisted by classical communication*, Phys. Rev. A **77**, 012332 (2008).
- [LPS06] N. Linden, S. Popescu, and J. A. Smolin, *Entanglement of Superpositions*, Phys. Rev. Lett. **97**, 100502 (2006).
- [LS98] M. Lewenstein and A. Sanpera, *Separability and Entanglement of Composite Quantum Systems*, Phys. Rev. Lett. **80**, 2261 (1998).
- [LZG+07] C.-Y. Lu, X.-Q. Zhou, O. Gühne, W.-B. Gao, J. Zhang, Z.-S. Yuan, A. Goebel, T. Yang, and J.-W. Pan, *Experimental entanglement of six photons in graph states*, Nat. Phys. **3**, 91 (2007).
- [Mas06] L. Masanes, *Asymptotic Violation of Bell Inequalities and Distillability*, Phys. Rev. Lett. **97**, 050503 (2006).
- [MLD08] L. Masanes, Y.-C. Liang, and A. C. Doherty, *All Bipartite Entangled States Display Some Hidden Nonlocality* Phys. Rev. Lett. **100**, 090403 (2008).
- [Mer90] N. D. Mermin, *Extreme quantum entanglement in a superposition of macroscopically distinct states*, Phys. Rev. Lett. **65**, 1838 (1990).
- [Mun99] W. J. Munro, *Optimal states for Bell-inequality violations using quadrature-phase homodyne measurements*, Phys. Rev. A **59**, 4197 (1999).
- [MP06] A. Miranowicz and M. Piani, *Comment on "Inseparability Criteria for Continuous Bipartite Quantum States"*, Phys. Rev. Lett. **97**, 058901 (2006).
- [NC00] M.A. Nielsen and I.L. Chuang, *Quantum Computation and Quantum Information* (Cambridge University Press, 2000).

## BIBLIOGRAPHY

## 115

- [NK01] M. Nielsen and J. Kempe, *Separable states are more disordered globally than locally*, Phys. Rev. Lett. **86**, 5184 (2001).
- [OF07] Y.-C. Ou and H. Fan, *Bounds on negativity of superpositions*, Phys. Rev. A **76**, 022320 (2007).
- [OPM06] A. Osterloh, G. Palacios, and S. Montangero, *Enhancement of pairwise entanglement via  $Z_2$  symmetry breaking*, Phys. Rev. Lett. **97**, 257201 (2006).
- [Per96a] A. Peres, *Collective tests for quantum nonlocality*, Phys. Rev. A **54**, 2685 (1996).
- [Per96b] A. Peres, *Separability Criterion for Density Matrices*, Phys. Rev. Lett. **77**, 1413 (1996).
- [Per99] A. Peres, *All Bell inequalities*, Found. Phys. **29**, 589 (1999).
- [PR97] S. Popescu and D. Rohrlich, *Thermodinamics and the measure of entanglement*, Phys. Rev. A **56**, 3319(R) (1997).
- [PFA07] D. Patanè, R. Fazio, and L. Amico, *Bound entanglement in the XY model*, New J. Phys. **9**, 322 (2007).
- [Pop95] S. Popescu, *Bell's Inequalities and Density Matrices: Revealing "Hidden" Nonlocality*, Phys. Rev. Lett. **74**, 2619 (1995).
- [PV98] M.B. Plenio and V. Vedral, *Teleportation, Entanglement and Thermodinamics in the Quantum World*, Contemp. Phys. **39**, 431 (1998).
- [PV05] M.B. Plenio and S. Virmani, *An introduction to entanglement measures*, Quant. Inf. Comp. **7**, 1 (2007).
- [RMH01] J. M. Raymond, M. Brune, and S. Haroche, *Manipulating quantum entanglement with atoms and photons in a cavity*, Rev. Mod. Phys. **73**, 565 (2001).
- [RVF+04] T. Roscilde, P. Verrucchi, A. Fubini, S. Haas, and V. Tognetti, *Studying Quantum Spin Systems through EntanglementEstimators*, Phys. Rev. Lett. **93**, 167203 (2004).
- [RVF+05] T. Roscilde, P. Verrucchi, A. Fubini, S. Haas, and V. Tognetti, *Entanglement and Factorized Ground States in Two-Dimensional Quantum Antiferromagnets* Phys. Rev. Lett. **94**, 147208 (2005).

- [Sch07] E. Schmidt, *Math. Ann.* **63**, 433 (1907);
- [Sch35] E. Schrödinger, Die gegenwärtige Situation in der Quantenmechanik, *Naturwissenschaften* **23**, 807, ibid 823, ibid 844 (2000). See a translation to english at J.A. Wheeler and W.H. Zurek, *Quantum Theory and Measurement*, (Princeton university Press, 1983).
- [Ste03] M. Steiner, *Generalized robustness of entanglement*, Phys. Rev. A **67**, 054305 (2003).
- [SK02] C. Simon and J. Kempe, *Robustness of multiparty entanglement*, Phys. Rev. A **65**, 052327 (2002).
- [SMDZ07] M. F. Santos, P. Milman L. Davidovich, and N. Zagury, *Direct measurement of finite-time disentanglement induced by a reservoir*, Phys. Rev. A **73**, 040305(R) (2006);
- [SV05] E. Shchukin and W. Vogel, *Inseparability Criteria for Continuous Bipartite Quantum States*, Phys. Rev. Lett. **95**, 230502 (2005).
- [SV06] E. Shchukin and W. Vogel, *Conditions for multipartite continuous-variable entanglement*, Phys. Rev. A **74**, 030302(R) (2006).
- [SV08] E. Shchukin and W. Vogel, *Quaternions, octonions and Bell-type inequalities*, arXiv:0803.0913v1 (2008).
- [TA06] G. Tóth and A. Acín, *Genuine tripartite entangled states with a local hidden-variable model*, Phys. Rev. A **74**, 030306 (2006).
- [Ter07] M. O. Terra Cunha, *The geometry of entanglement sudden death*, New J. Phys **9**, 273 (2007).
- [Ter00] B.M. Terhal, *Bell inequalities and the separability criterion*, Phys. Lett. A **271**, 319 (2000).
- [Ter02] B.M. Terhal, *Detecting entanglement*, Journal of Theoretical Computer Science **287**, 313-335 (2002).
- [TKGB07] G. Tóth, C. Knapp, O. Gühne, and H. J. Briegel, *Optimal spin squeezing inequalities detect bound entanglement in spin models*, Phys. Rev. Lett. **99**, 250405 (2007).
- [Ved03] V. Vedral, *Entanglement in the second-quantization formalism* Cent. Eur. J. Phys. **2**, 289 (2003).

- [VPRK97] V. Vedral, M. B. Plenio, M. A. Rippi, and P. L. Knight, *Quantifying entanglement*, Phys. Rev. Lett. **78**, 2275 (1997).
- [VP98] V. Vedral and M.B. Plenio, *Entanglement measures and purification procedures*, Phys. Rev. A **57**, 1619 (1998).
- [Ver02] F. Verstraete, *A study of entanglement in quantum information theory*, PhD Thesis, Katholieke Universiteit Leuven (2002).
- [Vid00] G. Vidal, *Entanglement monotones*, J. Mod. Opt. **47**, 355 (2000).
- [VT99] G. Vidal and R. Tarrach, *Robustness of entanglement*, Phys. Rev. A **59**, 141 (1999).
- [VW02] G. Vidal and R.F. Werner, *Computable measure of entanglement*, Phys. Rev. A **65**, 032314 (2002).
- [Wer89] R. F. Werner, *Quantum states with Einstein-Podolsky-Rosen correlations admitting a hidden-variable model*, Phys. Rev. A **40**, 4277 (1989).
- [WW01a] R. F. Werner and M. M. Wolf, *All-multipartite Bell-correlation inequalities for two dichotomic observables per site*, Phys. Rev. A **64**, 032112 (2001).
- [WW01b] R. F. Werner and M. M. Wolf, *Bell inequalities and entanglement*, Quant. Inf. and Comp. **3**, 1 (2001).
- [Woo98] W.K. Wootters, *Entanglement of Formation of an Arbitrary State of Two Qubits*, Phys. Rev. Lett. **80**, 2245 (1998).
- [WEGM04] T.-C. Wei, M. Ericsson, P.M. Goldbar, and W.J. Munro, *Connections between relative entropy of entanglement and geometric measure of entanglement*, Quant. Inf. and Comp. **4**, 252 (2004).
- [WG03] T.-C. Wei and P.M. Goldbart, *Geometric measure of entanglement and applications to bipartite and multipartite quantum states*, Phys. Rev. A **68**, 042307 (2003).
- [WHG+03] J. Wenger, M. Hafezi, F. Grosshans, R. Tualle-Brouri, and P. Grangier, *Maximal violation of Bell inequalities using continuous-variable measurements*, Phys. Rev. A **67**, 012105 (2003).
- [WNIA92] C. Weisbuch, M. Nishioka, A. Ishikawa, and Y. Arakawa, *Observation of the coupled exciton-photon mode splitting in a semiconductor quantum microcavity*, Phys. Rev. Lett. **69**, 3314 (1992).

- [Yam91] Y. Yamamoto, *Coherence, amplification, and quantum effects in semiconductor lasers*, John Wiley Sons (1991).
- [YC96] P. Y. Yu and M. Cardona, *Fundamentals of Semiconductors*, Springer-Verlag (1996).
- [YE04] T. Yu and J. H. Eberly, *Finite-time disentanglement via spontaneous emission* Phys. Rev. Lett. **93**, 140404 (2004).
- [YE06] T. Yu and J. H. Eberly, *Quantum open system theory: bipartite aspects*, Phys. Rev. Lett. **97**, 140403 (2006).
- [YE07] T. Yu and J. H. Eberly, *Many-body separability of warm qubits*, arXiv:0707.3215 (2007).
- [YYS07] C.-S. Yu, X.X. Yi, and H-S. Song, *Concurrence of superpositions*, Phys. Rev. A **75**, 022332 (2007).
- [XXH] Y. Xiang, S.-J. Xiong, F.-Y. Hong, *The bound of entanglement of superpositions with more than two components*, quant-ph/0706.1598.
- [Zur03] W. H. Zurek, *Decoherence and the transition from quantum to classical - REVISITED*, arXiv:quant-ph/0306072 (2003).
- [ZHSL98] K. Życzkowski, P. Horodecki, A. Sanpera and M. Lewenstein, *Volume of the set of separable states*, Phys. Rev. A **58**, 883 (1998).

## 4. Observation and measurement of entanglement

**Abstract:** Quantum theory of observation is enlightened.

**Keywords:** Observer, observed system, disentanglement

# Quantum theory of observation/Entanglement

---

According to classical physics, the state of a compound system is always determined by the list of the states of its components. Formally, we define the state space of the compound as the cartesian product of the state spaces of the components. If the state of the compound is known exactly, the states of the components are therefore necessarily known with the same accuracy. This is no longer true in quantum physics, because the state space of the compound is the tensor product of the state spaces of the components. For example, if a two-qubits system is in the state  $\frac{1}{\sqrt{2}}(|00\rangle + |11\rangle)$  one can not assign state vectors to the qubits taken separately. Each qubit is entangled with the other. This entanglement effect is purely quantum. It has no equivalent in classical physics. It is often considered, since Schrödinger (1935), as the quantum effect par excellence. Entanglement is at the heart of the great mystery of quantum superposition.

This chapter is the most important of the book because quantum entanglement is fundamental to explain the reality of observations.

## Definition

The state of a composite system AB ... Z is said to be separable when it is the product of the states of its components:

$$|\psi_{AB\dots Z}\rangle = |\psi_A\rangle|\psi_B\rangle\dots|\psi_Z\rangle$$

for a pure state,

$$\rho_{AB\dots Z} = \rho_A \rho_B \dots \rho_Z$$

for a mixed state.

A state is entangled when it is not separable. It is sometimes called an inseparable state.

## Interaction, entanglement and disentanglement

When two parts of a system interact, an initially separable state may become entangled. For example,  $CNOT[\frac{1}{\sqrt{2}}(|0\rangle + |1\rangle)|0\rangle] = \frac{1}{\sqrt{2}}(|00\rangle + |11\rangle)$

But interactions do not always lead to entanglement. CNOT does not entangle the states of the computation basis (for two qubits the computation basis is:  $|00\rangle, |01\rangle, |10\rangle, |11\rangle$ ). SWAP is an interaction that never entangles the separable states on which it acts:

$$SWAP|\alpha\rangle|\beta\rangle = |\beta\rangle|\alpha\rangle$$

When an interaction  $U$  transforms a separable state into an entangled state, it is in principle possible to return to the

initial separable state, provided that the dynamics of the interaction is reversible, because  $U^{-1}$  then represents a possible interaction. Almost all elementary interactions allow such temporal reversibility.

For example :

$$CNOT \frac{1}{\sqrt{2}}(|00\rangle + |11\rangle) = |00\rangle$$

CNOT is its own inverse:  $CNOT^{-1} = CNOT$ . Any state that has been entangled by CNOT becomes separable again if CNOT is applied a second time. When entanglement is thus destroyed, one can speak of disentanglement, or return to separability.

The Hadamard gate is very useful for modeling entanglement and disentanglement of qubits. From the computation basis, the combination of H on the first qubit followed by CNOT produces the basis of the Bell states:

$$CNOT(H_1|00\rangle) = \frac{1}{\sqrt{2}}(|00\rangle + |11\rangle) = |\beta_{00}\rangle$$

$$CNOT(H_1|01\rangle) = \frac{1}{\sqrt{2}}(|01\rangle + |10\rangle) = |\beta_{01}\rangle$$

$$CNOT(H_1|10\rangle) = \frac{1}{\sqrt{2}}(|00\rangle - |11\rangle) = |\beta_{10}\rangle$$

$$CNOT(H_1|11\rangle) = \frac{1}{\sqrt{2}}(|01\rangle - |10\rangle) = |\beta_{11}\rangle$$

The Bell states  $|\beta_{ij}\rangle$  are the simplest entangled states which can be conceived.

Two systems can get entangled without interacting directly, through a third system. For example, if in a three-qubits system, the second and the third both measure the first, the following can be obtained:

$$U \frac{1}{\sqrt{2}}(|0\rangle + |1\rangle)|00\rangle = \frac{1}{\sqrt{2}}(|000\rangle + |111\rangle)$$

Similarly, if the second qubit measures the first before being measured by the third, we can obtain:

$$\frac{1}{\sqrt{2}}(|0\rangle + |1\rangle)|00\rangle \rightarrow \frac{1}{\sqrt{2}}(|00\rangle + |11\rangle)|0\rangle \rightarrow \frac{1}{\sqrt{2}}(|000\rangle + |111\rangle)$$

If two qubits are initially entangled and if the first one interacts by a SWAP with a third, then there is transfer of entanglement:

$$\begin{aligned} SWAP_{13} \frac{1}{\sqrt{2}}(|00\rangle + |11\rangle)(\alpha|0\rangle + \beta|1\rangle) &= SWAP_{13} \frac{1}{\sqrt{2}}[\alpha(|000\rangle + |110\rangle) + \beta(|001\rangle + |111\rangle)] \\ &= \frac{1}{\sqrt{2}}[\alpha(|000\rangle + |011\rangle) + \beta(|100\rangle + |111\rangle)] = \frac{1}{\sqrt{2}}(\alpha|0\rangle + \beta|1\rangle)(|00\rangle + |11\rangle) \end{aligned}$$

The third qubit thus becomes entangled with the second without having interacted directly with it. The first qubit is disentangled through the SWAP with the third.

## Everett relative states

In general, an observation changes the observed system and the measuring apparatus from a separable state to an entangled state. For an ideal measurement:

$$U\left(\sum_{ij} \alpha_{ij}|i,j\rangle_S\right)|ready\rangle_A = \sum_{ij} \alpha_{ij}|i,j\rangle_S|i\rangle_A$$

There is no entanglement only if the observed system is in an eigenstate of the measurement.

After the observation,  $\frac{\sum_j \alpha_{ij}|i,j\rangle_S}{|\sum_j \alpha_{ij}|i,j\rangle_S|}$  is the state of the observed system relative, in Everett's sense, to the state  $|i\rangle_A$  of the measurement apparatus, and vice versa.

More generally, if  $\sum_{ij} \alpha_{ij}|a_i\rangle|b_j\rangle$  is the state of an AB system where the  $|a_i\rangle$  and the  $|b_j\rangle$  are any two orthonormal bases of A and B, then  $\frac{\sum_i \alpha_{ij}|a_i\rangle}{|\sum_i \alpha_{ij}|a_i\rangle|}$  is the relative state of A with respect to the state  $|b_j\rangle$  of B, and  $\frac{\sum_j \alpha_{ij}|b_j\rangle}{|\sum_j \alpha_{ij}|b_j\rangle|}$  is the relative state of B with respect to the state  $|a_i\rangle$  of A (Everett 1957).

For mathematical convenience, it is agreed that if the weight of  $|b_j\rangle$  is null in  $\sum_{ij} \alpha_{ij}|a_i\rangle|b_j\rangle$  the state of A relative to  $|b_j\rangle$  is the null vector  $\mathbf{0}$ . It must be distinguished from  $|0\rangle$  whose length is one, because the length of  $\mathbf{0}$  is zero. The vector  $\mathbf{0}$  is not a state vector. It is the only element of the vector space of states of a system that can not be identified with state of the system state.

$|\sum_i \alpha_{ij}|a_i\rangle|^2 = \sum_i |\alpha_{ij}|^2$  is the weight of the state  $|b_j\rangle$  of B in the state  $\sum_{ij} \alpha_{ij}|a_i\rangle|b_j\rangle$  of AB. Similarly,  $|\sum_j \alpha_{ij}|b_j\rangle|^2 = \sum_j |\alpha_{ij}|^2$  is the weight of the state  $|a_i\rangle$  of A.

A pure state  $|\psi\rangle$  of a system AB can always be decomposed as follows:

$$|\psi\rangle = \sum_i \sqrt{p_i}|a_i\rangle|b_i\rangle$$

where the  $|a_i\rangle$  are orthonormal vectors, as well as the  $|b_i\rangle$ . It is called a Schmidt decomposition. It is unique when the  $p_i$  are all different. It contains at least two terms if and only if  $|\psi\rangle$  is an entangled state.

For each  $i$ ,  $|a_i\rangle$  is the state of A relative to the state  $|b_i\rangle$  of B, and vice versa. They have the same weight  $p_i$  in  $|\psi\rangle$ .

$\sum_i (\sum_j \alpha_{ij}|i,j\rangle_S)|i\rangle_A$  is a Schmidt decomposition of the system SA. According to the Born rule, the weight  $\sum_j |\alpha_{ij}|^2$  of  $\sum_j \alpha_{ij}|i,j\rangle_S$  and of  $|i\rangle_A$  is the probability that the measurement provides the result  $i$ .

## The collapse of the state vector through observation is a disentanglement.

Most textbooks in quantum physics set forth the following two principles:

The evolution of the state vector is described by a unitary operator, or by the Schrödinger equation, as long as the studied system is not observed.

When the system is observed, its initial state  $|\psi\rangle$  before the observation becomes one of the states  $\frac{P(i)|\psi\rangle}{|P(i)|\psi\rangle|}$  where  $P(i) = \sum_j |ij\rangle\langle ij|$  is the projector on the subspace of eigenstates  $|ij\rangle$  of the result  $i$ . It is then said that the state vector

collapsed, a kind of quantum jump which moves the system from the state  $|\psi\rangle$  to the state  $\frac{P(i)|\psi\rangle}{|P(i)|\psi\rangle|}$ . We also say that it is a wave function collapse, because a wave function represents the components of a state vector in a position state basis.

After a measurement which has given the result  $i$ , the relative state of the observed system with respect to the observer system is  $\frac{P(i)|\psi\rangle}{|P(i)|\psi\rangle|}$ . The collapse of the state vector is therefore the transition from the initial state vector to the state vector relative, in Everett's sense, to the result of the measurement.

The collapse of the state vector through observation is a disentanglement because the observed system passes into an eigenstate of the measurement after the observation. If the measurement is exact, ie if there is only one state of the observed system pointed to by the measurement result, the disentanglement is complete. If the observed system was entangled with its environment, it is no longer so after the measurement. The observation thus destroys any previous entanglement of the observed system with its environment.

Distentanglement through observation explains why quantum physics makes excellent predictions from the calculation on pure states. As interactions between all parts of the Universe occur constantly, and as interactions are often entangling, everything should be entangled with everything, or almost so. Matter never ceases to interact with matter. All material beings generally have a long history of interactions, and therefore of entanglements, with all the other material beings they have encountered. How is it then that one can describe their states by pure states, separated from the rest of the Universe, and make accurate predictions from such a description ?

We know the quantum states of material beings only if we give ourselves conditions of observation which enable us to know them. Since from our points of view our observations are disentangling, we can ignore all entanglements preceding our observations, and thus attribute state vectors to the systems we observe.

## **Apparent disentanglement results from real entanglement between the observed system and the observer.**

The collapse of the state vector through observation can not be described by a unitary operator. We should therefore admit two kinds of evolution, one is unitary and occurs in the absence of observation, the other is not unitary and occurs during a measurement. But a measurement is a natural evolution. The principle of unitary evolution is universal. We assume that it describes all natural processes. We are therefore faced with a contradiction. The quantum jump, the collapse of the state vector, is a natural evolution, but it is not unitary.

Is quantum physics contradictory? Is it not possible to give a unified theory, which describes without contradiction, with the same principles, all the natural processes, whether or not there is observation?

One can believe that quantum physics is only an approximation, that the postulate of unitary evolution is not universal, that a new physics will explain in which cases the evolution is unitary, or almost, and in which other cases collapse of the state vector occurs. But until now, such a new physics, which surpasses and supplantes quantum physics does not exist. The various speculations on this subject have never produced real fruits.

The postulate of the reduction of the state vector denies the existence theorem of multiple destinies. If an observation really leads to the collapse of the state vector then we only have a single destiny. The postulate of the collapse of the state vector allows us to preserve our prejudice, that the other destinies do not exist. It is its only justification. There are no others. We introduce a contradiction into the heart of quantum theory because we do not want to believe in other destinies, because we do not accept that reality could be more than what we can directly observe.

To explain our observation results, the postulate of the collapse of the state vector is not necessary. The principle of unitary evolution and the entanglement between the observed system and the observer are sufficient to account for the measured probabilities. To understand it, it suffices to reason on conditional probabilities: what is the probability that an observation provides a result knowing the result of an earlier observation ?

Suppose that we do two successive measurements on the same system (Everett 1957), prepared initially in the state  $|\psi\rangle$ . After the two measurements, the overall system (observed system + measuring devices) is found in the following state:

$$\sum_{ij} (P_2(j)U_S P_1(i)|\psi\rangle)(U_{A_1}|i\rangle_1)|j\rangle_2$$

where the  $P_1(i)$  and  $P_2(j)$  are the projectors associated with the two successive measurements,  $U_S$  is the evolution operator of the observed system between the two measurements and  $U_{A_1}$  that of the first measuring device.

The probability of obtaining the result  $j$  with the second measurement, knowing that  $i$  was obtained with the first is:

$$\frac{Pr(ij)}{Pr(i)} = \frac{|P_2(j)U_S P_1(i)|\psi\rangle|^2}{|P_1(i)|\psi\rangle|^2}$$

This is the same probability as that which would be obtained if, immediately after the first measurement, the system had been in the state  $\frac{P_1(i)|\psi\rangle}{|P_1(i)|\psi\rangle|}$ .

Once we get the result  $i$  everything happens as if the state of the observed system had gone from the state  $|\psi\rangle$  to the state  $\frac{P_1(i)|\psi\rangle}{|P_1(i)|\psi\rangle|}$ , as if there had been a collapse of the state vector. The other states of the observed system, the  $\frac{P_1(i')|\psi\rangle}{|P_1(i')|\psi\rangle|}$  where  $i'$  is different from  $i$ , have no influence on subsequent measurements. If they exist, they are obtained in other destinies which have no influence on ours, since they have no influence on our observations.

If one takes quantum physics seriously, if one believes that it correctly describes reality, if one thus accepts the existence theorem of multiple destinies, one does not need the postulate of the collapse of the state vector. The principle of unitary evolution is sufficient to describe reality.

Depending on the point of view chosen, it can be said that the observations are entangling or disentangling. They are entangling because they lead to an entanglement between the observed system and the observer. They are disentangling because they lead to an apparent collapse of the state vector of the observed system.

Disentanglement through observation is only a subjective effect. The observation is disentangling only from the point of view of the observer. From an external point of view, on the contrary, an observation is generally entangling. It is precisely the entanglement between the observed system and the observer that produces the apparent collapse of the state vector, because after an observation an observer can only know the relative state, in Everett's sense, of the observed system. All other states can no longer influence subsequent observations. But it is only from the point of view

of the observer that the state vector of the observed system has been reduced to the state relative to the observer. The collapse of the state vector is only a kind of illusion, produced by our viewpoint of an entangled observer, who knows of reality only a tiny part, who can only know one destiny among myriads of others, all equally real.

## Can we see non-localized macroscopic states?

If a quantum system can be in the states  $|1\rangle$  and  $|2\rangle$ , it can also be in the state  $\alpha|1\rangle + \beta|2\rangle$ . For example,  $|1\rangle$  and  $|2\rangle$  can be two states of the moon at different positions. But the moon is never seen in different positions. A non-localized state of the moon such as  $\frac{1}{\sqrt{2}}(|1\rangle + |2\rangle)$  is never observed. The same is true for all macroscopic objects (Schrödinger 1935)

even if they are very small. (From the point of view of the biologist, a bacterium is microscopic, but from the point of view of the physicist, it is macroscopic, because it is made up of billions of atoms.)

Vision involves the formation of images. Each point of the image represents a point of an object in the visual field. If the object is not located, it can not have a clear and stable image. But perhaps we could see it sometimes in one position, sometimes in another. The apparent reduction of the state vector during an observation proves that it is not possible. If the object seen is initially unlocalized, it passes, from my point of view, into a localized state as soon as I see it at a defined position. If I repeat the observation several times, I will see it in the same place. The other components of the initial state vector can no longer be observed, once one of the components has been selected by an observation. Due to the entanglement by observation, the simple fact of seeing an object at a defined position suffices to destroy its initial non-localized state.

But this does not prove that it is impossible to observe non-localized macroscopic states (cf. 4.20), it only proves that it is impossible to see them.

## The quantum explanation of intersubjectivity

Since the Universe is in an entangled state, one can not in general attribute a truly defined state to each of its parts. The problem is not that we do not know the states of these parts, but that they are not defined, that they simply do not exist, at least according to the theory. However we know the Universe always by observing its parts. We can not know anything about it apart from the parts we observe. And when we have observed them we believe we know how they really are. Why say that we know their real state, whereas according to the theory such a state does not even exist ?

The response of quantum physics is essentially relativistic, in the sense that the observed reality is always relative to the observers. The beings actually present in the Universe do not have a single state defined absolutely, invariantly, ie the same for all observers. The theory does not attribute to them a single state, but many states, because the real state of a being is always relative to the state of another being.

If A, B and C are three beings, the state of A relative to a state of B is in general different from the state of A relative to a state of C. We conclude that B and C each have their reality. The representations of the world of all observers should therefore always be different. How is it then that we can agree on the same reality that we all observe?

Everett (1957) showed that communication between observers is sufficient to observe the same reality:

Suppose that A is observed by B which is then observed by C such that the information possessed by B on A is transmitted to C.

We argue on a simplified model: the states  $|a_i\rangle$  of A are the eigenstates associated with the pointer states  $|b_i\rangle$  of B,

which are themselves the eigenstates associated with the pointer states  $|c_i\rangle$  of C.

Starting from the initial state  $\sum_i \alpha_i |a_i\rangle$  of A, one obtains, after the observation of A by B, the state  $\sum_i \alpha_i |a_i\rangle |b_i\rangle$  of AB. After the observation of B by C, one obtains the state  $\sum_i \alpha_i |a_i\rangle |b_i\rangle |c_i\rangle$  of ABC. Before the communication between B and C, the state vector of A relative to a state of C is not defined, because A is entangled with B. We show below (cf. 4.15) that it can be defined as a mixed state, but it is not a state vector. After the communication between B and C, the state  $|a_i\rangle$  of A relative to a state  $|c_i\rangle$  of C is the same as the state of A relative to the state  $|b_i\rangle$  of B relative to the state  $|c_i\rangle$  of C. The reality of A is therefore the same for B and C. Quantum theory thus explains the possibility of intersubjectivity in an essentially relativistic universe.

## Einstein, Bell, Aspect and the reality of quantum entanglement

Suppose that two entangled qubits in the state  $\frac{1}{\sqrt{2}}(|00\rangle + |11\rangle)$  are very far from each other. One can therefore make

a measurement on one without touching the other. If we measure the first qubit, if it has  $|0\rangle$  and  $|1\rangle$  for eigenstates, we can deduce from the result of the measurement the state  $|0\rangle$  or  $|1\rangle$  of the second qubit, which is very far from the measuring instrument. Einstein concludes that this state must represent an element of reality which existed before the measurement (Einstein, Podolsky & Rosen 1935). An immediate instantaneous action of the first qubit or of the measuring instrument on the second qubit is excluded. It is contrary to the principles of physics which he has greatly contributed to establish. But the quantum equations do not assign a defined state to the second qubit before the measurement. According to Einstein, therefore, they do not completely describe reality, there must be hidden variables, that is, real quantities ignored by quantum theory, which must complete the quantum description of reality, necessarily incomplete.

Einstein could not believe that quantum physics gives a complete description of reality because he did not want to give up the principle of the separability of reality. All classical physics respects the principle that the state of the system is always to be identified with the list of states of its parts. To speak of an entangled state, of a defined state of a system in which the parts have no definite state, has no meaning in classical physics.

The existence of these hidden variables, postulated by Einstein, remained very hypothetical until Bell understood in 1964 how to put this hypothesis to the test of experience (Bell 1988). The experiment was made (Aspect, Grangier & Roger 1982, Gisin, Tittel, Brendel & Zbinden 1998, Gisin 2014) and the result is very clear: Einstein was wrong to believe that reality is necessarily separable. The entangled quantum states really exist and they completely describe reality, as far as we know.

One can understand the reasoning of Bell and the results obtained by Aspect by studying a system with two entangled qubits and considering two measuring instruments for each of them.

Let  $|\mathbf{x}^+\rangle = \frac{1}{\sqrt{2}}(|0\rangle + |1\rangle)$  and  $|\mathbf{x}^-\rangle = \frac{1}{\sqrt{2}}(|0\rangle - |1\rangle)$  be two new basis vectors (the names  $\mathbf{x}^+$  and  $\mathbf{x}^-$  come from the spin 1/2 theory).

$\{|0\rangle, |1\rangle\}$  and  $\{|\mathbf{x}^+\rangle, |\mathbf{x}^-\rangle\}$  are the two bases of eigenstates of the measuring instruments of the first qubit.

$\{|v^+\rangle, |v^-\rangle\}$  and  $\{|w^+\rangle, |w^-\rangle\}$  are the two bases of eigenstates of the measuring instruments of the second qubit.

At each iteration of the experiment, Alice chooses one of the two instruments and applies it to her qubit, Bob does the

same on the other qubit. There are therefore four possible experiences, which may have as results :

- $0v^+, 0v^-, 1v^+, 1v^-$
- $0w^+, 0w^-, 1w^+, 1w^-$
- $x^+v^+, x^+v^-, x^-v^+, x^-v^-$
- $x^+w^+, x^+w^-, x^-w^+, x^-w^-$

It seems that the Bell state  $\frac{1}{\sqrt{2}}(|00\rangle + |11\rangle)$  favors the basis  $\{|0\rangle, |1\rangle\}$  but it is an illusion :

$$\frac{1}{\sqrt{2}}(|x^+x^+\rangle + |x^-x^-\rangle) = \frac{1}{2\sqrt{2}}[(|0\rangle + |1\rangle)(|0\rangle + |1\rangle) + (|0\rangle - |1\rangle)(|0\rangle - |1\rangle)] = \frac{1}{\sqrt{2}}(|00\rangle + |11\rangle)$$

If one chooses :

$$|v^+\rangle = \cos(\pi/8)|0\rangle + \sin(\pi/8)|1\rangle$$

$$|v^-\rangle = \sin(\pi/8)|0\rangle - \cos(\pi/8)|1\rangle$$

$$|w^+\rangle = \cos(3\pi/8)|0\rangle + \sin(3\pi/8)|1\rangle$$

$$|w^-\rangle = \sin(3\pi/8)|0\rangle - \cos(3\pi/8)|1\rangle$$

one can positively correlate the eight following couples: **0** with  $v^+$  and  $w^-$ , **x**<sup>+</sup> with  $v^+$  and  $w^+$ , **1** with  $v^-$  and  $w^+$ , **x**<sup>-</sup> with  $v^-$  and  $w^-$ :

$$Pr(0v^+) = \frac{1}{2}|\langle 0v^+ | (|00\rangle + |11\rangle)|^2 = \frac{1}{2}\cos^2(\pi/8) > Pr(0)Pr(v^+) = \frac{1}{4}$$

The same result is found for the other seven couples. Their sum is greater than 3:

$$4\cos^2(\pi/8) \approx 3.414$$

Bell understood that such a result, predicted by quantum physics and empirically verifiable, is incompatible with the principle of separability of reality.

Since we have:

$$\frac{1}{\sqrt{2}}(|00\rangle + |11\rangle) = \frac{1}{\sqrt{2}}(|v^+v^+\rangle + |v^-v^-\rangle) = \frac{1}{\sqrt{2}}(|w^+w^+\rangle + |w^-w^-\rangle),$$

if Alice measured on the first qubit the states  $|v^+\rangle$  and  $|v^-\rangle$ , she could deduce Bob's results from hers, if he measured too the states  $|v^+\rangle$  and  $|v^-\rangle$  on the second qubit. The same holds for  $|w^+\rangle$  and  $|w^-\rangle$ . According to Einstein's criterion, there should therefore be elements of reality which determine Bob's results. As the roles of Alice and Bob are symmetrical, there should also be elements of reality that determine Alice's results. We should therefore be able to distribute the experiments into sixteen groups which correspond to the sixteen possible combinations of elements of reality. If the experiment is well done, these sixteen groups should always occur with the same probabilities. We can not measure these probabilities because quantum physics forbids measuring the four elements **0** or **1**, **x**<sup>+</sup> or **x**<sup>-</sup>, **v**<sup>+</sup> or **v**<sup>-</sup>, and **w**<sup>+</sup> or **w**<sup>-</sup>, of a combination. But if we accept Einstein's reasoning based on the postulate of separability, we must accept the existence of these sixteen probabilities.

The eight measurable probabilities of correlated couples can be considered as the expectation values of eight random variables. For example  $\Pr(0v^+)$  is the expectation value of the variable which equals 1 if  $0v^+$  is observed and zero otherwise. The sum of these eight variables is also a random variable whose expectation value is the sum of the eight expectation values of the summed variables. It is possible to verify on each of the sixteen combinations that this sum is always less than or equal to three. For example, it is three for the combination  $0x^+v^+w^+$ . Hence its expectation value is necessarily less than or equal to three. The principle of separability thus contradicts the quantum prediction which has been confirmed empirically.

## Co-presence without possible encounter

Is it possible to be in the same place without being able to meet?

Let two beings A and B be able to interact when they are nearby.  $|0\rangle_A$  and  $|0\rangle_B$  are states of A and B when they are in a place 0,  $|1\rangle_A$  and  $|1\rangle_B$  for another place 1. It is assumed that if they are in different places, they can not interact. So we have :

$$U|0\rangle_A|1\rangle_B = |0\rangle_A|1\rangle_B$$

$$U|1\rangle_A|0\rangle_B = |1\rangle_A|0\rangle_B$$

If they are initially in the entangled state  $\frac{1}{\sqrt{2}}(|0\rangle_A|1\rangle_B + |1\rangle_A|0\rangle_B)$ , then they will not interact with each other.

Proof :  $U[\frac{1}{\sqrt{2}}(|0\rangle_A|1\rangle_B + |1\rangle_A|0\rangle_B)] = \frac{1}{\sqrt{2}}(U|0\rangle_A|1\rangle_B + U|1\rangle_A|0\rangle_B) = \frac{1}{\sqrt{2}}(|0\rangle_A|1\rangle_B + |1\rangle_A|0\rangle_B)$ . End of proof.

However, there is a probability  $\frac{1}{2}$  to find A in the place 0, similarly for B. They are therefore both present in the place 0, at least partially, but they can not meet. Similarly for the place 1.

For example Alice and Bob have agreed to an appointment, but for security reasons they have not defined the place in advance. They use an entangled pair, assumed in the state  $\frac{1}{\sqrt{2}}(|0\rangle_a|0\rangle_b + |1\rangle_a|1\rangle_b)$ . Just before the rendezvous, each must observe his or her part of the pair and decide accordingly the place where they will meet. But unbeknownst to Alice and Bob, Charles is jealous and replaced the pair with another,  $\frac{1}{\sqrt{2}}(|0\rangle_a|1\rangle_b + |1\rangle_a|0\rangle_b)$ . Then Alice and Bob will go to their rendezvous without being able to meet there while being both present.

## Entangled space-time

Parts of a quantum system are generally conceived as material beings, particles, atoms, molecules, or larger objects. But at a more fundamental level, it seems that elementary particles and their compounds should be considered as forms of excitation of space, or of the quantum vacuum. The parts of the system are then conceived as regions of space. The state space of the whole space is the tensor product of the state spaces of the regions in which it has been decomposed. The state vector of the universe thus describes the entanglement between all regions of space (Wallace 2012). But it describes the multiple destinies of all beings in the universe. Most of these destinies are separated and can never meet, while they occur in the same space and sometimes in the same places. This poses a difficulty of principle: why say of two destinies that they pass by the same place if they can not meet there?

This makes sense because even if A and B can not meet in a certain place when they both pass through it, they can still meet each a third being C present in this place. C will never meet A and B at the same time, only one or the other, but not both. The initial destiny of C will bifurcate into two destinies, one where he meets A, the other B.

Everett's thesis is sometimes stated in a way that seems a little absurd: at each observation the universe of the observer would separate into several independent universes that would each correspond to a possible result. We then conceive the evolution of the universe as a tree in which each branch can be divided into several branches which can then be divided, and so on. This image of the tree is sometimes useful (cf. chapter 6) but it incorrectly suggests that there would be several spaces and several times, several branches of the flow of time and several spaces where they flow. Everett's thesis does not say anything like that. It takes quantum physics as it is, without adding any hypothesis. It therefore admits that there is a single space-time. It only notes that quantum physics attributes to material beings not one but many destinies which are all entangled in the same space-time.

## Action, reaction and no cloning

During the CNOT interaction it seems that the control qubit acts on the target qubit but not the reverse. This appearance is false. If the initial state of the control qubit is  $\alpha|0\rangle + \beta|1\rangle$ , the final state after the measurement is:

$$CNOT(\alpha|0\rangle + \beta|1\rangle) = \alpha|00\rangle + \beta|11\rangle$$

When  $\alpha$  and  $\beta$  are both nonzero, the control qubit does not remain in its initial state. It gets entangled with the target qubit.

In fact, there is a hidden symmetry in the CNOT quantum gate. With an appropriate change of basis, the first qubit becomes the target and the second the control (Nielsen & Chuang 2010): Let  $|x^+\rangle = \frac{1}{\sqrt{2}}(|0\rangle + |1\rangle)$  and  $|x^-\rangle = \frac{1}{\sqrt{2}}(|0\rangle - |1\rangle)$  be two new basis vectors (the names  $x^+$  and  $x^-$  come from the spin 1/2 theory). In this new basis, the *CNOT* operator is determined by:

$$CNOT|x^+x^+\rangle = |x^+x^+\rangle$$

$$CNOT|x^-x^+\rangle = |x^-x^+\rangle$$

$$CNOT|x^+x^-\rangle = |x^-x^-\rangle$$

$$CNOT|x^-x^-\rangle = |x^+x^-\rangle$$

The calculation is very simple. For example :

$$CNOT|x^+x^-\rangle = CNOT[\frac{1}{2}(|0\rangle + |1\rangle)(|0\rangle - |1\rangle)]$$

$$= CNOT[\frac{1}{2}(|00\rangle - |01\rangle + |10\rangle - |11\rangle)]$$

$$= \frac{1}{2}(|00\rangle - |01\rangle + |11\rangle - |10\rangle)$$

$$= \frac{1}{2}(|0\rangle - |1\rangle)(|0\rangle - |1\rangle) = |x^-x^-\rangle$$

A classical CNOT gate copies the information carried by the control bit to the target bit. It is a cloning of information. At first glance it seems that a quantum gate CNOT does the same thing with qubits. But this appearance is false. The quantum information carried by the control qubit is not copied to the target qubit. The cloning of quantum information is actually forbidden by quantum principles (Dieks 1982, Wootters & Zurek 1982). For quantum cloning, there should be an interaction U such that:

$$U|\phi\rangle|ready\rangle = |\phi\rangle|\phi\rangle$$

for all states  $|\phi\rangle$  of the cloned system. In particular, for two orthogonal states  $|\phi_1\rangle$  and  $|\phi_2\rangle$ :

$$U|\phi_1\rangle|ready\rangle = |\phi_1\rangle|\phi_1\rangle$$

$$U|\phi_2\rangle|ready\rangle = |\phi_2\rangle|\phi_2\rangle$$

But we do not have  $U(|\phi_1\rangle + |\phi_2\rangle)|ready\rangle = (|\phi_1\rangle + |\phi_2\rangle)(|\phi_1\rangle + |\phi_2\rangle)$  because the interaction is necessarily entangling:

$$U(|\phi_1\rangle + |\phi_2\rangle)|ready\rangle = |\phi_1\rangle|\phi_1\rangle + |\phi_2\rangle|\phi_2\rangle$$

Entanglement is responsible for the impossibility of quantum cloning.

## The ideal measurement of entangled states

If we observe separately the parts of an entangled system, we necessarily destroy their entanglement, since we are led to attribute to each a determinate state. How then can we observe entangled states without destroying them?

We want to make an ideal measurement whose eigenstates are the Bell states of a two-qubit system AB.

Two observer qubits C and D are used to measure the Bell states of the first two qubits A and B.

A first measurement method involves an interaction of A and B as follows (Kaye & Laflamme 2007):

$$U_1|00\rangle = |\alpha^+0\rangle$$

$$U_1|01\rangle = |\alpha^+1\rangle$$

$$U_1|10\rangle = |\alpha^-1\rangle$$

$$U_1|11\rangle = |\alpha^-0\rangle,$$

$$\text{where } |\alpha^+\rangle = \frac{1}{\sqrt{2}}(|0\rangle + |1\rangle) \text{ et } |\alpha^-\rangle = \frac{1}{\sqrt{2}}(|0\rangle - |1\rangle)$$

$U_1$  consists of operating the CNOT gate on AB and then the Hadamard H gate on A:

$$U_1 = H_A CNOT_{AB}$$

$U_1$  destroys the entanglement of the Bell states:

$$U_1|\beta_{00}\rangle = |00\rangle$$

$$U_1|\beta_{01}\rangle = |01\rangle$$

$$U_1|\beta_{10}\rangle = |10\rangle$$

$$U_1|\beta_{11}\rangle = |11\rangle$$

Then C and D measure the states  $|0\rangle$  and  $|1\rangle$  of A and B:

$$U_2 = CNOT_{AC}CNOT_{BD}$$

More explicitly:

$$U_2|0000\rangle = |0000\rangle$$

$$U_2|0100\rangle = |0101\rangle$$

$$U_2|1000\rangle = |1010\rangle$$

$$U_2|1100\rangle = |1111\rangle$$

The evolution  $U_1$  followed by  $U_2$  therefore gives for the Bell states of AB:

$$U_2U_1|\beta_{00}\rangle|00\rangle = |0000\rangle$$

$$U_2U_1|\beta_{01}\rangle|00\rangle = |0101\rangle$$

$$U_2U_1|\beta_{10}\rangle|00\rangle = |1010\rangle$$

$$U_2U_1|\beta_{11}\rangle|00\rangle = |1111\rangle$$

This is not yet an ideal measurement, because A and B have been disturbed. For them to return to their initial state, it is necessary to operate  $U_1^{-1} = CNOT_{AB}^{-1}H_A^{-1} = CNOT_{AB}H_A$  because CNOT and H are their own inverses.

The complete ideal measurement is therefore defined by:

$$U = U_1^{-1}U_2U_1 = CNOT_{AB}H_ACNOT_{AC}CNOT_{BD}H_ACNOT_{AB}$$

$$U|\beta_{00}\rangle|00\rangle = |\beta_{00}\rangle|00\rangle$$

$$U|\beta_{01}\rangle|00\rangle = |\beta_{01}\rangle|01\rangle$$

$$U|\beta_{10}\rangle|00\rangle = |\beta_{10}\rangle|10\rangle$$

$$U|\beta_{11}\rangle|00\rangle = |\beta_{11}\rangle|11\rangle$$

It is actually an ideal measurement of the Bell states of AB.

This method of measurement requires that A and B interact to be disentangled (if they are initially entangled), then they are measured separately, then they interact once more to get entangled again. If A and B are distant and can not interact directly, is it still possible to make an ideal measurement of their entangled states?

The following measurement process produces such a result. First, C is used to measure successively A and B with a CNOT interaction:

$$V_1 = CNOT_{BC}CNOT_{AC}$$

D is then used to measure A and B with an interaction W which measures the states  $|x^+\rangle$  and  $|x^-\rangle$ :

$$W|x^+0\rangle = |x^+0\rangle$$

$$W|x^+1\rangle = |x^+1\rangle$$

$$W|x^-0\rangle = |x^-1\rangle$$

$$W|x^-1\rangle = |x^-0\rangle$$

The measurement of A and B by D is defined by:

$$V_2 = W_{BD}W_{AD}$$

One can verify (the calculation is simple but a little tedious) that one gets an ideal measurement of the Bell states. Explicitly:

$$V|\beta_{00}\rangle|00\rangle = |\beta_{00}\rangle|00\rangle$$

$$V|\beta_{01}\rangle|00\rangle = |\beta_{01}\rangle|10\rangle$$

$$V|\beta_{10}\rangle|00\rangle = |\beta_{10}\rangle|01\rangle$$

$$V|\beta_{11}\rangle|00\rangle = |\beta_{11}\rangle|11\rangle$$

$$\text{where } V = V_2 V_1 = W_{BD}W_{AD}CNOT_{BC}CNOT_{AC}$$

So we have :

$$V = SWAP_{CD}U$$

## Why does not the measurement of entangled states enable us to observe our other destinies?

If I observe, by a CNOT measurement, a qubit prepared in the state  $\frac{1}{\sqrt{2}}(|0\rangle + |1\rangle)$ , the observation leads to the state

vector  $\frac{1}{\sqrt{2}}(|00\rangle + |11\rangle)$  where the second qubit registers the result of the measurement.  $\frac{1}{\sqrt{2}}(|00\rangle + |11\rangle)$  can be

interpreted as a superposition of two destinies, one where I get the result **0**, the other where I get the result **1**. If we take seriously quantum physics these destinies both exist. The observation of the qubit makes my destiny bifurcate into two separate destinies, but I know of only one. Is it possible, however, to verify the existence of this other destiny? If it exists, we would like to see it. Can we, as in *Fringe*, make a television that shows us other destinies?

It seems that the ideal measurement of entangled states enables us to observe these other destinies. After observing the first qubit, I place myself and it in front of a measuring device which detects our state of entanglement. In order to be sure that such an experiment (observation of a qubit prepared in the state  $\frac{1}{\sqrt{2}}(|0\rangle + |1\rangle)$  and ideal measurement of our entangled state) always puts us into an entangled state, I repeat it many times. If the entanglement measuring device informs me each time that we are in the expected entangled state, I shall have confirmation that other destinies

exist.

There is, however, one problem. When I make an observation, I am able to memorize it. So there is a part of me that keeps this information. At least it takes a qubit which remains in the same state. But the ideal measurement of the entanglement of the two qubits can disturb them. An ideal measurement does not disrupt the observed system only if it is in an eigenstate of the measurement.

Suppose that the observed qubit is initially in the state  $|0\rangle$ , this observation leads to the state vector  $|00\rangle$ . There is only one measurement result and therefore no bifurcation in several destinies. Since this state is not entangled, it is not an eigenstate of the ideal measurement of entangled states. If I place myself in front of a device that performs such a measurement, I will be disturbed. My qubit which recorded the first observation will not be able to retain its information. The proposed protocol, intended to verify the existence of another destiny, can not therefore function if I have properly memorized the result of my first observation.

This shows that we can not observe a destiny in which we have memorized observations different from those we have memorized in this destiny.

The apparent collapse of the state vector is enough to prove that we can not observe the other destinies, since after an observation everything happens as if the undetected components of the state vector no longer exist: they can no longer have effect on subsequent observations. The above reasoning clarifies this conclusion. It is the memorization of the results of observation which prevents us from observing destinies in which we have obtained other results.

An observer can not observe her other destinies, but we will show further (experiments of the "Schrödinger's cat" type) that her multiple destinies are in principle observable by a second observer. We can not observe our other destinies, but we can indirectly prove that they exist, since it is in principle possible to observe that another observer has several destinies.

## Reduced density operators

A reduced density operator represents the maximum information about a part of a system as long as the state of the remainder is ignored.

When the state  $|\psi\rangle$  of a system AB is given as a Schmidt decomposition:

$$|\psi\rangle = \sum_i \sqrt{p_i} |a_i\rangle |b_i\rangle$$

where the  $|a_i\rangle$  are orthonormal vectors, as well as the  $|b_i\rangle$ , the reduced density operators of  $|\psi\rangle\langle\psi|$  are :

$$\rho_A = \sum_i p_i |a_i\rangle\langle a_i|$$

and

$$\rho_B = \sum_i p_i |b_i\rangle\langle b_i|$$

In general, the reduced density operators are obtained by assigning to the basis states of a part of a system probabilities equal to their weight in the state of the system:

If AB is in the state  $\sum_{ij} \alpha_{ij} |a_i\rangle|b_j\rangle$  then :

$$\rho_A = \sum_i (\sum_j |\alpha_{ij}|^2) |a_i\rangle\langle a_i|$$

and

$$\rho_B = \sum_j (\sum_i |\alpha_{ij}|^2) |b_j\rangle\langle b_j|$$

$\rho_A$  is sufficient to determine all the probabilities of the observation results on A alone, when it is separated from B. We can therefore consider that it represents the mixed state of A .

The reduced density operators can be defined with the partial trace operation:

$$\rho_A = Tr_B(\rho_{AB})$$

and

$$\rho_B = Tr_A(\rho_{AB})$$

where  $Tr_X(O)$  is the partial trace on  $X$  of an operator  $O$ .

It can be defined as follows:

$$\text{Let be } O = \sum_{ijkl} O_{ijkl} |a_i\rangle|b_j\rangle\langle a_k|\langle b_l|$$

where the  $|a_i\rangle$  are a basis of the state space of A, and the  $|b_i\rangle$  a basis of the state space of B, then:

$$Tr_A(O) = \sum_{jlm} O_{mjml} |b_j\rangle\langle b_l|$$

and

$$Tr_B(O) = \sum_{ikm} O_{imkm} |a_i\rangle\langle a_k|$$

In particular :

$$Tr_A(O_A \otimes O_B) = Tr(O_A)O_B$$

and

$$Tr_B(O_A \otimes O_B) = Tr(O_B)O_A$$

If a  $\rho_{AB}$  density operator is separable ( $\rho_{AB} = \rho_A \otimes \rho_B$ ) then  $\rho_A$  and  $\rho_B$  are its reduced density operators.

Whether separable or not,  $\rho_{AB}$  is always sufficient to determine the reduced operators  $\rho_A$  and  $\rho_B$ . It can be concluded that the state of AB is sufficient to determine the states of A and B. With reduced density operators the states of the parts can be determined from the state of the whole. But this is not enough to make the mystery of entanglement

disappear, because if it represents an entangled state,  $\rho_{AB}$  is not determined by  $\rho_A$  and  $\rho_B$ .

For example, if  $|\psi\rangle = \frac{1}{\sqrt{2}}(|0\rangle_A|0\rangle_B + |1\rangle_A|1\rangle_B)$  then:

$$\rho_A = \frac{1}{2}(|0\rangle_A\langle 0|_A + |1\rangle_A\langle 1|_A)$$

and

$$\rho_B = \frac{1}{2}(|0\rangle_B\langle 0|_B + |1\rangle_B\langle 1|_B)$$

But  $|\psi\rangle\langle\psi|$  is entangled while  $\rho_A \otimes \rho_B$  is separable.

## Relative density operators

Let  $\rho_{AB}$  be the density operator of the system AB.

Let  $\rho'_B$  be any given density operator of B:

$$\rho'_B = \sum_i p_i |b_i\rangle\langle b_i|$$

The state  $\rho'_A$  of A relative to the state  $\rho'_B$  of B when AB is in the state  $\rho_{AB}$  is defined by:

$$\rho'_A = \sum_i p_i |a_i\rangle\langle a_i|$$

where the  $|a_i\rangle$  are the states of A relative to the states  $|b_i\rangle$  of B.

We can then define the relative states, generally mixed, of any part of the Universe with respect to any pure or mixed state of any other.

Let A and B be two parts of the Universe and E their environment. The state of the Universe is a density operator  $\rho_{ABE}$ . We can then define the state  $\rho'_{AE}$  of AE relative to any state  $\rho'_B$  of B. By partial trace one obtains then the state  $\rho'_A$  of A relative to the state  $\rho'_B$  of B:

$$\rho'_A = Tr_E(\rho'_{AE})$$

## Why do not entangled pairs enable us to communicate?

Let A and B be two parts of an AB system. It is assumed that they have interacted in the past and that AB is now in an entangled state where they are very far from each other. If we observe only one of the parts, and if we reason on the reduction of the state vector as if it were a real effect, we conclude that there should be an instantaneous action at a distance from the observed part on the unobserved one, because the state of B after the measurement is different from its previous state. It is then surprising that this effect, supposed to be real, does not enable us to communicate instantaneously at a distance. If there was really action, there should be a possibility of communication.

In general, whether the action is instantaneous or delayed, the entangled pairs never enable us to communicate in the way suggested by the reduction of the state vector. From this point of view quantum physics is not distinguished from classical physics. For there to be communication, or transport of information, there must be an action or an interaction

which travels at the speed of light or at a lower speed. When a distant part of an entangled pair is observed, there is no interaction with the unobserved part. No measurable effect of the former on the latter can be detected.

Formally, this lack of communication between parts results in the invariance of the reduced density operator of the unobserved part at the end of the observation. The unobserved part does not change its state, it is not disturbed by the observation of the other part. It is understood that the non-perturbed state is a mixed state. A reduced density operator determines all the probabilities of the measurements performed on a part (see 2.8) as long as there is no information on the results of the measurements performed on the other parts. As an observation does not change the reduced density operators of unobserved parts, it can have no measurable effect on them.

## Decoherence through entanglement

When a system is in a pure state, a superposition such as  $\sum_i \alpha_i |i\rangle$  is said to be coherent. It's almost a pleonasm. A true quantum superposition is always coherent. But a mixture of states  $|i\rangle$  with probabilities  $p_i$  is sometimes incorrectly called an incoherent superposition.

The formalism of density operators specifies this difference. The density operator of a coherent superposition is:

$$(\sum_i \alpha_i |i\rangle)(\sum_i \alpha_i^* \langle i|) = \sum_{ij} \alpha_i \alpha_j^* |i\rangle \langle j| \text{ while for an incoherent superposition it is:}$$

$$\sum_i p_i |i\rangle \langle i|$$

The non-diagonal elements  $\alpha_i \alpha_j^*$  of the density matrix of a coherent superposition thus make all the difference with an incoherent superposition. They are sometimes called the coherences of this density matrix.  $\alpha_i \alpha_j^*$  is the coherence between the states  $|i\rangle$  and  $|j\rangle$ .

When a measurement is ideal, the eigenstates of the measurement are not disturbed by the observation. On the other hand, any coherent superposition of eigenstates associated with distinct eigenvalues is disrupted: Let a system initially in the state  $\sum_i \alpha_i |i\rangle_S$ , where it has been assumed that the measurement results each have a single eigenstate, in order to simplify the writings. After the observation it is entangled with the measuring apparatus, because the final state of the global system is  $\sum_i \alpha_i |i\rangle_S |i\rangle_A$ .

After the measurement, the state of the observed system can be considered a mixture of the states associated with all the possible results. For an ideal measurement, we already know, with the Born rule, the density operator which represents this mixture, but it is worth doing the calculation in detail to compare it with interactions more general than ideal measurements:

$$\begin{aligned} \rho_S^f &= Tr_A[(\sum_i \alpha_i |i\rangle_S |i\rangle_A)(\sum_i \alpha_i^* \langle i|_S \langle i|_A)] = Tr_A(\sum_{ij} \alpha_i \alpha_j^* |i\rangle_S |i\rangle_A \langle j|_S \langle j|_A) \\ &= \sum_{ij} \alpha_i \alpha_j^* Tr_A(|i\rangle_S |i\rangle_A \langle j|_S \langle j|_A) = \sum_{ij} \alpha_i \alpha_j^* |i\rangle_S \langle j|_S Tr(|i\rangle_A \langle j|_A) \\ &= \sum_i \alpha_i \alpha_i^* |i\rangle_S \langle i|_S \end{aligned}$$

where the last equality comes from the fact that the  $|i\rangle_A$  are orthonormal.

Since the non-diagonal elements of the density matrix have disappeared, the coherence of the initial superposition has been destroyed. This effect of disturbance by measurement is called decoherence (Zurek 2003). In the particular case of an ideal measurement, the coherence of the superpositions of eigenstates associated with distinct results is completely destroyed by the measurement. Their decoherence is complete. On the other hand, the coherence of the superpositions of eigenstates associated with the same result is not destroyed by an ideal measurement. The subspaces of such eigenstates are free of decoherence.

If a system remains isolated, without interactions with its environment, there is no decoherence, because the evolution of an isolated system is unitary:

$$U\left(\sum_i \alpha_i |i\rangle\right) = \sum_i \alpha_i U|i\rangle$$

It follows that the coherences  $\alpha_i \alpha_j^*$  are conserved quantities, in the following sense: if a system is isolated the coherence between the final states  $U|i\rangle$  and  $U|j\rangle$  is equal to the coherence between the initial states  $|i\rangle$  and  $|j\rangle$ .

If a system S is disturbed by an environment E, the coherences are no longer necessarily conserved. They depend on the entanglement of S with its environment. It is sometimes believed that interactions or disturbances are sufficient to cause decoherence, but this is not entirely true. The SWAP gate for example is an interaction without entanglement. If the two qubits which interact with SWAP are in pure states, they remain in pure states. There is no loss of coherence, because there is no entanglement. Decoherence is measured by the degree of entanglement with the environment.

Let S be a system subject to the influence of an environment E. Let us consider two orthogonal states  $|j\rangle_S$  and  $|k\rangle_S$  of S. What is the degree of coherence  $|C_{jk}|^2$  between these two states?

The  $|i\rangle_S$  is an orthonormal basis of S which contains  $|j\rangle_S$  and  $|k\rangle_S$ . The  $|l\rangle_E$  are any orthonormal basis of E. Any pure state of the system SE can then be determined by:

$$|\psi\rangle = \sum_{il} \alpha_{il} |i\rangle_S |l\rangle_E = \sum_i |i\rangle_S \sum_l \alpha_{il} |l\rangle_E = \sum_i |i\rangle_S |\phi(i)\rangle_E$$

$$\text{where } |\phi(i)\rangle_E = \sum_l \alpha_{il} |l\rangle_E$$

The reduced density operator of S is:

$$\rho_S = Tr_E(|\psi\rangle\langle\psi|) = Tr_E\left(\sum_{ill'} \alpha_{il} \alpha_{i'l'}^* |i\rangle_S |l\rangle_E \langle i'|_S \langle l'|_E\right)$$

$$= \sum_{ill'} \alpha_{il} \alpha_{i'l'}^* |i\rangle_S \langle i'|_S$$

$$\text{We can deduce : } C_{jk} = \sum_l \alpha_{jl} \alpha_{kl}^* = \langle \phi(j) |_E \phi(k) \rangle_E$$

$|C_{jk}|^2$  is therefore equal to  $|\langle \phi(j) |_E \phi(k) \rangle_E|^2$ . It is a measure of the quantum resemblance between  $|\phi(j)\rangle_E$  et  $|\phi(k)\rangle_E$ . The more  $|\phi(j)\rangle_E$  and  $|\phi(k)\rangle_E$  are different, the more the coherence between  $|j\rangle_S$  and  $|k\rangle_S$  is decreased by the influence of the environment. If  $|\phi(j)\rangle_E$  is orthogonal to  $|\phi(k)\rangle_E$  the decoherence between  $|j\rangle_S$  et  $|k\rangle_S$  is complete and the entanglement between S et E is maximal. If  $|\phi(j)\rangle_E$  is equal to  $|\phi(k)\rangle_E$  the coherence between  $|j\rangle_S$  and  $|k\rangle_S$  is maximal and there is no entanglement between S and E for these two states of S. Entanglement is actually responsible

for decoherence.

## The Feynman Rules

When a system is not in an eigenstate of an ideal measurement, observation produces an entangled state between the observed system and the measuring apparatus:

$$U\left(\sum_i \alpha_i |i\rangle_S\right)|\text{ready}\rangle_A = \sum_i \alpha_i |i\rangle_S|i\rangle_A$$

where it has been assumed that the  $i$  results have only one eigenstate  $|i\rangle_S$  to simplify the writings.

The reduced density operator which represents the mixed state of the system observed after the measurement is therefore:

$$\sum_i |\alpha_i|^2 |i\rangle_S \langle i|_S$$

We conclude that an observation makes the observed system pass from a pure state to a mixed state when it is not an eigenstate of the measurement.

This explains the Feynman Rules for calculating probabilities in quantum physics (Feynman 1966):

Let a system which passes from an initial state  $a$  to a final state  $b$  via intermediate states  $i$ .

If the intermediate states  $i$  are not observed, we must sum the probability amplitudes  $[A(a \rightarrow i)A(i \rightarrow b)]$  of all paths  $a \rightarrow i \rightarrow b$  and then take the squared modulus of this sum to find the probability that the system will go from  $a$  to  $b$ :

$$Pr(a \rightarrow b) = \left| \sum_i A(a \rightarrow i)A(i \rightarrow b) \right|^2$$

If the intermediate states  $i$  are observed, we must sum the probabilities  $[Pr(a \rightarrow i)Pr(i \rightarrow b)]$  of all paths  $a \rightarrow i \rightarrow b$  to find the probability that the system will go from  $a$  to  $b$ :

$$Pr(a \rightarrow b) = \sum_i Pr(a \rightarrow i)Pr(i \rightarrow b)$$

$$\text{where } Pr(x \rightarrow y) = |A(x \rightarrow y)|^2$$

The first rule is typical of quantum physics. It results from the postulate of unitary evolution. The second rule is a classical rule of addition of probabilities. It results from decoherence through observation. When intermediate states  $i$  are observed, the observed system is represented by a mixture of states. The classical rule of addition of probabilities must then be applied. Entanglement by observation thus explains Feynman's second rule.

## The a posteriori reconstitution of interference patterns

The a posteriori reconstitution of interference patterns illustrates in a striking way the relativity, in the Everett sense, of the observed states with respect to the observer:

In a Mach-Zehnder interferometer, an observer qubit is placed on one of the photon trajectories. The evolution of the system can then be described by the operator:

$$H_1 CNOT_{12} H_1 |00\rangle = \frac{1}{2}(|00\rangle + |10\rangle + |01\rangle - |11\rangle)$$

$$= \frac{1}{2}[(|0\rangle + |1\rangle)|0\rangle + (|0\rangle - |1\rangle)|1\rangle] = |\psi\rangle$$

where the first qubit represents the photon and the second, the observer.

The reduced density operator of the photon at the output of the second beam splitter is:

$$\frac{1}{2}(|0\rangle\langle 0| + |1\rangle\langle 1|)$$

The photon therefore has a probability 1/2 of being absorbed by each of the detectors. The observation of the path followed by the photon thus destroyed the effect of interference between the two paths.

Then we apply the Hadamard gate to the observer qubit:

$$H_2|\psi\rangle = \frac{1}{2\sqrt{2}}[(|0\rangle + |1\rangle)(|0\rangle + |1\rangle) + (|0\rangle - |1\rangle)(|0\rangle - |1\rangle)]$$

$$= \frac{1}{\sqrt{2}}(|00\rangle + |11\rangle)$$

The relative states of the first qubit with respect to the second are therefore  $|0\rangle$  with respect to  $|0\rangle$  and  $|1\rangle$  with respect to  $|1\rangle$ . If we observe the second qubit, we can deduce the state of the first qubit. In this way it is possible to reconstruct an interference pattern by linking the observations of the two qubits. Such a reconstruction can be made even if the second qubit is observed long after the first.

It is sometimes said that the interference patterns are destroyed because of the disturbance by the probes placed on the followed paths. This is not entirely accurate since these patterns can be reconstructed after these disturbances have occurred. The probes do not necessarily destroy the interference patterns, but only the conditions of their observation. The entanglement of the object observed with the probes changes these conditions because the observed states are always states relative, in the sense of Everett, to the observer.

## The fragility of non-localized macroscopic states

A single photon is enough to destroy a non-localized macroscopic state, because of the decoherence through entanglement.

Suppose for example, a non-localized macroscopic state  $\frac{1}{\sqrt{2}}(|1\rangle_M + |2\rangle_M)$  and an incident photon in the state  $|0\rangle_p$ .

The photon may or may not be localized.

Suppose it is initially located near  $|1\rangle_M$ . After the interaction, the following state is obtained:

$$\frac{1}{\sqrt{2}}(|1\rangle_p|1'\rangle_M + |0\rangle_p|2\rangle_M)$$

$M$  being macroscopic, its localized state  $|1\rangle_M$  is very little affected by the impact of the photon.  $|1'\rangle_M$  is almost equal to  $|1\rangle_M$ , in the sense that their scalar product is not very different from 1. But this does not prevent the destruction of the non-localized state, because  $|1\rangle_p$  is in general very different from  $|0\rangle_p$ . If  $\langle 0_p | 1 \rangle_p$  is zero, the decoherence between the

states  $|1\rangle_M$  et  $|2\rangle_M$  is complete. The non-localized state is thus completely destroyed, because of the entanglement with a single photon.

If the photon is not initially localized, the interaction leads to the following state:

$$\frac{1}{\sqrt{2}}(|1\rangle_p|1'\rangle_M + |2\rangle_p|2'\rangle_M)$$

$|1\rangle_p$  is usually very different from  $|2\rangle_p$ . Again, if  $\langle 2_p|1\rangle_p$  is equal to zero, the decoherence is complete.

As long as the macroscopic objects are not in an ultra-cold vacuum, they are permanently impacted by very many particles, photons and molecules of the ambient air. It might be that only one of these particles is not sufficient to cause a complete decoherence of a non-localized state, if  $\langle 2_p|1\rangle_p$  is not close enough to zero. But a small number of incident particles is always sufficient for the decoherence to be complete. The decoherence of non-localized macroscopic states is therefore a very powerful and very rapid effect. It is almost impossible to escape. The larger the objects, the more sensitive they are to this destruction of their non-localized states. Microscopic beings, on the other hand, particles and small molecules, are much less sensitive because they can propagate over great distances without interacting, or with very little interacting, with other particles or molecules.

Even in an ultra-cold vacuum, non-localized macroscopic states undergo a very rapid decoherence if they are not ultra-cold themselves, because they emit photons with which they are entangled.

Non-localized macroscopic states are very fragile, because generally, macroscopic objects can not be isolated, or not very well, and because their non-localized states are destroyed by the entanglement with the environment. Localized macroscopic states are not as fragile, because the interactions are always local. Everything happens as if the macroscopic objects were permanently observed by their environment. Since the interactions are local, the localized states can be eigenstates of this observation. If it was an ideal measurement, they would not be disturbed. The locality of interactions selects the localized states among all the states of a macroscopic object because they are the most robust, the less disturbed by their environment (Joos, Zeh & ... 2003, Zurek 2003, Schlosshauer 2007).

## Experiments of the "Schrödinger's cat" type

Quantum principles do not prohibit the observation of quantum superpositions of macroscopic states. They only predict that such observations are very difficult, because it is necessary to isolate the observed system to protect it from decoherence by its environment.

Schrödinger invented an unfortunately rather sinister thought experiment to illustrate the very counterintuitive character of the principle of quantum superposition, which he helped to discover, since this principle necessarily accompanies his famous equation. A cat is enclosed in a box equipped with a diabolical device: a radioactive atom is coupled to a vial of poison which will only spread if the atom decays. It is assumed that the half-life of the atom is one hour and that at the beginning of the experiment it has been verified that the atom has not disintegrated. The experiment consists in leaving the cat enclosed for an hour and then opening the box (Schrödinger 1935).

If the box is completely isolated from its environment, this experiment can be described with a unitary operator on a system of a qubit and a qutrit. The qubit represents the atom, which can be in the state  $|0\rangle$  if it has disintegrated, and  $|1\rangle$  otherwise. The qutrit represents all the rest of the box: the disintegrating product, if present, the poison vial, the cat and the box itself.  $|\text{alive}_0\rangle$  is the state of the box and its contents, except the atom, at the beginning of the experiment when the cat is alive,  $|\text{alive}\rangle$ , the state of the box and its contents except the atom at the end of the experiment if the cat

is alive,  $|dead\rangle$ , if it is dead. The experiment is then described by:

$$U|1, alive_0\rangle = \frac{1}{\sqrt{2}}(|1, alive\rangle + |0, dead\rangle)$$

The state of the system at the end of the experiment is therefore an entangled state between the atom, the cat and the rest of the box, where the cat is simultaneously dead and alive.

Any experiment which prepare and observe a state such as  $\frac{1}{\sqrt{2}}(|alive\rangle + |dead\rangle)$  for a macroscopic system is called an experiment of the "Schrödinger's cat" type. Obviously it is not necessary to kill a cat.

Schrödinger's original experiment does not prepare the state  $\frac{1}{\sqrt{2}}(|alive\rangle + |dead\rangle)$  of the cat, but only an entangled state between the cat and its environment. In order to prepare the state  $\frac{1}{\sqrt{2}}(|alive\rangle + |dead\rangle)$ , one should completely isolate the cat from its environment and put the diabolic device in its belly. But a living being can not survive in ultracold vacuum, so it can never be in a state like  $\frac{1}{\sqrt{2}}(|alive\rangle + |dead\rangle)$ .

Schrödinger's thought experiment shows that in principle nothing prevents the application of the principle of quantum superposition to a macroscopic system, provided that it can be perfectly isolated.

An experiment of the "Schrödinger cat" type has never yet been realized with a truly macroscopic system, because we do not know how to isolate them sufficiently from their environment. On the other hand, it can be realized in various ways with mesoscopic objects, small systems of particles, atoms or molecules.

The excitation modes of an electromagnetic cavity are the quantum states of the photons which it contains. Haroche and his collaborators are able to manufacture a cavity where they can prepare, manipulate and observe quite freely the quantum states they imagine. Cavity states are prepared and observed using giant atoms which function as microscopic probes. They have thus realized a "Schrödinger's cat" type experiment with an ultra-cold cavity containing several photons.

Some quantum states of the electromagnetic field resemble very much classical states, especially if they contain on average many photons. They are called Glauber states.

A mode of the electromagnetic field is mathematically similar to a harmonic oscillator, because the field oscillates periodically like any other oscillator. In quantum physics the accessible energies of a harmonic oscillator are quantified. They correspond to the number of photons excited in a mode of an electromagnetic cavity. When the energy of an oscillator is very large with respect to the energy difference between two successive states, it is possible to construct quantum states which resemble very much the classical states of an oscillator. They can have precisely defined position and momentum. These are the Glauber states. They are not states with a definite number of photons, the Fock states, which are purely quantum, which have no equivalent in classical physics, even if they contain a very large number of photons. Glauber states are also called "coherent states".

A Glauber state can be prepared simply by briefly coupling the initially empty cavity to a conventional source of electromagnetic radiation. One can arrange for the giant atom to disrupt the field in the cavity by causing a phase shift of the Glauber state, as if an oscillator had been moved without changing its energy, much as if the atom had given a shot on the field. According to its initial state  $|g\rangle$  or  $|e\rangle$ , the atom causes a phase shift in opposite directions (Haroche &

Raimond 2006, pp.377- 378). The interaction between the atom and the cavity is described by:

$$U|g\rangle|G_0\rangle = |g\rangle|G_\phi\rangle$$

$$U|e\rangle|G_0\rangle = e^{-i\phi}|e\rangle|G_{-\phi}\rangle$$

where  $|G_0\rangle$  is the initial Glauber state and  $|G_\phi\rangle$  the Glauber state obtained by a phase shift of  $\phi$ .

If the atom is prepared in the state  $\frac{1}{\sqrt{2}}(|g\rangle + |e\rangle)$  one obtains thus :

$$U\frac{1}{\sqrt{2}}(|g\rangle + |e\rangle)|G_0\rangle = \frac{1}{\sqrt{2}}(|g\rangle|G_\phi\rangle + e^{-i\phi}|e\rangle|G_{-\phi}\rangle)$$

Since the conditions of the experiment enable to reach values of  $\phi$  greater than a radian, the state obtained can be considered as a state of the "Schrödinger's cat" type for the system atom + field. In order to prepare the state  $\frac{1}{\sqrt{2}}(|G_\phi\rangle + |G_{-\phi}\rangle)$  of the cavity, it is sufficient to put the atom initially in the state  $\frac{1}{\sqrt{2}}(|g\rangle + |e\rangle)$  and then observe it

at the output of the cavity in one of the states  $\frac{1}{\sqrt{2}}(|g\rangle + e^{-i\phi}|e\rangle)$  or  $\frac{1}{\sqrt{2}}(|g\rangle - e^{-i\phi}|e\rangle)$ .

If, for example, it has been observed at output in the state  $\frac{1}{\sqrt{2}}(|g\rangle + e^{-i\phi}|e\rangle)$

the state of the cavity relative to the observation is:

$$\frac{1}{\sqrt{2}}(|G_\phi\rangle + |G_{-\phi}\rangle)$$

since

$$\begin{aligned} U\frac{1}{\sqrt{2}}(|g\rangle + |e\rangle)|G_0\rangle &= \frac{1}{\sqrt{2}}(|g\rangle|G_\phi\rangle + e^{-i\phi}|e\rangle|G_{-\phi}\rangle) \\ &= \frac{1}{2\sqrt{2}}[(|g\rangle + e^{-i\phi}|e\rangle)(|G_\phi\rangle + |G_{-\phi}\rangle) + (|g\rangle - e^{-i\phi}|e\rangle)(|G_\phi\rangle - |G_{-\phi}\rangle)] \end{aligned}$$

In order to verify that the desired "Schrödinger's cat" state has been properly prepared, the observation system uses homodyne detection (Haroche & Raimond 2006, pp.374-375).

By proceeding this way Haroche and his collaborators have prepared many "Schrödinger's cat" states and they have observed their fragility. They were able to verify empirically the theory of decoherence through entanglement with the environment. The tiny perturbations by the ultracold and very well isolated cavity are sufficient to destroy very quickly the "cat of Schrödinger" states even if they contain a small number of photons.

The following thought experiment, modeled on the previous one, shows how to prepare and observe a non-localized macroscopic state of a mirror. Experimenting poses great difficulties, because the mirror must be perfectly isolated from its environment. Any interaction between the mirror and its environment can destroy the non-localized state that one wishes to observe.

We assume that a state  $|1\rangle_m$  of a mirror is in unstable equilibrium. If it is struck by a photon in the  $|1\rangle_p$  state, it falls into the  $|0\rangle_m$  state, while the reflected photon passes into the state  $|2\rangle_p$ . If the mirror is initially in the state  $|0\rangle_m$ , it

does not affect the photon. The following measurement process is thus obtained:

$$U|1\rangle_m|1\rangle_p = |0\rangle_m|2\rangle_p$$

$$U|0\rangle_m|1\rangle_p = |0\rangle_m|1\rangle_p$$

To prepare the non-localized macroscopic state  $\frac{1}{\sqrt{2}}(|0\rangle_m + |1\rangle_m)$  we make use of a photon prepared (by means of a beam splitter for example) in a state  $\frac{1}{\sqrt{2}}(|0\rangle_p + |1\rangle_p)$  where  $|0\rangle_p$  is a state in which the photon does not interact with the mirror. Having prepared the mirror in the state  $|1\rangle_m$  we get:

$$\begin{aligned} U \frac{1}{\sqrt{2}}|1\rangle_m(|0\rangle_p + |1\rangle_p) &= \frac{1}{\sqrt{2}}(|1\rangle_m|0\rangle_p + |0\rangle_m|2\rangle_p) \\ &= \frac{1}{2}[(|0\rangle_m + |1\rangle_m)(|0\rangle_p + |2\rangle_p) + (|0\rangle_m - |1\rangle_m)(|2\rangle_p - |0\rangle_p)] \end{aligned}$$

If the photon is then detected (with a beam splitter followed by a photodetector) in the state  $\frac{1}{\sqrt{2}}(|0\rangle_p + |2\rangle_p)$ , we have prepared the state  $\frac{1}{\sqrt{2}}(|0\rangle_m + |1\rangle_m)$  of the mirror. With this non-localized macroscopic state and a new photon in the state  $|1\rangle_p$  we get:

$$U \frac{1}{\sqrt{2}}(|0\rangle_m + |1\rangle_m)|1\rangle_p = \frac{1}{\sqrt{2}}|0\rangle_m(|1\rangle_p + |2\rangle_p)$$

If the experiment is repeated many times with a detector capable of detecting the photon in the state  $\frac{1}{\sqrt{2}}(|1\rangle_p + |2\rangle_p)$ , this will always be detected. It can be concluded that the non-localized state of the mirror was observed.

This example is mainly theoretical. Experimenting poses great difficulties, because the mirror must be perfectly isolated from its environment. Any interaction between the mirror and its environment can destroy the non-localized state that one wishes to observe.

Experiments of the "Schrödinger's cat" type are therefore in principle feasible. It is possible in principle to observe superpositions of different macroscopic states.

### **Is the existence theorem of multiple destinies empirically verifiable?**

In the experiment imagined above, the mirror in unstable equilibrium can be considered as an observation system, designed to detect and record the presence of a photon. This experiment makes it possible to verify the existence of the multiple destinies of an observation system. We deduce that the existence theorem of multiple destinies is empirically verifiable. But this surprising conclusion is accompanied by severe restrictions.

The observer system must be completely isolated from its environment, so in ultracold ultrahigh vacuum. If such isolation is not perfect, decoherence by the environment is enough to destroy the state of superposition of destinies whose existence one wishes to verify. We can imagine chambers capable of perfectly isolating a living being, but it is practically infeasible. Even the isolation of very small systems, much less sensitive to their environment, is usually very difficult.

Another fundamental reason prevents us from observing the multiple destinies of a living being. For a superposition of two observational results to be observable, these results must be recorded in a reversible way, so that they can be "forgotten" by the observer system. In the above experiment, the final state  $|0\rangle_m$  of the mirror did not keep track of previous states  $|0\rangle_m$  and  $|1\rangle_m$  by which it has simultaneously passed. This is general. For a state  $|\psi_0\rangle$  to be observable, we need a detector and an initial state  $|0\rangle_d$  such that  $|\psi_0\rangle|0\rangle_d$  lead to  $|\psi_1\rangle|1\rangle_d$ , where  $|1\rangle_d$  is the state of the detector when it detected  $|\psi_0\rangle$ , and  $|\psi_1\rangle$  is the final state of the observed system. If  $|\psi_0\rangle$  is a superposition of observation results,  $\frac{1}{\sqrt{2}}(|a\rangle + |b\rangle)$  for example, the results obtained  $a$  and  $b$  can not both be stored in the state  $|\psi_1\rangle$ . At least one

of the two results, and perhaps both, has been cleared.  
recorded, the superposition of different destinies is not observable. As the destinies of living beings are successions of processes and irreversible observations, their superpositions are not observable. The existence of the multiple destinies of living beings is therefore not empirically verifiable, because of the irreversibility of living processes.

---



## Observation of Measurement-Induced Entanglement and Quantum Trajectories of Remote Superconducting Qubits

N. Roch,<sup>1,\*</sup> M. E. Schwartz,<sup>1</sup> F. Motzoi,<sup>2</sup> C. Macklin,<sup>1</sup> R. Vijay,<sup>3</sup> A. W. Eddins,<sup>1</sup> A. N. Korotkov,<sup>4</sup> K. B. Whaley,<sup>2</sup> M. Sarovar,<sup>5</sup> and I. Siddiqi<sup>1</sup>

<sup>1</sup>Quantum Nanoelectronics Laboratory, Department of Physics, University of California, Berkeley, California 94720, USA

<sup>2</sup>Department of Chemistry, University of California, Berkeley, California 94720, USA

<sup>3</sup>Department of Condensed Matter Physics and Materials Science, Tata Institute of Fundamental Research, Mumbai 400005, India

<sup>4</sup>Department of Electrical Engineering, University of California, Riverside, California 92521, USA

<sup>5</sup>Scalable and Secure Systems Research (08961), Sandia National Laboratories, Livermore, California 94550, USA

(Received 8 February 2014; published 28 April 2014)

The creation of a quantum network requires the distribution of coherent information across macroscopic distances. We demonstrate the entanglement of two superconducting qubits, separated by more than a meter of coaxial cable, by designing a joint measurement that probabilistically projects onto an entangled state. By using a continuous measurement scheme, we are further able to observe single quantum trajectories of the joint two-qubit state, confirming the validity of the quantum Bayesian formalism for a cascaded system. Our results allow us to resolve the dynamics of continuous projection onto the entangled manifold, in quantitative agreement with theory.

DOI: 10.1103/PhysRevLett.112.170501

PACS numbers: 03.67.Bg, 42.50.Dv, 42.50.Lc, 85.25.Dq

Entanglement—the property that binds two independent objects into a single, highly correlated, nonseparable system—is a hallmark of quantum theory. Entanglement schemes for superconducting qubits have traditionally relied on direct qubit-qubit coupling [1,2], cavity-mediated interactions [3], photon-mediated interactions [4], or autonomous cooling [5]. Measurement, in contrast, has traditionally been viewed as a means to restore classical behavior: a quantum system, once observed, is projected onto a single measurement basis state. However, in certain cases, it is possible to design [6–11] a measurement that projects onto an entangled state, thereby purifying, rather than destroying, quantum correlations. Such a measurement has recently been used to entangle two superconducting qubits coupled to the same microwave resonator [12].

Measurement-induced entanglement is a particularly important resource in spatially separated quantum systems, for which no local interactions and therefore no direct methods of creating entanglement exist. Such remote entanglement has been demonstrated using optical photons in several atomic systems [13–15] and nitrogen vacancy centers [16], but has remained elusive for superconducting qubits, which operate in the microwave regime. In this Letter, we demonstrate measurement-induced entanglement between two superconducting qubits, each dispersively [17] coupled to a separate cavity for readout and separated by 1.3 meters of ordinary coaxial cable, by engineering a continuous measurement for which one of the three outcomes is a Bell state [18]. Unlike previous experiments in spatially separated quantum systems, in which the detection of individual spontaneous fluorescence events reveals whether or not entanglement has been

generated, we employ time-continuous measurements [19]. This allows us to access the ensemble-averaged dynamics of entanglement generation, which are well described by a statistical model and by a full master-equation treatment. Furthermore, our measurement efficiency is sufficiently high to resolve the individual quantum trajectories in the ensemble [20], thus enabling the observation of the stochastic evolution of a joint two-qubit state under measurement. This functionality sheds new light on the fundamental interplay between entanglement, measurement, and decoherence in a quantum network.

Our experimental apparatus consists of two superconducting transmon qubits placed in spatially separated copper waveguide cavities (three-dimensional transmon architecture) [21]. Each cavity is wound with a superconducting bias coil to enable tuning of the qubit frequency. A weakly coupled port is used for transmission measurements and single qubit control, and a strongly coupled port enables qubit state readout. The strongly coupled ports of the two cavities are connected via two microwave circulators and 1.3 meters of coaxial cable to enable directional transfer of information from cavity 1 to cavity 2 [Fig. 1(a)]. The entire apparatus is contained within an absorptive shield and a Cryoperm magnetic shield to suppress spurious radiation and noise. Qubit and cavity parameters are described in detail in the supplemental information [22].

A joint qubit state measurement can be performed by sequentially driving the cavities in reflection with a near-resonant microwave tone at frequency  $\omega_m$  that can be described by a classical complex amplitude  $\alpha_{in}$ . For a single qubit measured in reflection, the output state is given by  $\alpha_{out} = r^\pm \alpha_{in}$ , where the reflection coefficient  $r^\pm$  is given by

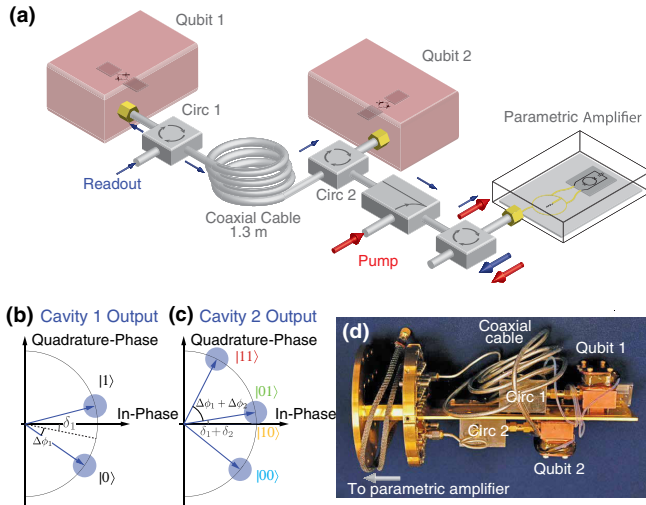


FIG. 1 (color online). Experimental setup. (a) Simplified representation of the experimental setup. (b) and (c) Schematic of the phase shift acquired by a coherent state sequentially measuring first qubit 1 (b) and then qubit 2 (c) in reflection. (d) Picture of the base-temperature setup.

$$r^\pm = \frac{\kappa - 2i(\omega_r - \omega_m \pm \chi)}{\kappa + 2i(\omega_r - \omega_m \pm \chi)}, \quad (1)$$

and the signifier + (−) represents the single qubit state  $|0\rangle$  ( $|1\rangle$ ) [22]. Here,  $\omega_r$  is the bare cavity frequency;  $\kappa$  is the cavity decay rate, and  $\chi$  is the dispersive shift. The measurement tone acquires a qubit state-dependent phase shift  $\phi^\pm = \text{Arg}[\alpha_{\text{out}}^\pm]$ . For the following analysis, it is convenient to define the average and relative phase shifts,  $\delta = (1/2)(\phi^+ + \phi^-)$  and  $\Delta\phi = (1/2)(\phi^+ - \phi^-)$ , respectively [see Fig. 1(b)]. For a sequential reflective measurement of two qubits, the output coherent state becomes  $\alpha_{\text{out}} = \sqrt{\eta_{\text{loss}}} r_1^\pm r_2^\pm \alpha_{\text{in}}$ , where  $\eta_{\text{loss}} \approx 0.81$  represents the efficiency of power transfer between the two cavities. In the general case,  $\Delta\phi_1 \neq \Delta\phi_2$  and the phase shifts corresponding to the four basis states  $|00\rangle$ ,  $|01\rangle$ ,  $|10\rangle$ , and  $|11\rangle$  are all distinct; the associated measurement decoheres any quantum superposition of states and projects the system into one of the four basis states. However, if we carefully engineer the cavities and the dispersive coupling [22], there exists  $\omega_m$  such that  $\Delta\phi_1 = \Delta\phi_2$ . In this situation, the phase shifts associated with states  $|01\rangle$  and  $|10\rangle$  are identical and equal to  $\delta_1 + \delta_2$ ; the measurement therefore cannot decohere a quantum superposition of  $|01\rangle$  and  $|10\rangle$  [shown schematically in Fig. 1(c)]. We use a superconducting parametric amplifier [23] to measure the acquired phase shift, realizing a high-fidelity homodyne measurement characterized by a quantum efficiency  $\eta_{\text{meas}} = 0.4 \pm 0.10$ . Figure 2(a) shows a sample time-domain trace of the homodyne signal

$$V_m(t_m) = \frac{1}{t_m} \int_0^{t_m} V(t) dt, \quad (2)$$

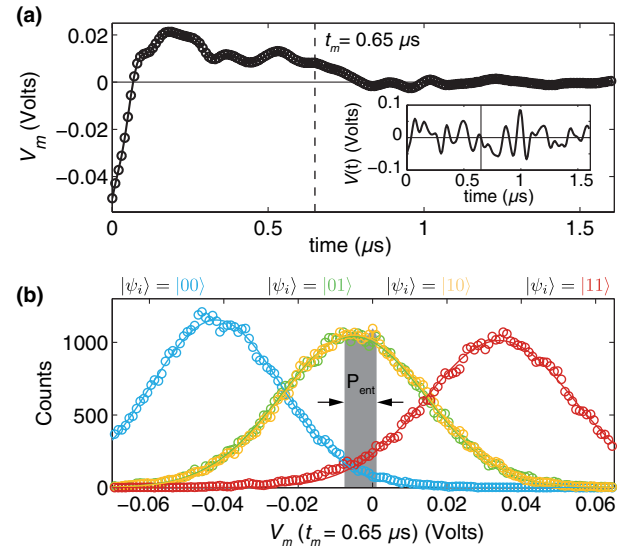


FIG. 2 (color online). Demonstration of indistinguishability between  $|01\rangle$  and  $|10\rangle$  computational states during measurement. (a) Example of the temporal evolution of the measurement signal  $V_m$ . The inset shows the associated instantaneous voltage  $V(t)$ . (b) Histogram of  $V_m$  for each of the four computational states  $|00\rangle$ ,  $|01\rangle$ ,  $|10\rangle$ , and  $|11\rangle$ . The range of data postselected for tomographic reconstruction at  $t_m = 0.65 \mu$ s is represented as a shaded grey area.

where  $V$  is the instantaneous voltage (inset). We verify that our joint readout cannot distinguish between  $|01\rangle$  and  $|10\rangle$  by sequentially preparing and then measuring the four basis states. Figure 2(b) represents histograms of  $V_m$  for a measurement time  $t_m = 0.65 \mu$ s. The states  $|00\rangle$  and  $|11\rangle$  are well separated, while the histograms for  $|01\rangle$  and  $|10\rangle$  are fully overlapping, as desired. This enables us to postselect measurement instances that correspond to occupation of the odd-parity manifold without destroying coherence within that manifold and therefore to probabilistically generate entanglement.

We control the rate of entanglement generation

$$\Gamma_{\text{meas}} = \frac{1}{2} \eta_{\text{meas}} \eta_{\text{loss}} |\alpha_{\text{in}}|^2 \sin(2\Delta\phi)^2 \quad (3)$$

by adjusting the measurement strength via the average intracavity photon number  $\bar{n}_1 = (1/2)(\bar{n}_1^+ + \bar{n}_1^-)$  where for each cavity  $i$  [22]

$$\bar{n}_i^\pm = \frac{\kappa_i}{(\kappa_i/2)^2 + (\omega_i - \omega_m \pm \chi_i)^2} |\alpha_{\text{in}}|^2. \quad (4)$$

A photon number  $\bar{n}_1 = 1.2$  results in  $\Gamma_{\text{meas}}/2\pi \approx 210$  kHz, which sets the characteristic time scale of entanglement generation  $\tau_{\text{meas}} \equiv 1/\Gamma_{\text{meas}} \approx 750$  ns. Thus, the dynamics of the measurement process, which are significantly faster than qubit decay rates, can be readily resolved using conventional digital electronics.

To generate and verify entanglement, we implement a sequence of three readout protocols and two qubit rotations.

We first perform a projective readout ( $\bar{n}_1 = 6.2$  and  $1 \mu\text{s}$  readout length) to postselect the  $|00\rangle$  ground state [24]. We then perform  $R_y^{\pi/2}$  rotations on both qubits to create the equal superposition state  $(1/2)(|00\rangle + |01\rangle + |10\rangle + |11\rangle)$ . The second readout, which is done in the weak regime and with varying  $t_m$ , stochastically steers the system toward  $|00\rangle$ ,  $|11\rangle$ , or the Bell state  $(1/\sqrt{2})(|01\rangle + |10\rangle)$ , as documented in the measurement output  $V_m$ . We then apply one of a set of 30 tomographic rotations immediately followed by a strong readout. We repeat this process 8000 times for each tomographic rotation and for each  $t_m$  to form a single well-averaged data set; we generate an error margin by taking the average and standard deviation of 17 data sets. To produce the density matrix of the postselected entangled state for each time  $t_m$ , we choose an entanglement probability  $p_{\text{ent}}$  to constitute the entangled state based on  $V_m(t_m)$  [shown in the grey shaded region in Fig. 2(b) for  $t_m = 0.65 \mu\text{s}$ ], and tomographically reconstruct the density matrix using a maximum-likelihood estimator [22]. For perfectly separated histograms, 50% of the counts will lie in the odd-parity subspace, but we utilize  $p_{\text{ent}} = 10\%$  to compensate for imperfect measurement efficiency.

The ability to perform time-continuous measurements enables us to directly observe the ensemble dynamics of the emergence of entanglement. Writing the two-qubit density matrix as  $\rho = \sum_{ijkl} \rho_{ij,kl} |ij\rangle \langle kl|$ , we can estimate concurrence [25] using the simplified formula [26]  $C \approx \max(0, |\rho_{01,10}| - \sqrt{\rho_{00,00}\rho_{11,11}})$  to characterize the quality of the entanglement during this process. This simplified formula holds when the only nonnegligible off-diagonal elements are  $\rho_{01,10}$  and its conjugate, which is applicable to our setup since the high distinguishability between  $|00\rangle$ ,

$|11\rangle$  and the  $\{|01\rangle, |10\rangle\}$  manifold results in rapid decay of all other off-diagonal elements. Concurrence ranges from zero (for a separable or mixed state) to one (for a maximally entangled two-qubit state) and is greater than zero for all nonseparable two-qubit states [25]. Maximizing  $C$  requires limiting decoherence within the odd-parity manifold, and minimizing stray counts of  $|00\rangle$  and  $|11\rangle$  by maximizing the signal-to-noise ratio (SNR), defined by the ratio of the separation of the Gaussian histograms [in Fig. 2(b)] to their width, or

$$\text{SNR} \sim 2|\alpha_{\text{in}}| \sin(2\Delta\phi) \sqrt{\eta_{\text{loss}}\eta_{\text{meas}}t_m}. \quad (5)$$

Figure 3 shows the evolution of the concurrence as a function of  $t_m$ . The inset shows the evolution of the relevant density matrix elements (the diagonal elements, representing population probabilities, and the off-diagonal element  $\rho_{01,10}$ , representing the coherence of the odd-parity subspace).

We note three qualitative regimes: SNR-dominated evolution, stabilization, and decay due to decoherence. Since SNR is proportional to  $\sqrt{t_m}$ , it dominates the evolution at short times  $t_m < 0.75\tau_{\text{meas}}$ . Here, the dynamics are governed by changes to population probabilities, i.e., the increase of  $\rho_{01,01}$  and  $\rho_{10,10}$  and the decrease of  $\rho_{00,00}$  and  $\rho_{11,11}$  in the postselected ensemble. The rapid decay of  $\rho_{00,00}$  and  $\rho_{11,11}$  compared to  $\rho_{01,10}$  results in growth of concurrence in this regime. For intermediate times ( $0.75\tau_{\text{meas}} < t_m < 1.25\tau_{\text{meas}}$ ), the SNR improvement rate decreases and decoherence begins to take a more noticeable effect. Decoherence is caused by intrinsic dephasing of the qubits  $\Gamma_{2,i}^* = 1/T_{2,i}^*$  and by  $\eta_{\text{loss}}$ , which contributes an

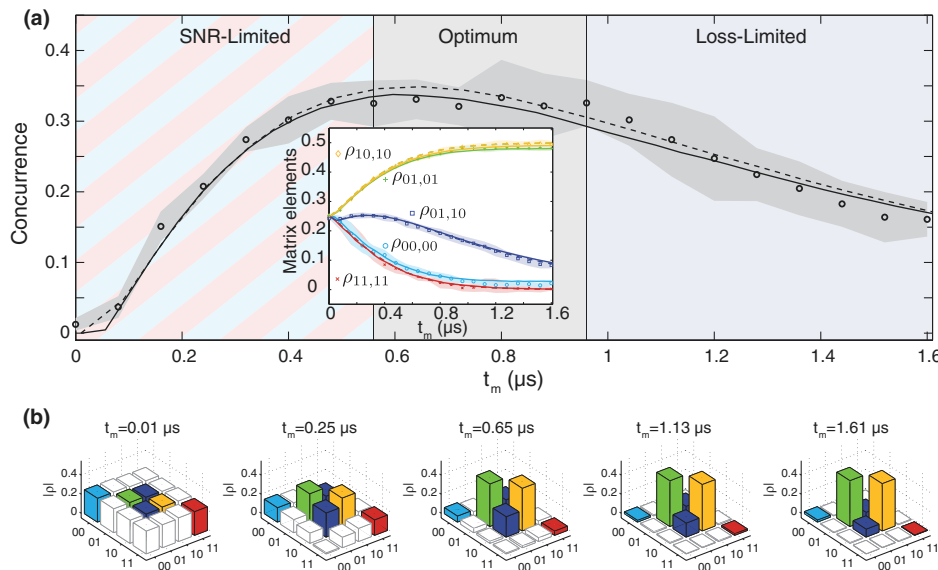


FIG. 3 (color online). Generation and verification of entanglement between two spatially separated superconducting qubits. (a) Concurrence of the entangled state as a function of  $t_m$ . The inset displays the evolution of the basis state populations ( $\rho_{00,00}$ , etc.) and odd-parity coherence ( $\rho_{01,10}$ ). The shaded region represents the standard deviation centered about the average (circles). Dashed lines are theoretical simulations based on a Bayesian approach, and solid lines are calculated using a rigorous master equation; in both cases, no fitting parameters are used [22]. (b) Full-density matrices of the postselected entangled subspace for increasing  $t_m$ .

additional measurement-induced dephasing of the first qubit at a rate

$$\Gamma_{\text{loss}} \simeq 2(1 - \eta_{\text{loss}})|\alpha_{\text{in}}|^2 \sin(\Delta\phi)^2. \quad (6)$$

At intermediate times, the SNR improvement rate and  $\Gamma_{\text{loss}}$  are roughly equal, and hence, the concurrence reaches a maximum value of 0.35. This value is comparable to what was obtained recently using optical communications [15,16]; however, thanks to our time-continuous measurement scheme, the rate at which a qubit-qubit-entangled state is created is orders of magnitude higher ( $\Gamma_{\text{creation}}/2\pi = 1 \text{ kHz}$ ). For longer times ( $t_m > 1.25\tau_{\text{meas}}$ ), the density matrix evolution is dominated by decoherence, which eventually drives the system into an incoherent mixture of  $|01\rangle$  and  $|10\rangle$ .

These ensemble dynamics are well described both by a simple statistical model (dashed lines) and by a rigorous master-equation treatment (solid lines) [22]. The models, which account for the chief technical limitations of our scheme (i.e., the inefficiencies  $\eta_{\text{loss}}$ , the losses between the cavities, and  $\eta_{\text{meas}}$ , the finite detection efficiency), indicate that reasonable technical improvements could lead to

concurrence of 70%, which is comparable to recent single-cavity experiments [12].

Our high-efficiency continuous measurement allows us to go one step further in decomposing the dynamics of measurement-induced entanglement: we can directly observe the individual quantum trajectories [20,27] of our two-qubit system, using a Bayesian update process. In this formalism,  $V_m(t)$  contains partial quantum state information that allows us to update our estimate of the instantaneous quantum state of the two-qubit system. To validate the Bayesian update for a single trajectory, we generate a mapping  $V_m \mapsto \rho(V_m)$ : at each time  $t_m$ , we collect all trajectories with similar weak measurement outcomes,  $V(t_m)$ , and perform a conditional tomographic state reconstruction of those trajectories [see Fig. 4(a)]. We then use this mapping to convert the measured voltage  $V_m(t)$  for a *single* experimental realization into  $\rho(t)$  and thus reconstruct the quantum trajectory of the system [20]. Figure 4(b) illustrates three typical trajectories, in which the system is projected onto a Bell state or onto the non-entangled states  $|00\rangle$  or  $|11\rangle$ . We see excellent agreement between the tomographic reconstructions of the trajectories and theoretical predictions based on Bayesian updates and a master equation treatment. The observation of these

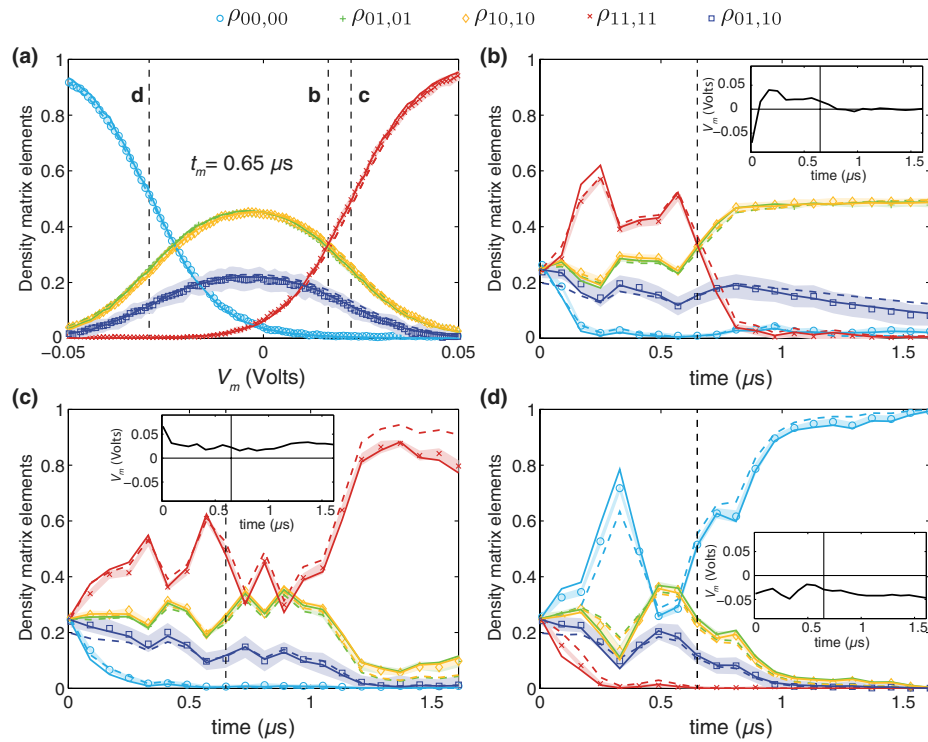


FIG. 4 (color online). Resolving single quantum trajectories for cascaded quantum systems. (a) Absolute value of the density matrix elements conditioned on the measured voltage  $V_m$  for  $t_m = 0.65 \mu\text{s}$  and  $\bar{n}_1 = 1.2$ , presenting an instantaneous mapping  $V_m \mapsto \rho(V_m)$ . The shaded region represents the standard deviation about the average (circles); dashed lines (respectively, solid lines) are theoretical simulations based on a Bayesian approach (respectively, on a full master equation) without fitting parameter [22]. (b)–(d) Examples of reconstructed quantum trajectories for diagonal and principal off-diagonal density matrix elements. The dots represent tomographic reconstruction based on the mapping  $V_m \mapsto \rho(V_m)$  for every  $t_m$ . The dashed lines are Bayesian estimations based on the measured  $V_m(t)$  (insets). The solid lines for the full master equation were obtained by running 100000 instances of the stochastic differential equation with 1-ns resolution and averaging the obtained populations conditioned on  $V_m$  at  $t_m$  [22].

quantum trajectories shows the novelty and strength of our continuous measurement scheme. Our experiment thus demonstrates the validity of quantum trajectory theories for cascaded quantum systems [28,29], which describe the conditioned evolution of distributed quantum systems.

Our experiments demonstrate that quantum entanglement can be established between distant systems that interact only through a coherent signal propagating along low-loss electrical wires, a functionality that will be integral to the realization of complex, distributed quantum networks. We take advantage of the versatility of continuous measurement to monitor the dynamics of entanglement generation and demonstrate quantitative agreement to a theoretical model that captures the experimental details of the physical circuit [22]. Moreover, our characterization of the state of the joint system under continuous measurement suggests the feasibility of future *continuous* feedback stabilization of entanglement [30,31]. Further technical improvements in quantum efficiency, coherence times, and transmission characteristics hold the promise of on-demand, stabilized remote entanglement—a powerful resource for quantum information processing.

N. R. and M. E. S. contributed equally to this work. We thank E. M. Levenson-Falk, K. W. Murch, D. H. Slichter, D. M. Toyli, and S. J. Weber for discussions. This research was supported in part by the U.S. Army Research Office, the Intelligence Advanced Research Projects Activity (IARPA). M. E. S. acknowledges support from the Fannie and John Hertz Foundation. R. V. acknowledges support from the Government of India. A. N. K. acknowledges support from ARO under MURI W911NF-11-1-0268. Sandia National Laboratories is a multiprogram laboratory managed and operated by Sandia Corporation, a wholly owned subsidiary of Lockheed Martin Corporation, for the United States Department of Energy's National Nuclear Security Administration under Contract No. DE-AC04-94AL85000.

\*Present address: CNRS and Université Grenoble Alpes, Institut Néel, 38042 Grenoble, France.

nicolas.roch@neel.cnrs.fr

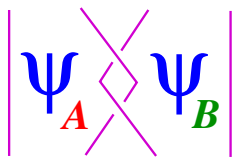
- [1] M. Steffen, M. Ansmann, R. C. Bialczak, N. Katz, E. Lucero, R. McDermott, M. Neeley, E. M. Weig, A. N. Cleland, and J. M. Martinis, *Science* **313**, 1423 (2006).
- [2] A. Dewes, F. R. Ong, V. Schmitt, R. Lauro, N. Boulant, P. Bertet, D. Vion, and D. Esteve, *Phys. Rev. Lett.* **108**, 057002 (2012).
- [3] L. DiCarlo, J. M. Chow, J. M. Gambetta, L. S. Bishop, B. R. Johnson, D. I. Schuster, J. Majer, A. Blais, L. Frunzio, S. M. Girvin, and R. J. Schoelkopf, *Nature (London)* **460**, 240 (2009).
- [4] A. F. van Loo, A. Fedorov, K. Lalumiére, B. C. Sanders, A. Blais, and A. Wallraff, *Science* **342**, 1494 (2013).
- [5] S. Shankar, M. Hatridge, Z. Leghtas, K. M. Sliwa, A. Narla, U. Vool, S. M. Girvin, L. Frunzio, M. Mirrahimi, and M. H. Devoret, *Nature (London)* **504**, 419 (2013).
- [6] R. Ruskov and A. N. Korotkov, *Phys. Rev. B* **67**, 241305 (2003).
- [7] H.-A. Engel and D. Loss, *Science* **309**, 586 (2005).
- [8] B. Trauzettel, A. N. Jordan, C. W. J. Beenakker, and M. Büttiker, *Phys. Rev. B* **73**, 235331 (2006).
- [9] C. L. Hutchison, J. M. Gambetta, A. Blais, and F. K. Wilhelm, *Can. J. Phys.* **87**, 225 (2009).
- [10] K. Lalumiére, J. M. Gambetta, and A. Blais, *Phys. Rev. A* **81**, 040301 (2010).
- [11] F. Helmer and F. Marquardt, *Phys. Rev. A* **79**, 052328 (2009).
- [12] D. Risté, M. Dukalski, C. A. Watson, G. de Lange, M. J. Tiggelman, Y. M. Blanter, K. W. Lehnert, R. N. Schouten, and L. DiCarlo, *Nature (London)* **502**, 350 (2013).
- [13] C. W. Chou, H. de Riedmatten, D. Felinto, S. V. Polyakov, S. J. van Enk, and H. J. Kimble, *Nature (London)* **438**, 828 (2005).
- [14] J. Hofmann, M. Krug, N. Ortegel, L. Gérard, M. Weber, W. Rosenfeld, and H. Weinfurter, *Science* **337**, 72 (2012).
- [15] D. L. Moehring, P. Maunz, S. Olmschenk, K. C. Younge, D. N. Matsukevich, L.-M. Duan, and C. Monroe, *Nature (London)* **449**, 68 (2007).
- [16] H. Bernien, B. Hensen, W. Pfaff, G. Koolstra, M. S. Blok, L. Robledo, T. H. Taminiau, M. Markham, D. J. Twitchen, L. Childress, and R. Hanson, *Nature (London)* **497**, 86 (2013).
- [17] A. Wallraff, D. I. Schuster, A. Blais, L. Frunzio, J. Majer, M. Devoret, S. M. Girvin, and R. J. Schoelkopf, *Phys. Rev. Lett.* **95**, 060501 (2005).
- [18] J. Kerckhoff, L. Bouts, A. Silberfarb, and H. Mabuchi, *Phys. Rev. A* **79** (2009).
- [19] M. Hatridge, S. Shankar, M. Mirrahimi, F. Schackert, K. Geerlings, T. Brecht, K. M. Sliwa, B. Abdo, L. Frunzio, S. M. Girvin, R. J. Schoelkopf, and M. H. Devoret, *Science* **339**, 178 (2013).
- [20] K. W. Murch, S. J. Weber, C. Macklin, and I. Siddiqi, *Nature (London)* **502**, 211 (2013).
- [21] H. Paik, D. I. Schuster, L. S. Bishop, G. Kirchmair, G. Catelani, A. P. Sears, B. R. Johnson, M. J. Reagor, L. Frunzio, L. I. Glazman, S. M. Girvin, M. H. Devoret, and R. J. Schoelkopf, *Phys. Rev. Lett.* **107**, 240501 (2011).
- [22] See Supplemental Material at <http://link.aps.org-supplemental/10.1103/PhysRevLett.112.170501> for further information on the theoretical modeling and experimental details.
- [23] M. Hatridge, R. Vijay, D. H. Slichter, J. Clarke, and I. Siddiqi, *Phys. Rev. B* **83**, 134501 (2011).
- [24] J. E. Johnson, C. Macklin, D. H. Slichter, R. Vijay, E. B. Weingarten, J. Clarke, and I. Siddiqi, *Phys. Rev. Lett.* **109**, 050506 (2012).
- [25] W. K. Wootters, *Phys. Rev. Lett.* **80**, 2245 (1998).
- [26] L. Jakóbczyk and A. Jamróz, *Phys. Lett. A* **347**, 180 (2005).
- [27] P. Campagne-Ibarcq, E. Flurin, N. Roch, D. Darson, P. Morfin, M. Mirrahimi, M. H. Devoret, F. Mallet, and B. Huard, *Phys. Rev. X* **3**, 021008 (2013).
- [28] H. J. Carmichael, *Phys. Rev. Lett.* **70**, 2273 (1993).
- [29] C. W. Gardiner, *Phys. Rev. Lett.* **70**, 2269 (1993).
- [30] M. Sarovar, H.-S. Goan, T. Spiller, and G. Milburn, *Phys. Rev. A* **72**, 062327 (2005).
- [31] S. G. Hofer, D. V. Vasilyev, M. Aspelmeyer, and K. Hammerer, *Phys. Rev. Lett.* **111**, 170404 (2013).

# Measuring Quantum Entanglement

John Cardy

University of Oxford

Max Born Lecture  
University of Göttingen, December 2012



- Quantum Entanglement is one of the most fascinating and counter-intuitive aspects of Quantum Mechanics
- its existence was first recognised in early work of the pioneers of quantum mechanics<sup>1</sup>
- it is the basis of the celebrated Einstein-Podolsky-Rosen paper<sup>2</sup> which argued that its predictions are incompatible with locality

---

<sup>1</sup>Schrödinger E (1935). "Discussion of probability relations between separated systems". Mathematical Proceedings of the Cambridge Philosophical Society **31** (4): 555-563. Communicated by M Born

<sup>2</sup>Einstein A, Podolsky B, Rosen N (1935). "Can Quantum-Mechanical Description of Physical Reality Be Considered Complete?". Phys. Rev. **47** (10): 777-780.

- this was part of Einstein's programme to refute the probabilistic interpretation of quantum mechanics<sup>171</sup> due to Born and others

*“Die Quantenmechanik ist sehr achtunggebietend. Aber eine innere Stimme sagt mir, daß das noch nicht der wahre Jakob ist. Die Theorie liefert viel, aber dem Geheimnis des Alten bringt sie uns kaum näher. Jedenfalls bin ich überzeugt, daß der Alte nicht würfelt.”<sup>3</sup>*

“Quantum mechanics is certainly impressive. But an inner voice tells me that it is not yet the real thing. The theory tells us a lot, but it does not bring us any closer to the secrets of the ancients. I, at any rate, am convinced that the old fellow does not play dice.”

---

<sup>3</sup>Letter to Max Born, 4 December 1926

- this was part of Einstein's programme to refute the probabilistic interpretation of quantum mechanics<sup>172</sup> due to Born and others

*“Die Quantenmechanik ist sehr achtunggebietend. Aber eine innere Stimme sagt mir, daß das noch nicht der wahre Jakob ist. Die Theorie liefert viel, aber dem Geheimnis des Alten bringt sie uns kaum näher. Jedenfalls bin ich überzeugt, daß der Alte nicht würfelt.”<sup>3</sup>*

“Quantum mechanics is certainly impressive. But an inner voice tells me that it is not yet the real thing. The theory tells us a lot, but it does not bring us any closer to the secrets of the ancients. I, at any rate, am convinced that the old fellow does not play dice.”

- Bell<sup>4</sup> showed that EPR's explanation, involving hidden variables, is inconsistent with the predictions of quantum mechanics – this was subsequently tested experimentally

---

<sup>3</sup>Letter to Max Born, 4 December 1926

- in this talk I am going to assume that conventional quantum mechanics (and the Copenhagen interpretation) holds and will address the questions:
  - what is quantum entanglement and is there a universal measure of the amount of entanglement?
  - how does this behave for systems with many degrees of freedom?
  - how might it be measured experimentally?

# A simple example

174

- a system consisting of two qubits (spin- $\frac{1}{2}$  particles) with a basis of states

$$(|\uparrow\rangle_A, |\downarrow\rangle_A) \times (|\uparrow\rangle_B, |\downarrow\rangle_B)$$

- Alice observes qubit A, Bob observes qubit B
- the state

$$|\Psi\rangle = \frac{1}{\sqrt{2}} (|\uparrow\rangle_A |\uparrow\rangle_B + |\downarrow\rangle_A |\downarrow\rangle_B)$$

is entangled: before Alice measures  $\sigma_A^z$ , Bob can obtain either result  $\sigma_B^z = \pm 1$ , but after she makes the measurement the state in B collapses and Bob can only get one result

- moreover this still holds if the subsystems A and B are far apart (the EPR paradox)

- an entangled state is different from a classically correlated state, eg with density matrix

$$\rho = \frac{1}{2} |\uparrow\rangle_A |\uparrow\rangle_B |A\langle \uparrow | + \frac{1}{2} |\downarrow\rangle_A |\downarrow\rangle_B |A\langle \downarrow |$$

- in both cases

$$\langle \sigma_A^z \sigma_B^z \rangle = 1$$

but for the entangled state

$$\langle \sigma_A^x \sigma_B^x \rangle = 1$$

while it vanishes for the classically correlated state

# Entanglement of pure states

176

- is there a good way of characterising the degree of entanglement (of pure states)?
- Schmidt decomposition theorem: any state in  $\mathcal{H}_A \otimes \mathcal{H}_B$  can be written

$$|\Psi\rangle = \sum_j c_j |\psi_j\rangle_A |\psi_j\rangle_B \quad (\text{S})$$

where the states are orthonormal,  $c_j > 0$ , and  $\sum_j c_j^2 = 1$

- the  $c_j^2$  are the eigenvalues of the reduced density matrix

$$\rho_A = \text{Tr}_B |\Psi\rangle\langle\Psi|$$

- if there is only one term in (S),  $|\Psi\rangle$  is unentangled
- if all the  $c_j$  are equal,  $|\Psi\rangle$  is maximally entangled

- a suitable measure is the entanglement entropy

$$S_A = - \sum_j c_j^2 \log c_j^2 = -\text{Tr}_A \rho_A \log \rho_A = S_B$$

- it is zero for unentangled states and maximal when all the  $c_j$  are equal
- it is convex:  $S_{A_1 \cup A_2} \leq S_{A_1} + S_{A_2}$
- it is basis-independent

- it increases under Local Operations and Classical Communication



- even for many-body systems it is often computable (analytically, or numerically by density matrix renormalization group methods or matrix product states)
- but it is not the only such measure: eg the Rényi entropies

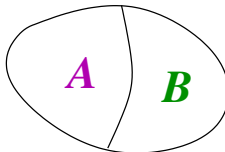
$$S_A^{(n)} \propto -\log \text{Tr}_A \rho_A^n$$

are equally useful, and for different  $n$  give information about the whole entanglement spectrum of  $\rho_A$

- consider a system whose degrees of freedom are extended in space, e.g. a quantum magnet described by the Heisenberg model with hamiltonian

$$H = \sum_{r,r'} J(r - r') \vec{\sigma}(r) \cdot \vec{\sigma}(r')$$

- the temperature is low enough so the system is in the ground state  $|0\rangle$  of  $H$



- suppose  $A$  is a large but finite region of space: what is the degree of entanglement of the spins within  $A$  with the remainder in  $B$ ?
- since  $S_A = S_B$  it can't be  $\propto$  the volume of  $A$  or  $B$
- in fact in almost all cases we have the area law:

$$S_A \sim C \times \text{Area of boundary}$$

where  $D$  is the dimensionality of space. The constant  $C$  is  $\propto 1/(\text{lattice spacing})^{D-1}$  and is non-universal in general.

- entanglement occurs only near the boundary

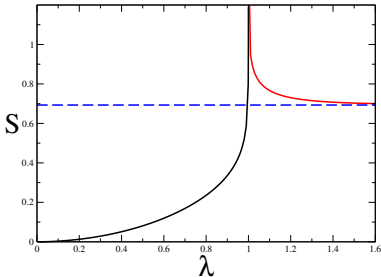
# One dimension

182

- when  $D = 1$  something interesting happens: the constant is proportional to a logarithm

$$S_A \sim C \log(\text{correlation length } \xi)$$

- now the constant  $C$  is dimensionless and *universal*
- at a quantum critical point  $\xi$  diverges and so does the entanglement entropy



- measuring entropy of many-body systems is conceptually difficult: even at finite temperature we do it by integrating the specific heat
- however the situation is better for the Rényi entropies

$$S_{\textcolor{red}{A}}^{(n)} \propto -\log \text{Tr} \rho_{\textcolor{red}{A}}^n = -\log \sum_j c_j^{2n}$$

- to simplify the discussion assume  $n = 2$  and consider two independent identical copies of the whole system, so the composite system is in the state

$$|\Psi\rangle_1 |\Psi\rangle_2 = \sum_{j_1} \sum_{j_2} c_{j_1} c_{j_2} |\psi_{j_1}\rangle_{\textcolor{red}{A}1} |\psi_{j_1}\rangle_{\textcolor{green}{B}1} |\psi_{j_2}\rangle_{\textcolor{red}{A}2} |\psi_{j_2}\rangle_{\textcolor{green}{B}2}$$

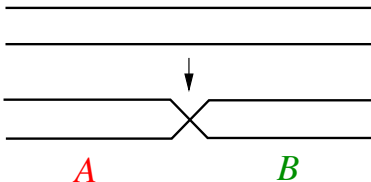
- let  $\mathfrak{S}$  be a ‘swap’ operator which interchanges the states in  $A_1$  with those in  $A_2$  but leaves states in  $B_1$  and  $B_2$  the same:

$$\mathfrak{S} |\psi_{j_1}\rangle_{A1} |\psi_{j_1}\rangle_{B1} |\psi_{j_2}\rangle_{A2} |\psi_{j_2}\rangle_{B2} = |\psi_{j_2}\rangle_{A1} |\psi_{j_1}\rangle_{B1} |\psi_{j_1}\rangle_{A2} |\psi_{j_2}\rangle_{B2}$$

- then

$$\left( {}_1\langle \Psi | {}_2\langle \Psi | \right) \mathfrak{S} \left( |\Psi\rangle_1 |\Psi\rangle_2 \right) = \sum_j c_j^4 = \text{Tr} \rho_A^2$$

- on a system with local interactions,  $\mathfrak{S}$  can be implemented locally as a quantum switch: eg a 1D quantum chain:  
**185**



- initially the two decoupled chains have a hamiltonian  $H = H_1 + H_2$  with a ground state  $|0\rangle = |\Psi\rangle_1|\Psi\rangle_2$
- after the switch, the hamiltonian is  $H' = \mathfrak{S}H\mathfrak{S}^{-1}$ , with a ground state  $|0\rangle' = \mathfrak{S}|0\rangle$  with the same energy
- we need to measure the overlap

$$M = \langle 0|0\rangle' = \text{Tr } \rho_A^2$$

- two proposals for how to do this:

- 5

- prepare the system in ground state  $|0\rangle$  of  $H$
- flip the switch so the new hamiltonian is  $H'$
- the system finds itself in a higher energy state than  $|0\rangle'$  and decays to this eg by emission of quasiparticles
- decay rate  $\propto |M|^2$

- 6

- introduce tunnelling between  $|0\rangle$  and  $|0\rangle'$ , equivalent to adding a term  $\propto \mathfrak{S}$  to the hamiltonian
- the tunnelling amplitude is  $\propto M$
- this can be detected by preparing in one state and observing Rabi oscillations

---

<sup>5</sup>JC, Phys. Rev. Lett. **106**, 150404, 2011

6Abanin DA and Demler E, Phys. Rev. Lett. **109**, 020504, 2012

- entanglement is a fascinating and useful property of quantum mechanics
- entropy is a useful measure of entanglement for characterising many-body ground states (and also in quantum information theory)
- in principle it can be measured in condensed matter or cold atom experiments

- entanglement is a fascinating and useful property of quantum mechanics
- entropy is a useful measure of entanglement for characterising many-body ground states (and also in quantum information theory)
- in principle it can be measured in condensed matter or cold atom experiments
- although the theory tells us a lot *die Alten* still have many secrets!

Article | Published: 02 December 2015

# Measuring entanglement entropy in a quantum many-body system

Rajibul Islam, Ruichao Ma, Philipp M. Preiss, M. Eric Tai, Alexander Lukin, Matthew Rispoli & Markus Greiner

*Nature* 528, 77–83 (03 December 2015) | Download Citation

## Abstract

---

Entanglement is one of the most intriguing features of quantum mechanics. It describes non-local correlations between quantum objects, and is at the heart of quantum information sciences. Entanglement is now being studied in diverse fields ranging from condensed matter to quantum gravity. However, measuring entanglement remains a challenge. This is especially so in systems of interacting delocalized particles, for which a direct experimental measurement of spatial entanglement has been elusive. Here, we measure entanglement in such a system of itinerant particles using quantum interference of many-body twins. Making use of our single-site-resolved control of ultracold bosonic atoms in optical lattices, we prepare two identical copies of a many-body state and interfere them. This enables us to directly measure quantum purity, Rényi entanglement entropy, and mutual information. These experiments pave the way for using entanglement to characterize quantum phases and dynamics of strongly correlated many-body systems.

## References

---

1. Horodecki, R., Horodecki, P., Horodecki, M. & Horodecki, K. Quantum entanglement. *Rev. Mod. Phys.* **81**, 865 (2009)
2. Aspect, A. Bell's inequality test: more ideal than ever. *Nature* **398**, 189–190 (1999)
3. Nielsen, M. A. & Chuang, I. L. *Quantum Computation and Quantum Information* (Cambridge Univ. Press, 2010)
4. Amico, L., Fazio, R., Osterloh, A. & Vedral, V. Entanglement in many-body systems. *Rev. Mod. Phys.* **80**, 517 (2008)
5. Calabrese, P. & Cardy, J. Entanglement entropy and conformal field theory. *J. Phys. A* **42**, 504005 (2009)
6. Nishioka, T., Ryu, S. & Takayanagi, T. Holographic entanglement entropy: an overview. *J. Phys. A* **42**, 504008 (2009)
7. Eisert, J., Cramer, M. & Plenio, M. B. Colloquium: area laws for the entanglement entropy. *Rev. Mod. Phys.* **82**, 277 (2010)

8. Kitaev, A. & Preskill, J. Topological entanglement entropy. *Phys. Rev. Lett.* **96**, 110404 (2006)
9. Levin, M. & Wen, X.-G. Detecting topological order in a ground state wave function. *Phys. Rev. Lett.* **96**, 110405 (2006)
10. Jiang, H.-C., Wang, Z. & Balents, L. Identifying topological order by entanglement entropy. *Nature Phys.* **8**, 902–905 (2012)
11. Zhang, Y., Grover, T. & Vishwanath, A. Entanglement entropy of critical spin liquids. *Phys. Rev. Lett.* **107**, 067202 (2011)
12. Isakov, S. V., Hastings, M. B. & Melko, R. G. Topological entanglement entropy of a Bose–Hubbard spin liquid. *Nature Phys.* **7**, 772–775 (2011)
13. Vidal, G., Latorre, J. I., Rico, E. & Kitaev, A. Entanglement in quantum critical phenomena. *Phys. Rev. Lett.* **90**, 227902 (2003)
14. Bardarson, J. H., Pollmann, F. & Moore, J. E. Unbounded growth of entanglement in models of many-body localization. *Phys. Rev. Lett.* **109**, 017202 (2012)
15. Daley, A. J., Pichler, H., Schachenmayer, J. & Zoller, P. Measuring entanglement growth in quench dynamics of bosons in an optical lattice. *Phys. Rev. Lett.* **109**, 020505 (2012)
16. Schuch, N., Wolf, M. M., Verstraete, F. & Cirac, J. I. Entropy scaling and simulability by matrix product states. *Phys. Rev. Lett.* **100**, 030504 (2008)
17. Bloch, I., Dalibard, J. & Nascimbène, S. Quantum simulations with ultracold quantum gases. *Nature Phys.* **8**, 267–276 (2012)
18. Blatt, R. & Roos, C. F. Quantum simulations with trapped ions. *Nature Phys.* **8**, 277–284 (2012)
19. Aspuru-Guzik, A. & Walther, P. Photonic quantum simulators. *Nature Phys.* **8**, 285–291 (2012)

20. Houck, A. A., Türeci, H. E. & Koch, J. On-chip quantum simulation with superconducting circuits. *Nature Phys.* **8**, 292–299 (2012)
- 
21. Bouwmeester, D., Pan, J.-W., Daniell, M., Weinfurter, H. & Zeilinger, A. Observation of three-photon Greenberger–Horne–Zeilinger entanglement. *Phys. Rev. Lett.* **82**, 1345–1349 (1999)
- 
22. Gühne, O. & Tóth, G. Entanglement detection. *Phys. Rep.* **474**, 1–75 (2009)
- 
23. James, D. F. V., Kwiat, P. G., Munro, W. J. & White, A. G. Measurement of qubits. *Phys. Rev. A* **64**, 052312 (2001)
- 
24. Pan, J.-W. et al. Multiphoton entanglement and interferometry. *Rev. Mod. Phys.* **84**, 777 (2012)
- 
25. Häffner, H. et al. Scalable multiparticle entanglement of trapped ions. *Nature* **438**, 643–646 (2005)
- 
26. Ekert, A. K. et al. Direct estimations of linear and nonlinear functionals of a quantum state. *Phys. Rev. Lett.* **88**, 217901 (2002)
- 
27. Moura Alves, C. & Jaksch, D. Multipartite entanglement detection in bosons. *Phys. Rev. Lett.* **93**, 110501 (2004)
- 
28. Bakr, W. S. et al. Probing the superfluid–to–Mott insulator transition at the single-atom level. *Science* **329**, 547–550 (2010)
- 
29. Brun, T. A. Measuring polynomial functions of states. *Quantum Inform. Comput.* **4**, 401–408 (2004)
- 
30. Bovino, F. A. et al. Direct measurement of nonlinear properties of bipartite quantum states. *Phys. Rev. Lett.* **95**, 240407 (2005)
- 
31. Walborn, S. P., Ribeiro, P. S., Davidovich, L., Mintert, F. & Buchleitner, A. Experimental determination of entanglement with a single measurement. *Nature* **440**, 1022–1024 (2006)

32. Schmid, C. *et al.* Experimental direct observation of mixed state entanglement. *Phys. Rev. Lett.* **101**, 260505 (2008)
- 
33. Horodecki, R. & Horodecki, M. *et al.* Information-theoretic aspects of inseparability of mixed states. *Phys. Rev. A* **54**, 1838 (1996)
- 
34. Mintert, F. & Buchleitner, A. Observable entanglement measure for mixed quantum states. *Phys. Rev. Lett.* **98**, 140505 (2007)
- 
35. Li, H. & Haldane, F. D. M. Entanglement spectrum as a generalization of entanglement entropy: identification of topological order in non-abelian fractional quantum Hall effect states. *Phys. Rev. Lett.* **101**, 010504 (2008)
- 
36. Hong, C. K., Ou, Z. Y. & Mandel, L. Measurement of subpicosecond time intervals between two photons by interference. *Phys. Rev. Lett.* **59**, 2044 (1987)
- 
37. Kaufman, A. M. *et al.* Two-particle quantum interference in tunnel-coupled optical tweezers. *Science* **345**, 306–309 (2014)
- 
38. Lopes, R. *et al.* Atomic Hong–Ou–Mandel experiment. *Nature* **520**, 66–68 (2015)
- 
39. Cramer, M. *et al.* Spatial entanglement of bosons in optical lattices. *Nat. Commun.* **4**, 2161 (2013)
- 
40. Fukuhara, T. *et al.* Spatially resolved detection of a spin-entanglement wave in a Bose–Hubbard chain. *Phys. Rev. Lett.* **115**, 035302 (2015)
- 
41. Bartlett, S. D. & Wiseman, H. M. Entanglement constrained by superselection rules. *Phys. Rev. Lett.* **91**, 097903 (2003)
- 
42. Schuch, N., Verstraete, F. & Cirac, J. I. Nonlocal resources in the presence of superselection rules. *Phys. Rev. Lett.* **92**, 087904 (2004)
- 
43. Palmer, R. N., Moura Alves, C. & Jaksch, D. Detection and characterization of multipartite entanglement in optical lattices. *Phys. Rev. A* **72**, 042335 (2005)

- 
44. Wolf, M. M., Verstraete, F., Hastings, M. B. & Cirac, J. I. Area laws in quantum systems: mutual information and correlations. *Phys. Rev. Lett.* **100**, 070502 (2008)
- 
45. Terhal, B. M., DiVincenzo, D. P. & Leung, D. W. Hiding bits in Bell states. *Phys. Rev. Lett.* **86**, 5807–5810 (2001)
- 
46. Vidal, G. Efficient simulation of one-dimensional quantum many-body systems. *Phys. Rev. Lett.* **93**, 040502 (2004)
- 
47. Trotzky, S. et al. Probing the relaxation towards equilibrium in an isolated strongly correlated one-dimensional Bose gas. *Nature Phys.* **8**, 325–330 (2012)
- 
48. Trotzky, S., Chen, Y.-A., Schnorrberger, U., Cheinet, P. & Bloch, I. Controlling and detecting spin correlations of ultracold atoms in optical lattices. *Phys. Rev. Lett.* **105**, 265303 (2010)
- 
49. Pichler, H., Bonnes, L., Daley, A. J., Läuchli, A. M. & Zoller, P. Thermal versus entanglement entropy: a measurement protocol for fermionic atoms with a quantum gas microscope. *New J. Phys.* **15**, 063003 (2013)
- 
50. Rigol, M., Dunjko, V. & Olshanii, M. Thermalization and its mechanism |for generic isolated quantum systems. *Nature* **452**, 854–858 (2008)
- 
51. Zanardi, P. & Paunković, N. Ground state overlap and quantum phase transitions. *Phys. Rev. E* **74**, 031123 (2006)
- 

## Acknowledgements

---

We thank D. Abanin, J. I. Cirac, M. Cramer, A. Daley, A. DelMaestro, E. Demler, M. Endres, S. Gopalakrishnan, M. Headrick, A. Kaufman, M. Knap, T. Monz, A. Pal, H. Pichler, S. Sachdev, B. Swingle, P. Zoller, and M. Zwierlein for useful discussions. This work was supported by grants from the Gordon and Betty Moore Foundations EPiQS Initiative (grant GBMF3795) , the NSF through the Center for Ultracold Atoms, the Army Research Office with funding

from the DARPA OLE programme and a MURI programme, an Air Force Office of Scientific Research MURI programme, and an NSF Graduate Research Fellowship (to M.R.).

## Author information

---

### Affiliations

*Department of Physics, Harvard University, Cambridge, Massachusetts 02138, USA*

Rajibul Islam, Ruichao Ma, Philipp M. Preiss, M. Eric Tai, Alexander Lukin, Matthew Rispoli & Markus Greiner

## Further reading

---

Entanglement certification from theory to experiment - <https://doi.org/10.1038/s42254-018-0003-5>

Nicolai Friis, Giuseppe Vitagliano [...] Marcus Huber  
*Nature Reviews Physics* (2019)

---

Neural-network quantum state tomography - <https://doi.org/10.1038/s41567-018-0048-5>

Giacomo Torlai, Guglielmo Mazzola [...] Giuseppe Carleo  
*Nature Physics* (2018)

---

Universality in volume-law entanglement of scrambled pure quantum states -  
<https://doi.org/10.1038/s41467-018-03883-9>

Yuya O. Nakagawa, Masataka Watanabe [...] Sho Sugiura  
*Nature Communications* (2018)

---

Engineering of entanglement and spin state transfer via quantum chains of atomic spins at large separations - <https://doi.org/10.1038/s41598-018-32145-3>

Dmitry I. Bazhanov, Ilia N. Sivkov & Valeri S. Stepnyuk  
Scientific Reports (2018)

---

Non-classical correlations in two quantum dots coupled in a coherent resonator field under decoherence - <https://doi.org/10.1007/s11128-018-2052-1>

A.-B. A. Mohamed & A.-S. F. Obada  
*Quantum Information Processing* (2018)

# Measuring entanglement entropy through the interference of quantum many-body twins

Rajibul Islam, Ruichao Ma, Philipp M. Preiss, M. Eric Tai, Alexander Lukin, Matthew Rispoli, Markus Greiner

*Department of Physics, Harvard University, Cambridge, MA 02138, USA*

(Dated: September 4, 2015)

Entanglement is one of the most intriguing features of quantum mechanics. It describes non-local correlations between quantum objects, and is at the heart of quantum information sciences. Entanglement is rapidly gaining prominence in diverse fields ranging from condensed matter to quantum gravity. Despite this generality, measuring entanglement remains challenging. This is especially true in systems of interacting delocalized particles, for which a direct experimental measurement of spatial entanglement has been elusive. Here, we measure entanglement in such a system of itinerant particles using quantum interference of many-body twins. Leveraging our single-site resolved control of ultra-cold bosonic atoms in optical lattices, we prepare and interfere two identical copies of a many-body state. This enables us to directly measure quantum purity, Rényi entanglement entropy, and mutual information. These experiments pave the way for using entanglement to characterize quantum phases and dynamics of strongly-correlated many-body systems.

At the heart of quantum mechanics lies the principle of superposition: a quantum system can be in several states at the same time. Measurement on such a superposition state will exhibit randomness in the outcomes. This quantum randomness is fundamental in nature, unlike classical randomness that arises when the observer has incomplete knowledge or ignores information about the system, as when throwing dice or flipping coins. In a many-body quantum system, quantum superposition between various possible configurations often results in a correlated randomness in the measurement outcomes of different parts of the system. These correlated subsystems are then said to be entangled [1]. The non-local correlations between entangled subsystems prompted Einstein to describe entanglement as ‘spooky action at a distance’ [2], and were shown by Bell to be inconsistent with reasonable local theories of classical hidden variables [3]. Later, it was realized that entanglement could be used as a resource to perform tasks not possible classically, with applications in computation [4, 5], communication [6], and simulating the physics of strongly correlated quantum systems [7].

In few level quantum systems, entangled states have been investigated extensively for studying the foundations of quantum mechanics [8] and as a resource for quantum information applications [5, 9]. Recently, it was realized that the concept of entanglement has broad impact in many areas of quantum many-body physics, ranging from condensed matter [10] to high energy field theory [11] and quantum gravity [12]. In this general context, entanglement is most often quantified by the entropy of entanglement [1] that arises in a subsystem when the information about the remaining system is ignored. This entanglement entropy exhibits qualitatively different behavior than classical entropy and has been used in theoretical physics to probe various properties of the many-body system. In condensed matter physics, for example, the scaling behavior [13] of entanglement entropy allows distinguishing between phases that cannot be characterized by symmetry properties, such as topological states of matter [14–16] and spin liquids [17, 18]. Entanglement entropy can be used to probe quantum criticality [19] and non-equilibrium dynamics [20, 21], and to determine whether efficient numerical techniques for computing many-body physics exist [22]. Despite the growing importance of entanglement in theoreti-

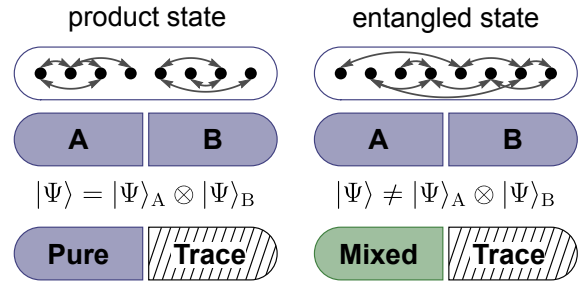


Figure 1. **Bipartite entanglement and partial measurements.** A generic pure quantum many-body state has quantum correlations (shown as arrows) between different parts. If the system is divided into two subsystems A and B, the subsystems will be bipartite entangled with each other when quantum correlations span between them (right column). Only with no bipartite entanglement present, the partitioned system  $|\psi_{AB}\rangle$  can be described as a product of subsystem states  $|\psi_A\rangle$  and  $|\psi_B\rangle$  (left column). A path for measuring the bipartite entanglement emerges from the concept of partial measurements: ignoring all information about subsystem B (indicated as “Trace”) will put subsystem A into a statistical mixture, to a degree given by the amount of bipartite entanglement present. Finding ways of measuring the many-body quantum state purity of the system and comparing that of its subsystems would then enable measurements of entanglement. For an entangled state, the subsystems will have less purity than the full system.

cal physics, current condensed matter experiments do not have a direct probe to detect and measure entanglement. Synthetic quantum systems such as cold atoms [23, 24], photonic networks [25], and some microscopic solid state devices [26] have unique advantages: their almost arbitrary control and detection of single particles, experimental access to relevant dynamical time scales, and isolation from the environment. In these systems, specific entangled states of few qubits, such as the highly entangled Greenberger-Horne-Zeilinger (GHZ) state [27] have been experimentally created and detected using witness operators [28]. However, entanglement witnesses are state specific. An exhaustive method to measure entanglement of an arbitrary state requires reconstructing the quantum state using tomography [29]. This has been accomplished in small

systems of photonic qubits [30] and trapped ion spins [31], but there is no known scheme to perform tomography for systems involving itinerant delocalized particles. With multiple copies of a system, however, one can use quantum many-body interference to quantify entanglement even in itinerant systems [21, 32, 33].

In this work, we take advantage of the precise control and readout afforded by our quantum gas microscope [34] to prepare and interfere two identical copies of a four-site Bose-Hubbard system. This many-body quantum interference enables us to measure quantities that are not directly accessible in a single system, e.g. quadratic functions of the density matrix [21, 32, 33, 35–38]. Such non-linear functions can reveal entanglement [1]. In our system, we directly measure the quantum purity, Rényi entanglement entropy, and mutual information to probe the entanglement in site occupation numbers.

## BIPARTITE ENTANGLEMENT

To detect entanglement in our system, we use a fundamental property of entanglement between two subsystems (bipartite entanglement): ignoring information about one subsystem results in the other becoming a classical mixture of pure quantum states. This classical mixture in a density matrix  $\rho$  can be quantified by measuring the quantum purity, defined as  $\text{Tr}(\rho^2)$ . For a pure quantum state the density matrix is a projector and  $\text{Tr}(\rho^2) = 1$ , whereas for a mixed state  $\text{Tr}(\rho^2) < 1$ . In case of a product state, the subsystems  $A$  and  $B$  of a many-body system  $AB$  described by a wavefunction  $|\psi_{AB}\rangle$  (Fig. 1) are individually pure as well, i.e.  $\text{Tr}(\rho_A^2) = \text{Tr}(\rho_B^2) = \text{Tr}(\rho_{AB}^2) = 1$ . Here the reduced density matrix of  $A$ ,  $\rho_A = \text{Tr}_B(\rho_{AB})$ , where  $\rho_{AB} = |\psi_{AB}\rangle\langle\psi_{AB}|$  is the density matrix of the full system.  $\text{Tr}_B$  indicates tracing over or ignoring all information about the subsystem  $B$ . For an entangled state, the subsystems become less pure compared to the full system as the correlations between  $A$  and  $B$  are ignored in the reduced density matrix,  $\text{Tr}(\rho_A^2) = \text{Tr}(\rho_B^2) < \text{Tr}(\rho_{AB}^2) = 1$ . Even if the many-body state is mixed ( $\text{Tr}(\rho_{AB}^2) < 1$ ), it is still possible to measure entanglement between the subsystems [1]. It is sufficient [39] to prove this entanglement by showing that the subsystems are less pure than the full system, i.e.

$$\begin{aligned} \text{Tr}(\rho_A^2) &< \text{Tr}(\rho_{AB}^2), \\ \text{Tr}(\rho_B^2) &< \text{Tr}(\rho_{AB}^2). \end{aligned} \quad (1)$$

These inequalities provide a powerful tool for detecting entanglement in the presence of experimental imperfections. Furthermore, quantitative bounds on the entanglement present in a mixed many-body state can be obtained from these state purities [40].

Eq.(1) can be framed in terms of entropic quantities [1, 39]. A particularly useful and well studied quantity is the  $n$ -th order Rényi entropy,

$$S_n(A) = \frac{1}{1-n} \log \text{Tr}(\rho_A^n). \quad (2)$$

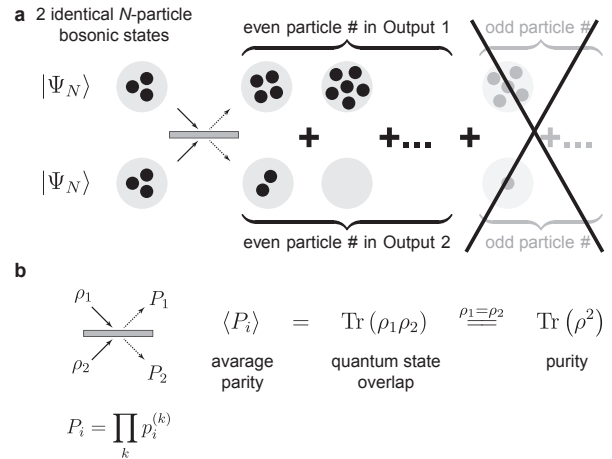


**Figure 2. Measurement of quantum purity with many-body bosonic interference of quantum twins.** **a.** When two  $N$  particle bosonic systems that are in identical pure quantum states are interfered on a 50%-50% beam splitter, they always produce output states with even number of particles in each copy. This is due to the destructive interference of odd outcomes and represents a generalized Hong-Ou-Mandel interference, in which two identical photons always appear in pairs after interfering on a beam splitter. **b.** If the input states  $\rho_1$  and  $\rho_2$  are not perfectly identical or not perfectly pure, the interference contrast is reduced. In this case the expectation value of the parity of particle number  $\langle P_i \rangle$  in output  $i = 1, 2$  measures the quantum state overlap between the two input states. For two identical input states  $\rho_1 = \rho_2$ , the average parity  $\langle P_i \rangle$  therefore directly measures the quantum purity of the states. We only assume that the input states have no relative macroscopic phase relationship.

From Eq. (2), we see that the second-order ( $n = 2$ ) Rényi entropy and purity are related by  $S_2(A) = -\log \text{Tr}(\rho_A^2)$ .  $S_2(A)$  provides a lower bound for the von Neumann entanglement entropy  $S_{VN}(A) = S_1(A) = -\text{Tr}(\rho_A \log \rho_A)$  extensively studied theoretically. The Rényi entropies are rapidly gaining importance in theoretical condensed matter physics, as they can be used to extract information about the “entanglement spectrum” [41] providing more complete information about the quantum state than just the von Neuman entropy. In terms of the second-order Rényi entropy, the sufficient conditions to demonstrate entanglement [1, 39] become  $S_2(A) > S_2(AB)$ , and  $S_2(B) > S_2(AB)$ , i.e. the subsystems have more entropy than the full system. These entropic inequalities are more powerful in detecting certain entangled states than other inequalities like the Clauser-Horne-Shimony-Holt (CHSH) inequality [36, 39].

## MEASUREMENT OF QUANTUM PURITY

The quantum purity and hence the second-order Rényi entropy can be directly measured by interfering two identical and independent copies of the quantum state on a 50%-50% beam splitter [21, 32, 33, 36]. For two identical copies of a bosonic Fock state, the output ports always have even parti-

cle number, as illustrated in Fig. 2a. This is due to the destructive interference of all odd outcomes. If the system is composed of multiple modes, such as internal spin states or various lattice sites, the total number parity  $P_i = \prod_k p_i^{(k)}$  is equal to unity in the output ports  $i = 1, 2$ . Here the parity for mode  $k$ ,  $p_i^{(k)} = \pm 1$  for even or odd number of particles, respectively. The well known Hong-Ou-Mandel (HOM) interference of two identical single photons [42] is a special case of this scenario. Here a pair of indistinguishable photons incident upon different input ports of a 50%-50% beam splitter undergoes bosonic interference such that both photons always exit from the same output port. In general, the average parity measured in the many-body bosonic interference on a beam splitter probes the quantum state overlap between the two copies  $\langle P_i \rangle = \text{Tr}(\rho_1 \rho_2)$ , where  $\rho_1$  and  $\rho_2$  are the density matrices of the two copies respectively and  $\langle \dots \rangle$  denotes averaging over repeated experimental realizations or over identical systems, as shown in Fig. 2b. Hence, for two identical systems, i.e. for  $\rho_1 = \rho_2 = \rho$ , the average parity for both output ports ( $i = 1, 2$ ) equals the quantum purity of the many-body state [21, 32, 33],

$$\langle P_i \rangle = \text{Tr}(\rho^2). \quad (3)$$

Equation (3) represents the most important theoretical foundation behind this work – it connects a quantity depending on quantum coherences in the system to a simple observable in the number of particles. It holds even without fixed particle number, as long as there is no definite phase relationship between the copies (Supplementary material). From Eqs. (1) and (3), detecting entanglement in an experiment reduces to measuring the average particle number parity in the output ports of the multi-mode beam splitter.

We probe entanglement formation in a system of interacting  $^{87}\text{Rb}$  atoms on a one dimensional optical lattice with a lattice constant of 680 nm. The dynamics of atoms in the lattice is described by the Bose-Hubbard Hamiltonian,

$$H = -J \sum_{\langle i,j \rangle} a_i^\dagger a_j + \frac{U}{2} \sum_i n_i(n_i - 1), \quad (4)$$

where  $a_i^\dagger$ ,  $a_i$  and  $n_i = a_i^\dagger a_i$  are the bosonic creation and annihilation operators, and the number of atoms at site  $i$ , respectively. The atoms tunnel between neighboring lattice sites (indicated by  $\langle i,j \rangle$ ) with a rate  $J$  and experience an onsite repulsive interaction energy  $U$ . The Planck's constant  $\hbar$  is set to 1 and hence both  $J$  and  $U$  are expressed in Hz. The dimensionless parameter  $U/J$  is controlled by the depth of the optical lattice. Additionally, we can superimpose an arbitrary optical potential with a resolution of a single lattice site by using a spatial light modulator (SLM) as an amplitude hologram through a high resolution microscope (Supplementary material). This microscope also allows us to image the number parity of each lattice site independently [34].

To initialize two independent and identical copies of a state with fixed particle number  $N$ , we start with a low entropy 2D Mott insulator with unity filling in the atomic limit [34] and deterministically retain a plaquette of  $2 \times N$  atoms while

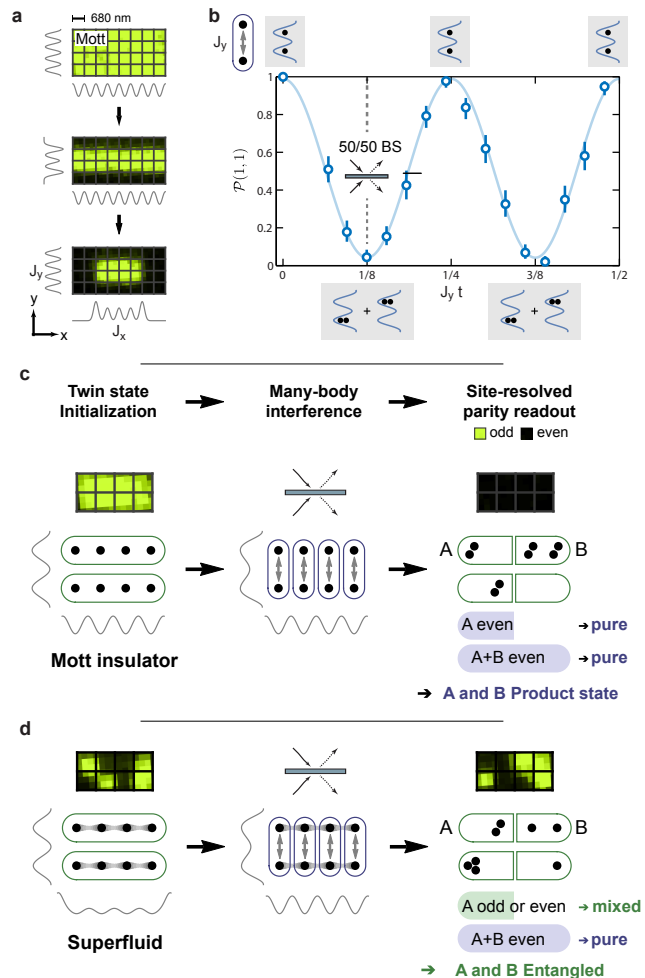


**Figure 3. Many-body interference to probe entanglement in optical lattices.** **a.** A high resolution microscope is used to directly image the number parity of ultra cold bosonic atoms on each lattice site (raw images: green = odd, black = even). Two adjacent 1D lattices are created by combining an optical lattice and potentials created by a spatial light modulator (SLM). We initialize two identical many-body states by filling the potentials from a low entropy 2D Mott insulator. The tunneling rates  $J_x$ ,  $J_y$  can be tuned independently by changing the depth of the potential. **b.** The atomic beam splitter operation is realized in a tunnel coupled double well potential. An atom, initially localized in one of the wells, delocalizes with equal probability into both the wells by this beam splitter. Here, we show the atomic analog of the HOM interference of two states. The joint probability  $\mathcal{P}(1,1)$  measures the probability of coincidence detection of the atoms in separate wells as a function of normalized tunnel time  $J_y t$ , with the single particle tunneling  $J_y = 193(4)$  Hz. At the beam splitter duration ( $J_y t = 1/8$ ) bosonic interference leads to a nearly vanishing  $\mathcal{P}(1,1)$  corresponding to an even parity in the output states. This can be interpreted as a measurement of the purity of the initial Fock state, here measured to be  $\approx 0.90(4)$ . The data shown here are averaged over two independent double wells. The blue curve is a maximum likelihood fit to the data, and the error-bars reflect  $1\sigma$  statistical error. **c.** When two copies of a product state, such as the Mott insulator in the atomic limit are interfered on the beam splitter, the output states contain even number of particles globally (full system) as well as locally (subsystem), indicating pure states in both. **d.** On the other hand, for two copies of an entangled state, such as a superfluid state, the output states contain even number of particles globally (pure state) but a mixture of odd and even outcomes locally (mixed state). This directly demonstrates entanglement.

removing all others (Supplementary material). This is illustrated in Fig. 3a. The plaquette of  $2 \times N$  atoms contains two copies (along the  $y$ -direction) of an  $N$ -atom one-dimensional system (along the  $x$ -direction), with  $N = 4$  in this figure. The desired quantum state is prepared by manipulating the depth of the optical lattice along  $x$ , varying the parameter  $U/J_x$  where  $J_x$  is the tunneling rate along  $x$ . A box potential created by the SLM is superimposed onto this optical lattice to constrain the dynamics to the sites within each copy. During the state preparation, a deep lattice barrier separates the two copies and makes them independent of each other.

The beam splitter operation required for the many-body interference is realized in a double well potential along  $y$ . The dynamics of atoms in the double well is likewise described by the Bose-Hubbard hamiltonian, Eq. (4). A single atom, initially localized in one well, undergoes coherent Rabi oscillation between the wells with a Rabi frequency of  $J = J_y$  (oscillation frequency in the amplitude). At discrete times during this evolution,  $t = t_{BS} = \frac{1}{8J_y}, \frac{3}{8J_y}, \dots$ , the atom is delocalized equally over the two wells with a fixed phase relationship. Each of these times realizes a beam splitter operation, for which the same two wells serve as the input ports at time  $t = 0$  and output ports at time  $t = t_{BS}$ . Two indistinguishable atoms with negligible interaction strength ( $U/J_y \ll 1$ ) in this double well will undergo interference as they tunnel. The dynamics of two atoms in the double well is demonstrated in Fig. 3b in terms of the joint probability  $\mathcal{P}(1,1)$  of finding them in separate wells versus the normalized time  $J_y t$ . The joint probability  $\mathcal{P}(1,1)$  oscillates at a frequency of  $772(16)$  Hz =  $4J_y$ , with a contrast of about 95(3)%. At the beam splitter times,  $\mathcal{P}(1,1) \approx 0$ . The first beam splitter time,  $tJ_y = \frac{1}{8}$  is used for all the following experiments, with  $\mathcal{P}(1,1) \approx 0.05(2)$ . This is a signature of bosonic interference of two indistinguishable particles [43, 44] akin to the photonic HOM interference [42]. This high interference contrast indicates the near-perfect suppression of classical noise and fluctuations and includes an expected 0.6% reduction due to finite interaction strength ( $U/J_y \approx 0.3$ ). The results from this interference can be interpreted as a measurement of the quantum purity of the initial Fock state as measured from the average parity (Eq.(3)),  $\langle P_i \rangle = 1 - 2 \times \mathcal{P}(1,1) = 0.90(4)$ , where  $i = 1, 2$  are the two copies.

## ENTANGLEMENT IN THE GROUND STATE

The Bose-Hubbard model provides an interesting system to investigate entanglement. In optical lattice systems, a lower bound of the spatial entanglement has been previously estimated from time-of-flight measurements [46] and entanglement dynamics in spin degrees-of-freedom has been investigated with partial state reconstruction [47]. Here, we directly measure entanglement in real space occupational particle number in a site-resolved way. In the strongly interacting, atomic limit of  $U/J_x \gg 1$ , the ground state is a Mott insulator corresponding to a Fock state of one atom at each lattice site. The quantum state has no spatial entanglement with respect to any partitioning in this phase – it is in a prod-

uct state of the Fock states. As the interaction strength is reduced adiabatically, atoms begin to tunnel across the lattice sites, and ultimately the Mott insulator melts into a superfluid with a fixed atom number. The delocalization of atoms create entanglement between spatial subsystems. This entanglement originates [48–50] from correlated fluctuations in the number of particles between the subsystems due to the super-selection rule that the total particle number in the full system is fixed, as well as coherence between various configurations without any such fluctuation.

To probe the emergence of entanglement, we first prepare the ground state of Eq. (4) in both the copies by adiabatically lowering the optical lattice potential along  $x$ . Then we freeze the tunneling along  $x$  without destroying the coherence in the many-body state and apply the beam splitter along  $y$ . Finally, we rapidly turn on a very deep 2D lattice to suppress all tunneling and detect the atom number parity (even = 1, odd = -1) at each site. We construct the parity of a spatial region by multiplying the parities of all the sites within that region. The average parity over repeated realizations measures the quantum purity, both globally and locally according to Eq. (3), enabling us to determine the second-order Rényi entropy globally and for all possible subsystems. In the atomic Mott limit (Fig. 3c), the state is separable. Hence, the interference signal between two copies should show even parity in all subsystems, indicating a pure state with zero entanglement entropy. Towards the superfluid regime (Fig. 3d), the buildup of entanglement leads to mixed states in subsystems, corresponding to a finite entanglement entropy. Hence, the measurement outcomes do not have a pre-determined parity. Remarkably, the outcomes should still retain even global parity, indicating a pure global state. Higher entropy in the subsystems than the global system cannot be explained classically and demonstrates bipartite entanglement.

Experimentally, we find exactly this behavior for our two 4-site Bose-Hubbard systems (Fig. 4). We observe the emergence of spatial entanglement as the initial atomic Mott insulator melts into a superfluid. The measured quantum purity of the full system is about 0.6 across the Mott to superfluid crossover, corresponding to a Rényi entropy,  $S_2(AB) \approx 0.5$ . The measured purity deep in the superfluid phase is slightly reduced, likely due to the reduced beam splitter fidelity in presence of increased single sites occupation number, and any residual heating. The nearly constant global purity indicates high level of quantum coherence during the crossover. For lower interaction strength  $U/J_x$  (superfluid regime) we observe that the subsystem Rényi entropy is higher than the full system,  $S_2(A) > S_2(AB)$ . This demonstrates the presence of spatial entanglement in the superfluid state. In the Mott insulator regime ( $U/J_x \gg 1$ ),  $S_2(A)$  is lower than  $S_2(AB)$  and proportional to the subsystem size, consistent with a product state.

In these experiments, we post-select outcomes of the experiment for which the total number of atoms detected in both copies is even. This constitutes about 60% of all the data, and excludes realizations with preparation errors, atom loss during the sequence, or detection errors (Supplementary material). The measured purity is consistent with an imperfect

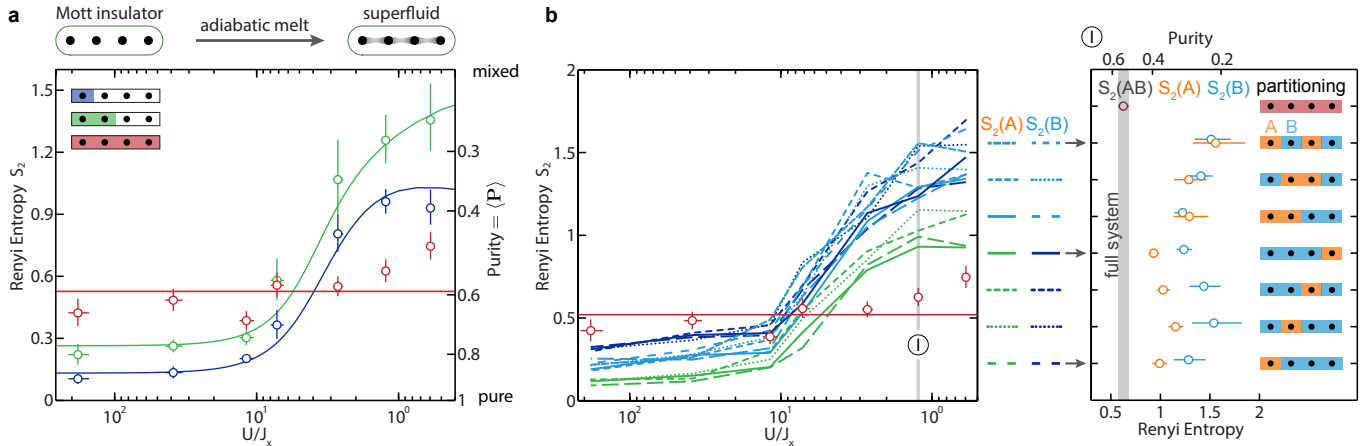


**Figure 4. Entanglement in the ground state of the Bose-Hubbard model.** We study the Mott insulator to superfluid transition with four atoms on four lattice sites in the ground state of the Bose-Hubbard model, Eq. (4). **a.** As the interaction strength  $U/J_x$  is adiabatically reduced the purity of the subsystem  $A$  (green and blue, inset),  $\text{Tr}(\rho_A^2)$ , become less than that of the full system (red). This demonstrates entanglement in the superfluid phase, generated by coherent tunneling of bosons across lattice sites. In terms of the second-order Rényi entanglement entropy,  $S_2(A) = -\log \text{Tr}(\rho_A^2)$ , the full system has less entropy than its subsystems in this state. In the Mott insulator phase ( $U/J_x \gg 1$ ) the full system has more Rényi entropy (and less purity) than the subsystems, due to the lack of sufficient entanglement and a contribution of classical entropy. The circles are data and the solid lines are theory calculated from exact diagonalization. The only free parameter is an added offset, assumed extensive in system size and consistent with the average measured entropy in the full system. **b.** Second-order Rényi entropy of all possible bi-partitioning of the system. For small  $U/J_x$ , all subsystems (data points connected by green and blue lines) have more entropy than the full system (red circles), indicating full multipartite entanglement [45] between the four lattice sites. The residual entropy in the Mott insulating regime is from classical entropy in the experiment, and extensive in the subsystem size. Right: The values of all Renyi entropies of the particular case of  $U/J_x \approx 1$  are plotted, to demonstrate spatial multipartite entanglement in this superfluid.

beam splitter operation alone, suggesting significantly higher purity for the many-body state. The measured entropy is thus a sum of an extensive classical entropy due to the imperfections of the beam splitter and any entanglement entropy.

Our site resolved measurement simultaneously provides information about all possible spatial partitionings of the system. Comparing the purity of all subsystems with that of the full system enables us to determine whether a quantum state has genuine spatial multipartite entanglement where every site is entangled with each other. Experimentally we find that this is indeed the case for small  $U/J_x$  (Fig. 4b). In the superfluid phase, all possible subsystems have more entropy than the full system, demonstrating full spatial multipartite entanglement between all four sites [33, 45]. In the Mott phase ( $U/J_x \gg 1$ ), the measured entropy is dominated by extensive classical entropy, showing a lack of entanglement.

By measuring the second-order Rényi entropy we can calculate other useful quantities, such as the associated mutual information  $I_{AB} = S_2(A) + S_2(B) - S_2(AB)$ . Mutual information exhibits interesting scaling properties with respect to the subsystem size, which can be key to studying area laws in interacting quantum systems [51]. In some cases, such as in the ‘data hiding states’ [52], mutual information is more appropriate than the more conventional two point correlators which might take arbitrarily small values in presence of strong correlations. Mutual information is also immune to present extensive classical entropy in the experiments, and hence is practically useful to experimentally study larger systems. In our experiments (Fig. 5a), we find that for the Mott insula-

tor state ( $U/J_x \gg 1$ ), the entropy of the full system is the sum of the entropies for the subsystems. The mutual information  $I_{AB} \approx 0$  for this state, consistent with a product state in the presence of extensive classical entropy. At  $U/J_x \approx 10$ , correlations between the subsystems begin to grow as the system adiabatically melts into a superfluid, resulting in non-zero mutual information,  $I_{AB} > 0$ .

It is instructive to investigate the scaling of Rényi entropy and mutual information with subsystem size [13, 51] since in larger systems they can characterize quantum phases, for example by measuring the central charge of the underlying quantum field theory [11]. Figure 5b shows these quantities versus the subsystem size for various partitioning schemes with a single boundary. For the atomic Mott insulator the Rényi entropy increases linearly with the subsystem size and the mutual information is zero, consistent with both a product state and classical entropy being uncorrelated between various sites. In the superfluid state the measured Rényi entropy curves are asymmetric and first increase with the system size, then fall again as the subsystem size approaches that of the full system. This represents the combination of entanglement entropy and the linear classical entropy. This non-monotonicity is a signature of the entanglement entropy, as the entropy for a pure state must vanish when the subsystem size is zero or the full system. The asymmetry due to classical entropy is absent in the mutual information.

The mutual information between two subsystems comes from the correlations across their separating boundary. For a four site system, the boundary area ranges from one to three

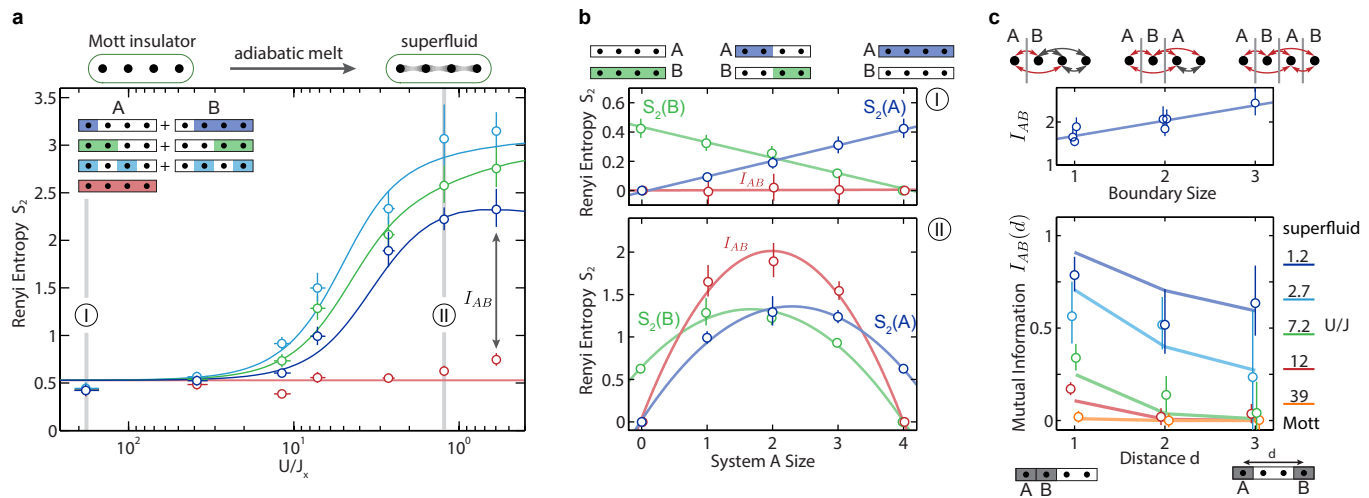


**Figure 5. Rényi Mutual information in the ground state.** Contribution from the extensive classical entropy in our measured Rényi entropy can be factored out by constructing the mutual information  $I_{AB} = S_2(A) + S_2(B) - S_2(AB)$ . Mutual information takes into account all correlations [51] between the subsystems  $A$  and  $B$ . **a.** We plot the summed entropy  $S_2(A) + S_2(B)$  (in blue, green and light blue corresponding to the partitions shown) and the entropy of the full system  $S_2(AB)$  (in red) separately. Mutual information is the difference between the two, as shown by the arrow for a partitioning scheme. In the Mott insulator phase ( $U/J_x \gg 1$ ) the sites are not correlated, and  $I_{AB} \approx 0$ . Correlations start to build up for smaller  $U/J_x$ , resulting in a non-zero mutual information. The theory curves are from exact diagonalization, with added offsets consistent with the extensive entropy in the Mott insulator phase. **b.** Classical and entanglement entropies follow qualitatively different scaling laws in a many-body system. Top - In the Mott insulator phase classical entropy dominates and  $S_2(A)$  and  $S_2(B)$  follow a volume law- entropy increases with the size of the subsystem. The mutual information  $I_{AB} \approx 0$ . Bottom -  $S_A$ ,  $S_B$  show non-monotonic behavior, due to the dominance of entanglement over classical entropy, which makes the curves asymmetric.  $I_{AB}$  restores the symmetry by removing the classical uncorrelated noise. **c.** Top - More correlations are affected (red arrow) with increasing boundary area, leading to a growth of mutual information between subsystems. The data points are for various partitioning schemes shown in Fig. 4b. Bottom-  $I_{AB}$  as a function of the distance  $d$  between the subsystems shows the onset and spread of correlations in space, as the Mott insulator adiabatically melts into a superfluid.

for various partitioning schemes. Among those schemes with a single boundary maximum mutual information in the superfluid is obtained when the boundary divides the system symmetrically (Fig. 5a). Increasing the boundary size increases the mutual information, as more correlations are interrupted by the partitioning (Fig. 5c).

Mutual information also elucidates the onset of correlations between various sites as the few-body system crosses over from a Mott insulator to a superfluid phase. In the Mott insulator phase ( $U/J_x \gg 1$ ) the mutual information between all sites vanish (Fig. 5c, bottom). As the particles start to tunnel only the nearest neighbor correlations start to build up ( $U/J_x \approx 12$ ) and the long range correlations remain negligible. Further into the superfluid phase, the correlations extend beyond the nearest neighbor and become long range for smaller  $U/J_x$ . These results suggest disparate spatial behavior of the mutual information in the ground state of an uncorrelated (Mott insulator) and a strongly correlated phase (superfluid). For larger systems this can be exploited to identify quantum phases and the onset of quantum phase transitions.

## NON-EQUILIBRIUM ENTANGLEMENT DYNAMICS

Away from the ground state, the non-equilibrium dynamics of a quantum many-body system is often theoretically intractable. This is due to the growth of entanglement beyond the access of numerical techniques such as the time dependent Density Matrix Renormalization Group (DMRG) theory [53, 54]. Experimental investigation of entanglement may shed valuable light onto non-equilibrium quantum dynamics. Towards this goal, we study a simple system: two particles oscillating in a double well [43, 55]. This non-equilibrium dynamics are described by the Bose-Hubbard model. The quantum state of the system oscillates between unentangled (particles localized in separate wells) and entangled states in the Hilbert space spanned by  $|1, 1\rangle$ ,  $|2, 0\rangle$  and  $|0, 2\rangle$ . Here,  $|m, n\rangle$  denotes a state with  $m$  and  $n$  atoms in the two subsystems (wells), respectively. Starting from the product state  $|1, 1\rangle$  the system evolves through the maximally entangled states  $|2, 0\rangle + |0, 2\rangle \pm |1, 1\rangle$  and the symmetric HOM-like state  $|2, 0\rangle + |0, 2\rangle$ . In the maximally entangled states the subsystems are completely mixed, with a probability of 1/3 to have zero, one, or two particles. The system then returns to the initial product state  $|1, 1\rangle$  before re-entangling. In our experiment, we start with a Mott insulating state ( $U/J_x \gg 1$ ), and suddenly quench the interaction parameter to a low value,

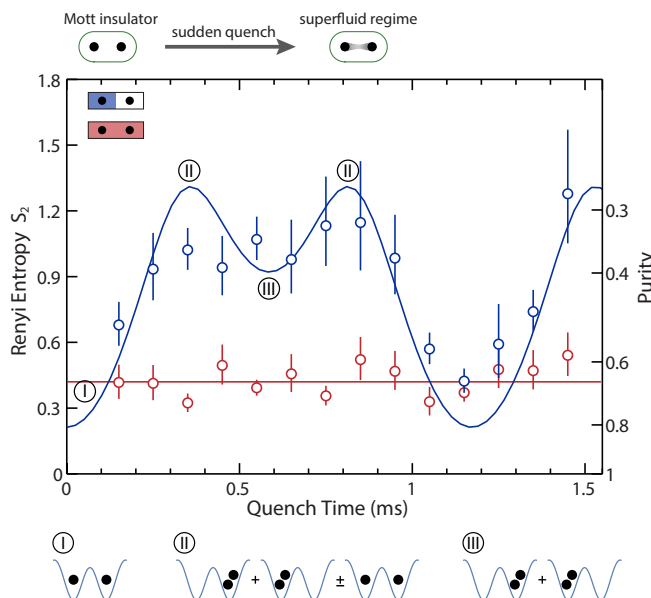


**Figure 6. Entanglement dynamics in quench** Entanglement dynamics of two atoms in two sites after a sudden quench of the Hamiltonian from a large value of  $U/J_x$  to  $U/J_x \approx 0.3$ , with  $J_x \approx 210$  Hz. Here, ‘quench time’ refers to the duration that the atoms spend in the shallow double well, after the initial sudden quench. The system oscillates between Mott insulator like state (I) and quenched superfluid states (II, III). The growth of bipartite entanglement in the superfluid state is seen by comparing the measured Rényi entropy of the single site subsystem (blue circles) to that of the two site full system (red circles). The solid lines are the theory curves with vertical offsets to include the classical entropy introduced by experimental imperfections.

$U/J_x \approx 0.3$ . The non-equilibrium dynamics is demonstrated (Fig. 6) by the oscillation in the second-order Rényi entropy of the subsystem, while the full system assumes a constant value originating from classical entropy. This experiment also demonstrates entanglement in HOM-like interference of two massive particles.

## SUMMARY AND OUTLOOK

In this work, we perform a direct measurement of quantum purity, the second-order Rényi entanglement entropy, and mutual information in a Bose-Hubbard system. Our measurement scheme does not rely on full density matrix reconstruction or the use of specialized witness operators to detect entanglement. Instead, by preparing and interfering two identical copies of a many-body quantum state, we probe entan-

glement with the measurement of only a single operator. Our experiments represent an important demonstration of the usefulness of the many-body interference for the measurement of entanglement. It is straight forward to extend the scheme to fermionic systems [56] and systems with internal degrees of freedom [33]. By generalizing the interference to  $n$  copies of the quantum state [35], arbitrary observables written as  $n$ -th order polynomial function of the density matrix, e.g.  $n > 2$  order Rényi entropies, can be measured.

With modest technical upgrades to suppress classical fluctuations and residual interactions, it should be possible to further improve the beam splitter fidelity enabling us to work with significantly larger systems. Mutual information is an ideal tool for exploring these larger systems as it is insensitive to any residual extensive classical entropy. For high entropy of a sub-system, corresponding to low state purity, the number of measurements required to reach a desired precision is high. However, in contrast to tomographic methods, this scheme would not require additional operations for larger systems. Moreover, the single site resolution of the microscope allows us to simultaneously obtain information about all possible subsystems, to probe multipartite entanglement.

For non-equilibrium systems, entanglement entropy can grow in time (indefinitely in infinite systems). This leads to interesting many-body physics, such as thermalization in closed quantum systems [57]. The long time growth of entanglement entropy is considered to be a key signature of many-body localized states [20] arising in presence of disorder. The ability to measure the quantum purity for these systems would allow experimental distinction of quantum fluctuations and classical statistical fluctuations.

More generally, by starting with two different quantum states in the two copies this scheme can be applied to measure the quantum state overlap between them. This would provide valuable information about the underlying quantum state. For example, the many-body ground state is very sensitive to perturbations near a quantum critical point. Hence, the overlap between two ground states with slightly different parameters (such as  $U/J$  in the Bose-Hubbard hamiltonian) could be used as a sensitive probe of quantum criticality [58]. Similarly the overlap of two copies undergoing non-equilibrium evolution under different perturbations can be used to probe temporal correlation functions in non-equilibrium quantum dynamics.

We thank J. I. Cirac, M. Cramer, A. Daley, A. DelMaestro, M. Endres, S. Gopalakrishnan, A. Kaufman, M. Knap, A. Pal, H. Pichler, B. Swingle, and P. Zoller for useful discussions. Supported by grants from the Gordon and Betty Moore Foundations EPiQS Initiative (grant GBMF3795), NSF through the Center for Ultracold Atoms, the Army Research Office with funding from the DARPA OLE program and a MURI program, an Air Force Office of Scientific Research MURI program, and an NSF Graduate Research Fellowship (M.R.).

[1] R. Horodecki, P. Horodecki, M. Horodecki, and K. Horodecki, “Quantum entanglement,” *Reviews of Modern Physics*, vol. 81,

no. 2, p. 865, 2009.

[2] A. Einstein, B. Podolsky, and N. Rosen, “Can quantum-

- mechanical description of physical reality be considered complete?,” *Physical review*, vol. 47, no. 10, p. 777, 1935.
- [3] J. S. Bell, “On the einstein-podolsky-rosen paradox,” *Physics*, vol. 1, no. 3, pp. 195–200, 1964.
- [4] P. W. Shor, “Polynomial-time algorithms for prime factorization and discrete logarithms on a quantum computer,” *SIAM journal on computing*, vol. 26, no. 5, pp. 1484–1509, 1997.
- [5] M. A. Nielsen and I. L. Chuang, *Quantum computation and quantum information*. Cambridge university press, 2010.
- [6] C. H. Bennett, G. Brassard, C. Crépeau, R. Jozsa, A. Peres, and W. K. Wootters, “Teleporting an unknown quantum state via dual classical and einstein-podolsky-rosen channels,” *Physical review letters*, vol. 70, no. 13, p. 1895, 1993.
- [7] R. P. Feynman, “Simulating physics with computers,” *International journal of theoretical physics*, vol. 21, no. 6/7, pp. 467–488, 1982.
- [8] A. Aspect, “Bell’s inequality test: more ideal than ever,” *Nature*, vol. 398, no. 6724, pp. 189–190, 1999.
- [9] T. D. Ladd, F. Jelezko, R. Laflamme, Y. Nakamura, C. Monroe, and J. L. OBrien, “Quantum computers,” *Nature*, vol. 464, no. 7285, pp. 45–53, 2010.
- [10] L. Amico, R. Fazio, A. Osterloh, and V. Vedral, “Entanglement in many-body systems,” *Reviews of Modern Physics*, vol. 80, no. 2, p. 517, 2008.
- [11] P. Calabrese and J. Cardy, “Entanglement entropy and conformal field theory,” *Journal of Physics A: Mathematical and Theoretical*, vol. 42, no. 50, p. 504005, 2009.
- [12] T. Nishioka, S. Ryu, and T. Takayanagi, “Holographic entanglement entropy: an overview,” *Journal of Physics A: Mathematical and Theoretical*, vol. 42, no. 50, p. 504008, 2009.
- [13] J. Eisert, M. Cramer, and M. B. Plenio, “Colloquium: Area laws for the entanglement entropy,” *Reviews of Modern Physics*, vol. 82, no. 1, p. 277, 2010.
- [14] A. Kitaev and J. Preskill, “Topological entanglement entropy,” *Physical review letters*, vol. 96, no. 11, p. 110404, 2006.
- [15] M. Levin and X.-G. Wen, “Detecting topological order in a ground state wave function,” *Physical review letters*, vol. 96, no. 11, p. 110405, 2006.
- [16] H.-C. Jiang, Z. Wang, and L. Balents, “Identifying topological order by entanglement entropy,” *Nature Physics*, vol. 8, no. 12, pp. 902–905, 2012.
- [17] Y. Zhang, T. Grover, and A. Vishwanath, “Entanglement entropy of critical spin liquids,” *Physical review letters*, vol. 107, no. 6, p. 067202, 2011.
- [18] S. V. Isakov, M. B. Hastings, and R. G. Melko, “Topological entanglement entropy of a bose-hubbard spin liquid,” *Nature Physics*, vol. 7, no. 10, pp. 772–775, 2011.
- [19] G. Vidal, J. I. Latorre, E. Rico, and A. Kitaev, “Entanglement in quantum critical phenomena,” *Physical Review Letters*, vol. 90, no. 22, p. 227902, 2003.
- [20] J. H. Bardarson, F. Pollmann, and J. E. Moore, “Unbounded growth of entanglement in models of many-body localization,” *Phys. Rev. Lett.*, vol. 109, p. 017202, Jul 2012.
- [21] A. Daley, H. Pichler, J. Schachenmayer, and P. Zoller, “Measuring entanglement growth in quench dynamics of bosons in an optical lattice,” *Physical review letters*, vol. 109, no. 2, p. 020505, 2012.
- [22] N. Schuch, M. M. Wolf, F. Verstraete, and J. I. Cirac, “Entropy scaling and simulability by matrix product states,” *Phys. Rev. Lett.*, vol. 100, p. 030504, Jan 2008.
- [23] I. Bloch, J. Dalibard, and S. Nascimbène, “Quantum simulations with ultracold quantum gases,” *Nature Physics*, vol. 8, no. 4, pp. 267–276, 2012.
- [24] R. Blatt and C. Roos, “Quantum simulations with trapped ions,” *Nature Physics*, vol. 8, no. 4, pp. 277–284, 2012.
- [25] A. Aspuru-Guzik and P. Walther, “Photonic quantum simulators,” *Nature Physics*, vol. 8, no. 4, pp. 285–291, 2012.
- [26] A. A. Houck, H. E. Türeci, and J. Koch, “On-chip quantum simulation with superconducting circuits,” *Nature Physics*, vol. 8, no. 4, pp. 292–299, 2012.
- [27] D. Bouwmeester, J.-W. Pan, M. Daniell, H. Weinfurter, and A. Zeilinger, “Observation of three-photon greenberger-horne-zeilinger entanglement,” *Phys. Rev. Lett.*, vol. 82, pp. 1345–1349, Feb 1999.
- [28] O. Gühne and G. Tóth, “Entanglement detection,” *Physics Reports*, vol. 474, no. 1, pp. 1–75, 2009.
- [29] D. F. James, P. G. Kwiat, W. J. Munro, and A. G. White, “Measurement of qubits,” *Physical Review A*, vol. 64, no. 5, p. 052312, 2001.
- [30] J.-W. Pan, Z.-B. Chen, C.-Y. Lu, H. Weinfurter, A. Zeilinger, and M. Żukowski, “Multiphoton entanglement and interferometry,” *Reviews of Modern Physics*, vol. 84, no. 2, p. 777, 2012.
- [31] H. Häffner, W. Hänsel, C. Roos, J. Benhelm, M. Chwalla, T. Körber, U. Rapol, M. Riebe, P. Schmidt, C. Becher, et al., “Scalable multiparticle entanglement of trapped ions,” *Nature*, vol. 438, no. 7068, pp. 643–646, 2005.
- [32] A. K. Ekert, C. M. Alves, D. K. Oi, M. Horodecki, P. Horodecki, and L. C. Kwek, “Direct estimations of linear and nonlinear functionals of a quantum state,” *Physical review letters*, vol. 88, no. 21, p. 217901, 2002.
- [33] C. M. Alves and D. Jaksch, “Multipartite entanglement detection in bosons,” *Physical review letters*, vol. 93, no. 11, p. 110501, 2004.
- [34] W. S. Bakr, A. Peng, M. E. Tai, R. Ma, J. Simon, J. I. Gillen, S. Foelling, L. Pollet, and M. Greiner, “Probing the superfluid-to-mott insulator transition at the single-atom level,” *Science*, vol. 329, no. 5991, pp. 547–550, 2010.
- [35] T. A. Brun, “Measuring polynomial functions of states,” *Quantum Information & Computation*, vol. 4, no. 5, pp. 401–408, 2004.
- [36] F. A. Bovino, G. Castagnoli, A. Ekert, P. Horodecki, C. M. Alves, and A. V. Sergienko, “Direct measurement of nonlinear properties of bipartite quantum states,” *Physical review letters*, vol. 95, no. 24, p. 240407, 2005.
- [37] S. Walborn, P. S. Ribeiro, L. Davidovich, F. Mintert, and A. Buchleitner, “Experimental determination of entanglement with a single measurement,” *Nature*, vol. 440, no. 7087, pp. 1022–1024, 2006.
- [38] C. Schmid, N. Kiesel, W. Wieczorek, H. Weinfurter, F. Mintert, and A. Buchleitner, “Experimental direct observation of mixed state entanglement,” *Phys. Rev. Lett.*, vol. 101, p. 260505, Dec 2008.
- [39] R. Horodecki et al., “Information-theoretic aspects of inseparability of mixed states,” *Physical Review A*, vol. 54, no. 3, p. 1838, 1996.
- [40] F. Mintert and A. Buchleitner, “Observable entanglement measure for mixed quantum states,” *Physical review letters*, vol. 98, no. 14, p. 140505, 2007.
- [41] H. Li and F. D. M. Haldane, “Entanglement spectrum as a generalization of entanglement entropy: Identification of topological order in non-abelian fractional quantum hall effect states,” *Phys. Rev. Lett.*, vol. 101, p. 010504, Jul 2008.
- [42] C. Hong, Z. Ou, and L. Mandel, “Measurement of subpicosecond time intervals between two photons by interference,” *Physical Review Letters*, vol. 59, no. 18, p. 2044, 1987.
- [43] A. Kaufman, B. Lester, C. Reynolds, M. Wall, M. Foss-Feig, K. Hazzard, A. Rey, and C. Regal, “Two-particle quantum interference in tunnel-coupled optical tweezers,” *Science*, vol. 345,

- no. 6194, pp. 306–309, 2014.
- [44] R. Lopes, A. Imanaliev, A. Aspect, M. Cheneau, D. Boiron, and C. I. Westbrook, “Atomic hong-ou-mandel experiment,” *Nature*, vol. 520, no. 7545, pp. 66–68, 2015.
- [45] R. Palmer, C. M. Alves, and D. Jaksch, “Detection and characterization of multipartite entanglement in optical lattices,” *Physical Review A*, vol. 72, no. 4, p. 042335, 2005.
- [46] M. Cramer, A. Bernard, N. Fabbri, L. Fallani, C. Fort, S. Rosi, F. Caruso, M. Inguscio, and M. Plenio, “Spatial entanglement of bosons in optical lattices,” *Nature communications*, vol. 4, 2013.
- [47] T. Fukuhara, S. Hild, J. Zeiher, P. Schauß, I. Bloch, M. Endres, and C. Gross, “Spatially resolved detection of a spin-entanglement wave in a bose-hubbard chain,” *Phys. Rev. Lett.*, vol. 115, p. 035302, Jul 2015.
- [48] F. Verstraete and J. I. Cirac, “Quantum nonlocality in the presence of superselection rules and data hiding protocols,” *Phys. Rev. Lett.*, vol. 91, p. 010404, Jul 2003.
- [49] S. D. Bartlett and H. M. Wiseman, “Entanglement constrained by superselection rules,” *Physical review letters*, vol. 91, no. 9, p. 097903, 2003.
- [50] N. Schuch, F. Verstraete, and J. I. Cirac, “Nonlocal resources in the presence of superselection rules,” *Physical review letters*, vol. 92, no. 8, p. 087904, 2004.
- [51] M. M. Wolf, F. Verstraete, M. B. Hastings, and J. I. Cirac, “Area laws in quantum systems: mutual information and correlations,” *Physical review letters*, vol. 100, no. 7, p. 070502, 2008.
- [52] D. P. DiVincenzo, D. W. Leung, and B. M. Terhal, “Quantum data hiding,” *Information Theory, IEEE Transactions on*, vol. 48, no. 3, pp. 580–598, 2002.
- [53] G. Vidal, “Efficient simulation of one-dimensional quantum many-body systems,” *Physical Review Letters*, vol. 93, no. 4, p. 040502, 2004.
- [54] S. Trotzky, Y.-A. Chen, A. Flesch, I. P. McCulloch, U. Schollwöck, J. Eisert, and I. Bloch, “Probing the relaxation towards equilibrium in an isolated strongly correlated one-dimensional bose gas,” *Nature Physics*, vol. 8, no. 4, pp. 325–330, 2012.
- [55] S. Trotzky, Y.-A. Chen, U. Schnorrberger, P. Cheinet, and I. Bloch, “Controlling and detecting spin correlations of ultracold atoms in optical lattices,” *Physical review letters*, vol. 105, no. 26, p. 265303, 2010.
- [56] H. Pichler, L. Bonnes, A. J. Daley, A. M. Läuchli, and P. Zoller, “Thermal versus entanglement entropy: a measurement protocol for fermionic atoms with a quantum gas microscope,” *New Journal of Physics*, vol. 15, no. 6, p. 063003, 2013.
- [57] M. Rigol, V. Dunjko, and M. Olshanii, “Thermalization and its mechanism for generic isolated quantum systems,” *Nature*, vol. 452, no. 7189, pp. 854–858, 2008.
- [58] P. Zanardi and N. Paunković, “Ground state overlap and quantum phase transitions,” *Physical Review E*, vol. 74, no. 3, p. 031123, 2006.

## SUPPLEMENTARY MATERIAL

### I. MEASURING ENTANGLEMENT ENTROPY WITH QUANTUM INTERFERENCE

The quantification of entanglement requires the measurement of non-linear functionals of a quantum state  $\rho$ , such as

the  $n$ -th order Rényi entropy  $S_n = -\ln \text{Tr}(\rho^n)$  [1]. A general scheme to measure  $\text{Tr}(\rho^n)$  is to measure the shift operator  $V_n$  acting on  $n$ -copies of the many-body system. The shift operator  $V_n$  re-orders the quantum states when acting on a collection of  $n$  states,

$$V_n |\psi_1\rangle |\psi_2\rangle \dots |\psi_n\rangle = |\psi_n\rangle |\psi_1\rangle \dots |\psi_{n-1}\rangle. \quad (\text{S.1})$$

It can be shown that  $\text{Tr}(\rho^n) = \text{Tr}(V_n \rho^{\otimes n})$  [2].

We focus on the experimentally relevant case of  $n = 2$ . The shift operator is then simply the SWAP operator which exchanges any two quantum states:

$$V_2 (|\psi_1\rangle \otimes |\psi_2\rangle) = |\psi_2\rangle \otimes |\psi_1\rangle \quad (\text{S.2})$$

Two successive applications of the SWAP operator leave the system unchanged,  $V_2^2 = \mathbb{1}$ . Therefore  $V_2$  has eigenvalues  $\pm 1$ , corresponding to subspaces of the 2-copy system that are symmetric or antisymmetric with respect to the state exchange. The SWAP operator may act on individual modes (e.g. lattice sites) or the entire quantum system, and operations on different modes commute. The following short proof[4]

$$\begin{aligned} \text{Tr}(V_2 \rho_1 \otimes \rho_2) &= \text{Tr} \left( V_2 \sum_{ijkl} \rho_{ij}^{(1)} \rho_{kl}^{(2)} |i\rangle \langle j| \otimes |k\rangle \langle l| \right) \\ &= \text{Tr} \left( \sum_{ijkl} \rho_{ij}^{(1)} \rho_{kl}^{(2)} |k\rangle \langle j| \otimes |i\rangle \langle l| \right) \\ &= \sum_{ijkl} \rho_{ij}^{(1)} \rho_{kl}^{(2)} \delta_{kj} \delta_{il} = \sum_{ik} \rho_{ik}^{(1)} \rho_{ki}^{(2)} = \text{Tr}(\rho_1 \rho_2) \end{aligned} \quad (\text{S.3})$$

shows that the overlap of two quantum states  $\rho_1$  and  $\rho_2$  is given by the expectation value of the SWAP operator on the product space of the two states. Consider from now on the case where the two state are identical ( $\rho_1 = \rho_2 = \rho$ ), then the expectation value of  $V_2$  gives the purity  $\text{Tr}(\rho^2)$ . Further if we have two copies of a pure state then  $\text{Tr}(\rho^2) = 1 = \text{Tr}(V_2 \rho \otimes \rho)$ , hence the combined 2-copy state is symmetric and can be expressed in the symmetric basis comprised of states

$$\left\{ \prod_{i,j} (a_{1,i}^\dagger - a_{2,i}^\dagger)^{2p_i} (a_{1,j}^\dagger + a_{2,j}^\dagger)^{q_j} |\text{vac}\rangle \right\} \quad \text{with } p, q = 0, 1, 2, \dots \quad (\text{S.4})$$

where  $a_{1(2),i}^\dagger$  is the creation operation of mode  $i$  in copy 1(2). If the two copies undergo a discrete Fourier transformation of the form (for simplicity dropping the mode indices)

$$\begin{aligned} (a_1^\dagger + a_2^\dagger)/\sqrt{2} &\rightarrow a_1^\dagger \\ (a_1^\dagger - a_2^\dagger)/\sqrt{2} &\rightarrow a_2^\dagger \end{aligned} \quad (\text{S.5})$$

then the basis states in Eq.S.4 will end up having  $2 \times p_i$  particles in mode  $i$  of copy 2. In other words a symmetric state, as is the case for 2 pure identical copies, will always have even

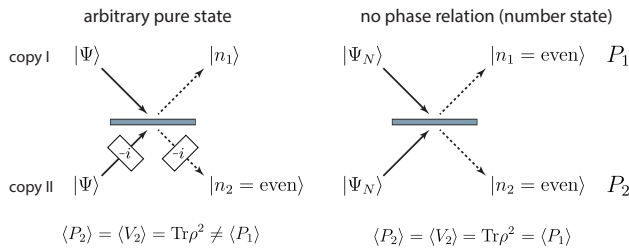


**Figure 7. Beamsplitter for many-body interference.** *Left:* With the beamsplitter operation and proper phase shift operations, one can directly measure quantum purity by measuring the average parity in output port 2 of the beamsplitter. For pure identical incident states, the atom number is always even in output 2. *Right:* In the experiment, we interfere states with well-defined particle number  $N$  or subsystems of such states. No macroscopic phase relationship exists between the input states, and the phase shifts in the input/output ports have no physical significance. Both outputs are equivalent and may be used to measure the expectation value  $\langle V_2 \rangle$  of the SWAP operator.

number of particles in copy 2 after the transformation. The symmetric and anti-symmetric subspaces of the SWAP operator are identified by the parity of atom number in copy 2 after a discrete Fourier transform, and the average parity directly measures the state purity,  $\langle P_2 \rangle = \text{Tr}\rho^2$ .

Our microscope experiments then allows us to probe entanglement in an optical lattice by comparing the local purity  $\text{Tr}\rho_{A(B)}^2$  to the global purity  $\text{Tr}\rho^2$  for a system partitioned into subsystems  $A$  and  $B$ . The entanglement is quantified by the entropy of the reduced density matrix  $\rho_A = \text{Tr}_B(\rho)$ , and the measured purity  $\text{Tr}\rho^2$  gives directly the 2nd order Rényi entropy  $S_2 = -\ln \text{Tr}\rho^2$ . This scheme is proposed in [2] and made explicit for measurements with beamsplitter operations in optical lattices in [3] and [4], giving Rényi entropy of arbitrary order  $n$ .

Using controlled tunneling in a double-well potential, we can implement the beamsplitter transformation for bosonic atoms (see next section):

$$\begin{aligned} a_1^\dagger &\rightarrow (a_1^\dagger + ia_2^\dagger)/\sqrt{2} \\ a_2^\dagger &\rightarrow (ia_1^\dagger + a_2^\dagger)/\sqrt{2} \end{aligned} \quad (\text{S.6})$$

where a  $\pi/2$ -phase ( $i$ ) is associated with each tunneling event across the double-well. Note that this transformation is *not* equivalent to the Fourier transform in Eq. (S.5). It's easy to verify that the Fourier transform is realized with the following protocol sequence of the beamsplitter operation and relative phase shift operations:

1. A  $-\pi/2$  phase shift ( $-i$ ) on copy 2
2. The beamsplitter operation in Eq. (S.6)
3. Another  $-\pi/2$  phase shift on copy 2

The inclusion of the additional phase shifts are important to correctly map the symmetric (antisymmetric) eigenstates

of the SWAP operator onto states with even (odd) atom number parity in output port 2 of the beamsplitter. The resulting protocol is valid for measuring purity of any general many-body state. In the classical limit where the incident states are two identical coherent states with well-defined identical phases, the inclusion of the proper phase factors in input 2 ensures that the states interfere destructively in output 2. In this port, the total number of bosons is always zero and therefore even, so the measured parity  $\langle V \rangle = 1$  correctly gives  $\rho_1 = \rho_2$  and  $\text{Tr}\rho^2 = 1$ . This situation is analogous to the interference of two phase-stabilized laser beams on a 50/50 beamsplitter, which may result in zero intensity in one output for the correct choice of incident phases. Away from the classical limit, for example as the input states become number squeezed states with decreasing uncertainty in atom number but increasing fluctuation in phase, atoms start to appear in output port 2 after the protocol but only in pairs (even parity) as long as the input states remain pure and identical.

The protocol also works when there is no global phase relationship between the interfering many-body states. Such as in our current experiments when the two copies are prepared each as an independent quantum state with a fixed number of atoms, so there is no well-defined phase. There are also no defined phases when the incident states to the beamsplitter are subsystems partitioned out of bigger systems. In either case, step 1 of the above protocol has no physical meaning in the absence of a defined phase and might be omitted from the experiment without changing the resulting state after the transformation. The *in-situ* fluorescence imaging of our microscope detects parity of the atom number on each lattice site which is phase-insensitive, so step 3 is also redundant. The beamsplitter operation in the double-well alone is thus sufficient to implement the mapping of SWAP operator eigenstates onto states with even or odd atom number parity. The two output ports are then equivalent and the purity measurements may be obtained from the atom numbers on either side of the double-well after the many-body interference sequence.

## II. IMPLEMENTATION OF THE BEAMSPLITTER OPERATION

### A. Projected double-well potentials

In addition to a square lattice, optical potentials are generated by projecting light onto the atoms using a digital micro-mirror device (DMD). The DMD is used as an amplitude hologram in a Fourier plane of our high resolution imaging system so that wavefronts with arbitrary phase and amplitude may be created with single-site resolution [5]. We use blue-detuned coherent light at  $\lambda = 762$  nm to generate a potential with a double-well profile along  $x$  and a smoothed flat top profile along  $y$ :

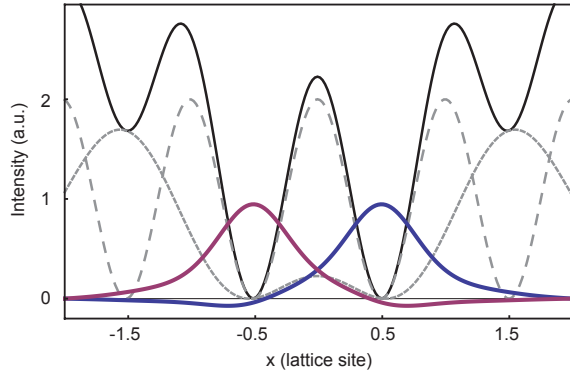


**Figure 8. Double-well potential for the beamsplitter.** The intensity profile of the projected potential (Eq.S.7, gray short-dashed), the lattice (gray long-dashed), and the combined potential for the beam splitter operation (black solid). Also shown are sketches of the amplitude of the ground band Wannier wavefunctions (blue, purple) in each well at the beamsplitter depth.

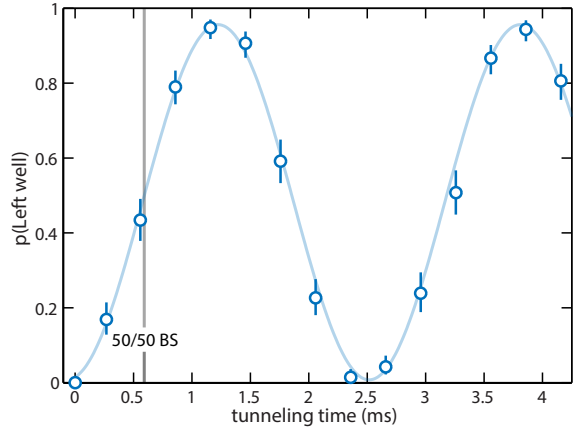


**Figure 9. Rabi oscillations in the double-well.** A single particle is initialized on the right side of the doublewell and oscillates coherently between the two wells with fitted tunneling rate  $J = 193(4)$  Hz and contrast of 95(1)%.

$$V(x, y) = V_{dw} \left( e^{-\frac{(x-1.5)^2}{0.95^2}} - 0.52e^{-\frac{x^2}{0.9^2}} + e^{-\frac{(x+1.5)^2}{0.95^2}} \right)^2 \times \left( \arctan \left( \frac{y+18}{5.5} \right) - \arctan \left( \frac{y-18}{5.5} \right) \right)^2 \quad (\text{S.7})$$

where  $x$  and  $y$  are in units of the lattice spacing and  $V_{dw}$  is the potential depth of the projected double-well.

The beamsplitter operation is realized by controlled tunneling in the combined potential of the above projected potential and a shallow  $x$ -lattice, as depicted in Fig. 8. We choose depths  $V_{dw} = 1.7 E_r$  and  $V_{latt} = 2 E_r$ , for which we observe tunneling rate  $J = 193(4)$  Hz during the beam-splitter operation (Fig. 9), in reasonable agreement with a band structure calculation predicting  $J = 170$  Hz. The discrepancy is likely due to uncertainty in the lattice depth, which is calibrated using amplitude modulation spectroscopy at  $V_{latt} \approx 40 E_r$ . Here  $E_R = 1240$  Hz is the recoil energy of the optical lattice. In the beamsplitter potential, the energy gap to the first excited band is  $\approx 1.3$  kHz, and states outside the ground band do not contribute significantly to the dynamics.

## B. Sources of error for the beamsplitter

*a. Potential imperfections* The leading order imperfection of the projected double-well potential are imperfect zero-crossings in the electric field, resulting in energy offsets between the two sides of the double-well. At the double-well depth for our beamsplitter operation, we observe offsets of 50 Hz or less, which do not significantly affect the Hong-Ou-Mandel (HOM) interference contrast (see Fig. 10).

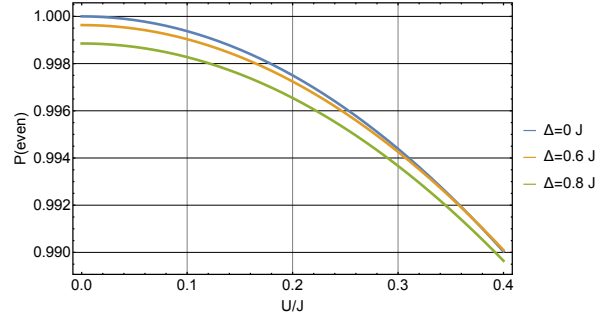


**Figure 10. Fidelities of the beamsplitter operation.** Finite interactions and energy offsets due to imperfections in the double-well potential reduce the Hong-Ou-Mandel interference contrast, as measured by the probability to detect even atom numbers at the beamsplitter time  $tJ = \frac{\pi}{4}$ . For a beamsplitter operation starting with one atom on each side of the double-well and typical experimental parameters  $J = 240$  Hz,  $U = 70$  Hz and offset  $\Delta = 50$  Hz (corresponding to  $U/J = 0.3$  and  $\Delta/J = 0.2$  ), the interference contrast is expected to be reduced by  $\sim 0.6\%$ . This calculation does not take the effects of higher bands into account.

*b. Alignment stability* The successful loading of atoms from the lattice into the double-well potential is sensitive to long-term and shot-to-shot position drifts between the lattice and the double-well. We minimize such drifts by imaging the lattice and double-well potential at the end of each experimental run and feeding back on the position of the double-well with a piezo-actuated mirror. We achieve a relative position stability of 0.04 sites RMS or less. To lowest order the position drift creates an energy offset between the two sides of the combined double-well potential. At the chosen depths for the beamsplitter operation, a relative shift of 0.1 sites leads to an offset of  $\approx 20$  Hz.

*c. Interaction effects* Interactions during the beamsplitter operation potentially reduce the HOM interference con-

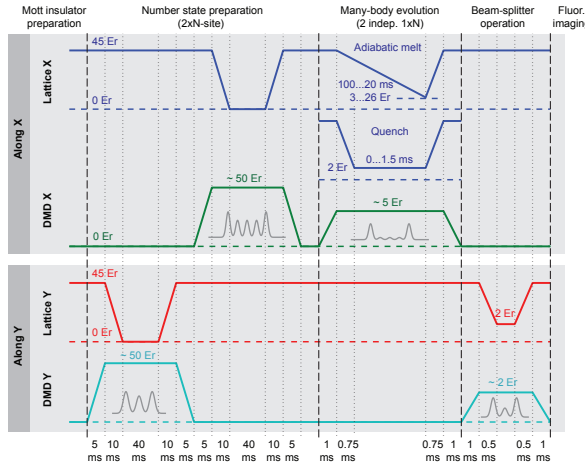


**Figure 11. Experimental sequence.** Schematic showing the ramps of the  $x$ - and  $y$ -lattices and the projected potential from the DMD. The profiles of the DMD potentials are sketched in the direction of interest, while the other direction always has a smoothed flattop profile across the region of interest. Ramps are exponential in depth as a function of time. See text for details.

trast. We minimize interactions by performing all experiments in a weak out-of-plane confinement of  $\omega_z = 2\pi \times 800$  Hz. During the beamsplitter operation we achieve an interaction of  $U = 2\pi \times 70$  Hz (measured with photon-assisted tunneling in a deep double-well and extrapolated to lower depths), corresponding to  $u = U/J = 0.3$ . This residual interaction reduces the HOM interference contrast by  $\sim 0.6\%$  (see Fig. 10).

*d. Coherent admixture of higher bands* Interactions of two particles on the same site distort the particles' wavefunctions and coherently admix higher bands. This wavefunction is thus different from that of a single particle, restoring some distinguishability to the bosonic atoms. The dominant contribution of higher bands occurs in the  $z$ -direction, along which the confinement is weakest, and the second excited band is admixed to the wavefunction. The admixture is  $\epsilon \approx (\frac{U}{2\omega_z})^2 = (\frac{2\pi \times 70\text{Hz}}{2 \times 2\pi \times 800\text{Hz}})^2 = 0.2\%$ . HOM interference contrast is thus reduced by less than 1%.

### III. EXPERIMENTAL SEQUENCE

Our experiments start with a single-layer two-dimensional Mott insulator of  $^{87}\text{Rb}$  atoms in a deep lattice ( $V_x = V_y = 45E_r$ ) with 680 nm spacing as described in previous work. The following sequence is illustrated in Fig. 11.

*State preparation* We deterministically prepare a plaquette of  $2 \times 2$  or  $2 \times 4$  atoms from a Mott insulator with unity occupancy. We first superimpose onto the deep lattice an optical potential with a double-well profile of depth  $\approx 50E_r$  along  $y$  and a smooth flattop profile along  $x$ , and subsequently turn off the lattice in the  $y$ -direction. The two troughs of the double-well are aligned with two neighboring lattice sites so only two

rows of atoms are trapped, while all other atoms leave the system along tubes in the  $y$ -direction. A blue-detuned Gaussian beam with waist  $w \approx 50 \mu\text{m}$  and  $\lambda = 755$  nm provides the anti-confinement to remove atoms outside the double-well efficiently in 40 ms. The  $y$ -lattice is then ramped back to its initial depth and the double-well removed, leaving a block of width 2 sites and length  $\sim 10$  sites populated with one atom each. The above procedure is then repeated with a double- or quadruple-well potential along the  $x$  direction, leaving a deterministically loaded block of  $2 \times 2$  or  $2 \times 4$  atoms in the lattice. The lattices and double-well potentials are ramped smoothly to avoid heating the atoms to excited bands of the lattice.

At the end of the state preparation sequence, the fidelity of unit occupancy is  $94.6(2)\%$  per site, limited primarily by the fidelity of the initial Mott insulator and losses during the state preparation. We verify independently that defects are predominantly empty, not doubly occupied sites.

*Evolution in independent copies* For studying the ground state entanglement using the  $2 \times 4$  block (Figure. 4 & 5 in the main text), we turn on an optical potential with two narrow Gaussian peaks separated by four lattice sites along the  $x$  direction and flat-top along  $y$ . This confines the atoms inside the 4-site "box potential". The  $x$  lattice is then ramped down adiabatically to various final depths from 26 to  $3E_r$ . The ramp in depth is exponential in time with a duration of 200 ms from 45 to  $3E_r$ . The  $y$ -lattice is kept at  $45E_r$  so that tunneling along  $y$  is negligible and the two copies evolve independently.

For quench dynamics using the  $2 \times 2$  block, we use a double-well potential along  $x$  with  $V_{dw} = 2E_r$  to prevent atoms from leaving the 2-site system. The  $x$  lattice is ramped from  $45E_r$  to  $2E_r$  in 0.75 ms and held for a variable time. The presence of the double-well slightly modifies the values of  $U$  and  $J$  from values in a lattice only, yielding  $U/J = 0.3$  during the hold time.

*Beamsplitter operation and imaging* Right before the beamsplitter operation, the  $x$ -lattice is ramped back to  $45E_r$  in 0.75 ms to suppress tunneling within each copy. A double-well potential along  $y$  is superimposed onto the lattice. The  $y$ -lattice is then ramped down to  $2E_r$  in 0.5 ms and atoms are allowed to tunnel in independent double-wells between the two copies for 0.34 ms, implementing the beam splitter transformation before the  $y$ -lattice is returned to its initial depth of  $45E_r$  in 0.5 ms.

Subsequently, we pin the atoms in a deep lattice and obtain fluorescence images with single-lattice-site resolution. Our detection scheme is sensitive only to the parity of the site occupation number.

### IV. DATA ANALYSIS

*Post-selection* Before data analysis we post-select outcomes of the experiment for which the total number of atoms detected within the plaquette ( $2 \times 2$  or  $2 \times 4$  sites) is even. Outcomes outside this subset of data indicate either state preparation errors, atom loss during the sequence, or detection errors. We furthermore reject all realizations for which we detect atoms in the  $20 \times 20$  block surrounding

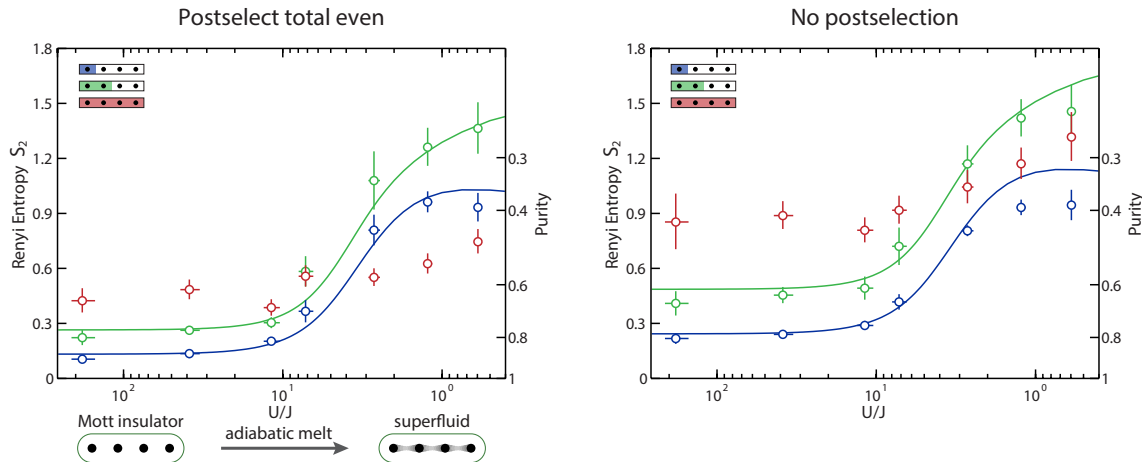


**Figure 12. Rényi entropy of the 4-site system and its subsystems with and without postselection.** The postselection process removes classical entropy and reduces the entropy of the full system (red) from  $\sim 0.9$  to  $\sim 0.5$ . Note that even without postselection the entropy of the half-chain (green) rises above the full system entropy, indicating bipartite entanglement. Theory curves are exact diagonalizations shifted vertically by the mean classical entropy per site calculated from the full system entropy.

the region of interest, most likely corresponding to atoms being lost from the plaquette during the sequence. Note that a combination of multiple errors (e.g. failure to load atoms on two sites) may lead to an unsuccessful run of the experiment being included in the post-selected data.

For experiments on the  $2 \times 2$  plaquette we typically retain 80% of the data, and 60% for the  $2 \times 4$  plaquette.

*Calculating Purity and Entropy* For the full many-body state and each subsystem of interest we calculate  $p_{\text{odd}}$ , the probability of measuring a total odd number of atoms after the beamsplitter operation within the post-selected data. The quantum mechanical purity and second-order Rényi entropy are then given by

$$\text{Tr}(\rho^2) = 1 - 2p_{\text{odd}} \quad (\text{S.8})$$

$$S_2(\rho) = -\log(\text{Tr}(\rho^2)) \quad (\text{S.9})$$

We average the calculated purity  $\text{Tr}(\rho^2)$  over both copies and over equivalent partitions. For instance, the single-site entropy reported in Fig. 4a of the main text is the mean over the first and last site of each copy of the 4-site system. From the variance of the parity in each subsystem and the covariance between subsystems we obtain the statistical standard error of the mean parity, taking into account possible correlations between regions. The reported error bars are the quadrature sum of the statistical error and the standard deviation of mean parities over the averaged regions. This procedure accounts for residual inhomogeneities between the copies and along the chains.

Errorbars in  $U/J$  correspond to a typical uncertainty in the optical lattice depth of  $\pm 2\%$ .

*Full system purity* For the  $2 \times 4$  plaquette, the initial state purity is reduced from 1 due to the presence of thermal holes in the initial Mott insulating state. Assuming all even sites are holes, the loading statistics for the  $2 \times 4$  plaquette are:

N atoms	loading probability $p(N)$
8	0.66(1)
7	0.27(1)
6	0.052(4)

i.e. the postselected subset of total even data contains  $\frac{0.052}{0.052+0.66} = 7\%$  of events with 6 atoms total. The inclusion of outcomes with 6 atoms reduces the purity of the initial state to 0.94, corresponding to a Rényi entropy of 0.06. The expected full system purity in the Mott insulator state is thus limited by the finite 95(3)% fidelity of the beamsplitter operation on each site and approximately given by the product of individual purities,  $P = \prod_k p^{(k)} = 0.90^4 \approx 0.66$ , in good agreement with the experimentally measured purity in Fig. 4a.

*Fitting procedure* To determine the contrast of single-particle Rabi oscillations (Fig.9) and HOM-interference (Fig. 3b in main text) we use a Bayesian inference for the fit to the measured parity, which is more robust than a least-squares fit in situations where error probabilities are small and the visibility close to 1. This approach prevents unphysical fits that extend past the possible bounds of the measurement and appropriately adjusts the error bars for points measured to lie near the physical bound. For each time point, we report the median and the  $1\sigma(68\%)$  confidence interval of a Beta-distribution  $\beta(p, m, N)$  for  $m$  successful outcomes in  $N$  experimental runs. The fitted sine curves in Fig. 1 are maximum-likelihood fits to the Beta-distributions at each time point, which are determined by maximizing the product of all the Beta-distributions where the fitted curve samples them. [6]

- 
- [1] F. Mintert, Entanglement measures as physical observables. *Appl. Phys. B* **89**, 493?497 (2007).
  - [2] A. K. Ekert, C. M. Alves, D. K. L. Oi, M. Horodecki, P. Horodecki, and L. C. Kwek, Direct estimations of linear and nonlinear functionals of a quantum state. *Phys. Rev. Lett.* **88**, 217901 (2002).
  - [3] C. Moura Alves and D. Jaksch, Multipartite Entanglement Detection in Bosons. *Phys. Rev. Lett.* **93**, 110501 (2004).
  - [4] A. J. Daley, H. Pichler, J. Schachenmayer, and P. Zoller, Measuring entanglement growth in quench dynamics of bosons in an optical lattice. *Phys. Rev. Lett.* **109**, 020505 (2012).
  - [5] P. Zupancic, Dynamic holography and beamshaping using digital micromirror devices. *Master's thesis*, Ludwig-Maximilians-Universität München (2013).
  - [6] K. Audenaert and S. Scheel, Accessing the purity of a single photon by the width of the Hong-Ou-Mandel interference, *New J. Phys.* **12**, 113052 (2009).

## 5. Generation of entanglement

**Abstract:** A possible way is application of a laser beam to a nonlinear crystal (parametric down-conversion). Other ways are also shown.

**Keywords:** Laser, optical nonlinearity, nonlinear crystal, parametric down-conversion

## GEDENTQOPT Report Summary

Project ID: [258647](#)

Funded under: [FP7-IDEAS-ERC](#)

Country: Spain

### Final Report Summary - GEDENTQOPT (Generation and detection of many-particle entanglement in quantum optical systems)

Quantum Information Science has become one of the major research fields in physics, to a large extent due to the recent breakthroughs in manipulating the quantum states of cold atoms, trapped ions, and photons. As experimentalists create larger and larger coherent quantum systems, new theoretical methods are needed. On the one hand, meaningful goals must be set for the quantum experiments, by determining the quantum states that are useful for quantum information processing applications. On the other hand, new methods are needed for the verification of the experimentally created state, since full tomography of the quantum state is not possible for state-of-the-art system sizes.

During the last decade, quantum entanglement has been intensively studied within quantum information science and has also appeared as a natural goal of recent quantum experiments. Because of that the theoretical background of detecting entanglement has been rapidly developing. However, most of this development concentrated on bipartite or few-party entanglement, while today's experiments typically involve many particles. Thus, as one of the most interesting part of quantum optics and quantum information, I chose to study multi-partite entanglement theory, with a stress on creation and generation of many-particle entanglement.

As planned in the grant proposal, with external collaborators, we developed Permutationally Invariant Quantum State Tomography, a method for scalable tomography of multipartite quantum systems. The number of measurements needed scale polynomially with the system size, while the scaling is exponential for full state tomography. Our method has been tested in a four-qubit experiment and in a six-qubit experiment with photons, creating Dicke states, in the group of H. Weinfurter in the Max Planck Institute for Quantum Optics in Munich. Our tomographic procedure is one of the few possible choices in many-particle systems with an individual access to the particles, for example, in trapped cold ion quantum registers, photonic systems or, in the near future, optical lattice quantum registers. The above collaboration yielded further results on quantum tomography, concerning the long standing problem of handling the negative eigenvalues of the density matrix obtained experimentally.

In the second part of the project, we considered many-particle systems in which only collective observables can be measured. We determined the full set of spin squeezing inequalities for ensembles of particles with a spin larger than 1/2. Our entanglement conditions are very useful, since most of the experiments are done with such particles. Our set of conditions is a complete set in the sense than no new conditions can be found that detect more entangled states than ours in the large particle number limit. As recent experiments focus more and more on entanglement in cold atomic ensembles, we hope that these inequalities will be used to detect entanglement in the vicinity of important quantum states such as singlets, Dicke states and planar squeezed states.

Connected to one of the entanglement conditions mentioned above, in collaboration with M. W. Mitchell (ICFO, Barcelona), we proposed a spin squeezing procedure, based on a spin squeezing of all the three collective spin observables, that creates a many-body singlet state. We also considered the use of this state for gradient magnetometry and the related problem of modeling the dynamics of large atomic systems analytically. The squeezing of all the three spin components, together with a necessary feedback step followed by incoherent pumping, has been realized experimentally in cold atoms in the group of M. W. Mitchell.

We also developed entanglement conditions that can detect the depth of entanglement close to Dicke states with spin-squeezing inequalities. These have been applied in the cold gas experiments of the group of Prof. C. Klempf at the University of Hannover, Germany. 28-particle entanglement has been detected in an 8000 atoms. Dicke states are quantum states very promising metrologically, since they are more robust to particle loss than Greenberger-Horne-Zeilinger (GHZ) states, while they still make possible to reach, apart from a constant factor, the Heisenberg limit.

The third part of the project was about theoretical issues in quantum metrology. We succeeded to connect multipartite entanglement to quantum metrology and show that genuine multipartite entanglement is needed to achieve the maximum precision in very general metrological tasks in a linear interferometer. This was a missing piece in understanding why this type of entanglement is important. Connected to these findings, experiments have been carried out that detected the entanglement of a quantum state based on the metrological performance of the state in cold atoms (group of C. Klemp, Hannover), and detected multipartite entanglement in photons also based on the metrological usefulness of the quantum state (group of H. Weinfurter, Munich).

We also showed that the quantum Fisher information, a fundamental quantity in quantum metrology, is the convex roof of the variance. This is a very important result, since convex roofs so far appeared only concerning entanglement measures. We used this fact to develop methods to estimate the quantum Fisher information based on few measurements. We also worked out an efficient method to obtain convex roofs numerically.

## Reported by

---

UNIVERSIDAD DEL PAIS VASCO/ EUSKAL HERRIKO UNIBERTSITATEA  
Spain

## Subjects

---

[Physical sciences and engineering - Scientific Research](#)

Last updated on 2017-06-20

## Review article

## Open Access

Nobuyuki Matsuda and Hiroki Takesue\*

# Generation and manipulation of entangled photons on silicon chips

DOI 10.1515/nanoph-2015-0148

Received November 28, 2015; revised January 23, 2016; accepted February 9, 2016

**Abstract:** Integrated quantum photonics is now seen as one of the promising approaches to realize scalable quantum information systems. With optical waveguides based on silicon photonics technologies, we can realize quantum optical circuits with a higher degree of integration than with silica waveguides. In addition, thanks to the large nonlinearity observed in silicon nanophotonic waveguides, we can implement active components such as entangled photon sources on a chip. In this paper, we report recent progress in integrated quantum photonic circuits based on silicon photonics. We review our work on correlated and entangled photon-pair sources on silicon chips, using nanoscale silicon waveguides and silicon photonic crystal waveguides. We also describe an on-chip quantum buffer realized using the slow-light effect in a silicon photonic crystal waveguide. As an approach to combine the merits of different waveguide platforms, a hybrid quantum circuit that integrates a silicon-based photon-pair source and a silica-based arrayed waveguide grating is also presented.

**Keywords:** integrated quantum photonics; quantum optics; entanglement; silicon photonics; quantum information.

## 1 Introduction

Optical waveguide technologies have emerged as promising platforms for quantum information processing systems using

photons [1–3]. The use of waveguides provides increased phase stability and enables the integration of larger numbers of quantum gates in a limited area. With the use of waveguides, several quantum tasks have been implemented, from basic quantum optic experiments [1, 4, 5] to sophisticated quantum information processing such as Shor's algorithm [6], quantum walks [7, 8], and boson sampling [9–14]. In the future, it is expected that such quantum functional circuits will be integrated on chip with other devices such as photon sources [15, 16], functional circuits [17, 18], buffers [19], and detectors [20–23], so that we can realize all optical quantum processors, as shown in Figure 1 [19].

Silica waveguides were first employed as devices for quantum communication [24–26] and then as a platform for quantum computation [1]. Silica waveguides have been developed as a technology to fabricate devices for optical fiber communication for several decades [27], and thus, the fabrication technology is matured. As a result, the loss per unit length of a typical silica waveguide is currently much smaller than that of waveguides based on other materials. On the other hand, as a typical silica waveguide has a relatively large effective area, the bending radius of a silica waveguide is relatively large (typically larger than a millimeter [28]), leading to a larger device size. In addition, it is relatively difficult to realize an active device based on nonlinear-optical effect, such as a photon-pair source on a silica chip, because of the small nonlinearity of silica waveguides. Note that there have been several reports of photon-pair generation [29–31] using femtosecond laser direct written silica waveguides [32].

With silicon photonics technologies, we can implement a variety of quantum functions on waveguides. One such technology is the silicon wire waveguide (SWW), which is a single-crystal, single-mode silicon waveguide typically about 400 nm wide and 200 nm thick. Because of this small cross-section, together with the large nonlinear refractive index of silicon, we can observe an enhanced nonlinear coefficient  $\gamma$  (/W/m) [33] that is much larger than that of a silica waveguide. Several groups have already reported the generation of correlated [15] and entangled [16] photon pairs using an SWW.

\*Corresponding author: Hiroki Takesue, NTT Basic Research Laboratories, NTT Corporation, 3-1 Morinosato Wakamiya, Atsugi, Kanagawa, 243-0198, Japan, e-mail: takesue.hiroki@lab.ntt.co.jp  
**Nobuyuki Matsuda:** NTT Basic Research Laboratories, NTT Corporation, 3-1 Morinosato Wakamiya, Atsugi, Kanagawa, 243-0198, Japan; and Nanophotonics Center, NTT Corporation, 3-1 Morinosato Wakamiya, Atsugi, Kanagawa, 243-0198, Japan

Edited by Benjamin J. Eggleton and Tara Dorrian

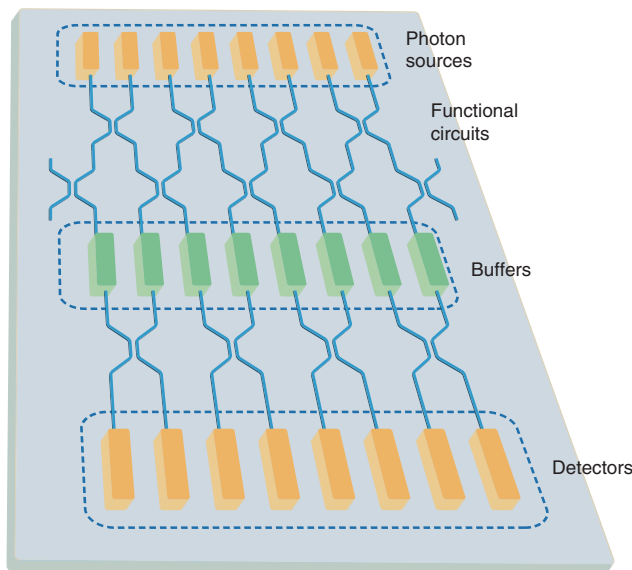


**Figure 1:** Conceptual diagram of a photonic quantum processor based on integrated quantum photonics.

In this paper, we review the recent progress in integrated quantum photonics based on silicon photonics technologies. Section 2 describes a monolithic polarization entangled photon-pair source on a silicon chip. In Section 3, we describe efforts for realizing ultrasmall correlated and entangled photon-pair sources, based on a silicon photonic crystal (PhC) technology. In Section 4, we introduce a novel function – an on-chip single-photon buffer – realized using PhC technology. We then describe a hybrid approach to integrate active function based on an SWW and a passive function based on a silica waveguide so that we can realize sophisticated photonic quantum information systems. In Section 6, we provide a brief summary.

## 2 Polarization entangled photon-pair source on a silicon chip

Quantum states of photons can be encoded in polarizations, paths, orbital-angular momentum, frequencies, and temporal positions of light. Of these, a polarization state provides a two-level photonic system, which is easy to manipulate with commercial bulk optics such as waveplates. Hence, it has been at the heart of many quantum information experiments [34–38]. To integrate a polarization-encoded quantum information system on a chip, it is necessary to develop the building blocks, including a polarization entanglement photon-pair source [39, 40].

However, the integration of optical circuits makes handling the polarization slightly more challenging. This is because it is difficult to eliminate the polarization-mode walk-off in a nonlinear waveguide completely [41], which degrades the polarization-encoded quantum states. To compensate for the walk-off, polarization entanglement sources using on-chip waveguides require extra off-chip components [42–46].

We demonstrated the first polarization-entangled photon-pair source fully integrated on a chip as shown in Figure 2 [47]. It consists of two SWW photon-pair sources connected by an ultrasmall silicon polarization rotator [48, 49]. The SWWs have a silicon core that is 400 nm wide, 200 nm high, and 1.5 mm long. The silicon polarization rotator has 30- $\mu\text{m}$ -long off-axis double cores. The inner and outer cores are a silicon wire (200 nm wide and 200 nm high) and a  $\text{SiO}_x\text{N}_y$  waveguide (840 nm wide and 840 nm high), respectively. The SWWs and the polarization rotator are connected by 10- $\mu\text{m}$ -long tapered silicon wires. The undercladdings and overcladdings are  $\text{SiO}_2$ . For efficient coupling with external optical fibers, both ends of the device are equipped with spot-size converters that are based on an inverted taper structure of the silicon core.

The SWWs and the spot-size converters were fabricated by electron beam lithography and electron cyclotron resonance plasma etching. An 840-nm-thick silicon

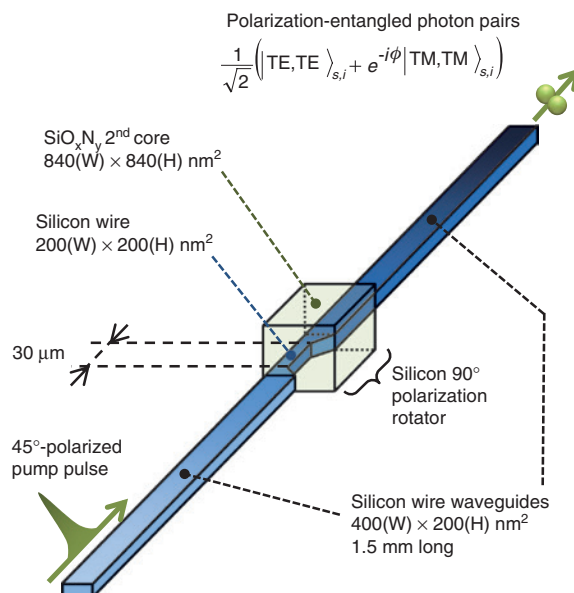


**Figure 2:** A polarization entangled photon pair source fabricated on a silicon-on-insulator substrate. The device consists of two silicon wire waveguide photon pair sources and a silicon-wire-based polarization rotator. The silicon substrate and the  $\text{SiO}_2$  overcladdings and undercladdings are not shown for clarity [47].

oxynitride film with a refractive index of 1.60 was deposited by the plasma-enhanced chemical vapor deposition, and the second core of the silicon polarization rotator was formed by reactive ion etching with fluoride gas.

In an SWW, a correlated pair of signal and idler photons is created following the annihilation of two pump photons via spontaneous four-wave mixing (FWM) arising from the bound-electronic  $\chi^{(3)}$  nonlinearity of the silicon core. Due to the high  $\chi^{(3)}$  nonlinearity of silicon in the telecommunication band (e.g. more than 100 times higher than that of silica) and the submicrometer scale mode field diameter [50, 51], correlated photons can be efficiently generated via spontaneous FWM in an SWW [15, 16, 52, 53]. Moreover, the Raman noise photons in a single-crystalline silicon core, which exhibit a sharp spectral peak that is 15.6 THz away from the pump frequency, can be easily eliminated with wavelength filters. Hence, low-noise correlated photons can be efficiently generated in an SWW [54].

Figure 3A shows the wavelength dependence of FWM efficiency in an SWW for cases where the pump, signal, and idler fields are all in the transverse-electric (TE) or transverse-magnetic (TM) mode. We obtained the data via a stimulated FWM experiment [55, 56], where we used two independent wavelength-tunable continuous wave (CW) lasers for the pump and stimulating signal field and observed the overall output spectrum including the generated idler field. Here, the signal wavelength (vertical axis) was scanned while the pump wavelength was fixed. We see that the idler components satisfied the energy conservation of the FWM  $2\omega_p = \omega_s + \omega_i$ , where  $\omega_{p,s,i}$  denotes the frequencies of the pump, signal, and idler fields. Due to a difference in the lateral field confinements and dispersions between the TE and TM modes, the FWM efficiently occurred for the all-TE condition in our SWW.

In the silicon polarization rotator [48], the off-axis double core structure induces two orthogonal eigenmodes with the polarization axis tilted  $\pm 45^\circ$  to the horizon and slightly different refractive indices as shown in Figure 3B. This birefringence provides an on-chip waveplate with fixed birefringence axes. The polarization rotation of a linearly polarized input field depends on the length of the rotator. We used a rotator with a length of 30  $\mu\text{m}$ , which provided a zeroth-order polarization rotation angle of  $86.7 \pm 0.1^\circ$  and a polarization extinction ratio exceeding 20 dB for a TE-polarized CW laser at around 1551-nm wavelength [47]. Hence, the rotator served as an on-chip polarization converter between the TE and TM modes, which was the function required for our polarization entanglement source. The insertion loss of the rotator is approximately 1 dB [48].

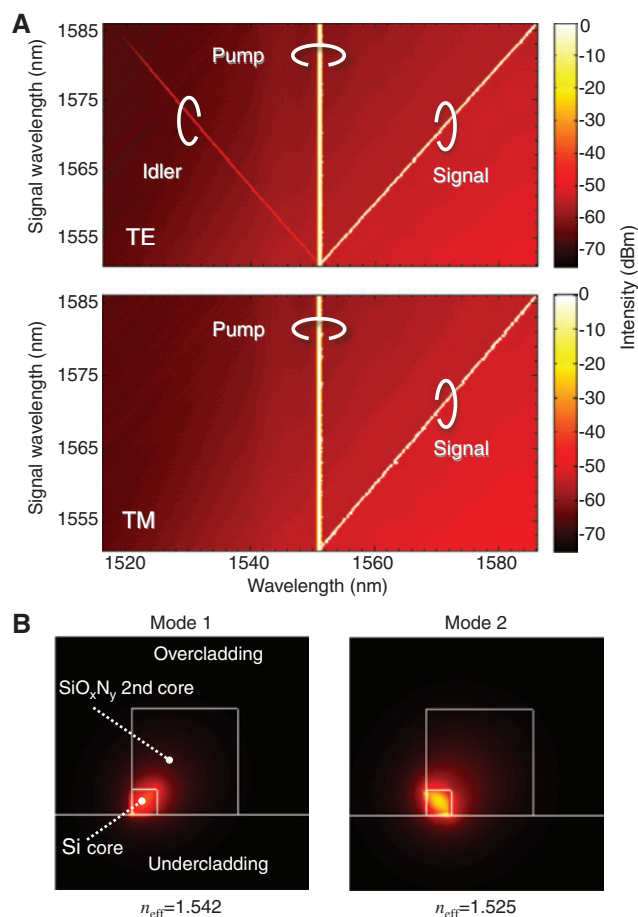


**Figure 3:** (A) Polarization dependence of the FWM efficiency in an SWW, investigated via stimulated FWM experiment. The density plots show the observed spectrum as a function of the center wavelength of the CW laser used for stimulating signal field. (B) The eigenmodes in the silicon polarization rotator, numerically simulated with a mode solver. Corresponding eigenvalues (effective refractive indices) are also shown. Figures from Ref. [47].

Pump pulses with  $+45^\circ$  linear polarization are injected into the polarization entanglement source. Then the input is decomposed into the TE and TM modes in the waveguides. In the first SWW, only the TE-polarized component of the pump pulses creates photon pairs in the TE mode because of the abovementioned polarization dependence. The polarization state of the correlated photons is then converted to the TM mode by the polarization rotator. At the same time, the silicon polarization rotator converts the polarization of TM-polarized pump pulses to TE; these pump pulses create TE-polarized correlated photons in the second SWW. Due to the quantum interference between the photon pairs created in the first and second SWWs, we obtain the following polarization entangled state of photons:

$$|\psi\rangle = \frac{1}{\sqrt{2}}(|TE, TE\rangle_{sj} + e^{-i\phi}|TM, TM\rangle_{sj}), \quad (1)$$

at the output end of the device. Here,  $\phi$  is a fixed relative phase. The configuration automatically equalizes the two amplitudes and thus provides a maximally entangled state. This is because the reduction of the pairs created in the first SWW from the waveguide loss in the second SWW is equivalent to the reduction of the pairs to be created in the second SWW owing to the loss of the TM component of the input pump pulses in the first SWW [47].

The operation is similar to that of a widely used polarization entanglement source utilizing  $\chi^{(2)}$  nonlinear crystals designed for spontaneous parametric down conversion under type I phase matching [40]. The source consists of two nonlinear crystals cascaded with  $90^\circ$  orientation, and horizontally and vertically polarized photon pairs are created in each crystal. In our case, instead of cascading two crystals with  $90^\circ$  orientation, we rotated the polarization between the two SWWs. Thus, the device is designed to be symmetric as regards the polarizations with respect to the midpoint of the device. This structure eliminates the degradation of the output entangled state caused by polarization-dependent walk-offs and losses in the waveguide [47].

The experimental setup is shown in Figure 4A. We input pump pulses with a temporal width of 80 ps and a repetition rate of 100 MHz, obtained by an intensity modulation of a CW laser operated at a wavelength of 1551.1 nm. The polarization of the input pulses was set to be  $+45^\circ$  linear polarization. The in-coupled pump peak power was 128 mW. The output signal and idler photons were collected by a lensed fiber and subsequently separated with the wavelength-division-multiplexing filter after they had passed through the notch filters for the pump field rejection. The bandwidth of each channel was 0.14 nm (18 GHz). The time correlated events of the photons were detected with the two InGaAs single-photon avalanche diodes (SPADs) (id210, ID Quantique) and a time-interval analyzer (TIA).

We then performed quantum state tomography on the generated photons [57] by carrying out a polarization-correlation measurement with the polarization analyzers. The reconstructed density matrix  $\rho$  of the photons obtained with the maximum-likelihood estimation is shown in Figure 4B. We clearly observed off-diagonal components with amplitudes as high as those of the diagonal components, indicating a high purity of the state. To evaluate the degree of entanglement, we estimated the fully entangled fraction  $F(\rho) = \max_{\Psi} \langle \Psi | \rho | \Psi \rangle$ , where the maximum is taken over all maximally entangled states

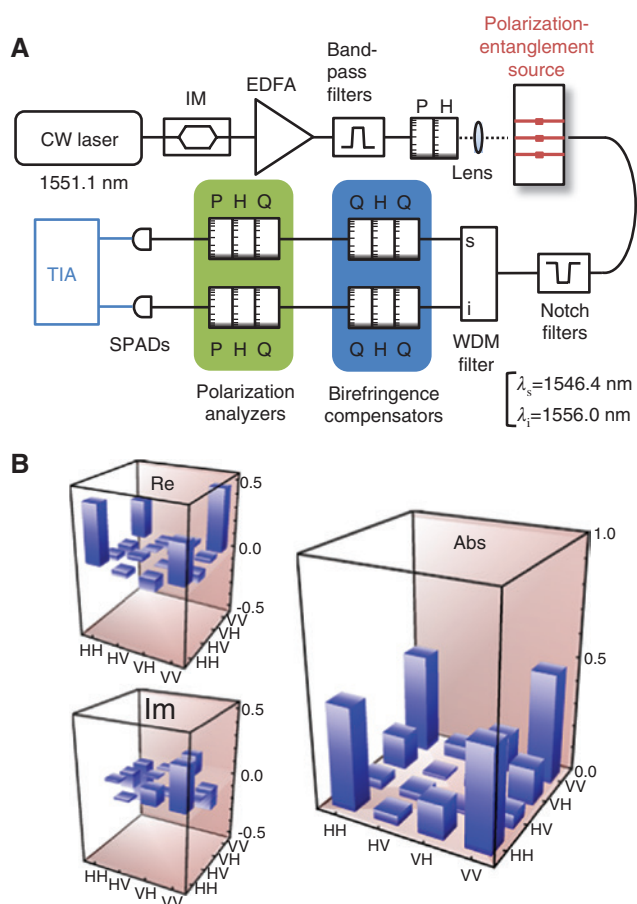


**Figure 4:** (A) Experimental setup for the measurement of polarization entanglement from the chip. IM: intensity modulator, EDFA: Erbium-doped fiber amplifier, P: polarizer, H: half-wave plate, Q: quarter-wave plate, WDM filter: wavelength-division multiplexing filter. Dashed and solid lines show free-space optical path and electrical connection. (B) The reconstructed density matrix of the two-photon polarization state generated from the chip. H and V represent the TE and TM modes, respectively [47].

$|\Psi\rangle$  [58, 59]. The obtained  $F(\rho) = 0.91 \pm 0.02$ . Hence, we have successfully generated photons with a high degree of polarization entanglement using the on-chip source. The imperfect fidelity was considered to be mainly due to the wavelength-dependent polarization rotation at the spot-size converters.

Following this work, many researchers demonstrated on-chip polarization entangled sources based on other device architectures and materials. Ollslager et al. [60] generated polarization entanglement using two SWWs that were monolithically connected by a two-dimensional (2D) vertical grating coupler. Lv et al. [61] generated polarization entanglement by means of the birefringence of a single SWW. Various polarization entanglement sources based on an  $\chi^{(2)}$  nonlinear waveguide made of (Al)GaAs have also been demonstrated [62–66]; these experiments

employing the direct band-gap materials paved the way to the realization of a polarization entanglement source driven by current injection [67, 68]. These results show important steps toward the realization of an integrated quantum information system using the polarizations of light.

In order to realize a polarization-encoded quantum information processor on chip, we need to develop polarization analysis functions, namely the manipulation and projection of polarization states on a chip. Recently, such functions have been achieved using a lithium niobate waveguide modulator [69] and low-birefringence silica waveguides [70–72].

### 3 Ultrasmall correlated and entangled photon-pair sources using PhC coupled-resonator optical waveguides

We used chip-scale SWWs as a bright and low-noise source of correlated photons. However, further downsizing of the photon source is of great importance in a view to realizing quantum information processing systems with higher integration density. Such integration includes a multiplexed single-photon source [73–76], which was proposed to realize a near-deterministic heralded single-photon source from probabilistic photon-pair sources based on spontaneous parametric processes. The source is a bundle of many identical heralded single-photon sources, each of which generates photon pairs at a low rate ( $\sim 0.01$  pairs/pulse). The whole system provides single photons at a certain period while the multiple pair generation rate is suppressed. This scheme requires many independent photon-pair sources connected with single-photon routing technology. Thus, increasing the integration density of photon-pair sources is required. Another promising approach to realize a near deterministic heralded single-photon source is to employ a temporal multiplexing configuration [77]. This configuration will avoid the size constraints in the spatial multiplexing described above, though at the expense of the reduced repetition frequency of the “triggered” single photons.

A simple solution for further downsizing is to enhance the optical nonlinearity of the photon-pair source per unit size. An effective way to achieve this is to slow down the group velocity of light in a medium  $v_g$  [78–81]. This is because the light-matter interaction time can be prolonged by the slow propagation of light. Furthermore,

the slow-light mode compresses the optical field longitudinally so that its peak intensity increases, leading to a further enhancement of nonlinearity. Because of these effects, the nonlinear constant  $\gamma$  of an optical waveguide is proportional to  $n_g^2$ , where  $n_g = c/v_g$  is the group index of the guided mode. Hence, we can significantly increase the nonlinearity and thereby the photon-pair generation rate via the spontaneous FWM ( $\propto \gamma^2$ ) by using the slow light effect.

Slow-light enhancement has been investigated particularly in relation to a silicon photonics platform, where mature nanofabrication technologies allow us to engineer the group velocity of light. Slow-light modes in silicon PhC line defect waveguides [82, 83], and coupled-resonator optical waveguides (CROWs) [84] based on Si microring resonators [85] have been shown to enhance the efficiency of spontaneous FWM. We have demonstrated slow-light enhancement [86] using a CROW consisting of PhC cavities based on mode-gap confinement [87, 88]. The cavity exhibits an ultrahigh  $Q$  value and wavelength-sized confinement of light, which enabled us to realize a low-loss and highly nonlinear waveguide. In the following, we review our recent work related to the PhC-based CROW and its application to the photon-pair sources [86, 89–91].

Figure 5 shows a schematic of our CROW fabricated on an air-bridged 2D silicon PhC slab with a triangular lattice of air holes [89]. Lattice constant  $a$  is 420 nm, the hole radius is  $0.25a$ , and the slab thickness is  $0.25a$ . Each cavity is formed by a local width modulation of a barrier line defect with a width of  $0.98\sqrt{3}a$  (W0.98) along the  $\Gamma$ -K direction. The red and green holes are shifted by 8 and 4 nm, respectively, in plane toward the outside. This yields optical cavities with a cavity  $Q$  as high as  $10^6$  and a mode volume of  $1.7(\lambda/n)^3$  [87, 88].

In a CROW, the collective resonance of the identical cavities exhibits Bloch modes, whose bandwidth is much larger than that of each cavity linewidth. The mode follows a dispersion relation given by

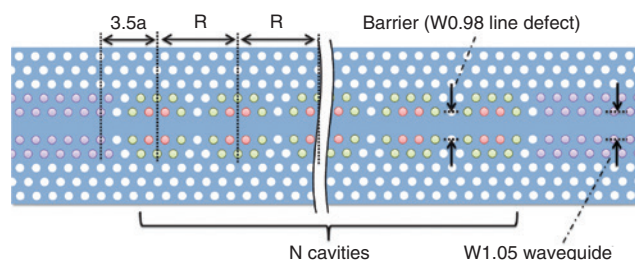


**Figure 5:** A CROW consisting of photonic-crystal mode gap nanocavities.

The positions of the red and green holes are shifted by 8 and 4 nm toward the outside, respectively [89].

$$\omega = \omega_0(1 + \Delta + \kappa_1 \cos(KR)) \quad (2)$$

under the tight-binding approximation [84]. Here,  $\kappa_1$  is nearest neighbor coupling strength between cavities,  $\omega_0$  is the center frequency of each cavity,  $\Delta$  is the center frequency offset of the band from  $\omega_0$ , and  $R$  is cavity pitch. This band formation for photons is analogous to electronic band formation of atoms in a crystal lattice. The bandwidth of the supermode is  $2\omega_0\kappa_1$ , and at center frequency  $\omega = \omega_0$ , the group-velocity dispersion is zero and the group velocity becomes  $v_g = \frac{d\omega}{dK} = \omega_0\kappa_1 R$ . Thus, we can

control  $v_g$  by designing  $\kappa_1$  and  $R$ . CROWs consisting of more than a 100 resonators have been developed using short waveguide elements [92], microring resonators [93, 94], microdisk resonators [95], and PhC cavities [87]. So far, a  $v_g$  value as small as  $c/170$  for an optical pulse has been realized using a PhC-based CROW [87].

To couple the light to our CROW, access waveguides consisting of W1.05 line-defect waveguides and SWWs (not shown) were fabricated. Intercavity distance was apodized at the CROW-waveguide connection. Reference waveguides, where the CROW section was replaced with a W1.05 line defect waveguide, were also fabricated on the same chip. The reference waveguide had  $n_g \sim 5$ .

Figure 6A shows linear transmission spectra of the CROWs (with  $R=5a$  and cavity number  $N=200$  and 400) and the reference waveguide, measured with a wavelength-tunable CW laser at TE polarization [89]. Each CROW exhibited a clear passband with isolations of over 30 dB. The loss comprised fiber-waveguide coupling loss (-8 dB/facet), waveguide propagation loss (-2 dB/mm), and additional loss at waveguide-CROW connections (-1 dB/facet).

The CROW with  $N=200$  exhibited a transmission bandwidth of 6 nm, from which  $\kappa_1$  was estimated to be  $1.9 \times 10^{-3}$  from Eq. (2). The value agreed well with that obtained from CROWs with smaller  $N$  (5 and 10) [87]. This indicated that the slow-light mode was extended toward the region over 100 cavities, where it was less influenced by structural fluctuation due to fabrication error. A statistical analysis [96, 97] revealed that the light transport in our CROW is less relevant than in a localized or diffusive transport regime [89]. On the other hand, we saw a decrease in the transmission bandwidth for  $N=400$ . This was because of degradation of the light transport characteristics, which was also indicated by the statistical analysis in the corresponding wavelength region [89]. However, the signature of the ballistic transport held in the wavelength region surrounded by the dashed lines in Figure 6A, where we could observe slow-light

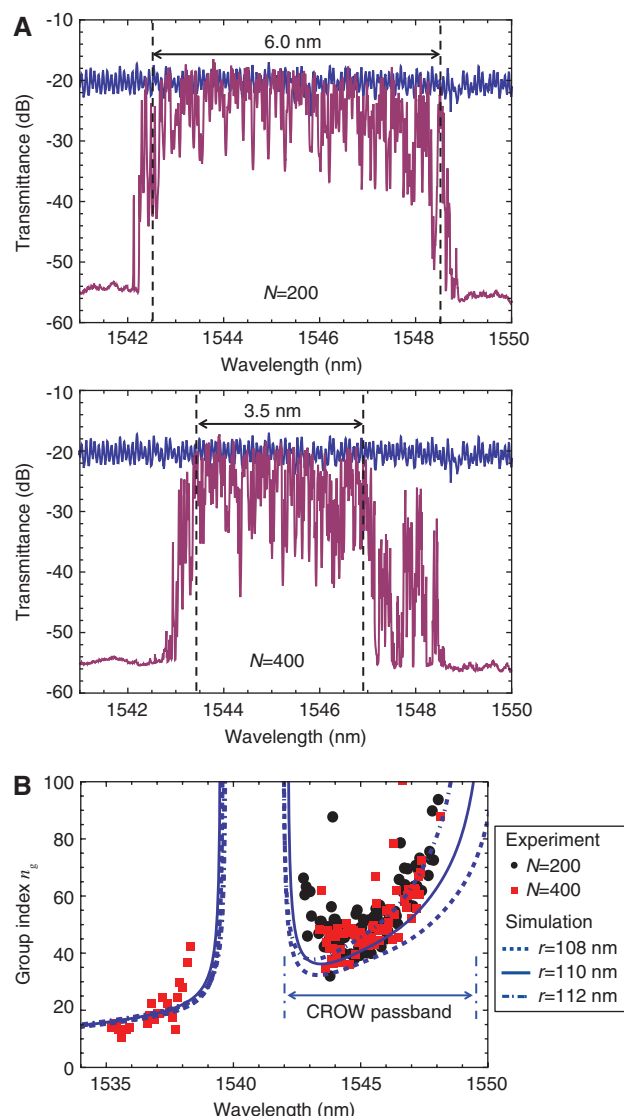


**Figure 6:** (A) Transmission spectra of CROWs (red curves) and a W1.05 line-defect waveguide (blue curves). (B) Measured group index spectra for CROWs with various cavity numbers along with the numerical simulation results based on the plane-wave expansion method. Figures from Ref. [89].

propagation without significant pulse distortion [19] (see Section 4).

The dispersion properties of the CROWs were investigated with the pulsed time-of-flight method [89]. Plots in Figure 6B show the measured  $n_g$  spectra. The data were extracted from the transit time difference of optical pulses (duration: 80 ps) between the CROWs and the reference waveguides. A slow-light mode with  $n_g \sim 40$  was obtained at around the band center. In addition, the  $n_g$  values were independent of the cavity number  $N$  as expected.

However, the dispersion curve was asymmetric with respect to the center of the CROW passband, distinct from

the shape given by Eq. (2). This is because the tight-biding model assumes that the resonator eigenmodes are nondispersive. In our case, the cavity confinement was based on the modulation of the line defect, whose mode exhibited dispersion. In fact,  $v_g$  at the band center was estimated to be  $c/65$  from Eq. (2), which is distinct from the observed value at around the band center. Lian et al. [98] explained this by introducing an energy dependence in  $\kappa_1$ . Another reason for the discrepancy is the effect of the next-nearest-neighbor coupling between cavities, which was investigated by Caselli et al. [99].

To confirm that the observed modes were induced by our CROW structure shown in Figure 5, we performed a numerical simulation of the dispersion, namely, the photonic band structure, with a three-dimensional vector plane-wave expansion method using BandSOLVE (Synopsys, Inc., Mountain View, CA USA) [89]. The results are shown as curves in Figure 6B. The numerical results showed good agreement with the experimental data, including the asymmetric shape. The mode at the wavelength region shorter than the minigap at around 1540 nm appeared due to the band folding of the original line-defect mode at the CROW periodicity of  $R=5a$ . This also well explained the experimental data.

Using the CROW, we investigated the slow-light enhancement of  $\chi^{(3)}$  nonlinearity for the correlated photon-pair generation [86]. In doing so, we performed the stimulated FWM experiment as described in Section 2. The observed FWM spectra are shown as a density plot in Figure 7. The pump and signal powers coupled to the waveguides were 1.6 and 0.5 mW, respectively. In both cases, we observed the idler wavelength component satisfying the energy conservation of the FWM. However, the CROW exhibited the brighter idler peaks, thanks to the slow-light-enhanced nonlinearity. From the result, we estimated nonlinear constant  $\gamma$  of the CROW to be 7200/W/m at  $n_g=36$  and 13,000/W/m at  $n_g=49$ . These values are much larger than that of an SWW (typically 200–300/W/m). Indeed, this is the first experimental observation of a  $\gamma$  value exceeding 10,000/W/m in a silicon-core nonlinear waveguide. Note that we used a CROW sample different from the one used in the stimulated FWM experiment above (but with the same specifications).

Next, we undertook the photon-pair generation experiment via the spontaneous FWM in our CROW [90]. Figure 8A shows the experimental setup. We obtained pump pulses centered at 1545.4 nm with a pulse duration of 130 ps and repetition rate of 100 MHz using a setup similar to that shown in Figure 4A. The output pulses containing correlated photons were collected with a lensed fiber. Notch filters with a suppression bandwidth of

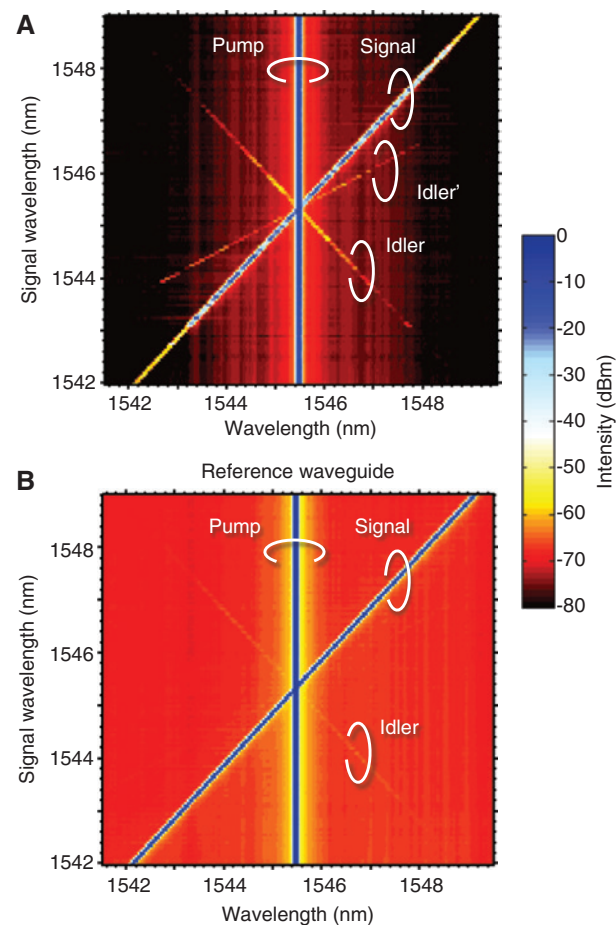


**Figure 7:** Stimulated FWM spectra using (A) the CROW with  $N=200$  and (B) the W1.05 reference waveguide. The line labeled Idler' in (A) was generated as a result of frequency conversion of the “pump” via FWM pumped by the “signal” [86].

1.0 nm centered at the pump wavelength were introduced for the pump field rejection. Then, the photon pairs were separated by the arrayed waveguide grating (AWG) into different fiber channels with a transmission bandwidth of 0.2 nm (25 GHz). The pump-to-signal (or -idler) detuning was chosen to be 0.8 nm, which was within the FWM bandwidth as seen in Figure 7A. After further noise suppression, the photons were received by the single photon counting modules (SPCMs), and their temporal correlation was analyzed by the TIA. The overall transmittance of the filtration system was approximately -6 dB, while the transmittance at the pump wavelength was <-130 dB.

Figure 8B shows the estimated photon-pair rate at the output ends of the waveguides as a function of the in-coupled average power of the pump pulses. The measurement time was 120 s for each data point for good statistics. We were able to successfully observe the slow-light enhancement of the photon-pair generation rate in our CROW. Indeed, the generation rate was almost two orders of

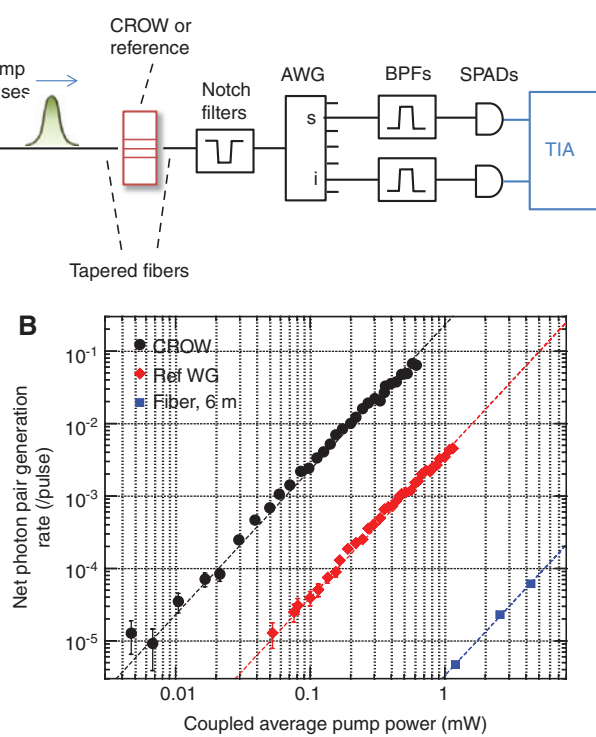


**Figure 8:** (A) Experimental setup for correlated photon pair generation from the CROW. AWG: arrayed-waveguide grating. (B) Net photon pair generation rate from various waveguides as a function of the in-coupled average pump power. Dashed lines represent fitting results using Eq. (3) [90].

magnitude larger than that with the reference line-defect waveguide. The photon-pair generation in 6-m fiber links for the measurement was negligible.

Under the slowly varying envelope approximation, we obtain the photon-pair generation rate per pump pulse  $\mu_c$  via spontaneous FWM as

$$\mu_c = \Delta\nu\Delta t(\gamma P_{\text{peak}} L_{\text{eff}})^2 \quad (3)$$

when the pump-to-signal (or -idler) detuning is within the FWM bandwidth, where  $\Delta\nu$  is the bandwidth of the wavelength filters for the signal and idler channels,  $\Delta t$  is the temporal width of the pump pulses, and  $P_{\text{peak}}$  is the pump peak power.  $L_{\text{eff}}$  is the loss-averaged effective waveguide length associated with  $L_{\text{eff}} = (1 - e^{-\alpha L})/\alpha$ , where  $\alpha$  is the attenuation coefficient.

The dashed lines in Figure 8B show the fittings using Eq. (3). One can see that the experimental data exhibited good power-squared dependence. From the fitted function for the CROW, we obtained a  $\gamma$  of 9000/W/m, which was in good agreement with that obtained via the stimulated FWM experiment. This value was ~30 times larger than that of standard SWWs [53]. In other words, the

photon-pair generation rate of our CROW was  $10^3$  times larger than in an SWW per unit length.

We also verified the nonclassicality of the photon pairs from the CROW by testing the violation of the Zou-Wang-Mandel inequality, which is valid for classical correlation [100]. We have successfully demonstrated the violation by 20 standard deviations. Hence, we confirmed the generation of nonclassical photon pairs from the CROW based on the PhC nanocavities [90].

Furthermore, we have demonstrated the generation of time-bin entangled photons from the CROW [91]. The experimental setup is shown in Figure 9A. A 60-ps, 1-GHz clock coherent pulse train with a wavelength of 1545.5 nm was launched into the CROW with  $N=200$ . Through the slow-light enhanced SFWM in the CROW, we generated high-dimensional time-bin entangled photon pairs whose state is given by

$$|\Psi\rangle = \sum_{k=1}^{N_c} |k\rangle_s |k\rangle_i, \quad (4)$$

where  $N_c$  is the number of pump pulses where coherence is preserved and  $|k\rangle_x$  denotes a quantum state where a single photon is at the  $k$ th temporal slot in mode  $x$  ( $=s$ : signal,  $i$ : idler). The photons from the CROW were passed through filters similar to the ones in Figure 8A and launched into 1-bit delayed Mach-Zehnder interferometers for Franson

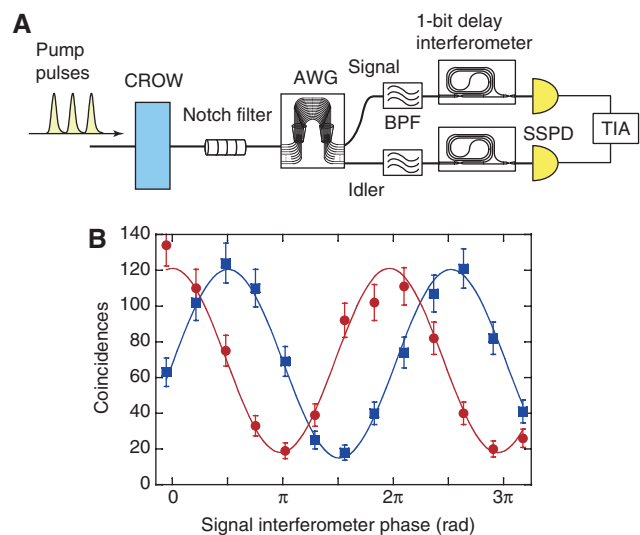


**Figure 9:** Time-bin entangled photon-pair generation using the CROW.

(A) Experimental setup. SSPD: superconducting single-photon detector. The wavelengths of the signal and idler channels were 1544.6 and 1546.2 nm, respectively. The photon bandwidth was 0.1 nm, limited by the bandwidth of the AWG. (B) Two-photon interference fringes. Squares: idler interferometer phase at 0, circles:  $\pi/2$ .

interferometry measurement [101]. The obtained two-photon interference fringes are shown in Figure 9B, where we observed clear sinusoidal modulations of coincidences for two nonorthogonal measurement bases for the idler photons. The visibilities of the fringes were  $78.0 \pm 3.9\%$  (idler interferometer phase 0) and  $74.1 \pm 4.8\%$  ( $\pi/2$ ), which indicates that we obtained an entangled state that can violate Bell's inequality. This was the first observation of quantum entanglement generated from a slow-light waveguide.

## 4 On-chip quantum buffer

In the photonic quantum circuit shown in Figure 1, synchronization of photons at functional circuits is crucial for obtaining quantum interference. Such integration becomes more difficult as the integration density increases and the circuits are further scaled down. A buffer can store a photon for a certain amount of time so that we can adjust the arrival time of a photon at each circuit. Inclusion of such a buffer enables a flexible circuit design. In addition, we may be able to realize a fully programmable integrated quantum optical circuit if we use a tunable buffer together with other active elements such as optical switches.

We can realize an integrated single-photon buffer by using the slow-light effect in optical waveguides [79, 80, 93]. We demonstrated a single-photon buffer on a silicon chip using the PhC-based CROW with the number of cavities  $N=400$  (inset of Figure 10) [19]. The total length of the CROW was 840  $\mu\text{m}$ . A 10- $\mu\text{m}$  PhC line-defect waveguide

was placed at each end of the CROW. The transmission spectrum of the CROW moved to longer wavelength as we increased the chip temperature, and the dependence was measured to be  $\sim 0.07 \text{ nm}/^\circ\text{C}$ .

The experimental setup for observing photon buffering is shown in Figure 10. A photon-pair source based on spontaneous FWM in a dispersion shifted fiber emitted photon pairs whose wavelengths were 1546.7 (signal) and 1555.53 (idler) nm. The bandwidth of the photons was 0.2 nm. The signal photon was coupled to the silicon chip that included the CROW and the reference waveguide using lensed fibers. The reference waveguide (the W1.05 line defect) was used as the temporal reference when measuring the delay caused by the CROW. The signal photons outputs from the chip were received by a superconducting single-photon detector (SSPD), while the idler photons were directly detected by a second SSPD. The detection signals from the SSPDs were input into a time interval analyzer as the start and stop signals, respectively.

Figure 11A and B shows the histograms obtained in the time interval analysis. We observed the largest peaks at the relative delay near 0, which correspond to the coincidences caused by the signal and idler photons that form correlated pairs. From these data, the cross-correlation  $g_{si}^{(2)}(0)=P_{si}/P_s P_i$  [ $P_{si}$ : coincidence detection probability,  $P_s$  ( $P_i$ ): signal (idler) photon detection probability], with which we can quantify the strength of intensity correlation between photons [102], was obtained as  $3.25 \pm 0.06$  for the CROW and  $3.10 \pm 0.05$  for the reference waveguide. Note that  $g_{si}^{(2)}(0) > 2$  implies the existence of nonclassical intensity correlation [102]. The cross-correlation value was  $3.22 \pm 0.05$  when we removed the chip, suggesting that the nonclassical intensity correlation was preserved even after the single photon had travelled through as many as 400 high-Q nanocavities without any degradation.

The coincidences at the main peaks correspond to the temporally resolved detection events of the single photons heralded by the detection of idler photons. Thus, we could measure the delay time of the signal photons in the CROW by observing the temporal shift of the main peaks. An enlarged image of the main peaks in Figure 11A and B is shown in Figure 11C, where we can observe a clear separation of the two peaks. This result shows that the CROW stored the single photon for  $151.1 \pm 0.5$  ps. The group index  $n_g$  of the reference waveguide was  $\sim 5$ , which means that the speed of the pulsed photon in the CROW was decreased to 1/59 of the light speed in a vacuum.

We can also tune the buffer time with the CROW. As stated above, the transmission spectrum of the CROW moved as we changed the chip temperature. This implies that we can shift the dispersion characteristic of the

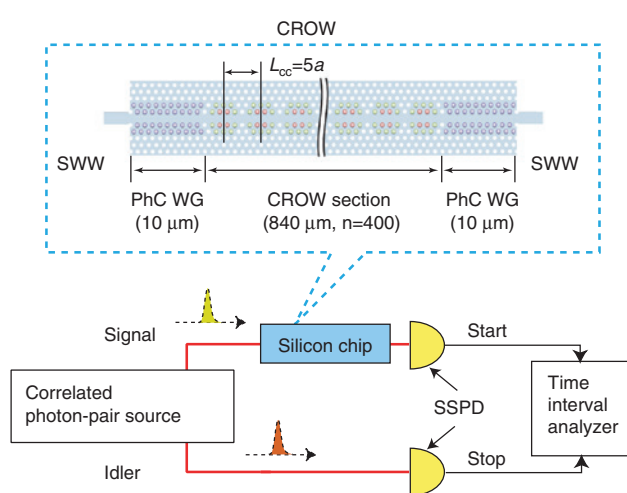


**Figure 10:** Setup for observing photon buffering.  
Inset: CROW consisting of PhC nanocavities.

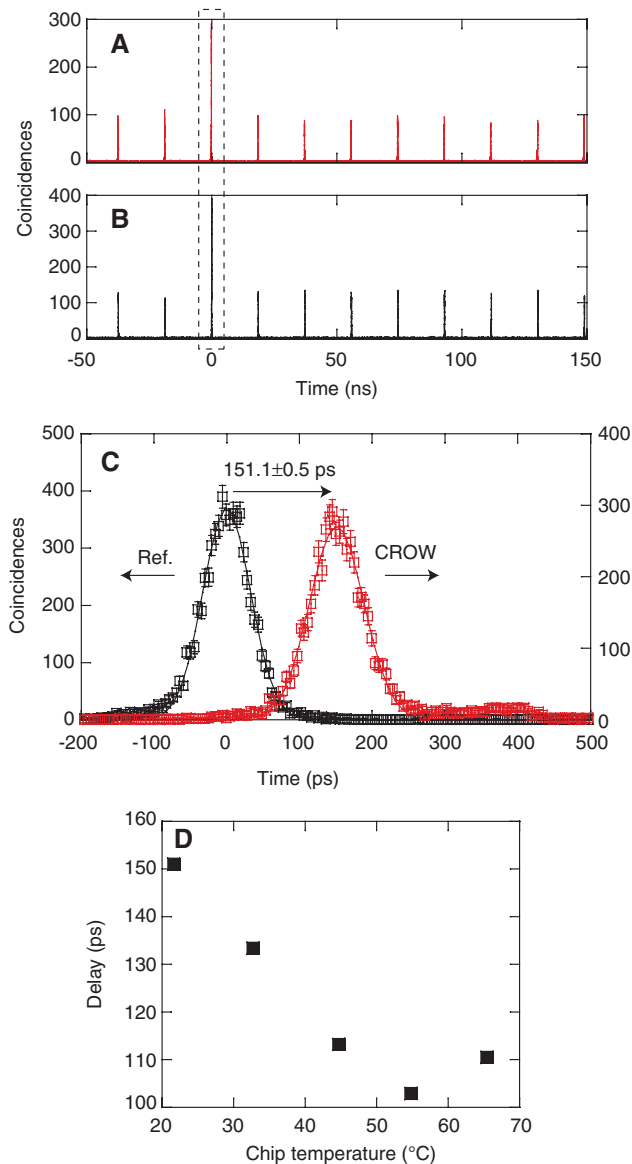


**Figure 11:** On-chip buffer experimental results.

(A, B) Time interval histograms when the signal photons passed through the (A) CROW and (B) reference waveguide. (C) Enlarged main peaks observed in dashed box in (A) and (B). The red and black squares show the histograms obtained with the CROW and the reference waveguide, respectively. (D) Delay caused by the CROW as a function of chip temperature [19].

CROW by changing the temperature. In fact, we observed a change in the delay time when varying the chip temperature in a measurement similar to the one from which we obtained the data shown in Figure 11C. The experimentally obtained delay time as a function of the chip temperature is shown in Figure 11D. Thus, we could tune the buffer time by  $\sim 50$  ps with a waveguide as short as 840  $\mu$ m. Note that we need 1.5-cm variable delay for 50-ps tunability in free space.

## 5 Silicon-silica hybrid waveguide platform for integrated quantum photonics

As we discussed so far, intensive studies are under way with the aim of developing on-chip quantum information devices, such as the processor shown in Figure 1. To fully exploit the advantages of integrated photonics, it would be ideal to integrate these different components on a single substrate. Motivated by this, many researchers have recently demonstrated the hybrid integration of different quantum-optical components [103–109]. Hence, the stage of integrated quantum photonics research is now moving to hybrid integration on a chip.

Among the building blocks, quantum circuits can be realized by using integrated waveguides with cores made of silicon [18, 108, 110], GaAs [111], or silica-based materials [1, 10, 13, 112]. Of these approaches, silica-based waveguide technology has realized planar lightwave circuits with a significantly large scale for classical optical communication [113, 114]; this capability will facilitate the construction of large-scale quantum circuits. In this context, a research group including an author of this paper has recently realized a silica-based universal linear optical circuit, which is capable of implementing any unitary operations to path-encoded quantum states with full reprogrammability [17]. In addition, the low nonlinearity of silica [115] helps in avoiding the generation of unwanted photons by the intense pump fields used for photon-pair generation in quantum light sources. To exploit these advantages, integrating quantum light sources and silica waveguides is an attractive approach for constructing on-chip quantum information systems.

As stated above, silicon waveguides are useful as photon-pair sources. To incorporate the advantage of silicon with that of silica-based quantum circuits, we have realized a silicon-silica monolithic integration platform as shown in Figure 12 [116]. The platform consists of a silicon and silicon-rich silica ( $\text{SiO}_x$ ) waveguides that are adiabatically interconnected with spot-size converters [117, 118]. The  $\text{SiO}_x$  waveguides have a core-cladding index contrast of  $\sim 3\%$ . The coupling loss at the spot-size converter interface is as small as  $-0.35$  dB per connection [119].

We investigated the photon-pair generation property of the silicon-silica monolithic waveguide platform. From experiments using waveguides with various lengths, we confirmed that most of the photon pairs were generated in the silicon waveguide region. Hence, the contribution of our silica-based waveguide to unnecessary photon generation was negligible as expected. Furthermore, the

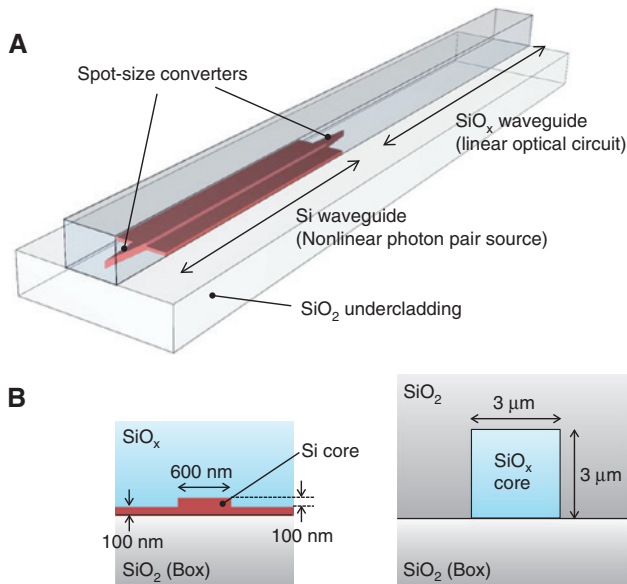


**Figure 12:** (A) Silicon-silica monolithic waveguide platform for integrating photonic quantum information devices. The silica overcladding and silicon substrate are not displayed for clarity. (B) Cross-sectional views of each waveguide section [116].

nonlinearity of the silicon waveguide  $\gamma$  was estimated to be  $161/\text{W/m}$ , which is as high as that of silicon waveguides fabricated without the  $\text{SiO}_x$  deposition process [53].

Toward full-scale integration, an important step is the integration of a photon-pair source with its interface, namely, a photon-pair demultiplexer. Using the monolithic platform, we constructed a chip capable of generating and demultiplexing quantum correlated photons [89]. Figure 13A is a schematic diagram of the monolithic device together with the experimental setup. In the device, correlated photon pairs were created via spontaneous FWM in an SWW with a length of 1.37 cm and subsequently spectrally separated by the on-chip  $\text{SiO}_x$  AWG into different output channels. The AWG had 16 output channels designed to have a 200-GHz channel spacing.

In the experiment, we obtained pump pulses centered at 1560.5 nm with a pulse duration of 200 ps and repetition rate of 100 MHz using a setup similar to that shown in Figure 4A. Photons were collected from a pair of waveguides that were three channels away from the center output port. The transmission spectra of the two AWG outputs are shown in Figure 13B. The 3-dB passband widths of the transmission windows are approximately 80 GHz. The spot-size converter interfaced the silicon waveguide and the AWG. The output optical fields were collected by optical fibers with a high numerical aperture integrated on a V-groove array. Then the photons were introduced into spectral filters, each of which consisted

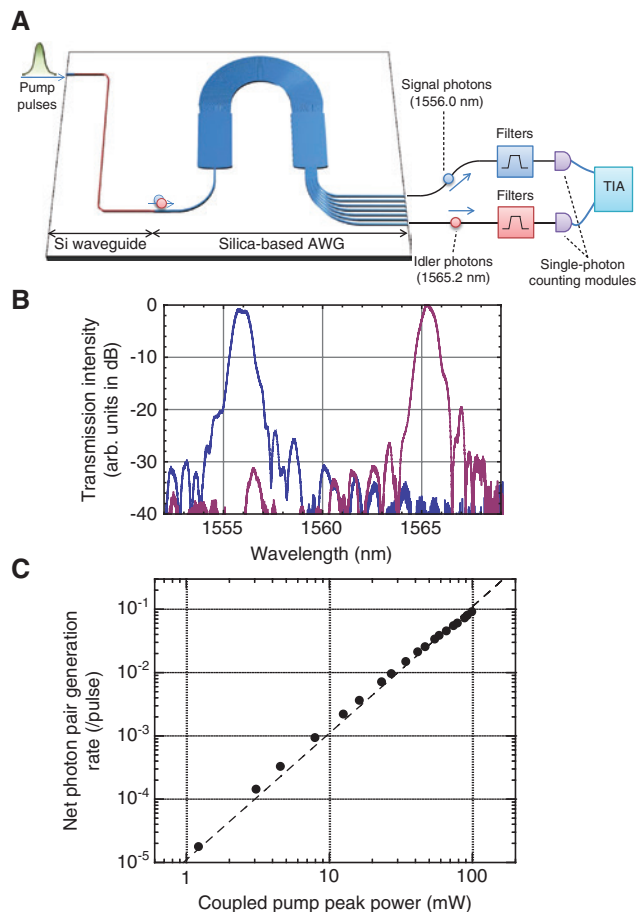


**Figure 13:** (A) A chip housing a silicon waveguide photon pair source and a silica-based AWG, illustrated with the experimental setup. (B) Transmission spectra from the on-chip AWG output ports used for the collection of the photon pairs. (C) Net photon pair generation rate as a function of pump peak power [116].

of a fiber-Bragg-grating notch filter and a band-pass filter (BPF) for the suppression of residual pump fields. The 3-dB bandwidth of the BPF  $\Delta\nu$  was 100 GHz, which covered the AWG passbands. The photons were received by InGaAs SPADs and a coincidence measurement was performed. The overall transmittance of the filters was -2.8 dB and the AWG insertion loss was -7.7 dB.

Figure 13C shows the net photon-pair generation rate estimated from the experiment as a function of the pump peak power. The data exhibited good power-squared dependence, indicating photon-pair generation via the spontaneous FWM process. The solid line shows the estimation obtained with Eq. (3) using the same  $\gamma=161/\text{W/m}$  obtained above and the insertion loss of the AWG. The experimental result agreed well with the calculation.

The chip can be used as a compact correlated photon pair source and will be useful for the construction of a multiplexed single-photon source [103] and for

wavelength-division multiplexing quantum communication technologies [120]. The silica-based AWG can provide an interface between a silicon-based photon pair source and silica-based functional circuits [17]. The wavelength-multiplexing capability would be useful for harnessing high-dimensional quantum states on a chip [121, 122]. An integration with high-speed optical switches using a silicon-LiNbO<sub>3</sub> hybrid integration approach is attractive for realizing a quantum information system with further functionality [123].

## 6 Summary and discussion

We have reviewed the recent progress in integrated quantum photonics based on silicon photonics technologies. We have described a monolithic integration of a polarization entangled photon pair source based on an SWW as an example of a quantum optical circuit that integrates several optical devices to realize a quantum function. We have also described our efforts to develop ultracompact photon sources based on silicon PhC technologies, which will be useful for realizing an on-demand single-photon source based on the heralding approach. As a novel function that will be useful for flexible design of integrated quantum optical circuits, we have presented an experiment on an integrated quantum buffer realized with silicon PhC. Finally, we have shown a hybrid approach, with which we can combine the advantages of silica and silicon platforms.

We have developed both polarization and time-bin entangled photon-pair sources. An advantage of polarization qubits is that we can utilize schemes developed in previous free-space quantum information experiments, including various quantum gates based on polarization beam splitters. On the other hand, the majority of waveguide devices show polarization-dependent loss and dispersion, which makes it relatively challenging to build a large-scale system based on polarization qubits. Time-bin qubits are potentially useful for waveguides with polarization dependence, but they have not been studied intensively for complex quantum information experiments. Thus, further investigations to develop various functional circuits based on time-bin qubits are needed. As such an investigation, a two-qubit operation of time-bin qubits has been demonstrated using an optical switch based on a lithium niobate waveguide [124].

The topics introduced here are the basic elements for a photonic quantum system on silicon chips. Therefore, an important future work is to integrate these elements. It

is relatively straightforward to combine SWWs and silicon PhC waveguides on the same chip, and in fact, our CROWs are integrated with SWWs. The use of the hybrid integration described in Section 5 enables us to combine low-loss functional circuits based on silica waveguides with other functions realized on silicon waveguides, including the SWWs and PhC waveguides. The choice of elements depends on the purpose of the system. For example, the polarization entangled photon-pair source introduced in Section 2 will be useful for realizing polarization-qubit-based quantum systems on chips, while ultra-small photon-pair sources based on CROW are advantageous for larger scale quantum systems based on path or time-bin encoding. In addition, it is also possible to use the CROW for systems based on the polarization encoding by incorporating the polarization diversity technique reported in Ref. [49]. When integrated with the various functional circuits and on-chip detectors developed so far, we expect that the technologies shown here will contribute to the realization of quantum processors based on fully integrated quantum optical circuits.

**Acknowledgments:** The authors thank K. Yamada, T. Tsuchizawa, H. Fukuda, T. Watanabe, H. Nishi, E. Kuramochi, H. Taniyama, M. Notomi, H. Le Jeannic, P. Karkus, W.J. Munro, K. Shimizu, and Y. Tokura for their collaborations. The work presented here was supported in part by a Grant-in-Aid for Scientific Research (No. 22360034) from the Japan Society for the Promotion of Science.

## References

- [1] Politi A, Cryan MJ, Rarity JG, Yu S, O'Brien JL. Silica-on-silicon waveguide quantum circuits. *Science* 2008;320:646–9.
- [2] O'Brien JL, Furusawa A, Vucčković J. Photonic quantum technologies. *Nat Photon* 2009;3:687–95.
- [3] Ladd TD, Jelezko F, Laflamme R, Nakamura Y, Monroe C, O'Brien JL. Quantum computers. *Nature* 2010;464:45–53.
- [4] Metcalf BJ, Thomas-Peter N, Spring JB, Kundys D, Broome MA, Humphreys PC, Jin X-M, Barbieri M, Kolthammer WS, Gates JC, Smith BJ, Langford NK, Smith PGR, Walmsley IA. Multiphoton quantum interference in a multiport integrated photonic device. *Nat Commun* 2013;4:1356.
- [5] Matthews JCF, Politi A, Stefanov A, OBrien JL. Manipulation of multiphoton entanglement in waveguide quantum circuits. *Nat Photon* 2009;3:346E50.
- [6] Politi A, Matthews JCF, OBrien JL. Shorâs quantum factoring algorithm on a photonic chip. *Science* 2009;325:1221.
- [7] Peruzzo A, Lobino M, Matthews JCF, Matsuda N, Politi A, Poulios K, Zhou X-Q, Lahini Y, Ismail N, Wörhoff K, Bromberg Y, Silberberg Y, Thompson MG, O'Brien JL. Quantum walks of correlated photons. *Science* 2010;329:1500–3.

- [8] Crespi A, Osellame R, Ramponi R, Giovannetti V, Fazio R, Sansoni L, De Nicola F, Sciarrino F, Mataloni P. Anderson localization of entangled photons in an integrated quantum walk. *Nat Photon* 2013;7:322–8.
- [9] Broome MA, Fedrizzi A, Rahimi-Keshari S, Dove J, Aaronson S, Ralph TC, White AG. Photonic boson sampling in a tunable circuit. *Science* 2013;339:794–8.
- [10] Spring JB, Metcalf BJ, Humphreys PC, Kolthammer WS, Jin X-M, Barbieri M, Datta A, Thomas-Peter N, Langford NK, Kundys D, Gates JC, Smith BJ, Smith PGR, Walmsley IA. Boson sampling on a photonic chip. *Science* 2013;339:798–801.
- [11] Tillmann M, Dakić B, Heilmann R, Nolte S, Szameit A, Walther P. Experimental boson sampling. *Nat Photon* 2013;7:540–4.
- [12] Crespi A, Osellame R, Ramponi R, Brod DJ, Galvão EF, Spagnolo N, Vitelli C, Maiorino E, Mataloni P, Sciarrino F. Integrated multimode interferometers with arbitrary designs for photonic boson sampling. *Nat Photon* 2013;7:545–9.
- [13] Spagnolo N, Vitelli C, Bentivegna M, Brod DJ, Crespi A, Flamini F, Giacomini S, Milani G, Ramponi R, Mataloni P, Osellame R, Galvão EF, Sciarrino F. Experimental validation of photonic boson sampling. *Nat Photon* 2014;8:615–20.
- [14] Bentivegna M, Spagnolo N, Vitelli C, Flamini F, Viggianiello N, Latminal L, Mataloni P, Brod DJ, Galvão EF, Crespi A, Ramponi R, Osellame R, Sciarrino F. Experimental scattershot boson sampling. *Sci Adv* 2015;1:3.
- [15] Sharping JE, Lee KF, Foster MA, Turner AC, Schmidt BS, Lipson M, Gaeta AL, Kumar P. Generation of correlated photons in nanoscale silicon waveguide quantum circuits. *Opt Express* 2006;14:12388–93.
- [16] Takesue H, Tokura Y, Fukuda H, Tsuchizawa T, Watanabe T, Yamada K, Itabashi S. Entanglement generation using silicon wire waveguide. *Appl Phys Lett* 2007;91:201108.
- [17] Carolan L, Harrold C, Sparrow C, Martín-López E, Russell NJ, Silverstone JW, Shadbolt PJ, Matsuda N, Oguma M, Itoh M, Marshall GD, Thompson MG, Matthews JCF, Hashimoto T, O'Brien JL, Laing A. Universal linear optics. *Science* 2015;349:711.
- [18] Harris NC, Steinbrecher GR, Mower J, Lahini Y, Prabhu M, Baehr-Jones T, Hochberg M, Lloyd S, Englund D. Bosonic transport simulations in a large-scale programmable nanophotonic processor. *arxiv:1507.06406 [quant-ph]*.
- [19] Takesue H, Matsuda N, Kuramochi E, Munro WJ, Notomi M. An on-chip coupled resonator optical waveguide single-photon buffer. *Nat Comm* 2013;4:2725.
- [20] Sprengers JP, Gaggero A, Sahin D, Jahanmirinejad S, Frucci G, Mattioli F, Leoni R, Beetz J, Lermer M, Kamp M, Höfling S, Sanjines R, Fiore A. Waveguide superconducting single-photon detectors for integrated quantum photonic circuits. *Appl Phys Lett* 2011;99:18110.
- [21] Pernice WH, Schuck C, Minaeva O, Li M, Goltsman GN, Sergienko AV, Tang HX. High-speed and high-efficiency travelling wave single-photon detectors embedded in nanophotonic circuits. *Nat Commun* 2012;3:1325.
- [22] Sahin D, Gaggero A, Zhou Z, Jahanmirinejad S, Mattioli F, Leoni R, Beetz J, Lermer M, Kamp M, Höfling S, Fiore A. Waveguide photon-number-resolving detectors for quantum photonic integrated circuits. *Appl Phys Lett* 2013;103:111116.
- [23] Najafi F, Mower J, Harris N, Bellei F, Dane A, Lee C, Kharel P, Marsili F, Assefa S, Berggren KK, Englund D. On-chip detection of non-classical light by scalable integration of single-photon detectors. *Nat Commun* 2015;6:5873.
- [24] Honjo T, Inoue K, Takahashi H. Differential-phase-shift quantum key distribution experiment with a planar light-wave circuit Mach-Zehnder interferometer. *Opt Lett* 2004;29:2797–9.
- [25] Nambu Y, Hatanaka T, Nakamura K. BB84 quantum key distribution system based on silica-based planar lightwave circuits. *Jpn J Appl Phys* 2004;43:L1109–10.
- [26] Takesue H, Inoue K. Generation of 1.5-μm band time-bin entanglement using spontaneous fiber four-wave mixing and planar lightwave circuit interferometers. *Phys Rev A* 2005;72:041804(R).
- [27] Kawachi M. Silica waveguides on silicon and their application to integrated-optic components. *Opt Quantum Electron* 1990;22:391E16.
- [28] Takahashi H. High performance planar lightwave circuit devices for large capacity transmission. *Opt Express* 2011;19:B173–80.
- [29] Spring JB, Salter PS, Metcalf BJ, Humphreys PC, Moore M, Thomas-Peter N, Barbieri M, Jin X-M, Langford NK, Steven Kolthammer W, Booth MJ, Walmsley IA. On-chip low loss heralded source of pure single photons. *Opt Express* 2013;21:13522.
- [30] Spring JB, Salter P, Mennea P, Metcalf B, Humphreys PC, Moore M, Gates JC, Thomsa-Peter N, Barbieri M, Jin X-M, Langford NK, Kolthammer SW, Smith PG, Booth M, Smith BJ, Walmsley IA. Quantum interference of multiple on-chip heralded sources of pure single photons. *Quantum Information and Measurements* 2014, paper QW1B, 2014.
- [31] Yan Z, Duan Y, Helt LG, Ams M, Withford MJ, Steel MJ. Generation of heralded single photons beyond 1100 nm by spontaneous four-wave mixing in a damage-stressed femtosecond laser written waveguide. *Appl Phys Lett* 2015;107:231106.
- [32] Psaila ND, Thomson RR, Bookey HT, Shen S, Chiodo N, Osellame R, Cerullo G, Jha A, Kar AK. Supercontinuum generation in an ultrafast laser inscribed chalcogenide glass waveguide. *Opt Express* 2007;15:15776–81.
- [33] Agrawal GP. Nonlinear fiber optics, 3rd ed. Academic, 2011.
- [34] Gisin N, Ribordy G, Tittel W, Zbinden H. Quantum cryptography. *Rev Mod Phys* 2002;74:145–95.
- [35] Knill E, Laflamme R, Milburn GJ. A scheme for efficient quantum computation with linear optics. *Nature* 2001;409:46E2.
- [36] Pittman TB, Jacobs BC, Franson JD. Probabilistic quantum logic operations using polarization beam splitters. *Phys Rev A* 2001;64:062311.
- [37] Walther P, Resch KJ, Rudolph T, Schenck E, Weinfurter H, Vedral V, Aspelmeyer M, Zeilinger A. Experimental one-way quantum computing. *Nature* 2005;434:169–76.
- [38] Kok P, Munro WJ, Nemoto K, Ralph TC, Dowling JP, Milburn GJ. Linear optical quantum computing with photonic qubits. *Rev Mod Phys* 2007;79:135–74.
- [39] Kwiat PG, Mattle K, Weinfurter H, Zeilinger A, Sergienko AV, Shih Y. New high-intensity source of polarization-entangled photon pairs. *Phys Rev Lett* 1995;75:4337–41.
- [40] Kwiat PG, Waks E, White AG, Appelbaum I, Eberhard PH. Ultrabright source of polarization-entangled photons. *Phys Rev A* 1999;60:R773.
- [41] Yamada K. Silicon photonic wire waveguides: fundamentals and applications. *Silicon Photon II* 2011;119:1–29.
- [42] Lim HC, Yoshizawa A, Tsuchida H, Kikuchi K. Stable source of high quality telecom-band polarization-entangled photon-pairs based on a single, pulse-pumped, short PPLN waveguide. *Opt Express* 2008;16:12460–8.

- [43] Takesue H, Fukuda H, Tsuchizawa T, Watanabe T, Yamada K, Tokura Y, Itabashi S. Generation of polarization entangled photon pairs using silicon wire waveguide. *Opt Express* 2008;16:5721–7.
- [44] Suhara T, Nakaya G, Kawashima J, Fujimura M. Quasi-phase-matched waveguide devices for generation of postselection-free polarization entangled twin photons. *IEEE Photon Technol Lett* 2009;21:1096–8.
- [45] Martin A, Issautier A, Herrmann H, Sohler W, Ostrowsky DB, Alibart O, Tanzilli S. A polarization entangled photon-pair source based on a type-II PPLN waveguide emitting at a telecom wavelength. *New J Phys* 2010;12:103005.
- [46] Arahira S, Namekata N, Kishimoto T, Yaegashi H, Inoue S. Generation of polarization entangled photon pairs at telecommunication wavelength using cascaded  $\chi^{(2)}$  processes in a periodically poled LiNbO<sub>3</sub> ridge waveguide. *Opt Express* 2011;19:16032–43.
- [47] Matsuda N, Le Jeannic H, Fukuda H, Tsuchizawa T, Munro WJ, Shimizu K, Yamada K, Tokura Y, Takesue H. A monolithically integrated polarization entangled photon pair source on a silicon chip. *Sci Rep* 2012;2:817.
- [48] Fukuda H, Yamada K, Tsuchizawa T, Watanabe T, Shinojima H, Itabashi S. Polarization rotator based on silicon wire waveguides. *Opt Express* 2008;16:2628–35.
- [49] Fukuda H, Yamada K, Tsuchizawa T, Watanabe T, Shinojima H, Itabashi S. Silicon photonic circuit with polarization diversity. *Opt Express* 2008;16:4872–80.
- [50] Leuthold J, Koos C, Freude W. Nonlinear silicon photonics. *Nat Photon* 2010;4:535–44.
- [51] Zhang L, Agrawal A, Kimerling LC, Michel J. Nonlinear group IV photonics based on silicon and germanium: from near-infrared to mid-infrared. *Nanophotonics* 2014;3:247E68.
- [52] Clemmen S, Phan Huy K, Bogaerts W, Baets RG, Emplit Ph, Massar S. Continuous wave photon pair generation in silicon-on-insulator waveguides and ring resonators. *Opt Exp* 2009;17:16558–70.
- [53] Takesue H. Entangled photon pair generation using silicon wire waveguides. *EIEEJ Sel Top Quant* 2012;18:1722E732.
- [54] Harada K, Takesue H, Fukuda H, Tsuchizawa T, Watanabe T, Yamada K, Tokura Y, Itabashi S. Generation of high-purity entangled photon pairs using silicon wire waveguide. *Opt Express* 2008;16:20368–73.
- [55] Fukuda H, Yamada K, Shoji T, Takahashi M, Tsuchizawa T, Watanabe T, Takahashi J, Itabashi S. Four-wave mixing in silicon wire waveguides. *Opt Express* 2005;13:4629–37.
- [56] Foster MA, Turner AC, Sharping JE, Schmidt BS, Lipson M, Gaeta AL. Broad-band optical parametric gain on a silicon photonic chip. *Nature* 2006;441:960E63.
- [57] James DFV, Kwiat PG, Munro WJ, White AG. Measurement of qubits. *Phys Rev A* 2001;64:052312.
- [58] Modlawska J, Grudka A. Increasing singlet fraction with entanglement swapping. *Phys Rev A* 2008;78:032321.
- [59] Badzigg P, Horodecki M, Horodecki P, Horodecki R. Local environment can enhance fidelity of quantum teleportation. *Phys Rev A* 2000;62:012311.
- [60] Olislager L, Safiou I, Clemmen S, Huy KP, Bogaerts W, Baets R, Emplit P, Massar S. Silicon-on-insulator integrated source of polarization-entangled photons. *Opt Lett* 2013;38:1960–2.
- [61] Lv N, Zhang W, Guo Y, Zhou Q, Huang Y, Peng J. 1.5  $\mu\text{m}$  polarization entanglement generation based on birefringence in silicon wire waveguides. *Opt Lett* 2013;38:2873–6.
- [62] Orieux A, Eckstein A, Lematre A, Filloux P, Favero I, Leo G, Coudreau T, Keller A, Milman P, Ducci S. Direct bell states generation on a III-V semiconductor chip at room temperature. *Phys Rev Lett* 2013;110:160502.
- [63] Horn RT, Kolenderski P, Kang D, Abolghasem P, Scarcella C, Frera AD, Tosi A, Helt LG, Zhukovsky SV, Sipe JE, Weihs G, Helmy AS, Jennewein T. Inherent polarization entanglement generated from a monolithic semiconductor chip. *Sci Rep* 2013;3:2314.
- [64] Vallés A, Hendrych M, Svozilík J, Machulka R, Abolghasem P, Kang D, Bijlani BJ, Helmy AS, Torres JP. Generation of polarization-entangled photon pairs in a Bragg reflection waveguide. *Opt Express* 2013;21:10841–9.
- [65] Kang D, Kim M, He H, Helmy AS. Two polarization-entangled sources from the same semiconductor chip. *Phys Rev A* 2015;92:013821.
- [66] Kang D, Anirban A, Helmy AS. Monolithic semiconductor chips as a source for broadband wavelength-multiplexed polarization entangled photons. *arXiv:1511.00903 [quant-ph]*.
- [67] Hayat A, Ginzburg P, Orenstein M. Observation of two-photon emission from semiconductors. *Nat Photon* 2008;2:238–41.
- [68] Boitier F, Orieux A, Autebert C, Lematre A, Galopin E, Manquest C, Sirtori C, Favero I, Leo G, Ducci S. Electrically injected photon-pair source at room temperature. *Phys Rev Lett* 2014;112:183901.
- [69] Bonneau D, Lobino M, Jiang P, Natarajan CM, Tanner MG, Hadfield RH, Dorenbos SN, Zwillaer V, Thompson MG, O'Brien JL. Fast path and polarization manipulation of telecom wavelength single photons in lithium niobate waveguide devices. *Phys Rev Lett* 2012;108:053601.
- [70] Sansoni L, Sciarrino F, Vallone G, Mataloni P, Crespi A, Ramponi R, Osellame R. Polarization and entangled state measurement on a chip. *Phys Rev Lett* 2010;105:200503.
- [71] Crespi A, Ramponi R, Osellame R, Sansoni L, Bongianni I, Sciarrino F, Vallone G, Mataloni P. Integrated photonic quantum gates for polarization qubits. *Nat Commun* 2011;2:566.
- [72] Corrielli G, Crespi A, Geremia R, Ramponi R, Sansoni L, Santinelli A, Mataloni P, Sciarrino F, Osellame R. Rotated waveplates in integrated waveguide optics. *Nat Commun* 2014;5:4249.
- [73] Migdall AL, Branning D, Castelletto S. Tailoring single-photon and multiphoton probabilities of a single-photon on-demand source. *Phys Rev A* 2002;66:053805.
- [74] Ma X.-S, Zotter S, Kofler J, Jennewein T, Zeilinger A. Experimental generation of single photons via active multiplexing. *Phys Rev A* 2011;83:043814.
- [75] Collins MJ, Xiong C, Rey IH, Vo TD, He J, Shahnia S, Reardon C, Krauss TF, Steel MJ, Clark AS, Eggleton BJ. Integrated spatial multiplexing of heralded single-photon sources. *Nat Commun* 2013;4:2582.
- [76] Xiong C, Vo TD, Collins MJ, Li J, Krauss TF, Steel MJ, Clark AS, Eggleton BJ. Bidirectional multiplexing of heralded single photons from a silicon chip. *Opt Lett* 2013;38:5176–9.
- [77] Pittman TB, Jacobs BC, Franson JD. Single photons on pseudodemand from stored parametric down-conversion. *Phys Rev A* 2002;66:042303.
- [78] Notomi M, Yamada K, Shinya A, Takahashi J, Takahashi C, Yokohama I. Extremely large group-velocity dispersion of line-defect waveguides in photonic crystal slabs. *Phys Rev Lett* 2001;87:253902.
- [79] Krauss TF. Slow light in photonic crystal waveguides. *J Phys D Appl Phys* 2007;40:2666–70.

- [80] Baba T. Slow light in photonic crystals. *Nature Photon* 2008;2:465–73.
- [81] Monat C, de Sterke M, Eggleton BJ. Slow light enhanced nonlinear optics in periodic structures. *J Opt* 2010;12:104003.
- [82] Xiong C, Monat C, Clark AS, Grillet C, Marshall GD, Steel MJ, Li J, O’Faolain L, Krauss TF, Rarity JG, Eggleton BJ. Slow-light enhanced correlated photon pair generation in a silicon photonic crystal waveguide. *Opt Lett* 2011;36:3413–5.
- [83] Xiong C, Collins MJ, Steel MJ, Krauss TF, Eggleton BJ, Clark AS. Photonic crystal waveguide sources of photons for quantum communication applications. *IEEE J Sel Top Quant* 2015; 21:1–10.
- [84] Yariv A, Xu Y, Lee RK, Scherer A. Coupled-resonator optical waveguide: a proposal and analysis. *Opt Express* 1999;24:711–3.
- [85] Davanço M, Ong JR, Shehata AB, Tosi A, Agha I, Assefa S, Xia F, Green WMJ, Mookherjea S, Srinivasan K. *Appl Phys Lett* 2012;100:261104.
- [86] Matsuda N, Kato T, Harada K, Takesue H, Kuramochi E, Taniyama H, Notomi M. Slow light enhanced optical nonlinearity in a silicon photonic crystal coupled-resonator optical waveguide. *Opt Express* 2011;19:19861–74.
- [87] Notomi M, Kuramochi E, Tanabe T. Large-scale arrays of ultrahigh-Q coupled nanocavities. *Nat Photon* 2008;2:741–7.
- [88] Kuramochi E, Notomi M, Mitsugi S, Shinya A, Tanabe T, Watanabe T. Ultrahigh-Q photonic crystal nanocavities realized by the local width modulation of a line defect. *Appl Phys Lett* 2006;88:041112.
- [89] Matsuda N, Kuramochi E, Takesue H, Notomi M. Dispersion and light transport characteristics of large-scale photonic-crystal coupled nanocavity arrays. *Opt Lett* 2014;39:2290–3.
- [90] Matsuda N, Takesue H, Shimizu K, Tokura Y, Kuramochi E, Notomi M. Slow light enhanced correlated photon pair generation in photonic-crystal coupled-resonator optical waveguides. *Opt Express* 2013;21:8596–604.
- [91] Takesue H, Matsuda N, Kuramochi E, Notomi M. Entangled photons from on-chip slow light. *Sci Rep* 2014;4:3913.
- [92] Mookherjea S, Park JS, Yang S-H, Bandaru PR. *Nat Photon* 2008;2:90.
- [93] Xia F, Sekaric L, Vlasov Y. *Nat Photon* 2007;1:65.
- [94] Cooper ML, Gupta G, Schneider MA, Green WMJ, Assefa S, Xia F, Gifford DK, Mookherjea S. *Opt Lett* 2010;35:3030.
- [95] Luo X, Poon AW. *Opt Express* 2009;17:23617.
- [96] Cooper ML, Gupta G, Schneider MA, Green WMJ, Assefa S, Xia F, Vlasov YA, Mookherjea S. Statistics of light transport in 235-ring silicon coupled-resonator optical waveguides. *Opt Express* 2010;18:26505.
- [97] Sapienza L, Thyrrstrup H, Stobbe S, Garcia PD, Smolka S, Lodahl P. Cavity quantum electrodynamics with anderson-localized modes. *Science* 2010;327:1352–5.
- [98] Lian J, Sokolov S, Yüce E, Combré S, De Rossi A, Mosk AP. Dispersion of coupled mode-gap cavities. *Opt Lett* 2015;40:4488–91.
- [99] Caselli N, Riboli F, La China F, Gerardino A, Li L, Linfield EH, Pagliano F, Fiore A, Intonti F, Gurioli M. Tailoring the photon hopping by nearest and next-nearest-neighbour interaction in photonic arrays. *ACS Photonics* 2015;2:565–71.
- [100] Zou XY, Wang LJ, Mandel L. Violation of classical probability in parametric down-conversion. *Opt Commun* 1991;84:351–4.
- [101] Franson JD. Bell inequality for position and time. *Phys Rev Lett* 1989;62:2205E208.
- [102] Kuzmich A, Bowen WP, Boozer AD, Boca A, Chou CW, Duan L-M, Kimble HJ. Generation of nonclassical photon pairs for scalable quantum communication with atomic ensembles. *Nature* 2003;423:731–4.
- [103] Meany T, Ngah LA, Collins MJ, Clark AS, Williams RJ, Eggleton BJ, Steel MJ, Withford MJ, Alibart O, Tanzilli S. Hybrid photonic circuit for multiplexed heralded single photons. *Laser Photonics Rev* 2014;8:L42–6.
- [104] Silverstone JW, Bonneau D, Ohira K, Suzuki N, Yoshida H, Iizuka N, Ezaki M, Natarajan CM, Tanner MG, Hadfield RH, Zwiller V, Marshall GD, Rarity JG, O’Brien JL, Thompson MG. On-chip quantum interference between silicon photon-pair sources. *Nature Photon* 2014;8:104–8.
- [105] Jöns KD, Rengstl U, Oster M, Hargart F, Heldmaier M, Bou-nouar S, Ulrich SM, Jetter M, Michler P. Monolithic on-chip integration of semiconductor waveguides, beam splitters and single-photon sources. *arXiv:1403.7174 [quant-ph]*.
- [106] Prtljaga N, Coles RJ, O’Hara J, Royall B, Clarke E, Fox AM, Skolnick MS. Monolithic integration of a quantum emitter with a compact on-chip beam-splitter. *Appl Phys Lett* 2014;104:231107.
- [107] Harris NC, Grassani D, Simbula A, Pant M, Galli M, Baehr-Jones T, Hochberg M, Englund D, Bajoni D, Galland C. Integrated source of spectrally filtered correlated photons for large-scale quantum photonic systems. *Phys Rev X* 2014;4:041047.
- [108] Silverstone JW, Santagati R, Bonneau D, Strain MJ, Sorel M, O’Brien JL, Thompson MG. Qubit entanglement between ring-resonator photon-pair sources on a silicon chip. *Nat Commun* 2015;6:7948.
- [109] Murray E, Ellis DJP, Meany T, Floether FF, Lee JP, Griffiths JP, Jones GAC, Farrer I, Ritchie DA, Bennett AJ, Shields AJ. Quantum photonics hybrid integration platform. *Appl Phys Lett* 2015;107:171108.
- [110] Bonneau D, Engin E, Ohira K, Suzuki N, Yoshida H, Iizuka N, Ezaki M, Natarajan CM, Tanner MG, Hadfield RH, Dorenbos SN, Zwiller V, O’Brien JL, Thompson MG. Quantum interference and manipulation of entanglement in silicon wire waveguide quantum circuits. *New J Phys* 2012;14:045003.
- [111] Wang J, Santamato A, Jiang P, Bonneau D, Engin E, Silverstone JW, Lermer M, Beetz J, Kamp M, Höfling S, Tanner MG, Natarajan CM, Hadfield RH, Dorenbos SN, Zwiller V, O’Brien JL, Thompson MG. Gallium arsenide (GaAs) quantum photonic waveguide circuits. *Opt Commun* 2014;327:49–55.
- [112] Smith BJ, Kundys D, Thomas-Peter N, Smith PGR, Walmsley IA. Phase-controlled integrated photonic quantum circuits. *Opt Express* 2009;17:13516–25.
- [113] Sohma S, Watanabe T, Ooba N, Itoh M, Shibata T, Takahashi H. Silica-based PLC type 32E2 optical matrix switch. *ECOC* 2006;1–2.
- [114] Hibino Y. Recent advances in high-density and large-scale AWG multi/demultiplexers with higher index-contrast silica-based PLCs. *IEEE J Sel Top Quant* 2002;8:1090–101.
- [115] Matsuda N, Shimizu R, Mitsumori Y, Kosaka H, Edamatsu K. Observation of optical-fibre Kerr nonlinearity at the single-photon level. *Nature Photon* 2009;3:95–8.

- [116] Matsuda N, Karkus P, Nishi H, Tsuchizawa T, Munro WJ, Takesue H, Yamada K. On-chip generation and demultiplexing of quantum correlated photons using a silicon-silica monolithic photonic integration platform. *Opt. Express* 2014;22:22831–40.
- [117] Nishi H, Tsuchizawa T, Watanabe T, Shinojima H, Park S, Kou R, Yamada K, Itabashi S. Monolithic integration of a silica-based arrayed waveguide grating filter and silicon variable optical attenuators based on p-i-n carrier-injection structure. *Appl Phys Express* 2010;3:102203.
- [118] Tsuchizawa T, Yamada K, Watanabe T, Sungbong P, Nishi H, Kou R, Shinojima H, Itabashi S. Monolithic integration of silicon-, germanium-, and silica-based optical devices for telecommunications applications. *IEEE J Sel Top Quant* 2011;17:516–25.
- [119] Hiraki T, Nishi H, Tsuchizawa T, Kou R, Fukuda H, Takeda K, Ishikawa Y, Wada K, Yamada K. Si-Ge-silica monolithic integration platform and its application to a 22-Gb/s 16-ch WDM receiver. *Photonics J IEEE* 2013;5:4500407.
- [120] Yoshino K, Fujiwara M, Tanaka A, Takahashi S, Nambu Y, Tomita A, Miki S, Yamashita T, Wang Z, Sasaki M, Tajima A. High-speed wavelength-division multiplexing quantum key distribution system. *Opt Lett* 2012;37:223–5.
- [121] Schaeff C, Polster R, Lapkiewicz R, Fickler R, Ramelow S, Zeilinger A. Scalable fiber integrated source for higher-dimensional path-entangled photonic quNits. *Opt Express* 2012;20:16145–53.
- [122] Schaeff C, Polster R, Huber M, Ramelow and Zeilinger A. Experimental access to higher-dimensional entangled quantum systems using integrated optics. *Optica* 2015;2:523–9.
- [123] Yamazaki H, Yamada T, Goh T, Sakamaki Y, Kaneko A. 64 QAM modulator with a hybrid configuration of silica PLCs and LiNbO<sub>3</sub> phase modulators. *IEEE Photon Technol Lett* 2010;22:344–6.
- [124] Takesue H. Entangling time-bin qubits with a switch. *Phys Rev A* 2014;89:062328.

## Entangled Photons: Generation, Observation, and Characterization

To cite this article: Keiichi Edamatsu 2007 *Jpn. J. Appl. Phys.* **46** 7175

## Entangled Photons: Generation, Observation, and Characterization

Keiichi EDAMATSU\*

Research Institute of Electrical Communication, Tohoku University, 2-1-1 Katahira, Aoba-ku, Sendai 980-8577, Japan

(Received May 21, 2007; accepted August 12, 2007; published online November 6, 2007)

Entanglement is one of the essential resources of quantum information and communication technology. Photons are the most popular and promising media to manipulate entanglement. In this review article, concepts and progress in the generation, observation, and characterization of entangled photons are presented. Starting from underlying theoretical concepts, a historical review on the generation of entangled photons is given. Particularly, recent results on the generation of polarization-entangled photons from semiconductor sources are reviewed and discussed. [DOI: [10.1143/JJAP.46.7175](https://doi.org/10.1143/JJAP.46.7175)]

KEYWORDS: entanglement, photon, quantum optics, quantum information, quantum communication

### 1. Introduction

Quantum information and communication technology (QICT) is one of the most direct and novel applications of quantum mechanics. Many researchers in the areas of pure and applied physics, mathematics, informatics and so on, are attracted by this fascinating research field. Entanglement, i.e., nonlocal quantum correlation between two or more quantum-mechanical objects, is one of the key issues in QICT. Thus, the development of techniques to generate, process, distribute, and characterize entanglement is of great importance in the field.

Entanglement was first but implicitly discussed by Einstein, Podolsky, and Rosen (EPR) in 1935,<sup>1)</sup> aiming at an objection to quantum mechanics. In the 1960s, an existence criterion of such nonlocal quantum correlation was formalized by Bell's inequality<sup>2)</sup> and its generalization known as CHSH-Bell's inequality.<sup>3)</sup> From the 1960s through the 1980s, several experiments<sup>4–9)</sup> had been carried out to test Bell's inequality; they had demonstrated the violation of Bell's inequality and thus manifested the existence of nonlocal quantum correlations brought about by entanglement. In these experiments, the researchers used photon pairs emitted from atomic cascades in which the emitted photon pairs have entanglement in their polarization states. Following to such pioneering studies to generate entangled photons from atomic sources, a number of methods to generate entangled photons have been proposed. As far as materials are concerned, atoms, various optical nonlinear crystals, optical fibers, and semiconductors have been used to generate entangled photons. Parametric down-conversion in optical nonlinear crystals has been the most popular and powerful method of obtaining entangled photons since the late 1980s.<sup>10–14)</sup> Most recently, entangled photon generation using semiconductor materials<sup>15–19)</sup> has attracted attention because of its potential for the realization of entangled photon-emitting diodes in the near future. The highly effective generation of entangled photons will be essential to advance quantum information and communication protocols that require a large number of entangled objects as their primary resources. Thus, the generation, observation and characterization of such a large number of entangled photons are also hot topics in the fields of experimental as well as theoretical QICT.

To date, various massive quantum objects such as

protons,<sup>20–22)</sup> atoms,<sup>23)</sup> and trapped ions<sup>24,25)</sup> have been used to demonstrate entanglement. Furthermore, entanglement between macroscopic objects such as superconducting circuits<sup>26)</sup> and atomic ensembles<sup>27)</sup> has also been demonstrated. However, in practice, it is still very difficult to maintain the entanglement of such massive objects because of its fragility in standard environments. Photons are the most promising and practical media to generate, process, and distribute entanglement because quantum states, including entanglement, encoded in photons are comparatively robust against environments.

In this review article, methods of generating, observing, and characterizing entangled photons are reviewed and discussed. Of particular interest is the polarization-entangled photon pairs, i.e., photons that are entangled in their polarization states. In §2, we present a brief review of the representation and physical coding of entanglement. In §3, we review and discuss the methods of generating entangled photon pairs, such as atomic sources, parametric down-conversion, and semiconductor sources. In §4 and §5, we describe the methods of observing and characterizing the entanglement. In these sections, our recent results on the generation of entangled photons from a semiconductor material<sup>15,19)</sup> are presented as an example. In §6, other topics and applications concerning entanglement held by photons are briefly described. I hope this review will encourage readers who have general interest in applied physics to look at the underlying technology of QICT, which uses entanglement as one of its essential resources.

### 2. Representation of Entangled States

“Entanglement” is a word that presents the concept of nonlocal quantum correlations between two or more quantum-mechanical systems. Quantum systems that can hold entanglement may be either two-level (qubit) systems such as electron spins and photon polarizations, or continuous variable systems such as position-momentum,<sup>1,28)</sup> which appears in the original EPR paradox,<sup>1)</sup> and quadrature variance.<sup>29)</sup> Furthermore, entanglement shared by more than two quantum systems, i.e., multipartite entanglement, is also a hot topic. However, here, we focus on the most simple and primary entangled system, i.e., entanglement shared by two qubits.

#### 2.1 Bell states

Let  $|0\rangle_A$ ,  $|1\rangle_A$  and  $|0\rangle_B$ ,  $|1\rangle_B$  be the orthogonal bases of qubits in two distinguishable systems labeled by A and B.

\*E-mail address: eda@riec.tohoku.ac.jp

An example of entangled states  $|\psi\rangle$  between the two systems is

$$\begin{aligned} |\psi\rangle &= \frac{1}{\sqrt{2}}(|0\rangle_A|0\rangle_B + e^{i\theta}|1\rangle_A|1\rangle_B) \\ &\equiv \frac{1}{\sqrt{2}}(|00\rangle + e^{i\theta}|11\rangle), \end{aligned} \quad (1)$$

where  $\theta$  is the phase difference between  $|00\rangle$  and  $|11\rangle$ . The state such as (1) cannot be written as a direct product of the two separate systems A and B. This means that the two systems are no longer independent but hold quantum correlation between them. In such a state, as we will see later, each system (A or B) is in a complete statistical mixture between  $|0\rangle$  and  $|1\rangle$ , but keeping the coherence between  $|00\rangle$  and  $|11\rangle$  expressed by the phase  $\theta$ .

The *Bell bases* or *Bell states* are the four orthogonal bases, i.e.,

$$|\Phi^\pm\rangle = \frac{1}{\sqrt{2}}(|00\rangle \pm |11\rangle), \quad (2)$$

$$|\Psi^\pm\rangle = \frac{1}{\sqrt{2}}(|01\rangle \pm |10\rangle), \quad (3)$$

that hold complete entanglement. Any 2-qubit state is expressed by a linear combination of the Bell states. For instance, the state (1) is a linear combination of  $|\Phi^+\rangle$  and  $|\Phi^-\rangle$ . In the Bell states,  $|\Psi^-\rangle$  is antisymmetric with respect to the transposition of the systems A and B, whereas the other three are symmetric. The former is called singlet or the *EPR state*, whereas the latter is called triplets.

The state such as (1) and Bell states hold the highest degree of entanglement in the 2-qubit system. Thus, they are called *maximally entangled states*. On the contrary, such a state

$$|\psi\rangle = \sqrt{p}|00\rangle + \sqrt{1-p}|11\rangle \quad (4)$$

has a lower degree of entanglement when  $p \neq 1/2$ , and thus it is called the *nonmaximally entangled state*. In particular, it has no entanglement when  $p = 0, 1$ .

## 2.2 Pure and mixed states: density matrix representation

The Bell states as well as the states (1) and (4) are *pure states* that are expressed by the linear combination of the basis vectors. When the states lose phase coherence between the bases, or decohere in other words, they also lose their degree of entanglement and are called *mixed states*. So as to express quantum systems including mixed states in general, we introduce the density matrix representation

$$\rho = \sum_i p_i |\psi_i\rangle\langle\psi_i|, \quad (5)$$

where  $p_i$  is the probability that the system is in state  $|\psi_i\rangle$ . For instance, the density matrix of the system in a maximally entangled pure state expressed by eq. (1) becomes

$$\begin{aligned} \rho &= |\psi\rangle\langle\psi| \\ &= \frac{1}{2}(|00\rangle + e^{i\theta}|11\rangle)(\langle 00| + e^{-i\theta}\langle 11|) \\ &= \frac{1}{2} \begin{pmatrix} 1 & 0 & 0 & e^{-i\theta} \\ 0 & 0 & 0 & 0 \\ 0 & 0 & 0 & 0 \\ e^{i\theta} & 0 & 0 & 1 \end{pmatrix}. \end{aligned} \quad (6)$$

In this matrix representation, we used  $|00\rangle$ ,  $|01\rangle$ ,  $|10\rangle$ , and  $|11\rangle$  as a basis set of the 2-qubit system. Each diagonal element of the density matrix represents the probability, i.e., population, that the system is in a corresponding basis state, and the off-diagonal elements represent the coherence that the system holds between the basis states. The density matrix in eq. (6) has the off-diagonal elements  $|00\rangle\langle 11|$  and  $|11\rangle\langle 00|$  whose absolute values are the same as those of the diagonal elements  $|00\rangle\langle 00|$  and  $|11\rangle\langle 11|$ , showing that it has full coherence between  $|00\rangle$  and  $|11\rangle$ .

On the other hand, the density matrix of the system that has only a classical correlation in a 1 : 1 statistical mixture of the pure states  $|00\rangle$  and  $|11\rangle$  is

$$\begin{aligned} \rho &= \frac{1}{2}(|00\rangle\langle 00| + |11\rangle\langle 11|) \\ &= \frac{1}{2} \begin{pmatrix} 1 & 0 & 0 & 0 \\ 0 & 0 & 0 & 0 \\ 0 & 0 & 0 & 0 \\ 0 & 0 & 0 & 1 \end{pmatrix}, \end{aligned} \quad (7)$$

in which the off-diagonal elements are all 0, indicating that the mixed state lacks a phase relationship between the constituent states,  $|00\rangle$  and  $|11\rangle$ . Furthermore, the density matrix of a statistical mixture where all the basis states  $|00\rangle$ ,  $|01\rangle$ ,  $|10\rangle$ , and  $|11\rangle$  are equally mixed becomes

$$\rho = \frac{1}{4}I = \frac{1}{4} \begin{pmatrix} 1 & 0 & 0 & 0 \\ 0 & 1 & 0 & 0 \\ 0 & 0 & 1 & 0 \\ 0 & 0 & 0 & 1 \end{pmatrix}. \quad (8)$$

This state is called the *fully mixed state*. In addition, the density matrix of a  $(1-a) : a$  statistical mixture of the Bell state  $|\Phi^+\rangle$  and the fully mixed state in eq. (8) becomes

$$\begin{aligned} \rho &= \frac{1-a}{2}(|00\rangle + |11\rangle)(\langle 00| + \langle 11|) + \frac{a}{4}I \\ &= \frac{1}{2} \begin{pmatrix} 1-a/2 & 0 & 0 & 1-a \\ 0 & a/2 & 0 & 0 \\ 0 & 0 & a/2 & 0 \\ 1-a & 0 & 0 & 1-a/2 \end{pmatrix}. \end{aligned} \quad (9)$$

This state is called the *Werner state*.<sup>30)</sup>

Note that the state of each constituent qubit in a maximally entangled state is a fully mixed state. The density matrix of the qubit is obtained by the partial tracing of the whole system with respect to the rest other than the qubit concerned. For instance, the density matrix  $\rho_A$  of the qubit A in the maximally entangled 2-qubit system (6) is obtained by the partial tracing of the 2-qubit density matrix with respect to B:

$$\begin{aligned} \rho_A &= \text{Tr}_B\{\rho\} \\ &= \frac{1}{2} \begin{pmatrix} 1 & 0 \\ 0 & 1 \end{pmatrix}. \end{aligned} \quad (10)$$

This is the fully mixed state in the 1-qubit system.

Thus, in general, quantum states including pure and mixed states are characterized by density matrices. As discussed in §5, we can evaluate the degree of entanglement in terms of a number of measures that are calculated from the density matrix.

### 2.3 Coding of qubits and entanglement on photon polarization

Qubits are implemented on any physical states that can be regarded as two-level states. With regard to photons, there are still several ways to implement qubits. The two most important implementations of photonic qubits are *polarization qubits* and *time-bin qubits*. Polarization qubits have been used to investigate various kinds of principal experiments on entanglement, such as the tests of Bell's inequality. Time-bin qubits are mainly applied to quantum communication protocols such as quantum cryptography<sup>31)</sup> because of their compatibility with optical fiber transmission. Here, we focus on the implementation and use of polarization qubits and discuss the entanglement between them. For readers who have interest in other kinds of qubits including time-bin qubits, it would be helpful to see, for instance, ref. 31.

In classical optics, the polarization of light corresponds to the direction of the electric (or magnetic) field amplitude of an electromagnetic wave. In free space, the electromagnetic wave is transverse and thus the polarization has two degrees of freedom, i.e.,  $x$  and  $y$ , assuming that the electromagnetic wave propagates along  $z$ . Any pure polarization states are expressed by the two-dimensional unit vector

$$\mathbf{a} = \begin{pmatrix} a_x \\ a_y \end{pmatrix}, \quad (11)$$

where  $a_x$  ( $a_y$ ) is the  $x$  ( $y$ ) component of the normalized field amplitude, and  $\|\mathbf{a}\|^2 = |a_x|^2 + |a_y|^2 = 1$ . Note that the  $z$  component is missing because of the transverse nature of the field. From the quantum mechanical viewpoint, a quantum associated with a three-dimensional vector field has triply degenerated internal degree of freedom, i.e., spin  $s = 1$ .<sup>32,33)</sup> Although a photon is a spin-1 ( $s = 1$ ) particle, the state for  $s_z = 0$  is missing because of the massless and transverse nature of a photon in free space. Thus, the polarization state for a single photon behaves as a two-level system, obeying SU(2) algebra just like an electron spin. If we take two orthogonal linear polarization states,  $|x\rangle$  and  $|y\rangle$ , as its bases, any polarization state  $|\psi\rangle$  can be expressed by their superposition

$$|\psi\rangle = c_x|x\rangle + c_y|y\rangle \equiv \begin{pmatrix} c_x \\ c_y \end{pmatrix}, \quad (12)$$

where  $\langle\psi|\psi\rangle = |c_x|^2 + |c_y|^2 = 1$ . The classical meaning of eq. (12) is straightforward by comparing with eq. (11). Thus, we can regard the quantum state of the photon polarization as a qubit;

$$|x\rangle = \begin{pmatrix} 1 \\ 0 \end{pmatrix} \equiv |0\rangle, \quad |y\rangle = \begin{pmatrix} 0 \\ 1 \end{pmatrix} \equiv |1\rangle. \quad (13)$$

It is very common for experimentalists to express the polarization states on the basis of their laboratory coordinates where photons propagate on a level with the ground. Horizontal and vertical polarization states,  $|H\rangle$  and  $|V\rangle$ , respectively, are used as the bases;

$$|H\rangle = \begin{pmatrix} 1 \\ 0 \end{pmatrix}, \quad |V\rangle = \begin{pmatrix} 0 \\ 1 \end{pmatrix}. \quad (14)$$

Diagonal ( $\pm 45^\circ$ ) linear polarization states,  $|D^+\rangle$  and  $|D^-\rangle$ , are

$$|D^+\rangle = \frac{1}{\sqrt{2}} \begin{pmatrix} 1 \\ 1 \end{pmatrix}, \quad |D^-\rangle = \frac{1}{\sqrt{2}} \begin{pmatrix} 1 \\ -1 \end{pmatrix}. \quad (15)$$

Left and right circular polarization states,  $|L\rangle$  and  $|R\rangle$ , are

$$|L\rangle = \frac{1}{\sqrt{2}} \begin{pmatrix} 1 \\ i \end{pmatrix}, \quad |R\rangle = \frac{1}{\sqrt{2}} \begin{pmatrix} 1 \\ -i \end{pmatrix}. \quad (16)$$

Since the polarization state for a single photon is regarded as a qubit, the combination of polarization states of a pair of photons, which hereafter we refer to as the two-photon polarization state, expresses two qubits. The bases of the two-photon polarization states are  $|HH\rangle$ ,  $|HV\rangle$ ,  $|VH\rangle$ , and  $|VV\rangle$ , where  $|\psi_A\psi_B\rangle$  represents the state in which the polarization states of photons A and B are  $|\psi_A\rangle$  and  $|\psi_B\rangle$ , respectively. By using this expression, the polarization-entangled Bell states are expressed by

$$|\Phi^\pm\rangle = \frac{1}{\sqrt{2}} (|HH\rangle \pm |VV\rangle), \quad (17)$$

$$|\Psi^\pm\rangle = \frac{1}{\sqrt{2}} (|HV\rangle \pm |VH\rangle). \quad (18)$$

It is worth noting the expression of Bell states on the bases other than  $|H\rangle$  and  $|V\rangle$ . For example, we obtain

$$|HH\rangle + |VV\rangle = |LR\rangle + |RL\rangle, \quad (19)$$

$$|HH\rangle - |VV\rangle = |LL\rangle + |RR\rangle, \quad (20)$$

$$|HV\rangle + |VH\rangle = |LL\rangle - |RR\rangle, \quad (21)$$

$$|HV\rangle - |VH\rangle = |LR\rangle - |RL\rangle, \quad (22)$$

from simple transformations. Note that the representation of each triplet state (19)–(21) depends on the bases, whereas that of the singlet state (22) is independent. For instance, the triplet state (19) exhibits a positive correlation (parallel polarizations) in the H–V bases while having negative correlation (counter-circular polarizations) in the L–R bases.

### 3. Generation of Entangled Photons

#### 3.1 Atomic sources

In the early years, trials were made to generate polarization-entangled photons using pair creation of gamma-ray photons produced by positron annihilation.<sup>34,35)</sup> However, the absence of good polarizers in the gamma-ray region gave no dependable evidence of the entanglement. The first reliable source that experimentally manifested the entanglement was cascaded two-photon emission from a single atom.

The polarization correlation of photons emitted from such atomic cascades was investigated using calcium<sup>4,5,8,9)</sup> and mercury<sup>6,7)</sup> atoms. For example, a diagram of the atomic cascade in calcium is shown in Fig. 1. The atom is excited from its ground state  $|g\rangle = (4s^2 \ ^1S_0)$  to the excited state  $|e\rangle = (4p^2 \ ^1S_0)$  by two-photon excitation.<sup>8)</sup> The excited state consists of two excited 4p electrons forming zero total angular momentum ( $J = 0$ ). Thus, the angular momentum part of the excited state is

$$|e\rangle = \frac{1}{\sqrt{3}} (|+1\rangle_A |-1\rangle_B - |0\rangle_A |0\rangle_B + |-1\rangle_A |+1\rangle_B), \quad (23)$$

where  $|m\rangle_i$  denotes the state of each excited electron ( $i = A$  or  $B$ ) represented by the orbital magnetic quantum number  $m$ . The excited state decays to the intermediate state  $|i\rangle =$

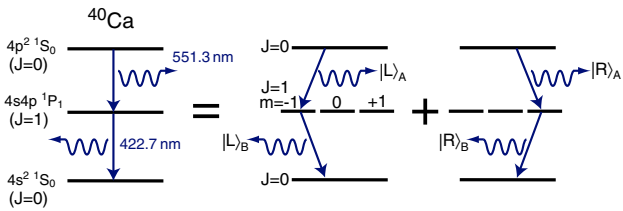


Fig. 1. (Color online) Schematic diagram of entangled photon pair emission via atomic cascade in calcium.

( $4s4p \ ^1P_1$ ) by emitting a visible photon A (wavelength  $\lambda = 551.3 \text{ nm}$ ). The intermediate state is triply degenerate, having orbital magnetic quantum numbers  $m = -1, 0$ , and  $+1$ . The intermediate state decays back to the ground state  $|g\rangle$  by emitting another photon B ( $\lambda = 422.7 \text{ nm}$ ). In this scheme, the total angular momentum  $J$  of the atom changes as  $J = 0 \rightarrow 1 \rightarrow 0$ . Assuming that the two photons are emitted along the quantization axis, the second term in eq. (23) does not contribute to the optical transition. As a result, if we observe the two photons emitted to opposite directions, the photon pair is entangled so that their polarization state is the maximally entangled state

$$\begin{aligned} |\psi\rangle &= \frac{1}{\sqrt{2}} (|L\rangle_A |L\rangle_B + |R\rangle_A |R\rangle_B) \\ &\equiv \frac{1}{\sqrt{2}} (|LL\rangle + |RR\rangle), \end{aligned} \quad (24)$$

where L and R denote the polarization state (L: left circular, R: right circular) of each photon. The polarization entangled state (24) can be rewritten in linear polarization bases as

$$|\psi\rangle = \frac{1}{\sqrt{2}} (|HH\rangle - |VV\rangle), \quad (25)$$

where H and V denote horizontal and vertical linear polarizations, respectively. Thus, from this atomic cascade, the generation of entangled photons in the triplet Bell state is expected. In practice, Aspect *et al.* performed the test of CHSH-Bell's inequality (see §4.2) utilizing the photons thus generated.<sup>8,9)</sup> In their experiments, the obtained  $S$  was  $S = 2.697 \pm 0.015$ ,<sup>9)</sup> exhibiting a violation of the inequality. This is the first clear demonstration of the generation of entangled photon pairs.

Although this method for generating entangled photons was pioneering, it is rather hard to collect the emitted pairs efficiently, because the photons are emitted randomly to a whole solid angle. Also, handling single atoms is not very useful for applications to general experiments. Thus, the atomic cascade has not been frequently used in practical quantum info-communication experiments, in spite of its honor as the first entangled photon source.

### 3.2 Parametric down-conversion

Parametric down-conversion (PDC) is a nonlinear optical process in which a pump light is converted into two (signal and idler) lights in a crystal with  $\chi^{(2)}$  optical nonlinearity.<sup>36)</sup> Spontaneous parametric down-conversion, parametric fluorescence in other words, has been observed since the 1960s.<sup>37,38)</sup> From a quantum optical point of view, PDC is a process in which twin daughter photons are produced simultaneously from a parent photon,<sup>39)</sup> as shown in Fig. 2.

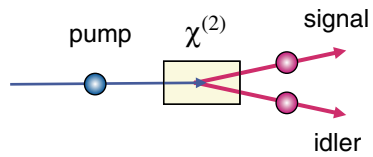


Fig. 2. (Color online) Illustration of the parametric down-conversion in  $\chi^{(2)}$  nonlinear crystal.

The interaction Hamiltonian  $H$  of this process is expressed by<sup>36)</sup>

$$H = \hbar g (\hat{a}_1^\dagger \hat{a}_2^\dagger \hat{a}_0 + \hat{a}_0^\dagger \hat{a}_2 \hat{a}_1), \quad (26)$$

where  $\hat{a}_i^\dagger$  and  $\hat{a}_i$  are the creation and annihilation operators for the pump ( $i = 0$ ), signal ( $i = 1$ ), and idler ( $i = 2$ ) modes, respectively, and  $g$  is the coupling constant. The first and second terms in eq. (26) represent PDC and its inverse, i.e., sum frequency generation, respectively. In the continuous-wave approximation, the sum frequency of the signal and idler lights must be the same as the pump light frequency. Also, a phase matching condition must be fulfilled so that each light wave generated is in phase at every point in the nonlinear crystal. These conditions are represented by

$$\omega_0 = \omega_1 + \omega_2, \quad (27)$$

$$\mathbf{k}_0 = \mathbf{k}_1 + \mathbf{k}_2, \quad (28)$$

where  $\omega_i$  and  $\mathbf{k}_i$  are the frequencies and wave vectors of the lights, respectively. These conditions are regarded as energy and momentum conservations of the photons concerned. As a result, the signal and idler photons have natural correlations in energy and momentum. In addition, the emission of the signal and idler photons should be simultaneous in practical conditions. The correlations in eqs. (27) and (28) were confirmed by observations including the simultaneous detection of the photon pairs.<sup>39)</sup> Because of these characteristics, PDC has been used frequently as a pair photon source for various types of two-photon interferometry,<sup>40)</sup> such as Hong-Ou-Mandel interference.<sup>41)</sup>

In the generation of polarization-entangled photons, it is essential to consider the polarization states of the photon pairs generated by PDC. There are two types of phase matching conditions in PDC, depending on the polarization states. One is called type-I phase matching or type-I PDC, in which the generated signal and idler photons have parallel polarizations. The other is called type-II, where the signal and idler photons have perpendicular polarizations. Both types can be used to generate photon pairs that are entangled in their polarization. The pioneering work to generate the polarization-entangled state from PDC utilized type-I phase matching, combined with the use of a nonpolarizing beam splitter (a half-reflecting, half-transmitting mirror, independent of polarization).<sup>10,11)</sup> In these experiments, as shown in Fig. 3, the polarization of one of the photons was rotated to obtain two orthogonally polarized photons, and then the two photons are combined at the beam splitter. When two photons having  $|H\rangle$  and  $|V\rangle$  polarizations are combined at the beam splitter, the resultant two-photon polarization state  $|\psi\rangle$  after the beam splitter is<sup>11)</sup>

$$|\psi\rangle = \frac{1}{\sqrt{2}} (|H\rangle_A + i|H\rangle_B) \otimes \frac{1}{\sqrt{2}} (-i|V\rangle_A + |V\rangle_B)$$

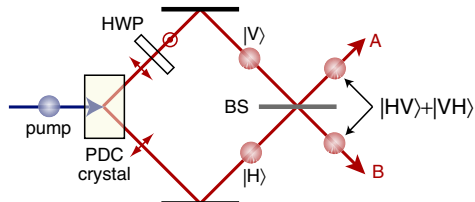


Fig. 3. (Color online) Generation of polarization-entangled photon pairs using type-I parametric down-conversion (PDC) and a beamsplitter (BS). The polarization of one of the photons emitted from PDC was rotated by a half-wave plate (HWP) to obtain a pair of orthogonally polarized photons. Then, the photon pair is combined at BS. Under the condition that the photon pair is separated into the two output ports, A and B, the state is entangled as eq. (30).

$$= \frac{1}{2} (|H\rangle_A |V\rangle_B + |V\rangle_A |H\rangle_B - i|H\rangle_A |V\rangle_A + i|V\rangle_B |H\rangle_B), \quad (29)$$

where A and B denote the two output ports of the beamsplitter. This state is a product state and thus is *not* entangled. However, if we select the events in which the two photons separate into the two output ports, A and B, the resultant state consists of the first two terms in eq. (29):

$$|\psi\rangle = \frac{1}{\sqrt{2}} (|HV\rangle + |VH\rangle). \quad (30)$$

This is the maximally entangled state. The technique involves the so-called *postselection* procedure, in which the desired state (30) is selected from the whole generated state (29). The selection procedure is probabilistic (success probability = 1/2) and thus it is inappropriate for applications such as the loophole-free Bell's inequality test.<sup>42</sup> Nevertheless, this was the first experimental demonstration of polarization-entangled photons generated from PDC. Later, a similar technique was applied to type-II PDC.<sup>12</sup>

In 1995, Kwiat *et al.* reported the polarization entanglement between the photons generated from a crystal in type-II PDC,<sup>13</sup> without the use of postselection. As shown in Fig. 4, under a particular type-II phase matching condition, signal and idler photons are emitted along the two conical surfaces: one for signal photons that have horizontal polarization, and the other for idler photons that have vertical polarization. The two conical surfaces cross with each other at two directions, A and B, where the signal and idler photons are emitted so that when one is emitted to A, the other is emitted to B, and *vice versa*. Thus, the polarization state of the

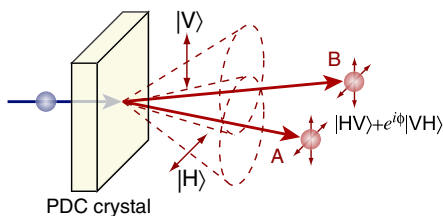


Fig. 4. (Color online) Generation of polarization-entangled photon pairs via type-II parametric down-conversion. Photons having horizontal (|H>) and vertical (|V>) linear polarizations are emitted along the two conical surfaces. A pair of photons emitted to the crossing directions of the two cones is entangled.

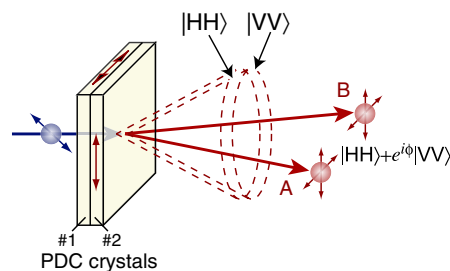


Fig. 5. (Color online) Generation of polarization-entangled photon pairs via type-I parametric down-conversion. Two crystals, i.e., #1 and #2 whose optic axes are aligned in perpendicular planes are pumped by 45°-polarized photons so that they emit photon pairs having |HH> and |VV> polarizations, respectively.

photons simultaneously emitted to the two directions should be

$$|\psi\rangle = \frac{1}{\sqrt{2}} (|HV\rangle + e^{i\theta}|VH\rangle). \quad (31)$$

The phase  $\theta$  between the two terms in eq. (31) can be adjusted by placing an additional birefringent phase shifter in one of the optical paths after the crystal. This method was used in the first experimental demonstration of quantum teleportation.<sup>43</sup>

Another method to generate entangled photons from PDC was also invented by Kwiat *et al.* in 1999.<sup>14</sup> In this method, two identical crystals operated with type-I phase matching are used; they are oriented with their optic axes aligned in perpendicular planes. As shown in Fig. 5, when the two crystals are illuminated by a 45°-polarized pump beam, the signal and idler photons are emitted together from either crystal, #1 or #2. Crystal #1 emits signal and idler photons with horizontal polarization, whereas crystal #2 emits photons with vertical polarization. The two cones along which the photons are emitted from each crystal are coaxial and almost identical, or indistinguishable, if the crystals are sufficiently thin. Thus, the polarization state of the emitted photons is the superposition of the two cases, i.e.,

$$|\psi\rangle = \frac{1}{\sqrt{2}} (|HH\rangle + e^{i\theta}|VV\rangle). \quad (32)$$

The phase  $\theta$  between the two terms in eq. (32) can be adjusted by controlling, for instance, the relative phase between the horizontal and vertical components of the pump beam. This method is more efficient than the method using type-II phase matching described earlier, because the photons emitted into larger solid angles are entangled. Thus, this method has been frequently used in various basic experiments of QICT.

In both methods described above, note that the two states [ $|HV\rangle$  and  $|VH\rangle$  in eq. (31),  $|HH\rangle$  and  $|VV\rangle$  in eq. (32)] should be indistinguishable except for their polarization. This means that the spatiotemporal modes for the two states should be identical. In birefringent materials, the group velocity of light pulses depends on their polarization and thus the wave packets of the generated photons split from each other depending on their polarization. If the separation of the photon wave packets is larger than their temporal width, which is on the order of the inverse spectral width

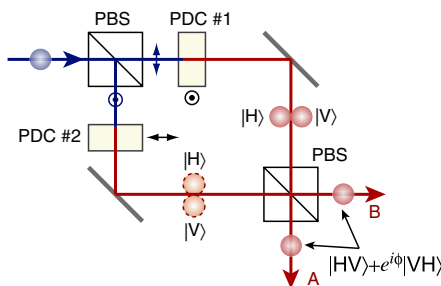


Fig. 6. (Color online) Generation of polarization-entangled photon pairs using two type-II PDC crystals in Mach-Zehnder interferometer.

(in the typical experimental condition, the temporal width is on the order of 100 fs), it causes the distinguishability that results in the degradation of entanglement. Thus, the thickness of the nonlinear crystal should be sufficiently small so that the separation of the photon wave packets is sufficiently small compared with their temporal width. It is effective to insert additional birefringent crystals to compensate the separation of the photon wave packets.<sup>44–46</sup>

Another method utilizing PDC to generate polarization-entangled photons is to place nonlinear crystal(s) in an interferometer.<sup>42,47–53</sup> Figure 6 shows an example of how to generate polarization-entangled photons using type-II PDC in a Mach-Zehnder interferometer.<sup>54</sup> In the interferometer, signal and idler photons are emitted from either PDC crystal, #1 or #2. The 45°-polarized pump beam is divided by a polarization beamsplitter (PBS), which reflects and transmits photons in vertical and horizontal polarizations, respectively. The pump beam then illuminates two nonlinear crystals whose optic axes are oriented orthogonally, one vertically and the other horizontally. Each crystal emits photon pairs consisting of one horizontally and one vertically polarized photons. The wave packets of the photon pairs are combined at the PBS again; if PDC crystal #1 emits photon pairs, the output state will be  $|H\rangle_A|V\rangle_B$ , and if PDC crystal #2 emits photons, the state will be  $|V\rangle_A|H\rangle_B$ . Thus, the output state from the interferometer is the superposition of the two cases, i.e., the same state as in eq. (31). The phase  $\theta$  can be adjusted by changing the path length difference between the two arms of the interferometer. This interferometric scheme presents the principle of generating entanglement, i.e., the superposition of the two states that interfere with each other. However, the stability of the interferometer, which is sensitive to environmental perturbation, limits the performance of entanglement. In this context, Sagnac interferometers have been used to obtain stable entangled photons.<sup>52,53</sup>

PDC using a natural optical nonlinear crystal has limitation in its working wavelength and efficiency because the phase matching condition depends on the natural dispersion of birefringence. Quasi-phase-matching (QPM) using periodically poled nonlinear crystals is a powerful technique to extend the applicability of nonlinear wavelength conversion. QPM using periodically poled lithium niobate (PPLN)<sup>50,51,55</sup> and periodically poled potassium titanyl phosphate (PPKTP)<sup>49,53,56–58</sup> has been applied to the generation of entangled photons via PDC. In particular, PPLN waveguides are used for the efficient generation of entangled photons in the telecom wavelength region (1.3 and 1.5 μm),<sup>50,51,55</sup> aiming at applying to quantum cryptography.

### 3.3 Semiconductor sources

Semiconductor sources that can generate nonclassical light are desirable because of their potential for various applications to QICT. For instance, the ability of single photon emitters is essential in keeping the security of quantum cryptography protocols such as BB84.<sup>31,59</sup> Semiconductor quantum dots (QDs) are very useful in generating single photons. When excited electron and hole pairs, or excitons, are confined together in a nanometer-sized QD, a strong interaction takes place between them. As a result, emission energies associated with exciton recombination depend on the number of excitons in a QD. One can distinguish the single exciton emission, i.e., emission from a single electron-hole pair in a QD, by discriminating its photon energy using a monochromator. Thus, a single QD acts as a single atom, emitting only one photon at a time. The single photon emission is evident from the observation of photon *antibunching*, i.e., ideally no probability of observing multiple photons at the same time. The antibunching of photons was observed in the emission from a single Na atom<sup>60</sup> in the 1970s. In 2000, the antibunched photon emission from a single QD was experimentally confirmed. Michler *et al.* observed for the first time the antibunching of emitted photons from a single CdSe QD.<sup>61</sup> Following this pioneering study, a number of results were reported on this phenomenon.<sup>62,63</sup> Note that the single photon emitter in a wavelength region for optical communication was readily achieved.<sup>64</sup> Some of these studies used pulsed excitation by which the emitted single photons are “clocked”, so that one can expect the regulated timing of the single photons. As mentioned above, the main application of these single photon sources is supposed to be quantum cryptography. In addition, a novel idea utilizing such clocked single photons is to prepare a pair of entangled photons.<sup>65</sup> In the experiment, two sequent single photons were used; the polarization of one of the photons was rotated by 90° and the timing of the photon was delayed for a single clock period in order to prepare two orthogonally polarized, temporally overlapped photons. These photons were then combined by a nonpolarized beamsplitter, just as in the case using PDC shown in Fig. 3. Thus, the resultant two-photon polarization state is the same as eq. (29). After the postselection that chooses the events in which two photons separate into two output ports, A and B, the selected state results in eq. (30). In this scheme, it is important that two photons emitted from a single QD are indistinguishable from each other so that quantum second-order interference between them takes place. To do so, the spectral width of the emitted photon should be a Fourier-transformed limit of the exciton lifetime. In other words, pure dephasing on the exciton wavefunction should be negligible in the exciton lifetime. This condition can be achieved in currently available QD samples with good quality.

In addition to the entangled photon generation based on the single photon emission described above, the excitonic system in a single QD can be used for the direct generation of entangled photon pairs. In this scheme, as shown in Fig. 7, cascaded two-photon emission from a biexciton, i.e., a bound state of two excitons, is used.<sup>66</sup> Similarly to the atomic cascade described in §3.1, the biexciton decays into the ground state via an exciton state emitting two sequent

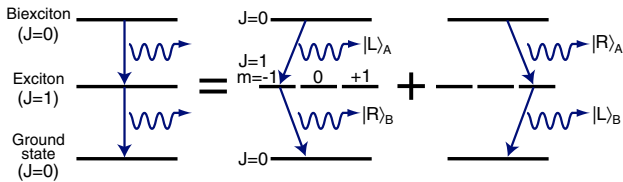


Fig. 7. (Color online) Schematic diagram of entangled photon generation via cascade emission from biexciton.

photons. The lowest bound state of the biexciton has zero total angular momentum ( $J = 0$ ); the angular momentum part of the biexciton is expressed by eq. (23). The optically allowed (bright) exciton is  $J = 1$  and the ground state is  $J = 0$ . Thus, the change in the angular momentum of the biexciton cascade is the same as that of the atomic cascade, i.e.,  $J = 0 \rightarrow 1 \rightarrow 0$ , showing that the emitted photon pair has polarization entanglement:

$$\begin{aligned} |\psi\rangle &= \frac{1}{\sqrt{2}} (|LR\rangle + |RL\rangle) \\ &= \frac{1}{\sqrt{2}} (|HH\rangle + |VV\rangle). \end{aligned} \quad (33)$$

We assumed here that we observe the two photons emitted to the same direction, whereas we assumed in eqs. (24) and (25) that we observe the two photons emitted to opposite directions.

In spite of the theoretical prediction described above, entangled photon generation from semiconductor QD has not been successful until most recently, mainly for the following reason. Most of self-organized QDs have small asymmetry in shape that induces the splitting of the exciton energy levels depending on their polarizations. In practice, it is quite common that the spectra of single QD emission (biexciton as well as exciton emission) splits into two components depending on the polarizations.<sup>67,68)</sup> The splitting causes the distinguishability between the photon pairs emitted from the biexciton cascade depending on the polarization. Let the two principal axes of the polarization be set as H and V. Note that the two-photon polarization state is no longer the superposition of the two, as shown in eq. (33), but the statistical mixture of  $|H\rangle_A|H\rangle_B$  and  $|V\rangle_A|V\rangle_B$ . The density matrix representation of the state is

$$\rho = \frac{1}{2} (|HH\rangle\langle HH| + |VV\rangle\langle VV|), \quad (34)$$

which is the mixed state presented in eq. (7). The state shows a classical correlation when the polarization was observed along its principal axes; it however does not exhibit any correlation when observed, for instance, in circular polarization or  $\pm 45^\circ$  polarization bases. Thus, the state in eq. (34) is not entangled. Such a mixed state of the two-photon polarization was observed experimentally.<sup>69)</sup> Most recently, two experimental groups have reported the generation of polarization-entangled photons from a single QD.<sup>16-18)</sup> The two groups took different approaches to realize the entanglement. One used QDs having reduced asymmetry and added an in-plane magnetic field to match the spectra for H and V polarizations.<sup>16,17)</sup> The other used spectral filtering of the emission spectra selecting identical

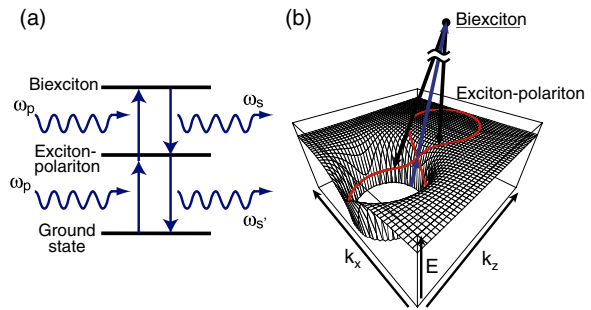


Fig. 8. (Color online) Schematic diagram of biexciton-resonant hyper parametric scattering (RHPS). (a) A simple picture that explains how two pump photons (frequency:  $\omega_p$ ) are converted to two scattered photons ( $\omega_s$ ,  $\omega_{s'}$ ). (b) Diagram taking account of the exciton–polariton dispersion drawn in two dimensions of momentum space. The curve on the polariton-dispersion surface indicates the states on which the phase-matching condition can be satisfied.

spectra from the overlapping spectral range of the two polarized emissions.<sup>18)</sup>

Entangled photon pairs can also be generated using biexcitons in a bulk semiconductor crystal, via the process called biexciton-resonant hyper parametric scattering (RHPS).<sup>15,19)</sup> In this process, as shown in Fig. 8, two pump photons (frequency:  $\omega_p$ ) create the biexciton by resonant two-photon excitation. The biexciton decays into the ground states emitting two scattered photons ( $\omega_s$ ,  $\omega_{s'}$ ). The photon pairs thus generated also have the polarization entanglement in eq. (33), reflecting the zero angular momentum of the biexciton. Although the RHPS, or resonant two-photon Raman scattering in other words, has been extensively studied since the 1970s,<sup>70-77)</sup> the applicability of the process to the generation of entangled photons has been theoretically pointed out only recently.<sup>78)</sup> RHPS is a  $\chi^{(3)}$  nonlinear process concerning four photons, whereas PDC discussed in §3.2 is a  $\chi^{(2)}$  nonlinear process concerning three photons. In RHPS, the photons concerned must obey a certain phase matching condition, as in PDC. Since the photons in the crystal form exciton–polaritons as a consequence of a strong exciton–photon interaction, the phase matching condition must take the dispersion of the exciton–polariton into account.<sup>70-77)</sup> The result is that the two scattered photons are emitted along the two almost identical conical surfaces, as in the type-I PDCs case shown in Fig. 5. In §4, we see an example of the observation of entangled photons generated from RHPS in the CuCl crystal. In addition, recent theoretical studies have predicted that RHPS will be markedly enhanced in a microcavity<sup>79,80)</sup> or films having specific thickness.<sup>81)</sup> In this context, RHPS in the CuCl film has been demonstrated experimentally.<sup>82)</sup>

### 3.4 Other sources

As described in §3.2, the most popular method to obtain entangled photon pairs is PDC, a second order ( $\chi^{(2)}$ ) optical nonlinear process in which a parent photon is converted into twin daughter photons. Higher-order nonlinear processes, e.g.,  $\chi^{(3)}$ , are also applicable to obtaining entangled photon pairs; nevertheless, the efficiency of such higher-order processes is very low unless somehow enhanced. RHPS is one of the examples of such  $\chi^{(3)}$  processes that utilize

electronic resonance to enhance its efficiency. Moreover, the strong spatiotemporal confinement of light in optical microcavities and optical waveguide structures can enhance the  $\chi^{(3)}$  optical nonlinear process. Dispersion-shifted fibers (DSFs) are used to generate correlated photon pairs via hyper parametric scattering (HPS), or spontaneous four-wave mixing in other words.<sup>83,84)</sup> In this technique, the pump wavelength is set close to the zero-dispersion wavelength of the DSF so as to avoid the longitudinal separation of the pump, signal, and idler photon pulses. Thus, the  $\chi^{(3)}$  interaction can be considerably enhanced by the spatiotemporal confinement of the photon pulses in the DSF. Recently, polarization<sup>85)</sup> and time-bin<sup>86)</sup> entanglements have been demonstrated using photon pairs thus generated. In addition, photonic crystal fibers were also applied to the generation of correlated photons.<sup>87–91)</sup> One of the remaining problems of these techniques is the presence of background noise originating mainly from spontaneous Raman scattering.<sup>84,87)</sup> The suppression of Raman noise by cooling fibers can improve performance.<sup>92,93)</sup> Most recently, correlated photon generation in nanoscale silicon waveguides, in which the Raman noise is expected to be much smaller, has also been reported.<sup>94)</sup> Such devices are compatible with conventional technologies in telecom wavelength and thus are promising in practical QICT.

#### 4. Observation of Entanglement

##### 4.1 Polarization correlation measurement

In order to observe and evaluate entanglement held by photon pairs, we must perform (i) simultaneous measurement of physical quantities of constituent photons and (ii) analysis of correlation between them. For instance, in the observation of polarization entanglement, projection measurement of the two-photon polarization state incorporating coincidence measurement is necessary, as shown in Fig. 9. Let the polarization states of the photons selected by the two polarization analyzers in the figure be  $\alpha$  and  $\beta$ . For instance,  $\alpha$  and  $\beta$  may be H, V, L, or R. Thus, the two-photon polarization state onto which the state is projected is  $|\alpha\rangle_A|\beta\rangle_B \equiv |\alpha\beta\rangle$ . The probability  $p_{\alpha\beta}$  that finds the system (density matrix:  $\rho$ ) in the polarization state  $|\alpha\beta\rangle$  is

$$p_{\alpha\beta} = \text{Tr}\{\rho|\alpha\beta\rangle\langle\alpha\beta|\}. \quad (35)$$

If the polarization state of the photon pair is in a pure state  $|\psi\rangle$ ,  $\rho = |\psi\rangle\langle\psi|$  and

$$p_{\alpha\beta} = |\langle\alpha\beta|\psi\rangle|^2. \quad (36)$$

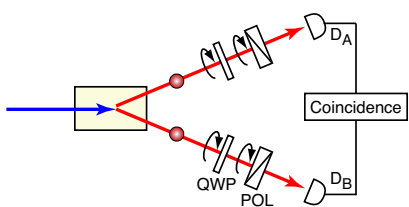


Fig. 9. (Color online) Schematic illustration of apparatus for measuring polarization entanglement. A polarization analyzer consisting of a quarter wave plate (QWP) and a polarizer (POL) in each path projects the polarization of each photon onto a certain polarization state. Coincident events from a pair of photon detectors ( $D_A$ ,  $D_B$ ) are recorded as coincidence signals for various polarization combinations.

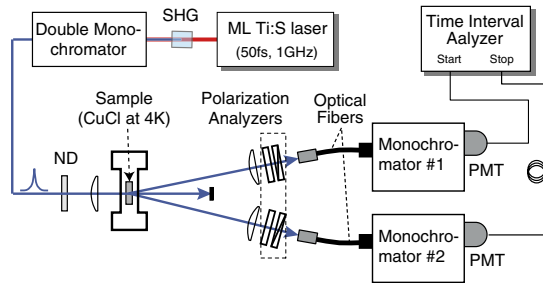


Fig. 10. (Color online) Schematic illustration of experimental setup for observing entangled photon pairs generated from RHPS in CuCl crystal. SHG: second harmonic generation. ND: neutral density filter. PMT: photon counting photomultiplier.

The rate of coincidence measurement of the photon pairs in which the polarization state is projected onto  $|\alpha\beta\rangle$  is proportional to  $p_{\alpha\beta}$ . For example, if the state is in the entangled state in eq. (33), it is expected that the projection measurement gives equal probabilities 1/2 for LR, RL, HH, and VV polarization combinations. Note that if the state is in the mixed state in eq. (34), which has only a classical correlation, it shows a perfect correlation in the linear polarization bases (H, V) but no correlation in the circular bases (L, R).

Figure 10 shows the experimental setup used to observe entangled photon pairs generated from RHPS in the CuCl crystal.<sup>19)</sup> In this experiment, a femtosecond mode-locked Ti:sapphire laser having a 1 GHz repetition rate was used as a pump source. The high-repetition pumping is essential for the reduction of accidental background signals. The second harmonics of the pump light was then spectrally filtered by a zero-dispersion double monochromator to be in the two-photon resonance with the lowest biexciton ( $h\nu = 3.186$  eV). The output light from the monochromator was focused on the sample through an ND filter. In order to suppress the accidental coincidence of uncorrelated photons, the pump power was set to approximately  $10 \mu\text{W}$ . The emitted photons from the sample are fed into the optical multimode fibers connected to the two monochromators. Using the polarization analyzers consisting of a quarter wave plate and a polarizer in front of each fiber, we carried out the polarization projection measurement as described above. Monochromators #1 and #2 select the photons having appropriate photon energies satisfying the phase-matching condition (see Fig. 8). The photons are detected by the two photomultipliers, and the time-interval analyzer records the difference in arrival time between the photons. Signals at the same arrival time, i.e., at zero delay time, are the coincidence signals between the photon pairs originating from a biexciton, whereas others are accidental coincidences between independent photons.

Figure 11 shows an example of the polarization correlation measurements thus obtained.<sup>19)</sup> In the figure, histograms of the coincidence count rate are shown for a set of polarization combinations, as a function of delay time  $\tau$  between two photons detected. In the histogram, the central peak at  $\tau = 0$  is the correlated two-photon coincidence signal originating from a biexciton. Thus, the polarization correlation of this central peak presents the quantum correlation. On the other hand, the noisy background signals

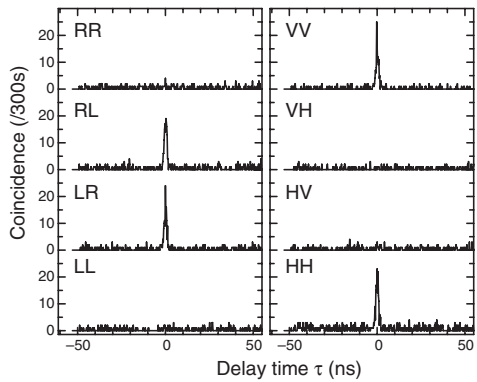


Fig. 11. Time correlation histograms of photon pairs generated from RPHS in CuCl crystal. Polarization correlation measurements were made in circular (L, R) and linear (H, V) polarization bases. The central peak at  $\tau = 0$  is the correlated two-photon coincidence signal originating from one biexciton. The background signal at  $\tau \neq 0$  results from the uncorrelated photons.

that appear at  $\tau \neq 0$  originate from uncorrelated photons generated by independent pump pulses (interval: 1 ns) and have no polarization correlations. In these histograms, it is clear that the coincidence signals at  $\tau = 0$  appear for counter-circular (LR and RL) or parallel (HH and VV) polarization combinations, in consistent with the theoretical prediction in eq. (33).

#### 4.2 Violation of Bell's inequality

In connection with the violation of Bell's inequality, the polarization correlation for the Bell states (2) and (3) is worth noting. If we measure the polarization states in linear polarization bases, the polarization state  $|\alpha\beta\rangle$  onto which the state is projected is described by  $|\theta_A\theta_B\rangle$  where

$$|\theta_A\theta_B\rangle \equiv (\cos\theta_A|H\rangle_A + \sin\theta_A|V\rangle_A) \otimes (\cos\theta_B|H\rangle_B + \sin\theta_B|V\rangle_B). \quad (37)$$

The probability  $p(\theta_A, \theta_B)$  that finds the systems in the polarization state  $|\theta_A\theta_B\rangle$  can be easily calculated:

$$p(\theta_A, \theta_B) = \begin{cases} \frac{1}{2} \cos^2(\theta_A \mp \theta_B) & \text{for } |\Phi^\pm\rangle \\ \frac{1}{2} \sin^2(\theta_A \pm \theta_B) & \text{for } |\Psi^\pm\rangle. \end{cases} \quad (38)$$

The observation of these relationships is used to examine the polarization-entanglement when one can expect that the two-photon polarization states are one of the Bell states.

A more explicit and quantitative proof of the violation of Bell's inequality is to examine the inequality proposed by Clauser, Horne, Shimony, and Holt (CHSH) in 1969.<sup>3)</sup> According to the CHSH theory, Bell's inequality can be written as

$$S = |E(\theta_A, \theta_B) - E(\theta_A, \theta'_B) + E(\theta'_A, \theta_B) + E(\theta'_A, \theta'_B)| \leq 2, \quad (39)$$

and  $E(\theta_A, \theta_B)$  is given by

$$E(\theta_A, \theta_B) = \frac{C(\theta_A, \theta_B) + C(\theta_A^\perp, \theta_B^\perp) - C(\theta_A^\perp, \theta_B) - C(\theta_A, \theta_B^\perp)}{C(\theta_A, \theta_B) + C(\theta_A^\perp, \theta_B^\perp) + C(\theta_A^\perp, \theta_B) + C(\theta_A, \theta_B^\perp)}, \quad (40)$$

where  $C(\theta_A, \theta_B)$  is the coincidence count for each polar-

ization angle and  $\theta_i^\perp \equiv \theta_i + 90^\circ$ . The Bell states clearly violate the inequality in eq. (39); for instance, if we calculated the value of  $S$  in eq. (39) for the state  $|\Phi^+\rangle$  substituting  $p(\theta_A, \theta_B)$  in eq. (38) for  $C(\theta_A, \theta_B)$ , we obtain  $S = 2\sqrt{2} > 2$  at  $\theta'_A - \theta_A = 45^\circ$ ,  $\theta_B - \theta_A = 22.5^\circ$ , and  $\theta'_B - \theta_A = 67.5^\circ$ . Other Bell states also violate the inequality with  $S = 2\sqrt{2}$ .

In order to confirm experimentally that the generated photon pairs actually violate CHSH-Bell's inequality (39), we must measure the polarization correlation for 16 combinations of analyzer setting ( $\theta_A = 0, 45, 90, 135^\circ$ ;  $\theta_B = 22.5, 67.5, 112.5, 157.5^\circ$ ). From the measurements similar to those in Fig. 11, coincidence counts  $C(\theta_A, \theta_B)$  were recorded for the 16 polarization combinations. From the result, an  $S$  value of  $2.34 \pm 0.1 > 2$  was obtained. It is clear that the  $S$  apparently violates Bell's inequality by more than 3 times the standard deviation. Although the obtained  $S$  violates Bell's inequality, the obtained  $S$  was smaller than the ideal value  $2\sqrt{2}$  for the Bell state  $|\Phi^+\rangle$ . This indicates the degradation of entanglement to some extent, as characterized and discussed in the next section. By using SPDC, a greater violation of Bell's inequality has been achieved.<sup>13,14)</sup>

#### 5. Characterization of Entanglement

##### 5.1 Quantum state tomography

As discussed in §2.2, any 2-qubit state is expressed by a density matrix. Polarization entanglement between two photons is also evaluated from their density matrix. The density matrix for the entangled state in eq. (33) generated from a biexciton is expressed as

$$\rho = \frac{1}{2}(|HH\rangle + |VV\rangle)(\langle HH| + \langle VV|) = \frac{1}{2} \begin{pmatrix} 1 & 0 & 0 & 1 \\ 0 & 0 & 0 & 0 \\ 0 & 0 & 0 & 0 \\ 1 & 0 & 0 & 1 \end{pmatrix}. \quad (41)$$

In this matrix representation,  $|HH\rangle$ ,  $|HV\rangle$ ,  $|VH\rangle$ , and  $|VV\rangle$  are used as a basis set. The maximally entangled state holds full coherence between the constituent bases and thus the diagonal ( $|HH\rangle\langle HH|$  and  $|VV\rangle\langle VV|$ ) and off-diagonal ( $|HH\rangle\langle VV|$  and  $|VV\rangle\langle HH|$ ) elements have the same absolute value 1/2 in the density matrix (41).

In order to obtain experimentally the density matrix of two-photon polarization states, we must observe the polarization correlation described in §4.1 for various polarization combinations. Then, using the procedure called *quantum state tomography*,<sup>95)</sup> or simply *state tomography*, we can reconstruct the density matrix that is estimated from the experimental data. The number of bases, or the dimension of Hilbert space, of a 2-qubit system is  $2 \times 2 = 4$ , and thus the minimal number of polarization combinations in the correlation measurement required to reconstruct the density matrix is  $4^2 = 16$ . Mathematically, we can reconstruct the density matrix from the 16 combinations of the experimental data by linear algebra. In practice, however, errors and noises in the experimental data usually make the reconstructed density matrix unreliable; sometimes it produces unphysical density matrices that have, for instance, negative eigenvalues. In such cases, we should reconstruct the density matrix from more than 16 experimental data by maximum

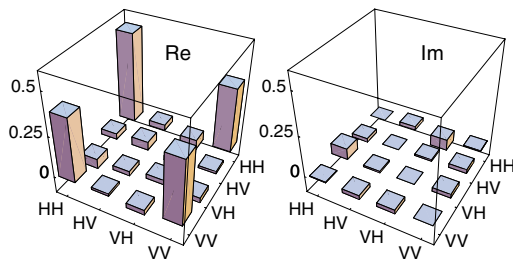


Fig. 12. (Color online) Reconstructed two-photon polarization density matrix for photon pairs generated from RPHS in CuCl.

likelihood estimation<sup>95</sup> so that the resultant density matrix is not unphysical.

Figure 12 shows a histogram of the reconstructed density matrix of the two-photon polarization state of the photon pairs generated by RPHS in the CuCl crystal.<sup>19</sup> To obtain the density matrix, data of 22 combinations in polarization correlation measurements, including those shown in Fig. 11, are used. The diagonal elements reflect the polarization correlation in the linear polarization bases (HH, HV, VH, and VV) in Fig. 11 and the off-diagonal elements show the coherence between them. We observe that the values of the diagonal elements ( $|HH\rangle\langle HH|$  and  $|VV\rangle\langle VV|$ ) and off-diagonal elements ( $|HH\rangle\langle VV|$  and  $|VV\rangle\langle HH|$ ) are close to 0.5 and those of the other elements are almost zero. Thus, we observe that the experimentally reconstructed density matrix closely resembles the expected one shown in eq. (41).

Strictly speaking, however, there are some deviations from the ideal one indicating that the entanglement is degraded to some extent by, for instance, the imperfection of the source and disturbance from the environment. The first signature of the degradation is an imbalance between the coefficients of  $|HH\rangle$  and  $|VV\rangle$ , as in the nonmaximally entangled state (4). The degradation appears in a density matrix as an imbalance of the diagonal elements,  $|HH\rangle\langle HH|$  and  $|VV\rangle\langle VV|$ . This degradation comes from the experimental condition in which we expect a geometrical imbalance between the intensities of H and V polarizations of the generated photons.<sup>19,73-75</sup> The second signature is the appearance of diagonal elements  $|HV\rangle\langle HV|$  and  $|VH\rangle\langle VH|$  that are not expected to appear originally. This indicates that noise approximated by the fully mixed state (8) is mixed up to the observed state. Such noise comes from the accidental coincidence signals originating from uncorrelated photons. As described in §2.2, when the fully mixed state is mixed to the maximally entangled state (41), the state becomes the Werner state (9). The third signature of the degradation, which is not significant in our reconstructed density matrix, is a disordered phase relationship between  $|HH\rangle$  and  $|VV\rangle$ . In this case, the amount of off-diagonal elements,  $|HH\rangle\langle VV|$  and  $|VV\rangle\langle HH|$ , becomes smaller. The extreme case of the phase disorder results in the classical mixed state (7) in which all the off-diagonal elements are 0. Thus, by analyzing the density matrix, we can make an estimation of the degree of entanglement and the origins of its degradation.

The fidelity ( $F$ ), defined by

$$F \equiv \langle \psi | \rho | \psi \rangle, \quad (42)$$

is a measure that evaluates the closeness of the state expressed by the density matrix  $\rho$  to the ideal pure state  $|\psi\rangle$ . More generally, the fidelity of the state  $\rho$  to the state expressed by a density matrix  $\rho_0$  is defined by

$$F \equiv (\text{Tr} \sqrt{\sqrt{\rho_0} \rho \sqrt{\rho_0}})^2. \quad (43)$$

$F$  takes a value in the range from 0 to 1. It is obvious that  $F = 1$  for the ideal state:  $\rho = \rho_0$ . The fidelity of the classical mixed states in eq. (7), which holds a classically maximal correlation, to the maximally entangled state (1) is  $F = 0.5$ ; this is the upper bound of the fidelity of any classical states to the maximally entangled state.

The fidelity of the reconstructed density matrix shown in Fig. 12 to the ideal maximally entangled state in eq. (33) is calculated to be  $F = 0.85$ . Since the fidelity of classical states should not exceed 0.5 as described above, the result shows that the observed two-photon polarization state has true entanglement beyond the classical limit. If one considers a state that models the degradation of entanglement assuming an imbalance of the polarization at the source and the mixture of noise originating from uncorrelated photons, the fidelity of the reconstructed density matrix to the model state is 0.94. This means that the degradation of entanglement in the observed state is almost expressed by the two origins modeled in the analysis. Note that part of such degradation can be compensated by local filtering of the polarization, i.e., by *entanglement distillation*.<sup>96</sup>

## 5.2 Quantitative measures of entanglement

A density matrix contains all information on a quantum state. However, it has so many elements that it is not convenient for the direct and simple measurement of entanglement. To date, a number of measures for the quantitative evaluation of entanglement have been proposed. Bell's inequality is one of such measures. *Entanglement of formation* ( $E_F$ ), or *ebit*, is a measure of entanglement; 1 ebit corresponds to a pair of qubit in a maximally entangled state and  $E_F$  quantifies how much ebit can be constructed from the state concerned, or how much ebit is necessary to construct the state, by the use of local operation and classical communication (LOCC).<sup>97</sup> *Concurrence*<sup>98</sup> ( $C$ ) and *tangle*<sup>99</sup> ( $T \equiv C^2$ ) are also used as quantitative measures of entanglement. In general, it is difficult to obtain  $E_F$  directly from a density matrix. In a 2-qubit system, however,  $C$  and  $T$  can be calculated from a density matrix and then we can obtain  $E_F$ .<sup>98</sup> For example, the values of  $C$ ,  $T$ , and  $E_F$  obtained from the density matrix shown in Fig. 12 are 0.75, 0.56, and 0.65, respectively.<sup>19</sup>  $E_F$  means that if we have 100 sets of the two-photon state, we can obtain 65 pairs of maximally entangled photons via LOCC. Taking account of the fact that  $E_F = 0$  for the classically correlated state (7), we observe that our state shown in Fig. 12 has a considerably high degree of entanglement, even though it is not perfect.

These entanglement measures are in principle obtained from a density matrix. However, we must obtain a large number of correlation measurement sets, at least more than the number of matrix elements, to reconstruct the density matrix. Thus, density matrix reconstruction is impractical for a large number of qubit systems because the number of measurement sets that is necessary for the density matrix reconstruction rapidly increases with increasing number of

qubits; we need  $(2^n)^2 = 4^n$  measurement sets for the  $n$ -qubit system. On the other hand, more efficient methods using such as *entanglement witness*<sup>100,101</sup> to evaluate entanglement have been proposed and performed.<sup>102,103</sup> These are expected to be powerful for the evaluation of entanglement in larger systems.

## 6. Entanglement beyond Qubits

In this article, we have focused on the entanglement shared by a pair of photons. The polarization entanglement, as well as the time-bin entanglement, shared by a pair of photons is categorized into the most simple class, i.e., 2-qubit entanglement. In addition to this most simple class, photons can have other kinds of entanglement, such as entanglement in continuous variables, and that in discrete states with more than two degrees of freedom (*qudit*). Entanglement in quadrature variance<sup>29</sup> was experimentally demonstrated and applied to unconditional quantum teleportation.<sup>104</sup> However, the entanglement in quadrature variance is essentially encoded to ensemble states of photons, but not to a single photon pair. An example of a continuous variable entanglement in a pair of photons is *energy-time entanglement*, an analogue to EPR's position-momentum entanglement. Suppose that a pair of daughter photons are generated by PDC from a parent photon that has a certain photon energy  $\hbar\omega_0$ . As a result of the energy conservation in eq. (27), the daughter photons have photon energies  $\hbar\omega_A$  and  $\hbar\omega_B$  that satisfy the relation

$$\hbar\omega_0 = \hbar\omega_A + \hbar\omega_B. \quad (44)$$

If we express the energy eigenstates of each photon as  $|\omega\rangle_i$  ( $i = A$  or  $B$ ), the two photon state  $|\psi\rangle$  is entangled so that

$$|\psi\rangle = \int f(\omega) |\omega\rangle_A |\omega_0 - \omega\rangle_B d\omega, \quad (45)$$

where  $f(\omega)$  is a function that describes the distribution of the complex amplitude of the down-converted photons. This is referred to as energy-time entanglement. The concept is close to EPR's original idea,<sup>1</sup> which concerns momentum and position, instead of energy and time. Franson proposed to investigate the energy-time entanglement using a pair of spatially separated interferometers,<sup>105</sup> known as a Franson interferometer. He predicted that the energy-time entangled state in eq. (45) results in interdependent interference fringes between the two separate interferometers,<sup>105</sup> and the prediction was demonstrated experimentally.<sup>106</sup>

Another important example of entanglement between photons is *photon-number entanglement*. Suppose we have  $N$  photons and separate them into two paths, A and B. If we express the photon number eigenstates (Fock states) of each path as  $|n\rangle_i$ , the total state  $|\psi\rangle$  is expressed as

$$|\psi\rangle = \sum_{n=0}^N c_n |n\rangle_A |N-n\rangle_B, \quad (46)$$

where  $c_n$  is the distribution amplitude. Of particular interest is the case that  $c_n = 0$  other than  $n = 0$  or  $N$ , i.e.,

$$|\psi\rangle = \frac{1}{\sqrt{2}} (|N\rangle_A |0\rangle_B + |0\rangle_A |N\rangle_B). \quad (47)$$

This particular photon-number entangled state is often called *NOON state*. It was theoretically predicted that the NOON

state would exhibit interference fringes that have  $N$  times smaller period than the classical wavelength ( $\lambda$ ) of light. In other words, the NOON state behaves as if it had "de Broglie wavelength"  $\lambda/N$ .<sup>107</sup> Such reduced wavelength of the NOON state has been experimentally demonstrated for  $N = 2$ ,<sup>108</sup> 3,<sup>109</sup> and 4.<sup>110,111</sup> It would be possible to use the NOON state in realizing high-resolution quantum imaging beyond the classical diffraction limit.<sup>112,113</sup>

Furthermore, twin photons generated by PDC have a strong spatial correlation. In the ideal one-dimensional case, the state is expressed by a form of *spatial entanglement*

$$|\psi\rangle = \int f(x) |x\rangle_A |x\rangle_B dx, \quad (48)$$

where  $|x\rangle_i$  expresses the state in which the photon  $i$  ( $i = A$  or  $B$ ) is generated at  $x$ .<sup>114,115</sup> This entanglement is attributed to the property of the twin photons; they are generated at the same place in the nonlinear crystal. Similar to the NOON state, the state in eq. (48) also exhibits diffraction and interference patterns as if the twin photons had the wavelength  $\lambda/2$ .<sup>114-116</sup> In addition to the spatial entanglement, the twin photons have a strong correlation in their momenta, i.e., *momentum entanglement*, which is a consequence of the momentum conservation in eq. (28) in PDC. The spatial and momentum entanglements, which again are very close to EPR's original idea,<sup>1</sup> are essentially concerned with continuous variables. However, using the spatial or momentum entanglement combined with a number ( $N$ ) of slits, apertures, or optical fibers, one can generate useful entanglement in  $N$ -dimensional qudit systems.<sup>117,118</sup>

As mentioned in §2.3, the polarization of a photon is interpreted as its spin angular momentum. A photon has another degree of angular momentum, i.e., the orbital angular momentum associated with Laguerre-Gaussian modes of the light beam. Entanglement has also been found between the angular momenta of photon pairs generated by PDC.<sup>119</sup> In this case, the degree of freedom of the angular momentum is not limited to 2, and thus it can present entanglement in a qudit system.

Finally, *hyperentanglement*, i.e., multiple combination of entanglement encoded in different physical quantities such as polarization, spatial modes (position or momentum), orbital angular momentum, and energy-time, held in a pair of photons has recently been investigated.<sup>120,121</sup> A photon pair in the hyperentangled state can contain multiple copies of a certain entangled state encoded in different degrees of freedom. Taking advantage of this multivariate character, one can characterize the entanglement between the photon pairs using local measurements on either one of the constituent photons.<sup>122</sup>

These kinds of entanglement between photons, some of which are in continuous variables and others with more than two degrees of freedom, would present novel interesting phenomena beyond those expected for a simple 2-qubit entanglement.

## 7. Summary

We have discussed the generation, observation, and characterization of entangled photons. Among the various media thus far developed for handling entanglement, photons are the most versatile and practical media by which

we can generate, process, and distribute entanglement. Photon-pair polarization is the most simple yet versatile system on which 2-qubit entanglement is encoded. Although in this article, we have not mentioned multipartite entanglement between more than two qubits, one can produce such multipartite entanglement from two entangled photon pairs or more. To date, entanglement in up to six photons has been achieved experimentally.<sup>123)</sup> Furthermore, technologies of processing entanglement, such as distillation, swapping, purification, and concentration<sup>96,124–126)</sup> are of crucial importance to practical applications in QICT. Polarization-entangled photons have been used in all these fundamental experiments.

From the first realization of entangled photons using atomic sources, many studies of the generation and observation of entangled photons have been carried out. One of the most successful and popular methods to date has been the use of PDC. Recently, QPM technology has been used to enhance the potential and flexibility of PDC in entangled photon generation. Semiconductor sources, which have been demonstrated most recently, have opened the way of realizing entangled photon-emitting diodes. Moreover, fiber-based sources are attracting interest because of their potential in telecom wavelength. Such practical sources of entangled photons are one of the key technologies in the development of QICT and thus will be attracting our interest.

## Acknowledgments

The author is grateful to Professors T. Itoh, H. Ishihara, M. Nakayama, and H. Ohno for their helpful discussion. Our experimental work described in this article was carried out with Drs. G. Oohata and R. Shimizu, and was supported in part by CREST of Japan Science and Technology Agency (JST), ERATO Semiconductor Spintronics Project of JST, SCOPE of the Ministry of Internal Affairs and Communications, and a Grant-in-Aid for Creative Scientific Research (17GS1204) of the Japan Society for the Promotion of Science.

- 1) A. Einstein, B. Podolsky, and N. Rosen: *Phys. Rev.* **47** (1935) 777.
- 2) J. S. Bell: *Physics (N.Y.)* **1** (1964) 195.
- 3) J. F. Clauser, M. A. Horne, A. Shimony, and R. A. Holt: *Phys. Rev. Lett.* **23** (1969) 880.
- 4) C. A. Kocher and E. D. Commins: *Phys. Rev. Lett.* **18** (1967) 575.
- 5) S. J. Freedman and J. F. Clauser: *Phys. Rev. Lett.* **28** (1972) 938.
- 6) J. F. Clauser: *Phys. Rev. Lett.* **36** (1976) 1223.
- 7) E. S. Fry and R. C. Thompson: *Phys. Rev. Lett.* **37** (1976) 465.
- 8) A. Aspect, P. Grangier, and G. Roger: *Phys. Rev. Lett.* **47** (1981) 460.
- 9) A. Aspect, P. Grangier, and G. Roger: *Phys. Rev. Lett.* **49** (1982) 91.
- 10) Y. H. Shih and C. O. Alley: *Phys. Rev. Lett.* **61** (1988) 2921.
- 11) Z. Y. Ou and L. Mandel: *Phys. Rev. Lett.* **61** (1988) 50.
- 12) T. E. Kiess, Y. H. Shih, A. V. Sergienko, and C. O. Alley: *Phys. Rev. Lett.* **71** (1993) 3893.
- 13) P. G. Kwiat, K. Mattle, H. Weinfurter, A. Zeilinger, A. V. Sergienko, and Y. Shih: *Phys. Rev. Lett.* **75** (1995) 4337.
- 14) P. G. Kwiat, E. Waks, A. G. White, I. Appelbaum, and P. H. Eberhard: *Phys. Rev. A* **60** (1999) R773.
- 15) K. Edamatsu, G. Oohata, R. Shimizu, and T. Itoh: *Nature* **431** (2004) 167.
- 16) R. M. Stevenson, R. J. Young, P. Atkinson, K. Cooper, D. A. Ritchie, and A. J. Shields: *Nature* **439** (2006) 179.
- 17) R. J. Young, R. M. Stevenson, P. Atkinson, K. Cooper, D. A. Ritchie, and A. J. Shields: *New J. Phys.* **8** (2006) 29.
- 18) N. Akopian, N. H. Lindner, E. Poem, Y. Berlitzky, J. Avron, D.

- Gershoni, B. D. Gerardot, and P. M. Petroff: *Phys. Rev. Lett.* **96** (2006) 130501.
- 19) G. Oohata, R. Shimizu, and K. Edamatsu: *Phys. Rev. Lett.* **98** (2007) 140503.
- 20) M. Lamehi-Racht and W. Mittig: *Phys. Rev. D* **14** (1976) 2543.
- 21) C. Polachic, C. Rangacharyulu, A. van den Berg, S. Hamieh, M. Harakeh, M. Hunyadi, M. de Huu, H. Wörche, J. Heyse, C. Bäumer, D. Frekers, S. Rakers, J. A. Brooke, and P. Busch: *Phys. Lett. A* **323** (2004) 176.
- 22) H. Sakai, T. Saito, T. Ikeda, K. Itoh, T. Kawabata, H. Kuboki, Y. Maeda, N. Matsui, C. Rangacharyulu, M. Sasano, Y. Satou, K. Sekiguchi, K. Suda, A. Tamii, T. Uesaka, and K. Yako: *Phys. Rev. Lett.* **97** (2006) 150405.
- 23) E. Hagley, X. Maître, G. Nogues, C. Wunderlich, M. Brune, J. M. Raimond, and S. Haroche: *Phys. Rev. Lett.* **79** (1997) 1.
- 24) Q. A. Turchette, C. S. Wood, B. E. King, C. J. Myatt, D. Leibfried, W. M. Itano, C. Monroe, and D. J. Wineland: *Phys. Rev. Lett.* **81** (1998) 3631.
- 25) C. A. Sackett, D. Kielpinski, B. E. King, C. Langer, V. Meyer, C. J. Myatt, M. Rowe, Q. A. Turchette, W. M. Itano, D. J. Wineland, and C. Monroe: *Nature* **404** (2000) 256.
- 26) M. Steffen, M. Ansmann, R. Bialczak, N. Katz, E. Lucero, R. McDermott, M. Neeley, E. Weig, A. Cleland, and J. Martinis: *Science* **313** (2006) 1423.
- 27) B. Julsgaard, A. Kozhekin, and E. S. Polzik: *Nature* **413** (2001) 400.
- 28) L. Vaidman: *Phys. Rev. A* **49** (1994) 1473.
- 29) S. L. Braunstein and H. J. Kimble: *Phys. Rev. Lett.* **80** (1998) 869.
- 30) R. F. Werner: *Phys. Rev. A* **40** (1989) 4277.
- 31) N. Gisin, G. Ribordy, W. Tittel, and H. Zbinden: *Rev. Mod. Phys.* **74** (2002) 145.
- 32) J. J. Sakurai: *Advanced Quantum Mechanics* (Addison-Wesley, Reading, MA, 1967) Sect. 2.3.
- 33) L. Mandel and E. Wolf: *Optical Coherence and Quantum Optics* (Cambridge University Press, Cambridge, U.K., 1995) Sect. 10.6.
- 34) E. Bleuler and H. L. Bradt: *Phys. Rev.* **73** (1948) 1398.
- 35) C. S. Wu and I. Shaknov: *Phys. Rev.* **77** (1950) 136.
- 36) L. Mandel and E. Wolf: *Optical Coherence and Quantum Optics* (Cambridge University Press, Cambridge, U.K., 1995) Sect. 22.4.
- 37) S. E. Harris, M. K. Oshman, and R. L. Byer: *Phys. Rev. Lett.* **18** (1967) 732.
- 38) D. Magde and H. Mahr: *Phys. Rev. Lett.* **18** (1967) 905.
- 39) D. C. Burnham and D. L. Weinberg: *Phys. Rev. Lett.* **25** (1970) 84.
- 40) L. Mandel: *Rev. Mod. Phys.* **71** (1999) S274.
- 41) C. K. Hong, Z. Y. Ou, and L. Mandel: *Phys. Rev. Lett.* **59** (1987) 2044.
- 42) P. G. Kwiat, P. H. Eberhard, A. M. Steinberg, and R. Y. Chiao: *Phys. Rev. A* **49** (1994) 3209.
- 43) D. Bouwmeester, J. Pan, K. Mattle, M. Eibl, H. Weinfurter, and A. Zeilinger: *Nature* **390** (1997) 575.
- 44) A. G. White, D. F. V. James, P. H. Eberhard, and P. G. Kwiat: *Phys. Rev. Lett.* **83** (1999) 3103.
- 45) A. G. White, D. F. V. James, W. J. Munro, and P. G. Kwiat: *Phys. Rev. A* **65** (2001) 012301.
- 46) Y. Nambu, K. Usami, Y. Tsuda, K. Matsumoto, and K. Nakamura: *Phys. Rev. A* **66** (2002) 033816.
- 47) D. Branning, W. Grice, R. Erdmann, and I. A. Walmsley: *Phys. Rev. A* **62** (2000) 013814.
- 48) Y.-H. Kim, M. V. Chekhova, S. P. Kulik, M. H. Rubin, and Y. Shih: *Phys. Rev. A* **63** (2001) 062301.
- 49) M. Fiorentino, G. Messin, C. E. Kuklewicz, F. N. C. Wong, and J. H. Shapiro: *Phys. Rev. A* **69** (2004) 041801.
- 50) A. Yoshizawa and H. Tsuchida: *Electron. Lett.* **39** (2003) 621.
- 51) A. Yoshizawa and H. Tsuchida: *Jpn. J. Appl. Phys.* **44** (2005) L375.
- 52) B.-S. Shi and A. Tomita: *Phys. Rev. A* **69** (2004) 013803.
- 53) T. Kim, M. Fiorentino, and F. N. C. Wong: *Phys. Rev. A* **73** (2006) 012316.
- 54) Y.-H. Kim, S. P. Kulik, and Y. Shih: *Phys. Rev. A* **63** (2001) 060301.
- 55) S. Tanzilli, W. Tittel, H. De Riedmatten, H. Zbinden, P. Baldi, M. DeMicheli, D. B. Ostrowsky, and N. Gisin: *Eur. Phys. J. D* **18** (2002) 155.
- 56) M. Pelton, P. Marsden, D. Ljunggren, M. Tengner, A. Karlsson, A. Fragemann, C. Canalias, and F. Laurell: *Opt. Express* **12** (2004) 3573.

- 57) M. Fiorentino, C. E. Kuklewicz, and F. N. C. Wong: Opt. Express **13** (2005) 127.
- 58) B.-S. Shi and A. Tomita: New J. Phys. **8** (2006) 38.
- 59) C. H. Bennet and G. Brassard: Proc. IEEE Int. Conf. Computers, Systems, and Signal Processing, Bangalore, India, 1984, p. 176.
- 60) H. J. Kimble, M. Dagenais, and L. Mandel: Phys. Rev. Lett. **39** (1977) 691.
- 61) P. Michler, A. Imamoglu, M. D. Mason, P. J. Carson, G. F. Strouse, and S. K. Buratto: Nature **406** (2000) 968.
- 62) C. Santori, M. Pelton, G. Solomon, Y. Dale, and Y. Yamamoto: Phys. Rev. Lett. **86** (2001) 1502.
- 63) Z. Yuan, B. E. Kardynal, R. M. Stevenson, A. J. Shields, C. J. Lobo, K. Cooper, N. S. Beattie, D. A. Ritchie, and M. Pepper: Science **295** (2002) 102.
- 64) K. Takemoto, Y. Sakuma, S. Hirose, T. Usuki, N. Yokoyama, T. Miyazawa, M. Takatsu, and Y. Arakawa: Jpn. J. Appl. Phys. **43** (2004) L993.
- 65) D. Fattal, K. Inoue, J. Vuckovic, C. Santori, G. S. Solomon, and Y. Yamamoto: Phys. Rev. Lett. **92** (2004) 037903.
- 66) O. Benson, C. Santori, M. Pelton, and Y. Yamamoto: Phys. Rev. Lett. **84** (2000) 2513.
- 67) D. Gammon, E. S. Snow, B. V. Shanabrook, D. S. Katzer, and D. Park: Phys. Rev. Lett. **76** (1996) 3005.
- 68) R. J. Young, R. M. Stevenson, A. J. Shields, P. Atkinson, K. Cooper, D. A. Ritchie, K. M. Groom, A. I. Tartakovskii, and M. S. Skolnick: Phys. Rev. B **72** (2005) 113305.
- 69) C. Santori, D. Fattal, M. Pelton, G. S. Solomon, and Y. Yamamoto: Phys. Rev. B **66** (2002) 045308.
- 70) M. Inoue and E. Hanamura: J. Phys. Soc. Jpn. **41** (1976) 1273.
- 71) F. Henneberger and J. Voigt: Phys. Status Solidi B **76** (1976) 313.
- 72) F. Bechstedt and F. Henneberger: Phys. Status Solidi B **81** (1977) 211.
- 73) F. Henneberger, K. Henneberger, and J. Voigt: Phys. Status Solidi B **83** (1977) 439.
- 74) T. Itoh and T. Suzuki: J. Phys. Soc. Jpn. **45** (1978) 1939.
- 75) F. Henneberger, J. Voigt, and E. Gutsche: J. Lumin. **20** (1979) 221.
- 76) B. Hönerlage, R. Lévy, J. B. Grun, C. Klingshirn, and K. Bohnert: Phys. Rep. **124** (1985) 161.
- 77) M. Ueta, H. Kanzaki, K. Kobayashi, Y. Toyozawa, and E. Hanamura: *Excitonic Processes in Solids* (Springer-Verlag, Berlin, 1986) Chaps. 2 and 3, and references therein.
- 78) S. Savasta, G. Martino, and R. Girlanda: Solid State Commun. **111** (1999) 495.
- 79) H. Ajiki and H. Ishihara: Phys. Status Solidi C **3** (2006) 2440.
- 80) H. Ajiki and H. Ishihara: J. Phys. Soc. Jpn. **76** (2007) 053401.
- 81) M. Bamba and H. Ishihara: Phys. Status Solidi C **3** (2006) 3460.
- 82) M. Nakayama, T. Nishioka, S. Wakaiki, G. Oohata, K. Mizoguchi, D. Kim, and K. Edamatsu: Jpn. J. Appl. Phys. **46** (2007) L234.
- 83) M. Fiorentino, P. L. Voss, J. E. Sharping, and P. Kumar: IEEE Photonics Technol. Lett. **14** (2002) 983.
- 84) K. Inoue and K. Shimizu: Jpn. J. Appl. Phys. **43** (2004) 8048.
- 85) H. Takesue and K. Inoue: Phys. Rev. A **70** (2004) 031802.
- 86) H. Takesue and K. Inoue: Phys. Rev. A **72** (2005) 041804.
- 87) J. Sharping, J. Chen, X. Li, P. Kumar, and R. Windeler: Opt. Express **12** (2004) 3086.
- 88) J. Rarity, J. Fulconis, J. Dalgall, W. Wadsworth, and P. Russell: Opt. Express **13** (2005) 534.
- 89) J. Fulconis, O. Alibart, W. Wadsworth, P. Russell, and J. Rarity: Opt. Express **13** (2005) 7572.
- 90) O. Alibart, J. Fulconis, G. K. L. Wong, S. G. Murdoch, W. J. Wadsworth, and J. G. Rarity: New J. Phys. **8** (2006) 67.
- 91) J. Fan, A. Migdall, and L. J. Wang: Opt. Lett. **30** (2005) 3368.
- 92) H. Takesue and K. Inoue: Opt. Express **13** (2005) 7832.
- 93) H. Takesue: Opt. Express **14** (2006) 3453.
- 94) J. E. Sharping, K. F. Lee, M. A. Foster, A. C. Turner, B. S. Schmidt, M. Lipson, A. L. Gaeta, and P. Kumar: Opt. Express **14** (2006) 12388.
- 95) D. F. V. James, P. G. Kwiat, W. J. Munro, and A. G. White: Phys. Rev. A **64** (2001) 052312.
- 96) P. G. Kwiat, S. Barraza-Lopez, A. Stefanov, and N. Gisin: Nature **409** (2001) 1014.
- 97) C. H. Bennett, D. P. DiVincenzo, J. A. Smolin, and W. K. Wootters: Phys. Rev. A **54** (1996) 3824.
- 98) W. K. Wootters: Phys. Rev. Lett. **80** (1998) 2245.
- 99) V. Coffman, J. Kundu, and W. K. Wootters: Phys. Rev. A **61** (2000) 052306.
- 100) M. Horodecki, P. Horodecki, and R. Horodecki: Phys. Lett. A **223** (1996) 1.
- 101) M. Lewenstein, B. Kraus, J. I. Cirac, and P. Horodecki: Phys. Rev. A **62** (2000) 052310.
- 102) O. Guhne, P. Hyllus, D. Bruss, A. Ekert, M. Lewenstein, C. Macchiavello, and A. Sanpera: Phys. Rev. A **66** (2002) 062305.
- 103) M. Bourennane, M. Eibl, C. Kurtsiefer, S. Gaertner, H. Weinfurter, O. Guhne, P. Hyllus, D. Bruss, M. Lewenstein, and A. Sanpera: Phys. Rev. Lett. **92** (2004) 087902.
- 104) A. Furusawa, J. L. Sørensen, S. L. Braunstein, C. A. Fuchs, H. J. Kimble, and E. S. Polzik: Science **282** (1998) 706.
- 105) J. D. Franson: Phys. Rev. Lett. **62** (1989) 2205.
- 106) P. G. Kwiat, A. M. Steinberg, and R. Y. Chiao: Phys. Rev. A **47** (1993) R2472.
- 107) J. Jacobson, G. Björk, I. Chuang, and Y. Yamamoto: Phys. Rev. Lett. **74** (1995) 4835.
- 108) K. Edamatsu, R. Shimizu, and T. Itoh: Phys. Rev. Lett. **89** (2002) 213601.
- 109) M. W. Mitchel, J. S. Lundeen, and A. M. Steinberg: Nature **429** (2004) 161.
- 110) P. Walther, J.-W. Pan, M. Aspelmeyer, R. Ursin, S. Gasparoni, and A. Zeilinger: Nature **429** (2004) 158.
- 111) T. Nagata, R. Okamoto, J. L. O'Brien, K. Sasaki, and S. Takeuchi: Science **316** (2007) 726.
- 112) A. N. Boto, P. Kok, D. S. Abrams, S. L. Braunstein, C. P. Williams, and J. P. Dowling: Phys. Rev. Lett. **85** (2000) 2733.
- 113) D. Strekalov and J. Dowling: J. Mod. Opt. **49** (2002) 519.
- 114) R. Shimizu, K. Edamatsu, and T. Itoh: Phys. Rev. A **67** (2003) 041805.
- 115) R. Shimizu, K. Edamatsu, and T. Itoh: Phys. Rev. A **74** (2006) 013801.
- 116) M. D'Angelo, M. V. Chekhova, and Y. Shih: Phys. Rev. Lett. **87** (2001) 013602.
- 117) L. Neves, G. Lima, J. G. A. Gomez, C. H. Monken, C. Saavedra, and S. Padua: Phys. Rev. Lett. **94** (2005) 100501.
- 118) M. N. O'Sullivan-Hale, I. A. Khan, R. W. Boyd, and J. C. Howell: Phys. Rev. Lett. **94** (2005) 220501.
- 119) A. Mair, A. Vaziri, G. Weihs, and A. Zeilinger: Nature **412** (2001) 313.
- 120) J. T. Barreiro, N. K. Langford, N. A. Peters, and P. G. Kwiat: Phys. Rev. Lett. **95** (2005) 260501.
- 121) M. Barbieri, C. Cinelli, P. Mataloni, and F. D. Martini: Phys. Rev. A **72** (2005) 052110.
- 122) S. P. Walborn, P. H. Souto Ribeiro, L. Davidovich, F. Mintert, and A. Buchleitner: Nature **440** (2006) 1022.
- 123) C.-Y. Lu, X.-Q. Zhou, O. Guhne, W.-B. Gao, J. Zhang, Z.-S. Yuan, A. Goebel, T. Yang, and J.-W. Pan: Nat. Phys. **3** (2007) 91.
- 124) J.-W. Pan, D. Bouwmeester, H. Weinfurter, and A. Zeilinger: Phys. Rev. Lett. **80** (1998) 3891.
- 125) J.-W. Pan, S. Gasparoni, R. Ursin, G. Weihs, and A. Zeilinger: Nature **423** (2003) 417.
- 126) T. Yamamoto, M. Koashi, S. K. Ozdemir, and N. Imoto: Nature **421** (2003) 343.



**Keiichi Edamatsu** is a Professor of Research Institute of Electrical Communication, Tohoku University. He was born in Sendai, Miyagi in 1959. He received B.S., M.S., and D.S. degrees in Physics from Tohoku University. He was a Research Associate in Department of Applied Physics, Faculty of Engineering, Tohoku University, a Visiting Associate in Norman Bridge Laboratory of Physics, California Institute of Technology, and an Associate Professor in Division of Materials Physics, Graduate School of Engineering Science, Osaka University. He is a member of the Physical Society of Japan and Optical Society of America. His current research interests are solid-state photophysics, quantum optics, and quantum information/communication science.

## 6. Influence on entanglement

**Abstract:** Influence can be detected using Bell inequality.

**Keywords:** Bell inequality

## Quantum "spooky action at a distance" travels at least 10,000 times faster than light



Brian Dodson (<https://newatlas.com/author/brian-dodson/>) | March 11th, 2013

4 PICTURES



The speed of entanglement dynamics is at least 10,000 times faster than light according to Prof. Juan Yin and colleagues ( Photo: Shutterstock (<http://www.shutterstock.com/pic.mhtml?id=72688813>))

Quantum entanglement, one of the odder aspects of quantum theory, links the properties of particles even when they are separated by large distances. When a property of one of a pair of entangled particles is measured, the other "immediately" settles down into a state compatible with that measurement. So how fast is "immediately"? According to research by Prof. Juan Yin and colleagues at the University of Science and Technology of China in Shanghai, the *lower limit* to the speed associated with entanglement dynamics - or "spooky action at a distance" - is at least 10,000 times faster than light.

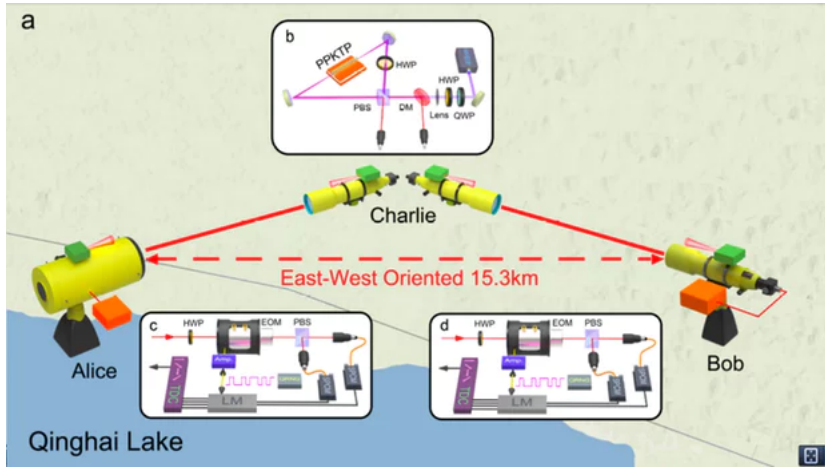
Despite playing a vital role in the development of quantum theory, Einstein felt philosophically at odds with its description of how the universe works. His famous quote that "God does not play dice" hints at his level of discomfort with the role of probability in quantum theory. He believed there exists another level of reality in which all of physics would be deterministic, and that quantum mechanics would turn out to be a description that emerges from the workings of that level - rather like a traffic jam emerges from the independent motions of a large number of cars.



Niels Bohr and Albert Einstein debating quantum theory in the mid 1920s

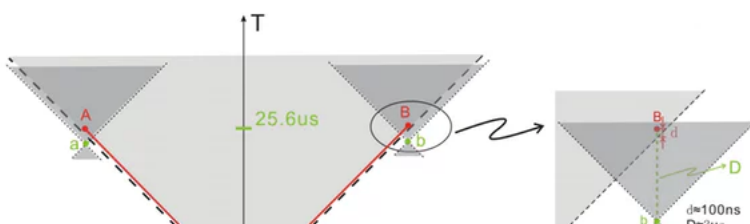
In 1935 Einstein and his coworkers discovered quantum entanglement lurking in the equations of quantum mechanics, and realized its utter strangeness. This lead to the EPR paradox introduced by Einstein, Podolsky and Rosen. The EPR paradox stated that the only ways of explaining the effects of quantum entanglement were to assume the universe is nonlocal, or that the true basis of physics is hidden (otherwise known as a hidden-variable theory). Nonlocality in this case means that events occurring to entangled objects are linked even when the events cannot communicate through spacetime, spacetime having the speed of light as a limiting velocity. Nonlocality is also known as spooky action at a distance (Einstein's phrase).

Einstein, as the primary prophet of relativity theory, was revolted by the notion of nonlocality, and hence regarded the EPR result as a demonstration that underlying quantum mechanics was a deterministic hidden-variable theory. On this occasion, however, Einstein was wrong.



So is the spooky action at a distance associated with entanglement actually instantaneous, or does it simply has a very large propagation speed? This seems a fair question to ask, and it's the challenge that was taken up by Prof. Yin's group. In their experiment, Alice and Bob (stars of many quantum adventures) were sent to two locations separated by 15.3 km (9.6 miles). Charlie, located equal distances from Alice and Bob, generated a pair of entangled photons, then sent one to Alice and one to Bob. The difference in the distance the photons traveled between Charlie and Alice and between Charlie and Bob was less than about 10 cm (4 in). All three of our participants have synchronized, highly accurate clocks. Charlie generates a pair of entangled photons, and records the time.

Both Alice and Bob have a mechanism for measuring the polarization of the incoming photons, but both mechanisms have randomly rotating polarization filters, so over time all polarization directions are measured, and at no time is there a correlation between Alice and Bob's polarization directions. When Alice detects a photon, she records the polarization and the time at which the measurement was made. When Bob measures his photon, he also records the polarization and the time of arrival.



Later the three get together to compare notes. Alice's and Bob's measurements were made at the same time, to within about 0.35 nanoseconds, and the decision on which way the polarization direction of their devices would point was decided about 3 microseconds before the photons arrived at the detectors. If Alice and Bob always measured the same polarization direction, the entanglement influence traveled 15.3 km in less than the possible difference in the measurement times they recorded (0.35 ns). If, on the other hand, the entanglement influence traveled more slowly, Alice and Bob would measure randomly different polarization directions.

Prof Yin's experiment, which was a bit more complicated in detail than the above simplification, observed no difference in polarization direction. The time it would take light to travel between Alice and Bob was about 50  $\mu$ s, while the action of the entanglement dynamics had to be less than 0.35 ns. The minimum speed of the entanglement influence is just the one divided by the other, or 144,500 times the speed of light. However, a number of factors go into the interpretation of the results, which reduce the lower limit of the speed of entanglement influence to about 10,000 times the speed of light.

Notice that this result does not eliminate the possibility that the influence of entanglement actually is instantaneous - it merely sets a limit saying how close the influence must be to infinitely fast. Another possibility that is gaining credence is that entanglement dynamics may operate external to time, or at least may ignore time as it ignores distance.

Niels Bohr, one of the prime developers of quantum theory, once said that those who are not shocked when they first encounter quantum theory cannot possibly have understood it. Eighty years later, this is still true, and applies even to those of us who first encountered quantum theory decades ago. It has been refined into an amazing tool, but we are woefully lacking in the ability to say how the world can work this way. Hope springs eternal.

Source: *Bounding the speed of 'spooky action at a distance'* - arXiv.org  
[\(PDF\)](http://arxiv.org/pdf/1303.0614v1.pdf)

# Undoing the effect of loss on quantum entanglement

Alexander E. Ulanov, Ilya A. Fedorov, Anastasia A. Pushkina, Yury V. Kurochkin, Timothy C. Ralph & A. I. Lvovsky

*Nature Photonics* 9, 764–768 (2015) | Download Citation

## Abstract

---

Entanglement distillation, the purpose of which is to probabilistically increase the strength and purity of quantum entanglement, is a primary element of many quantum communication and computation protocols. It is particularly necessary in quantum repeaters in order to counter the degradation of entanglement that inevitably occurs due to losses in communication lines. Here, we distil the Einstein–Podolsky–Rosen state of light, the workhorse of continuous-variable entanglement, using noiseless amplification. The advantage of our technique is that it permits recovering a macroscopic level of entanglement, however low the initial entanglement or however high the loss may be. Experimentally, we recover the original entanglement level after one of the Einstein–Podolsky–Rosen modes has experienced a loss factor of 20. The level of entanglement in our distilled state is higher than that achievable by direct transmission of any state through a similar loss channel. This is a key step towards realizing practical continuous-variable quantum communication protocols.

## References

---

1. Nielsen, M. & Chuang, I. *Quantum Computation and Quantum Information* (Cambridge Univ. Press, 2000).
2. Bennett, C. H. et al. Purification of noisy entanglement and faithful teleportation via noisy channels. *Phys. Rev. Lett.* **76**, 722–725 (1996).
3. Braunstein, S. L. & van Loock, P. Quantum information with continuous variables. *Rev. Mod. Phys.* **77**, 513–577 (2005).
4. Reid, M. D. Demonstration of the Einstein–Podolsky–Rosen paradox using nondegenerate parametric amplification. *Phys. Rev. A* **40**, 913–923 (1989).
5. Weedbrook, C. et al. Gaussian quantum information. *Rev. Mod. Phys.* **84**, 621–669 (2012).
6. Ralph, T. C. & Lund, A. P. Nondeterministic noiseless linear amplification of quantum systems. *AIP Conf. Proc.* **1110**, 155–160 (2009).
7. Takahashi, H. et al. Entanglement distillation from Gaussian input states. *Nature Photon.* **4**, 178–181 (2010).
8. Kurochkin, Y., Prasad, A. S. & Lvovsky, A. I. Distillation of the two-mode squeezed state. *Phys. Rev. Lett.* **112**, 070402 (2014).

9. Bartley, T. J. & Walmsley, I. A. Directly comparing entanglement-enhancing non-Gaussian operations. *New J. Phys.* **17**, 023038 (2015).
10. Chrzanowski, H. M. et al. Measurement-based noiseless linear amplification for quantum communication. *Nature Photon.* **8**, 333–338 (2014).
11. Andersen, U. L., Neergaard-Nielsen, J. S., van Loock, P. & Furusawa, A. Hybrid discrete- and continuous-variable quantum information. *Nature Phys.* **11**, 713–719 (2015).
12. Xiang, G. Y., Ralph, T. C., Lund, A. P., Walk, N. & Pryde, G. J. Heralded noiseless linear amplification and distillation of entanglement. *Nature Photon.* **4**, 316–319 (2010).
13. Ferreyrol, F. et al. Implementation of a nondeterministic optical noiseless amplifier. *Phys. Rev. Lett.* **104**, 123603 (2010).
14. Zavatta, A., Fiurasek, J. & Bellini, M. A high-fidelity noiseless amplifier for quantum light states. *Nature Photon.* **5**, 52–60 (2010).
15. Kosis, S., Xiang, G. Y., Ralph, T. C. & Pryde, G. J. Heralded noiseless amplification of a photon polarization qubit. *Nature Phys.* **9**, 23–28 (2013).
16. Pegg, D., Phillips, L. & Barnett, S. Optical state truncation by projection synthesis. *Phys. Rev. Lett.* **81**, 1604–1606 (1998).
17. Babichev, S. A., Ries, J. & Lvovsky, A. I. Quantum scissors: teleportation of single-mode optical states by means of a nonlocal single photon. *Europhys. Lett.* **64**, 1–7 (2003).
18. Lvovsky, A. I. & Mlynek, J. Quantum-optical catalysis: generating nonclassical states of light by means of linear optics. *Phys. Rev. Lett.* **88**, 250401 (2002).
19. Mičuda, M. et al. Noiseless loss suppression in quantum optical communication. *Phys. Rev. Lett.* **109**, 180503 (2012).

- 
20. Ourjoumtsev, A., Dantan, A., Tualle-Brouri, R. & Grangier, P. Increasing entanglement between Gaussian states by coherent photon subtraction. *Phys. Rev. Lett.* **98**, 030502 (2007).
- 
21. Kumar, R. *et al.* Versatile wideband balanced detector for quantum optical homodyne tomography. *Opt. Commun.* **285**, 5259–5267 (2012).
- 
22. Huisman, S. R. *et al.* Instant single-photon Fock state tomography. *Opt. Lett.* **34**, 2739–2741 (2009).
- 
23. Vidal, G. & Werner, R. F. Computable measure of entanglement. *Phys. Rev. A* **65**, 032314 (2002).
- 
24. Pan, J. W., Gasparoni, S., Ursin, R., Weihs, G. & Zeilinger, A. Experimental entanglement purification of arbitrary unknown states. *Nature* **423**, 417–422 (2003).
- 
25. Ralph, T. C. Quantum error correction of continuous-variable states against Gaussian noise. *Phys. Rev. A* **84**, 022339 (2011).
- 
26. Eisert, J., Browne, D. E., Scheel, S. & Plenio, M. B., Distillation of continuous-variable entanglement with optical means. *Ann. Phys. (Leipz.)* **311**, 431–458 (2004).
- 
27. Datta, A. *et al.* Compact continuous-variable entanglement distillation. *Phys. Rev. Lett.* **108**, 060502 (2012).
- 
28. Berry, D. W. & Lvovsky, A. I. Linear-optical processing cannot increase photon efficiency. *Phys. Rev. Lett.* **105**, 203601 (2010).
- 
29. Berry, D. W. & Lvovsky, A. I. Preservation of loss in linear-optical processing. *Phys. Rev. A* **84**, 042304 (2011).
- 

## Acknowledgements

The authors thank G. Adesso for discussions and the Russian Quantum Center for support. A.L. is supported by the National Science and Engineering Research Council of Canada and is a fellow of the Canadian Institute for Advanced Research. T.C.R.'s research is funded by the Australian Research Council Centre of Excellence for Quantum Computation and Communication Technology (project no. CE110001027).

## Author information

---

### Alexander E. Ulanov & Ilya A. Fedorov

These authors contributed equally to this work

### Affiliations

Russian Quantum Center, 100 Novaya St., Skolkovo, Moscow 143025, Russia

Alexander E. Ulanov, Ilya A. Fedorov, Anastasia A. Pushkina, Yury V. Kurochkin & A. I. Lvovsky

Institute of Fundamental and Frontier Sciences, University of Electronic Science and Technology, Chengdu, Sichuan 610054, China

Alexander E. Ulanov & A. I. Lvovsky

Moscow Institute of Physics and Technology, Institutsky Lane 9, Dolgoprudny 141700, Russia  
Alexander E. Ulanov & Anastasia A. Pushkina

P.N. Lebedev Physics Institute, Leninskiy Prospect 53, Moscow 119991, Russia  
Ilya A. Fedorov, Anastasia A. Pushkina & A. I. Lvovsky

Centre for Quantum Computation and Communication Technology, School of Mathematics and Physics, University of Queensland, Brisbane, Queensland 4072, Australia

Timothy C. Ralph

Institute for Quantum Science and Technology, University of Calgary, Calgary Alberta T2N 1N4, Canada

A. I. Lvovsky

A. I. Lvovsky

## Further reading

---

Avoiding disentanglement of multipartite entangled optical beams with a correlated noisy channel - <https://doi.org/10.1038/srep44475>

Xiaowei Deng, Caixing Tian [...] Changde Xie  
Scientific Reports (2017)

---

Surpassing the no-cloning limit with a heralded hybrid linear amplifier for coherent states  
- <https://doi.org/10.1038/ncomms13222>

Jing Yan Haw, Jie Zhao [...] Ping Koy Lam  
Nature Communications (2016)

---

Efficient entanglement distillation without quantum memory -  
<https://doi.org/10.1038/ncomms11720>

Daniela Abdelkhalek, Mareike Syllwasschy [...] Roman Schnabel  
Nature Communications (2016)

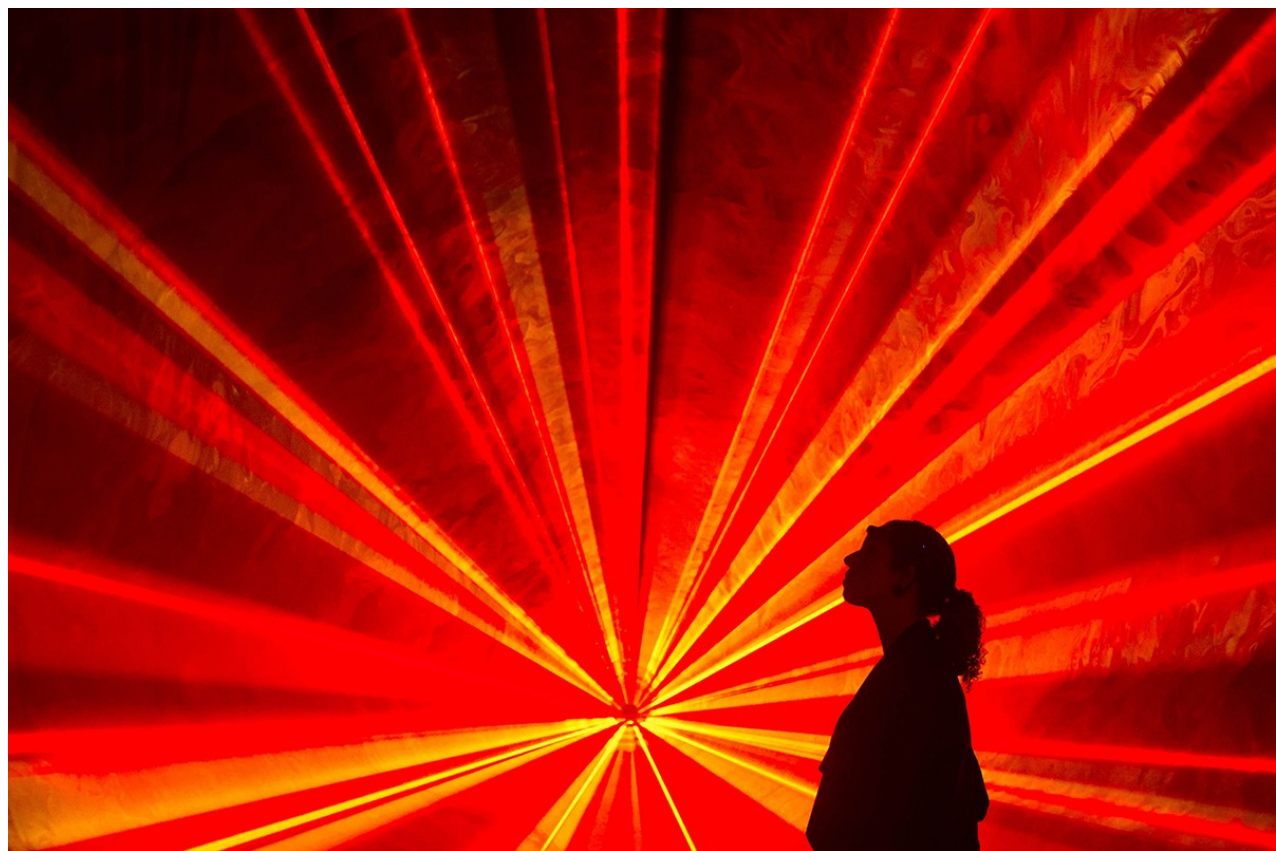
---

Loss-tolerant state engineering for quantum-enhanced metrology via the reverse Hong-Ou-Mandel effect - <https://doi.org/10.1038/ncomms11925>

Alexander E. Ulanov, Ilya A. Fedorov [...] A. I. Lvovsky  
Nature Communications (2016)

DAILY NEWS 19 May 2017

# A classic quantum test could reveal the limits of the human mind



A quantum test could tell us what minds are made of  
Dominic Lipinski/PA

By Anil Ananthaswamy

consciousness. If such an experiment showed deviations from quantum mechanics, it could provide the first hints that our minds are potentially immaterial.

Spooky action at a distance was Einstein's phrase for a quantum effect called entanglement. If two particles are entangled, then measuring the state of one particle seems to instantly influence the state of the other, even if they are light years apart.

But any signal passing between them would have to travel faster than the speed of light, breaking the cosmic speed limit. To Einstein, this implied that quantum theory was incomplete, and that there was a deeper theory that could explain the particles' behaviour without resorting to weird instantaneous influence. Some physicists have been trying to find this deeper theory ever since.

## **Demonstrating Descartes**

In 1964, physicist John Bell paved the way for testing whether the particles do in fact influence each other. He devised an experiment that involves creating a pair of entangled particles and sending one towards location A and the other to location B. At each point, there is a device that measures, say, the spin of the particle.

The setting on the device – for example, whether to measure the particle's spin in the +45 or -45 degree direction – is chosen using random number generators, and in such a way that it's impossible for A to know of B's setting and vice-versa at the time of the measurement.

The measurements are done for numerous entangled pairs. If quantum physics is correct and there is indeed spooky action at a distance, then the results of these measurements would be correlated to a far greater extent than if Einstein was correct. All such experiments so far have supported quantum physics.

However, some physicists have argued that even the random number generators may not be truly random. They could be governed by some underlying physics that we don't yet understand, and this so-called "super-determinism" could explain the observed correlations.

Now, Lucien Hardy at the Perimeter Institute in Canada suggests that the measurements at A and B can be controlled by something that could potentially be separate from the material world: the human mind.

"[French philosopher Rene] Descartes put forth this mind-matter duality, [where] the mind is outside of regular physics and intervenes on the physical world," says Hardy.

## **Question of free will**

To test this idea, Hardy proposed an experiment in which A and B are set 100 kilometres apart.

If the amount of correlation between these measurements doesn't tally with previous Bell tests, it implies a violation of quantum theory, hinting that the measurements at A and B are being controlled by processes outside the purview of standard physics.

"[If] you only saw a violation of quantum theory when you had systems that might be regarded as conscious, humans or other animals, that would certainly be exciting. I can't imagine a more striking experimental result in physics than that," Hardy says. "We'd want to debate as to what that meant."

Such a finding would stir up debate about the existence of free will. It could be that even if physics dictated the material world, the human mind not being made of that same matter would mean that we could overcome physics with free will. "It wouldn't settle the question, but it would certainly have a strong bearing on the issue of free will," says Hardy.

Nicolas Gisin at the University of Geneva in Switzerland thinks Hardy's proposal makes "plenty of sense", but he's sceptical of using unstructured EEG signals to switch settings on devices. That's akin to using the brain as a random number generator, says Gisin. He would rather see an experiment where the conscious intent of humans is used to perform the switching – but that would be experimentally more challenging.

Either way, he wants to see the experiment done. "There is an enormous probability that nothing special will happen, and that quantum physics will not change," says Gisin. "But if someone does the experiment and gets a surprising result, the reward is enormous. It would be the first time we as scientists can put our hands on this mind-body or problem of consciousness."

**Journal reference:** *arXiv*, DOI: 1705.04620v1

## 7. Death and revival of entanglement

**Abstract:** Any interaction that leads to the entangled system to get entangled with yet more degrees of freedom.

**Keywords:** Degree of freedom

## What processes cause the collapse of a wavefunction and break entanglement?

This question states that measuring the spin of an entangled particle causes the collapse of the wavefunction and thus the entanglement is broken.

Then this question states that we don't know what exactly is the cause for the collapse of wavefunctions.

However, what processes are known to collapse the wavefunction, and specifically break entanglement?

So measuring the spin collapses the wavefunction. What else does?

- Chemical processes?
- Presence in magnetic field without a screen (similar to Stern-Gerlach experiment)?
- Irradiation of some form?
- Heating?

### EDIT

Given comments that the collapse of the wavefunction is still not understood, I'd like to emphasize experimental observations.

Also, given that the collapse of a wavefunction may or may not be an artificial construct, can we focus on what processes have been observed to destroy entanglement?

(From what I understand of current theory, entanglement is only broken by the resolution/collapse of the wavefunction, thus asking "what has been observed to collapse the wavefunction" and "what has been observed to break entanglement" should be questions with the same answers.)

[quantum-mechanics](#) [wavefunction](#) [quantum-entanglement](#) [measurement-problem](#) [wavefunction-collapse](#)

2 Any interaction that leads to the entangled system to get entangled with yet more degrees of freedom. Then if you only consider the original degrees of freedom, the system has to be described using a density matrix, it then looks like as if the wavefunction has collapsed breaking the original entanglements. – [Count Iblis](#) Mar 20 '17 at 22:10

This is not a question about entanglement; you could ask exactly the same questions about an unentangled state. – [WillO](#) Mar 20 '17 at 22:12

3 [Interpretations of quantum mechanics](#) disagree whether collapse of the wave function is a physical process or an artifact of theoretical description. If it is an artifact nothing can "cause" it because it is only a manner of speaking. What is known is what can "prepare" a system to undergo collapse (whatever it is or isn't), any interaction with environment that causes decoherence. "Environment" can be any system with many degrees of freedom, i.e. "classical". – [Conifold](#) Mar 20 '17 at 23:15

2 As the [Wikipedia article on the Measurement Problem](#) makes clear, this is an open problem in quantum mechanics - and indeed this question is pretty much equivalent to the measurement problem. – [Emilio Pisanty](#) Mar 26 '17 at 20:55

## 3 Answers

Since you already talk about Stern-Gerlach, I suspect that the focus of your question is more about at which point in existing experimental techniques the collapse occurs, and not about learning existing techniques. In Stern-Gerlach that would be the deflection, not the screen, because this is where the spin value gets to be determined. If I got the question right, then the general answer is "at the point in the experiment where the studied property gets a specific value and superposition ends".

Also: Measuring is interacting with the system under study. There is nothing special putting measurement apart from any other physical process. This means that any interaction of the original system with anything else in the universe will break the wavefunction, preparing a new state.

I think the most concise (and entertaining) answer was the first comment ([source](#)) in the first of your links:

Basically, for observations to happen, there has to be an interaction between particles, or as the post put it less/more(?) eloquently, whenever a physicist says "observe", mentally replace it with "hit with sh\*t".

# Entanglement, symmetry breaking and collapse: correspondences between quantum and self-organizing dynamics

*Francis Heylighen*

Center Leo Apostel,  
Vrije Universiteit Brussel, Pleinlaan 2,  
1050 Brussel, Belgium  
fheylich@vub.ac.be

**Abstract:** Quantum phenomena are notoriously difficult to grasp. The present paper first reviews the most important quantum concepts in a non-technical matter: superposition, uncertainty, collapse of the wave function, entanglement and non-locality. It then tries to clarify these concepts by examining their analogues in complex, self-organizing systems. These include bifurcations, attractors, emergent constraints, order parameters and non-local correlations. They are illustrated with concrete examples that include Rayleigh-Bénard convection, social self-organization and Gestalt perception of ambiguous figures. In both cases, quantum and self-organizing, the core process appears to be a symmetry breaking that irreversibly and unpredictably “collapses” an ambiguous state into one of a number of initially equivalent “eigenstates” or “attractors”. Some speculations are proposed about the non-linear amplification of quantum fluctuations of the vacuum being ultimately responsible for such symmetry breaking.

**Keywords:** quantum processes, self-organization, entanglement, collapse of the wave function, symmetry breaking, bifurcation

## 1. Introduction

Quantum mechanics is a theory notorious for the fact that the phenomena it describes are highly counterintuitive. What makes it particularly difficult for us to imagine what happens is that these phenomena belong to a microworld that we can never hope to perceive with our senses. Moreover, their description uses a highly abstract mathematical formalism (operators in Hilbert spaces) that has no clear counterpart in other, more intuitive theories of the physical world. Nevertheless, we may be able to understand these quantum phenomena better if we could find analogues of them in the

macroworld in which we live. One recently developed example of this approach is quantum cognition (Aerts, 2009; Bruza, Wang, & Busemeyer, 2015): establishing a correspondence between cognitive processes in our brain and quantum mechanisms. But the brain is an extremely complex system of which we as yet do not understand too much. Therefore, it is not yet clear in how far the apparent similarities between cognitive and quantum structures will help us to elucidate either the one or the other.

The present article proposes to examine the analogies between quantum systems and systems that are still complex, but not as complex as the brain, and to which we have a more direct access, both empirically and theoretically. I am referring to what is known as complex systems, complex adaptive systems, or self-organizing systems (Ball, 2012; Heylighen, 2009). These are systems that consist of many interacting components, typically modeled as “agents”, that are distributed in space. Agents can be molecules, people, insects, or neurons. Local interactions between agents commonly give rise to globally coordinated behavior, as exemplified by the movement of birds in a swarm, ants in a colony, or fish in a shoal. Such emergence of order or coherence is called *self-organization* (Ashby, 1962; Haken, 1977; Heylighen, 2001). This is a non-linear process that tends to amplify tiny fluctuations into macroscopic differences. As a result, such complex processes are typically unpredictable and difficult to control—a property they share with quantum systems. But, as I will elaborate in the remainder of this paper, the similarities go much deeper.

I will first briefly review the most characteristic and poorly understood concepts of quantum mechanics, such as non-locality, entanglement and collapse of the wave function, in a non-technical manner. I will then review related concepts in complex systems theory. Using examples, I will try to establish a correspondence between each of the core quantum concepts and its counterpart in complexity. Finally, I will make some suggestions about how this correspondence may help us to understand the counterintuitive aspects of quantum theory.

## 2. Core quantum concepts

Probably the most fundamental difference between a quantum theory and a classical theory of some physical system is that the quantum model obeys the superposition principle (Dirac, 1981; Heylighen, 1990). This means that for any two states  $a$  and  $b$  of the system that can be distinguished there exists some third state  $a + b$ , called a *superposition* of  $a$  and  $b$ . This superposition state has properties that somehow combine the properties of  $a$  with those of  $b$ . In other words, this state is not in between  $a$  and  $b$ , it is somehow both  $a$  and  $b$ . For example, suppose that the possible states of your system are  $|black\rangle$  and  $|white\rangle$ . Classically, you might expect that there exists a separate, “in-between” state, such as  $|grey\rangle$ . But in a quantum theory, there would always be a superposition state  $|black\rangle + |white\rangle$ , which would sometimes appear as black and sometimes as white, but never as grey.

The name “superposition” comes from the representation of quantum states as wave functions. Here, quantum systems are viewed as waves that spread out over space, with different intensities (ultimately determining the probabilities of finding the system) in different positions. Superposing two waves means that you add the intensities for each of the positions to get the total

intensity of the combined wave for that position. If one wave would have a non-zero intensity only in region  $a$  (meaning that the probability to find it outside that region is nil) and the other in region  $b$ , then the superposed wave would be present in both  $a$  and  $b$ , but nowhere else—no matter how far apart these two regions are. This means that the particle is in a sense distributed across these two regions, somehow being in both at the same time.

This operation of addition of wave functions is straightforwardly generalized to the addition of vectors, which form an equivalent mathematical representation of quantum states. The superposition principle can then be expressed by the fact that the set of all states of a quantum system defines a particular type of vector space, called “Hilbert space”. This means that any linear combination of states (vectors) defines another possible state (vector) in the state space of the system. Still, we do not need the Hilbert space formalism to understand the core concept of superposition: for any two distinct states of the system there exists at least one other state that is neither the one, nor the other, but that somehow has the properties of both. This ambivalence creates an intrinsic indeterminacy at the heart of any quantum theory.

But how can something be both black and white at the same time? Ultimately, the ambiguity is resolved by the process of observation. When an experiment is performed to ascertain what the color of the system is, the result can only be one of the colors. That means that the superposition state black + white will give either the result “white” or the result “black”. However, we cannot predict beforehand which result it will be. This brings us to another core feature of the quantum theory: *uncertainty* or *indeterminacy*. A state such that the property to be observed has a determinate value is called an “eigenstate” of the observable property. If the system is not in a superposition state, but in such an eigenstate (e.g. it is in the state black), then the probability of the result black will be 1. However, since there are many more superpositions than eigenstates, in the most general case, a quantum system will be in a superposition state for the particular feature we want to determine. Therefore, we cannot say which result the observation will produce. Given the specific form of the vector or wave function, we can merely calculate the probabilities of the different outcomes.

On the other hand, if an observation is repeated, the result will not change: black remains black. This is explained in the quantum formalism by the *projection postulate*. The vector black + white is orthogonal neither to the black vector nor to the white vector. When the observation is made, it is somehow projected onto one of its orthogonal component vectors, the eigenstates white or black. Once projected onto, say, black, the state has effectively become identical to the one it was projected upon (because a state only depends on the direction of the vector, not its length). So now it is 100% black, without ambiguity.

This process is traditionally called the *collapse of the wave function*. Suppose that the wave function (which is a representation of a state equivalent to the vector representation) is spread out over two separate regions, one corresponding to black, one to white. Performing the operation of observation forces the wave to choose one of the two possible outcomes, white or black. That means that after the observation it is fully concentrated in one region, say black, while it has vanished from the other region. The wave has “collapsed” from a wider region, covering both black and white, to a smaller one, covering only black.

This “projection” or “collapse” is presented in quantum mechanics as an abstract mathematical operation, not as a concrete physical process. Therefore, the collapse is assumed to happen *instantaneously*, even though in practice the experiment needed to make an observation will of course need some time to take place. Yet, the quantum theory says nothing about what is supposed to happen during that time; it only describes the state before (superposition state) and after (projected state) that operation. Thus, the collapse of the wave function is another highly mysterious and counterintuitive quantum property: it is as if the wave “jumps” instantaneously from one region to another one without passing through any intermediate regions. This will lead us to another bizarre quantum feature: non-locality.

*Entanglement* is a quantum property that follows straight from superposition (Horodecki, Horodecki, Horodecki, & Horodecki, 2009). Assume that you have two quantum systems (typically particles),  $x$  and  $y$ . Each of them can be in a particular state, e.g.  $|x\text{-black}\rangle$ , and  $|y\text{-white}\rangle$ . The state of the compound system is then  $|x\text{-black}\rangle|y\text{-white}\rangle$ . But this compound state, describing the system consisting of both  $x$  and  $y$ , also obeys the superposition principle. Therefore, the compound system can be in the superposition state:

$$|x\text{-black}\rangle|y\text{-white}\rangle + |x\text{-white}\rangle|y\text{-black}\rangle.$$

This means that if you observe  $x$  and find the result black, the compound state will have collapsed to the first part of the sum:  $|x\text{-black}\rangle|y\text{-white}\rangle$ . Therefore, any further observation of  $y$  will necessarily produce the result white. However, if the first observation of  $x$  had found white as result, the collapse of the wave function would have forced the observation of  $y$  to produce black. In this case, we say that the components  $x$  and  $y$  are *entangled*, because the observation of the one cannot be separated from the observation of the other. Before the observation, both  $x$  and  $y$  could have produced the result white or black. But once a result for one of the components is determined, the one for the other is determined as well. The results mutually determine each other, and cannot be disentangled.

A final quantum concept we need to introduce is *non-locality* (Wiseman, 2006). Suppose that components  $x$  and  $y$  are separated by a distance in space. For example,  $x$  might reside in Brussels, and  $y$  in Tokyo. Assume that both systems are entangled, i.e. their compound state is a superposition of two states each characterized by different individual values (black, white) for each of the components. An observation of  $x$  in Brussels will determine the value of its property (say, black). But because the collapse of the wave function is instantaneous, this means that at the same time the value of  $y$  in Tokyo will become determined (in this case to white). The outcomes of the two experiments are correlated: whenever the one results in black, the other one will necessarily result in white. The distance between the two components of the system is completely irrelevant to this process. Therefore, it does not depend on their locality: the collapse is non-local. It is as if quantum observation processes ignore distance or space. The state of the compound system is simply smeared out or distributed across different locations, no matter how far or how near the locations are from each other.

At first sight, non-locality contradicts the basic principle of relativity theory, which says that signals cannot travel faster than the speed of light. The instantaneity of the collapse implies that the

state of  $y$  is reduced to black the very moment the one of  $x$  is determined to be white. This leaves no time for a signal to travel from Brussels to Tokyo that would “tell” the particle  $y$  that it should collapse to its black state. Yet, numerous experiments with entangled systems that are observed simultaneously have confirmed that such a collapsed outcome indeed results before any signal traveling with a speed not faster than light could have reached the second component (Aspect, 2007). Does quantum theory then prove relativity theory to be wrong? Not at all, because whatever is transmitted between the two components is not a “signal”, in the sense that it cannot be used to transfer information from the one location to the other. This has been proven mathematically using different versions of the quantum formalism (Eberhard & Ross, 1989; Ghirardi, Grassi, Rimini, & Weber, 1988).

We can understand this result more intuitively by noting that an observer in Tokyo cannot determine whether the component on that side has collapsed because of some measurement in Brussels. When the Tokyo observer measures the property of the component, s/he will find “black” with 50% probability, no matter whether a previous measurement was or was not performed in Brussels. Finding “black” in Tokyo may mean that the Brussels observer found “white” and thus collapsed the Tokyo component to its “black” state just before the Tokyo experiment. But it may equally mean that the Tokyo observer collapsed the system to its “black” state in Tokyo, before any Brussels experiment took place. The local experiment in Tokyo or Brussels cannot ascertain whether an experiment in the other location has or has not taken place. Only after we bring together the results of several such experiments in both locations will we be able to infer from the correlations between their results that the components were entangled. And that bringing together still requires the transmission of information with a velocity not higher than the speed of light, meaning that relativity theory is not contradicted...

In summary, what we need to remember from quantum theory is that systems can be in some indeterminate *superposition* state, which is neither one thing or its opposite, nor something in between, but in a sense both things at the same time. Moreover, the result from observing such a superposition state is fundamentally *uncertain*, and can only be predicted statistically. After the observation, the superposition state “collapses” to the eigenstate that corresponds to the value measured, and remains in that state when the observation is repeated. This *collapse* is instantaneous, even when the components of the system observed are arbitrarily far apart. The components of a system in a superposition state are said to be *entangled*. The collapse means that entangled components instantaneously influence each other’s state, independently of the distance between them, a feature called *non-locality*.

### 3. Core concepts of complex dynamics

The theory of complex systems is as yet much less developed than quantum mechanics. Thus, its concepts are more diverse, less clearly defined and less integrated into a coherent theory. There is in particular no overall formalism, like the one defined for quantum mechanics by the axioms formulated by von Neumann. Therefore, I will here merely present a selection of what I consider to

be some of its more fundamental ideas, with a focus on those that seem most similar to quantum concepts.

Complex systems consist of many components that undergo many, non-trivial interactions, so that they are impossible to separate or reduce to independent aspects or properties (Heylighen, 2009; Heylighen, Cilliers, & Gershenson, 2007). Therefore, it is in general not possible for an observer to collect complete information about the state of the system. Statistical mechanics has developed dependable methods to model systems, such as gases, that have many components but that lack such intricate, non-linear interactions and dependencies. Since it is impossible to measure the position and velocity of each individual gas molecule, we cannot determine the full “microstate” of the system. However, since a gas is statistically homogeneous, a large array of such molecules can be accurately described by macroscopic properties such as volume, temperature and pressure, together determining the “macrostate” of the system. A macrostate is simply a class of microstates that are considered equivalent, in the sense that e.g. the average velocity of the molecules in each of the microstates composing a macrostate is the same. Thus, a macrostate may not provide full information about the details of the system, but it is not ambiguous, in the sense that it can normally be clearly established in which of two macrostates the system resides. Macrostates do not overlap, and a particular microstate belongs to either one or another of the distinguishable macrostate. Therefore, there is no equivalent of superpositions for macrostates.

This assumption of independence of observable states can no longer be made for complex systems. This is because we not only cannot observe the microscopic properties of each component; we also cannot determine their macroscopic interactions. This is a general feature of non-linear systems that is technically known as “sensitive dependence on initial conditions”, and more informally as “the butterfly effect” (Hilborn, 2004). Non-linearity means that the effects of interactions are not proportional to their causes. This may result in an amplification of effects such that microscopic differences too small to be observed eventually produce huge, macroscopic differences. Thus, we may have two states of the system that are macroscopically indistinguishable initially (they belong to the same “macrostate”), but that still produce macroscopically distinct result after some observation is performed. For example, a state with or without the movement of a butterfly wing may result in either a hurricane or no hurricane.

Another example would be the prediction of elections through polls: when the differences in percentage of vote intentions are small enough, it becomes impossible to predict which of the candidates will get a majority. This is not just because the polls do not collect enough data: the collection and publishing of the data itself may affect the result, which is why in most countries it is forbidden to publish poll results just before the election. Even without this “observer effect”, the non-linear interactions between voters influencing each other’s preferences so that they change the intentions they expressed during the poll can magnify tiny fluctuations into swings large enough to carry the majority.

In such cases, we can say that the properties of the macrostate (as determined by polls) are indeterminate: a further observation (e.g. an actual election) can produce one of several results (e.g. either candidate *a* or candidate *b* is elected). Initially, the system is in the equivalent of a *superposition* state: *a* + *b*. After the observation, the state has collapsed to one of the possible

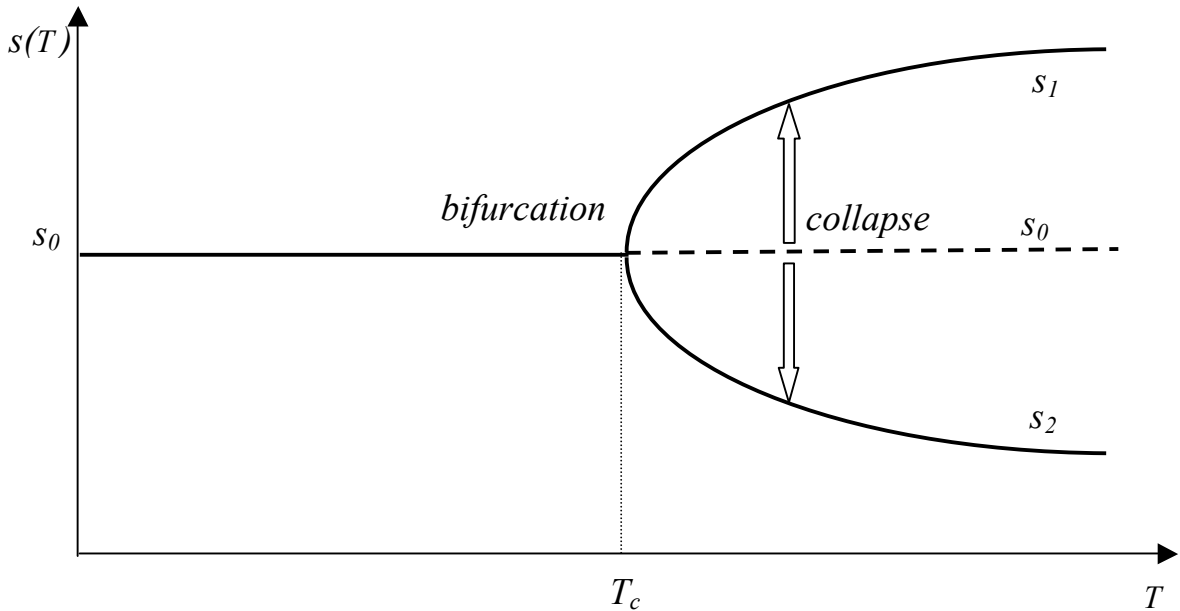


**Fig. 1:** the equilibrium state  $s$  of a system as a function of an order parameter  $T$ . As  $T$  reaches the critical value  $T_c$ , the number of possible states bifurcates into  $s_1$  and  $s_2$ , while the original state  $s_0$  becomes unstable. This instability implies that beyond the bifurcation point,  $s_0$  must “collapse” into either  $s_1$  or  $s_2$ , thus breaking the symmetry between the options.

outcomes: *a* or *b*. Before the observation, we were *uncertain* about the result, and able at most to estimate a probability for each of the possible outcomes. But once the result was produced, it is definitive or irreversible.

This intuitive illustration can be made more precise using the mathematical notion of a *bifurcation* (Nicolis & Prigogine, 1977). Assume that you have a dynamic system governed by a differential or difference equation that describes the state  $s$  as a function of time  $t$ :  $s(t)$ . The equilibrium solutions of the equation are the ones for which  $s$  is constant:  $s(t) = s_0$ . Assume that these solutions depend on a parameter  $T$  (commonly called “order parameter”) that characterizes the dynamics. In typical non-linear systems, like the Bénard convection that we will discuss further, there is a single solution for low values of  $T$  (see Fig. 1). However, as the value of  $T$  increases, you reach a point where the equation has two stable solutions:  $s_1$  and  $s_2$ . The point in parameter space where the number of solutions changes is called the bifurcation point. The equilibrium solution  $s_0$  still exists beyond that point but it is no longer stable: the tiniest perturbation or fluctuation away from the state  $s_0$  makes the system shift immediately to one of the stable solutions,  $s_1$  or  $s_2$ , where it then remains.

This shift from the unstable equilibrium  $s_0$  to one of the stable states  $s_1$  or  $s_2$  can be seen as a “collapse” of the superposition state  $s_1 + s_2$ , “projecting” it to one of its component states  $s_1$  or  $s_2$ . The increase of the order parameter  $T$  beyond the bifurcation point plays the role of an observation, which forces the system to make a choice between one of the “eigenstates” of this observation. Assuming that  $s_1$  and  $s_2$  are equivalent solutions, this choice for the one over the other can be seen as a *symmetry breaking* (Castellani, 2003). It is as if the system when arriving at the bifurcation is forced to decide whether to go left ( $s_1$ ) or right ( $s_2$ ), since it cannot continue straight on its  $s_0$  course (which would be the only way to maintain the left-right symmetry). Like in the quantum case, this process is

both unpredictable in its result and irreversible, in the sense that once the choice for one of the states  $s_1$  or  $s_2$  is made, the system remains in that state for any similar “observation”.

More generally, a dynamic system is characterized by a number of *attractors*: regions in its state space that it can enter but not leave, and that do not contain smaller such regions (Heylighen, 2001; Milnor, 2006). Stable states like  $s_1$  and  $s_2$  are zero-dimensional, point attractors. Limit cycles, which commonly occur in non-linear, far-from-equilibrium systems, are one-dimensional attractors. But attractors can have any number of dimensions, including fractal. An attractor  $A$  is surrounded by its *basin of attraction*  $B(A)$ . This consists of all the states in the state space whose trajectory ends up in the attractor  $A$ . The boundaries between basins correspond to bifurcation points (such as the unstable state  $s_0$ ): a system on such a boundary has to make a choice about which of the two adjacent basins  $B(A_1)$  or  $B(A_2)$ , and therefore attractors  $A_1$  or  $A_2$ , it will enter.

A system that has reached an attractor is *constrained* in its further evolution, because its trajectory by definition cannot leave that attractor and move to a different attractor or basin. It has lost part of its freedom. If the state space has dimension  $n$ , and the attractor dimension  $k < n$ , then the system has lost  $n - k$  of its degrees of freedom. If the system consists of different components, this means that the components in general can no longer move independently of each other. For example, assume that the system consists of two components, each with  $m$  degrees of freedom. Then the system as a whole has  $n = 2 \times m$  degrees of freedom. After reaching the attractor, it has  $k < 2 \times m$  degrees of freedom, implying that its components can no longer fully use their own  $m$  degrees of freedom: the movement of one component through its state space will constrain the movement of the other: their movements can no longer be separated.

As an example, consider two billiard balls, each able to move on a 2-dimensional billiard table. The two-ball system thus has  $2 \times 2 = 4$  degrees of freedom. Assume that the balls are magnetic, so that they attract each other. After some independent movements across the table, they are likely to come so close together that they can no longer resist the attractive force and end up sticking together. This produces a two-ball assembly shaped like a figure 8. This stuck together configuration is an attractor for the system, as the balls no longer can separate and thus recover their independent movement. This shape-8 configuration can still move as a whole on the billiard table: 2 degrees of freedom. Moreover, it can still rotate around its axis: 1 degree of freedom. However, the balls have lost the freedom to vary the distance between them. Thus, the system now has only 3 degrees of freedom. Using quantum terminology, we could say that the balls have become entangled. Whenever we observe the position of one of the balls, we can deduce that the other ball is at a fixed distance of that position. If we were uncertain about the position of the two balls, a measurement of a single ball not only reduces our uncertainty about that ball, but also about the other one.

Thus, quantum entanglement corresponds to the complex systems phenomenon of a global constraint. This constraint on the whole forces the components of the system to behave in a coordinated manner (*downward causation*), while defining an *emergent property* (in this case the angle of rotation). Such an emergent property characterizes the way the components cohere or depend on each other, while being undefined at the level of the separate components. Therefore, it cannot be reduced to the properties of these components (Bedau, 2002; Heylighen et al., 2007).

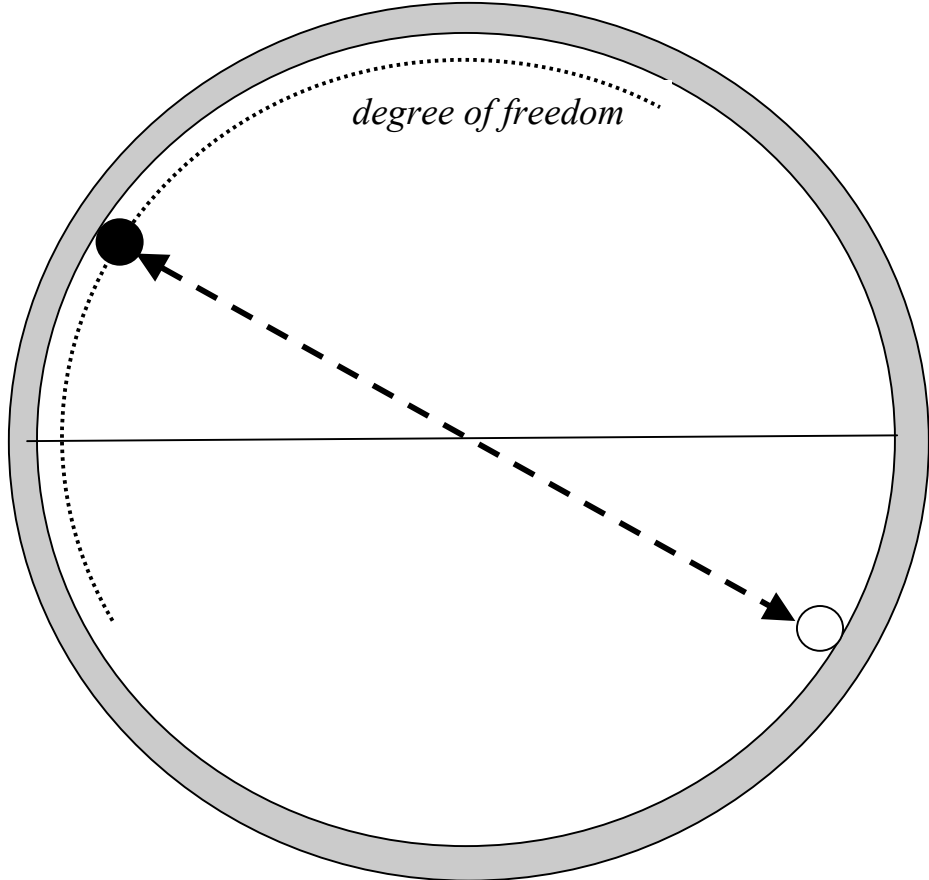


**Fig. 2:** a system consisting of two mutually repelling billiard balls on a round table. The system has one degree of freedom: the position of one of the balls along the perimeter (the other ball is always on the opposite side). Observing one ball to be in the upper or left half of the circle “collapses” the state of the second ball to the lower or right half.

This example does not yet illustrate non-locality, as the balls remain in local contact. Let us then imagine two billiard balls that repel each other, e.g. because they have the same electrostatic charge. Let us assume for simplicity that the billiard table has a round, circular shape. When the two balls are dropped at random positions on the table, the repulsive force will make them move away as far as possible from each other, until they reach the circular border of the table, where they will remain at opposite ends (Fig. 2). The balls can still move along the circle, but always together so that the distance between them remains maximal. That means that they are “entangled” in such a way that together they have only a single degree of freedom left: their position along the circle. An observer who would examine the upper half ( $\uparrow$ ) of the circle, and find ball  $x$  there would be able to deduce that another observer examining the lower half ( $\downarrow$ ) at exactly the same instant would find the ball  $y$  there. Vice versa, if the first observer would find  $y$  in the upper section, it would follow that the second observer would find  $x$  in the lower section.

We could describe this situation as a superposition of the eigenstates of this observation:

$$|x \uparrow\rangle |y \downarrow\rangle + |x \downarrow\rangle |y \uparrow\rangle$$

The discovery of  $x$  in the top section  $\uparrow$  would collapse this superposition to the first part of the above sum, thus also collapsing the state of  $y$  to being present in the lower half. Note that if instead we had measured the presence of ball  $x$  in the left half of the circle  $|x\leftarrow\rangle$ , then we would be certain that ball  $y$  would be in the right half  $|y\rightarrow\rangle$ . The reason is that the constraint upon the two-component system merely says that the one component must be opposite to the other, so that their centre of mass always remains in the middle of the circle. This is similar to the classic example of quantum entanglement (Wiseman, 2006), where the constraint is that the total spin of the system consisting of  $x$  and  $y$  must be zero, meaning that spin up for  $x$  implies spin down for  $y$ , while spin left for  $x$  implies spin right for  $y$ . Such a global constraint creates a coherence or correlation between the parts of the system.

Since  $x$  and  $y$  are spatially separated, the correlation between their states is non-local. Of course, the correlation was initially created by a local interaction (between electrostatic forces). Yet, the same applies to non-local correlations in quantum systems, where the components first need to interact locally before their states can become entangled (e.g. particles with opposite spins are created from the decay of a single spin zero system).

This example may still appear too simple, given that an observer could in principle observe the positions of both balls at the same time. Let us then investigate a more complex system, where macroscopically observable properties emerge from non-observable, microscopic interactions.

## 4. Rayleigh-Bénard convection

Rayleigh-Bénard convection (Bodenschatz, Pesch, & Ahlers, 2000; Nicolis & Prigogine, 1977) is a classic example of self-organization in which a complex system reaches a bifurcation point, after which it settles in a new, coherent regime in which its initially independent components have become non-locally correlated. The phenomenon appears in a liquid that is heated evenly from below while it cools down evenly at its surface. The heat added to the bottom layer of the liquid must be transported to the top layer in order to be dissipated at the cool surface. Initially, this heat transport can take place by conduction, in which the molecules in the warmer liquid at the bottom pass on their kinetic energy to adjacent molecules until it reaches the surface. But as the heating is increased, the gradient or temperature difference  $T$  between bottom and surface eventually becomes too large, and conduction is no longer sufficient. Transport of the heat can now only happen by *convection*: warmer (and thus lighter) liquid from the bottom floating up to the surface where it can release its heat to the cooler air above, while cooler (and thus heavier) liquid sinks down to the warmer bottom, where it collects heat.

These opposite movements at first sight create a conflict: the cool liquid moving down obstructs the warm liquid moving up. The “solution” to the conflict is that the movements of liquid coordinate so as to produce a circular flow: warm liquid flows up in one spot, cools down at the surface, moves sideways to a different spot where it now joins a cool, downward flow that reaches the bottom; there it warms up again, moves sideways in the opposite direction, back to the spot

where it joins the initial upward flow, and so on (Fig. 3). This produces a “roll” of liquid circulating between surface and bottom. If the container is sufficiently large, the liquid will self-organize into a series of such parallel rolls, or, depending on the shape of the container, hexagonal cells. For simplicity, we will here examine the case of the rolls, so that we can depict the whole system in two dimensions: vertical, representing the temperature gradient, and horizontal, representing the points where rolls start and end. A roll rotating in a clockwise manner will normally be adjacent to a roll that rotates counterclockwise, and vice versa. Thus, the liquid spontaneously subdivides into a series of coordinated, parallel rolls

First, we can note that the flows in the different regions of the container are correlated. If we know the width of a roll (which will depend on the properties of the liquid and the container), then it suffices to know the speed and direction of flow in one region to derive the speed and the flow in any other region. Initially, a single roll may form somewhere in the liquid, but as its upwards and downward flows rub against the adjacent liquid, this part of the system too will start to move in the same direction, creating a parallel roll, which in turn will pass on its direction of movement to its neighboring region, until the whole container is filled with coordinated rolls. Thus, the correlation between neighboring regions propagates until it covers the whole system. This feature of self-organization in which a local order spreads can be expressed by the *correlation length*: the average distance over which parts of the system are still correlated. As self-organization propagates further, correlation length increases until it reaches the full size of the system. At that moment, the order is no longer *local*, but *global* or *distributed*. Using quantum terminology, we might say that the correlation has become non-local: if we know the direction of flow in one region, then we can instantly deduce the direction of flow in any other region, no matter how far apart these regions are.

A second crucial feature is that the direction of flow is not determined by the initial state of the system. The temperature difference  $T$  plays the role of an order parameter: as its value increases, the system moves from an equilibrium state  $s_0$  without convection flows to a bifurcation (Fig. 1), with two possible outcomes: a clockwise flow  $s_1$  and a counterclockwise flow  $s_2$ . The state  $s_0$  without flow becomes unstable after the bifurcation point. Therefore, the system will have to “choose” one of the two options  $s_1$  or  $s_2$ . This is normally caused by an unobservably small, microscopic fluctuation, which makes that perhaps a few more liquid molecules move up rather than down in one particular spot. Because of the instability caused by the temperature gradient, this fluctuation is magnified into a macroscopic flow, driven by the heat energy that is continuously added to the liquid from below and that maintains the system far from equilibrium. As a result, the symmetry between clockwise and counterclockwise—or up and down—is broken: the system has opted for the one and rejected the other.

Let us represent this using a simplified quantum formalism. Consider a single convection roll, which we divide into a left-hand side ( $x$ ) and a right-hand side ( $y$ ). If the liquid is in the clockwise regime  $s_1$ , then it moves upward on the left of the roll:  $|x \uparrow\rangle$ , and downward on the right:  $|y \downarrow\rangle$  (Fig. 3):

$$s_1 = |x \uparrow\rangle |y \downarrow\rangle$$

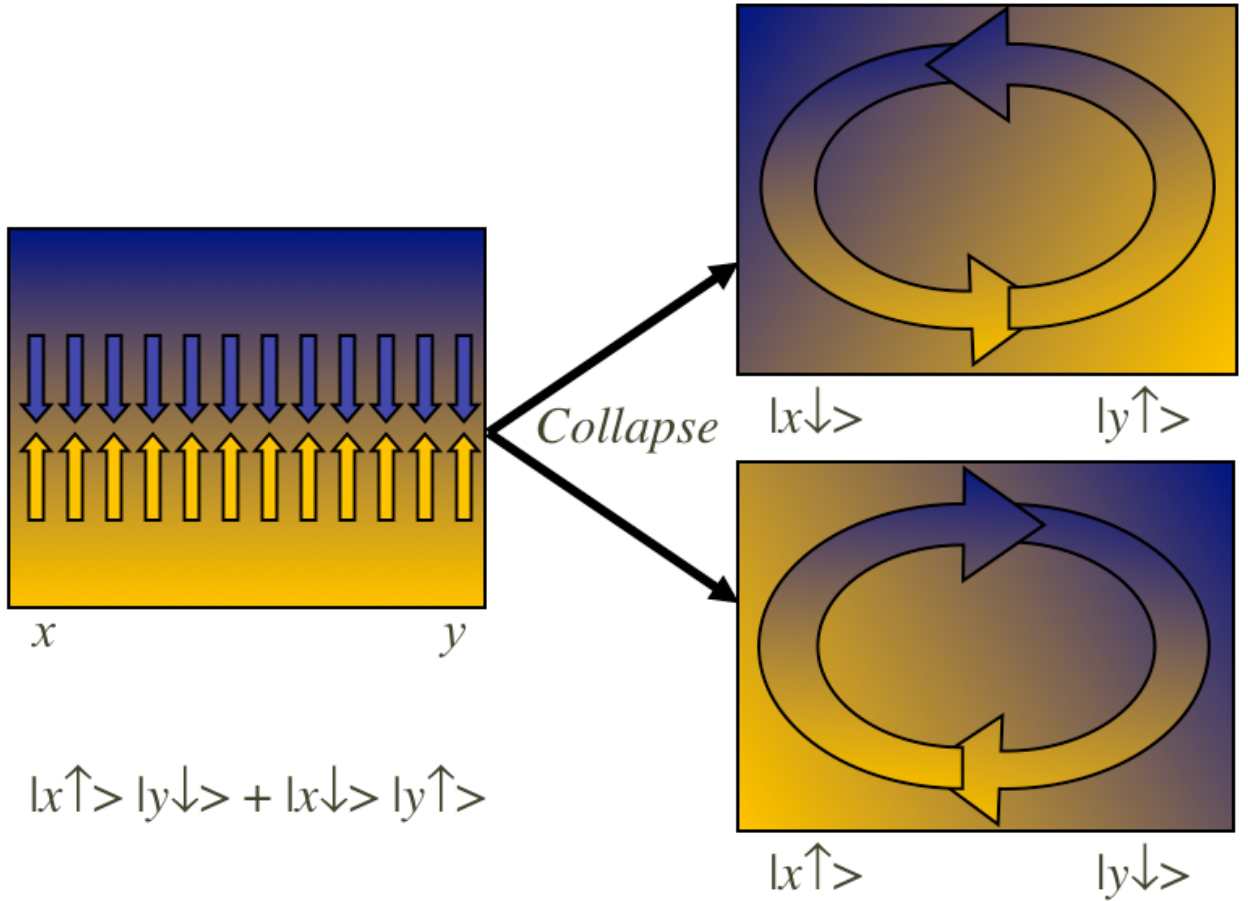


**Fig. 3:** The Rayleigh-Bénard instability. As the temperature difference between bottom (light, yellow) and top (dark, blue) of a liquid increases, heat must be transported by a convection flow (arrows). There are two possible solutions to this problem, a clockwise flow (bottom-right picture) and a counterclockwise flow (top-right). In the first, cold liquid moves down on the left side ( $x$ ) of the container, and up on the right ( $y$ ) side:  $|x\uparrow\rangle |y\downarrow\rangle$ , and vice-versa for the second. The original, unstable configuration can be seen as a superposition of both states that must collapse to one of them.

Vice versa for the counterclockwise regime:

$$s_2 = |x\downarrow\rangle |y\uparrow\rangle$$

Let us go back to the unstable regime  $s_0$  where the convection flow has not yet started and the symmetry between left and right has not yet been broken. We argued earlier that this “undecided” state on the border between two basins of attraction could be seen as a superposition of the two attractor states at the center of these basins:

$$s_0 = s_1 + s_2 = |x\uparrow\rangle |y\downarrow\rangle + |x\downarrow\rangle |y\uparrow\rangle$$

This superposition describes an entanglement between the two regions  $x$  (left) and  $y$  (right). When the value of the order parameter  $T$  is increased, this state will collapse to either  $s_1$  or  $s_2$ . That means that

the two separate regions  $x$  and  $y$  simultaneously opt for a certain flow direction, but such that the one is always the opposite of the other.

Note that this is similar to the classic Einstein-Podolsky-Rosen situation in which the spin of two entangled particles  $x$  and  $y$  is measured (Wiseman, 2006). Because their total spin is 0, any measurement establishing that the one has spin up  $|x \uparrow\rangle$  instantaneously collapses the other one to its spin-down state  $|y \downarrow\rangle$ . However, what creates the true “paradox” in this EPR set-up is that the observer could as well have measured a different property, such as the spin in the left-right direction. Here too a result of “left” for the one would have implied a collapse to “right” for the other, and vice versa.

Complementary properties are properties that cannot be observed simultaneously. For example, the set-up necessary to measure the wavelike properties of an electron (such as its momentum  $p$ ) is incompatible with the set-up necessary to measure its particle-like properties (such as its position  $x$ ). Therefore, the wave and particle aspects of quantum systems are said to be *complementary*: whenever we see the one, we cannot see the other, yet both are necessary to fully understand the behavior of the system. A precise observation result for one of a pair of complementary properties (like position and momentum, or spin in the vertical and in the horizontal directions) implies that the result for the other one becomes completely indeterminate. This is a more general formulation of the famous Heisenberg uncertainty principle (where  $\Delta x$  represents the uncertainty in the measurement of position  $x$ ):

$$\Delta x \cdot \Delta p \geq h/4\pi$$

Can we find an equivalent of complementary properties that describe the emergence of a convection roll? Up to now, we distinguished the flow directions: clockwise  $s_1$  and counterclockwise  $s_2$ . But the system is also characterized by the temperature difference between the lower layer of the liquid and the higher layer. This difference is driven by the parameter  $T$  (temperature difference between heated bottom and cool surface). However, it also depends on the state of system. In the state  $s_0$  without convection, there is a large temperature difference, because heat cannot travel easily from bottom to top. In the states  $s_1$  and  $s_2$ , on the other hand, there is a small temperature difference, because warm liquid from the bottom is continuously transported to the cool surface, and vice versa (Fig. 3). The greater the heating and thus  $T$ , the faster the warm water will move to the surface to mix with the cooler water there. Thus, in the convection states there is a constant mixing of temperature layers that compensates for any increases in  $T$ . If an observation consists in registering the temperature in the lower and higher layers of the liquid, then we might say that the size of  $T$  is not observable in the convection state, while its value is clearly determined in the equilibrium state  $s_0$ . Let us for simplicity distinguish two “eigenstates” of the observable  $T$ :  $|T\text{-large}\rangle$  and  $|T\text{-small}\rangle$  (where “small”  $T$  is still large enough to sustain convection). In that case, the convection state  $s_1$ , which is an eigenstate for the observable “direction of flow”, becomes a superposition state for the observable  $T$ :

$$s_1 = |T\text{-large}\rangle + |T\text{-small}\rangle$$

Bringing back the convection state to the equilibrium state  $s_0$  would in a sense “collapse” the superposition, because in this state we find either  $|T\text{-large}\rangle$  or  $|T\text{-small}\rangle$ . This might be achieved as follows. We could temporarily interrupt the convection flow by inserting parallel horizontal plates that stop the liquid from moving in the vertical direction. After the plates have been inserted, we can measure the temperature difference between upper and lower layer, and determine whether the result of this observation is  $|T\text{-large}\rangle$  or  $|T\text{-small}\rangle$ . But in this state we can no longer determine the result of the complementary observation  $|x\uparrow\rangle$  or  $|x\downarrow\rangle$ , because there is no flow. After the removal of the plates, the state will collapse again to one of the two flow states  $s_1$  or  $s_2$ , but the result will be uncertain. Thus, the two observations of flow direction and temperature gradient are complementary, and a determinate result for the one implies an indeterminate one for the other. It would be an interesting exercise to check whether such a system could be made to violate the Bell inequalities that are the classic way to characterize quantum non-locality (Wiseman, 2006), just like the Bell-violating macroscopic system proposed by Aerts (1982).

## 5. Other examples of complex phenomena

There are many similar examples of self-organization in complex systems that exhibit quantum-like properties. A straightforward analogue to Bénard convection can be found in the lanes that spontaneously form in pedestrian traffic (Helbing, 2001; Helbing & Molnar, 1998). Assume that a crowd of people needs to pass through a relatively narrow space, such as a street or square, but that half of the people move in one direction (say north to south) and half in the opposite direction (south to north). Initially, we are in a state of friction or mutual obstruction, as people will constantly need to change course in order not to bump into others. However, after a while their movements become more coordinated, as people moving in a given direction will start to follow each other, while staying out of the way of the people moving in the opposite direction. Thus, the available space self-organizes into two or more parallel “lanes”, so that people in one lane all move in one direction, while those in the adjacent lane move in the opposite direction. This is similar to the liquid splitting up in parallel upward and downward flows, albeit it with the difference that individuals reaching the end of a lane/flow do not change direction and come back via the adjacent lane. Still, the initial separation between the lanes exhibits a similar kind of bifurcation dynamics, given that the same lane could have been used for either north-south or south-north traffic.

Initially, both options are equally likely, and it is some unpredictable fluctuation that will break the symmetry, making that in a given lane a few more people move in one direction than the other. As people tend to follow others that move in the same direction in order to avoid collisions, this chance fluctuation will be amplified until it dominates the length of the lane. Again, we could say that the initially uncoordinated movement corresponds to an indeterminate superposition state, which then “collapses” to one of several possible eigenstates characterized by a determinate flow for a given lane. The order parameter that forces the collapse in this case is the density of pedestrian traffic: the more people try to cross a given area, the more friction will be caused by people bumping

into each other, and therefore the more people will tend to follow others moving in the same direction.

Such self-organization through the non-linear amplification of microscopic fluctuations is what Prigogine called “order through fluctuations” (Nicolis & Prigogine, 1977). The symmetry breaking that it forces can be understood through what is called a “winner-takes-all” dynamics. This describes a situation in which several possible configurations are competing to take over a given assembly of components (such as molecules, drops of liquid, or people). The amplification is typically caused by a positive feedback or chain reaction in which the number of new “recruits” to the spreading configuration is proportional to the number that is already there, so that its growth is exponential. Components are typically recruited the moment a majority of their neighbors has been recruited. The first configuration to start growing will recruit most components, and thus extend the neighborhood in which it can make more recruits. Thus, it will encroach upon any configuration that started later and that therefore was able to recruit only a smaller number of neighbors. As a result, the first configuration (or the one that for some other reason managed to grow more quickly) will eventually overtake and erase any rival configurations. Thus, there will be a single “winner” that takes over all the components.

A classic example of this type of dynamics is opinion formation in a social group. Suppose that initially people have different opinions, but that they are inclined to conform to the opinion of their neighbors. If by chance, a small group of neighbors have the same opinion, their influence on their neighbors will be larger than the one of other neighbors that all have different opinions. Thus, the group will grow. Because of the positive feedback dynamics sketched above, eventually they will overtake the whole group so that everyone will settle on the same opinion, a process called “conformist transmission” (Henrich & Boyd, 1998). Similar dynamics can be seen in the Ising model for magnetization, in which spins tend to align to the direction of spin (up or down) of their neighbors. Depending on how sensitive spins are to random fluctuations and to the influence of their neighbors, this may lead either to irregular zones in which molecules locally have the same spin, which is different from the one in other zones, or to a completely homogeneous outcome in which spins are globally aligned. In all these cases, we start from an indeterminate state where spins or opinions are randomly distributed, which then “collapses” to a single direction or opinion, thus breaking the symmetry of the initially homogeneous distribution, while creating a global correlation between all the regions.

A similar dynamics seems to occur in the brain. According to the global workspace theory, which is increasingly supported by empirical evidence (Dehaene, 2014; Sergent & Dehaene, 2009), we become conscious of some perception or thought when it manages to win the competition for attention from rival stimuli. It thus comes to dominate the “global workspace”, which is a kind of central neuronal crossroads from which commands are broadcasted to other parts of the brain. Many subconscious processes go on in parallel, but from those that reach the global workspace only the “winner-taking-all” can dominate consciousness. That is why consciousness is sequential: we can only be fully conscious of a single thought at a time, even while the subconscious activity in our neural networks outside the workspace is massively parallel.

This is illustrated by a classic example that has clear similarities to both quantum processes and self-organization: Gestalt perception (Kruse & Stadler, 2012; Stadler & Kruse, 1990). Our consciousness does not see images as detailed arrays of pixels, parts or nuances, but as coherent wholes: clear figures with an unambiguous interpretation that are called “Gestalts”. When an image is ambiguous, in the sense that it can be interpreted in more than one way, we are normally aware of only a single interpretation at a time. Well-known examples of such ambiguous figures are a shape that looks like either a rabbit or a duck, or one that resembles either a vase or two people’s profiles facing each other. While we are able to perceive both Gestalts, we cannot do so simultaneously. Only one Gestalt can win the competition for global workspace domination.

Such an ambiguous figure can be represented as a superposition state, e.g.  $|\text{rabbit}\rangle + |\text{duck}\rangle$ . But consciousness functions like a quantum observation that can only perceive eigenstates:  $|\text{rabbit}\rangle$  or  $|\text{duck}\rangle$ . The process of reaching a conscious interpretation “collapses” the superposition state to one of the eigenstates, and this in an intrinsically unpredictable manner.

The implied symmetry breaking is perhaps illustrated most clearly by another ambiguous figure, the Necker cube (Fig. 4). This is a two-dimensional geometrical figure consisting of two connected squares, which the brain tends to interpret as a view on a three-dimensional cube. However, there are two ways of “seeing” the cube, one in which the left square appears as the front side of the cube (implying that the right square represents the back side), and one in which the right square appears as the front. The two interpretations are perfectly symmetrical, and there is no reason why the one would be preferred to the other. Yet, the winner-takes-all dynamics implies that only one can be present in consciousness at a given time. Thus, the initial symmetry must be broken, in a way that is intrinsically unpredictable.

This example also illustrates non-locality. Suppose we decompose the figure into left and right squares. Because of their connecting lines, the squares are “entangled”. The initial state of our perception, before it reaches consciousness, is as yet indeterminate as to which square will appear as “front” and which as “back”. Thus, we might describe it as a superposition state:

$$|\text{left-front}\rangle |\text{right-back}\rangle + |\text{left-back}\rangle |\text{right-front}\rangle$$

The operation of reaching consciousness collapses this state to one of the two eigenstates. Thus, the perception of the left square as being “front” forces the state of the right square to instantaneously collapse to “back”. But left and right are separated by a finite distance, so this process is in a sense “non-local”.

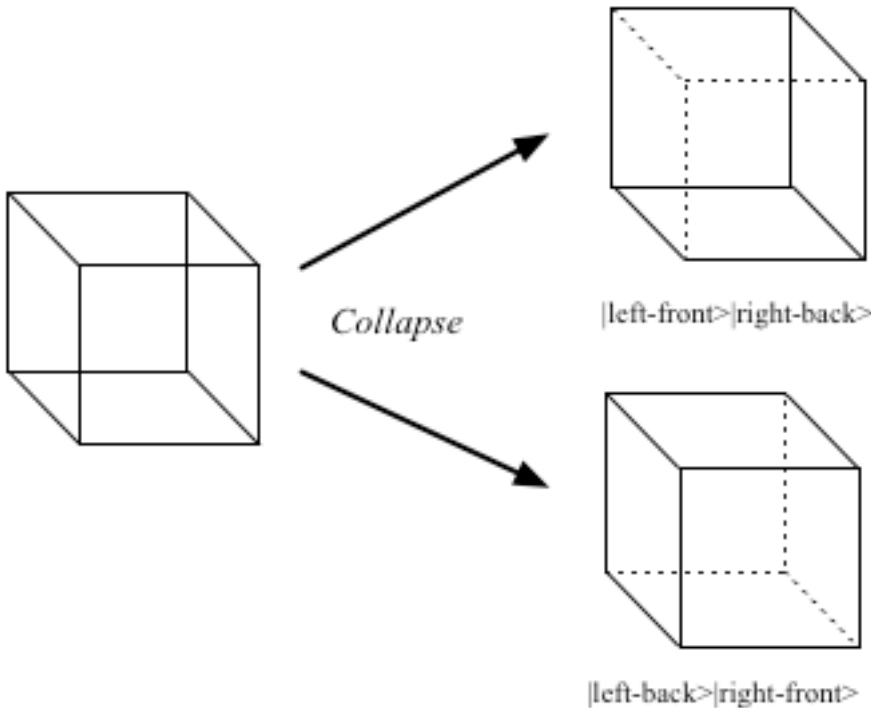


**Fig. 4:** The Necker cube perceptual instability. The figure with the two connected, parallel squares on the left is interpreted by the brain as a view on a cube. However, there are two ways to “collapse” the ambiguous figure: either into a cube where the left square represents the front of the cube (top-right picture), and the right square the back, or a cube where front and back are switched (bottom-right picture).

## 6. Some reflections on quantum field theory

The above examples seem to make a good case for a parallelism between complex processes of self-organization and quantum observation processes. The question is whether this correspondence points to a fundamentally shared dynamics. Let us therefore examine the differences between the two domains, and see whether these can be eliminated. A first difference, the instantaneity of collapse in the quantum realm vs. an extended process of self-organization, is perhaps less fundamental than it appears. We noted earlier that a quantum observation is only instantaneous as a mathematical operation, but that its physical realization always has a finite duration. We also noted that at no point is information transmitted from one part of the system to another at a speed faster than light. The same applies to self-organization, where correlations between distant regions may emerge very fast, because of non-linear amplification, but the propagation of order or alignment still uses local interactions and therefore needs a finite time to reach all regions. Yet, once the correlation is global, we can forget about the finite process that produced it, and immediately deduce the state of one component from our observation of another one.

Another difference between the two types of processes is that the one is induced by an observation, while the other happens spontaneously—albeit typically driven by the change in value of an order parameter affecting the system. An observation implies an interaction between the

quantum system being measured and some apparatus or set-up that necessarily affects the system being measured. In that sense, an observation can be seen as an external dynamics imposed by some observer on the system that forces the system to “collapse” and thus make a choice between the eigenstates that make up its initial superposition state. This does not look fundamentally different from the dynamics externally induced by the change of an order parameter that forces it to choose between attractors. This point is confirmed by the more recent interpretation of wave function collapse as a process of “decoherence” (Joos et al., 2013; Zurek, 2003), in which the noisy interactions between the quantum system and its environment gradually erase the coherence that existed between the different parts of the superposition state or wave function.

This brings us to a fundamental question: what causes the system to choose for one option rather than another? If we assume perfect symmetry between the options, in the sense that none of the solutions is in any way preferable to the others, then there does not seem to be a cause. Such spontaneous symmetry breaking (Castellani, 2003) appears like a fundamentally indeterministic, uncaused process, or what I have previously called a “distinction creation” (Heylighen, 1989, 1990; Heylighen et al., 2007). In self-organization, the cause is normally assumed to be some microscopic, unobservable fluctuation (Nicolis & Prigogine, 1977), similar to the random distribution of molecular movements that cause Brownian motion in a liquid. The equivalent in quantum mechanics would be a hidden variable, a microscopic property that we cannot observe but that affects the outcome of the observation. However, the Bell theorem has established that if hidden variables are responsible for the paradoxes of entanglement, then these hidden variables must be non-local (Wiseman, 2006), which would contradict some of the deepest principles underlying physical theories. Therefore, hidden variables are generally rejected as an explanation for quantum indeterminacy.

Aerts has proposed an elegant hypothesis to resolve the problem: the hidden measurement approach (Aerts, 1998). This assumes that the unobservable properties that determine the outcome of an observation are not hiding inside the quantum system, but inside the measuring apparatus. This makes sense, given that a microscopic quantum system, such as an electron, hardly offers any “room” to hide anything, while an observation apparatus constitutes a complex, macroscopic system of which we can never determine the full microstate. Since the outcome of the measurement depends on both system and apparatus, it seems reasonable to assume that different, albeit non-distinguishable, microstates for the same apparatus would result in different outcomes.

To make things more concrete, Aerts proposes a toy model that illustrates how the hidden measurement approach might give rise to some of the probability distributions predicted by quantum theory. In this model, the (deterministic) state of the quantum system is somehow registered on a particular spot along an elastic string that is extended inside the apparatus. (This can be visualized with the set-up in Fig. 2, where we imagine that one of the balls, representing the system, would “fall” onto the horizontal line that represents the “string”). But the apparatus can only register two possible outcomes (eigenstates), “spin-left” or “spin-right”. This happens when the string breaks in two. If the spot is found on the left piece of string, the registered outcome is “spin-left”, and vice versa. The indeterminacy is introduced by the fact that we do not know where along its length the string will break.

This model actually provides a beautifully simple illustration of our initial problem of symmetry breaking. When the tension on a string is increased, there will inevitably come a moment when the string will break, thus creating a distinction or differentiation. Let us assume that the string is homogeneous: every segment is as strong as any other segment. Therefore, there are no a priori “weak spots” that would break under a lower tension than the other regions. Because the string is elastic, no matter where the tension is exerted, this tension will spread evenly over all segments. Indeed, imagine that the tension would be higher in segment *A*, so that *A* would be extended more. That means that *A* will pull harder on its neighboring segment *B* which is as yet less extended, and thus has more elastic capacity to absorb the tension, until it is equally tense as *A*. Thus, any local inhomogeneity would immediately be globally diffused, so that the tension remains homogeneous. But that means that any segment of the string is just as likely (or unlikely) to break as any other. Yet, as the tension is increased, the string has to break in a particular spot, which therefore is selected out of a continuum of equivalent spots. This is similar to the symmetry breaking during a bifurcation, with the increasing tension playing the role of the order parameter forcing the system to make a choice. The only difference is that in this case the number of possible choices is continuously infinite, rather than finite.

In an actual macroscopic experiment, we would explain the symmetry breaking by some microscopic inhomogeneity in the rubber of the string, or perhaps a fluctuation in the distribution of molecular forces in the string. In quantum mechanics, we attribute it to some peculiarity of the observation process, perhaps explainable by the way the apparatus perturbs the system. But there is a deeper theory suggesting that the symmetry breaking is truly spontaneous, and does not need any external factors: (relativistic) *quantum field theory* (Mandl & Shaw, 2010). The mathematics of this theory is so complex that no one really seems to have dared to propose a systematic or intuitive interpretation of its results. Yet, these results are so amazingly wide-ranging and empirically accurate that it is probably the most reliable theory in the whole of science. But we do not need to understand the mathematical derivation to appreciate some of the phenomena it explains.

Perhaps the best-known case is radioactive decay: a radioactive atom is by definition unstable, which means that it may disintegrate into smaller particles at any moment in time. However, it is impossible to determine at which time such decay will happen. We only know that there is a fixed probability for an atom to decay during a given time interval. The half-life of an isotope denotes the interval for which that probability is exactly 50%. That means that after that period, about half of the atoms in a sample will have decayed. Yet, these atoms were absolutely identical as far as the forces responsible for radioactivity are concerned. The initial homogeneity or symmetry between the atoms has been broken: some have decayed, others have survived. But here we cannot find any internal or external cause responsible for this difference: no observation, no order parameter, no microscopic inhomogeneity, no perturbation... has affected the atoms. Each atom on its own, independently of outside influences, has decided at some random moment to either fall apart or remain.

A less well-known, but actually more common, example of such an intrinsically indeterministic process is the “quantum jump” through which an excited atom or molecule falls back to a lower level of energy. Any energy level higher than the ground state is unstable, and will

eventually fall back to its ground level while emitting one or more photons to carry away the excess energy. However, the time of this decay and the direction in which the photon is emitted are essentially unpredictable. Ironically, although the emission of such “quanta” of energy is what gave quantum mechanics its name, the process cannot be explained within conventional quantum mechanics. Indeed, the evolution of a quantum state as described by the Schrödinger equation is intrinsically continuous, while discontinuities only appear when an observation collapses the state to an eigenstate. But the discontinuous emission of a photon by an excited state happens spontaneously, without any observation taking place. It therefore has to be explained by quantum field theory.

The only “cause” for such symmetry breaking this theory proposes is a so-called *quantum fluctuation of the vacuum*. In field theory, a vacuum is the zero-energy state of the field. Any positive energy injected into the field creates an “excitation”, which classically takes the form of a wave, but quantum mechanically can be interpreted as a particle (e.g. a photon). Now, the Heisenberg uncertainty principle for the complementary properties of time and energy states that when time intervals become arbitrarily small, the uncertainty on the energy present in that time interval becomes arbitrarily large. That means that if we consider the vacuum across a sufficiently short interval, the energy present during that interval can take on values large enough to produce “virtual particles”. These are excitations of the field that are so short-lived that we cannot directly observe them, because they decay almost as soon as they appeared. But during their brief life, they can interact with a system such as an atom in an excited state, and trigger the decay of that state. Thus, quantum field theory suggests that even emptiness or nothingness (i.e. absence of any energy, matter or other differentiating feature) can temporarily fluctuate by randomly producing virtual particles or waves that affect unstable systems, and that may force them to “collapse”.

How does this relate to self-organization? A typical self-organizing system, such as a liquid or an array of spins, consists of many interacting components distributed across space. Through local interactions, a change in the state of a component tends to propagate to its neighboring components, thus spreading like a wave across the medium. Examples of such waves are the “phonons”, which are particle-like vibrations propagating in some solid medium. This medium is discrete, consisting of separate components, such as molecules. A field is a continuous medium, but that can be seen as the limit of such a discrete medium when the distance between the components goes to zero. For example, it has been shown that the classic Ising model, which is used to illustrate the self-organization of magnetization via the propagation of magnetic alignment between neighboring spins, becomes isomorphic to a quantum electromagnetic field in such a limit. Thus, fields and complex dynamic systems appear like different ways to model a dynamics of fluctuation and propagation, where fluctuation plays the role of the initial event that precipitates the symmetry breaking, while propagation across a medium is the mechanism that amplifies this random change, and creates a new coherence or coordination between remote regions. A classic application of this in physics are phase transitions, such as the transition from (disordered) liquid to (coherent) solid, which can be modeled using both non-linear statistical mechanics and an equivalent of QFT (Zinn-Justin, 1996).

Quantum phenomena	Complex dynamics/self-organization
Superposition state	Indeterminate state
Uncertainty	Bifurcation
Wave function collapse	Reaching of attractor
Entanglement	Emergent constraint
Non-locality	Non-local correlations
Observation	Order parameter
Symmetry breaking	Symmetry breaking
Eigenstate	Attractor state

Table 1: some correspondences between quantum and self-organizing phenomena.

## 7. Conclusion

We have investigated the correspondence between fundamental aspects of quantum theory and related phenomena in the emerging theory of complex, self-organizing systems (Table 1). On the one hand, this helps us to better grasp the often counterintuitive behavior of quantum systems, because we now can see how they are analogous to macroscopic phenomena with which we have more direct experience. It also suggests new methods to perhaps analyze that behavior at a deeper level. Vice-versa, the analogy with quantum mechanics suggest new ways of looking at complex phenomena, such as the self-organization of cognitive or social structures, thus extending the program that was initiated by quantum cognition (Aerts, 2009; Aerts, Gabora, Sozzo, & Veloz, 2011; Bruza et al., 2015).

Quantum phenomena at the deepest level are characterized by the superposition principle. It implies that for any two states with determinate characteristics there exists a superposition state for which these same characteristics are indeterminate, meaning that an observation may produce either the one or the other result, in an unpredictable manner. This uncertainty is mirrored in complex systems by the phenomenon of bifurcation, which notes that under changes of an order parameter stable solutions may multiply, forcing the system to “choose” one of a number of a priori equivalent states. In both quantum and complex dynamics, the initially indeterminate state appears to “collapse” into one of the determinate outcomes, where it then remains. This means that the outcome is an attractor or eigenstate of the process that precipitated the collapse. The choice of one among several equivalent outcomes in both cases defines a symmetry breaking. In complex dynamics, this symmetry breaking appears to be initiated by a microscopic fluctuation, while in quantum mechanics it may be caused by the microscopic perturbation induced by the observation apparatus, or more fundamentally by the fluctuations of the vacuum implied by the Heisenberg uncertainty principle.

In self-organizing systems, the “collapse” into an attractor state produces a global or emergent constraint that induces a correlation between the components of the system. This is similar to the

“entanglement” that can occur between the components of a quantum system, when the system as a whole is constrained to obey a global condition, such as having a total spin of 0. Such correlations are non-local, in the sense that the states of spatially remote components depend on each other, and a determinate observation outcome (collapse) for the one forces a complementary outcome for the other, even when their individual states are initially indeterminate. It is not yet clear whether the correlations in self-organizing systems can exhibit the same paradoxical property expressed by the violation of the Bell inequalities that characterizes quantum non-locality (Aerts, 1982). This and the role of quantum fluctuations of the vacuum in triggering symmetry breaking appear like promising issues for further research.

## References

- Aerts, D. (1982). Example of a macroscopical classical situation that violates Bell inequalities. *Lettere Al Nuovo Cimento (1971–1985)*, 34(4), 107–111.
- Aerts, D. (1998). The hidden measurement formalism: what can be explained and where quantum paradoxes remain. *International journal of theoretical physics*, 37(1), 291–304.
- Aerts, D. (2009). Quantum structure in cognition. *Journal of Mathematical Psychology*, 53(5), 314–348.
- Aerts, D., Gabora, L., Sozzo, S., & Veloz, T. (2011). Quantum structure in cognition: fundamentals and applications. *arXiv preprint arXiv:1104.3344*.
- Ashby, W. R. (1962). Principles of the self-organizing system. In H. von Foerster & G. W. Zopf (Eds.), *Principles of Self-Organization* (pp. 255–278). Pergamon Press. Retrieved from <http://csis.pace.edu/~marchese/CS396x/Computing/Ashby.pdf>
- Aspect, A. (2007). Quantum mechanics: to be or not to be local. *Nature*, 446(7138), 866.
- Ball, P. (2012). *Why Society is a Complex Matter: Meeting Twenty-first Century Challenges with a New Kind of Science* (2012th ed.). New York: Springer.
- Bedau, M. (2002). Downward causation and the autonomy of weak emergence. *Principia*, 6(1), 5. Retrieved from

<http://search.proquest.com/openview/e32baabe9f7b694db698fab5a4a17062/1?pq-origsite=gscholar&cbl=2026966>

Bodenschatz, E., Pesch, W., & Ahlers, G. (2000). Recent Developments in Rayleigh-Bénard Convection. *Annual Review of Fluid Mechanics*, 32(1), 709–778. doi:10.1146/annurev.fluid.32.1.709

Bruza, P. D., Wang, Z., & Busemeyer, J. R. (2015). Quantum cognition: a new theoretical approach to psychology. *Trends in cognitive sciences*, 19(7), 383–393.

Castellani, E. (2003). On the meaning of symmetry breaking. *Symmetries in physics: Philosophical reflections*, 321–334.

Dehaene, S. (2014). *Consciousness and the Brain: Deciphering How the Brain Codes Our Thoughts*. Penguin.

Dirac, P. A. M. (1981). *The principles of quantum mechanics*. Oxford university press.

Eberhard, P. H., & Ross, R. R. (1989). Quantum field theory cannot provide faster-than-light communication. *Foundations of Physics Letters*, 2(2), 127–149. doi:10.1007/BF00696109

Ghirardi, G. C., Grassi, R., Rimini, A., & Weber, T. (1988). Experiments of the EPR Type Involving CP -Violation Do not Allow Faster-than-Light Communication between Distant Observers. *EPL (Europhysics Letters)*, 6(2), 95. doi:10.1209/0295-5075/6/2/001

Haken, H. (1977). *Synergetics: an introduction: nonequilibrium phase transitions and self-organization in physics, chemistry, and biology*. Springer.

Helbing, D. (2001). Traffic and related self-driven many-particle systems. *Reviews of modern physics*, 73(4), 1067. Retrieved from [http://rmp.aps.org/abstract/RMP/v73/i4/p1067\\_1](http://rmp.aps.org/abstract/RMP/v73/i4/p1067_1)

Helbing, D., & Molnar, P. (1998). Self-organization phenomena in pedestrian crowds. *arXiv preprint cond-mat/9806152*. Retrieved from <http://arxiv.org/abs/cond-mat/9806152>

Henrich, J., & Boyd, R. (1998). The Evolution of Conformist Transmission and the Emergence of Between-Group Differences. *Evolution and Human Behavior*, 19(4), 215–241.

- Heylighen, F. (1989). Causality as Distinction Conservation: a theory of predictability, reversibility and time order. *Cybernetics and Systems*, 20(5), 361–384. doi:10.1080/01969728908902213
- Heylighen, F. (1990). Classical and nonclassical representations in physics II: quantum mechanics. *Cybernetics and Systems*, 21(5), 477–502. doi:10.1080/01969729008902255
- Heylighen, F. (2001). The science of self-organization and adaptivity. *The Encyclopedia of Life Support Systems*, 5(3), 253–280. Retrieved from <http://pespmc1.vub.ac.be/Papers/EOLSS-Self-Organiz.pdf>
- Heylighen, F. (2009). Complexity and Self-Organization. *Encyclopedia of Library and Information Sciences*, Third Edition (pp. 1215–1224). Taylor & Francis. Retrieved from <http://www.tandfonline.com/doi/abs/10.1081/E-ELIS3-120043869>
- Heylighen, F., Cilliers, P., & Gershenson, C. (2007). Complexity and Philosophy. In J. Bogg & R. Geyer (Eds.), *Complexity, science and society* (pp. 117–134). Oxford: Radcliffe Publishing,. Retrieved from <http://arxiv.org/abs/cs/0604072>
- Hilborn, R. C. (2004). Sea gulls, butterflies, and grasshoppers: A brief history of the butterfly effect in nonlinear dynamics. *American Journal of Physics*, 72(4), 425–427. Retrieved from <http://scitation.aip.org/content/aapt/journal/ajp/72/4/10.1119/1.1636492>
- Horodecki, R., Horodecki, P., Horodecki, M., & Horodecki, K. (2009). Quantum entanglement. *Reviews of modern physics*, 81(2), 865.
- Joos, E., Zeh, H. D., Kiefer, C., Giulini, D. J., Kupsch, J., & Stamatescu, I.-O. (2013). *Decoherence and the appearance of a classical world in quantum theory*. Springer Science & Business Media.
- Kruse, P., & Stadler, M. (2012). *Ambiguity in Mind and Nature: Multistable Cognitive Phenomena*. Springer Science & Business Media.
- Mandl, F., & Shaw, G. (2010). *Quantum Field Theory*. John Wiley & Sons.
- Milnor, J. W. (2006). Attractor. *Scholarpedia*, 1(11), 1815. doi:10.4249/scholarpedia.1815

- Nicolis, G., & Prigogine, I. (1977). *Self-organization in nonequilibrium systems: From dissipative structures to order through fluctuations*. Wiley, New York.
- Sergent, C., & Dehaene, S. (2009). PSYCHOLOGICAL SCIENCE Research Article Is Consciousness a Gradual Phenomenon? Evidence for an All-or-None Bifurcation During the Attentional Blink.
- Stadler, M., & Kruse, P. (1990). Theory of Gestalt and Self-organization. *Self-Steering and Cognition in Complex Systems. Gordon and Breach, New York*, 142–169.
- Wiseman, H. M. (2006). From Einstein's theorem to Bell's theorem: a history of quantum non-locality. *Contemporary Physics*, 47(2), 79–88.
- Zinn-Justin, J. (1996). *Quantum field theory and critical phenomena*. Clarendon Press.
- Zurek, W. H. (2003). Decoherence, einselection, and the quantum origins of the classical. *Reviews of modern physics*, 75(3), 715.

# Phase-Controlled Collapse and Revival of Entanglement of Two Interacting Qubits

Vladimir S. Malinovsky

*MagiQ Technologies, Inc., 171 Madison Avenue, Suite 1300, New York, New York 10016, USA*

Ignacio R. Sola

*Departamento de Química Física I, Universidad Complutense, 28040 Madrid, Spain*

(Received 9 September 2005; revised manuscript received 12 December 2005; published 6 February 2006)

We demonstrate the strong dependence of the entanglement dynamics of two distinguishable qubits in a trap on the relative phase of the pulses used for excitation. We show that the population and entanglement exhibits collapses and full revivals when the initial distribution of phonons is a coherent state.

DOI: 10.1103/PhysRevLett.96.050502

PACS numbers: 03.67.Mn, 03.65.Ud, 03.67.Pp, 42.50.Vk

One of the most promising systems to build a quantum computer is based on trapped ions [1,2]. Recently, several schemes of coherent manipulation of the quantum states of trapped ions have been developed [3–6]. Here we consider a scheme for creating and controlling entanglement of two qubits in a linear trap, or in other words, two two-level quantum systems coupled to a harmonic bath. In our setup, the two-qubit system must have independently addressable transitions. There are two different strategies to create the entanglement: by individually addressing each system or by means of simultaneous indistinguishable excitation. Both cases were found promising, since even hot ions were shown to be useful for quantum computation [7–9], owing to the independence of the effective coupling on the vibrational (phonon) quantum number.

The basic system underlying the two-qubit manipulation involves a four-level system in closed-loop configuration, shown in Fig. 1. When each coupling can be addressed independently, new forms of control are possible. Recently, we have shown that the relative phase between the pulses can be used to control population dynamics as well as to prepare entangled states [10], by virtue of quantum interference between two pathways connecting the initial and target states [11]. Obviously, population dynamics and entanglement depend on many parameters of the system. In most experimental setups (for instance, trapped ions) the system is addressed by means of fully overlapping cw fields, so that the Rabi flopping depends only on the pulse area. Then, it is still possible to gain a higher finesse in the manipulation of the quantum system by introducing an externally controllable relative phase. In this work we show that the relative phase between the pulses has far more important influence on the population dynamics and entangled state manipulation when the qubits are coupled to a harmonic trap. For properly chosen relative phases one can observe either Rabi oscillations according to the Mølmer-Sørensen scheme [7–9] (the relative phase is zero) or collapse and revival phenomena, as in the well-known Jaynes-Cummings model [12,13] (the phase is not equal to zero). Additionally, the phase could be used to control the time of operation of quantum gates.

Let us consider the dynamics of two distinguishable qubits in a one-dimensional harmonic trap. We assume that the two additional degrees of freedom are suppressed, and we neglect decoherence effects caused, for instance, by spontaneous decay. The collective motion of, e.g., atoms or ions will be defined by an effective harmonic trap potential, with the Hamiltonian

$$\hat{H}_0 = \nu \left( \hat{a}^\dagger \hat{a} + \frac{1}{2} \right) + \sum_i \frac{E_2^{(i)}}{2} (I - \sigma_{zi}) + J \sigma_{z1} \sigma_{z2}, \quad (1)$$

where  $\nu$  is the frequency of the vibrational motion,  $E_2^{(i)}$  is the transition energy in the  $i$  qubit (for instance, the excited internal state of the ions or atoms),  $\sigma_{zi}$  are Pauli matrices, and  $\hat{a}^\dagger$ ,  $\hat{a}$  are the vibrational ladder operators (all parameters in atomic units,  $\hbar = 1$ ). We allow here interaction between the qubits, which in a simple case can be treated as an effective spin-spin coupling Hamiltonian, where  $J$  is the coupling constant.

The interaction of the qubits with the external fields can be written in the following form:  $V_i = -\sum_j \Omega_j(t) \times \cos[\omega_j t + \phi_j - \eta_j(\hat{a}^\dagger + \hat{a})] \sigma_{xi} + \text{H.c.}$ , where  $\omega_j$ ,  $\phi_j$  are the laser frequency and phase,  $\Omega_j(t)$  is the Rabi frequency [14],  $\eta_j = k_j / \sqrt{4m\omega_t}$  is the Lamb-Dicke parameter

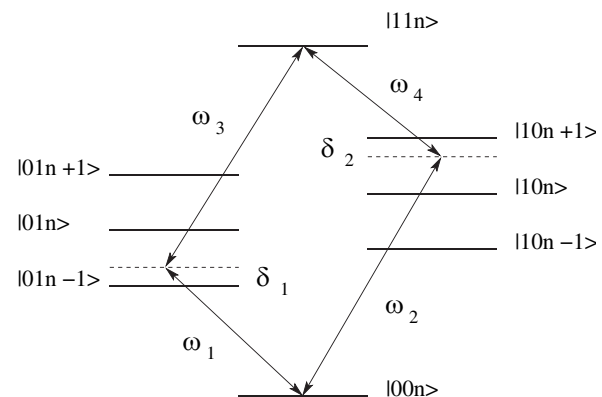


FIG. 1. Schematic of a four-level system for two qubits with distinguishable interactions in a linear trap.

ter,  $\omega_t$  is the trap frequency,  $m$  is the ion mass, and  $k_j$  is the laser wave vector.

Owing to the interaction between the qubits, the transition frequencies of the four-level system are different in general, depending on the specific system realization. As particular examples, the interaction between qubits gives rise to blockade effects known as dipole blockade in atomic systems [15] and it also takes place in semiconductor quantum dots [16]. In a very general approach, we consider here excitation of the trapped two-qubit system by four off-resonant fields driving the following transitions:  $|00n\rangle \xrightarrow{\Omega_1(t)} |01n-1\rangle \xrightarrow{\Omega_3(t)} |11n\rangle$  and  $|00n\rangle \xrightarrow{\Omega_2(t)} |01n+1\rangle \xrightarrow{\Omega_4(t)} |11n\rangle$  (Fig. 1), where “0” or “1” denotes the qubit state and  $n$  is the vibrational quantum number. The Hamiltonian for the total wave function  $|\psi\rangle = a_1|00n\rangle + a_2|11n\rangle + b_1|01n-1\rangle + b_2|10n+1\rangle$  in the rotating wave approximation has the form

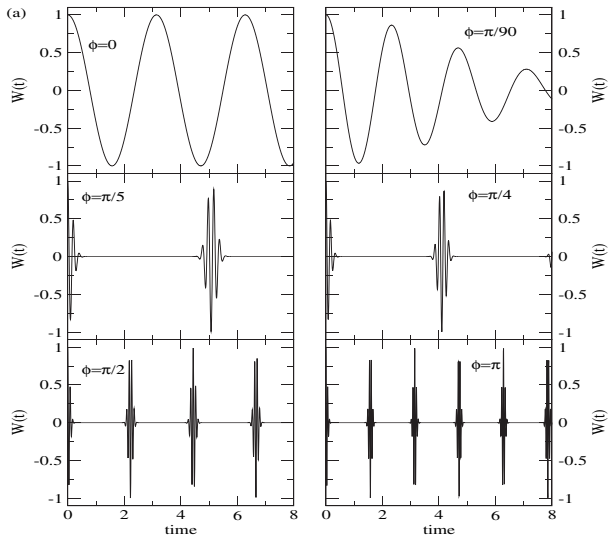
$$H = -\frac{1}{2} \begin{pmatrix} 0 & \Omega_{1,n} & \Omega_{2,n+1} & 0 \\ \Omega_{1,n}^* & -2\delta_1 & 0 & \Omega_{3,n} \\ \Omega_{2,n+1}^* & 0 & -2\delta_2 & \Omega_{4,n+1} \\ 0 & \Omega_{3,n}^* & \Omega_{4,n+1}^* & 0 \end{pmatrix}, \quad (2)$$

where  $\Omega_{i,n} = \eta_i \Omega_{i,0}(t) e^{i\phi_i} \sqrt{n}$ , and  $\delta_{1,2}$  are the detunings including energy level shifts due to spin-spin interaction.

By choosing the phases  $b_1 \rightarrow b_1 e^{-i\phi_1}$ ,  $b_2 \rightarrow b_2 e^{-i\phi_2}$ , and  $a_2 \rightarrow a_2 e^{-i(\phi_1+\phi_3)}$ , after adiabatic elimination (off-resonant excitation) of the  $b_i$  amplitudes, we obtain the following equation in the case of completely overlapped pulses,  $\Omega_{i,0}(t) = \Omega_0(t)$ :

$$H = -\frac{\eta^2 \Omega_0^2(t)}{4} \begin{pmatrix} \frac{n}{\delta_1} + \frac{n+1}{\delta_2} & \frac{n}{\delta_1} + \frac{n+1}{\delta_2} e^{i\phi} \\ \frac{n}{\delta_1} + \frac{n+1}{\delta_2} e^{-i\phi} & \frac{n}{\delta_1} + \frac{n+1}{\delta_2} \end{pmatrix}, \quad (3)$$

where  $\phi = \phi_4 + \phi_2 - \phi_1 - \phi_3$  is the effective phase



difference between the two distinct two-photon couplings, and we assume  $\eta_1 \approx \eta_2 = \eta$ .

Finally, choosing detunings as  $\delta_2 = -\delta_1 = \delta_0$  we obtain

$$H = -\frac{\eta^2 \Omega_0^2(t)}{4\delta_0} \begin{pmatrix} 1 & i\alpha^* \\ -i\alpha & 1 \end{pmatrix}, \quad (4)$$

where  $\alpha = [(2n+1)\sin(\phi/2) + i\cos(\phi/2)]$ .

In Eq. (4) the ac Stark shifts do not depend on the vibrational quantum number, but the effective Rabi frequency is still a function of  $n$ . At  $\phi = 0$ , Eq. (4) reproduces the well-known Mølmer-Sørensen Hamiltonian of trapped ions [7–9], while at  $\phi = \pi$  the effective Rabi frequency is linearly proportional to  $2n+1$ . The coupling between states  $|00n\rangle$  and  $|11n\rangle$  depends on the relative phase,  $\phi$ . Only at  $\phi = 0$  the coupling between the internal states does not depend on the motional states. As a result, one observes Rabi oscillations between the ground and the excited electronic states even if the motional state is not a single Fock state.

The solution of the Schrödinger equation with the Hamiltonian of Eq. (4) for arbitrary phase is  $a_1 = \cos[\varepsilon_n S(t)]$  and  $a_2 = \alpha \sin[\varepsilon_n S(t)]/\varepsilon_n$ , where  $S(t) = \eta^2 \int_0^t dt' \Omega_0^2(t')/4\delta_0$  and  $\varepsilon_n = [1 + 4n(n+1)\sin^2(\phi/2)]^{1/2}$ .

To demonstrate the effect of the relative phase we now consider the cw regime, that is, when  $\Omega_0(t) = \Omega_0$  is time independent. In general, when the initial state of the phonons is not a single Fock state, one has to average the results over the corresponding state distribution. Here we consider two particular situations: coherent and thermal state of the phonons. Averaging using the coherent state distribution,  $P_c(n) = e^{-\bar{n}} \bar{n}^n / n!$ , where  $\bar{n}$  is the average number of phonons, we obtain for the population inversion

$$W(t) = \sum_{n=0}^{\infty} P_c(n) (|a_1|^2 - |a_2|^2) = \sum_{n=0}^{\infty} P_c(n) \cos[2gt\varepsilon_n], \quad (5)$$

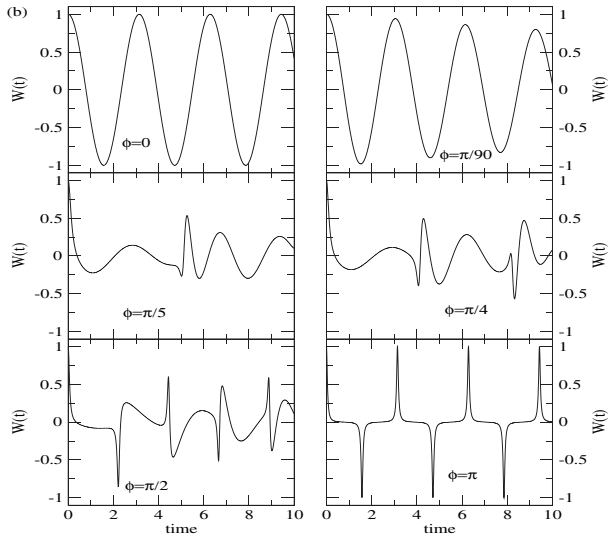


FIG. 2. Population inversion dynamics,  $W(t)$ , of the qubits at various relative phases,  $\phi$ : (a) for the initial coherent state of phonons with average number  $\bar{n} = 25$ ; (b) for the initial thermal distribution of phonons with average number  $\bar{n} = 5$ .

where  $g = \eta^2 \Omega_0^2 / 4\delta_0$ . It can be seen that at  $\phi = 0$  the dynamics of the system does not depend on the vibrational quantum number, as it was shown in Refs. [7–9], and we observe simple Rabi oscillations with frequency defined by  $2g$ . However, in general the Rabi frequencies depend on the vibrational quantum number  $n$ ,  $G_n = 2g\varepsilon_n$ .

To our knowledge, there is no general analytic solution for the summations in Eq. (5). However, in the limit of  $\bar{n} \gg 1$  the summation can be done exactly, and we obtain the analytic form for population inversion  $W(t) = e^{-2\bar{n}\sin^2(\tau/2)} \cos(\bar{n}\sin\tau)$ , where  $\tau = 4gt \sin(\phi/2)$ . The envelope function,  $e^{-2\bar{n}\sin^2(\tau/2)}$ , shows that all revivals in this model imply the exact regeneration of the initial value, that is, full revivals.

Using the analytic expressions for the probability amplitudes [Eq. (5)], we estimate the time period of the Rabi oscillations  $t_R$ , the collapse time  $t_c$ , and the interval between revivals  $t_r$  [17].  $t_R$  is defined by the inverse of the Rabi frequency at  $n = \bar{n}$ ,  $G_{\bar{n}} = 2g\varepsilon_{\bar{n}}$ . Therefore, we obtain  $t_R \sim G_{\bar{n}}^{-1} = [2g\varepsilon_{\bar{n}}]^{-1}$ . In the limit  $\bar{n} \gg 1$ , one obtains  $t_R \sim 1/4g\bar{n}\sin(\phi/2)$ .

The Rabi oscillations take place until a collapse time, when the oscillations related to different vibrational states become uncorrelated. Since the root-mean-square deviation for the coherent state  $\langle \Delta n \rangle$  is equal to  $\sqrt{\bar{n}}$ , we estimate the collapse time using the condition  $t_c(G_{\bar{n}+\sqrt{\bar{n}}} - G_{\bar{n}-\sqrt{\bar{n}}}) \sim 1$ . Finally, for  $\bar{n} \gg 1$ , we obtain  $t_c = [8g\sqrt{\bar{n}}\sin(\phi/2)]^{-1}$ .

The revival of the oscillations takes place when the phases of the neighboring  $n$ 's differ by  $2\pi$ . Using  $G_{\bar{n}}$  we find for the time interval between revivals  $t_r = 2\pi m/[G_{\bar{n}} - G_{\bar{n}-1}] \sim \pi m/[2g\sin(\phi/2)]$ , where  $m = 1, 2, \dots$ . Figure 2(a) shows the population dynamics for different values of the relative phase after averaging over

the coherent state distribution. The results are in perfect agreement with our estimates above.

In the case of a thermal distribution of the phonons, we have to perform the averaging over the one-mode Bose-Einstein distribution,  $P_t(n) = \bar{n}^n / (1 + \bar{n})^{n+1}$ , where  $\bar{n}$  is the average number of phonons. The analysis follows as previously, although the delocalization of the thermal distribution in terms of vibrational quantum number  $n$  (the main difference between coherent and thermal states) makes it impossible, in general, to apply any suitable approximation, even in the limit of  $\bar{n} \gg 1$ .

Figure 2(b) shows the population dynamics for different values of the relative phase after averaging over the thermal distribution. Here again, we observe Rabi oscillations with the frequency  $2g$  at  $\phi = 0$ , but the population dynamics becomes absolutely uncorrelated at  $\phi \neq 0$  on a longer time scale. It is interesting to see that as  $\phi \rightarrow \pi$ , the periodicity of the population dynamics (with frequency  $2g$ ) is again restored. The time between peaks does not depend on the average number of phonons, and we observe perfect revival of the envelope function. However, the width of the peaks decreases when the average number of phonons increases.

To quantify the degree of entanglement, we construct the density matrix  $\rho$  and calculate the concurrence  $C(t)$  [18–22]. According to the general expression for the case of two qubits  $A$  and  $B$ ,  $C(t) = \max(0, \sqrt{\lambda_1} - \sqrt{\lambda_2} - \sqrt{\lambda_3} - \sqrt{\lambda_4})$ , where  $\lambda_i$  are the eigenvalues of the matrix  $\rho = \rho(\sigma_y^A \otimes \sigma_y^B)\rho^*(\sigma_y^A \otimes \sigma_y^B)$ .

Figure 3 shows the dynamics of entanglement in the two-qubit system at various values of the relative phase. For coherent states the concurrence fully revives at any value of the relative phase [Fig. 3(a)]. The relative phase controls the revival time and the width of the reviving comb. The collapse of population inversion correlates

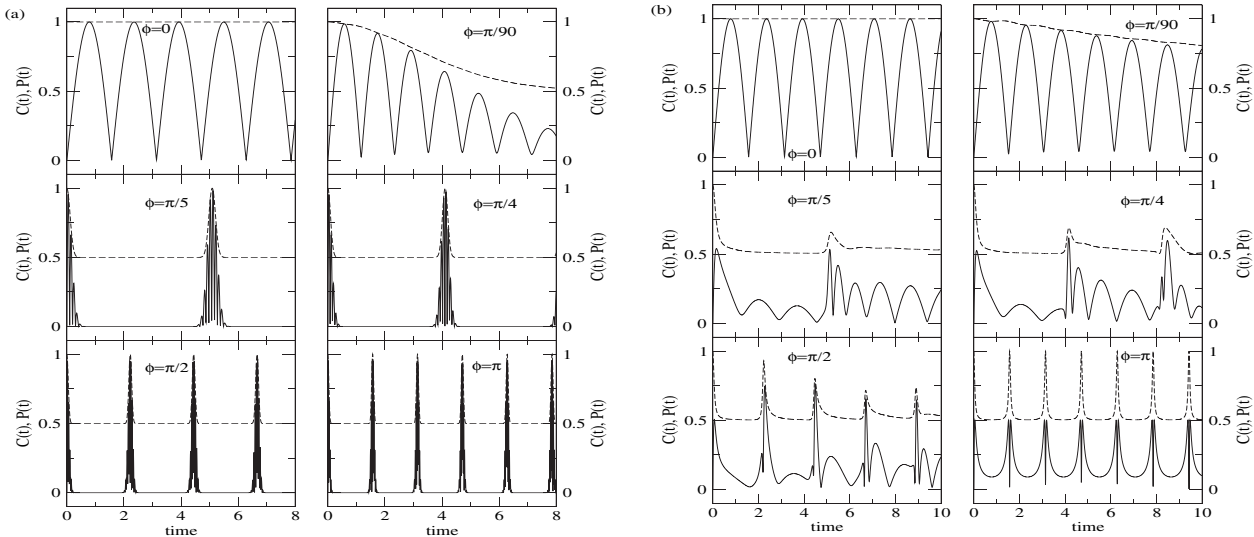


FIG. 3. Concurrence  $C(t)$  (solid line) and Renyi entropy  $P(t)$  (dashed line) in a system of two trapped qubits as a function of time at various relative phases,  $\phi$ : (a) for the initial coherent state of phonons with average number  $\bar{n} = 25$ ; (b) for the initial thermal distribution of phonons with average number  $\bar{n} = 5$ .

with the collapse of the concurrence, clearly revealing the decoherence of the system.

The degree of entanglement for the case of the thermal distribution behaves as in the coherent state at  $\phi = 0$ , or at very small values of the relative phase [compare Figs. 3(a) and 3(b)]. However, for larger  $\phi$  the lack of correlation in the population dynamics is reflected in the concurrence. In this case, the correlation between the population inversion dynamics and the concurrence is less obvious than previously. In fact, the concurrence never reaches unity in contrast to the population inversion and the Renyi entropy,  $P(t) = \text{Tr}[\rho^2]$ , which can be used as a measure of system purity. For the case of coherent states the Renyi entropy revives completely [see Fig. 3(a)], in agreement with our estimations. An interesting fact is that even for the thermal distribution at  $\phi = \pi$  the entropy revives completely; that is, the system “becomes” pure [Fig. 3(b)].

In conclusion, we have demonstrated the fundamental role of the relative phase of the fields for creating entanglement in a two distinguishable qubit system of trapped atoms or ions. We have shown that, only in the case of zero relative phase, the dynamics of the system exhibits Rabi oscillations and does not depend on the motional states. In general, the dynamics is qualitatively different. There are collapses and revivals in the dynamics of the internal states of the qubits when the phonons of the trap are in a coherent state, and the dynamics is chaotic for a thermal distribution of the phonons, except when the relative phase is zero or  $\pi$ . Since coherent distributions experience full revivals with phase-controlled Rabi frequencies, we believe they could be used as two-qubit gates, with the additional advantage that the speed of the gate could be easily controlled.

The phase-induced collapse and revival of entanglement could be experimentally observed with current technology. The most difficult part in the setup is the ability to address independently the transitions in the qubit system. We believe that the first potential candidates are trapped ions in inhomogeneous magnetic fields [23,24] and Rydberg atoms in ponderomotive optical lattices [25]. The energy shifts due to the effective spin-spin coupling can vary from several Hz, as in the modified ion trap proposed by Mintert and Wunderlich [23], up to tens of MHz for Rydberg atoms [25]. By choosing magnetic sublevels of the ions (atoms) for the qubit, the effect of decoherence (spontaneous decay) can be neglected on the time scale of an order of few milliseconds or even seconds [7,8]. Using Rabi frequencies  $\sim 100$  kHz we predict up to six almost perfect revivals during  $20\text{--}22\ \mu\text{s}$  for a coherent state of phonons with average number  $\bar{n} = 10$ . Novel developments in quantum information processing based on quantum dots and superconducting qubits could also have suitable parameters to observe these effects [26]. The importance of the phase shows that additional care should be taken over the relative phase of the fields when the distinguishable qubits are not

in a single Fock state. The phase should be locked to zero if one wants to apply a  $\pi$ -pulse technique for quantum logic operations, since even a small change in the phase introduces phonon-induced decoherence in the system dynamics.

The authors thank Chris Monroe, Luming Duan, Georg Raithel, Paul Haljan, and Winfried Hensinger for helpful, stimulating discussions. I. R. S. acknowledges financial support from the Dirección General de Investigación of Spain under Project No. BQU2002-00173.

- 
- [1] J. I. Cirac and P. Zoller, Phys. Rev. Lett. **74**, 4091 (1995).
  - [2] J. I. Cirac and P. Zoller, Nature (London) **404**, 579 (2000).
  - [3] C. A. Sackett *et al.*, Nature (London) **404**, 256 (2000).
  - [4] D. Kielpinski, C. Monroe, and D.J. Wineland, Nature (London) **417**, 709 (2002).
  - [5] F. Schmidt-Kaler *et al.*, Nature (London) **422**, 408 (2003).
  - [6] D. Leibfried *et al.*, Nature (London) **422**, 412 (2003).
  - [7] K. Mølmer and A. Sørensen, Phys. Rev. Lett. **82**, 1835 (1999).
  - [8] A. Sørensen and K. Mølmer, Phys. Rev. Lett. **82**, 1971 (1999).
  - [9] A. Sørensen and K. Mølmer, Phys. Rev. A **62**, 022311 (2000).
  - [10] V.S. Malinovsky and I.R. Solá, Phys. Rev. Lett. **93**, 190502 (2004); Phys. Rev. A **70**, 042304 (2004); **70**, 042305 (2004); Quantum Inf. Comput. **5**, 364 (2005).
  - [11] P.W. Brumer and M. Shapiro, *Principles of the Quantum Control of Molecular Processes* (Wiley & Sons, Hoboken, 2003).
  - [12] E.T. Jaynes and F.W. Cummings, Proc. IEEE **51**, 89 (1963); M. Tavis and F.W. Cummings, Phys. Rev. **170**, 379 (1968).
  - [13] B.W. Shore and P.L. Knight, J. Mod. Opt. **40**, 1195 (1993).
  - [14] For Raman excitation schemes the Rabi frequency can be replaced by the effective Rabi frequency.
  - [15] D. Jaksch *et al.*, Phys. Rev. Lett. **85**, 2208 (2000); M.D. Lukin *et al.*, *ibid.* **87**, 037901 (2001).
  - [16] X. Li *et al.*, Science **301**, 809 (2003).
  - [17] M.O. Scully and M.S. Zubairy, *Quantum Optics* (Cambridge University Press, Cambridge, 1997).
  - [18] S. Hill and W.K. Wootters, Phys. Rev. Lett. **78**, 5022 (1997).
  - [19] W.K. Wootters, Phys. Rev. Lett. **80**, 2245 (1998).
  - [20] P. Runqta, V. Buzek, C.M. Caves, M. Hillery, and G.J. Milburn, Phys. Rev. A **64**, 042315 (2001).
  - [21] T. Yu and J.H. Eberly, Phys. Rev. B **66**, 193306 (2002).
  - [22] T. Yu and J.H. Eberly, Phys. Rev. B **68**, 165322 (2003).
  - [23] F. Mintert and C. Wunderlich, Phys. Rev. Lett. **87**, 257904 (2001).
  - [24] D. Mc Hugh and J. Twamley, Phys. Rev. A **71**, 012315 (2005).
  - [25] S.K. Dutta *et al.*, Phys. Rev. Lett. **85**, 5551 (2000).
  - [26] A. Wallraff *et al.*, Nature (London) **431**, 162 (2004).

## Abstract

In this paper, the dynamics of entanglement is investigated in the presence of a noisy environment. We reveal its revival behavior and probe the mechanisms of this behavior via an information-theoretic approach. By analyzing the correlation distribution and the information flow within the composite system including the qubit subsystem and a noisy environment, it has been found that the subsystem-environment coupling can induce the quasi-periodic entanglement revival. Furthermore, the dynamical relationship among tripartite correlations, bipartite entanglement and local state information is explored, which provides a new insight into the non-Markovian mechanisms during the evolution.

## Introduction

---

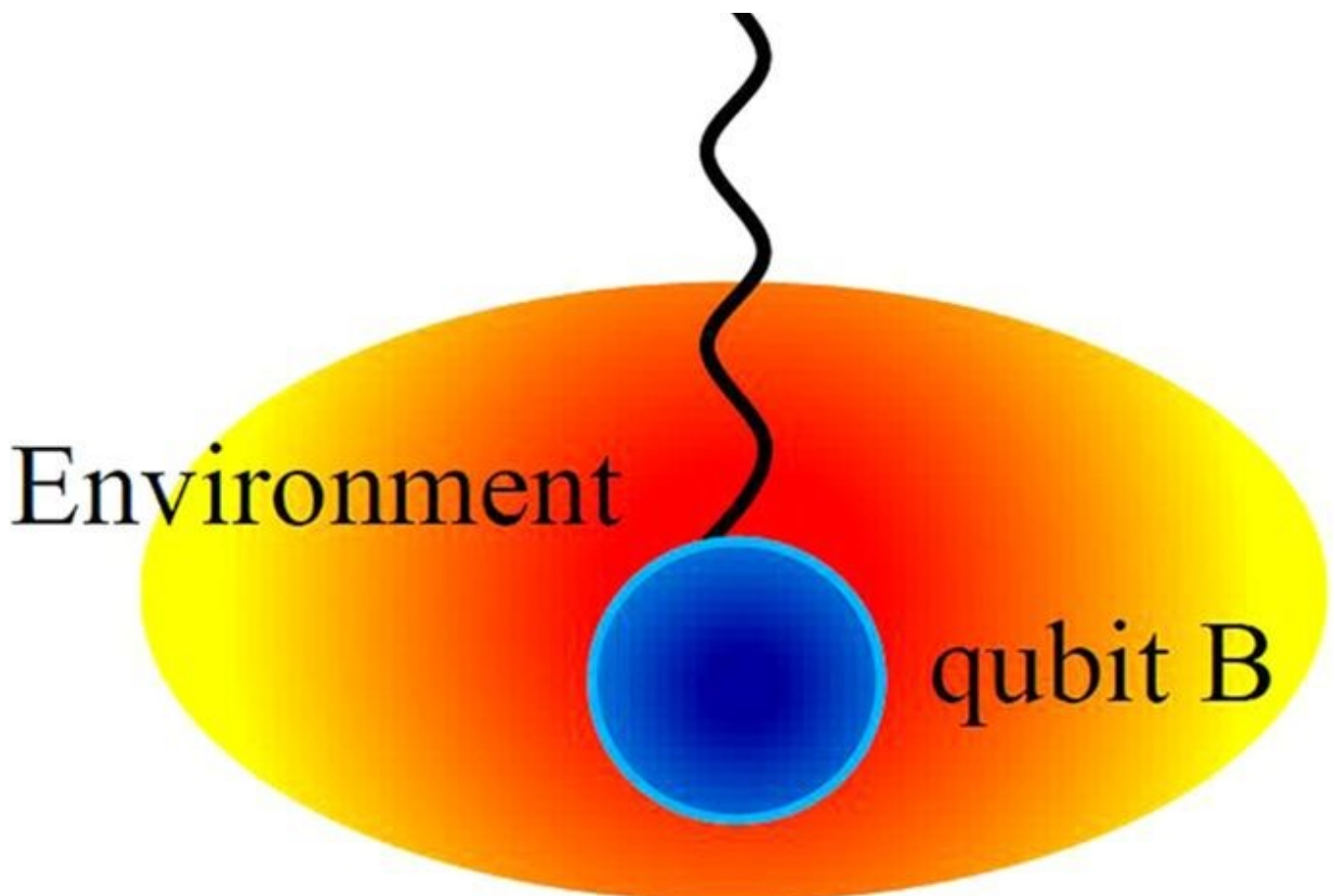
As it is well known, the existence of quantum correlations in composite systems is recognized as one of the most fundamental features of the quantum theory, which can distinguish the quantum realm from the classical one<sup>1,2,3,4</sup>. Conceptually,

interactions between the quantum system and environment.

On the other hand, it has been verified that the entanglement in an open quantum system is characterized by some specific phenomena, such as sudden death and revival within the noisy environments<sup>20,21,22,23,24,25</sup>. Mazzola *et al.* have found that the revivals of entanglement after a finite time period of complete disappearance can be expected when the system is coupled with a common non-Markovian environment. Up to now, a few interpretations of these revivals have been offered: one of the interpretations is that quantum memory of the environment can inherently influence on the coherence of quantum system<sup>26,27</sup>; another is that the environment is considered as a control device, and the interactions between quantum system and non-Markovian environment can create quantum correlation<sup>28,29,30,31,32,33</sup>. Here, we will focus on pursuing the intrinsic mechanisms concerning the revivals of entanglement.

In this paper, we will explore the non-Markovian mechanisms of the revivals of environment by means of the information-theoretic point of view. It turns out that the dynamical interplay between quantum subsystem and noisy environment can induce the quasi-periodic entanglement revivals and information flows. Furthermore, we observe explicit dynamical relationships among the genuine tripartite correlations, bipartite entanglement and local state information. At last, we provide the origin of these relationships in terms of the flow of information among the different constituents involved in the composite system.

environment is in the vacuum state. For clarity, the model sketch of the total system is depicted in Fig. 1, where the noisy environment is turned to a non-Markovian environment which can be realized by an electromagnetic field with a single-mode cavity. In fact, the model can be viewed as a tripartite composite system, one part composed by the two qubits and the other part by the non-Markovian environment, which can be similarly treated as a qubit.



The two qubits are initially entangled and a local non-Markovian environment only interacts with the qubit  $B$ , whereas qubit  $A$  is isolated.

In this case, we consider the dynamical map for the single qubit coupled with the local non-Markovian environment, which can be described by the interaction Hamiltonian<sup>23</sup>

$$H = \omega_0 \sigma_+ \sigma_- + \sum_i \omega_i b_i^\dagger b_i + (\sigma_+ B + \sigma_- B^\dagger), \quad (1)$$

non-Markovian environment interacting with the qubit. In ref. 34, the local non-Markovian environment at zero temperature can be quantized as an electromagnetic field in a high-Q cavity with the following effective spectral density

$$J(\omega) = \frac{1}{2\pi} \frac{\gamma_0 \lambda^2}{(\omega_0 - \omega)^2 + \lambda^2}, \quad (2)$$

where the parameters  $\lambda$  and  $\gamma_0$  define the spectral width of the environment and the decay rate of the excited state of the qubit, respectively, linked with the environment correlation time  $\tau_B$ , the relaxation time  $\tau_R$  by  $\tau_B \approx 1/\lambda$  and  $\tau_R \approx 1/\gamma_0$ . We provide the detailed proofs of this quantization in the part of Methods. Particularly, their relative magnitudes typically determine a Markovian ( $\lambda > 2\gamma_0$ ) and a non-Markovian ( $\lambda < 2\gamma_0$ ) regime, respectively<sup>35</sup>. We will focus on the non-Markovian regime in terms of  $\lambda = 0.1$  and  $\gamma_0 = 1$  in the remainder of our work.

In the following, we use the general notation  $\{|0\rangle, |1\rangle\}$  as the computational basis of the qubit. Then, the dynamical map for the single qubit evolved within the non-Markovian regime can be described by the reduced density matrix<sup>23,36</sup>

$$\rho(t) = \begin{pmatrix} \rho_{00}(0)P_t & \rho_{01}(0)\sqrt{P_t} \\ \rho_{10}(0)\sqrt{P_t} & \rho_{11}(0) + \rho_{00}(0)(1 - P_t) \end{pmatrix}, \quad (3)$$

$P_t$  is an oscillation term describing the fact that the decay of the qubit' excited state is induced by the interaction between the qubit subsystem and the environment. For the effective spectral density  $J(\omega)$  in Eq. (2), within the non-Markovian regime  $P_t$  can be

Upon the above preliminaries, we now proceed by discussing about the revivals of entanglement within the local non-Markovian environment. In this regard, the initial state is prepared in the Bell-like state

$$|\varphi\rangle_{AB} = \alpha|01\rangle + \sqrt{1 - \alpha^2}|10\rangle. \quad (5)$$

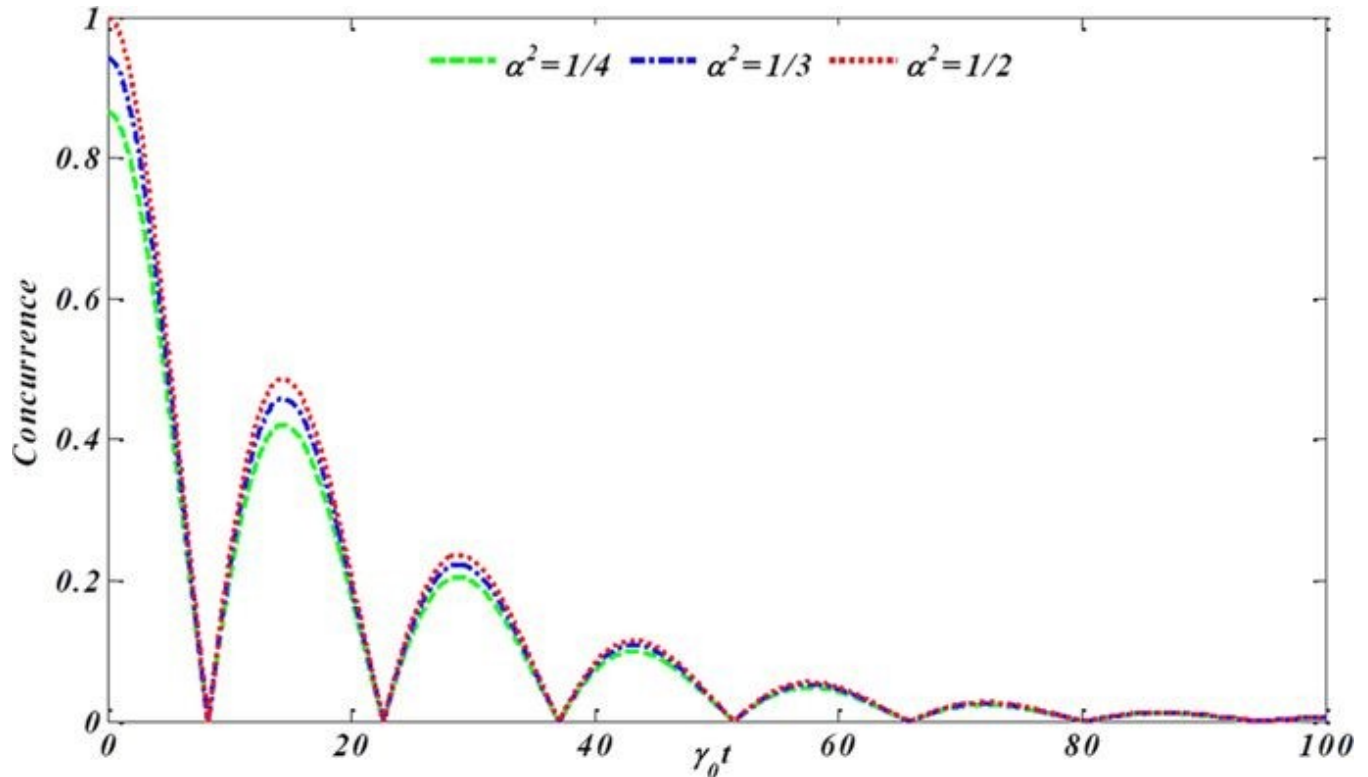
The state is maximally entangled when the condition  $|\alpha| = 1/\sqrt{2}$  is satisfied.

When only qubit B interacts with the local non-Markovian environment E, we can obtain the time-evolved state of the composite system in terms of the reduced density matrix for the single qubit shown in Eq. (3) as

$$|\varphi(t)\rangle_{ABE} = \alpha\sqrt{P_t}|010\rangle + \alpha\sqrt{1 - P_t}|001\rangle + \sqrt{1 - \alpha^2}|100\rangle. \quad (6)$$

By taking the partial trace of  $|\varphi(t)\rangle_{ABE}$  over the degrees of freedom of the environment E, one can readily obtain the reduced density matrix  $\rho_{AB}(t)$  for the qubit subsystem. Subsequently, we will concentrate on observing the dynamics of its entanglement. In this work, the Wootters' concurrence  $C(\rho) = \max \{0, \sqrt{\xi_1} - \sqrt{\xi_2} - \sqrt{\xi_3} - \sqrt{\xi_4}\}$  is employed as the measurement of the entanglement<sup>6</sup>. The parameters  $\xi_i$  are the decreasing eigenvalues of matrix  $\rho\tilde{\rho}$ , where  $\tilde{\rho} = (\sigma_y^A \otimes \sigma_y^B)\rho^*(\sigma_y^A \otimes \sigma_y^B)$  is the spin-flip matrix.

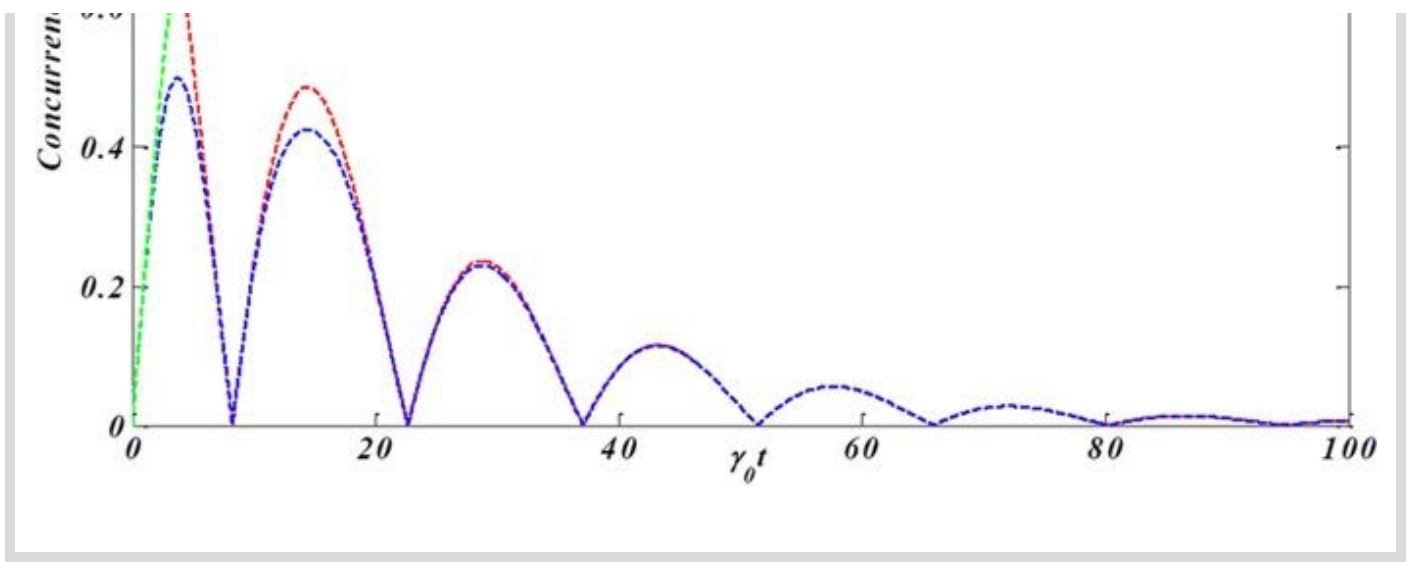
In Fig. 2, we plot the dynamics behaviors of concurrence  $C(\rho_{AB}(t))$  for the qubit subsystem as a function of the scaled time  $\gamma_0 t$  within the non-Markovian regime for the different state parameter  $\alpha$ . It has been shown that the concurrence exhibits damped



### Mechanisms of entanglement revivals

In this section, we aim to explore the mechanism of the entanglement revival via an information-theoretic approach. The composite system illustrated in Fig. 1 can be described by a standard decoherence paradigm of a quantum system (qubit A) correlated with a measurement apparatus (qubit B) which in turn interacts with an environment (E)<sup>37,38,39</sup>. That is to say, the environment can also affect the qubit A via the qubit B. Then, we can divide the composite system  $|\varphi\rangle_{ABE}$  into three bipartite subsystems, namely, AB, AE and BE. To explore the intrinsic mechanisms, we will mainly focus on how the entanglement is distributed among all the bipartite constituents of  $|\varphi\rangle_{ABE}$  during the evolution. The corresponding flow of information

$C_{AE}$  arise immediately when the concurrence  $C_{AB}$  decreases. Moreover,  $C_{AB}$  and  $C_{AE}$  show a striking opposition behavior in the limit of finite time, such that the maxima of  $C_{AB}$  coincides with the minima of  $C_{AE}$ , and vice versa. On the other hand,  $C_{AB}$  and  $C_{BE}$  behaviors are the similar each other in the most of the evolution. It deserves noting that the decrease of  $C_{AE}$  is not enough to compensate for the increase of  $C_{AB}$  or  $C_{BE}$  in the course of the first revival of  $C_{AB}$ . Next, we will explicitly give our explanation for this. To do so, we will probe the flow of information, searching for a possible relation between bipartite entanglement and genuine tripartite correlations present in the composite system.



In this context, we use a recently introduced measure of genuine tripartite correlations<sup>40,41,42,43</sup>. Given a tripartite system {A,B,E}, the genuine tripartite correlations  $v(\rho_{ABE})$  reads<sup>44</sup>

$$v(\rho_{ABE}) = I(\rho_{ABE}) - I_{loc}(\rho_i) - I_{max}(\rho_{ij}), \quad (7)$$

where

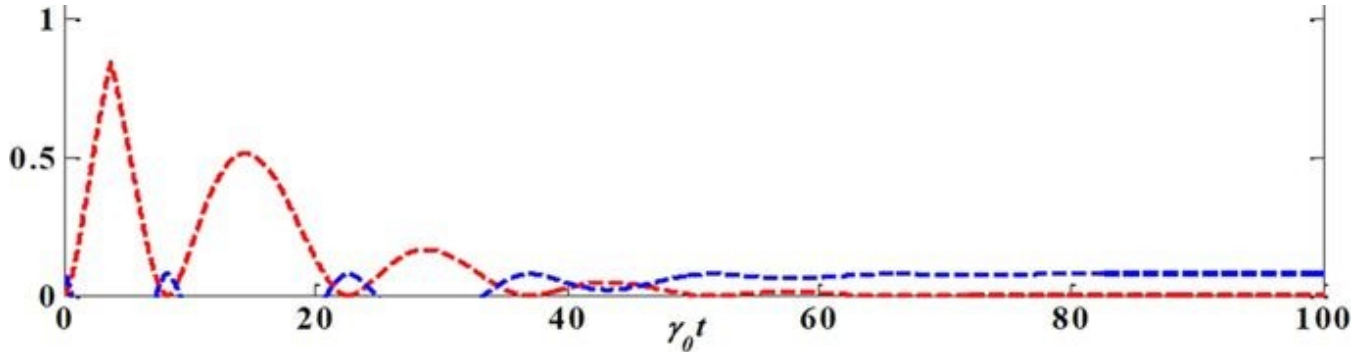
$$I(\rho_{ABE}) = \ln d - S(\rho_{ABE}) \quad (8)$$

is the total state information measured by the mutual information living in the Hilbert space of dimension  $d$  with the von Neumann entropy  $S(\bullet)$ ,

$$I_{loc}(\rho_i) = I(\rho_A) + I(\rho_B) + I(\rho_E) \quad (9)$$

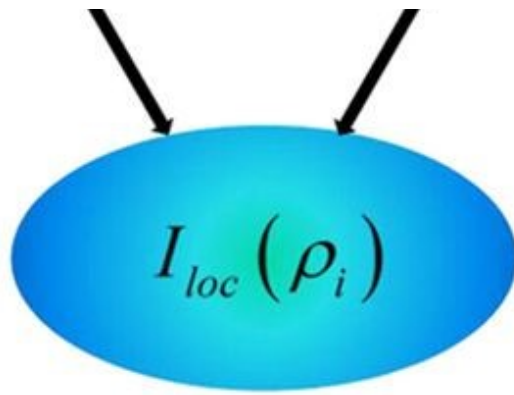
information stored locally in each part, the maximal bipartite information in the system and its genuine tripartite correlations.

Next, let us analyze the flow of information among all the constituents for our composite system. The dynamical evolution of all the relevant quantities involved in Eq. (7) versus  $\gamma_0 t$  within the non-Markovian regime is shown in Fig. 4. First of all, the total state information measured by  $I(\rho_{ABE})$  always keeps a constant value because the composite system is closed. Secondly, the information is stored in the bipartite, genuine tripartite correlations and/or local state information, which, in particular, is periodically transferred back and forth among them. Finally, more importantly, the maximal bipartite correlations  $I_{\max}(\rho_{ij})$  and the genuine tripartite correlations  $v(\rho_{ABE})$  show a striking opposition behavior, i.e. the information stored in the  $v(\rho_{ABE})$  transfers to the  $I_{\max}(\rho_{ij})$ , which induces the revival of entanglement.



Genuine tripartite correlations  $u(\rho_{ABE})$ , maximal bipartite correlations  $I_{\max}(\rho_{ij})$ , local state information  $I_{loc}$  and total state information  $I(\rho_{ABE})$  versus the scaled time  $\gamma_0 t$  within the non-Markovian regime for the maximal initial state  $\alpha = 1/\sqrt{2}$ .

To describe how the information flows among all constituents of the composite system we shall reanalyze its configuration. It turns out that  $v(\rho_{ABE})$  is shared among three different subsystems: two qubit-subsystems and noisy environment. It is worth noting that  $I_{\max}(\rho_{ij})$  is a hybrid quantity since it may or may not involve the subsystem E during maximization of any possible two-party reduced states. Moreover,  $I_{loc}(\rho_i)$  is a manifest form of information stored in the system. On the other hand,  $I_{loc}(\rho_i)$  can affect dynamics of  $I_{\max}(\rho_{ij})$  and  $v(\rho_{ABE})$  with certainty, due to the case that the local information stored in each party can evolve into bipartite and genuine tripartite correlations. At the same time, the bipartite correlations  $I(\rho_{AE})$ ,  $I(\rho_{AB})$  and  $I(\rho_{BE})$  can also affect the dynamics of  $v(\rho_{ABE})$  or  $I_{loc}(\rho_i)$ . To sum up, all of them can transform each other and the corresponding flow of information is shown in Fig. 5.



To attain a better quantitative understanding the information flow, we here will study the derivatives of three quantities  $\frac{dv(\rho_{ABE})}{dt}$ ,  $\frac{dI_{max}(\rho_{ij})}{dt}$  and  $\frac{dI_{loc}(\rho_i)}{dt}$ . Particularly, during their evolutions there are two consecutive time-intervals, namely  $T^{(1)} = [0, t^*]$  and  $T^{(2)} = [t^*, t^M]$ , which are particularly imperative, with  $t^*$  being the time instant when the first maximum of  $v(\rho_{ABE})$  is reached and  $t^M$  is the instant of the subsequent minimum of  $v(\rho_{ABE})$ . Having this in mind, one can obtain the explicit expressions of these derivatives in each time interval. Note that the two-qubit system and noisy environment are initially decoupled, such that the initial amount of correlations present in the overall system depends only on the qubit subsystem. So, in the interval  $T^{(1)}$  the maximal bipartite correlations is  $I(\rho_{AB})$  and  $\frac{dS(\rho_{ABE})}{dt} = 0$  (total system is closed), then

$$\begin{aligned}\frac{dI_{loc}(\rho_i)}{dt} &= -\frac{d}{dt}S(\rho_A) - \frac{d}{dt}S(\rho_B) - \frac{d}{dt}S(\rho_E), \\ \frac{dI_{max}(\rho_{ij})}{dt} &= \frac{d}{dt}S(\rho_A) + \frac{d}{dt}S(\rho_B) - \frac{d}{dt}S(\rho_{AB}), \\ dv(\rho_{ABE}) &= d \dots \quad d \dots \quad \dots\end{aligned}$$

interval  $T^{(2)}$ , so that

$$\begin{aligned}\frac{dv(\rho_{ABE})}{dt} &= \frac{d}{dt}S(\rho_B) + \frac{d}{dt}S(\rho_{AE}), \\ \frac{dI_{\max}(\rho_{ij})}{dt} &= \frac{d}{dt}S(\rho_A) + \frac{d}{dt}S(\rho_E) - \frac{d}{dt}S(\rho_{AE}), \\ \frac{dI_{loc}(\rho_i)}{dt} &= -\frac{d}{dt}S(\rho_A) - \frac{d}{dt}S(\rho_B) - \frac{d}{dt}S(\rho_E).\end{aligned}\quad (12)$$

These equations can quantify the information fluxes  $v(\rho_{ABE}) \rightarrow I_{\max}(\rho_{ij})$ ,  $v(\rho_{ABE}) \rightarrow I_{loc}(\rho_i)$  and  $I_{\max}(\rho_{ij}) \rightarrow I_{loc}(\rho_i)$ . After  $t^M$ , due to the quasi-periodicity of the dynamics, all the information fluxes repeat new cycles.

## Conclusions

---

Here, we have investigated the dynamics behaviors of entanglement when the single qubit of bipartite subsystem interacts with a local non-Markovian environment. It turns out that the qubit subsystem-environment coupling can induce damped oscillations and revivals for the entanglement, which gradually decay to a stable value. Furthermore, by analyzing the correlation distribution and the flow of information among all the constituents of the composite system, we have illustrated the non-Markovian mechanisms of these revival behaviors. To gain a quantitative understanding of the information flow, explicit dynamical relationships among the genuine tripartite correlations, bipartite correlations and local state information via the methodologies of

## Proofs of the quantization for the local non-Markovian environment

From refs 19 and 30 we find that the non-Markovian environment can be actually quantized as the single-mode electromagnetic field in the high-Q cavity with an effective spectral density at zero temperature. Usually, the dynamics of the system-environment interactions can be described by master equations derived from perturbation theory.

To quantize the electromagnetic field in the high-Q cavity, it is convenient to begin with the classical description of the field based on the Maxwell's equations. For simplicity, we do not list them here. The classical Hamiltonian for the electromagnetic field in a cavity resonator is<sup>45</sup>

$$H = \frac{1}{2} \sum_i \left( m_i \omega_i^2 q_i^2 + m_i \dot{q}_i^2 \right) = \frac{1}{2} \sum_i \left( m_i \omega_i^2 q_i^2 + \frac{p_i^2}{m_i} \right), \quad (13)$$

where  $q_i (i = 1, 2, 3, \dots)$  is the mode amplitude,  $p_i = m_i \dot{q}_i$  is the canonical momentum of the  $i$ th mode,  $m_i$  is a constant with the dimension of mass, and  $\omega_i = i\pi c/L$  is the cavity eigenfrequency with  $L$  the cavity resonator length.

The present problem with respect to the quantization of the electromagnetic field in the high-Q cavity can be solved by identifying  $q_i$  and  $p_i$  as operators which obey the commutation relations

$$[q_i, p_{i'}] = i\hbar \delta_{ii'}, \quad [q_i, q_{i'}] = [p_i, p_{i'}] = 0. \quad (14)$$

with the commutation relations between  $a_i$  and  $a_i^\dagger$

$$[a_i, a_{i'}^\dagger] = \delta_{ii'}, \quad [a_i, a_{i'}] = [a_i^\dagger, a_{i'}^\dagger] = 0. \quad (17)$$

For the single-mode electromagnetic field, i.e.,  $i = 1$ , the Hamiltonian is

$$H = \hbar\omega \left( a_1^\dagger a_1 + \frac{1}{2} \right) \quad (18)$$

with the commutation relations  $[a_1, a_1^\dagger] = 1$ . Subsequently, by solving the Schrödinger equation one can obtain the eigenvalues and eigenstates of the Hamiltonian shown in Eq. (18). Therefore, it turns out that one can achieve the quantization of the local non-Markovian environment.

A natural way to describe the dynamics of an open quantum system is to regard it as an interaction between the system and environment, which together form a closed quantum system. The dynamics of the closed quantum system can be described by a unitary transform. In general, based on the general notation  $\{|0\rangle, |1\rangle\}$  the dynamical map for the single qubit evolved in environment can be described as<sup>1</sup>

$$U(t)|0\rangle_S|0\rangle_E \rightarrow |0\rangle_S|0\rangle_E, \quad (19)$$

$$U(t)|1\rangle_S|0\rangle_E \rightarrow \sqrt{P_t}|1\rangle_S|0\rangle_E + \sqrt{1-P_t}|0\rangle_S|1\rangle_E, \quad (20)$$

where  $U(t)$  is the time evolution operator of the environment,  $|0\rangle_E$  indicates the

$$\rho(t) = U(t)(\rho_S \otimes \rho_E)U^\top(t). \quad (21)$$

One can obtain the reduced density matrix for any bipartite subsystems by performing a partial trace over the remaining subsystem.

Moreover, the entanglement is quantified by the Wootters' concurrence. For the X-type structures of the density matrix, we have a simpler expression<sup>19,46</sup>

$$C(\rho^X) = 2 \max \left\{ 0, \sqrt{\rho_{14}\rho_{41}} - \sqrt{\rho_{22}\rho_{33}}, \sqrt{\rho_{23}\rho_{32}} - \sqrt{\rho_{11}\rho_{44}} \right\}, \quad (22)$$

where  $\rho_{ij}$  are the elements of density matrix  $\rho^X$ . Based on the definition in Eq. (22), one can derive the concurrence for different bipartite subsystems,

$$\begin{aligned} C_{AB} &= 2 \max \{ 0, \alpha \sqrt{P_t(1-\alpha^2)} \}, \\ C_{AE} &= 2 \max \{ 0, \alpha \sqrt{(1-P_t)(1-\alpha^2)} \}, \\ C_{BE} &= 2 \max \{ 0, \alpha^2 \sqrt{P_t(1-P_t)} \}. \end{aligned} \quad (23)$$

From the above equations, one can readily find that the bipartite concurrences  $C_{ij}$  are only the functions of state parameter  $\alpha$  and environment strength  $P_t$ . And  $C_{ij}$  can exhibit the distribution of entanglement among the different bipartite subsystems. Furthermore, we can also derive the genuine tripartite correlations  $v(\rho_{ABE})$  for the tripartite composite system {A,B,E}, namely,

$$v(\rho_{ABE}) = \min \{ S(\rho_{AB}) + S(\rho_E), S(\rho_{BE}) + S(\rho_A), S(\rho_{AE}) + S(\rho_B) \} - S(\rho_{ABE}), \quad (24)$$

where  $S(\rho) = -\text{Tr}(\rho \log_2 \rho)$  is the von Neumann entropy. So we can get the desired

## References

---

1. Nielsen, M. A. & Chuang, I. L. *Quantum Computation and Quantum Information*. Cambridge University Press, Cambridge, England (2000).
  2. Einstein, A., Podolsky, B. & Rosen, N. Can quantum-mechanical description of physical reality be considered complete ? *Phys. Rev.* **47**, 777 (1935).
  3. Niset, J. & Cerf, N. J. Multipartite nonlocality without entanglement in many dimensions. *Phys. Rev. A* **74**, 052103 (2006).
  4. Piani, M., Horodecki, P. & Horodecki, R. No-Local-Broadcasting Theorem for Multipartite Quantum Correlations. *Phys. Rev. Lett.* **100**, 090502 (2008).
-

- 
8. Harrow, A. Hayden, P. & Leung, D. Superdense coding of quantum states. *Phys. Rev. Lett.* **92**, 187901 (2004).
9. Lo, H. K., Curty, M. & Tamaki, K. Secure quantum key distribution. *Nat. Photonics* **8**, 595–604 (2014).
10. Wang, D. et al. Efficient and faithful remote preparation of arbitrary three- and four-particle W-class entangled states, *Quantum Inf. Process.* **14**, 2135–2151 (2015).
11. Wang, D. et al. Practical single-photon-assisted remote state preparation with non-maximally entanglement. *Quantum Inf. Process.* doi: 10.1007/s11128-016-1346-4
12. Yu, T. & Eberly, J. H. Sudden Death of Entanglement. *Science* **323**, 598 (2009).
13. Modi, K. et al. The classical-quantum boundary for correlations: discord and related measures. *Rev. Mod. Phys.* **84**, 1655 (2012).
14. Xu, J. S. et al. Experimental investigation of classical and quantum correlations under decoherence. *Nat. Commun.* **1**, 7 (2010).
15. Werlang, T. et al. Robustness of quantum discord to sudden death. *Phys. Rev. A* **80**, 024103 (2009).
-

19. Shi, J. D. et al. Revival and robustness of Bures distance discord under decoherence channels. *Phys. Lett. A* **380**, 843–847 (2016).
20. Buscemi, F. & Bordone, P. Time evolution of tripartite quantum discord and entanglement under local and nonlocal random telegraph noisy. *Phys. Rev. A* **87**, 042310 (2013).
21. Bordone, P., Buscemi, F. & Benedetti, C. Effect of Markova and non-Markova classical noisy on entanglement dynamics. *Fluct. Noisy Lett.* **11**, 1242003 (2012).
22. Benedetti, C. et al. Effect of classical environment noisy on entanglement and quantum discord dynamics. *Int. J. Quantum Inf.* **10**, 1241005 (2012).
23. Bellomo, B., Franco, R. Lo. & Compagno, G. Non-Markovian Effects on the Dynamics of Entanglement. *Phys. Rev. Lett.* **99**, 160502 (2007).
24. Bellomo, B. et al. Entanglement trapping in structured environments. *Phys. Rev. A* **78**, 060302(R) (2008).
25. Mazzola, L. et al. Sudden death and sudden birth of entanglement in common structured reservoirs. *Phys. Rev. A* **79**, 042302 (2009).
26. Franco, R. L. et al. Revival of quantum correlations without system-environment back-action. *Phys. Rev. A* **85**, 032318 (2012).
27. Xu, J. S. et al. Experimental recovery of quantum correlations in absence of

structured reservoirs. *Ann. Phys.* **327**, 2343–2353 (2012).

31. Ding, Z. Y., He, J. & Ye, L. Protecting tripartite entanglement in non-Markovian environments via quantum partially collapsing measurements. *Quantum Inf. Process.* doi: 10.1007/s11128-016-1342-8.
32. Rivas, Á., Huelga, S. F. & Plenio, M. B. Quantum non-Markovianity: characterization, quantification and detection. *Rep. Prog. Phys.* **77**, 094001 (2014).
33. Romero, K. M. F. & Franco, R. Lo Simple non-Markovian microscopic models for the depolarizing channel of a single qubit. *Phys. Scr.* **86**, 065004 (2012).
34. Garraway, B. M. Nonperturbative decay of an atomic system in a cavity. *Phys. Rev. A* **55**, 2290 (1997).
35. Fanchini, F. F. et al. Non-Markovian dynamics of quantum discord. *Phys. Rev. A* **81**, 052107 (2010).
36. Maniscalco, S. & Petruccione, F. Non-Markovian dynamics of a qubit. *Phys. Rev. A* **73**, 012111 (2006).
37. Zurek, W. H. Decoherence, einselection, and the quantum origins of the classical. *Rev. Mod. Phys.* **75**, 715 (2003).

- 
41. Zhao, L. M. et al. Genuine correlations of tripartite system, *Quantum Inf. Process* **12**, 2371–2383 (2013).
- 
42. Bennett, C. H. et al. Postulates for measures of genuine multipartite correlations. *Phys. Rev. A* **83**, 012312 (2011).
- 
43. Maziero, J. & Zimmer, F. M. Genuine multipartite system-environment correlations in decoherent dynamics. *Phys. Rev. A* **86**, 042121 (2012).
- 
44. Costa, A. C. S., Angelo, R. M. & Beims, M. W. Monogamy and backflow of mutual information in non-Markovian thermal baths, *Phys. Rev. A* **90**, 012322 (2014).
- 
45. Scully, O. M. & Zubairy, M. S. *Quantum optics*. Cambridge University Press, Cambridge, England (1997).
- 
46. Wang J. C. & Jing, J. L. System-environment dynamics of X-type states in noninertial frames. *Ann. Phys.* **327**, 283–291 (2015).
- 

## Acknowledgements

This work was supported by the National Science Foundation of China under Grants Nos 61275119, 11575001 and 11247256, and also by the fund of Anhui Provincial Natural Science Foundation (Grant No. 1508085QF139).

## About this article

---

### Publication history

**Received**

17 March 2016

**Accepted**

07 July 2016

**Published**

10 August 2016

**DOI**

<https://doi.org/10.1038/srep30710>



## 8. Effect of noise on entanglement

**Abstract:** Noise can brake entanglement above a noise threshold.

**Keywords:** Noise, noise threshold

## Effects of Noise on Entanglement Dynamics in Atom-Field Interactions

Hünkar Kayhan\*

Department of Physics, Abant Izzet Baysal University, Bolu-14280, Turkey

(Received on 01 April, 2008)

The entanglement dynamics in a system of the interaction of an atom with a single-mode cavity field in the presence of noise is studied by the Jaynes-Cummings model. Random phase telegraph noise is considered as the noise in the interaction and an exact solution to the model under this noise is obtained. The obtained solution is used to investigate the entanglement dynamics of the atom-field interaction. The mutual entropy is adopted for the quantification of the entanglement in the interaction. It is found that the entanglement is a non monotonic function of the intensity of the noise. The degree of the entanglement decreases to a minimum value for an optimal intensity of the noise and then increases for a sufficiently large intensity.

Keywords: Entanglement; Random phase telegraph noise; Mutual entropy

### 1. INTRODUCTION

Entanglement can display nonlocal correlations between quantum systems that have no classical counterpart. As a physical resource it plays a key role in Quantum Information Processing (QIP) [1–3]. Its preparation is thus a primary goal of this field. Real quantum systems will unavoidably interact with their surrounding environments. The main problem that must be overcome in QIP is decoherence, an effect that results from the coupling of the system to its surroundings or noise described by the stochastic processes associated with the system. The influence of noise (jump-type) on the atom-field interactions was first introduced by Burshtein [4, 5] in quantum optics. The simplest model of such jump-like processes is the two-state random telegraph. Eberly *et al* [6, 7] discussed laser-atom interactions that are subjected to two-state random (phase and frequency) telegraph noise.

The interaction of a two-level atom with a single-mode field which makes a single-photon transitions in an ideal cavity is described by the Jaynes-Cummings model (JCM) [8]. An employment of noise into the JCM was studied by Joshi *et al* [9–12]. In these works, the authors have treated the incorporation of noise into the JCM as the stochastic fluctuations in the atom-field coupling parameter (that is assumed to fluctuate in phase or in amplitude) with following possible physical reasons: The stochastic fluctuations associated with the coupling parameter in the cavity quantum electrodynamics may presumably be inherited from several reasons such as due to the source of the single-mode coherent cavity field or due to any variation in the mechanism of the production of Rydberg atom because of the instability in the atomic vapour production. Or, the motion of an ion in a harmonic trap interacting with a standing wave or a traveling wave may introduce another possibility for introducing the JCM with the stochastic fluctuations. Because, under a particular approximation [13], the equation of the motion for the ion in the trap may reduce to a similar form with the JCM. In this case, the fluctuations in the coupling coefficient can be considered both in the amplitude and the phase of the standing wave. Another possibility

for introducing the stochastic fluctuations in the JCM is that the fluctuations of vacuum Rabi frequency or the atom-field coupling coefficient are known to wash out the trapping states in the micromaser system. Such fluctuations are possible in the case of an electric field generated by rubidium deposits at the cavity coupling holes or the electric field between the adjacent crystal domains in the cavity walls made of niobium.

In this paper, the interaction of a two-level atom with a single-mode field is studied in the environment of the random phase telegraph noise (RPTN) by the JCM [12]. By the method introduced in this reference, an exact solution to the JCM under this noise is obtained. The obtained solution is used to investigate the entanglement dynamics of the atom-field interaction. The mutual entropy is adopted for the quantification of the entanglement in the interaction.

The organization of the paper is as follows; In section 2, the formulation of the problem is obtained. The JCM with the RPTN is introduced and an exact solution to the model under this noise is presented. In section 3, the results and discussions are given. The solution obtained in the previous section is applied to a system in which the atom is initially taken in a pure state and the field initially in a thermal state. The entanglement properties of the system under the RPTN are explored. Finally, in section 4, the conclusions are presented.

### 2. THE FORMULATION OF THE PROBLEM

#### 2.1. The Model and Solution

It is considered the interaction of a two-level atom described by spin-1/2 operators  $S_{\pm}, S_z$  with a single-mode of quantized radiation field described by the annihilation and the creation operators  $a, a^{\dagger}$ . For the sake of the simplicity, it is assumed that the field is in resonance with the atomic transition frequency  $\omega_0$ . In this case, the Hamiltonian of the system under the rotating wave approximation takes the form of ( $\hbar = 1$ )

$$H = \omega_0 S_z + \omega_0 a^{\dagger} a + (g^*(t) S_{+} a + g(t) S_{-} a^{\dagger}) \quad (1)$$

in which the interaction part is

$$H_{int} = (g^*(t) S_{+} a + g(t) S_{-} a^{\dagger}) \quad (2)$$

\*Electronic address: hunkar\_k@ibu.edu.tr

where  $g(t)$  is the coupling coefficient between the atom and the field and is time-dependent. In order to employ the RPTN into the problem, the nature of  $g(t)$  is considered to be completely stochastic which is defined as

$$g(t) = g_0 e^{i\phi(t)} \quad (3)$$

where  $g_0$  is a positive real constant for the amplitude and  $\phi(t)$  is a stochastic variable which fluctuates between different ar-

bitrary phases in a manner of jumps. The jumps are separated by the time intervals called the mean dwell time. It is considered that  $\phi(t)$ 's in the neighbouring intervals are not correlated. Then, the probability for finding  $\phi$  remains at any instant is the same. Therefore,  $\phi(t)$  is undergoing random continuous change of Markov type which allows to take the average over the stochastic fluctuations.

An exact solution of the system is obtained by the method introduced by Joshi [12]

$$\begin{aligned} \rho(\tau) \exp \frac{\tau}{\tau_0} &= \int U(\phi; \tau; 0) \rho(0) U^{-1}(\phi; \tau; 0) dQ(\phi) \\ &\quad + \frac{1}{\tau_0} \int \exp\left(\frac{t}{\tau_0}\right) \int U(\phi; \tau; t) \rho(t) U^{-1}(\phi; \tau; t) dQ(\phi) dt \end{aligned} \quad (4)$$

where  $dQ(\phi) = \frac{d\phi}{2\pi}$  and  $\tau_0$  is the mean dwell time. The mean dwell is the only factor which determines the strength/insensity of the noise. The shorter the mean dwell time means the stronger/the more intense noise. In this integral equation, the statistical average is taken over the stochastic variable  $\phi(t)$ . So,  $\rho(t)$  is the noise-averaged density matrix of the system. The most general solution of Eq. (4) for the atom-field interactions with RPTN may be obtained as follows;

One can obtain the unitary transformation in atomic bases  $|e\rangle$  and  $|g\rangle$  in the interaction picture as

$$U = \begin{pmatrix} \cos(\sqrt{aa^\dagger} g_0 t) & -i \frac{\sin(\sqrt{aa^\dagger} g_0 t)}{\sqrt{aa^\dagger}} a \exp(-i\phi) \\ -i \frac{\sin(\sqrt{a^\dagger a} g_0 t)}{\sqrt{a^\dagger a}} a^\dagger \exp(i\phi) & \cos(\sqrt{a^\dagger a} g_0 t) \end{pmatrix} \quad (5)$$

The most general expression of the atom-field state at  $t = 0$  can be written as

$$\rho(0) = \sum_{m,n=0} \{ \rho_{mn}^{++}(0) |me\rangle\langle ne| + \rho_{mn}^{--}(0) |mg\rangle\langle ng| + \rho_{mn}^{+-}(0) |me\rangle\langle ng| + \rho_{mn}^{-+}(0) |mg\rangle\langle ne| \} \quad (6)$$

During the interaction, this state will evolve in time into the state

$$\rho(t) = \sum_{m,n=0} \{ \rho_{mn}^{++}(t) |me\rangle\langle ne| + \rho_{mn}^{--}(t) |mg\rangle\langle ng| + \rho_{mn}^{+-}(t) |me\rangle\langle ng| + \rho_{mn}^{-+}(t) |mg\rangle\langle ne| \} \quad (7)$$

where the diagonal elements are

$$\begin{aligned} \rho_{mn}^{++}(t) &= \langle me | \rho(t) | ne \rangle \\ \rho_{mn}^{--}(t) &= \langle mg | \rho(t) | ng \rangle \end{aligned} \quad (8)$$

and the off-diagonal elements are

$$\begin{aligned} \rho_{mn}^{+-}(t) &= \langle me | \rho(t) | ng \rangle \\ \rho_{mn}^{-+}(t) &= \langle mg | \rho(t) | ne \rangle \end{aligned} \quad (9)$$

From these terms, one may obtain the integral expressions for these elements as

$$\begin{aligned} \rho_{mn}^{++}(\tau) \exp(\tau/\tau_0) &= \rho_{mn}^{++}(0) \cos \alpha_m \tau \cos \alpha_n \tau + \rho_{m+1n+1}^{--}(0) \sin \alpha_m \tau \sin \alpha_n \tau \\ &\quad + \frac{1}{\tau_0} \int_0^\tau dt \exp(t/\tau_0) \{ \rho_{mn}^{++}(t) \cos \alpha_m (\tau-t) \cos \alpha_n (\tau-t) \\ &\quad + \rho_{m+1n+1}^{--}(t) \sin \alpha_m (\tau-t) \sin \alpha_n (\tau-t) \} \end{aligned} \quad (10)$$

$$\begin{aligned} \rho_{mn}^{--}(\tau) \exp(\tau/\tau_0) &= \rho_{mn}^{--}(0) \cos \beta_m \tau \cos \beta_n \tau + \rho_{m-1n-1}^{++}(0) \sin \beta_m \tau \sin \beta_n \tau \\ &+ \frac{1}{\tau_0} \int_0^\tau dt \exp(t/\tau_0) \{ \rho_{mn}^{--}(t) \cos \beta_m (\tau-t) \cos \beta_n (\tau-t) \\ &+ \rho_{m-1n-1}^{++}(t) \sin \beta_m \sin \beta_n (\tau-t) \} \end{aligned} \quad (11)$$

$$\begin{aligned} \rho_{mn}^{+-}(\tau) \exp(\tau/\tau_0) &= \rho_{mn}^{+-}(0) \cos \alpha_m \tau \cos \beta_n \tau \\ &+ \frac{1}{\tau_0} \int_0^\tau dt \exp(t/\tau_0) \{ \rho_{mn}^{+-}(t) \cos \alpha_m (\tau-t) \cos \beta_n (\tau-t) \} \end{aligned} \quad (12)$$

$$\begin{aligned} \rho_{mn}^{-+}(\tau) \exp(\tau/\tau_0) &= \rho_{mn}^{-+}(0) \cos \beta_m \tau \cos \alpha_n \tau \\ &+ \frac{1}{\tau_0} \int_0^\tau dt \exp(t/\tau_0) \{ \rho_{mn}^{-+}(t) \cos \beta_m (\tau-t) \cos \alpha_n (\tau-t) \} \end{aligned} \quad (13)$$

where,  $\alpha_{m-1} = \beta_m = g_0 \sqrt{m}$ .

By using the Laplace transformation technique, the following expressions from the above equations can be obtained as

$$\rho_{mn}^{++}(s) = \frac{(s+1/T)\rho_{mn}^{++}(0)[(s+1/T)^2 + \Omega_{mn}^+]}{s^4 + 3s^3/T + (2\Omega_{mn}^+ + 3/T^2)s^2 + (1/T^3 + (3\Omega_{mn}^+ - \Gamma_{mn})/T)s + A_{mn}} \quad (14)$$

$$\rho_{mn}^{--}(s) = \frac{(s+1/T)\{\rho_{mn}^{--}(0)[(s+1/T)^2 + \Theta_{mn}^+] + \rho_{m-1n-1}^{++}(0)\Lambda_{mn}\}}{s^4 + 3s^3/T + (2\Theta_{mn}^+ + 3/T^2)s^2 + (1/T^3 + (3\Theta_{mn}^+ - \Lambda_{mn})/T)s + B_{mn}} \quad (15)$$

$$\rho_{mn}^{+-}(s) = \frac{(s+1/T)\rho_{mn}^{+-}(0)[(s+1/T)^2 + \Upsilon_{mn}^+]}{s^4 + 3s^3/T + (2\Upsilon_{mn}^+ + 3/T^2)s^2 + (1/T^3 + 3\Upsilon_{mn}^+/T)s + C_{mn}} \quad (16)$$

$$\rho_{mn}^{-+}(s) = \frac{(s+1/T)\rho_{mn}^{-+}(0)[(s+1/T)^2 + \Upsilon_{mn}^-]}{s^4 + 3s^3/T + (2\Pi_{mn}^+ + 3/T^2)s^2 + (1/T^3 + 3\Pi_{mn}^+/T)s + D_{mn}} \quad (17)$$

where  $T = \tau_0$ ,  $\Omega_{mn}^\pm = \alpha_m^2 \pm \alpha_n^2$ ,  $\Gamma_{mn} = 2\alpha_m \alpha_n$ ,  $\Theta_{mn}^\pm = \beta_m^2 \pm \beta_n^2$ ,  $\Lambda_{mn} = 2\beta_m \beta_n$ , and  $\Upsilon_{mn}^\pm = \alpha_m^2 \pm \beta_n^2$  and  $\Pi_{mn}^\pm = \beta_m^2 \pm \alpha_n^2$ . And also

$$\begin{aligned} A_{mn} &= (\Omega_{mn}^+/T^2 - \Gamma_{mn}/T^2 + \Omega_{mn}^-) \\ B_{mn} &= (\Theta_{mn}^+/T^2 - \Lambda_{mn}/T^2 + \Theta_{mn}^-) \\ C_{mn} &= (\Upsilon_{mn}^+/T - (\Upsilon_{mn}^-)^2/T) \\ D_{mn} &= (\Pi_{mn}^+/T - (\Pi_{mn}^-)^2/T) \end{aligned}$$

The inverse Laplace transformation gives an exact solution to the atom-field system as

$$\rho_{mn}^{++}(t) = \sum_{j=1}^4 \frac{(\lambda_j + 1/T)[\rho_{mn}^{++}(0)[(\lambda_j + 1/T)^2 + \Omega_{mn}^+]] + \rho_{m-1n-1}^{++}(0)\Gamma_{mn}}{\prod_{k \neq j}(\lambda_j - \lambda_k)} \exp(\lambda_j t) \quad (18)$$

$$\rho_{mn}^{--}(t) = \sum_{j=1}^4 \frac{(\lambda_j + 1/T)[\rho_{mn}^{--}(0)[(\lambda_j + 1/T)^2 + \Theta_{mn}^+]] + \rho_{m-1n-1}^{++}(0)\Lambda_{mn}}{\prod_{k \neq j}(\lambda_j - \lambda_k)} \exp(\lambda_j t) \quad (19)$$

where the  $\lambda_j$ 's are the roots of the equations

$$\lambda_j^4 + 3\lambda_j^3/T + (2\Omega_{mn}^+ + 3/T^2)\lambda_j^2 + (1/T^3 + (3\Omega_{mn}^+ - \Gamma_{mn})/T)\lambda_j + A_{mn} = 0 \quad (20)$$

and

$$\lambda_j^4 + 3\lambda_j^3/T + (2\Theta_{mn}^+ + 3/T^2)\lambda_j^2 + (1/T^3 + (3\Theta_{mn}^+ - \Lambda_{mn})/T)\lambda_j + B_{mn} = 0 \quad (21)$$

respectively.

And the other two terms are

$$\rho_{mn}^{+-}(t) = \sum_{j=1}^4 \frac{(\lambda_j + 1/T)\rho_{mn}^{+-}(0)[(\lambda_j + 1/T)^2 + \Upsilon_{mn}^+]}{\prod_{j \neq k}(\lambda_j - \lambda_k)} \exp(\lambda_j t) \quad (22)$$

$$\rho_{mn}^{-+}(t) = \sum_{j=1}^4 \frac{(\lambda_j + 1/T)\rho_{mn}^{-+}(0)[(\lambda_j + 1/T)^2 + \Pi_{mn}^+]}{\prod_{j \neq k}(\lambda_j - \lambda_k)} \exp(\lambda_j t) \quad (23)$$

where the  $\lambda_j$  s are the roots of equations

$$\lambda_j^4 + 3\lambda_j^3/T + (2\Upsilon_{mn}^+ + 3/T^2)\lambda_j^2 + (1/T^3 + 3\Upsilon_{mn}^+/T)\lambda_j + C_{mn} = 0 \quad (24)$$

and

$$\lambda_j^4 + 3\lambda_j^3/T + (2\Pi_{mn}^+ + 3/T^2)\lambda_j^2 + (1/T^3 + 3\Pi_{mn}^+/T)\lambda_j + D_{mn} = 0 \quad (25)$$

respectively.

Eqs. (18), (19), (22) and (23) describe the dynamics of the atom-field interactions that are subjected to the random phase telegraph noise.

### 3. RESULTS AND DISCUSSION

The exact solution given by Eqs. (18), (19), (22) and (23) for the RPTN is now used to investigate the entanglement properties of the system. For this, the atom is initially taken in a pure state as

$$|\psi_a(0)\rangle = (\lambda|e\rangle + \sqrt{1 - |\lambda|^2}|g\rangle) \quad (26)$$

where  $\lambda$  is the atomic state distribution with  $0 \leq |\lambda| \leq 1$  and the field is initially taken in a thermal state

$$\rho_f(0) = \sum_{n=0} P_n |n\rangle \langle n| \quad (27)$$

where the thermal field at some temperature of the cavity  $Te$  with the probability distribution  $P_n$  in the number states  $|n\rangle$  being given by,

$$P_n = \frac{1}{(1 + \bar{n})} \left( \frac{\bar{n}}{1 + \bar{n}} \right)^n \quad (28)$$

where  $\bar{n} = \{e^{\beta\omega} - 1\}^{-1}$  is the initial mean photon number in the cavity,  $\beta = 1/k_B Te$  and  $k_B$  is Boltzmann's constant. In this case, the initial atom-field state at  $t = 0$  becomes

$$\rho^{af}(0) = \sum_{n=0} P_n \{ |\lambda|^2 |ne\rangle \langle ne| + (1 - |\lambda|^2) |ng\rangle \langle ng| \lambda \sqrt{1 - |\lambda|^2} |ne\rangle \langle ng| + \lambda^* \sqrt{1 - |\lambda|^2} |ng\rangle \langle ne| \} \quad (29)$$

From Eq. (29), it is clear that  $\rho_{nn}^{++}(0) = P_n |\lambda|^2$ ,  $\rho_{nn}^{--}(0) = P_n (1 - |\lambda|^2)$ ,  $\rho_{nn}^{+-}(0) = P_n \lambda \sqrt{1 - |\lambda|^2}$ ,  $\rho_{nn}^{-+}(0) = P_n \lambda^* \sqrt{1 - |\lambda|^2}$ . With these initial conditions, one can obtain the solution of the system. In this case, the atom-field system will evolve in time into the state

$$\rho^{af}(t) = \sum_{n=0} \{ \rho_{nn}^{++}(t) |ne\rangle \langle ne| + \rho_{nn}^{--}(t) |ng\rangle \langle ng| + \rho_{nn}^{+-}(t) |ne\rangle \langle ng| + \rho_{nn}^{-+}(t) |ng\rangle \langle ne| \} \quad (30)$$

The dimension of the system described by Eq. (30) is  $2 \otimes \infty$ . In fact, there is no known an entanglement measure to quant-

ify such systems. For the quantification of the entanglement

in the system, it is adopted the mutual entropy of the system  $S(A : F)$  which is defined as  $S(A : F) = S(A) + S(F) - S(AF)$ . Here,  $S(A)$  and  $S(F)$  are the entropies of the atom and the field, respectively and  $S(AF)$  is the entropy of the atom-field system. In order to calculate the entropies, the dimension of the system  $n_{dim}$  is taken in such a way that the probability distribution of the field reaches to unity approximately, that is,  $\sum_{n=0}^{n_{dim}} P_n \cong 1$  [14].

The entropy of a system is defined as

$$S = - \sum_i \lambda_i \log \lambda_i \quad (31)$$

$$\rho^a(t) = \sum_{n=0} \rho_{nn}^{++}(t) |e\rangle\langle e| + \sum_{n=0} \rho_{nn}^{--}(t) |g\rangle\langle g| + \sum_{n=0} \rho_{nn}^{+-}(t) |e\rangle\langle g| + \sum_{n=0} \rho_{nn}^{-+}(t) |g\rangle\langle e| \quad (32)$$

And the time-dependent elements of the density matrix of the field becomes

$$\rho_{nn}^f(t) = \rho_{nn}^{++}(t) + \rho_{nn}^{--}(t) \quad (33)$$

The effects of the RPTN on the entanglement dynamics of the atom-field interaction are depicted in Figs. (1)-(4).

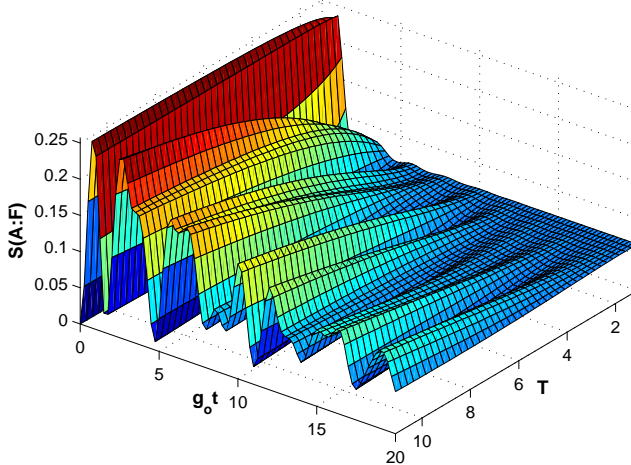


FIG. 1: The mutual entropy as the function of the time  $g_0 t$  and the mean dwell time  $T$  (in the unit of  $1/g_0$ ) for the large values of the mean dwell time.  $\lambda = 1/\sqrt{2}$  and  $\bar{n} = 0.1$ .

In Figs. (1) and (2), the mutual entropy  $S(A : F)$  of the system is plotted as the function of time  $g_0 t$  and the mean dwell time  $T$ . In Fig. (1), it is clear that the entanglement between the atom and the field reaches its maximum value then decays and eventually will disappear in a finite time interval that depends on the strength/intensity of the noise determined by the mean dwell time. As the value of mean dwell time  $T$  increases, the strength and the lifetime of the entanglement increases. Because, as  $T$  increases, the effects of the noise on

where  $\lambda_i$ s are the non-zero eigenvalues of the density matrix of the system. The density matrix of the atom (and the field) can be found by tracing out the joint density matrix of the system described by Eq. (30) over the degree of freedom of the field (and the atom). So, the time evolution of the density matrix of the atom becomes

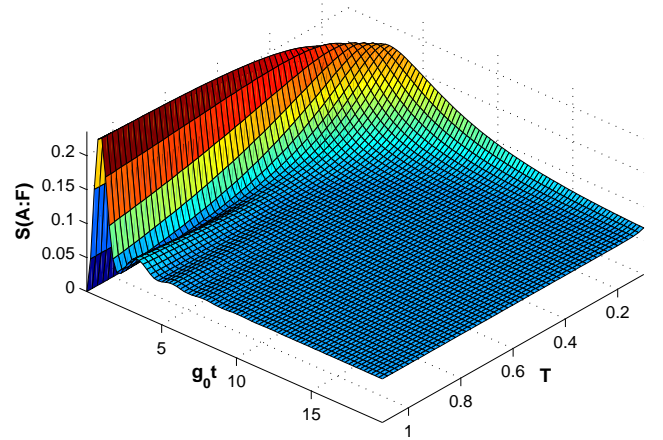


FIG. 2: The mutual entropy as the function of the time  $g_0 t$  and the mean dwell time  $T$  (in the unit of  $1/g_0$ ) for the small values of the mean dwell time.  $\lambda = 1/\sqrt{2}$  and  $\bar{n} = 0.1$ .

the interaction weakens. Since the intensity/strength of the noise is determined by the mean dwell time, the decoherence mechanism becomes faster as the mean dwell time is shorter. So, it seems that there is a monotonous relation between the strength of the noise (the mean dwell time) and the degree of the entanglement. But, for the sufficiently small values of the mean dwell time, the decrease in the mean dwell time (the increase in the strength of the noise) does not induce a decrease in the degree of the entanglement, instead causes an increase in the degree as shown by Fig. (2). This may be explained as; when the changes in the phase (jump-like) are very fast, the system can not follow all the phase changes and can not respond them completely. So, it only feels the averages of the phase changes. In this case, the entanglement becomes more robust against the noise. Thus, the entanglement is a non-

monotonic function of the intensity of the noise. The degree of the entanglement decreases to a minimum value for an optimal intensity of the noise and then increases for a sufficiently large intensity. This situation resembles the stochastic resonance in which the response of a non-linear system to a weak periodic driving can be enhanced when supplemented with a noisy field of certain optimal intensity [15].

In addition, as also shown by Fig. (3), as  $T \rightarrow \infty$ , the effect of the noise disappears and one reaches the entanglement dynamics in the usual JCM [16], in which the entanglement is present at all times and never goes to zero due to the interaction, except at  $t = 0$ .

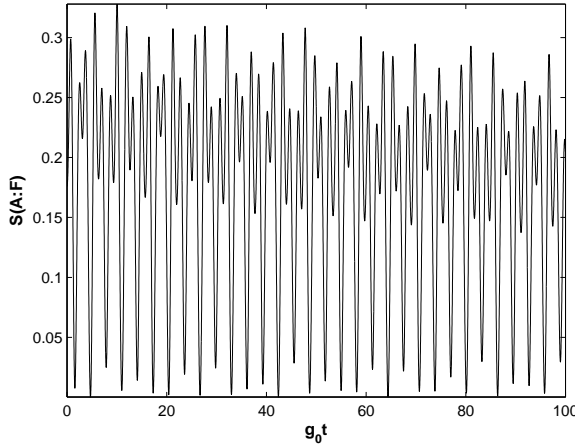


FIG. 3: The mutual entropy as the function of the time  $g_0 t$ .  $\lambda = 1/\sqrt{2}$ ,  $\bar{n} = 0.1$  and  $T \rightarrow \infty$ .

As to the influence of the parameters of the system on the entanglement dynamics, Fig. (4) shows the effects of these parameters, atomic state distribution  $\lambda$  and the average photon number  $\bar{n}$ , on the entanglement dynamics in the presence of the RPTN. The entanglement is obviously the most powerful when the atom is initially in the excited state ( $\lambda = 1$ ) and is the weakest when the atom is initially in the ground state ( $\lambda = 0$ ), as expected. As the value of  $\lambda$  increases, the entanglement becomes stronger. In addition, as the value of  $\bar{n}$  increases, equivalently the temperature of the cavity increases, the system acts much like a classical statistical system. So, the strength of the entanglement falls down. But, unlike the non-noisy case, the entanglement of the system will disappear at any temperature of the cavity field no matter what, provided that the monotonous relation between the strength of the noise and the degree of the entanglement. So, the entanglement is very sensitive to the system parameters. The initial conditions of the system play important role on the entanglement dynamics for its strength and for its lifetime to die out.

In the interaction, there is a dephasing mechanism that accounts for the decay of the entanglement. This mechanism arises from the stochastic phase fluctuations of the atom-field coupling parameter. In the mechanism, the phase fluctuations affect only the dipole or the transverse relaxation mechanism of the system. There is not any type of dissipation in the en-

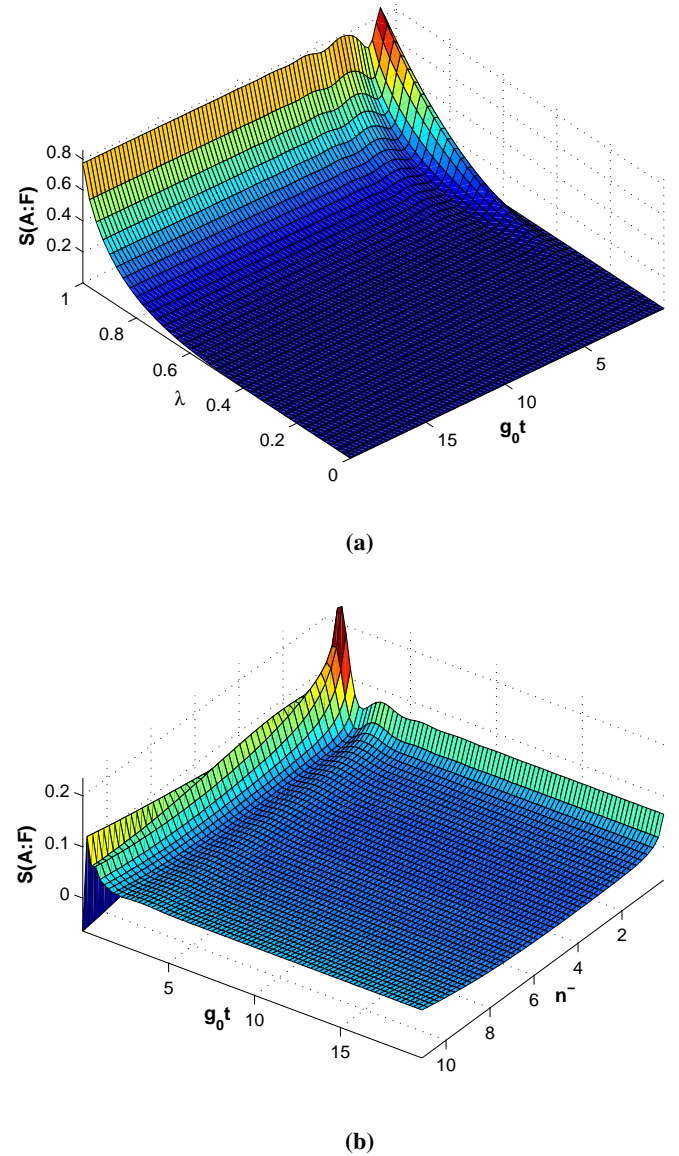


FIG. 4: The mutual entropy as the function of the time  $g_0 t$  and (a) the atomic state distribution  $\lambda$ .  $\bar{n} = 0.1$ . (b) the average photon number  $\bar{n}$ ,  $\lambda = 1/\sqrt{2}$ .  $T = 1$  for both.

ergy of the system. So, this dephasing mechanism is different from the usual dissipation mechanisms (such as cavity field damping and spontaneous emission decay or radiative damping of the system) which affects both the energy and the coherence of the system. So, RPTN causes another type of intrinsic decoherence in the JCM, in result the decay of quantum coherences. Milburn [17] proposed a model for intrinsic decoherence. In this model, intrinsic decoherence gives rise the destruction of the quantum coherence in the case that the physical properties of the system approaching a macroscopic level. In this type of dephasing mechanism, the constants of the motion remain constants of the motion and

hence stationary states remain stationary states. So, the dephasing mechanisms in these two cases display similar physical features (no energy dissipation and the decay of quantum coherences) but do not have the same origin. Jian *et.al* [18] used Milburn's model to investigate the effects of the intrinsic decoherence on the entanglement properties of the same relevant system. The exact solution in their work reveals that there is an obvious monotonous relation between intrinsic decoherence coefficient  $\gamma$  and the degree of the entanglement. For the small values of the coefficient  $\gamma \rightarrow 0$ , no entanglement emerges and for its large values  $\gamma \rightarrow \infty$ , the entanglement in usual JCM is obtained. Therefore, as though the dephasing mechanisms in these both cases display similar physical features (no energy dissipation and the decay of quantum coherences), the entanglement dynamics do not. The random phase telegraph noise induces a very special featured entanglement dynamics. Moreover, the noise considered in this study arises in a non-controllable manner. It is completely due to the stochastic behavior of the system itself, not due to an environment effect. There are some works devoted to the environmental noise. For example, one is about preventing or minimizing the influence of environmental noise in quantum information processing [19]. But, instead of attempting to shield the system from the environmental noise, Plenio and Huelga used a white noise to generate a controllable entanglement by incoherent sources [20]. The entanglement dynamics in their work displays a similar character with that of this work. The noise plays a constructive role in quantum information processing but the entanglement arises from a controllable situation. Similar aspects have also been considered elsewhere [21, 22]. In this paper, the revealed properties of the entanglement of the system under the random phase telegraph noise are uncontrollable and unaffected by the surrounding environment. Since the fluctuations in the system are quite random, the entanglement equivalently the information in the system fluctuates randomly.

#### 4. CONCLUSION

In this paper, the interaction of a two-level atom with a single-mode field is studied in the environment of the random phase telegraph noise analytically by the Jaynes-Cummings model. Random phase telegraph noise is considered as the noise which arises from the system itself not from its surrounding environment. It is quite due to the stochastic phase fluctuations in the atom-field coupling of the system. It causes another type of intrinsic decoherence in the JCM in a non-controllable manner. An exact solution to the model under this noise is obtained. The entanglement dynamics between the atom and the cavity field is explored by calculating the mutual entropy of the system. The noise manifests itself as a decay factor in the degree of entanglement in time due to a kind of dephasing mechanism which is different from the radiative damping of the atom. This dephasing mechanism affects only the dipole or the transverse relaxation mechanism of the system. The mean dwell time predominantly determines the strength as well as the lifetime of the entanglement. The entanglement is a non monotonic function of the intensity of the noise determined by the mean dwell time. The degree of the entanglement decreases to a minimum value for an optimal intensity of the noise and then increases for a sufficiently large intensity. In addition, the entanglement dynamics is very sensitive to the system parameters. The initial conditions of the system play important role on the entanglement dynamics for its strength and for its lifetime to die out. Unlike the non-noisy case, the entanglement of the system will disappear at any temperature of the cavity field no matter what provided that the monotonous relation between the intensity of the noise and the degree of the entanglement.

#### Acknowledgments

I am grateful to Aliekber Aktag for his help and discussion.

- [1] D. P. DiVincenzo, Science **270**, 255 (1995).
- [2] J. I. Cirac and P. Zoller, Nature (London) **404**, 579 (2000).
- [3] M. A. Nielsen and I. L. Chuang, *Quantum Computation and Quantum Information*, Cambridge University Press, Cambridge, England 2000.
- [4] A. I. Burshtein, Zh. Eksp. Teor. Fiz. **49**, 1362 (1966), [Sov. Phys. JETP **22**, 939 (1966)]; A. I. Burshtein and Yu. S. Oseledchik *ibid.* **51**, 1071 (1966) [*ibid.* **24**, 716 (1967)]; L. D. Zusman and A. I. Burshtein *ibid.* **61**, 976 (1971) [*ibid.* **34**, 520 (1972)].
- [5] A. I. Burshtein and Yu. S. Oseledchik *ibid.* **51**, (1966) 1071 [*ibid.* **24**, 716 (1967)]; L. D. Zusman and A. I. Burshtein *ibid.* **61**, 976 (1971) [*ibid.* **34**, 520 (1972)].
- [6] J. H. Eberly, K. Wodkiewicz, and B. W. Shore, Phys. Rev. A **30**, 2381 (1984).
- [7] K. Wodkiewicz, B. W. Shore, and J. H. Eberly, Phys. Rev. A **30**, 2390 (1984).
- [8] E. T. Jaynes, F. W. Cummings, Proc. IEEE **51**, 89 (1963).
- [9] A. Joshi, S. W. Lawande, Phys. Lett. A **184**, 390 (1994).
- [10] A. Joshi, S. W. Lawande, Phys. Rev. A **50**, 1692 (1994).
- [11] S. V. Lawande, A. Joshi, and Q. V. Lawande, Phys. Rev. A **52**, 619 (1995).
- [12] A. Joshi, J. mod. Optics **42**, 2561 (1995).
- [13] J. I. Cirac, P. R. Zoller, W. D. Phillips, Phys. Rev. A **46**, 2688 (1992); C. A. Blockley, D. F. Walls, H. Risken, Europhys. Lett. **17**, 509 (1992).
- [14] E. Boukobza, D. J. Tannor, Phys. Rev. A. **71**, 063821 (2005).
- [15] L. Gammaitoni *et al.*, Rev. Mod. Phys., **223**, 70 (1998).
- [16] S. Bose, I. Fuentes-Guridi, P. L. Knight, and V. Vedral, Phys. Rev. Lett. **87**, 050401 (2001).
- [17] G. J. Milburn, Phys. Rev. A. **44**, 5401 (1991).
- [18] ZHANG Jian, SHAO Bin, J. At. Mol. Phys. **23**, 417 (2006).
- [19] L.-M. Duan and G.-C. Guo, Phys. Rev. Lett. **79**, 1953 (1997); P. Zanardi, and M. Rasetti, *ibid.* **79**, 3306 (1997); D. A. Lidar, I. L. Chuang, and K. B. Whaley, *ibid.* **81**, 2594 (1998).
- [20] M. B. Plenio and S. F. Huelga, Phys. Rev. Lett. **88**, 197901 (2002).
- [21] A. Beige *et al.*, J. Mod. Opt. **47**, 2583 (2000);
- [22] M. S. Kim *et al.*, Phys. Rev. A **65**, 040101 (2002).

# Effect of excess noise on continuous variable entanglement sudden death and Gaussian quantum discord\*

Su Xiao-Long(苏晓龙)<sup>†</sup>

*State Key Laboratory of Quantum Optics and Quantum Optics Devices,  
Institute of Opto-Electronics, Shanxi University, Taiyuan 030006, China*

(Received 10 January 2013; revised manuscript received 6 March 2013)

A symmetric two-mode Gaussian entangled state is used to investigate the effect of excess noise on entanglement sudden death and Gaussian quantum discord with continuous variables. The results show that the excess noise in the channel can lead to entanglement sudden death of a symmetric two-mode Gaussian entangled state, while Gaussian quantum discord never vanishes. As a practical application, the security of a quantum key distribution (QKD) scheme based on a symmetric two-mode Gaussian entangled state against collective Gaussian attacks is analyzed. The calculation results show that the secret key cannot be distilled when entanglement vanishes and only quantum discord exists in such a QKD scheme.

**Keywords:** continuous variable, entanglement, quantum key distribution

**PACS:** 03.67.Hk, 03.67.Dd, 42.50.Dv, 42.50.-p

**DOI:** [10.1088/1674-1056/22/8/080304](https://doi.org/10.1088/1674-1056/22/8/080304)

## 1. Introduction

Quantum entanglement is a basic resource for quantum information processing. A troublesome problem in practical application is that quantum entanglement is sensitive to environment-induced loss. In the discrete variable case, it has been shown that entanglement can be completely lost after a finite time of interaction with the environment for a two-qubit system, which is known as entanglement sudden death (ESD).<sup>[1,2]</sup> The continuous variable (CV) system is an alternative system to investigate quantum information and has obtained remarkable progress.<sup>[3,4]</sup> It has been observed that losses may lead to ESD in Gaussian CV systems too.<sup>[5-7]</sup>

Quantum correlation, which is measured by quantum discord,<sup>[8]</sup> can also be used as the quantum resource in some types of quantum information processing tasks. It has been shown that some quantum computational tasks based on a single qubit can be carried out by separable (that is, non-entangled) states that nonetheless carries non-classical correlations.<sup>[9-11]</sup> Recently, quantum discord was extended to a two-mode Gaussian state.<sup>[12,13]</sup> A two-mode Gaussian state is entangled with Gaussian quantum discord  $D > 1$ , while when  $0 \leq D \leq 1$  it is either a separable or entangled state. Gaussian quantum discord has been experimentally demonstrated by several groups.<sup>[14-16]</sup>

Quantum key distribution (QKD) allows two legitimate parties, Alice and Bob, who are linked by a quantum channel and an authenticated classical channel, to establish the secret key only known by themselves. Generally CV QKD uses a Gaussian quantum resource state, such as entangled state, squeezed state, and modulated coherent state, as the resource state, along with a reconciliation and privacy amplification

procedure to distill the secret key.<sup>[4,17,18]</sup> In the practical applications, quantum channels not only are lossy, but also have excess Gaussian noises on the quadrature distribution. For a given tolerable channel efficiency  $T$ , there exists a lower limit for excess noise  $\delta$ , which is given by  $\delta < 2T$ .<sup>[19]</sup> CV QKD protocols have been shown to be unconditionally secure, that is, secure against arbitrary attacks<sup>[20]</sup> and have been proved to be unconditionally secure over long distance.<sup>[21]</sup> Besides the traditional one-way CV QKD scheme, a two-way CV QKD scheme has been proposed and proved to be able to tolerate more excess noise than one-way CV QKD scheme.<sup>[22,23]</sup> Recently, a CV QKD scheme with thermal states was also proposed and proved to be secure against collective Gaussian attacks.<sup>[24]</sup> The CV QKD exploiting coherent state<sup>[25-31]</sup> and entangled state<sup>[32-34]</sup> have been experimentally realized in recent years.

In Ref. [7], it is shown that a symmetric two-mode Gaussian entangled state is a fully robust state, which means that entanglement never vanishes with any type of loss in the channel. However, the practical quantum channels not only are lossy, but also have excess Gaussian noises. In this paper, we analyze the effect of the excess noise in the channel on ESD and Gaussian quantum discord of a symmetric two-mode Gaussian entangled state. The calculation shows that the excess noise in the channel is the key factor that leads to ESD for a symmetric two-mode Gaussian entangled state. The excess noise also leads to a decrease of the Gaussian quantum discord, but it never makes the quantum discord vanish.<sup>[12,13]</sup> As an example of practical application, the security of a QKD scheme based on a symmetric two-mode Gaussian entangled state is also analyzed. The relation among the secret key rate,

\*Project supported by the National Basic Research Program of China (Grant No. 2010CB923103), the National Natural Science Foundation of China (Grant Nos. 11174188 and 61121064), and the Fund from the Shanxi Scholarship Council of China (Grant No. 2012-010).

<sup>†</sup>Corresponding author. E-mail: [suxl@sxu.edu.cn](mailto:suxl@sxu.edu.cn)

© 2013 Chinese Physical Society and IOP Publishing Ltd

<http://iopscience.iop.org/cpb> <http://cpb.iphy.ac.cn>

entanglement, and quantum discord is analyzed. What we are interested in is whether the secret key can be distilled when entanglement vanishes and only quantum correlation exists. The calculation results show that it is impossible to distill the secret key when entanglement vanishes and only quantum correlation exists. It confirms that entanglement is a precondition for QKD with a two-mode Gaussian entangled state.<sup>[35]</sup> It also supplies a possible way to destroy, instead of eavesdrop, this type of CV QKD scheme where a two-mode Gaussian entangled state is used as a resource state.

The paper is organized as follows. In Section 2, the physical model used to investigate the effect of excess noise on CV ESD and Gaussian quantum discord is presented. In Section 3, the ESD and Gaussian quantum discord under influence of excess noise are analyzed. In Section 4, the security of CV QKD scheme based on a symmetric two-mode Gaussian entangled state is proved, and the relation between secret key rate, ESD, and Gaussian quantum discord is analyzed. In Section 5, we conclude the paper.

## 2. Physical model

The physical model used to analyze the effect of excess noise on ESD and Gaussian quantum discord is shown in Fig. 1. A symmetric two-mode Gaussian entangled state with a variance of  $V$ , such as a symmetric Einstein–Podolsky–Rosen (EPR) entangled state, is used as the resource state, which is distributed between Alice and Bob. One of the two-mode Gaussian states ( $\hat{b}$ ) is transmitted through a lossy channel, which is modeled by a beam splitter with transmission efficiency  $T$ . The excess noise in the channel is modeled by an environmental thermal state  $\rho_E$  with variance  $W$ , which corresponds to  $\delta = W - 1$  in Ref. [19] and  $\varepsilon = (W - 1)(1 - T)/T$  in Ref. [29].  $W = 1$  means there is no excess noise ( $\delta = 0$ ) in the channel, only loss exists. When  $W > 1$ , there is excess noise in the channel.

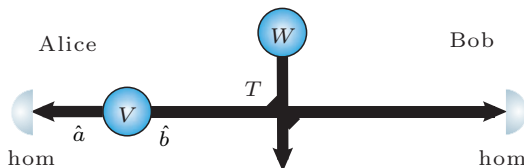


**Fig. 1.** (color online) Schematic plot of a symmetric two-mode Gaussian entangled state distributed between Alice and Bob through a lossy channel with excess noise. The transmission efficiency of quantum channel is modeled by a beam splitter with transmission  $T$ . Excess noise in the channel is modeled by an environmental thermal state  $\rho_E$  with variance  $W$ . Alice and Bob perform homodyne (hom) detection on the mode they hold, respectively.

The amplitude and phase quadratures of an optical mode  $\hat{a}$  is defined as  $\hat{X}_a = \hat{a} + \hat{a}^\dagger$  and  $\hat{Y}_a = (\hat{a} - \hat{a}^\dagger)/i$ , respectively. A Gaussian state is fully characterized by its covariance matrix. The covariance matrix is constructed using the following

definitions of its matrix elements

$$V_{lm} := \frac{1}{2} \langle \hat{O}_l \hat{O}_m + \hat{O}_m \hat{O}_l \rangle - \langle \hat{O}_l \rangle \langle \hat{O}_m \rangle, \quad (1)$$

$$V_{ll} = \langle \hat{O}_l^2 \rangle - \langle \hat{O}_l \rangle^2 := V(\hat{O}_l), \quad (2)$$

where  $\hat{O}_l$  is the  $l$ -th element of the quadrature row vector  $\hat{O} = (\hat{X}_1, \hat{Y}_1, \dots, \hat{X}_N, \hat{Y}_N)$  which describes the bosonic system of  $N$  modes. The covariance matrix of a symmetric two-mode Gaussian state is given by

$$\boldsymbol{\sigma} = \begin{pmatrix} V\mathbf{I} & C\mathbf{Z} \\ C\mathbf{Z} & V\mathbf{I} \end{pmatrix}, \quad (3)$$

where  $V = \cosh 2r$  with squeezing parameter  $r \in [0, \infty)$  is the noise variance of EPR entangled modes  $\hat{a}$  and  $\hat{b}$ ,  $C = \sqrt{V^2 - 1}$ ,  $\mathbf{I}$  and  $\mathbf{Z}$  are the Pauli matrices

$$\mathbf{I} = \begin{pmatrix} 1 & 0 \\ 0 & 1 \end{pmatrix}, \quad \mathbf{Z} = \begin{pmatrix} 1 & 0 \\ 0 & -1 \end{pmatrix}. \quad (4)$$

The entanglement between Alice and Bob is contaminated by loss and excess noise in the channel. After transmission, the amplitude and phase quadratures at Bob's station are given by

$$\hat{X}_B = \sqrt{T}\hat{X}_b + \sqrt{1-T}\hat{X}_W, \quad (5)$$

$$\hat{Y}_B = \sqrt{T}\hat{Y}_b + \sqrt{1-T}\hat{Y}_W, \quad (6)$$

where  $\hat{X}_W$  and  $\hat{Y}_W$  are the amplitude and phase quadratures of the environmental thermal state  $\rho_E$ . Then the covariance matrix of the two-mode Gaussian state distributed between Alice and Bob is given by

$$V_{AB} = \begin{pmatrix} V\mathbf{I} & C'\mathbf{Z} \\ C'\mathbf{Z} & V_B\mathbf{I} \end{pmatrix}, \quad (7)$$

where  $V_B = TV + (1 - T)W$ ,  $C' = \sqrt{T(V^2 - 1)}$ .

## 3. Entanglement and quantum discord of the system

The symplectic spectrum of a covariance matrix

$$\boldsymbol{\sigma} = \begin{pmatrix} \mathbf{A} & \mathbf{C} \\ \mathbf{C} & \mathbf{B} \end{pmatrix} \quad (8)$$

is given by<sup>[36,37]</sup>

$$\tilde{v}_\pm = \sqrt{\frac{\Delta \pm \sqrt{\Delta^2 - 4\det \boldsymbol{\sigma}}}{2}}, \quad (9)$$

where  $\mathbf{A}$  ( $\mathbf{B}$ ) denotes the covariance matrix of mode  $\hat{a}$  ( $\hat{b}$ ),  $\mathbf{C}$  contains correlations between quadratures of the two modes,  $\det \boldsymbol{\sigma}$  is the determinant of covariance matrix and  $\Delta = \det \mathbf{A} + \det \mathbf{B} + 2\det \mathbf{C}$ .

PPT criterion is a necessary and sufficient criterion for entanglement of a Gaussian state.<sup>[38,39]</sup> A Gaussian state is entangled iff  $\tilde{v}_- < 1$ , where  $\tilde{v}_-$  is the smallest symplectic eigenvalue of partially transposed covariance matrix for a two-mode Gaussian state, which is given by<sup>[36,37]</sup>

$$\tilde{v}_- = \sqrt{\frac{\tilde{\Delta} - \sqrt{\tilde{\Delta}^2 - 4\det \boldsymbol{\sigma}}}{2}}, \quad (10)$$

where  $\tilde{\Delta} = \det \mathbf{A} + \det \mathbf{B} - 2 \det \mathbf{C}$ . Substituting the corresponding terms of matrix  $\mathbf{V}_{AB}$  in Eq. (7) into Eq. (10), we can verify whether the two-mode Gaussian state is entangled or not after the transmission.

Quantum discord is defined as the difference between two quantum analogues of classically equivalent expression of the mutual information. The Gaussian quantum discord of a two-mode squeezed thermal state is given by<sup>[12]</sup>

$$D_{AB} = f(\sqrt{I_2}) - f(v_-) - f(v_+) + f\left(\frac{\sqrt{I_1} + 2\sqrt{I_1 I_2} + 2I_3}{1 + 2\sqrt{I_2}}\right), \quad (11)$$

where

$$f(x) = \left(x + \frac{1}{2}\right) \log_2 \left(x + \frac{1}{2}\right) - \left(x - \frac{1}{2}\right) \log_2 \left(x - \frac{1}{2}\right),$$

$I_1 = \det \mathbf{A}$ ,  $I_2 = \det \mathbf{B}$ , and  $I_3 = \det \mathbf{C}$ . When  $D_{AB} > 1$ , the state is an entangled state, while when  $0 \leq D_{AB} \leq 1$ , the state is either separable or entangled. When  $D_{AB} < 0$ , there is no quantum correlation, only classical correlation between two modes. Substituting the corresponding terms of matrix  $\mathbf{V}_{AB}$  in Eq. (7) into Eq. (11), we can calculate the Gaussian quantum discord between Alice and Bob.

Figure 2(a) shows the smallest symplectic eigenvalues of partially transposed covariance matrix for  $r = 0.35$  (3-dB quantum correlation, solid line) with  $W = 1$ ,  $r = 1.15$  (10-dB quantum correlation) with  $W = 1$  (dotted line), and  $W = 1.5$  (dashed line), respectively. For  $r = 0.35$  and  $r = 1.15$  with  $W = 1$ , we have  $\tilde{v}_- < 1$  at any transmission efficiency, which clearly shows that entanglement is robust against loss. When  $r = 1.15$  with  $W = 1.5$ , i.e. there is excess noise  $\delta = 0.5$  in the channel,  $\tilde{v}_-$  is larger than 1 when transmission efficiency is smaller than 0.2, which means that entanglement vanishes due to excess noise in the channel. This result confirms that excess noise can lead to ESD of a symmetric Gaussian entangled state. For avoiding ESD, we have to eliminate or minimize the excess noise in the transmission channel.

Figure 2(b) shows the Gaussian quantum discords for  $r = 0.35$  (solid line) with  $W = 1$ ,  $r = 1.15$  with  $W = 1$  (dotted line) and  $W = 1.5$  (dashed line), respectively. In all the cases, we see that Gaussian quantum discord increases with the increase of transmission efficiency of the channel. For  $r = 0.35$  with  $W = 1$ ,  $D_{AB}$  is always smaller than 1, which means that the transmitted state is either separable or entangled state. For  $r = 1.15$  with  $W = 1$  and  $W = 1.5$ ,  $D_{AB}$  is larger than 1 when transmission efficiency is larger than 0.68 and 0.85, respectively. It means that for higher transmission efficiency, the state is an entangled state ( $D_{AB} > 1$ ). With the decreasing of transmission efficiency and increasing of excess noise, the state may be turned into either separable or entangled state.

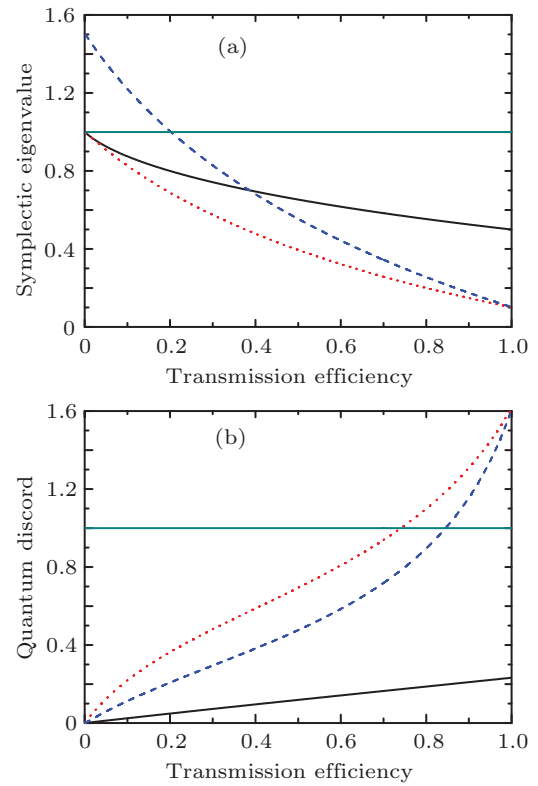


**Fig. 2.** (color online) (a) Symplectic eigenvalues with different variances of resource state and (b) Gaussian quantum discords with different variances of resource state. Dotted (red) and solid (black) lines in panels (a) and (b) correspond to  $r = 1.15$  and  $r = 0.35$  with  $W = 1$ , respectively. Dashed (blue) lines in panels (a) and (b) correspond to  $r = 1.15$  with  $W = 1.5$ .

#### 4. Security of the QKD with a symmetric two-mode Gaussian entangled state

As an example, we apply a symmetric two-mode Gaussian entangled state to be the resource state for a QKD scheme, which is shown in Fig. 3. In the QKD scheme, Alice holds mode  $\hat{a}$ , and transmits mode  $\hat{b}$  to Bob over the quantum channel with transmission efficiency  $T$ . Alice and Bob perform homodyne detection on their own beam randomly to measure amplitude or phase quadrature, respectively. The secret key is established by the quantum fluctuation of each quadrature. There are two advantages of this QKD scheme, one is that the true random numbers resulting from the quantum fluctuations are used to establish the secret key. The other is that no signal modulation is

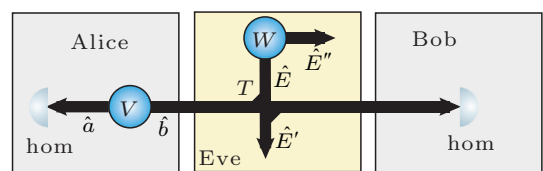


**Fig. 3.** (color online) Schematic of the QKD scheme with an EPR entangled state. The transmission efficiency of the quantum channel is modeled by a beam splitter with transmission  $T$ . Eve performs an entangling cloner attack, where the variance of the EPR state is  $W$ . Alice and Bob perform homodyne (hom) detection on the mode they hold, respectively.

needed in the QKD scheme. The proof-of-principle experimental demonstration of this QKD scheme has been demonstrated in Ref. [32], in which the post-selection technique is utilized to distill the secret key.<sup>[40]</sup>

We assume that Eve performs the entangling cloner attack,<sup>[41]</sup> which is the most important and practical example of a collective Gaussian attack,<sup>[20,42–44]</sup> to steal the information. She prepares an ancilla EPR entangled state with variance  $W$ . She keeps one mode  $\hat{E}''$  and mixes the other mode  $\hat{E}$  with the transmitted mode  $\hat{b}$  in the quantum channel by a beam splitter, leading to the output mode  $\hat{E}'$ . Eve's output modes are stored in a quantum memory and detected collectively at the end of the protocol. Eve's final measurement is optimized based on Alice and Bob's classical communication.

The 3-dB loss limit on the transmission line in the CV QKD<sup>[45]</sup> can be beaten with the reverse reconciliation<sup>[25]</sup> or the post-selection.<sup>[40]</sup> In reverse reconciliation, Alice attempts to guess what was received by Bob rather than Bob guessing what was sent by Alice. Such a reverse reconciliation protocol gives Alice an advantage over a potential eavesdropper Eve. In the following, we use the variable  $X$  to represent amplitude or phase quadrature of an optical mode to analyze the secret key without losing the generality.

In reverse reconciliation, the secret key rate is given by

$$K_{RR} = I(X_A : X_B) - I(X_B : E), \quad (12)$$

where

$$I(X_A : X_B) = H(X_B) - H(X_B | X_A) \quad (13)$$

is the mutual information between Alice and Bob, with

$$H(X_B) = (1/2) \log_2 V(X_B)$$

and

$$H(X_B | X_A) = (1/2) \log_2 V(X_B | X_A)$$

being the total and conditional Shannon entropies. Eve's information is given by

$$I(X_B : E) = S(E) - S(E | X_B), \quad (14)$$

where  $S(\cdot)$  is the von Neumann entropy. The von Neumann entropy of a Gaussian state  $\rho$  can be expressed in terms of its symplectic eigenvalues<sup>[46]</sup>

$$S(\rho) = \sum_{k=1}^n g(v_k), \quad (15)$$

where

$$g(v) = \left( \frac{v+1}{2} \right) \log_2 \left( \frac{v+1}{2} \right) - \left( \frac{v-1}{2} \right) \log_2 \left( \frac{v-1}{2} \right), \quad (16)$$

with  $v = \{v_1, \dots, v_n\}$  being the symplectic eigenvalues of Gaussian state  $\rho$ .

The conditional variance is defined as<sup>[47]</sup>  $V_{X|Y} = V(X) - |\langle XY \rangle|^2 / V(Y)$ . So Bob's conditional variance is given by

$$V_{B|A} = V_B - \frac{T(V^2 - 1)}{V}. \quad (17)$$

Then according to Eq. (13), we obtain the mutual information between Alice and Bob.

Eve interacts her mode  $\hat{E}$  with the transmitted mode  $\hat{b}$  on the beam splitter to eavesdrop information. The amplitude and phase quadratures of mode  $\hat{E}'$  are

$$\hat{X}_{E'} = \sqrt{T} \hat{X}_E - \sqrt{1-T} \hat{X}_b, \quad (18)$$

$$\hat{Y}_{E'} = \sqrt{T} \hat{Y}_E - \sqrt{1-T} \hat{Y}_b. \quad (19)$$

Eve's covariance matrix is made up from the modes  $\hat{E}'$  and  $\hat{E}''$ , which is

$$\mathbf{V}_E = \begin{pmatrix} e_v \mathbf{I} & \varphi \mathbf{Z} \\ \varphi \mathbf{Z} & W \mathbf{I} \end{pmatrix}, \quad (20)$$

where  $e_v = (1-T)V + TW$ ,  $\varphi = \sqrt{T(W^2 - 1)}$ .

The conditional covariance matrix  $\mathbf{V}_{E|X_B}$ , which represents the covariance matrix of a system where one of the modes has been measured by homodyne detection (in this case Bob), is given by<sup>[4,48,49]</sup>

$$\mathbf{V}_{E|X_B} = \mathbf{V}_E - (V_B)^{-1} \mathbf{D} \boldsymbol{\Pi} \mathbf{D}^T, \quad (21)$$

where

$$\boldsymbol{\Pi} = \begin{pmatrix} 1 & 0 \\ 0 & 0 \end{pmatrix}. \quad (22)$$

Here  $\mathbf{D}$  is the matrix describing the correlations between Eve's modes and Bob's mode, which is given by

$$\mathbf{D} = \begin{pmatrix} \langle \hat{E}' X_B \rangle \mathbf{I} \\ \langle \hat{E}'' X_B \rangle \mathbf{Z} \end{pmatrix} = \begin{pmatrix} \mu \mathbf{I} \\ \theta \mathbf{Z} \end{pmatrix}, \quad (23)$$

where  $\mu = \sqrt{T(1-T)(W-V)}$ ,  $\theta = \sqrt{(1-T)(W^2-1)}$ .

Substituting the corresponding terms of matrix in Eqs. (20) and (21) into Eq. (9), the symplectic eigenvalues of  $\mathbf{V}_E$  and  $\mathbf{V}_{E|X_B}$  are obtained. Then substituting these eigenvalues into Eqs. (15) and (16), we obtain  $S(E)$  and  $S(E|X_B)$ , which are substituted into Eq. (14) to calculate Eve's information. Finally, the secret key rate is obtained from Eq. (12).

Figure 4 shows the secret key rates for  $r = 0.35$  (solid line) with  $W = 1$ ,  $r = 1.15$  with  $W = 1$  (dotted line) and  $W = 1.5$  (dashed line), respectively. By comparing the secret key rates of different entanglement level, we see that the higher entanglement is, the higher the secret key rate is, which means that entanglement helps to increase the secret key rate. When the excess noise exists in the channel ( $W > 1$ ), for example,  $W = 1.5$ , the secret key can be distilled for  $T > 0.53$ . It means that Eve can destroy the secure communication between Alice and Bob by adding sufficient excess noise in the channel.

Comparing dashed lines in Fig. 2(a) and Fig. 4, we find that after entanglement died ( $T < 0.2$ ), none of any secret key

can be distilled, although the Gaussian quantum discord still exists ( $D_{AB} > 0$  in Fig. 2(b)). The results confirm that entanglement is a necessary precondition for CV QKD and point out that Gaussian quantum discord itself has no contribution to the secret key in such a CV QKD scheme.

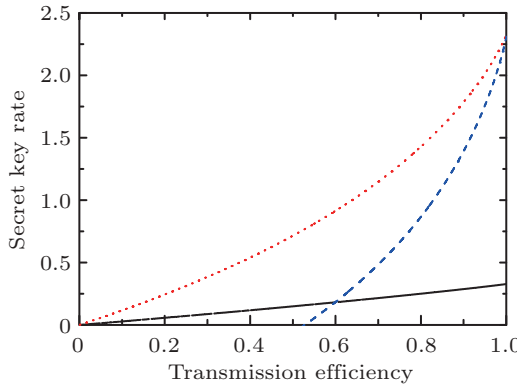


**Fig. 4.** (color online) Secret key rates with different variances of resource state. Dotted (red) and solid (black) lines correspond to  $r = 1.15$  and  $r = 0.35$  with  $W = 1$ , respectively. Dashed (blue) lines correspond to  $r = 1.15$  with  $W = 1.5$ .

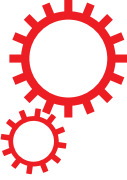
## 5. Conclusion

In conclusion, by considering a symmetric two-mode Gaussian entangled state transmitted through a lossy channel with excess noise, we show that excess noise in the channel can lead to ESD. Although the excess noise also decreases Gaussian quantum discord, it never totally vanishes. Therefore in order to distribute Gaussian entanglement over a long distance, we have to control the excess noise in the quantum channel. For CV QKD with a symmetric two-mode Gaussian entangled state, the secret key cannot be distilled when entanglement vanishes ( $\tilde{v}_- > 1$ ) and only Gaussian quantum discord exists ( $D_{AB} > 0$ ). The result supplies a possible way to destroy, instead of eavesdrop, the CV QKD with a symmetric two-mode Gaussian entangled state.

## References

- [1] Yu T and Eberly J H 2009 *Science* **323** 598
- [2] Almeida M P, De Melo F, Hor-Meyll M, Salles A, Walborn S P, Souto Ribeiro P H and Davidovich L 2007 *Science* **316** 579
- [3] Braunstein S L and Van Loock P 2005 *Rev. Mod. Phys.* **77** 513
- [4] Weedbrook C, Pirandola S, García-Patrón R, Cerf N J, Ralph T C, Shapiro J H and Lloyd S 2012 *Rev. Mod. Phys.* **84** 621
- [5] Coelho A S, Barbosa F A S, Cassemiro K N, Villar A S, Martinelli M, and Nussemzveig P 2009 *Science* **326** 823
- [6] Barbosa F A S, Coelho A S, De Faria A J, Cassemiro K N, Villar A S, Nussemzveig P and Martinelli M 2010 *Nat. Photon.* **4** 858
- [7] Barbosa F A S, De Faria A J, Coelho A S, Cassemiro K N, Villar A S, Nussemzveig P and Martinelli M 2011 *Phys. Rev. A* **84** 052330
- [8] Ollivier H and Zurek W H 2001 *Phys. Rev. Lett.* **88** 017901
- [9] Knill E and Laflamme R 1998 *Phys. Rev. Lett.* **81** 5672
- [10] Ryan C A, Emerson J, Poulin D, Negrevergne C and Laflamme R 2005 *Phys. Rev. Lett.* **95** 250502
- [11] Lanyon B P, Barbieri M, Almeida M P and White A G 2008 *Phys. Rev. Lett.* **101** 200501
- [12] Giorda P and Paris M G A 2010 *Phys. Rev. Lett.* **105** 020503
- [13] Adesso G and Datta A 2010 *Phys. Rev. Lett.* **105** 030501
- [14] Gu M, Chrzanowski H M, Assad S M, Symul T, Modi K, Ralph T C, Vedral V and Lam P K 2012 *Nat. Phys.* **8** 671
- [15] Blandino R, Genoni M G, Etesse J, Barbieri M, Paris M G A, Grangier P and Tualle-Brouri Rosa 2012 *Phys. Rev. Lett.* **109** 180402
- [16] Madsen L S, Berni A, Lassen M and Andersen U L 2012 *Phys. Rev. Lett.* **109** 030402
- [17] Chen J J, Han Z F, Zhao Y B, Gui Y Z and Guo G C 2006 *Physics* **35** 785 (in Chinese)
- [18] Zhu J, He G Q and Zeng G H 2007 *Chin. Phys.* **16** 1364
- [19] Namiki R and Hirano T 2004 *Phys. Rev. Lett.* **92** 117901
- [20] Renner R and Cirac J I 2009 *Phys. Rev. Lett.* **102** 110504
- [21] Leverrier A and Grangier P 2009 *Phys. Rev. Lett.* **102** 180504
- [22] Su X L, Jing J T, Pan Q and Xie C D 2006 *Phys. Rev. A* **74** 062305
- [23] Pirandola S, Mancini S, Lloyd S and Braunstein S L 2008 *Nat. Phys.* **4** 726
- [24] Weedbrook C, Pirandola S and Ralph T C 2012 *Phys. Rev. A* **86** 022318
- [25] Grosshans F, Van Assche G, Wenger J, Brouri R, Cerf N J and Grangier P 2003 *Nature* **421** 238
- [26] Lorenz S, Korolkova N and Leuchs G 2004 *Appl. Phys. B* **79** 273
- [27] Lance A M, Symul T, Sharma V, Weedbrook C, Ralph T C and Lam P K 2005 *Phys. Rev. Lett.* **95** 180503
- [28] Symul T, Alton D J, Assad S M, Lance A M, Weedbrook C, Ralph T C and Lam P K 2007 *Phys. Rev. A* **76** 030303
- [29] Lodewyck J, Bloch M, García-Patrón R, Fossier S, Karpov E, Diamanti E, Debuisschert T, Cerf N J, Tualle-Brouri R, McLaughlin S W and Grangier P 2007 *Phys. Rev. A* **76** 042305
- [30] Qi B, Huang L L, Qian L and Lo H K 2007 *Phys. Rev. A* **76** 052323
- [31] Shen Y, Zou H X, Tian L, Chen P X and Yuan J M 2010 *Phys. Rev. A* **82** 022317
- [32] Su X L, Wang W Z, Wang Y, Jia X J, Xie C D and Peng K C 2009 *Europhys. Lett.* **87** 20005
- [33] Eberle Tobias, Händchen Vitus, Duhme J, Franz T, Werner R F and Schnabel R arXiv: 1110.3977v1 [quant-ph]
- [34] Madsen L S, Usenko V C, Lassen M, Filip R and Andersen U L 2012 *Nature Commun.* **3** 1083
- [35] Curty M, Lewenstein M and Lütkenhaus N 2004 *Phys. Rev. Lett.* **92** 217903
- [36] Serafini A, Illuminati F and De Siena S 2004 *J. Phys. B: At. Mol. Opt. Phys.* **37** L21
- [37] Adesso G, Serafini A and Illuminati F 2004 *Phys. Rev. A* **70** 022318
- [38] Simon R 2000 *Phys. Rev. Lett.* **84** 2726
- [39] Werner R F and Wolf M M 2001 *Phys. Rev. Lett.* **86** 3658
- [40] Silberhorn Ch, Ralph T C, Lütkenhaus N and Leuchs G 2002 *Phys. Rev. Lett.* **89** 167901
- [41] Grosshans F, Cerf N J, Wenger J, Tualle-Brouri R and Grangier P 2003 *Quantum Inf. Comput.* **3** 535
- [42] Navascués M, Grosshans G and Acín A 2006 *Phys. Rev. Lett.* **97** 190502
- [43] García-Patrón R and Cerf N J 2006 *Phys. Rev. Lett.* **97** 190503
- [44] Pirandola S, Braunstein S L and Lloyd S 2008 *Phys. Rev. Lett.* **101** 200504
- [45] Grosshans F and Grangier P 2002 *Phys. Rev. Lett.* **88** 057902
- [46] Holevo A S, Sohma M and Hirota O 1999 *Phys. Rev. A* **59** 1820
- [47] Grangier P, Levenson J A and Poizat J P 1998 *Nature* **396** 537
- [48] Eisert J, Scheel S and Plenio M B 2002 *Phys. Rev. Lett.* **89** 137903
- [49] Fiurášek J 2002 *Phys. Rev. Lett.* **89** 137904

# SCIENTIFIC REPORTS



OPEN

## Effect of weak measurement on entanglement distribution over noisy channels

Received: 03 September 2015

Accepted: 12 February 2016

Published: 03 March 2016

Xin-Wen Wang<sup>1,2</sup>, Sixia Yu<sup>2</sup>, Deng-Yu Zhang<sup>1</sup> & C. H. Oh<sup>2</sup>

Being able to implement effective entanglement distribution in noisy environments is a key step towards practical quantum communication, and long-term efforts have been made on the development of it. Recently, it has been found that the null-result weak measurement (NRWM) can be used to enhance probabilistically the entanglement of a single copy of amplitude-damped entangled state. This paper investigates remote distributions of bipartite and multipartite entangled states in the amplitudedamping environment by combining NRWMs and entanglement distillation protocols (EDPs). We show that the NRWM has no positive effect on the distribution of bipartite maximally entangled states and multipartite Greenberger-Horne-Zeilinger states, although it is able to increase the amount of entanglement of each source state (noisy entangled state) of EDPs with a certain probability. However, we find that the NRWM would contribute to remote distributions of multipartite W states. We demonstrate that the NRWM can not only reduce the fidelity thresholds for distillability of decohered W states, but also raise the distillation efficiencies of W states. Our results suggest a new idea for quantifying the ability of a local filtering operation in protecting entanglement from decoherence.

It is well known that establishment of quantum entanglement among distant parties is a prerequisite for many quantum information protocols. Moreover, a necessary condition for perfectly implementing these tasks is that the shared entangled states among the users are maximally entangled pure states. In practice, however, unavoidable interactions of the entangled systems with environments during their distributions or storages would result in degradation of the entanglement among the users. In other words, the entanglement resources actually available are usually entangled mixed states, which would decrease the fidelities and efficiencies of quantum information processes.

To accomplish the aforementioned quantum information processing tasks, the communicators need to transform the noisy entangled states into maximally entangled pure states in advance. This raises a problem which is also of theoretical interest: How can maximally entangled pure states be extracted from shared entangled mixed states by local operations? One solution, at least in principle, is to use entanglement distillation protocols (EDPs) which function as distilling a small number of entangled pure or nearly pure states from a large number of entangled mixed states<sup>1–5</sup>. This means perfect or nearly perfect entanglement-based quantum information processing would be possible even in noisy environments by utilizing the idea of entanglement purification.

However, the EDPs do not work for the inseparable states whose fidelities or singlet fractions (which quantify how close the states are to maximally entangled states<sup>1,6</sup>) are less than some thresholds (e.g., 1/2 for two-qubit states<sup>1,2</sup>), except that they have some special forms or are hyperentangled<sup>6–11</sup>. Fortunately, Gisin<sup>12</sup> discovered that the amount of entanglement of an entangled mixed state could be raised probabilistically by local filtering operations, which has been proven in the experiment<sup>13</sup>. Moreover, local filtering could be used to make trace-preserving local operations assisted by classical communication so as to increase limitedly the fidelities of some low-fidelity entangled mixed states with entanglement unchanged<sup>14–18</sup>. These findings enable the entanglement of little-entangled particles (even with fidelities less than the thresholds) to be distillable, because they can be put through local filters, such that their fidelities are over the related thresholds, prior to being subjected to EDPs<sup>19</sup>.

<sup>1</sup>College of Physics and Electronic Engineering, Hengyang Normal University, Hengyang 421002, China. <sup>2</sup>Center for Quantum Technologies, National University of Singapore, 2 Science Drive 3, Singapore 117542. Correspondence and requests for materials should be addressed to X.-W.W. (email: xwwang@mail.bnu.edu.cn) or S.Y. (email: cqtys@nus.edu.sg) or C.H.O. (email: phyohch@nus.edu.sg)

Recently, purification of a single-copy entangled mixed state by local filtering operations has attracted considerable interest<sup>20–39</sup>, due to the fact that it does not involve multiparticle collective operations on multiple copies of source states and thus may reduce the experimental difficulty, as well as can act as a complement to entanglement distillation. The null-result weak measurement (NRWM, a local filtering operation)<sup>40</sup> is widely used to enhance the entanglement of various decohered states in amplitude-damping (AD) or generalized AD environments<sup>20–28</sup>. The experimental viability of implementing a NRWM and its reversal<sup>21,41–47</sup> indeed makes it an elegant approach to protecting entanglement. However, the filtering method cannot be applied for the direct production of entangled pure states<sup>48,49</sup>. To obtain maximally entangled pure states for perfect remote quantum information processing, EDPs are required. Then, a question arises, namely, is the NRWM beneficial to entanglement distribution among distant parties in terms of the efficiency of extracting maximally entangled states, although it can improve with a certain probability the entanglement of each source state (initial noisy entangled state) of the EDP? This paper is addressing such an issue.

We consider entanglement distribution over AD channels. The aim of the users is to share maximally entangled states. As mentioned before, to achieve remote distribution of maximally entangled states, we resort to the entanglement distillation. In previous literatures<sup>20–23</sup>, the NRWM was introduced to raise the amount of entanglement of a single-copy decohered state in AD environments. We here investigate the impact of the NRWM on entanglement distribution efficiencies (i.e., the efficiencies of distilling maximally entangled states) by using it to enhance the entanglement of each decohered state before starting the distillation procedures. We show that NRWMs would decrease distillation efficiencies of bipartite maximally entangled states and multipartite Greenberger-Horne-Zeilinger (GHZ) states<sup>50</sup>. The efficiency (also known as yield in literature) of an EDP is conventionally defined as the ratio of the number of obtained maximally entangled states to that of source states (inputs). Multipartite W-state<sup>51</sup> distribution, however, exhibits different behaviors and features. That is to say, the NRWM would contribute to increasing the efficiency of W-state distribution with the existing EDP or its generalization and reducing the fidelity threshold for distillability of the decohered W state. Our results indicate that the NRWM is not necessarily helpful to practical entanglement distributions, although it is able to increase the amount of entanglement of a single-copy noisy entangled state, and thus suggest a new approach to quantify the ability of a local filtering operation in protecting entanglement from decoherence.

The rest of this paper is organized as follows. In the Results section, we first demonstrate the uselessness of NRWMs to distributions of bipartite entangled states and multipartite GHZ states, and then discuss the effect of the NRWM on W-state distribution. We offer our conclusions in the Discussion section. Some technical bits are deferred to the Methods section.

## Results

**Bipartite entanglement distribution.** The quantum channel considered in this paper is the AD channel. AD decoherence is applicable to many practical qubit systems, including vacuum-single-photon qubit with photon loss, photon-polarization qubit traveling through a polarizing optical fiber or a set of glass plates oriented at the Brewster angle, atomic qubit with spontaneous decay, and superconducting qubit with zero-temperature energy relaxation. The action of the AD channel on a qubit  $l$  can be described by two Krauss operators<sup>52</sup>

$$\begin{aligned} K_0^{(l)} &= |0\rangle\langle 0| + \sqrt{\bar{d}_l}|1\rangle\langle 1|, \\ K_1^{(l)} &= \sqrt{d_l}|0\rangle\langle 1|, \end{aligned} \quad (1)$$

where  $d_l$  stands for the damping rate satisfying  $0 \leq d_l < 1$  and  $\bar{d}_l = 1 - d_l$ . The AD channel is trace preserving, that is,  $\sum_{j=0,1} K_j^{(l)\dagger} K_j^{(l)} = I$ . Note that  $d=0$  denotes the noise-free case, and it will not be considered in the following context.

Assume the initial entangled state to be distributed to Alice and Bob is a 2-qubit Bell state given by

$$|\psi\rangle = \frac{1}{\sqrt{2}}(|01\rangle + |10\rangle). \quad (2)$$

During the process of distributing or storing, the two qubits would experience AD decoherence with decoherence strength  $d_1$  and  $d_2$ , respectively. The original entangled pure state then degrades into a mixed state

$$\begin{aligned} \rho_d &= \sum_{i,j=0,1} K_i^{(1)} \otimes K_j^{(2)} |\psi\rangle\langle\psi| K_i^{(1)\dagger} \otimes K_j^{(2)\dagger} \\ &= \frac{1}{2}(\sqrt{\bar{d}_2}|01\rangle + \sqrt{\bar{d}_1}|10\rangle)(\sqrt{d_2}\langle 01| + \sqrt{d_1}\langle 10|) + \frac{1}{2}(d_1 + d_2)|00\rangle\langle 00|, \end{aligned} \quad (3)$$

where the superscripts of  $K_{i,j}$  denote the qubit indices. The concurrence (a universal entanglement measure for 2-qubit states<sup>53</sup>) of  $\rho_d$  is

$$C(\rho_d) = \sqrt{\bar{d}_1\bar{d}_2}. \quad (4)$$

As claimed and demonstrated in recently reports<sup>20–23</sup>, the concurrence of the decohered state  $\rho_d$  can be improved probabilistically by performing locally each qubit a weak measurement, accompanied by a bit flip operation before and after the weak measurement, respectively. The weak measurement is a kind of measurement that does not totally collapse the measured system. Practically, the weak measurement on a qubit can be done by monitoring its environment using a detector<sup>21,41–47</sup>. Whenever the detector registers an “excitation”, one knows that the qubit has totally collapsed into its ground state; if, however, there is no “excitation” (null result), one

knows that the qubit state is just renormalized. Mathematically, such a measurement can be described by two positive operators

$$\begin{aligned} M_0 &= \sqrt{1-w}|1\rangle\langle 1| + |0\rangle\langle 0|, \\ M_1 &= \sqrt{w}|1\rangle\langle 1|. \end{aligned} \quad (5)$$

If we discard the outcome of  $M_1$ , then  $M_0$  denotes the NRWM (null-result weak measurement) of strength  $w$  ( $0 \leq w < 1$ ), that partially collapses the system to the ground state. The NRWM in fact uses post-selection to selectively map the state of a qubit. If no outcome is discarded, the two operators  $M_1$  and  $M_0$  will describe a noisy effect. Considering that a flip operation  $\sigma^x$  (conventional Pauli operator) is preformed on the system before and after the NRWM  $M_0$ , respectively, the total process can be described by the operator

$$M_w = \sigma^x M_0 \sigma^x = \sqrt{w}|0\rangle\langle 0| + |1\rangle\langle 1|, \quad (6)$$

where  $\bar{w} = 1 - w$ . For convenience,  $M_w$  will be directly referred to as the NRWM operator. After Alice (holds the first qubit) and Bob (holds the second qubit) performing NRWMs of strength  $w_1$  and  $w_2$  on the entangled pairs, respectively, the state  $\rho_d$  becomes

$$\begin{aligned} \rho_w &= \frac{1}{P_w} M_{w_1} \otimes M_{w_2} \rho_d M_{w_1}^\dagger \otimes M_{w_2}^\dagger \\ &= \frac{(\sqrt{\bar{d}_2 \bar{w}_1}|01\rangle + \sqrt{\bar{d}_1 \bar{w}_2}|10\rangle)(\sqrt{\bar{d}_2 \bar{w}_1}\langle 01| + \sqrt{\bar{d}_1 \bar{w}_2}\langle 10|) + (d_1 + d_2)\bar{w}_1 \bar{w}_2|00\rangle\langle 00|}{(d_1 + d_2)\bar{w}_1 \bar{w}_2 + \bar{d}_2 \bar{w}_1 + \bar{d}_1 \bar{w}_2}, \end{aligned} \quad (7)$$

where  $P_w$  is the probability of getting the outcome of  $M_{w_1} \otimes M_{w_2}$ , i.e. the probability of successful event, given by

$$P_w = \text{Tr}(M_{w_1}^\dagger M_{w_1} \otimes M_{w_2}^\dagger M_{w_2} \rho_d) = \frac{1}{2}(d_1 + d_2)\bar{w}_1 \bar{w}_2 + \frac{1}{2}\bar{d}_2 \bar{w}_1 + \frac{1}{2}\bar{d}_1 \bar{w}_2. \quad (8)$$

Evidently,  $\rho_w$  is equivalent to  $\rho_d$  for  $w_1 = w_2 = 0$  that means no weak measurement is made. Naturally,  $P_w$  is then equal to 1. The concurrence of  $\rho_w$  can be calculated as

$$C(\rho_w) = \frac{\sqrt{\bar{d}_1 \bar{d}_2 \bar{w}_1 \bar{w}_2}}{P_w}. \quad (9)$$

$C(\rho_w)$  is larger than  $C(\rho_d)$  provided that  $\sqrt{\bar{w}_1 \bar{w}_2} > P_w$ . Such a condition can be satisfied for any  $d_1$  and  $d_2$  by choosing suitable  $w_1$  and  $w_2$ . For instance, the inequality always holds for  $w_1 = w_2$ . It is easy to see that when  $C(\rho_w) \rightarrow 1$  (corresponding to  $w \rightarrow 1$ ), the success probability  $P_w \rightarrow 0$ .

Although the entanglement established between Alice and Bob was improved by NRWMs, the shared entangled state is still not a maximally entangled pure state that is a prerequisite for some perfect quantum communications (e.g., teleportation). As mentioned before, the filtering operations cannot be, even in principle, applied for the direct production of maximally entangled states<sup>48,49</sup>. To obtain maximally entangled states, Alice and Bob need further to utilize EDPs.

Next, we investigate whether the NRWM can help Alice and Bob to raise the efficiency of getting maximally entangled states by transforming the decohered state  $\rho_d$  to  $\rho_w$  using NRWMs before starting the EDP. We will employ two EDPs, both of which enable bipartite maximally entangled pure states to be extracted from finite copies of  $\rho_w$  or  $\rho_d$  (corresponding to  $w_1 = w_2 = 0$  in  $\rho_w$ ). The first EDP will be called a two-copy EDP, because each round of distillation only involves two copies of input states<sup>6</sup>. The second EDP will be referred to as a bisection EDP, because each round of distillation except the first round divides the pairs of qubits into two blocks of equal length<sup>54</sup>. The bisection EDP is up to now the most efficient theoretical scheme for the amplitude-damped state  $\rho_d$  or  $\rho_w$ <sup>54</sup>, although it is much more difficult than the two-copy EDP in the experiment.

**Two-copy EDP.** Suppose there is a collection of groups of source entangled pairs  $\rho_w$ . Each group contains two pairs, one as the control pair and the other as the target pair. Each party of Alice and Bob holds one qubit of each pair. The EDP works as follows: (i) Alice and Bob apply, respectively, a local controlled-not (CNOT) gate between the two pairs of each group (i.e., the bilateral CNOT operation<sup>6</sup>), where the control pair comprises the two control qubits and the target one the two target qubits; (ii) they measure locally the target pair in the computational basis  $\{|0\rangle, |1\rangle\}$ ; (iii) they keep the control pair if they get the outcomes “11” (this means the success of extracting a maximally entangled state) and “00” (in this case, the control pair can be used for the second round of distillation), and discard it otherwise.

It can be easily verified that if the outcome of this measurement on a given target pair is “11”, then the corresponding control pair is left in the Bell state  $|\psi\rangle$  which can be used for faithful teleportation, etc. The probability of this event is

$$P_1 = \frac{2\bar{d}_1 \bar{d}_2 \bar{w}_1 \bar{w}_2}{[(d_1 + d_2)\bar{w}_1 \bar{w}_2 + \bar{d}_2 \bar{w}_1 + \bar{d}_1 \bar{w}_2]^2}. \quad (10)$$

Since each target pair has to be sacrificed for the measurement, the yield from this procedure is  $Y_{r_1} = P_1/2$ . As for the measurement outcome “00” of the target pair, the corresponding control pair is left in the state

$$\rho_{r_1} = \frac{(\bar{d}_2 \bar{w}_1 | 01) + (\bar{d}_1 \bar{w}_2 | 10)(\bar{d}_2 \bar{w}_1 \langle 01 | + \bar{d}_1 \bar{w}_2 \langle 10 |) + (d_1 + d_2)^2 (\bar{w}_1 \bar{w}_2)^2 | 00 \rangle \langle 00 |}{(d_1 + d_2)^2 (\bar{w}_1 \bar{w}_2)^2 + (\bar{d}_2 \bar{w}_1)^2 + (\bar{d}_1 \bar{w}_2)^2}. \quad (11)$$

The probability of this event is

$$P_0 = \frac{(d_1 + d_2)^2 (\bar{w}_1 \bar{w}_2)^2 + (\bar{d}_2 \bar{w}_1)^2 + (\bar{d}_1 \bar{w}_2)^2}{[(d_1 + d_2) \bar{w}_1 \bar{w}_2 + \bar{d}_2 \bar{w}_1 + \bar{d}_1 \bar{w}_2]^2}. \quad (12)$$

Evidently, two copies of  $\rho_{r_1}$  can be used for the second round of distillation following the procedure above. Then after  $m$  rounds of distillation procedure, the efficiency (total yield) of this EDP becomes

$$\begin{aligned} E'_f(\rho_w) &= Y_{r_1} + Y_{r_2} + \cdots + Y_{r_m}, \\ Y_{r_1} &= \frac{P_1}{2}, \\ Y_{r_m} &= \frac{Y_{r_{m-1}} (\bar{d}_1 \bar{d}_2 \bar{w}_1 \bar{w}_2)^{2^{m-2}}}{2 \{ [(d_1 + d_2) \bar{w}_1 \bar{w}_2]^{2^{m-1}} + (\bar{d}_2 \bar{w}_1)^{2^{m-1}} + (\bar{d}_1 \bar{w}_2)^{2^{m-1}} \}}, \quad (m > 1). \end{aligned} \quad (13)$$

Naturally, for a given EDP, the more entangled the source states are, the higher efficiency would be obtained. As a consequence, the value of  $E'_f$  in a general case (i.e.,  $w_1$  and  $w_2$  are not simultaneously equal to zero) can always be larger than that of it in the case  $w_1 = w_2 = 0$  for given  $d_1$  and  $d_2$ , because the source state  $\rho_w$  can be more entangled than  $\rho_d$ .

What will happen when considering the fact that the probability of getting  $\rho_w$  from  $\rho_d$  by NRWMs is not one but  $P_w$  given in Eq. (8)? Under this situation, the efficiency of the above entanglement distribution scheme, with NRWMs being performed in advance on each copy of  $\rho_d$ , should be

$$E_f(\rho_d) = P_w E'_f(\rho_w). \quad (14)$$

That is, the final efficiency is the product of the efficiencies of two stages: filtering and distillation protocol. If one does not recycle the state  $\rho_d$  corresponding to the aforementioned measurement outcome “00”, the efficiency  $E_f(\rho_d) = E_f^1(\rho_d) = P_w P_1/2$ . It is easy to prove that  $E_f^1(w_1 = w_2 = 0) > E_f^1(w_1 \neq 0, w_2 \neq 0)$  for arbitrarily given  $d_1$  and  $d_2$ . This means that the efficiency of the distillation scheme with NRWM is lower than that of the scheme without NRWM. Such a conclusion is still tenable in the case of any  $m$  rounds of distillation. As an example, we plot the efficiency  $E_f(\rho_d)$  for  $m = 10$  in Fig. 1. It can be seen from Fig. 1 that  $E_f(\rho_d)$  takes the maximum only when  $w_1 = w_2 = 0$  (that means no weak measurement) for any  $d_1$  and  $d_2$ . All the above results imply that the NRWM does not increase but decreases the efficiency of bipartite entanglement distribution, i.e., the efficiency of extracting the Bell state  $|\psi\rangle$  from the amplitude-damped state  $\rho_d$ . Thus, the NRWM would generate a negative impact on the bipartite entanglement distribution. The same conclusion will be obtained for the bisection EDP as shown in the next subsection.

We notice that some 2-qubit partially entangled pure states are more robust than the Bell state  $|\psi\rangle$  in terms of the singlet fractions of the decohered states when just one qubit interacts with the AD channel<sup>17,18</sup>. In this case, the efficiency of establishing maximally entangled states between Alice and Bob may be slightly improved by substituting the input Bell state  $|\psi\rangle$  for an appropriate 2-qubit partially entangled pure state. However, it will make no difference to the conclusion that the NRWM would reduce the efficiency of preparing nonlocal Bell states. As an example, we replace the initial Bell state  $|\psi\rangle$  by the nonmaximally entangled pure state  $|\psi'\rangle = \frac{1}{\sqrt{2-d}}|01\rangle + \sqrt{\frac{1-d}{2-d}}|10\rangle$  from which the maximum singlet fraction is obtained when only one qubit suffers from the AD noise<sup>17,18</sup>. By the same procedure as before and setting  $d_2 = 0$  (or  $d_1 = 0$ ), we obtain the final efficiency of establishing Bell states between Alice and Bob, as displayed in Fig. 2. Figure 2 indicates that the no-NRWM-scheme ( $w = 0$ ) still outperforms the NRWM-scheme ( $w > 0$ ) even using  $|\psi'\rangle$  as the initial state.

**Bisection EDP.** Let Alice and Bob share  $n$  copies of state  $\rho_w$ , where  $n$  is the power of two. For simplicity, we assume  $d_1 = d_2 = d$  and  $w_1 = w_2 = w$ . Then  $\rho_w^{\otimes n}$  can be conveniently written as

$$\begin{aligned} \rho_w^{\otimes n} &= t^n |\psi\rangle \langle \psi|^{\otimes n} + t^{(n-1)} \bar{t} [|\psi\rangle \langle \psi|^{\otimes(n-1)} |00\rangle \langle 00| + \cdots] \\ &\quad + t^{(n-2)} \bar{t}^2 [|\psi\rangle \langle \psi|^{\otimes(n-2)} |00\rangle \langle 00|^{\otimes 2} + \cdots] + \cdots \bar{t}^n |00\rangle \langle 00|^{\otimes n}, \end{aligned} \quad (15)$$

where

$$t = \frac{\bar{d}}{d\bar{w} + \bar{d}}, \quad (16)$$

$\bar{t} = 1 - t$ , and “...” in each square bracket denotes all permutations of the first term in the square bracket.

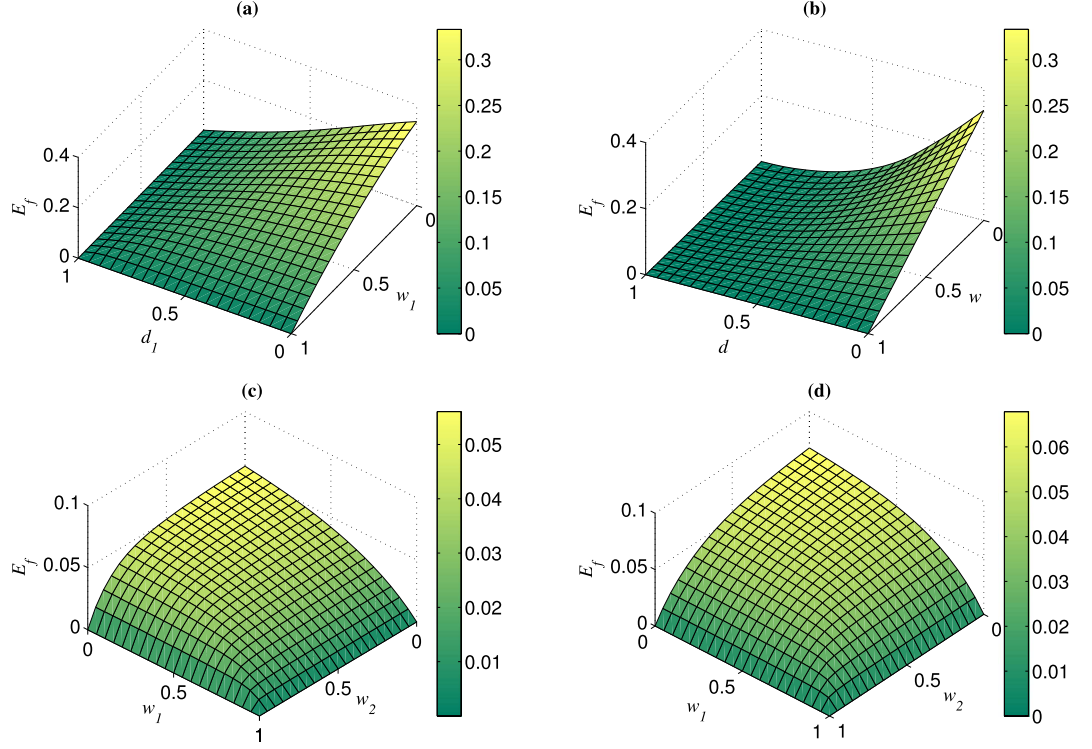


**Figure 1.** Variation in the bipartite entanglement distribution efficiency  $E_f$  with weak measurement strengths ( $w_1, w_2$ ) and channel damping rates ( $d_1, d_2$ ). Here the number of rounds is taken  $m = 10$ .  
**(a)**  $d_2 = 0 = w_2$ ; **(b)**  $d_1 = d_2 = d$  and  $w_1 = w_2 = w$ ; **(c)**  $d_1 = 0.3$  and  $d_2 = 0.7$ ; **(d)**  $d_1 = d_2 = 0.5$ .

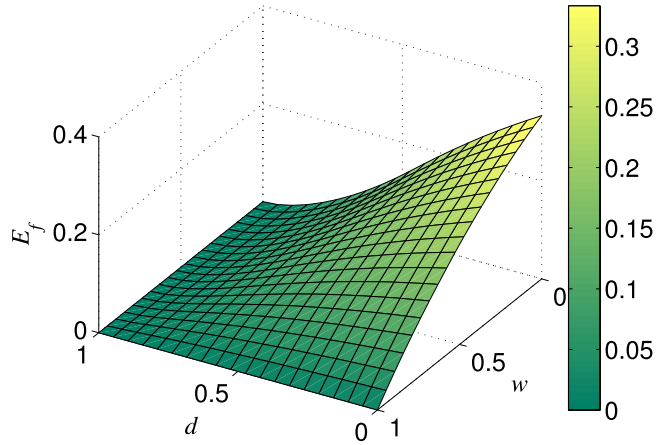


**Figure 2.** Dependence of the bipartite entanglement distribution efficiency  $E_f$  on the weak measurement strength  $w$  and channel damping rate  $d$  when using  $|\psi'\rangle = \frac{1}{\sqrt{2-d}}|01\rangle + \sqrt{\frac{1-d}{2-d}}|10\rangle$  as the initial state and just one qubit of it suffers from the AD noise.

Now both Alice and Bob project her/his part of the state  $\rho_w^{\otimes n}$  on a subspace spanned by vectors with definite number of “1”. That is, they perform their particles von Neumann measurements given by the sets of projectors

$$\left\{ M_a^n = \sum_{[x_a]=n, |x_a|=a} |x_a\rangle\langle x_a| \right\}, \quad (17)$$

$$\left\{ M_b^n = \sum_{|y_b|=n, |y_b|=b} |y_b\rangle\langle y_b| \right\}, \quad (18)$$

respectively, where  $|x_a|(|y_b|)$  denotes the Hamming weight of the string  $x_a(y_b)$  of  $[x_a] = n$  ( $[y_b] = n$ ) qubits and  $a, b \in \{0, 1, \dots, n\}$ . If Alice obtains the measurement outcome  $M_a^n$  and Bob obtains  $M_b^n$ , the state of the  $n$  pairs collapses into

$$\rho_{a,b}^{n,n} = \frac{1}{p(n, a, b)} \sum_{[x_a]=[y_a]=n, |x_a|=|y_a|=a}^{[x_b]=[y_b]=n, |x_b|=|y_b|=b} |x_a\rangle\langle x_a| \otimes |y_b\rangle\langle y_b| \quad (19)$$

with  $|x_a \oplus x_b| = |x_{a+b}|$  and  $|y_a \oplus y_b| = |y_{a+b}|$ , where “ $\oplus$ ” standing for modulo-2 sum of the bitwise of two strings  $x_a(y_a)$  and  $x_b(y_b)$ , e.g.,  $1000 + 0100 = 1100$ . The sign “ $\otimes$ ” in the above equation denotes the partition “Alice:Bob” of  $2n$  qubits and  $p(n, a, b)$  is given by

$$p(n, a, b) = \binom{n}{a+b} \binom{a+b}{a}. \quad (20)$$

The probability of this event is

$$P(n, a, b) = 2^{-a-b} t^{a+b} \bar{t}^{n-a-b} p(n, a, b). \quad (21)$$

If  $a + b = n$ , then Alice and Bob share a maximally entangled pure state of the rank

$$r_a^n = \binom{n}{a}, \quad (22)$$

which is equivalent to  $\log_2 r_a^n$  maximally entangled pairs of qubits. If any one of the equalities  $\{a = 0, a = n, b = 0, b = n\}$  holds, Alice and Bob share a separable state. In the remaining cases, the state  $\rho_{a,b}^{n,n}$  is inseparable in terms of the partition “Alice:Bob”, that is reusable in the second round of distillation. Using the bisection method (Alice and Bob divide the pairs of qubits into two blocks of equal length) in the following rounds of distillation, the total yield of such an EDP starting from the state  $\rho_w$  is given by<sup>54</sup>

$$E'_s(\rho_w) = \sum_{k=1}^m t^{2^k} [H(2^k) - H(2^{k-1})], \quad (23)$$

where  $m = \log_2 n$  and

$$H(x) = \frac{1}{x2^x} \sum_{l=0}^x \binom{x}{l} \log_2 \binom{x}{l}. \quad (24)$$

Considering the fact that the probability of obtaining  $\rho_w$  from the original decohered state  $\rho_d$  is  $P_w$  as Eq. (8) with  $d_1 = d_2 = d$  and  $w_1 = w_2 = w$ , the final efficiency of Alice and Bob sharing maximally entangled pure states should be

$$E_s(\rho_d) = P_w E'_s(\rho_w). \quad (25)$$

The efficiency  $E_s(\rho_d)$  as a function of  $d$  and  $w$  with  $n = 32$  is exhibited in Fig. 3. It can be seen that  $E_s(\rho_d)$  takes the maximum only when  $w = 0$  (that means no weak measurement) for an arbitrarily given  $d$ , and that the larger  $w$ , the lower  $E_s(\rho_d)$ . This result further justifies the fact that NRWMs would decrease the efficiency of distributing maximally entangled pairs to two distant parties. Note that although the total yield of the bisection EDP could be further improved by combining one-way hashing method after the first round of distillation<sup>54</sup>, it will not change the conclusion above, due to the fact that the yields of all rounds except the first round of distillation procedure are not related with the weak measurement parameter  $w$ . In addition, we can see from Figs. 1 and 3 that the decrease of  $E_s(\rho_d)$  caused by NRWMs in the bisection protocol is larger than that in the two-copy protocol. It implies that the more efficient the EDP is, the larger adverse impact the NRWM will have.

The negative influence of the NRWM on the above-mentioned bipartite entanglement distribution could be partly understood from that as follows. If putting the source states (original noisy states) through local filters prior to starting distillation procedure, then the final entanglement distribution efficiency is the product of the efficiencies of two stages: filtering and distilling. Although the NRWM could increase the yield of the second stage, it will decrease the success probability of the first stage (the probability is one when no weak measurement is performed). The competition of two opposite effects in two stages leads to the result above.

What is the case for multipartite entanglement distribution? In the next two sections, we will elucidate such a problem by discussing the impact of the NRWM on GHZ-state and W-state distributions, respectively.

**Multipartite GHZ-state distribution.** In this section, we investigate the effect of the NRWM on the efficiency of GHZ-state distribution in the AD environment based on multipartite EDPs. The existing GHZ-state distillation protocols only deal with “Werner-type” or GHZ-diagonal states and work in asymptotic ways<sup>55-58</sup>. It is not clear whether these protocols can be applied to amplitude-damped GHZ states which are not GHZ-diagonal

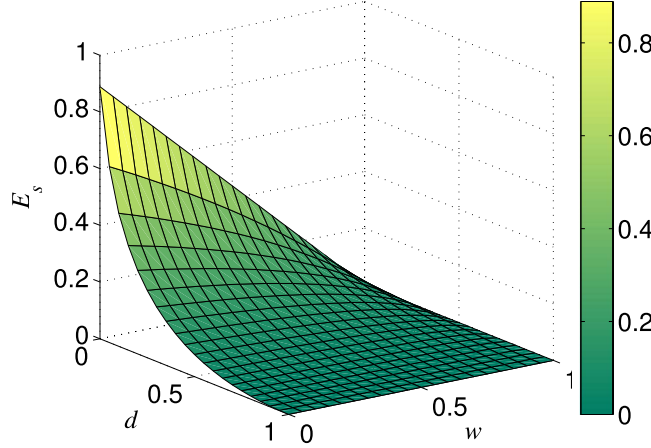


**Figure 3.** Variation in the bipartite entanglement distribution efficiency  $E_s$  with  $d$  and  $w$ . Here we take the number of source pairs  $n = 32$ .

states. We here present an efficient GHZ-state distillation protocol which is suitable for the scenario considered here. This protocol works out of asymptotic way, and can be regarded as a generalization of the aforementioned two-copy EDP for two qubits to a multipartite case. For clarity and simplicity, we here just discuss the case of 3-qubit GHZ-state distillation and distribution, and the obtained results can be extended to  $N$ -qubit GHZ states.

Suppose the initial 3-qubit GHZ state to be distributed to three distant parties is in the form

$$|GHZ\rangle = \frac{1}{\sqrt{2}}(|001\rangle + |110\rangle), \quad (26)$$

where the three qubits are not all parallel. After each qubit independently suffering the AD decoherence during the process of distribution or storage, the state  $|GHZ\rangle$  will degrade into an entangled mixed state denoted by  $\rho'_d$ . If assume the decoherence strength of every qubit is the same, the noisy GHZ state is in the form

$$\begin{aligned} \rho'_d = & \frac{1}{2}[d(1+d)|000\rangle\langle 000| + \bar{d}|001\rangle\langle 001| + dd\bar{d}|010\rangle\langle 010| \\ & + d\bar{d}|100\rangle\langle 100| + \bar{d}^2|110\rangle\langle 110| + \sqrt{\bar{d}^3}|001\rangle\langle 110| + \sqrt{\bar{d}^3}|110\rangle\langle 001|]. \end{aligned} \quad (27)$$

We now perform each qubit a NRWM described by the operator  $M_w$  given in (6). Under the successful event, the noisy GHZ state becomes  $\rho'_w$ , which can be obtained by multiplying each ‘‘0’’ or ‘‘0’’ of  $\rho'_d$  by the factor  $\sqrt{w}$  (e.g.,  $|000\rangle\langle 000| \rightarrow \bar{w}^3|000\rangle\langle 000|$ ). The success probability is

$$P'_w = \frac{\bar{w}}{2}[d(1+d)\bar{w}^2 + \bar{d}\bar{w} + 2d\bar{d}\bar{w} + \bar{d}^2]. \quad (28)$$

According to the analysis in ref. 25,  $\rho'_w$  could be more entangled than  $\rho'_d$  in terms of the measures of negativity and multipartite concurrence, and thus the fidelity of the former could also be higher than that of the latter<sup>29</sup>.

However, we shall show that the NRWM is not good for distilling pure GHZ states from noisy GHZ states. The proposed distillation protocol works as follows: (i) All the three parties take two copies of the input state  $\rho'_w$  (or  $\rho'_d$  with  $w = 0$ ); (ii) each one labels the first qubit control and the second target and perform a CNOT-gate operation on his/her two qubits; (iii) they measure their target qubits in the basis  $\{|0\rangle, |1\rangle\}$ ; (iv) they keep the control qubits if they get the outcome ‘‘111’’ (this means the success of extracting the pure GHZ state  $|GHZ\rangle$ ) or ‘‘000’’ (in this case, the control copy can be used for the second round of distillation), and discard it otherwise. Following the same processing as the bipartite two-copy EDP introduced above, we obtain the formula of the final distribution efficiency of the GHZ state  $|GHZ\rangle$ ,

$$\begin{aligned} E &= P'_w(Y_1 + Y_2 + \dots + Y_m), \\ Y_1 &= \frac{\bar{d}^3\bar{w}^3}{4(P'_w)^2}, \\ Y_m &= \frac{(\bar{d}\bar{w})^{3 \cdot 2^{m-2}} Y_{m-1}}{2\{(d(1+d)\bar{w}^3)^{2^{m-1}} + (\bar{d}\bar{w}^2)^{2^{m-1}} + 2(d\bar{d}\bar{w}^2)^{2^{m-1}} + (\bar{d}^2\bar{w})^{2^{m-1}}\}}, \quad (m > 1), \end{aligned} \quad (29)$$

where  $m$  denotes the number of rounds. The specific dependence of the efficiency  $E$  on the parameters  $d$  and  $w$  for  $m = 10$  is exhibited in Fig. 4. From Fig. 4, we can see that  $E$  takes the maximum value only when  $w = 0$  (that means no weak measurement) for any  $d$ . This result means that the NRWM is bad for the distribution of the

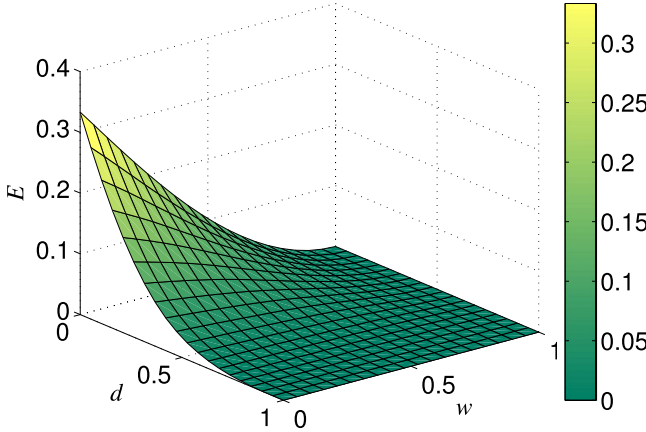


**Figure 4.** Dependence of the 3-qubit GHZ-state distribution efficiency  $E$  on the weak measurement strength  $w$  and channel damping rate  $d$ .

3-qubit GHZ state. We believe the conclusion is also applicable to  $N$ -qubit GHZ states. The origin of the negative influence of the NRWM on the GHZ-state distribution may be the same as that of Bell-state distribution.

**Multipartite W-state distribution.** Next, we discuss the role of the NRWM in the distribution of W states and show different phenomena from that observed before. The W state is a peculiar type of multipartite entangled state, and has attracted particular interest on its properties and applications<sup>51,59–64</sup>. Entanglement distillation of 3-qubit dephased and depolarized W states was studied in ref. 65. A EDP for the 3-qubit amplitude-damped W state has been proposed in ref. 66. Here, we show that the EDP in ref. 66 can be generalized to  $N$ -qubit W states, and that the yields of W-state distillation schemes could be improved by the aforementioned NRWM. Moreover, the fidelity thresholds for distillability of decohered W states could be reduced to near zero.

Suppose the perfect  $N$ -qubit W state

$$|W_N\rangle = \frac{1}{\sqrt{N}}(|0\cdots 01\rangle_N + |0\cdots 010\rangle_N + \cdots + |10\cdots 0\rangle_N) \quad (30)$$

is distributed to  $N$  parties (Alice, Bob, Charlie, …), but suffers typical decoherence as described by the local AD channel with the same damping rate  $d$ . Then the  $N$  parties initially share a noisy W state given by

$$\rho_d = \bar{d}|W_N\rangle\langle W_N| + d|0\cdots 0\rangle\langle 0\cdots 0|. \quad (31)$$

The fidelity of this noisy W state relative to the original pure W state is  $F = \bar{d}$ .

We show that the fidelity of  $\rho_d$  can be improved probabilistically by performing each qubit a NRWM described in Eq. (6). After each of the  $N$  parties performing a NRWM on the qubit he/she holds with a successful event, the state  $\rho_d$  becomes

$$\rho_w = F_w|W_N\rangle\langle W_N| + \bar{F}_w|0\cdots 0\rangle\langle 0\cdots 0|, \quad (32)$$

where the fidelity  $F_w = \bar{d}/(d\bar{w} + \bar{d})$  is the same as  $t$  in Eq. (16) and  $\bar{F}_w = 1 - F_w$ . The success probability is

$$p_w = \bar{w}^{N-1}(\bar{d} + d\bar{w}). \quad (33)$$

Obviously,  $F_w > F$  as long as the weak measurement strength  $w \neq 0$ . Thus the fidelity of a single copy of noisy W state  $\rho_d$  can be indeed enhanced by NRWMs by sacrificing a reduction in the probability. It is easy to see that when  $F_w \rightarrow 1$  (corresponding to  $w \rightarrow 1$ ), the success probability  $p_w \rightarrow 0$ .

We now demonstrate that the NRWM can improve the efficiency of distributing the  $N$ -qubit W state  $|W_N\rangle$  in the AD environment by employing the EDP for amplitude-damped W states. Suppose there are many groups of  $N$ -qubit amplitude-damped W states  $\rho_w$ . Each group contains two copies, one as the control copy and the other as the target copy.  $N$  qubits of each copy belong to  $N$  users (Alice, Bob, Charlie, …), respectively. The W-state distillation protocol is as follows: (i) the  $N$  users first perform, respectively, a local CNOT gate between two copies of each group, the control copy consists of the  $N$  control qubits and the target one the  $N$  target qubits; (ii) they then measure locally the qubits of the target copy in the computational basis  $\{|0\rangle, |1\rangle\}$ ; (iii) they keep the control copy if they get the measurement outcome “00…0”, and discard it otherwise. Depending on the outcome “00…0” known through classical communication, the  $N$  parties share another entangled mixed state

$$\rho_1 = F_1|W_N\rangle\langle W_N| + \bar{F}_1|0\cdots 0\rangle\langle 0\cdots 0|, \quad (34)$$

where the fidelity  $F_1$  of the noisy W state after the first step of distillation is given by

$$F_1 = \frac{F_w^2}{F_w^2 + N\bar{F}_w^2}. \quad (35)$$

The success probability is

$$p_1 = \frac{1}{N} F_w^2 + \bar{F}_w^2. \quad (36)$$

It is easy to prove that  $F_1 > F_w$  for  $F_w > N/(N+1)$ . If  $w = 0$ , meaning that no NRWM has been performed prior to the distillation operations, only  $d < 1/(N+1)$  can ensure  $F_1 > F_w (w=0) = F$ . It indicates that the EDP does not work if one directly use the decohered state  $\rho_d$  instead of  $\rho_w (w>0)$ , as the input of it when  $d \geq 1/(N+1)$ . As to the case of  $w > 0$ , however, the condition of  $F_1 > F_w$  (i.e.,  $F_w > \frac{N}{N+1}$ ) is  $d < 1/(N\bar{w}+1)$ . Evidently, the upper bound of  $d$  in this case could be close to unit by modulating  $w$  to be near to one. In other words, for any damping rate  $d$ , the NRWM would enable the above EDP to work, at least in principle, by meeting

$$w > \frac{(N+1)d - 1}{Nd}. \quad (37)$$

Note that the degree of weak measurement  $w$  can take any value from 0 to 1, and that the inequality (37) naturally holds for  $d < 1/(N+1)$ . Moreover, when  $d \geq 1/(N+1)$ , the larger  $d$  is, the larger  $w$  is required for satisfying the inequality (37).

So, for the case of  $d \geq 1/(N+1)$ , the NRWM is evidently beneficial to the distribution of the  $N$ -qubit W state  $|W_N\rangle$ , due to the fact that it can decrease the fidelity threshold for distillability of the decohered W state  $\rho_d$  from  $N/(N+1)$  to an arbitrarily small number. Whether the NRWM could still bring benefits in the regime of  $d < 1/(N+1)$  (keeping it in mind that the EDP can work with the absence of the NRWM under this case)? We next focus on discussing such a problem. It will be shown that the NRWM would contribute to raising the efficiency of the W-state distillation protocol for most values of  $d$  even in the range  $(0, \frac{1}{N+1})$ , which indicates that the entanglement distribution scheme with NRWM could outperform the scheme without NRWM in most region of  $d \in (0, \frac{1}{N+1})$ .

Based on the success of the first distillation step, the users can carry out the second recurrence step by using  $\rho_1$  as the input state. By the same token, they can carry on with the third, the fourth, and up to the  $m$ th recurrence step so that obtaining the nearly perfect W state. In each step, the input states are the states that are kept in the former step with successful events. The fidelity and success probability in each step comply with the recursion formulas (35) and (36) with  $F_w$  being substituted by the fidelity in the former step. Then after  $m$  steps, the fidelity  $F_m$  of the obtained state relative to the initial perfect W state  $|W_N\rangle$  and the corresponding efficiency  $E_m^{(N)}$  are given by

$$F_m = \frac{1}{1 + \lambda_m}, \quad (38)$$

$$\begin{aligned} E_m^{(N)} &= p_w \cdot \prod_{i=1}^m \frac{p_i}{2} = \bar{w}^{N-1} d (1 + \lambda_m) \prod_{i=0}^{m-1} \frac{1}{2N(1 + \lambda_i)}, \\ p_i &= \frac{1 + \lambda_i}{N(1 + \lambda_{i-1})^2} \quad (i = 1, 2, \dots, m), \\ \lambda_i &= \frac{1}{N} \left( N\bar{w} \frac{d}{\bar{d}} \right)^{2^i} \quad (i = 0, 1, \dots, m). \end{aligned} \quad (39)$$

Here  $p_i$  denotes the success probability in the  $i$ th step. If the fidelity  $F_m \geq 1 - \varepsilon$ , it means the users obtain a nearly perfect W state denoted by  $|W_N^\varepsilon\rangle$  and the W-state distribution succeeds. Following the iteration process as described above, the distribution of the  $N$ -qubit W state would be accomplished in several steps with finite copies of noisy W state  $\rho_d$ .

We now take  $\varepsilon = \varepsilon_0 = 10^{-6}$  as an example for detailed analysis. For clarity, we first consider  $N = 3$ . The required number of distillation steps  $m$  for getting the aim state  $|W_3^{\varepsilon_0}\rangle$  is given in Fig. 5 (see also Methods). From Fig. 5, we can see that for a given  $d$ , there always exists a region of  $w > 0$  in which the required distillation steps are less than that for the case with  $w = 0$ . It means that the NRWM can reduce the number of the distillation steps for obtaining the same expected state. The step-wise behavior in Fig. 5 implies that to arrive at the given fidelity threshold, those initial fidelities in a certain region need the same number of iteration steps. This is due to the fact that a smaller initial fidelity may lead to a faster increase in fidelity of the distilled state, which should result from nonlinearity of the iteration formula of fidelity (given in Eq. (35)) and the initial fidelity  $F_w(d, w)$  with respect to  $d$  and  $w$ . The advantage of the NRWM-scheme in distillation steps can not ensure its efficiency being higher than that of the no-NRWM-scheme. To judge whether the NRWM-scheme could be superior to the no-NRWM-scheme, we need to observe the ratio of the efficiency of the NRWM-scheme  $E_m^{(3)}(w \neq 0)$  to that of the no-NRWM-scheme  $E_{m'}^{(3)}(w = 0)$ , i.e.,

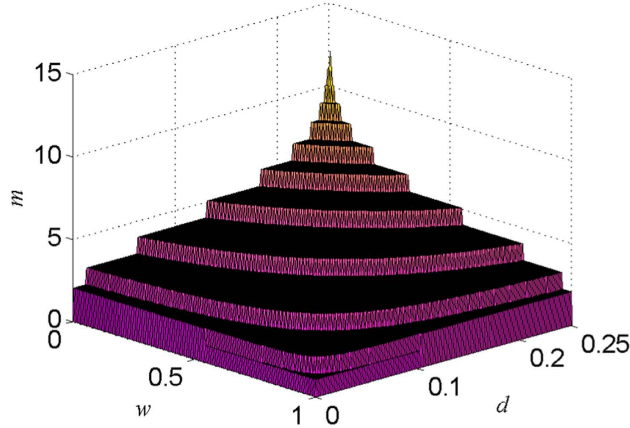


**Figure 5.** The number of distillation steps  $m$  needed for finally getting the aim state  $|W_3^{e_0}\rangle$ .

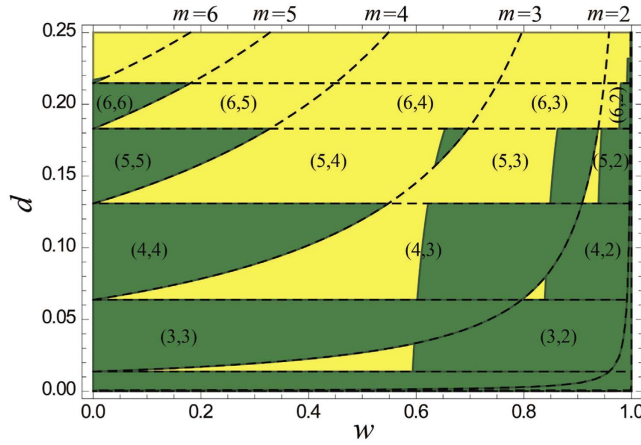


**Figure 6.** The ranges of  $d$  and  $w$  in which  $R^{(3)} > 1$  (yellow) or  $\leq 1$  (green) under the fidelity threshold  $1 - \varepsilon_0$ . The dashed curve lines and straight lines correspond, respectively, to  $3\bar{w}d/\bar{d} = C^{2^{-m}}$  and  $3d/\bar{d} = C^{2^{-m}}$  ( $C = 3\varepsilon_0/(1 - \varepsilon_0)$ ) with different  $m$  (see Methods). The pair-wise numbers  $(m', m)$  ( $m' \geq m$ ) denote that the no-NRWM-scheme and the NRWM-scheme involve, respectively,  $m'$  and  $m$  steps of distillation so that the final fidelity of the noisy W state exceeds the threshold  $1 - \varepsilon_0$  in the encircled regions (see Methods). Note that the no-NRWM-scheme involves only the parameter  $d$  in the region of  $(m', m)$ .

$$R^{(3)} = \frac{E_m^{(3)}(w \neq 0)}{E_{m'}^{(3)}(w = 0)}, \quad (40)$$

note that  $m \leq m'$  as shown in Fig. 5. The dependence of  $R^{(3)}$  on  $d$  and  $w$  is exhibited in Fig. 6, where the region with denotation  $(m', m)$  denotes that the no-NRWM-scheme and the NRWM-scheme at least involve, respectively,  $m'$  and  $m$  steps of distillation so that the final fidelity of the noisy W state exceeds the threshold  $1 - \varepsilon_0$ . It can be seen from Fig. 6 that the regions of  $R^{(3)} > 1$  are as follows: (i)  $(m' > 6, m > 2)$ ; (ii)  $(m' = 6, 6 > m \geq 3)$ ; (iii) most part of  $(m' = 5, 5 > m \geq 3)$ ; (iv) about half of  $(4, 3)$ ; (v) part of  $(m' \geq 3, m = 2)$ . It implies that when  $m = m'$  with  $m'$  being less than a threshold,  $R^{(3)} \leq 1$ . In other cases, however, the regularity of the sign of  $R^{(3)} - 1$  seems to be not clear. It is worth pointing out that the zig-zag behavior in Fig. 6 is well correspondent with the step-wise behavior in Fig. 5. Moreover, the non-ordered phenomenon in Fig. 6 should be related to the fact that  $F_m$  is non-linear with respect to  $d$  and  $w$ , and that  $E_m$  and thus  $R^{(3)}$  are nonmonotonic with respect to  $w$ . In a word, the ratio  $R^{(3)}$  could be larger than one for most values of  $d$  in the range  $(0, 1/4)$ . Thus the NRWM-scheme can indeed outperform the no-NRWM-scheme in most region of  $0 < d < 1/4$  in terms of the efficiency. Generally, the larger the degree of decoherence is, the clearer the superiority of the NRWM-scheme. Moreover, the fact that the NRWM is helpful to distributing W states does not mean the larger  $w$  the better. The optimal weak measurement strength  $w_o^{(3)}$  that maximizes the efficiency  $E_m^{(3)}$  for a given channel damping rate  $d \in (0, 1/4)$  is displayed in Fig. 7, where the inset gives the number of steps  $m$  needed for getting the aim state  $|W_3^{e_0}\rangle$  under the case of  $w = w_o^{(3)}$ . The jump

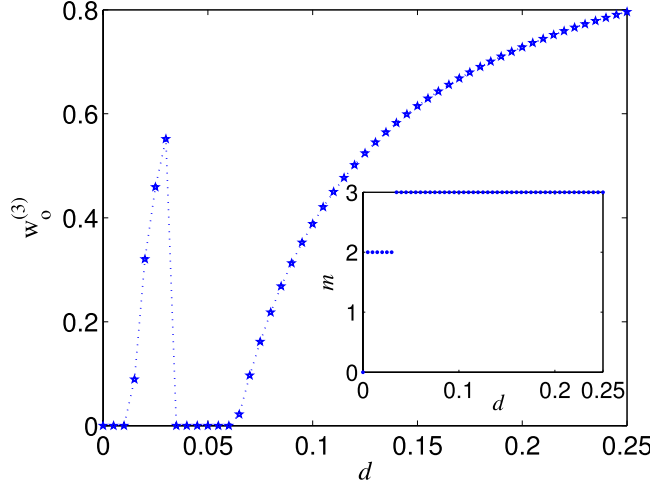


**Figure 7.** The optimal weak measurement strength  $w_0^{(3)}$  that maximizes the efficiency of getting the nearly perfect W state  $|W_3^{\varepsilon_0}\rangle$ . The inset shows the required number of distillation steps  $m$  for getting  $|W_3^{\varepsilon_0}\rangle$  under the optimal degree of weak measurement  $w_0^{(3)}$ .

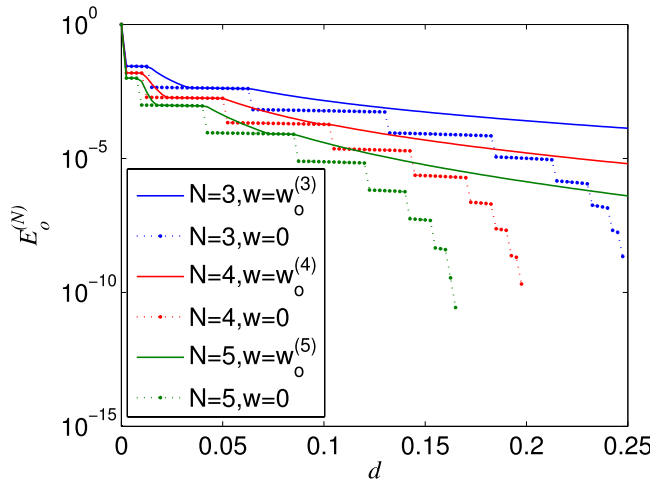


**Figure 8.** The efficiency  $E_0^{(N)}$  of distributing the nearly perfect  $N$ -qubit W state  $|W_N^{\varepsilon_0}\rangle$  to  $N$  distant parties in the AD environment. The solid lines denote the optimal NRWM-scheme and the dotted lines stand for the no-NRWM-scheme which works only for  $d < 1/(N+1)$ .

phenomenon in Fig. 7 is matching to  $R^{(3)} > 1$  in the bottom yellow region of Fig. 6. With the optimal NRWM, we can compute the best efficiency of 3-qubit W-state distribution  $E_0^{(3)}$  (see Fig. 8).

As for a general  $N$ , one can still verify that the efficiency of the EDP with NRWM could be higher than that of the scheme without NRWM for most values of  $d$  in the regime of  $d < 1/(N+1)$ . Furthermore, we can also find the optimal NRWM strength  $w_0^{(N)}$  that maximizes the efficiency of extracting a nearly perfect  $N$ -qubit W state  $|W_N^{\varepsilon_0}\rangle$  from the decohered state  $\rho_d$  for a given channel damping rate  $d$ , and then calculate the corresponding highest efficiency  $E_0^{(N)}$ . Note that  $w_0^{(N)}$  may be dependent on  $N$ . As examples, we show the optimal efficiencies  $E_0^{(N)}$  for  $N = 4, 5$  in Fig. 8. It can be seen that in the regime of  $d < 1/(N+1)$ , the efficiency of the scheme with NRWM is indeed higher than that of the scheme without NRWM for most values of  $d$ .

Finally, we give a brief discussion on the case of  $\varepsilon \rightarrow 0$ . Obviously,  $\varepsilon \rightarrow 0$  would lead to the fact that the entailed number of distillation steps tends to infinity. Then we obtain (see Methods)

$$\begin{aligned} \lim_{\varepsilon \rightarrow 0} R^{(N)} &= \lim_{m, m' \rightarrow \infty} \frac{E_m^{(N)}(w \neq 0)}{E_{m'}^{(N)}(w = 0)} \\ &\sim \bar{w}^{N-1} \exp \left[ \frac{1}{\ln 2} \int_{N\lambda'_0}^{N\lambda_0} \frac{\ln(2N + 2u)}{u \ln u} du \right], \end{aligned} \quad (41)$$

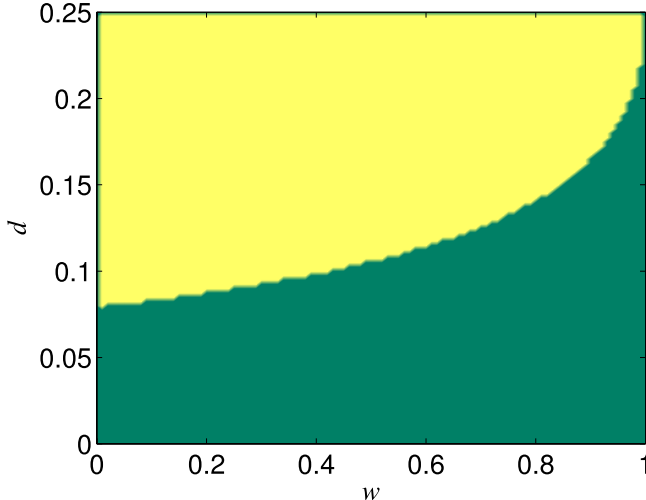


**Figure 9.** The ranges of  $d$  and  $w$  in which  $\lim_{\varepsilon \rightarrow 0} R^{(3)} > 1$  (yellow region) or  $\leq 1$  (green region).

where  $\lambda'_0 = d/\bar{d}$ . As an example, we give the ranges of  $d$  and  $w$  in which  $\lim_{\varepsilon \rightarrow 0} R^{(3)}$  is larger or less than one in Fig. 9. Figure 9 indicates that the ratio  $R^{(3)}$  of the efficiency of the NRWM-scheme to that of the no-NRWM-scheme could also be larger than one under the case of  $\varepsilon \rightarrow 0$  as long as the channel damping rate  $d$  is not too small. In addition, the larger  $d$  is, the clearer the advantage of the NRWM-scheme is. The same results could be obtained for  $N > 3$ .

The positive impact of the NRWM on the W-state distribution could be partly explained by the fact that its positive effect in the distillation phase can surpass its negative effect in the filtering phase when some conditions are satisfied.

### Discussion

Entanglement distillation is a good tool to prepare entangled pure states among distant parties in noisy environments by concentrating the entanglement of a large number of decohered states into a small number of entangled states. Local filtering may be another possible solution to overcoming decoherence of quantum systems. As claimed, a particular filter could be utilized to increase the amount of entanglement of a single-copy noisy entangled state with a certain probability. The filtering method, however, cannot be applied for direct production of an entangled pure state. The effect of filtering operations on protecting entanglement from decoherence would be far more exciting if they can be combined with EDPs to improve the efficiency of distributing entangled pure states to distant users who plan to implement remotely faithful quantum information tasks.

In this paper, we have investigated the possibility of improving the efficiency of distilling maximally entangled pure states from entangled mixed states in the AD environment by using the NRWM (a local filtering operation) which has recently been shown to be an effective method for enhancing probabilistically the entanglement of a single-copy amplitude-damped entangled state. We have shown that NRWMs would lead to the decrease of the distillation efficiencies of bipartite maximally entangled states and multipartite GHZ states. However, we found that the NRWM is beneficial to remote distributions of multipartite W states. We demonstrated that the NRWM can not only reduce the fidelity thresholds for distillability of decohered W states, but also raise the distillation efficiencies of W states. The different effects of the NRWM on the distillation efficiencies of W and GHZ states (or bipartite maximally entangled states) may be related to the fact that the former works in an asymptotic way but the latter does not.

Our results indicate that the NRWM is not necessarily helpful to practical entanglement distributions which aim at establishing maximally entangled pure (or nearly pure) states among distant parties, although it can increase to some extent the amount of entanglement of a single-copy entangled mixed state with a certain probability. This leads to a new criterion for measuring the usefulness of a local filter in protecting entanglement from decoherence. These findings are expected to inspire widespread interest on investigating the possibility of improving efficiencies of distributing entangled states in noisy environments by local filtering operations.

### Methods

**Methods of plotting.** Explanations on plotting Fig. 6 are given below. The purpose of the distillation is to make the final fidelity of the mixed W state  $F_m$  reach to the threshold  $1 - \varepsilon$  via the minimum number of distillation steps  $m$ . Thus  $m$  satisfies  $F_m \geq 1 - \varepsilon > F_{m-1}$  ( $m \geq 1$ ). Using Eq. (38), one can readily obtain

$$m = \left\lceil \log_2 \frac{\ln \frac{N\varepsilon}{1-\varepsilon}}{\ln(N\lambda_0)} \right\rceil. \quad (42)$$

Next, we take  $\varepsilon = \varepsilon_0$  and  $N = 3$  for explaining Fig. 6. With Eq. (42), we can obtain the equations of dashed curve lines in Fig. 6,

$$3\bar{w}\frac{d}{\bar{d}} = C^{2^{-m}}, \quad C = \frac{3\varepsilon_0}{1 - \varepsilon_0}. \quad (43)$$

In the region between neighbored two dashed curve lines with  $m$  and  $m - 1$ , the required number of distillation steps is  $m$  for the NRWM-scheme. The dashed straight lines parallel to  $w$  axis can be directly obtained by setting  $w = 0$  in Eq. (43). Note that  $w = 0$  corresponds to the no-NRWM-scheme. So, if  $C^{2^{-(m'-1)}} < 3d/\bar{d} \leq C^{2^{-m'}} (m' \geq 1)$ , the required number of distillation steps is  $m'$  for the no-NRWM-scheme. Then, the region surrounded by neighbored two straight lines and two curve lines satisfies  $C^{2^{-(m'-1)}} < 3\bar{w}d/\bar{d} \leq C^{2^{-m}}$  and  $C^{2^{-(m'-1)}} < 3d/\bar{d} \leq C^{2^{-m'}}$ , which is denoted by the pair-wise numbers  $(m', m)$  for short. By the way, the intersection points of curve and straight lines satisfy the equation  $\bar{w} = 3d/\bar{d}$ . In the region with denotation  $(m', m) (m < m'$ , as shown in Fig. 5), the entailed numbers of distillation steps are  $m'$  and  $m$  for the no-NRWM-scheme and the NRWM-scheme, respectively. It should be pointed out that  $m' = 0$  means no purification operation is needed, and that  $m = 0$  means purification task can be accomplished by only weak measurements. In the regions on and under the curve  $3\bar{w}d/\bar{d} = C, m = 0$ . If  $d \leq C/(3 + C)$ ,  $m'$  is equal to zero and thus  $m$  is also equal to zero. For any given  $m'$  and  $m$ , the boundary of  $R^{(3)} \leq 1$  can be obtained by solving, at least in principle, the inequality  $E_m \leq E_{m'}$ , i.e.,

$$2^{m'-m}x^2[3 + (xy)^{2^m}] \prod_{i=0}^{m'-1} (3 + y^{2^i}) \leq (3 + y^{2^{m'}}) \prod_{i=0}^{m-1} [3 + (xy)^{2^i}], \quad (44)$$

where  $x = \bar{w}$  and  $y = 3d/\bar{d}$ . If the inequality has no solution, it means  $R^{(3)} > 1$  within the total region  $(m', m)$ .

**Derivation of equation (41).** The derivation of Eq. (41) is given below. When  $m \rightarrow \infty$ , we have

$$\prod_{i=0}^{m-1} 2N(1 + \lambda_i) \rightarrow \exp \left[ \int_0^\infty \ln(2N + 2N\lambda_x) dx \right], \quad (45)$$

$$\lambda_m \rightarrow 0, \quad (46)$$

where the inequality  $N\lambda_0 < 1$  (because  $d < \frac{1}{N+1}$ ) has been utilized. Making two times of variable substitutions  $y = 2^x$  and  $u = (N\lambda_0)^y$ , one will get

$$\int_0^\infty \ln(2N + 2N\lambda_x) dx = \frac{1}{\ln 2} \int_{N\lambda_0}^\infty \frac{\ln(2N + 2u)}{u \ln u} du, \quad (47)$$

where  $\varepsilon \rightarrow 0$ . By substituting Eqs. (46) and (47) into Eq. (39), we obtain

$$\lim_{m \rightarrow \infty} E_m^{(N)}(w \neq 0) \approx \bar{w}^{N-1}\bar{d} \exp \left[ \frac{1}{\ln 2} \int_\varepsilon^{N\lambda_0} \frac{\ln(2N + 2u)}{u \ln u} du \right]. \quad (48)$$

Similarly, we can obtain

$$\lim_{m' \rightarrow \infty} E_{m'}^{(N)}(w = 0) \approx \bar{d} \exp \left[ \frac{1}{\ln 2} \int_\varepsilon^{N\lambda'_0} \frac{\ln(2N + 2u)}{u \ln u} du \right], \quad (49)$$

where  $\lambda'_0 = d/\bar{d}$ . Eq. (41) can be straightforwardly derived from Eqs. (48) and (49).

## References

1. Bennett, C. H., Brassard, G., Popescu, S., B. Schumacher, J. A. S. & Wootters, W. K. Purification of noisy entanglement and faithful teleportation via noisy channels. *Phys. Rev. Lett.* **76**, 722–725 (1996).
2. Deutsch, D. *et al.* Quantum privacy amplification and the security of quantum cryptography over noisy channels. *Phys. Rev. Lett.* **77**, 2818–2821 (1996).
3. Pan, J. W., Gasparoni, S., Ursin, R., Weihs, G. & Zeilinger, A. Experimental entanglement purification of arbitrary unknown states. *Nature* **423**, 417–422 (2003).
4. Reichle, R. *et al.* Experimental purification of two-atom entanglement. *Nature* **443**, 838–841 (2006).
5. Morimae, T. & Fujii, K. Secure entanglement distillation for double-server blind quantum computation. *Phys. Rev. Lett.* **111**, 020502 (2013).
6. Bennett, C. H., DiVincenzo, D. P., Smolin, J. A. & Wootters, W. K. Mixed-state entanglement and quantum error correction. *Phys. Rev. A* **54**, 3824–3851 (1996).
7. Chen, P. X., Liang, L. M., Li, C. Z. & Huang, M. Q. Necessary and sufficient condition for distillability with unit fidelity from finite copies of a mixed state: The most efficient purification protocol. *Phys. Rev. A* **66**, 022309 (2002).
8. Chen, P. X., Liang, L. M., Li, C. Z. & Huang, M. Q. Distilling multipartite pure states from a finite number of copies of multipartite mixed states. *Phys. Rev. A* **69**, 012308 (2004).
9. Czechlewski, M., Grudka, A., Horodecki, M., Mozrzymas, M. & Studziński, M. Distillation of entanglement by projection on permutationally invariant subspaces. *J. Phys. A: Math. Theor.* **45**, 125303 (2012).
10. Sheng, Y. B. & Deng, F. G. Deterministic entanglement purification and complete nonlocal bell-state analysis with hyperentanglement. *Phys. Rev. A* **81**, 032307 (2010).

11. Sheng, Y. B. & Zhou, L. Deterministic entanglement distillation for secure double-server blind quantum computation. *Sci. Rep.* **5**, 7815 (2015).
12. Gisin, N. Hidden quantum nonlocality revealed by local filters. *Phys. Lett. A* **210**, 151–156 (1996).
13. Kwiat, P. G., Barraza-Lopez, S., Stefanov, A. & Gisin, N. Experimental entanglement distillation and ‘hidden’ non-locality. *Nature* **409**, 1014–1017 (2001).
14. Verstraete, F. & Verschelde, H. Optimal teleportation with a mixed state of two qubits. *Phys. Rev. Lett.* **90**, 097901 (2003).
15. Bandyopadhyay, S. Origin of noisy states whose teleportation fidelity can be enhanced through dissipation. *Phys. Rev. A* **65**, 022302 (2002).
16. Badzia, P., Horodecki, M., Horodecki, P. & Horodecki, R. Local environment can enhance fidelity of quantum teleportation. *Phys. Rev. A* **62**, 012311 (2000).
17. Pal, R., Bandyopadhyay, S. & Ghosh, S. Entanglement sharing through noisy qubit channels: One-shot optimal singlet fraction. *Phys. Rev. A* **90**, 052304 (2014).
18. Bandyopadhyay, S. & Ghosh, A. Optimal fidelity for a quantum channel may be attained by nonmaximally entangled states. *Phys. Rev. A* **86**, 020304(R) (2012).
19. Horodecki, M., Horodecki, P. & Horodecki, R. Inseparable two spin-1/2 density matrices can be distilled to a singlet form. *Phys. Rev. Lett.* **78**, 574–577 (1997).
20. Sun, Q., Al-Amri, M., Davidovich, L. & Zubairy, M. Reversing entanglement change by a weak measurement. *Phys. Rev. A* **82**, 052323 (2010).
21. Kim, Y.-S., Lee, J.-C., Kwon, O. & Kim, Y.-H. Protecting entanglement from decoherence using weak measurement and quantum measurement reversal. *Nat. Phys.* **8**, 117–120 (2012).
22. Man, Z. X., Xia, Y. J. & An, N. B. Enhancing entanglement of two qubits undergoing independent decoherences by local pre- and postmeasurements. *Phys. Rev. A* **86**, 052322 (2012).
23. Man, Z. X., Xia, Y. J. & An, N. B. Manipulating entanglement of two qubits in a common environment by means of weak measurements and quantum measurement reversals. *Phys. Rev. A* **86**, 012325 (2012).
24. Siomau, M. & Kamli, A. A. Defeating entanglement sudden death by a single local filtering. *Phys. Rev. A* **86**, 032304 (2012).
25. Singh, U., Mishra, U. & Dhar, H. S. Enhancing robustness of multiparty quantum correlations using weak measurement. *Ann. Phys.* **350**, 50–68 (2014).
26. Liao, X. P., Fang, M. F., Fang, J. S. & Zhu, Q. Q. Preserving entanglement and the fidelity of three-qubit quantum states undergoing decoherence using weak measurement. *Chin. Phys. B* **23**, 020304 (2014).
27. Wang, S. C., Yu, Z. W., Zou, W. J. & Wang, X. B. Protecting quantum states from decoherence of finite temperature using weak measurement. *Phys. Rev. A* **89**, 022318 (2014).
28. Doustimotagh, N., Wang, S., You, C. & Long, G. L. Enhancement of quantum correlations between two particles under decoherence in finite-temperature environment. *Eur. Phys. Lett.* **106**, 60003 (2014).
29. Huang, Y. S. *et al.* Distillation of multipartite entanglement by local filtering operations. *Phys. Rev. A* **89**, 062320 (2014).
30. Ota, Y., Ashhab, S. & Nori, F. Entanglement amplification via local weak measurements. *J. Phys. A: Math. Theor.* **45**, 415303 (2012).
31. Xing, H. B., Yang, M., Dong, P., Fang, S. D. & Cao, Z. L. Enhancing and expanding remote photonic entanglement via local filtering operations. *Opt. Commun.* **321**, 205–210 (2014).
32. Verstraete, F., Dehaene, J. & DeMoor, B. Local filtering operations on two qubits. *Phys. Rev. A* **64**, 010101 (2001).
33. Kent, A., Linden, N. & Massar, S. Optimal entanglement enhancement for mixed states. *Phys. Rev. Lett.* **83**, 2656–2659 (1999).
34. Liang, Y. C., Masanes, L. & Doherty, A. C. Convertibility between two-qubit states using stochastic local quantum operations assisted by classical communication. *Phys. Rev. A* **77**, 012332 (2008).
35. Cen, L. X., Wu, N. J., Yang, F. H. & An, J. H. Local transformation of mixed states of two qubits to bell diagonal states. *Phys. Rev. A* **65**, 052318 (2002).
36. Wang, Z. W. *et al.* Experimental entanglement distillation of two-qubit mixed states under local operations. *Phys. Rev. Lett.* **96**, 220505 (2006).
37. Romero, J. L., Roa, L., Retamal, J. C. & Saavedra, C. Entanglement purification in cavity qed using local operations. *Phys. Rev. A* **65**, 052319 (2002).
38. Xu, X. Y., Xu, J. S., Li, C. F. & Guo, G. C. Measurement-induced quantum entanglement recovery. *Phys. Rev. A* **82**, 022324 (2010).
39. Orioux, A. *et al.* Experimental on-demand recovery of entanglement by local operations within non-markovian dynamics. *Sci. Rep.* **5**, 8575 (2015).
40. Wu, L.-A., Byrd, M. S. & Lidar, D. A. Efficient universal leakage elimination for physical and encoded qubits. *Phys. Rev. Lett.* **89**, 127901 (2002).
41. Korotkov, A. N. & Jordan, A. N. Undoing a weak quantum measurement of a solid-state qubit. *Phys. Rev. Lett.* **97**, 166805 (2006).
42. Katz, N. *et al.* Reversal of the weak measurement of a quantum state in a superconducting phase qubit. *Phys. Rev. Lett.* **101**, 200401 (2008).
43. Lee, J.-C., Jeong, Y.-C., Kim, Y.-S. & Kim, Y.-H. Experimental demonstration of decoherence suppression via quantum measurement reversal. *Opt. Express* **19**, 16309–16316 (2011).
44. Sherman, J. A. *et al.* Experimental recovery of a qubit from partial collapse. *Phys. Rev. Lett.* **111**, 180501 (2013).
45. Keane, K. & Korotkov, A. N. Simplified quantum error detection and correction for superconducting qubits. *Phys. Rev. A* **86**, 012333 (2012).
46. Schindler, P. *et al.* Undoing a quantum measurement. *Phys. Rev. Lett.* **110**, 070403 (2013).
47. Korotkov, A. N. & Keane, K. Decoherence suppression by quantum measurement reversal. *Phys. Rev. A* **81**, 040103 (2010).
48. Linden, N., Massar, S. & Popescu, S. Purifying noisy entanglement requires collective measurements. *Phys. Rev. Lett.* **81**, 3279–3282 (1998).
49. Kent, A. Entangled mixed states and local purification. *Phys. Rev. Lett.* **81**, 2839–2841 (1998).
50. Greenberger, D. M., Horne, M. A., Shimony, A. & Zeilinger, A. Bell’s theorem without inequalities. *Am. J. Phys.* **58**, 1131–1143 (1990).
51. Dür, W., Vidal, G. & Cirac, J. I. Three qubits can be entangled in two inequivalent ways. *Phys. Rev. A* **62**, 062314 (2000).
52. Nielsen, M. A. & Chuang, I. L. *Quantum Computation and Quantum Information*. (Cambridge Univ. Press, Cambridge, 2000).
53. Wootters, W. K. Entanglement of formation of an arbitrary state of two qubits. *Phys. Rev. Lett.* **80**, 2245–2248 (1998).
54. Czechlewski, M., Grudka, A., Ishizaka, S. & Wójcik, A. Entanglement purification protocol for a mixture of a pure entangled state and a pure product state. *Phys. Rev. A* **80**, 014303 (2009).
55. Murao, M., Plenio, M. B., Popescu, S., Vedral, V. & Knight, P. L. Multiparticle entanglement purification protocols. *Phys. Rev. A* **57**, R4075–R4078 (1998).
56. Chen, K. & Lo, H.-K. Multi-partite quantum cryptographic protocols with noisy ghz states. *Quantum Inf. Comput.* **7**, 689–715 (2007).
57. Aschauer, H., Dür, W. & Briegel, H.-J. Multiparticle entanglement purification for two-colorable graph states. *Phys. Rev. A* **71**, 012319 (2005).
58. Kruszynska, C., Miyake, A., Briegel, H. J. & Dür, W. Entanglement purification protocols for all graph states. *Phys. Rev. A* **74**, 052316 (2006).
59. Dür, W. Multipartite entanglement that is robust against disposal of particles. *Phys. Rev. A* **63**, 020303 (2001).

60. Wang, X. W., Su, Y. H. & Yang, G. J. Controlled teleportation against uncooperation of part of supervisors. *Quantum Inf. Process.* **8**, 319–330 (2009).
61. Wang, X. W. & Yang, G. J. Hybrid economical telecloning of equatorial qubits and generation of multipartite entanglement. *Phys. Rev. A* **79**, 062315 (2009).
62. An, N. B. Joint remote state preparation via w and w-type states. *Opt. Commun.* **283**, 4113–4117 (2010).
63. Agrawal, P. & Pati, A. Perfect teleportation and superdense coding with w states. *Phys. Rev. A* **74**, 062320 (2006).
64. Zheng, S. B. Splitting quantum information via w states. *Phys. Rev. A* **74**, 054303 (2006).
65. Miyake, A. & Briegel, H.-J. Distillation of multipartite entanglement by complementary stabilizer measurements. *Phys. Rev. Lett.* **95**, 220501 (2005).
66. Sun, L. L., Wang, H. F., Zhang, S. & Yeon, K. H. Entanglement purification for a three-qubit w-like state in amplitude damping. *J. Korean Phys. Soc.* **61**, 1938–1943 (2012).

### Acknowledgements

This work was supported by the Hunan Provincial Natural Science Foundation of China (Grant No. 2015JJ3029), the Scientific Research Fund of Hunan Provincial Education Department of China (Grant No. 15A028), and also funded by the Singapore Ministry of Education (partly through the Academic Research Fund Tier 3 Grant No. MOE2012-T3-1-009) and the National Research Foundation, Singapore (Grant No. WBS: R-710-000-008-271). X. W. Wang was also supported in part by the Government of China through CSC.

### Author Contributions

X.W.W. contributed to the initial idea. X.W.W. and S.Y. performed the computations. D.Y.Z. and C.H.O. discussed the results. All authors reviewed the manuscript.

### Additional Information

**Competing financial interests:** The authors declare no competing financial interests.

**How to cite this article:** Wang X. W. *et al.* Effect of weak measurement on entanglement distribution over noisy channels. *Sci. Rep.* **6**, 22408; doi: 10.1038/srep22408 (2016).



This work is licensed under a Creative Commons Attribution 4.0 International License. The images or other third party material in this article are included in the article's Creative Commons license, unless indicated otherwise in the credit line; if the material is not included under the Creative Commons license, users will need to obtain permission from the license holder to reproduce the material. To view a copy of this license, visit <http://creativecommons.org/licenses/by/4.0/>

## 9. Exploiting entanglement

**Abstract:** For example, entanglement can be exploited in communication channels with correlated noise.

**Keywords:** Communication channels, correlated noise

# Exploiting entanglement in communication channels with correlated noise

Jonathan Ball,<sup>1</sup> Andrzej Dragan,<sup>2</sup> and Konrad Banaszek<sup>1</sup>

<sup>1</sup>*Centre for Quantum Computation, Clarendon Laboratory,  
University of Oxford, Oxford OX1 3PU, United Kingdom*

<sup>2</sup>*Instytut Fizyki Teoretycznej, Uniwersytet Warszawski, Hoża 69, 00-681 Warszawa, Poland*

We develop a model for a noisy communication channel in which the noise affecting consecutive transmissions is correlated. This model is motivated by fluctuating birefringence of fiber optic links. We analyze the role of entanglement of the input states in optimizing the classical capacity of such a channel. Assuming a general form of an ensemble for two consecutive transmissions, we derive tight bounds on the classical channel capacity depending on whether the input states used for communication are separable or entangled across different temporal slots. This result demonstrates that by an appropriate choice, the channel capacity may be notably enhanced by exploiting entanglement.

PACS numbers: 03.67.Hk, 03.65.Yz, 42.50.Dv

## I. INTRODUCTION

Entanglement is a fragile feature of composite quantum systems that can easily diminish by uncontrollable interactions with the environment. At the same time however carefully crafted entangled states can protect quantum coherence from the deleterious effects of those random interactions. This idea underlies the principles of quantum error correcting codes that strengthen the optimism regarding the feasibility of implementing in practice complex quantum information processing tasks [1].

In this paper we demonstrate how quantum entanglement can help in the task of classical communication. To this end, we develop a simple model of a noisy communication channel, where the noise affecting consecutive transmissions is correlated. Within this model, we derive bounds on the classical channel capacity assuming either separable or entangled input states, and we show that using collective entangled states of transmitted particles leads to an enhanced capacity of the channel.

The motivation for our model comes from classical fiber optic communications [2]. In practice, light transmitted through a fiber optic link undergoes a random change of polarization induced by the birefringence of the fiber. The fiber birefringence usually fluctuates depending on the environmental conditions such as temperature and mechanical strain. At first sight, this makes the polarization degree of freedom unsuitable for encoding information, as the input polarization state gets scrambled on average to a completely mixed state. However, the birefringence fluctuations have a certain time constant which means that the transformation of the polarization state, though random, remains nearly the same on short time scales. Consider now sending a pair of photons whose temporal separation lies well within this time scale. Although the polarization state of each one of the photons when looked at separately becomes randomized, certain properties of the joint state remain preserved. For example, this is the case of the relative polarization of the second photon with respect to the first

one. We can therefore try to decode from the output whether the input polarizations were mutually parallel or orthogonal. This property cannot be determined perfectly, as in general we cannot tell whether two general quantum states are identical or orthogonal if we do not know anything else about them [3], but even the ability of providing a partial answer establishes correlations between the channel input and output that can be used to encode information into the polarization degree of freedom. The situation becomes even more interesting when we allow for entangled quantum states. Then the singlet polarization state of the two photons, when sent as the input, remains invariant under such perfectly correlated depolarization, and it can be discriminated unambiguously against the triplet subspace. Therefore we can encode one bit of information into the polarization state of two photons by sending either a singlet state or any of the triplet states. We shall see that these simple observations will also emerge from our general analysis of the channel capacity.

The first example of entanglement-enhanced information transmission over a quantum channel with correlated noise has been recently analyzed by Macchiavello and Palma [4]. Our model assumes a different form of correlations, and its high degree of symmetries has allowed us to perform optimization of the channel capacity over arbitrary input ensembles. Although we analyze only zero- and one-photon signals, we define the action of the channel in terms of the transformations of the bosonic annihilation operators, which sets up a framework for possible generalizations, such as use of multiphoton signals. This application of entanglement in classical communication is a distinct problem from entanglement-assisted classical capacity of noisy quantum channels studied by Bennett *et al.* in Ref. [5], where it has been shown that prior entanglement shared between sender and receiver can increase the classical capacity. We also note that the non-zero time constant of phase and polarization fluctuations can be used in robust protocols for long-haul quantum key distribution [6, 7].

Before passing on to a detailed discussion of the prob-

lem in the subsequent sections, let us introduce some basic notation. The action of a channel is described by a completely positive map [8] that we will denote by  $\Lambda(\cdot)$ . The sender selects messages from an input ensemble  $\{p_i, \hat{\varrho}_i\}$ , where  $p_i$  is the probability of sending the state  $\hat{\varrho}_i$  through the channel. The capacity of the channel is a function of the mutual information between the input ensemble and measurement outcomes at the receiving stations: it characterizes the strength of correlations between these two that are preserved by the channel. The mutual information itself involves a specific measurement scheme; however, it has a very useful upper bound in the form of the Holevo quantity that depends only on the output ensemble of states  $\{p_i, \Lambda(\hat{\varrho}_i)\}$  emerging from the channel [9]:

$$\chi = S \left( \sum_i p_i \Lambda(\hat{\varrho}_i) \right) - \sum_i p_i S(\Lambda(\hat{\varrho}_i)) \quad (1)$$

where  $S$  is the von Neumann entropy  $S(\hat{\varrho}) = -\text{Tr}(\hat{\varrho} \log_2 \hat{\varrho})$ . As we will see, in our model the Holevo quantity will provide a tight bound on the mutual information that could be achieved in practice using a simple measurement scheme. The classical channel capacity is obtained by assuming arbitrarily long sequences of possibly entangled input systems, and calculating the average capacity per single use of the channel. In our analysis, we will perform a restricted optimization by considering only two consecutive uses of the channel.

## II. CHANNEL DECOMPOSITION

We will start our discussion by proving a rather general lemma about channels that can be decomposed into a direct sum of maps acting on subspaces of the Hilbert space of the input systems. In physical terms, such channels remove quantum coherence between the components of the input state that belong to different subspaces, by zeroing the respective off-diagonal blocks of the density matrix characterizing the input state. This lemma will greatly simplify our further calculations.

*Lemma 1:* Suppose that we can decompose the Hilbert space  $\mathcal{H}$  of the system into a direct sum of subspaces

$$\mathcal{H} = \bigoplus_k \mathcal{H}^{(k)} \quad (2)$$

such that for an arbitrary input state  $\hat{\varrho}$  the state emerging from the channel  $\Lambda(\hat{\varrho})$  can be represented as

$$\Lambda(\hat{\varrho}) = \bigoplus_k \Lambda^{(k)}(\hat{\varrho}^{(k)}) \quad (3)$$

where  $\hat{\varrho}^{(k)} = \hat{\varrho}|_{\mathcal{H}^{(k)}}$  is the input state  $\hat{\varrho}$  truncated to the subspace  $\mathcal{H}^{(k)}$ , and each  $\Lambda^{(k)}$  is a certain trace-preserving completely positive map acting in the corresponding subspace  $\mathcal{H}^{(k)}$ . Then the optimal channel capacity can be

attained with an ensemble in which each state belongs to one of the subspaces  $\mathcal{H}^{(k)}$ .

*Proof:* Indeed, suppose that there is a state  $\hat{\varrho}$  that does not satisfy the above condition, i.e. it is defined on more than one subspace  $\mathcal{H}^{(k)}$ . We can replace it by a sub-ensemble  $\{\text{Tr}(\hat{\varrho}^{(k)}) ; \hat{\varrho}^{(k)}/\text{Tr}(\hat{\varrho}^{(k)})\}$ , obtained by truncating the state  $\hat{\varrho}$  to the subspaces  $\mathcal{H}^{(k)}$  and normalizing the resulting density matrices. In other words, whenever the sender is supposed to transmit  $\hat{\varrho}$ , she replaces it by one of the normalized truncated states  $\hat{\varrho}^{(k)}/\text{Tr}(\hat{\varrho}^{(k)})$  with the corresponding probability  $\text{Tr}(\hat{\varrho}^{(k)})$ . It is straightforward to verify that the average state obtained from such a subensemble is identical with  $\Lambda(\hat{\varrho})$ .

The above observation has a useful consequence when optimizing the Holevo bound on channel capacity. If the input ensemble is of the form discussed above, then it can be split into subensembles of states that belong to separate subspaces  $\mathcal{H}^{(k)}$ , with the probability distributions normalized to one within each subensemble, and  $p_k$  denoting the probability of sending a state from the  $k$ th subensemble. It is then easy to check that the Holevo quantity is given by the following expression:

$$\chi = \sum_k p_k \chi^{(k)} - \sum_k p_k \log_2 p_k, \quad (4)$$

where  $\chi^{(k)}$  is the Holevo quantity for the  $k$ th subensemble. Therefore, the maximization of the Holevo quantity can be performed in two steps. The first one is the optimization of each  $\chi^{(k)}$  separately, assuming an input ensemble restricted to the subspace  $\mathcal{H}^{(k)}$ . The second step consists of optimizing the probability distribution  $p_k$  with the normalization constraint  $\sum_k p_k = 1$ , and it can be performed explicitly using the method of Lagrange multipliers. Indeed, if we denote the Lagrange multiplier as  $\lambda$ , then differentiation over  $p_l$  yields:

$$0 = \frac{\partial}{\partial p_l} \left( \chi - \lambda \sum_k p_k \right) = \chi^{(l)} - \log_2 p_l - \frac{1}{\ln 2} - \lambda. \quad (5)$$

This formula allows us to express the probabilities  $p_l$  in terms of the Lagrange multiplier  $\lambda$  as:

$$p_l = 2^{\chi^{(l)} - 1/\ln 2 - \lambda}, \quad (6)$$

and furthermore summation over  $l$  and using the fact that  $\sum_l p_l = 1$  gives the value of the Lagrange multiplier as:

$$\lambda = \log_2 \left( \sum_l 2^{\chi^{(l)}} \right) - \frac{1}{\ln 2}. \quad (7)$$

Finally, inserting Eqs. (6) and (7) into Eq. (4) yields the maximum value of the Holevo quantity equal to:

$$\chi = \log_2 \left( \sum_k 2^{\chi^{(k)}} \right). \quad (8)$$

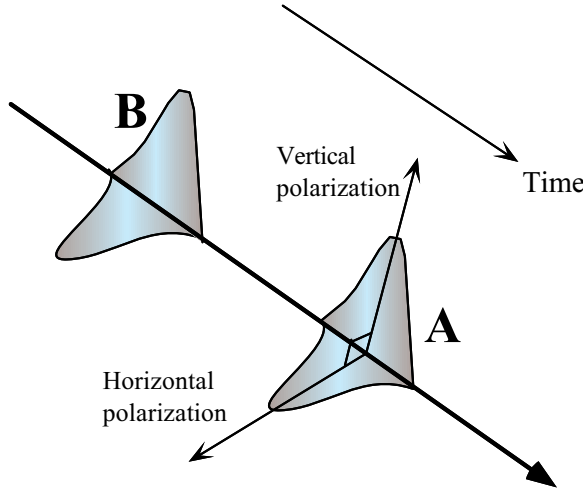


FIG. 1: Representation of two consecutive temporal slots labelled by  $A$  and  $B$ . The Hilbert space of each slot is spanned in our model by three states: the zero-photon state  $|0\rangle$  and two mutually orthogonal polarization states denoted by  $|\leftrightarrow\rangle$  and  $|\updownarrow\rangle$ .

We will later find this expression useful in calculating the channel capacity in our model. The physical reason for this is that we will be able to decompose the set of states used for communication into subensembles with a fixed number of photons, and then optimize the Holevo quantity separately in each subspace.

### III. DEPOLARIZATION MODEL

Let us now introduce a mathematical model for the random transformation of polarization during transmission through the channel. A general linear transformation between two annihilation operators corresponding to a pair of orthogonal modes is given by  $2 \times 2$  unitary matrices [10] that form the Lie group  $U(2)$ . In situations when only the relative phase between the two polarization modes is relevant, the overall phase of the transformation can be assumed to be fixed, which reduces the group of transformations to  $SU(2)$ . However, in our case the overall phase shift can vary between the consecutive temporal slots, and therefore we need to keep it as an independent parameter. We note that any  $U(2)$  matrix can be mapped onto a rotation in the three dimensional physical space. Such a rotation describes the corresponding transformation of the Poincaré sphere used to represent the polarization state of light in classical optics [11]. We will label elements of  $U(2)$  as  $\Omega$  and use a dot to denote the multiplication within the group. The  $U(2)$  group has a natural invariant integration measure which we assume is normalized to one  $\int d\Omega = 1$ . This measure defines a uniformly randomized distribution of polarization transformations that scrambles an arbitrary input polarization to a completely mixed one.

Suppose now that two consecutive temporal slots la-

belled by  $A$  and  $B$ , each comprising two orthogonal polarizations, are occupied by a joint state of radiation  $\hat{\rho}_{AB}$ , as shown schematically in Fig. 1. We will assume that the polarization transformation  $\Omega_A$  affecting the slot  $A$  is completely random, but that the transformation  $\Omega_B$  is correlated with the first one through a conditional probability distribution  $p(\Omega_B|\Omega_A)$ . The resulting transformation of the joint two-slot state is therefore given by the following completely positive map:

$$\Lambda(\hat{\rho}_{AB}) = \int d\Omega_A \int d\Omega_B p(\Omega_B|\Omega_A) \hat{U}(\Omega_A) \otimes \hat{U}(\Omega_B) \hat{\rho}_{AB} \hat{U}^\dagger(\Omega_A) \otimes \hat{U}^\dagger(\Omega_B). \quad (9)$$

Here  $\hat{U}(\Omega)$  is a unitary matrix acting in the Hilbert space of one of the slots that represents the polarization transformation  $\Omega$ . We will now assume that the conditional probability  $p(\Omega_B|\Omega_A)$  depends only on the relative transformation between the slots  $A$  and  $B$  and that it can consequently be represented as  $p(\Omega_B|\Omega_A) = p(\Omega_B \cdot \Omega_A^{-1})$ . In such a case, we can substitute the integration variables in the second integral according to  $\Omega_B = \Omega' \cdot \Omega_A$ , and make use of the invariance of the integration measure  $d\Omega_B = d\Omega'$ . This procedure shows that the map  $\Lambda$  can be represented as a composition of two maps:  $\Lambda = (\hat{1} \otimes \Lambda_{\text{dep}}) \circ \Lambda_{\text{perf}}$ . The first one of them,  $\Lambda_{\text{perf}}$ , acts on both the temporal slots and it depolarizes them in exactly the same way:

$$\Lambda_{\text{perf}}(\hat{\rho}_{AB}) = \int d\Omega \hat{U}(\Omega) \otimes \hat{U}(\Omega) \hat{\rho}_{AB} \hat{U}^\dagger(\Omega) \otimes \hat{U}^\dagger(\Omega) \quad (10)$$

The second map,  $\Lambda_{\text{dep}}$ , acts only on the slot  $B$ , and it introduces additional depolarization relative to the slot  $A$  according to the probability distribution  $p(\Omega')$ :

$$\Lambda_{\text{dep}}(\hat{\rho}_B) = \int d\Omega' p(\Omega') \hat{U}(\Omega') \hat{\rho}_B \hat{U}^\dagger(\Omega'). \quad (11)$$

We will assume later that the distribution  $p(\Omega')$  has sufficient symmetry to describe the action of the map  $\Lambda_{\text{dep}}$  in the relevant Hilbert space with the help of two simple parameters.

We now introduce a further simplification by imposing a condition that each temporal slot may contain at most one photon. Therefore the relevant Hilbert space for each slot is spanned by three states: the zero-photon state  $|0\rangle$ , and horizontally and vertically polarized one-photon states  $|\leftrightarrow\rangle$  and  $|\updownarrow\rangle$ . We can conveniently write the explicit form of the unitary transformation  $\hat{U}(\Omega)$  using the irreducible unitary representations of the group  $SU(2)$ . We will denote by  $\hat{D}^j(\Omega)$  a  $(2j+1) \times (2j+1)$  matrix that is a  $(2j+1)$ -dimensional representation of an  $SU(2)$  element obtained from  $\Omega$  by fixing the overall phase factor to one. These matrices are well known in the quantum theory of angular momentum as describing transformations of a spin- $j$  particle under the rotation group [12]. We will also denote by  $\alpha(\Omega)$  the overall phase

of the element  $\Omega$ . Then the unitary transformation of the input state corresponding to the polarization rotation  $\Omega$  is given by the matrix:

$$\hat{U}(\Omega) = \begin{pmatrix} \hat{\mathcal{D}}^0(\Omega) & 0 & 0 \\ 0 & e^{i\alpha(\Omega)} \hat{\mathcal{D}}^{1/2}(\Omega) & 0 \\ 0 & 0 & e^{i\alpha(\Omega)} \hat{\mathcal{D}}^{1/2}(\Omega) \end{pmatrix}. \quad (12)$$

In this formula, the one-dimensional representation  $\hat{\mathcal{D}}^0(\Omega)$  is identically equal to one, and  $e^{i\alpha(\Omega)} \hat{\mathcal{D}}^{1/2}(\Omega)$  is a  $2 \times 2$  unitary matrix itself; however, we will keep this more general notation in order to be able to use results from the theory of group representations. In particular, the following property of the rotation matrix elements will allow us to evaluate directly a number of expressions:

$$\int d\Omega [\mathcal{D}_{mn}^j(\Omega)]^* \mathcal{D}_{m'n'}^{j'}(\Omega) = \frac{1}{2j+1} \delta_{jj'} \delta_{mm'} \delta_{nn'}. \quad (13)$$

The action of the map  $\Lambda_{\text{perf}}$  on a joint two-slot state can be analyzed most easily if we decompose the com-

plete Hilbert space into a direct sum of subspaces with a fixed number of photons:  $\mathcal{H} = \mathcal{H}^{(0)} \oplus \mathcal{H}^{(1)} \oplus \mathcal{H}^{(2)}$ , where the upper index labels the number of photons. The zero-photon subspace is spanned by a single state  $|0_A 0_B\rangle$ . The one-photon space has a basis formed by four vectors:  $|\leftrightarrow_A 0_B\rangle$ ,  $|\downarrow_A 0_B\rangle$ ,  $|0_A \leftrightarrow_B\rangle$ , and  $|0_A \downarrow_B\rangle$ . Finally, in the two-photon subspace  $\mathcal{H}^{(2)}$  we will introduce a basis that consists of the singlet state  $|\Psi_-\rangle = (|\leftrightarrow_A \downarrow_B\rangle - |\downarrow_A \leftrightarrow_B\rangle)/\sqrt{2}$  and the three triplet states  $|\leftrightarrow_A \leftrightarrow_B\rangle$ ,  $|\Psi_+\rangle = (|\leftrightarrow_A \downarrow_B\rangle + |\downarrow_A \leftrightarrow_B\rangle)/\sqrt{2}$ , and  $|\downarrow_A \downarrow_B\rangle$ . The reason for this choice is that then the action of the tensor product  $\hat{\mathcal{D}}^{1/2}(\Omega) \otimes \hat{\mathcal{D}}^{1/2}(\Omega)$  on a two-photon state can be decomposed into the sum:  $\hat{\mathcal{D}}^{1/2}(\Omega) \otimes \hat{\mathcal{D}}^{1/2}(\Omega) = \hat{\mathcal{D}}^0(\Omega) \oplus \hat{\mathcal{D}}^1(\Omega)$  where  $\hat{\mathcal{D}}^0(\Omega)$  acts on the singlet state  $|\Psi_-\rangle$ , and  $\hat{\mathcal{D}}^1(\Omega)$  is a three-dimensional matrix acting in the triplet subspace. Using our decomposition of the complete Hilbert space, the action of the tensor product  $\hat{U}(\Omega) \otimes \hat{U}(\Omega)$  on a general two-slot state in the basis specified above is given by:

$$\hat{U}(\Omega) \otimes \hat{U}(\Omega) = \hat{\mathcal{D}}^0(\Omega) \oplus e^{i\alpha(\Omega)} \begin{pmatrix} \hat{\mathcal{D}}^{1/2}(\Omega) & 0 & 0 \\ 0 & 0 & 0 \\ 0 & 0 & 0 \end{pmatrix} \oplus e^{2i\alpha(\Omega)} \begin{pmatrix} \hat{\mathcal{D}}^0(\Omega) & 0 & 0 & 0 \\ 0 & \hat{\mathcal{D}}^1(\Omega) & 0 & 0 \\ 0 & 0 & \hat{\mathcal{D}}^1(\Omega) & 0 \\ 0 & 0 & 0 & \hat{\mathcal{D}}^1(\Omega) \end{pmatrix} \quad (14)$$

If we now insert this formula into Eq. (10), it can be easily seen that the invariant integration over the overall phase factor  $\alpha(\Omega)$  kills all the off-block diagonal elements of the density matrix that link different subspaces  $\mathcal{H}^{(k)}$ . In other words, all the coherence between states with different photon numbers is completely removed by the phase fluctuations. Furthermore, the operation  $\Lambda_{\text{dep}}$ , acting only on the second slot, does not mix subspaces with different photon numbers. Therefore the conditions of our lemma are satisfied and we can consider only states with a definite number of photons as elements of the input ensemble. Thus we need to calculate are three corresponding Holevo quantities  $\chi^{(0)}$ ,  $\chi^{(1)}$ , and  $\chi^{(2)}$  that can be combined into a Holevo bound for the overall channel capacity according to Eq. (8). This calculation forms the contents of the next section.

#### IV. CHANNEL CAPACITY

The communication capacity  $\chi^{(0)}$  of the zero-photon subspace itself  $\mathcal{H}^{(0)}$  is naturally zero, as we have only a single state  $|0_A 0_B\rangle$  at our disposal. This state can of course be used as an element of a larger ensemble thus contributing to the overall capacity. This fact is reflected in the form of Eq. (8), where  $\chi^{(0)} = 0$  indeed does increase the total value of  $\chi$ .

##### A. One-photon subspace

A less trivial problem to calculate is the capacity of the one-photon subspace. If we assume a normalized input state  $\hat{\rho}_{\text{in}}$  from the subspace  $\mathcal{H}^{(1)}$ , then the action of the channel  $\Lambda_{\text{perf}}$  restricted to this subspace is given by:

$$\Lambda_{\text{perf}}^{(1)}(\hat{\rho}_{\text{in}}) = \frac{1}{2} \begin{pmatrix} a & 0 & b & 0 \\ 0 & a & 0 & b \\ b^* & 0 & 1-a & 0 \\ 0 & b^* & 0 & 1-a \end{pmatrix} \quad (15)$$

where the parameters  $a$  and  $b$  are defined in terms if the input density matrix as:

$$\begin{aligned} a &= \langle \leftrightarrow_A 0_B | \hat{\rho}_{\text{in}} | \leftrightarrow_A 0_B \rangle + \langle \downarrow_A 0_B | \hat{\rho}_{\text{in}} | \downarrow_A 0_B \rangle \\ b &= \langle \leftrightarrow_A 0_B | \hat{\rho}_{\text{in}} | 0_A \leftrightarrow_B \rangle + \langle \downarrow_A 0_B | \hat{\rho}_{\text{in}} | 0_A \downarrow_B \rangle \end{aligned} \quad (16)$$

For the form of density matrix given in Eq. (15), the depolarizing channel  $\Lambda_{\text{dep}}$  affects only the off-diagonal elements  $b$  and  $b^*$ . We will assume that the symmetry of the distribution  $p(\Omega')$  is such that the effect of  $\Lambda_{\text{dep}}$  is a rescaling of these elements by a real parameter  $\eta'$  bounded between 0 and 1. It is now easy to check that the entropy of the one-photon state emerging from the channel can be written as

$$S(\Lambda(\hat{\rho}_{\text{in}})) = 1 + S\left(\begin{pmatrix} a & \eta'b \\ \eta'b^* & 1-a \end{pmatrix}\right) \quad (17)$$

where the  $2 \times 2$  matrix appearing in the second term can be interpreted as a state of a qubit. Therefore, the second term is bounded by 0 and 1, and consequently  $1 \leq S(\Lambda(\hat{\rho}_{\text{in}})) \leq 2$ . It is a straightforward observation that the Holevo quantity is bound from above by the difference between the maximum and the minimum possible entropies of states emerging from the channel. Therefore we obtain that  $\chi^{(1)} \leq 1$ . This inequality can be saturated simply by taking a one-photon state confined either to the first or to the second temporal slot, with an arbitrary polarization. Thus, the channel capacity is not enhanced in the one-photon sector.

## B. Two-photon subspace

The most interesting regime is when both the temporal slots are occupied by photons. As we will see below, in this case quantum correlations can then enhance the capacity of the channel. If we take a normalized input state  $\hat{\rho}_{\text{in}}$  from the two-photon subspace  $\mathcal{H}^{(2)}$ , then the map  $\Lambda_{\text{perf}}$  produces a Werner state [13]:

$$\Lambda_{\text{perf}}^{(2)}(\hat{\rho}_{\text{in}}) = \hat{W}_c, \quad (18)$$

where we have introduced the following notation:

$$\hat{W}_c = -c|\Psi_-\rangle\langle\Psi_-| + (1+c)\frac{\hat{1}}{4} \quad (19)$$

and we will use for  $c$  the name of the Werner parameter of the input state  $\hat{\rho}_{\text{in}}$ , defined as:

$$c = \frac{1}{3} - \frac{4}{3}\langle\Psi_-|\hat{\rho}_{\text{in}}|\Psi_-\rangle. \quad (20)$$

This result, derived previously in Ref. [13], can be verified independently using the property given in Eq. (13).

The second operation affecting the input state is the partially depolarizing channel  $\hat{1} \otimes \Lambda_{\text{dep}}$ . We will assume that the action of the map  $\Lambda_{\text{dep}}$  acting on the photon in the second temporal slot is simply isotropic depolarization shrinking the length of the Bloch vector by a factor  $\eta$  satisfying  $0 \leq \eta \leq 1$ . Such an operation preserves the Werner form of the transmitted state, and its only effect is the multiplication of the parameter  $c$  by the factor  $\eta$ . Thus, the state emerging from the channel is given by:

$$\Lambda^{(2)}(\hat{\rho}_{\text{in}}) = \hat{W}_{\eta c} \quad (21)$$

with the parameter  $c$  defined by the input state  $\hat{\rho}_{\text{in}}$  according to Eq. (20).

At this point the possibility of enhanced communication capacity by exploiting entanglement manifests itself. The difference between the separable and entangled alphabets can be seen by comparing the allowed ranges of the parameter  $c$ . The positivity of the input density matrix  $\hat{\rho}_{\text{in}}$  requires that

$$-1 \leq c \leq 1/3 \quad (22)$$

and this is the only condition if we consider the most general, possibly entangled input states. However, if the input states are restricted to *separable* ones, then as shown by Horodeccy [14], the allowed range for the parameter  $c$  is reduced to

$$-1/3 \leq c \leq 1/3. \quad (23)$$

This limitation will underlie the reduced channel capacity in the case of separable states.

As the two-photon states emerging from the channel are fully characterized by the Werner parameters of the respective input states, optimization of the Holevo quantity can be carried out over the ensemble  $\{q_j; c_j\}$  of the probabilities  $q_j$  of sending the  $j$ th state with the Werner parameter equal to  $-c_j$ . The output states emerging from the channel is therefore given by an ensemble of Werner states  $\{q_j; \hat{W}_{\eta c_j}\}$ . Because a statistical mixture of Werner states is also a Werner state with the average parameter:

$$\sum_j q_j \hat{W}_{\eta c_j} = \hat{W}_{\sum_j q_j \eta c_j}, \quad (24)$$

the Holevo quantity can be expressed with the help of a single real-valued function  $f(c)$ :

$$\begin{aligned} \chi^{(2)} &= S\left(\sum_j q_j \hat{W}_{\eta c_j}\right) - \sum_j q_j S(\hat{W}_{\eta c_j}) \\ &= f\left(\sum_j q_j \eta c_j\right) - \sum_j q_j f(\eta c_j) \end{aligned} \quad (25)$$

where the explicit form of the function  $f(c)$  is given by:

$$f(c) = 2 - \frac{3}{4}(1+c)\log_2(1+c) - \frac{1}{4}(1-3c)\log_2(1-3c). \quad (26)$$

The optimization of the Holevo quantity, which in principle needs to be performed over an arbitrarily large input ensemble of permitted quantum states, can be greatly simplified using the following observation.

*Lemma 2:* Let  $f(\gamma)$  be a concave function defined on a closed interval  $[\alpha, \beta]$ , and let  $q_j$  be a probability distribution for a set  $\gamma_j$  of real numbers taken from the range  $\alpha \leq \gamma_j \leq \beta$ . Then the following inequality holds:

$$\begin{aligned} &f\left(\sum_j q_j \gamma_j\right) - \sum_j q_j f(\gamma_j) \\ &\leq \sup_{\alpha \leq \gamma \leq \beta} \left( f(\gamma) - \frac{\beta - \gamma}{\beta - \alpha} f(\alpha) - \frac{\gamma - \alpha}{\beta - \alpha} f(\beta) \right). \end{aligned} \quad (27)$$

*Proof:* The concavity of the function  $f(c)$  implies that for every  $j$  we have:

$$f(\gamma_j) \geq \frac{\beta - \gamma_j}{\beta - \alpha} f(\alpha) + \frac{\gamma_j - \alpha}{\beta - \alpha} f(\beta). \quad (28)$$

If we now multiply the above equation by  $-q_j$ , perform the summation over  $j$ , and add a term  $\sum_j f(q_j \gamma_j)$  to both sides of the equation, we will obtain an inequality whose left hand side is identical with that of Eq. (27), and the right hand side is exactly the argument of the supremum for  $\gamma = \sum_j q_j \gamma_j$ . Obviously, this value of  $\gamma$  lies between  $\alpha$  and  $\beta$ , and consequently the supremum may only exceed the value obtained from this calculation. This confirms that Eq. (27) is indeed satisfied.

The above lemma reduces the whole problem of optimizing the Holevo bound to maximizing a one-parameter real-valued function that is the argument of the supremum on the right hand side of Eq. (27). Inserting the explicit form of the function  $f(\gamma)$  given in Eq. (26) and differentiating the resulting expression over  $\gamma$  shows that the supremum in the right hand side of Eq. (27) is attained for

$$\gamma_{\text{opt}} = \frac{1 - 2^{4\mu/3}}{3 + 2^{4\mu/3}} \quad (29)$$

where  $\mu = [f(\beta) - f(\alpha)]/(\beta - \alpha)$ .

As we have seen, the permitted range of the parameters  $c_j$  characterizing the states belonging to the input ensemble depends on whether we allow most general, possibly entangled states, or rather restrict the input to separable states only. If we assume that this range spans from  $c_{\min}$  to  $c_{\max}$ :

$$c_{\min} \leq c_j \leq c_{\max} \quad (30)$$

then we can easily apply Lemma 2 to the expression of the Holevo quantity  $\chi^{(2)}$  in terms of the function  $f(c)$  that has been given in the second line of Eq. (25). Taking  $\alpha = \eta c_{\min}$  and  $\beta = \eta c_{\max}$  and using the explicit value of the turning point derived in Eq. (29) yields the following bound:

$$\chi^{(2)} \leq \log_2(3+2^{4\mu/3}) - f(\eta c_{\min}) + \mu(\eta c_{\min} - 1/3) - 2 \quad (31)$$

where  $\mu$  is given in terms of the input ensemble characteristics as:

$$\mu = \frac{f(\eta c_{\max}) - f(\eta c_{\min})}{\eta(c_{\max} - c_{\min})}. \quad (32)$$

We will analyze in detail numerical values of the channel capacity in the next section. Before doing so, we will close this section by describing a simple intuitive picture of Lemma 2 that gives an additional insight into the form of the input ensemble.

### C. Graphical interpretation

The result of Lemma 2 can be visualized using the following geometrical reasoning depicted in Fig. 2. Consider a graph of the function  $f(\gamma)$  versus its argument  $\gamma$ . The numbers  $\gamma_j$  and the corresponding values of the function  $f$  are given by a set of points  $G_j = (\gamma_j, f(\gamma_j))$  in the

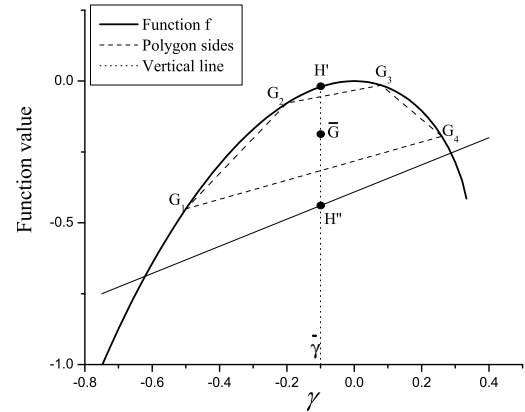


FIG. 2: The graphical representation the maximization procedure for the two-photon subspace. The set of points  $G_j$  corresponds to the output ensemble. The difference  $f(\gamma) - g(\gamma)$  over  $\gamma$  needs to be maximized over the interval  $[\alpha, \beta]$ .

plane of the graph. The probability distribution  $q_j$  for the arguments  $\gamma_j$  defines an average

$$\bar{G} = \left( \sum_j q_j \gamma_j, \sum_j q_j f(\gamma_j) \right) \quad (33)$$

that can be interpreted as a center of gravity for the system of points  $G_j$  that have been assigned respective masses  $q_j$ . Obviously, if the probability distribution is arbitrary, then this average can lie anywhere within the convex polygon spanned by the points  $G_j$ . Since the function  $f$  is strictly concave over the range considered, the whole polygon lies within the area bounded by the graph of the function  $f(\gamma)$  on one side, and a straight line connecting the points  $(\alpha, f(\alpha))$  and  $(\beta, f(\beta))$  on the other side. This straight line is given by a function  $g$  defined as:

$$g(\gamma) = \frac{\beta - \gamma}{\beta - \alpha} f(\alpha) + \frac{\gamma - \alpha}{\beta - \alpha} f(\beta). \quad (34)$$

The left hand side of Eq. (27) is now given by the length of a vertical line connecting  $\bar{G}$  with the point  $H' = (\bar{\gamma}, f(\bar{\gamma}))$  on the graph of the function  $f(\gamma)$ , where  $\bar{\gamma} = \sum_j q_j \gamma_j$ . Clearly, the line  $\bar{G}H'$  will be always equal in length or shorter than the line  $H'H''$  where the point  $H'' = (\bar{\gamma}, g(\bar{\gamma}))$  lies on the graph of the function  $g(\gamma)$ . Furthermore, in order to find the maximum possible length of the line  $H'H''$ , it is clear from this geometric construction that we need to maximize the difference  $f(\gamma) - g(\gamma)$  over  $\gamma$  belonging to the interval  $[\alpha, \beta]$ . This procedure is expressed explicitly in the right hand side of Eq. (27) and the parameter  $\mu$  introduced in the previous subsection is simply the gradient of the function  $g(\gamma)$ .

It is clearly seen from this geometric construction that enlarging the interval  $[\alpha, \beta]$  can only increase the value

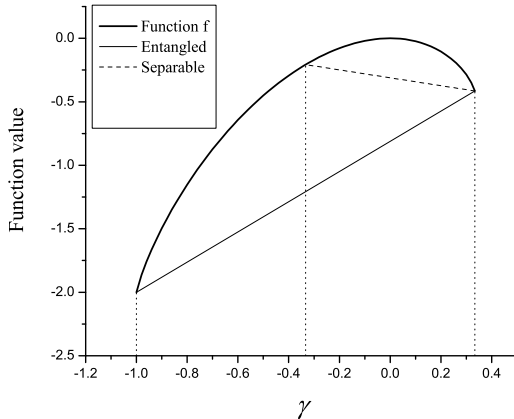


FIG. 3: Depiction of the optimal ensembles that maximize the Holevo quantity in both the general entangled case and the restricted separable case, for perfectly correlated noise ( $\eta = 1$ ). It is sufficient to take only two-element ensembles with the extreme points of the allowed interval. For general entangled states the interval is  $[-1, 1/3]$  whereas for the separable case the interval is  $[-1/3, 1/3]$

of the upper bound given in Eq. (27). This implies two rather straightforward observations. First, the use of entangled states should give a larger capacity compared to separable states. Secondly, a lower value of the parameter  $\eta$  meaning weaker correlations between consecutive polarization rotations results in a decreased channel capacity.

The graphical construction presented above also gives a simple recipe for constructing an output ensemble that saturates the bound on the Holevo quantity. It is sufficient to take a two-element ensemble with the extreme points of the allowed interval as the parameters of the Werner states emerging from the channel:  $\alpha = \eta c_{\min}$  and  $\beta = \eta c_{\max}$ . The optimal probabilities of using the two states need to be selected in such a way that the weighted sum of the points corresponding to these states gives the point  $\gamma_{\text{opt}}$  maximizing the difference  $f(\gamma) - g(\gamma)$ . Explicitly, these probabilities are respectively given by  $(\beta - \gamma_{\text{opt}})/(\beta - \alpha)$  and  $(\gamma_{\text{opt}} - \alpha)/(\beta - \alpha)$ . The actual graph of the function  $f(\gamma)$  with the permitted ranges of the Werner parameter for perfectly correlated noise and entangled and separable inputs is shown in Fig. 3.

## V. ATTAINABILITY AND IMPLEMENTATION

The Holevo quantity  $\chi$  is only an upper bound on the channel capacity and therefore is not necessarily attainable. Users of a communication channel need two relevant pieces of information. The first one is the optimal form of the input ensemble that should be used by the sender. The second one is a measurement scheme that should be employed at the output of the channel in order

to optimize the capacity.

Let us start by summarizing the results of the preceding section and specifying the input ensemble implied by these considerations. We have seen that in the zero- and one-photon subspaces the channel capacity cannot be enhanced by exploiting the polarization degree of freedom. Therefore as the elements of the input ensemble we can take for example states  $|0_A 0_B\rangle$ ,  $|\downarrow_A \downarrow_B\rangle$ , and  $|0_A \uparrow_B\rangle$ , where for concreteness we have fixed the polarization of single-photon states to vertical. The polarization degree of freedom starts to play a nontrivial role when both the temporal slots are occupied by photons. In this subspace, we need to select two input states characterized by the Werner parameters that are as distant as it is allowed by the constraints on the input ensemble. If we restrict ourselves to separable states, then according to Eq. (23) we need to take one separable state with  $c_{\min} = -1/3$  and another one with  $c_{\max} = 1/3$ . It is easy to verify using Eq. (20) that the pair of separable states satisfying this condition can be taken as  $|\uparrow_A \leftrightarrow_B\rangle$  and  $|\uparrow_A \uparrow_B\rangle$ . We thus see that in agreement with the simple picture developed in the introduction to this paper, the relevant quantity is the relative polarization of the photons occupying consecutive slots. If we allow for entangled input, then the lower limit for the Werner parameters of the input states shifts down to  $c_{\min} = -1$ . This value can be of course attained by taking the singlet state  $|\Psi_-\rangle$  itself as one element of the input ensemble, and any state with  $c_{\max} = 1/3$ , for example again  $|\uparrow_A \downarrow_B\rangle$  as the second one.

In order to complete the description of the communication protocol, we need to specify the measurement applied to the states emerging from the channel. This task can be decomposed into two steps. The first one is the determination of the total number of photons contained in the two slots and it can in principle be accomplished by a collective quantum non-demolition measurement [15] on all the modes involved that would determine the total photon number without destroying coherence between the modes. Depending on the outcome, the second step needs to be either finding the temporal slot occupied by a photon in the one-photon subspace which can be realized by direct temporally resolved detection, or discriminating between the states used to encode information in the two-photon subspace. It is easy to see that this discrimination takes a simple form in the case of perfectly correlated noise and entangled input states: we need to determine whether the received states belong to the singlet or the triplet subspace, which corresponds to a two-element projective measurement:

$$\begin{aligned}\hat{\mathcal{O}}_S &= |\Psi_-\rangle\langle\Psi_-| \\ \hat{\mathcal{O}}_T &= \hat{\mathbb{1}} - |\Psi_-\rangle\langle\Psi_-|\end{aligned}\quad (35)$$

It turns out that the same measurement saturates the Holevo bound also in the general case of any value of the parameter  $\eta$  with either entangled or separable input states. In Fig. 4(a) we depict conditional probabilities of obtaining the singlet or the triplet outcomes for a

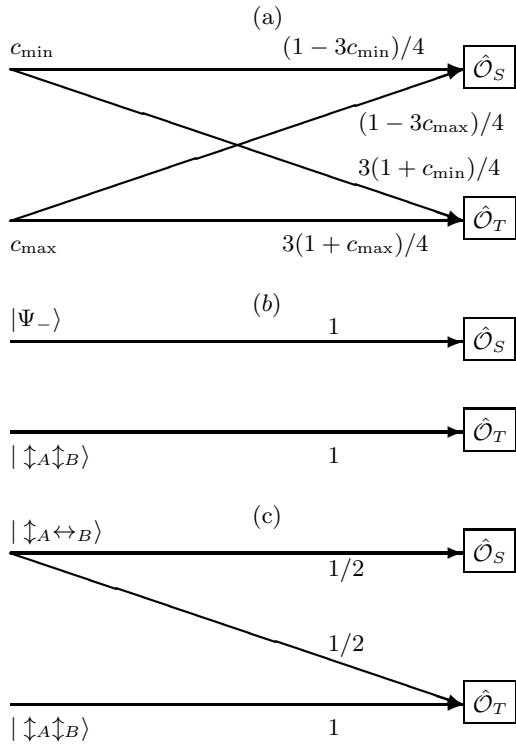


FIG. 4: Depiction of the outcomes of operator measurements  $\hat{O}_S$  and  $\hat{O}_T$ . The general case is shown in (a). For perfectly correlated noise, when the full range of allowed entangled states is employed, perfect distinguishability between the two inputs is possible as shown in (b). In the restricted separable states only regime, the diagram reduces to that shown in (c) and the emerging states are unable to be distinguished unambiguously.

two-element input ensemble characterized by Werner parameters  $c_{\min}$  and  $c_{\max}$ . A lengthy but straightforward calculation shows that if we take as the input probabilities the values discussed in the preceding section, the mutual information is given exactly by the right hand side of Eq. (31). Thus the described procedure indeed maximizes the channel capacity in the two-photon subspace.

It is instructive to compare the above diagram for optimal entangled and separable input ensembles in the case of perfect correlations  $\eta = 1$ . For the optimal entangled ensemble, shown in Fig. 4(b) we can distinguish perfectly between the two inputs as they belong to orthogonal subspaces even after the transmission. For the separable ensemble, the emerging states can no longer be perfectly discriminated as seen in Fig. 4(c).

The complete channel capacity obtained by combining Eq. (8) with the results of Sec. IV is shown as a function of  $\eta$  in Fig. 5. It is seen that using an entangled input ensemble gives a clear advantage over the separable states over the complete range of the correlation parameter  $\eta$ .

We note that the measurement discriminating between the singlet and the triplet subspaces can be implemented using the Braunstein-Mann scheme based on linear optics

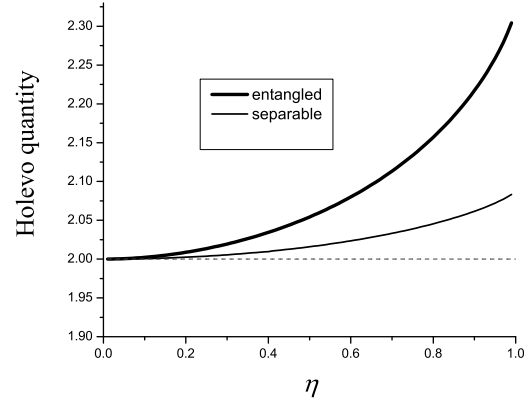


FIG. 5: Graph showing plot of  $\chi$  versus  $\eta$ . The channel capacity for the general case where entangled states are used is significantly greater than for the restricted case where only separable states are employed. The dashed line is the channel capacity when the polarization degree of freedom is not used at all.

[16], as we do not have to distinguish between all four Bell states. After overlapping temporally the received photons and interfering them on a 50:50 non-polarizing beam splitter, their detection in the same output port corresponds to a projection onto the triplet subspace, whereas measuring them in the separate output ports of the beam splitter identifies the singlet state.

## VI. CONCLUSIONS

We have introduced a model of a communication channel with correlated noise motivated by random birefringence fluctuations in a fiber optic link. Within this model, we have demonstrated that introducing quantum correlations between consecutive uses of the channel increases its capacity. This demonstrates how specifically quantum phenomena such as entanglement can be helpful in the task of transferring classical information. Making use of entanglement requires more complex preparation procedures that provide joint input states extending over a number of temporal slots. A related question is the role of collective quantum measurements on the output of the channel rather than detecting radiation in each of the slots individually and combining classical outcomes of separate measurements.

The action of the channel has been defined in terms of transformations of the bosonic field operators. This opens up a route towards interesting generalizations of the present work, for example including arbitrary multi-photon states. Another direction would be extending the model to an arbitrary number of temporal slots rather than just allowing for correlations between pairs of consecutive slots as in our example. It is easy to give a simple protocol showing that in this case the channel capacity

can be enhanced even further. Suppose that the sender generates a train of zero- and one-photon states with the same probabilities equal to one half. The first time she is to transmit a photon, she sends half of maximally entangled pair. In the second instance when a one photon should be transmitted, she sends the remaining member of the pair transforming it in such a way that the joint two-photon polarization state belongs either to the singlet or the triplet subspace. The receiver implements a polarization-independent quantum non-demolition measurement on each temporal slot. When a photon is detected, it needs to be stored until the arrival of the second member of a pair, when the discrimination between the singlet and the triplet subspaces can be performed with

the help of a joint measurement. If the fluctuations in random birefringence can be neglected over the temporal separation between the photons in a pair, this procedure allows one to encode one extra bit of information into each pair of transmitted photons. This gives the average channel capacity equal to 2.5 per a pair of temporal slots, enhancing further the optimal value shown in Fig. 5.

## ACKNOWLEDGEMENTS

This research was supported by EPSRC and Polish KBN.

- [1] M. A. Nielsen and I. L. Chuang, *Quantum Computation and Quantum Information* (Cambridge University Press, Cambridge, 2000).
- [2] A. Ghatak and K. Thyagarajan, *Introduction to Fiber Optics* (Cambridge University Press, Cambridge, 1998).
- [3] E. Kashefi, A. Kent, V. Vedral, and K. Banaszek, Phys. Rev. A **65**, 050304(R) (2002).
- [4] C. Macchiavello, G. M. Palma, Phys. Rev A **65**, 050301 (2002).
- [5] C. H. Bennett, P. W. Shor, J. A. Smolin, and A. V. Thapliyal, Phys. Rev. Lett. **83**, 3081 (1999).
- [6] Z. D. Walton, A. F. Abouraddy, A. V. Sergienko, B. E. A. Saleh, and M. C. Teich, Phys. Rev. Lett. **91**, 087901 (2003).
- [7] J.-C. Boileau, D. Gottesman, R. Laflamme, D. Poulin, and R. W. Spekkens, quant-ph/0306199.
- [8] P. Hausladen, R. Jozsa, B. Schumacher, M. Westmoreland, and W. K. Wootters, Phys. Rev. A **54**, 1869 (1996).
- [9] A. S. Holevo, Prob. Inf. Transm. **5**, 247 (1979).
- [10] R. A. Campos, B. E. A. Saleh, and M. C. Teich, Phys. Rev. A **40**, 1371 (1989).
- [11] M. Born and E. Wolf, *Principles of Optics*, 7th Ed. (Cambridge University Press, Cambridge, 1999).
- [12] D. M. Brink and G. R. Satchler, *Angular Momentum*, 2nd Ed. (Clarendon, Oxford, 1968).
- [13] R. F. Werner, Phys. Rev. A **40**, 4277 (1989).
- [14] R. Horodecki and M. Horodecki, Phys. Rev. A **54**, 1838 (1996).
- [15] P. Grangier, J. A. Levenson, and J.-P. Poizat, Nature **396**, 537 (1998).
- [16] S. L. Braunstein and A. Mann, Phys. Rev. A **51**, R1727 (1995)

# Quantifying and Exploiting Entanglement

by

Irfan Ali Khan

Submitted in Partial Fulfillment  
of the  
Requirements for the Degree  
Doctor of Philosophy

Supervised by  
Professor John C. Howell

Department of Physics and Astronomy  
The College  
Arts and Sciences

University of Rochester  
Rochester, New York

2006

*for my mother, my family, and my Chia-Ling*

# Curriculum Vitae

The author was born in Karachi, Pakistan on the 3rd September, 1978 where he obtained his primary and secondary education from the Karachi Grammar School. He then went to London, England in 1997 for further education. He obtained his Bachelors of Science with First Class Honours in Physics with Theoretical Physics from the Imperial College of Science, Technology and Medicine in 2000. He also obtained a Masters of Science in Quantum Fields and Fundamental Forces from Imperial College in 2001. He came to the University of Rochester in the fall of 2001 where he was recipient of the Marshak Fellowship in 2001 and 2002. At the University of Rochester he carried out his doctoral research in one- and two-photon quantum optics under the supervision of Professor John C. Howell.

## Publications

I. Ali Khan, C. Broadbent, and J. C. Howell, “Experimental Demonstration of Secure, Large Alphabet Quantum Key Distribution Using Energy Time Entanglement” *Phys. Rev. Lett.* (submitted)

I. Ali Khan, C. Broadbent, and J. C. Howell, “Experimental Demonstration of Entanglement Reduction and Restoration for Three Party Secret Sharing” *Phys. Rev. A* (submitted)

I. Ali Khan and J.C. Howell, “Experimental Demonstration of High Two-Photon Time-Energy Entanglement” *Phys. Rev. A* **73**, 031801 (2006).

M. N. O’Sullivan-Hale, I. Ali Khan, R. W. Boyd, and J.C. Howell, “Pixel Entanglement: Experimental Realization of Optically Entangled  $d = 3$  and  $d = 6$  Qudits” *Phys. Rev. Lett.* **94**, 220501 (2005).

I. Ali Khan and J. C. Howell, “Exploring the optimal sensitivity of sum-variance nonseparability criteria for spin-1/2 systems” *Phys. Rev. A* **70**, 062320 (2004).

I. Ali Khan and J.C. Howell, “Hong Ou Mandel Cloning: quantum copying without an ancilla” *Phys. Rev. A* **70**, 010303(R) (2004).

I. Ali Khan and J.C. Howell, “Reconciling Cloning Fidelities” *Quantum Information and Computation* **4**, 146 (2004).

## Presentations

I. Ali Khan, C. Broadbent, and J.C. Howell, “Experimental Demonstration of Large Alphabet Quantum Key Distribution Using Energy Time Entanglement” SPIE annual meeting, San Diego, CA \*\*Invited\*\* (August 2006)

I. Ali Khan, C. Broadbent, and J.C. Howell, “Experimental Demonstration of Large Alphabet Quantum Key Distribution Using Energy Time Entanglement” CLEO/QELS, Long Beach, CA \*\*Postdeadline\*\* (May 2006)

C. Broadbent, I. Ali Khan, and J.C. Howell, “Experimental Demonstration of Entanglement Reduction and Restoration for Three Party Secret Sharing” CLEO/QELS, Long Beach, CA (May 2006)

I. Ali Khan and J.C. Howell, “High Bandwidth Quantum Communication and EPR’s Paradox” SPIE annual meeting, San Diego, CA \*\*Invited\*\* (July 2005)

**CURRICULUM VITAE**

---

I. Ali Khan and J.C. Howell, "Experimental Demonstration of High Dimensional Time-Energy Entangled Two-Photon States" CLEO/QELS, Baltimore, MD (May 2005)

I. Ali Khan and J.C. Howell, "Momentum-position realization of the Einstein-Podolsky-Rosen paradox", SPIE annual meeting, Denver, CO \*\*Invited\*\* (July 2004)

I. Ali Khan and J.C. Howell, "Hong-Ou-Mandel Cloning: Quantum copying without an ancilla" CLEO/QELS, San Francisco, CA (May 2004)

I. Ali Khan and J.C. Howell, "Phase-Covariant Cloning" CLEO/QELS, Baltimore, MD \*\*Postdeadline\*\* (May 2003)

**Patents**

J.C. Howell and I. Ali Khan, "High Bandwidth Time-Energy Quantum Cryptography" *prov. pat. filed* Jan 10, 2006. Ref#1-11072-06010

# Acknowledgements

First and foremost I would like to thank my mother for giving me a wonderful past and a promising future. I thank my father for being there when I most needed him. I thank my family for making me who I am, and my friends for accepting who I have become.

I would like to acknowledge the support and guidance of my thesis advisor Professor John Howell. Professor Howell encourages discussion and an atmosphere of creativity that has allowed us group members to explore independent ideas, frequently yielding fruitful results. Professor Howell has always made himself available to answer questions and help out with experimental and conceptual difficulties. I learnt a great deal from Professor Howell during the process of setting up a new lab. I have greatly enjoyed Professor Howell's perpetual optimism and his infectious excitement for research.

I thank Professor Boyd for enlightening group meetings, and his invaluable advice on paper writing. I thank Professor Zubairy for very interesting discussions at SPIE 2004 and 2005.

I would like to thank my principal experimental collaborators Curtis Broad-

## ACKNOWLEDGEMENTS

---

bent and Colin O’Sullivan-Hale. Curtis possesses an energy, dynamism and initiative that made research an extremely pleasurable experience. I thank Colin for showing me the ropes of Fourier optics, and for wonderful discussions during our collaborations together. I would like to thank Michael Pack for sharing his encyclopedic knowledge with us, for always helping out, and for his profoundly quirky comments. I thank Ryan Camacho for his consistently cheerful mood and helpfulness around the lab, and a short collaboration on hot Rubidium cells. I thank Ryan Bennink and Sean Bentley for their help in getting our experiments underway.

I would like to thank Faisal Ahmad, my partner in crime, for sharing with me this stretch of life’s journey, and hopefully more. I thank Raja, Rafia and Sumera Ahmad for our conversations on scholarship, and our discussions on the opinions of my extreme *jahalat*. I thank Hasan Abbasi for first inspiring my interest in physics and pursuing a Ph.D. in this field.

I thank all the graduate students who have made the University of Rochester an enjoyable place to work. Sungjong Woo for liberating discussions, Marat Khavizov for companionship, and Palash and Vasudha Bharadwaj for relaxing evenings. I would like to thank the fine staff of the physics department for their excellent work in keeping the department running smoothly, and Barbara Warren for pointing me in the right direction these past five years.

I thank my brother Sultan, his wife Erum and their daughter Iman for taking

## ACKNOWLEDGEMENTS

---

care of me in England, and for letting me share in their lives. I thank my sisters Aida and Anokhi for always being there for me.

Finally, I would like to thank Chia-Ling for making life more colorful than I ever thought it could be. Together we have tried to experience the most of life. Because of Chia-Ling I now know how to ski, how to stroll in the park, how to use linux, and how to watch a garden blossom. I would also like to thank Chia-Ling for helping me with the formatting of this dissertation.

# Abstract

The aim of this work is to explore the characterization of various entangled parameters of the two-photon state that is created in the process of spontaneous parametric down-conversion, as well as to investigate the potential application of these two-photon states to quantum communication and quantum information processing. The parameters fall into two natural divisions, the discrete-variable and continuous-variable regimes.

Polarization-correlated photon pairs are used to explore the discrete-variable regime. Using these polarization-correlated photon pairs we investigate phase-covariant quantum cloning, sum-variance entanglement measures, and unambiguous state-discrimination. Phase-covariant quantum cloning is experimentally demonstrated to provide higher cloning fidelity than a universal quantum cloner. The simplicity of the practical implementation of this cloning method makes this cloner a useful addition to the quantum information and communication toolbox. Next, it is experimentally demonstrated that three, concatenating, sum-variance entanglement measures possess higher sensitivities than the popular Bell entanglement measure, while each requires fewer measurements than a Bell measurement

---

**ABSTRACT**

to obtain. Finally, it is demonstrated that unambiguous state-discrimination of nonorthogonal, bipartite entangled-states involves an analogous physical mechanism to that of entanglement distillation of bipartite entangled states. This physical mechanism is the basis of a two-qubit, three-party secret sharing protocol.

In the continuous variable regime, two-photon position-momentum entanglement and two-photon time-energy entanglement is explored. Entanglement between discrete regions of space (pixels) is demonstrated using transverse-momentum and position entanglement. Each photon is mapped onto as many as six pixels, where each pixel represents one level of a qudit state. Next, the number of information eigenmodes  $K$  of time-energy entanglement is investigated. Explicit measurements estimate  $K$  to be greater than 100, with theoretical estimates predicting a value of as high as  $1 \times 10^6$ . Finally, a protocol for large alphabet quantum key distribution is presented that uses energy-time entangled biphotons. Binned, high-resolution timing measurements are used to generate a large alphabet key of up to 1278 characters, while the security of the quantum channel is determined from the measured visibility of Franson interference fringes. Successful encryption and decryption is demonstrated for a generated key of  $\sim 5$  bits per photon, with a key bit error rate of  $\sim 10\%$ .

# Table of Contents

<b>1 Foreword</b>	<b>1</b>
<b>I Discrete-Variable Regime</b>	<b>5</b>
<b>2 Reconciling cloning fidelities</b>	<b>6</b>
2.1 Introduction . . . . .	7
2.2 Definition of Fidelity . . . . .	10
2.3 $N \rightarrow M$ Cloner . . . . .	15
2.4 2-level Ancilla . . . . .	17
2.5 Conclusion . . . . .	20
<b>3 Hong-Ou-Mandel Cloning: quantum copying without an ancilla</b>	<b>22</b>
3.1 Introduction . . . . .	23
3.2 Phase Covariant Cloner . . . . .	24
3.3 Experimental Demonstration . . . . .	29
3.4 Discussion . . . . .	33

---

**CONTENTS**

3.5 Conclusion . . . . .	34
<b>4 Exploring the optimal sensitivity of sum-variance nonseparability criteria for spin-1/2 systems</b>	<b>35</b>
4.1 Introduction . . . . .	36
4.2 Sum-Variance Inequalities . . . . .	39
4.3 Concatenating Measurements . . . . .	44
4.4 Experimental Demonstration . . . . .	46
4.5 Summary and Conclusion . . . . .	52
<b>5 Experimental Demonstration of Entanglement Reduction and Restoration for Three Party Secret Sharing</b>	<b>54</b>
5.1 Introduction . . . . .	55
5.2 Three Party Secret Sharing . . . . .	57
5.3 Experimental Setup . . . . .	62
5.4 Entanglement Reduction and Revival . . . . .	67
5.5 Summary and Conclusion . . . . .	69
<b>II Continuous-Variable Regime</b>	<b>72</b>
<b>6 Pixel Entanglement: Experimental Realization of Optically Entangled <math>d = 3</math> and <math>d = 6</math> Qudits</b>	<b>73</b>
6.1 Introduction . . . . .	74

---

**CONTENTS**

6.2 Entangled Pixels . . . . .	76
6.3 Experimental Demonstration . . . . .	78
6.4 Discussion . . . . .	83
6.5 Summary and Conclusion . . . . .	86
<b>7 Experimental Demonstration of High Two-Photon Time-Energy Entanglement</b>	<b>88</b>
7.1 Introduction . . . . .	89
7.2 Experimental Setup . . . . .	91
7.2.1 Time Correlation . . . . .	92
7.2.2 Energy Correlation . . . . .	96
7.2.3 Violation of EPR bound . . . . .	98
7.3 High Energy-Time Entanglement . . . . .	99
7.4 Discussion . . . . .	101
<b>8 Demonstration of Secure, Large-Alphabet QKD Using Continu- ous Variable Energy-Time Entangled Bipartite States</b>	<b>103</b>
8.1 Introduction . . . . .	104
8.2 Motivation . . . . .	105
8.3 Energy-Time Entanglement Protocol . . . . .	108
8.4 Experimental Demonstration . . . . .	110
8.5 Summary and Discussion . . . . .	118

<b>9 Conclusions</b>	<b>121</b>
<b>Bibliography</b>	<b>124</b>
<b>A Derivation of the time-domain biphoton wavefunction</b>	<b>133</b>
A.1 The biphoton wavefunction . . . . .	133
A.2 The time domain . . . . .	135
<b>B The Franson interferometer</b>	<b>138</b>
B.1 Entangled biphotons . . . . .	138
B.2 Classically correlated photons . . . . .	143
<b>C General expression for the <math>L_2</math> and <math>L_3</math> sum-variance inequalities</b>	<b>147</b>

## List of Tables

Table	Title	Page
4.1	The results of the various measurements for Werner-type noise. Only $L_3$ is violated in this example, showing its higher sensitivity.	51

# List of Figures

Figure	Title	Page
3.1	A linearly polarized photon in mode A interferes with a circularly polarized photon in mode B at a beam splitter. Phase-covariant cloning occurs when both photons are measured in the same output port of the beam splitter. . . . .	25
3.2	Schematic of the experimental setup. The downconverted photons are separated at the first PBS. The photon from arm A is circularly polarized when it is incident on the 50/50 BS. HOM interference occurs when the path lengths of arms A and B are matched, leading to cloning of the linearly polarized photon from arm B after post-selection. . . . .	30

3.3 The figures show the results of measuring same port coincidences with respect to path length mismatch for the four possible polarization combinations. The <i>position</i> axes are only for scale, and have a systematic offset of $\sim 0.08$ mm. Boson mode enhancement only occurs in A and C where both photons have the same polarizations, thus leading to the cloning effect. . . . .	32
4.1 The Bell-state ‘filter’. An interferometer is set up to simulate entanglement via post-selection. The quality of the entanglement can be varied by tuning the path-mismatch between the two arms using an optical trombone. . . . .	47
4.2 Entanglement is plotted for various two-photon interference visibilities. This is simply used as a convenient method of charting the entanglement, and is not intended to convey any deeper physical meaning. For a visibility of 0.32, $J_H$ can be seen to violate its bound while the Bell measurement does not, thus demonstrating its higher sensitivity. . . . .	50

- 5.1 A 405 nm, 40 mW cw diode laser pumps a 2 mm thick BBO crystal that is cut and oriented for degenerate type-II collinear down conversion. Charlie's half wave-plate and the quarter wave-plates in the Hong-Ou-Mandel interferometer are used for alignment purposes only. The quarter wave-plates following the 50/50 beamsplitter determine whether Charlie will send an attenuated  $|\psi_+\rangle$  or  $|\psi_-\rangle$  state. For the experiment only the  $|\psi_-\rangle$  state was generated at the Bell-state filter, and only one detector each was used by Alice and Bob. The quarter wave-plates in Charlie's P-filter determine the attenuation of the qubit sent to Bob. Alice restores the entanglement by orientation of the quarter wave-plates in her P-filter. . . . . 64
- 5.2 a) Maximally entangled coincidences (high visibility) and reduced entanglement coincidences (low visibility) per 20 second integration time vs.  $\Delta$ , the relative path delay in Alice's P-filter. b) Restored-entanglement, high-visibility coincidences per 20 second integration time vs.  $\Delta$ . The dashed line in both a) and b) indicates the background coincidences, 110, 56 and 37, respectively. As seen graphically, the high visibility entanglement can be reduced and then restored again. Different fringe periods are obtained for the three plots due to phase drifts in the P-filters (see text for details). 66

## LIST OF FIGURES

7.1 Schematic of the two-photon time-energy entangled source and analyzing devices. The Franson interferometer is used to measure the biphoton coherence time, while the monochromators are used to measure an upper bound of the two-photon spectral correlations. The beam diameter of the photons in the monochromators is increased to 3.85 mm using a 1:5 telescope, then diffracted off of a diffraction grating at an incidence angle of $\sim 20^\circ$ . $L_1$ and $L_2$ are lenses of 1 m and 750 mm focal lengths respectively. $\tau_A$ and $\tau_B$ are the path mismatch in arms A and B of the Franson interferometer respectively. . . . .	92
7.2 Data points depict the typical interference envelope which is observed in the coincidence rates of the Franson interferometer as a function of path mismatch. The solid line is the theoretical triangular envelope function which is calculated for a square biphoton wavefunction of coherence time $\pi/\Omega_f = 100$ fs. . . . .	95
7.3 Using ghost imaging we estimate the two-photon spectral correlation width as 0.048 nm (details in text). The curve is a theoretical fit to the experimental data (squares). . . . .	97

8.1 Experimental Setup. BS, FBS, VBS, and PPS, refer to a 50:50 beamsplitter, a fiber 50:50 beamsplitter, a variable beamsplitter made with a half wave plate and a polarizing beam splitter, and a passive power splitter, respectively. . . . .	109
8.2 Franson fringe visibility versus Eve's POVM resolution. The solid curve represents a gaussian POVM, while the dashed curve represents a rectangular-form POVM. A measured visibility of 95% corresponds to a POVM resolution of $\gtrsim 65$ ns, demonstrating nominal security (details in text). . . . .	112
8.3 An example of the binning procedure as outlined in the text. In this example we have used $I = 5$ , $M = 2$ and $D = 3$ . . . . .	114
8.4 Experimental key generation for a bin size of 192 ps. The size of the alphabet, $D$ , and the corresponding QDER can be varied by varying the index-parameter, $I$ , and sync-division-parameter, $M$ . An alphabet of over 150 characters was observed, with an associated QDER of $\sim 50\%$ . . . . .	115



# Chapter 1

## Foreword

Quantum superposition [1, 2] and quantum entanglement [2–4] are arguably the most defining characteristics of quantum physics that distinguish it from classical physics. Both of these characteristics have been tested extensively [5–18], and have inspired some exciting potential applications, for example quantum computing [19–30] and quantum cryptography [31–35]. Quantum computing could provide a more powerful method for solving difficult mathematical problems, and would allow for more efficient and accurate simulations of quantum processes. Quantum cryptography could enhance the security of networks, and help to protect against quantum computing attacks on many traditional security protocols.

In 1994 Peter Schor discovered one of the first significant algorithms for quantum computing, showing that large integers could be factored in polynomial time [36]. In other words, the time required to factor a large integer using Shor’s al-

---

gorithm increases polynomially with the size of the integer. Digital computers typically solve such problems in exponential time, i.e. the time required to factor a large integer increases exponentially with the size of the integer. Shor's algorithm was thus a clear demonstration of the potential advantages that quantum computers could provide in computational tasks. Apart from Shor's discovery, a number of quantum algorithms have been discovered which also exhibit a distinct advantage over their digital algorithm counterparts [37, 38].

Many contemporary cryptographic protocols utilize mathematical complexity as the basis of their security. One such protocol uses exactly the same mathematical problem addressed by Shor's algorithm, the problem of factoring large integers. The computational time required to solve this problem using digital computers is beyond practical limitations, hence providing the security of the process. However, using Shor's algorithm with a quantum computer, this problem could be solved within a meaningful amount of time, therefore rendering the protocol insecure. One could thus argue that most or all cryptographic protocols whose security is based on mathematical complexity will no longer be secure in the advent of mature quantum computers. The security of cryptographic protocols could be preserved by increasing the complexity of the mathematical problems beyond the capabilities of contemporary quantum computers. Alternatively, cryptographic protocols could be employed whose security is not dependent on mathematical complexity. One such promising candidate is quantum key distribution, where the

---

security is ideally guaranteed by the laws of quantum physics itself. Many quantum key distribution protocols utilise entangled particles to distribute secret keys with demonstrable, measurable security.

The first quantum-entangled correlations were demonstrated by Aspect *et al* in 1981 using radiative atomic cascade of calcium [8]. However, the source of choice for most two-photon experiments has been spontaneous parametric down-conversion [39–42]. This is because spontaneous parametric down-conversion provides a high brightness source of photon pairs that have a number of correlated variables [43]. Additionally, the central wavelength of down-conversion for the two-photon pairs can be chosen over a large spectrum of wavelengths. This large range of workable wavelengths allows for experiments to be performed at the  $\sim 1550$  nm telecom wavelength, as well as the  $\sim 450 - 900$  nm wavelengths. Experiments at the 1550 nm range demonstrate exciting potential applications over current fiber optic networks [44, 45]. Experiments at the  $\sim 450 - 900$  nm range take advantage of the highest quantum efficiency single photon detectors [46–48]. Additionally, many useful atomic resonances occur over the  $\sim 450 - 900$  nm range, opening up an avenue for exciting applications and physical research [49–53].

This dissertation consists of a compendium of experimental and theoretical investigations on the characterization and application of the two-photon state produced in the process of spontaneous parametric down-conversion. Some of the experiments were performed in collaboration with graduate students at the Uni-

versity of Rochester. The work in Chapter 6, ‘Pixel Entanglement: Experimental Realization of Optically Entangled  $d = 3$  and  $d = 6$  Qudits’, was performed in collaboration with M. O’Sullivan-Hale. The work in Chapters 5 and 8, ‘Experimental Demonstration of Entanglement Reduction and Restoration for Three Party Secret Sharing’ and ‘Demonstration of Secure, Large-Alphabet QKD Using Continuous Variable Energy-Time Entangled Bipartite States’, was performed in collaboration with C. Broadbent.

# Part I

# Discrete-Variable Regime

## Chapter 2

# Reconciling cloning fidelities

In most theoretical literature on quantum cloning, fidelity is defined in terms of density matrices by assuming clones which are produced in distinguishable spatial modes. Recent optical implementations of cloning, including the optical implementation in Chapter 3, do not produce clones in distinct spatial modes [54–56], therefore another simpler expression for fidelity was proposed. However, no clear theoretical justification was initially provided for the equivalence of the two expressions. It is important to be able to compare experimental results with theoretical predictions, therefore the theoretical justification is given in this chapter, along with the circumstances under which the two expressions for fidelity are equivalent. The two expressions for fidelity are shown to be equivalent for *all* symmetric  $N \rightarrow M$  quantum cloners, with the symmetry requirement being lifted for ancilla-free cloners. The fidelity is verified explicitly for the  $1 \rightarrow 2$  universal quan-

tum cloner based on stimulated emission proposed in [54], where the spatial indistinguishability of the output clones is also discussed.

## 2.1 Introduction

In 1982 Herbert proposed an interesting method of superluminal communication by attempting to utilize the non-locality of Quantum Mechanics theorized in entanglement between quantum particles [57]. However, apart from being a result of the corner stone of relativity, the upper limit of the speed of communication to that of light in vacuum also spares physicists the trouble of causality paradoxes. Hence the solution to Herbert's proposal was quick in coming in the form of the “no cloning theorem” by Wootters and Zurek [58], that states that it is impossible to *perfectly* clone an unknown pure quantum state.

This simple theorem resulted in the conception of quantum cryptography [31–34], while later clarification of the possibility of *imperfect cloning* led to the field of quantum cloning [59–65]. As well as being of central importance to quantum cryptography, cloning has become a topic of interest in the field of quantum computation [66] and in the foundations of quantum physics in general. Barnum *et. al.* [67] later extended the theory to the “no-broadcasting theorem” to include the impossibility of perfectly cloning mixed quantum states. In doing so the use of fidelity [68],  $F = \langle \Psi_{in} | \rho_{out} | \Psi_{in} \rangle$ , was introduced as a measure of similarity of

---

**2.1. INTRODUCTION**

two quantum states by comparing their respective density matrices, where  $\Psi_{in}$  is the input state, and  $\varrho_{out}$  is the density matrix of the cloned state.

The first theoretical model of a universal quantum cloner (UQC) was proposed by Bužek and Hillery [60] wherein unknown pure quantum states pointing anywhere on the Bloch sphere were copied equally well. The Hilbert-Schmidt norm was primarily used in that paper as a measure of cloning efficiency, however their UQC was also shown to have a fidelity of  $5/6$ . Since then the use of fidelity has become a popular method for characterizing cloners. The fidelity of  $5/6$  as an upper bound for  $1 \rightarrow 2$  universal quantum copying has since been proved via various methods [64, 65, 69], and indeed the method by Gisin [65] showed this to be the upper bound over which superluminal communication would be possible.

Bruß *et. al.* carefully characterized the cloning process, and re-derived the Bužek and Hillery cloner as the optimal UQC via constructive proof [69]. In fact, various other types of cloners have been proposed and their respective upper limits explored [70–72].

Experimental realizations of quantum cloning came only recently, with De Martini *et. al.* [73] and Lamas-Linares *et. al.* [55] demonstrating the first experimental UQC following a proposal to clone the polarization state of photons by Simon *et. al.* [54]. In the Simon *et. al.* proposal, however, the two output clones are not in spatially distinguishable modes, which leads to problems in defining fidelity in the popular density matrix formulation (as will be seen later).

---

**2.1. INTRODUCTION**

Hence, to circumvent this problem, the fidelity was re-defined in an intuitively appealing form as “the average of the relative frequency of photons with the correct polarization in the final state”.

Indeed, this simpler form predicted a fidelity of 5/6 for the proposed Simon *et. al.* cloner, and using the same definition of fidelity Lamas-Linares *et. al.* measured a fidelity of 5/6 in their experimental realization. Most recently, Fasel *et. al.* demonstrated an experimental QC via linear amplification, once again using the Simon *et. al.* definition to measure a fidelity of 5/6 [74]. The Simon *et. al.* definition of fidelity is used in Chapter 3 to measure the fidelity of an ancilla-free phase-covariant cloner.

In this chapter we explicitly show the equivalence of the two expressions of fidelity, and in which circumstances they can be used interchangeably. In the process we shall re-express the Simon *et. al.* fidelity in a form which is more conducive to experimental situations. It will be seen that the two definitions are indeed analogous for all symmetric cloners, with the symmetry requirement being lifted for ancilla-free cloners. Hence the use of the Simon *et. al.* definition of fidelity is justified in Chapter 3

## 2.2 Definition of Fidelity

The density matrix of a spin-1/2 pure state  $|\Psi\rangle$  can be most generally expressed as:

$$\varrho_{pure} = |\Psi\rangle\langle\Psi| = \frac{1}{2}(\mathbb{1} + \vec{s} \cdot \vec{\sigma}) \quad (2.1)$$

where  $\mathbb{1}$  is the identity matrix,  $\vec{s}$  is the Bloch vector of the state and  $\vec{\sigma}$  are the x, y and z Pauli matrices. The generality of this expression can be intuitively verified by observing that the identity gives the density matrix a trace of 1 while the Pauli matrices allow the Bloch vector to point anywhere within the Bloch sphere. For simplicity, we shall at first talk about only  $1 \rightarrow 2$  cloners, later extending our results to the  $N \rightarrow M$  case.

As shown in [69], when the conditions of unitarity, symmetry and isotropy are imposed on a UQC, the Bloch vector of the cloned qubits cannot rotate with respect to the original qubit. They do however shrink by a ‘shrinking factor’  $\eta$ , in keeping with the no-cloning theorem:

$$\varrho_{red.} = \frac{1}{2}(\mathbb{1} + \eta\vec{s} \cdot \vec{\sigma}) = \eta|\psi\rangle\langle\psi| + \frac{1}{2}(1 - \eta)\mathbb{1} \quad (2.2)$$

where  $|\psi\rangle$  is state of the original input qubit, and  $\varrho_{red.}$  is the density matrix of one of the cloned qubits. This reduction in the magnitude of the vector results in a mixed state of the two output clones. The symmetry requirement and the definition for a clone to be as close as possible to the original density matrix

---

**2.2. DEFINITION OF FIDELITY**

resulted in the following theoretical expression for local fidelity [69]:

$$F_T = \langle \psi | \varrho_{red.} | \psi \rangle \quad (2.3)$$

This definition is analogous to the one originally advocated by Schumacher [68] in that it is a measure of the similarity of the original and cloned density matrices.

In the Simon *et. al.* proposal [54], quantum cloning via stimulated emission was proposed wherein an expression for Fidelity was given based on “right” and “wrong” photons. We shall rewrite the definition in an analogous form which is more instructive in an experimental environment:

$$F_S = \frac{R_{Clones}}{R_{Clones} + R_{Noise}} = Prob(Clone) \quad (2.4)$$

where  $R_{Clones}$  and  $R_{Noise}$  are count rates of clones (right photons) and noise (wrong photons) respectively, and  $Prob(Clone)$  is the probability of any one count being a clone. One can see that this is exactly equivalent to the expression of fidelity used in Eq. (2.5) by Lamas-Linares *et. al.* [55]. What this implies is that in an experimental setting, by measuring the above rates one can easily calculate the fidelity of a cloner without needing to resort to density matrices.

However, to what extent is  $F_S$  truly representative of the density matrices of the input and output qubits? In order to answer this question let us first take a look at the example of a  $1 \rightarrow 2$  cloner. In the following example we have a general expression for the output field of a non-optimized universal cloner [69] with an

input signal of  $|0\rangle$ . Here, as well as in the rest of the paper, we shall only consider an input state of  $|0\rangle$  in order to avoid redundancy. We shall consider the general case of a UQC with a spin-1/2 machine state (or ancilla state), where one input state and one ‘blank’ state enters the cloner. The cloning process produces two clones, and alters the final state of the machine state. The output state  $|\varphi\rangle_{output}$  of the cloning process is given by

$$|\varphi\rangle_{output} = \alpha|00A\rangle + \beta(|01B_1\rangle + |10B_2\rangle) + \gamma|11C\rangle \quad (2.5)$$

where  $|00A\rangle \equiv |0\rangle_1 \otimes |0\rangle_2 \otimes |A\rangle_{machine}$ , where  $|0\rangle_1$  represents the first clone in state 0,  $|0\rangle_2$  represents the second clone in state 0,  $|A\rangle_{machine}$  represents the machine state in state A, and similarly for the other terms. Also, we have that

$$|\alpha|^2 X_A + |\beta|^2 (X_{B_1} + X_{B_2}) + |\gamma|^2 X_C = 1 \quad (2.6)$$

due to normalization, where  $X_A = \langle A|A\rangle$  etc, and  $|0\rangle$  and  $|1\rangle$  are assumed to be orthonormal. For generality we have lifted the normalization condition of the ancillary states as assumed in [69]. The ancilla states can be expressed in terms of a complete orthonormal basis spanning the D-dimensional Hilbert space of the ancilla:

$$|J\rangle = \sum_{i=1}^D \lambda_i^{(J)} |\lambda_i\rangle \quad (2.7)$$

---

**2.2. DEFINITION OF FIDELITY**


---

where  $J$  is a general ancilla state. Therefore

$$X_J = \langle J|J \rangle = \sum_{i=1}^D |\lambda_i^{(J)}|^2 = Tr\{|J\rangle\langle J|\}_{anc.} \quad (2.8)$$

where  $Tr\{\cdot\}_{anc.}$  implies tracing over the ancillary states. The last equality has been added for convenience in the rest of the paper.

It must be kept in mind that the two output qubits are in different modes (distinguishable). In this example the “right” photons of the output are in state  $|0\rangle$ . Observing the output field in Eq. (2.5) we note that with probability  $|\alpha|^2 X_A$  both output photons are in state  $|0\rangle$ , with probability  $|\beta|^2(X_{B_1} + X_{B_2})$  only one of the output photons is in state  $|0\rangle$ , and with probability  $|\gamma|^2 X_C$  none of the photons are in state  $|0\rangle$ . Using this in Eq. (2.4) gives us

$$\begin{aligned} F_S &= \frac{2|\alpha|^2 X_A + |\beta|^2(X_{B_1} + X_{B_2})}{2|\alpha|^2 X_A + 2|\beta|^2(X_{B_1} + X_{B_2}) + 2|\gamma|^2 X_C} \\ &= |\alpha|^2 X_A + |\beta|^2 \frac{(X_{B_1} + X_{B_2})}{2} \end{aligned} \quad (2.9)$$

due to the normalization condition in Eq. (2.6). Let us now compare this with  $F_T$  via the reduced density matrix of one of the clones (by tracing over the ancilla

---

**2.2. DEFINITION OF FIDELITY**


---

and the other clone):

$$\begin{aligned}
 \varrho_{red.} = & |\alpha|^2 |0\rangle\langle 0| \cdot Tr\{|A\rangle\langle A|\}_{anc.} \\
 & + |\gamma|^2 |1\rangle\langle 1| \cdot Tr\{|C\rangle\langle C|\}_{anc.} \\
 & + |\beta|^2 |1\rangle\langle 1| \cdot Tr\{|B_2\rangle\langle B_2|\}_{anc.} \\
 & + |\beta|^2 |0\rangle\langle 0| \cdot Tr\{|B_1\rangle\langle B_1|\}_{anc.} \\
 & + \alpha\beta^* |0\rangle\langle 1| \cdot Tr\{|A\rangle\langle B_2|\}_{anc.} \\
 & + \alpha^*\beta |1\rangle\langle 0| \cdot Tr\{|B_2\rangle\langle A|\}_{anc.} \\
 & + \gamma^*\beta |1\rangle\langle 0| \cdot Tr\{|B_1\rangle\langle C|\}_{anc.} \\
 & + \gamma\beta^* |0\rangle\langle 1| \cdot Tr\{|C\rangle\langle B_1|\}_{anc.}
 \end{aligned} \tag{2.10}$$

This gives

$$F_T = \langle 0 | \varrho_{red.} | 0 \rangle = |\alpha|^2 X_A + |\beta|^2 X_{B_1} \tag{2.11}$$

using Eq. (2.8). We can see that the only solution for  $F_S = F_T$  is  $X_{B_1} = X_{B_2}$ , i.e. the symmetric cloner. *Thus  $F_S$  is a valid measure of fidelity for all symmetric  $1 \rightarrow 2$  cloners.* It should be noted that no limits were placed on the dimensionality of the ancilla. It can be seen that this result also extends to *all*  $1 \rightarrow 2$  ancilla-free cloners.

## 2.3 N→M Cloner

This analysis can be extended to the general N→M cloner. Once again it must be kept in mind that each output clone is distinguishable. Let us assume without loss of generality that the input state of the clone =  $|[0]_N\rangle$ , i.e. N particles in state  $|0\rangle$ . In the same vein as above, the output of the cloner will be

$$|\varphi\rangle_{output} = \sum_{i=0}^M \beta_i \sum_{k=1}^{\frac{M!}{i!(M-i)!}} |[0]_i [1]_{M-i}\rangle^{(k)} |B_i^{(k)}\rangle \quad (2.12)$$

where we have summed over all the possible output states.  $|[0]_i [1]_{M-i}\rangle^{(k)}$  represents the k'th permutation of an output with ‘i’ clones in state  $|0\rangle$  and ‘M-i’ clones in state  $|1\rangle$ . There are  $\frac{M!}{i!(M-i)!}$  such distinguishable permutations. For generality, each permutation is associated with a distinct ancilla state  $|B_i^{(k)}\rangle$ . The states  $|0\rangle$  and  $|1\rangle$  are assumed to be orthonormal, and the normalization condition is now given by

$$\sum_{i=0}^M |\beta_i|^2 \sum_{k=1}^{\frac{M!}{i!(M-i)!}} X_{B_i^{(k)}} = 1 \quad (2.13)$$

### 2.3. N→M CLONER

---

Summing the number of “right” output states as before, the simplistic expression of fidelity gives us

$$\begin{aligned}
 F_S &= \frac{\sum_{i=0}^M i \cdot |\beta_i|^2 \cdot \sum_{k=1}^{\frac{M!}{i!(M-i)!}} X_{B_i^{(k)}}}{\sum_{i=0}^M M \cdot |\beta_i|^2 \cdot \sum_{k=1}^{\frac{M!}{i!(M-i)!}} X_{B_i^{(k)}}} \\
 &= \frac{1}{M} \sum_{i=0}^M i \cdot |\beta_i|^2 \cdot \sum_{k=1}^{\frac{M!}{i!(M-i)!}} X_{B_i^{(k)}}
 \end{aligned} \tag{2.14}$$

where the normalization condition in Eq. (2.13) was used in the second step.

Now, only the diagonal terms of the reduced density matrix contribute to  $F_T$ , therefore we shall ignore all off-diagonal elements in calculating the reduced density matrix of the first clone (i.e. the clone in the first output mode). In order to do this we will need to separate out the cases when the first mode is in state  $|0\rangle$ , and when it is in state  $|1\rangle$ . Let us consider the case where an output has ‘i’ clones in state  $|0\rangle$  and ‘M-i’ clones in state  $|1\rangle$ . Keeping the first mode in state  $|0\rangle$ , there are  $\frac{(M-1)!}{(i-1)!(M-i)!} = s$  ways to distribute the remaining clones in the remaining M-1 modes. We can specify the first ‘s’ permutations to fall within this category, while the remaining permutations have state  $|1\rangle$  in the first mode.

This allows us to write

$$\begin{aligned}
 \varrho_{red.} &= \sum_{i=1}^{M-1} |\beta_i|^2 \left\{ \sum_{k=1}^s |0\rangle\langle 0| X_{B_i^{(k)}} + \sum_{k=s+1}^{\frac{M!}{i!(M-i)!}} |1\rangle\langle 1| X_{B_i^{(k)}} \right\} \\
 &\quad + |\beta_0|^2 |1\rangle\langle 1| X_{B_0^{(1)}} + |\beta_M|^2 |0\rangle\langle 0| X_{B_M^{(1)}} + OffDiag...
 \end{aligned} \tag{2.15}$$

---

**2.4. 2-LEVEL ANCILLA**

which gives us

$$\begin{aligned}
 F_T &= |\beta_M|^2 X_{B_M^{(1)}} + \sum_{i=1}^{M-1} |\beta_i|^2 \sum_{k=1}^{\frac{(M-1)!}{(M-i)!(i-1)!}} X_{B_i^{(k)}} \\
 &= \sum_{i=1}^M |\beta_i|^2 \sum_{k=1}^{\frac{(M-1)!}{(M-i)!(i-1)!}} X_{B_i^{(k)}}
 \end{aligned} \tag{2.16}$$

Comparing this to Eq. (2.14), we see that the only solution to  $F_S = F_T$  is  $X_{B_i^{(a)}} = X_{B_i^{(b)}}$  for all a, b. *Therefore the two expressions for fidelity are equivalent for all  $N \rightarrow M$  symmetric cloners.* Once again, no limitations were made on the dimensionality of the ancilla. It should be noted that in the case of an ancilla-free system,  $X_{B_i^{(a)}} = 1$  for all i, a. Therefore the two expressions are equivalent for *all* ancilla-free cloners.

## 2.4 2-level Ancilla

Let us consider as an example that of a UQC with a 2-level ancilla, specifically that of the optimum UQC proposed by Bužek and Hillery [60]. Once again the signal is taken to be  $|0\rangle$ :

$$|\varphi\rangle_{output} = \sqrt{\frac{2}{3}}|00\rangle \otimes |\uparrow\rangle_A + \sqrt{\frac{1}{6}}(|01\rangle + |10\rangle) \otimes |\downarrow\rangle_A \tag{2.17}$$

where the subscript A specifies the ancilla. The simple expression for fidelity gives

us:

$$F_s = \frac{2 \times \frac{2}{3} + 1 \times \frac{2}{6}}{2 \times \frac{2}{3} + 2 \times \frac{2}{6}} = \frac{5}{6} \quad (2.18)$$

The reduced density matrix of the clone is

$$\rho_{red.} = \frac{5}{6}|0\rangle\langle 0| + \frac{1}{6}|1\rangle\langle 1| \quad (2.19)$$

It is a simple matter to check that the  $F_T$  gives the same result as  $F_S$ .

Now let us consider the Simon *et. al.* proposal of cloning via stimulated emission [54]. In this setup the signal beam is aligned on top of one of the output arms of a pumped type-II downconverting crystal whilst the downconverted photon in the other arm serves as the ancilla. Thus we must also take into consideration the characteristic that both the clones of the QC are in the same mode (spatially indistinguishable). Therefore

$$|00\rangle \rightarrow \sqrt{2}|2_0; 0_1\rangle \quad (2.20)$$

$$|01\rangle + |10\rangle \rightarrow 2|1_0; 1_1\rangle \quad (2.21)$$

$$|\uparrow\rangle_A \rightarrow |1\rangle_A \quad (2.22)$$

$$|\downarrow\rangle_A \rightarrow |0\rangle_A \quad (2.23)$$

where  $|2_0; 0_1\rangle$  represents two indistinguishable particles with polarization 0, and

---

**2.4. 2-LEVEL ANCILLA**

no particles with orthogonal polarization 1. Hence on normalization we get

$$|\varphi\rangle = \sqrt{\frac{1}{3}}(\sqrt{2}|2_0;0_1\rangle\otimes|1\rangle_A + |1_0;1_1\rangle\otimes|0\rangle_A) \quad (2.24)$$

We can see here explicitly that there is no way of calculating the reduced density matrix of an output clone in this formulation. On the other hand  $F_S$  gives us

$$F_S = \frac{2 \times \frac{2}{3} + 1 \times \frac{1}{3}}{2 \times \frac{2}{3} + 2 \times \frac{1}{3}} = \frac{5}{6} \quad (2.25)$$

which is what was purported by Simon *et. al.* [54] and experimentally verified by Lamas-Linares *et. al.* [55].

This is a compelling argument for the Simon *et. al.* proposal to qualify as a  $1 \rightarrow 2$  UQC, with a valid expression for fidelity of cloning. At this juncture, however, the distinction (or equivalence) between cloning and state discrimination needs to be addressed more clearly for this statement to be absolute. Operationally, in order for a device to qualify as a cloner, it is not unreasonable to demand that both output clones be in different modes to allow for manipulation of one clone independently of the other (modulo entanglement). This can be implemented in the Simon *et. al.* case by placing a 50/50 beam splitter in the output mode, and explicitly selecting different port coincidences. In theory, this could be achieved using a ‘QND filter’, where QND number measurements on both output ports of the BS could non-destructively select different port outputs. However, half

of all input signals are lost in this process. This gives us:

$$\begin{aligned} |2_0; 0_1\rangle &\rightarrow \frac{1}{\sqrt{2}}|00\rangle + \frac{1}{2}(|2_0; 0_1\rangle_C + |2_0; 0_1\rangle_D) \\ |1_0; 1_1\rangle &\rightarrow \frac{1}{2}(|01\rangle + |10\rangle) + \frac{1}{2}(|1_0; 1_1\rangle_C + |1_0; 1_1\rangle_D) \end{aligned} \quad (2.26)$$

where  $|1_0; 1_1\rangle_C$  represents one horizontal and one vertical photon in output port C of the BS etc. Plugging this into Eq. (2.24), discarding same port outputs, and normalizing we get:

$$|\varphi\rangle = \sqrt{\frac{2}{3}}|00\rangle \otimes |1\rangle_A + \sqrt{\frac{1}{6}}(|01\rangle + |10\rangle) \otimes |0\rangle_A \quad (2.27)$$

i.e. we get exactly the optimum  $1 \rightarrow 2$  UQC as given in Eq. (2.17).

## 2.5 Conclusion

It is important to have clear foundations on which to compare theoretical predictions with experimental results. Therefore, in this chapter we have clarified the equivalence of two expressions for fidelity, as well as the conditions under which the equivalency holds. In the case of pure input states the two expressions were shown to be equivalent for *all* symmetric  $N \rightarrow M$  QCs, with the symmetry requirement being lifted for ancilla-free  $N \rightarrow M$  QCs. With the knowledge of this

equivalence, we can safely proceed to use the Simon *et. al.* expression to measure the fidelity of an ancilla-free phase-covariant cloner in Chapter 3.

## Chapter 3

# Hong-Ou-Mandel Cloning: quantum copying without an ancilla

In this chapter we report the first experimental realization of an ancilla-free  $1 \rightarrow 2$  phase-covariant quantum cloner. The cloner is realized by interfering a linearly polarized photon, which we wish to clone with a circularly polarized photon at a beam splitter. The two-photon effect can be understood in light of Hong-Ou-Mandel interference. The fidelity of the cloner was measured as  $0.829 \pm 0.008$  for the  $0/90$  basis and  $0.835 \pm 0.006$  for the  $45/135$  basis, which is in good agreement with the theoretical prediction of  $5/6$  fidelity. The experimental scheme is straightforward and has a high cloning success rate.

### 3.1 Introduction

Since the proposal of the “no cloning” theorem by Wooters and Zurek, the field of quantum cloning has experienced immense interest and growth, owing mostly to the fact that the theorem should be more accurately labeled the “no-perfect-cloning” theorem. The inability to perfectly clone unknown quantum states initiated the development of quantum cryptography [31–34], and it has even been shown to be useful in quantum computing [66]. Theoretical aspects of quantum cloning have been studied for some time now; first in discrete [59–61, 75], then recently in continuous variable [62, 63] quantum systems. Success in experimental aspects and realizations of cloning, however, have only come relatively recently [54, 55, 73, 74].

Buzek and Hillery [60] proposed the first theoretical model of a universal quantum cloning machine (UQCM). In their original work, the universal quantum cloning machine takes a two-state particle in any arbitrary, unknown state and copies all possible states equally well. In other words, the fidelity (a measure of the quality of the copying procedure) is independent of the unknown input state. The best possible copying, or optimal fidelity, was derived by Buzek and Hillery to be  $5/6$  for a 1 to 2 copying procedure. This was later derived via constructive proof by Bruss *et. al.* [64].

In pursuing the universal cloner, Buzek and Hillery discovered that it was necessary to have an additional “ancilla bit” in order to realize the universal cloner.

This ancilla bit is sometimes referred to as the “machine” state or antyclone in the literature. However, in many instances, such as optimal eavesdropping on a BB84 cryptochannel, it is only necessary to clone arbitrary *linearly* polarized states instead of any possible polarized states (e.g., any elliptically polarized state). Restricting the cloning to only linearly polarized states dramatically simplifies the cloning requirements. As we show experimentally, cloning only linearly polarized photons does not require an ancilla bit. This type of restrictive cloning is referred to as phase covariant cloning [70–72, 76–79]. On a more formal level, phase covariant cloning is the study of restricted copying in which the symmetric cloning only occurs on a great circle of the Bloch sphere. In this work, the great circle is the linear polarization equator of the Bloch sphere. Further, the cloner presented here is nonperturbative, which ultimately means that the cloning procedure will occur with much higher repetition rate than in previous experiments.

## 3.2 Phase Covariant Cloner

In this work, the phase covariant cloner is achieved by interfering a linearly polarized photon we wish to clone with a circularly polarized photon at a beam splitter (as seen in Fig. 3.1). From a practical point of view, a circularly polarized photon has a 50% chance of being transmitted through (or absorbed in) a polarizer *regardless of the orientation of the polarizer*. This means that there is no preferred orientation of a circularly polarized photon in a linearly polarized basis.

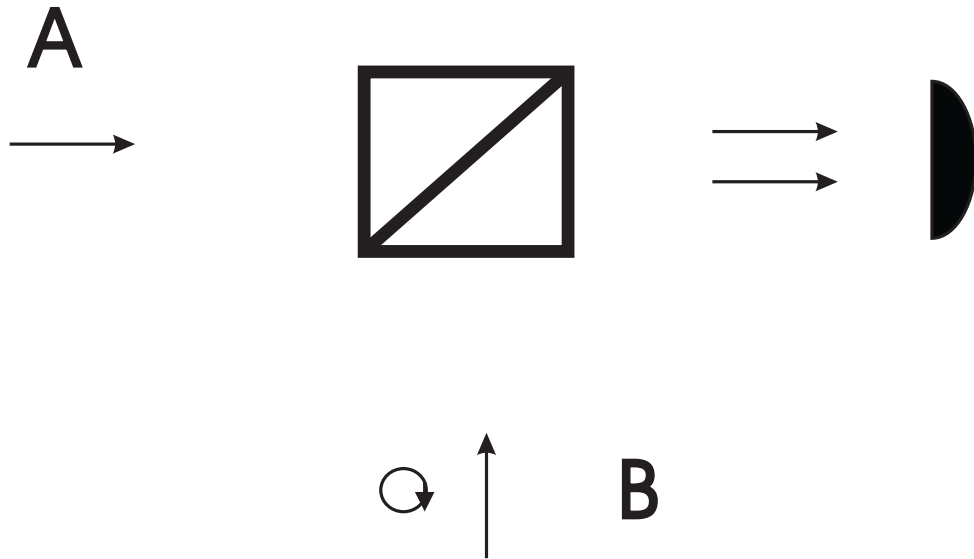


Figure 3.1: A linearly polarized photon in mode A interferes with a circularly polarized photon in mode B at a beam splitter. Phase-covariant cloning occurs when both photons are measured in the same output port of the beam splitter.

With this simple fact, interfering a linearly polarized photon with a circularly polarized photon then causes a “stimulated” two photon effect when both photons are measured with the same linear polarization orientation and in the same spatio-temporal mode and a “noise”-like term when the photons are measured with orthogonal linear polarizations. The cloner interference can be understood in light of the famous Hong-Ou-Mandel two-photon interference effect [39]. Interestingly, no additional ancilla photon is needed to achieve the same fidelity as the UQCM for the phase-covariant conditions of this cloner.

Recall that if two bosons are made indistinguishable in every quantum variable, they occupy the same quantum state and get a corresponding boson mode

---

**3.2. PHASE COVARIANT CLONER**

occupation enhancement. Therefore, if two photons (which are bosons) are made to be spatially and temporally indistinguishable at a beam splitter while having the same spectral and polarization orientation characteristics, they must both leave the same output port of the beam splitter. This two-photon behavior has been labelled Hong-Ou-Mandel interference [39] and has played a vital role in many remarkable experiments in quantum information such as teleportation [80], and dense coding [81]. However, the two photons will not interfere if they have orthogonal polarizations, even if all the other characteristics are the same (e.g., spectral, spatial and temporal) because they are distinguishable. Therefore, the two photons will behave independently at the beam splitter.

Consider the outcome when a circularly polarized photon interferes with a linearly polarized photon. For the moment, we are only interested in one output port of the 50/50 beam splitter. Also, we will assume that the two photons are distinguishable in some quantum variable such as temporal mode overlap. In other words, the photons arrive at the beam splitter at different times and are therefore distinguishable. Lastly, assume that the linearly polarized photon in mode A is horizontally polarized and that the photons will be measured in the horizontal/vertical basis. The wavefunction for the linearly polarized photon in the output port is  $|\Psi\rangle_1 = |1, 0\rangle_1$ , where the subscript 1 labels the linearly polarized photon and the ket  $|1, 0\rangle_1$  denotes that there is one horizontally polarized photon and zero vertically polarized photons. As a note, we will not worry about the nor-

malization of the wavefunction. The wavefunction in the same output port for the circularly polarized photon is given by  $|\Psi\rangle_2 = |1, 0\rangle_2 + i|0, 1\rangle_2$ . Without worrying about normalization, the circularly polarized wavefunction denotes that the circularly polarized photon can be decomposed into an equal amplitude superposition with both a horizontal and vertical component. The two-photon wavefunction is then given by the tensor product of the two individual wavefunctions

$$|\Psi\rangle = |\Psi\rangle_1 \otimes |\Psi\rangle_2 = |1, 0\rangle_1 \otimes (|1, 0\rangle_2 + i|0, 1\rangle_2). \quad (3.1)$$

As it is, this two-photon wavefunction is not very interesting. However, if one applies a quantum eraser to erase any distinguishable space-time information between the two photons in the same output port, the two-photon wavefunction then becomes

$$|\Psi\rangle = \sqrt{2}|2, 0\rangle + i|1, 1\rangle, \quad (3.2)$$

where it should be noted that the  $\sqrt{2}$  is now in front of the first ket. This factor is a result of the boson mode enhancement and leads to the stimulated enhancement needed for cloning. The other ket is the noise term which has an analog to spontaneous emission in an orthogonal mode of a linear amplifier. If on the other hand, the linearly polarized photon (to be cloned) is vertically polarized, the two-photon wavefunction is given by

$$|\Psi\rangle = |1, 1\rangle + i\sqrt{2}|0, 2\rangle. \quad (3.3)$$

---

**3.2. PHASE COVARIANT CLONER**

Using the sum-frequency technique proposed by Simon *et. al.* [54, 82] the fidelity is computed by adding all the contributions with the same polarization as the incoming linearly polarized photon and dividing by all the contributions. From the wavefunction it can be seen that there is twice the probability of measuring both photons in the same polarization mode as to measure one photon in each polarization mode. The fidelity is then computed to be

$$F = \frac{2 \times 2 + 1 \times 1}{2 \times 2 + 1 \times 2} = \frac{5}{6}, \quad (3.4)$$

which is the same as the optimal universal cloning fidelity.

As asserted, the cloning should be independent of the linear polarization of the incoming photon. Suppose the incoming linearly polarized photon is horizontal in a *new* primed basis (a basis which can be achieved by rotating the linear analyzers). The wavefunction is written as  $|\Psi\rangle'_1 = |1, 0\rangle'_1$ , where the ' denotes that the wavefunction is written in the primed basis. The important aspect of this phase-covariant cloner is that the circularly polarized photon can be written as  $|\Psi\rangle_2 = |1, 0\rangle'_2 + i|0, 1\rangle'_2$  in the new basis. Thus, applying the quantum eraser, the two-photon wavefunction in the primed basis is given by

$$|\Psi\rangle = \sqrt{2}|2, 0\rangle' + i|1, 1\rangle', \quad (3.5)$$

which yields the same cloning fidelity as the unprimed basis. We arrive at the very

---

**3.3. EXPERIMENTAL DEMONSTRATION**

important conclusion that the cloning is independent of the linear polarization basis.

A more careful analysis of the input-output relations of the beam splitter reveal that ideally the probability that both photons will be measured in the same output port is 75%. It should be kept in mind that due to symmetry cloning occurs with equal probability in both exit ports of the beam splitter. This statistically means 3/4 of the time a cloning event will occur if a circularly polarized photon enters one input port at the same time that a linearly polarized photon enters the other input port of a 50/50 beam splitter. Thus, two-photon postselection is needed to observe the cloning. Ideally, this implies that single photons on demand can be cloned with single photons on demand with high success probability. This very high success rate can be contrasted with stimulated emission in a crystal, where the perturbative (meaning that there is a small probability that an entangled pair will be created when a signal photon enters the crystal) three-photon postselection success is very low. However, this latter system could be improved dramatically if one and only one pair of entangled photons can be created on demand.

### **3.3 Experimental Demonstration**

We report on an experimental demonstration of the phase covariant cloner using collinear type-II parametric down conversion (a schematic of the experiment is shown in Fig. 3.2). The spontaneously emitted pair of photons, having orthogo-

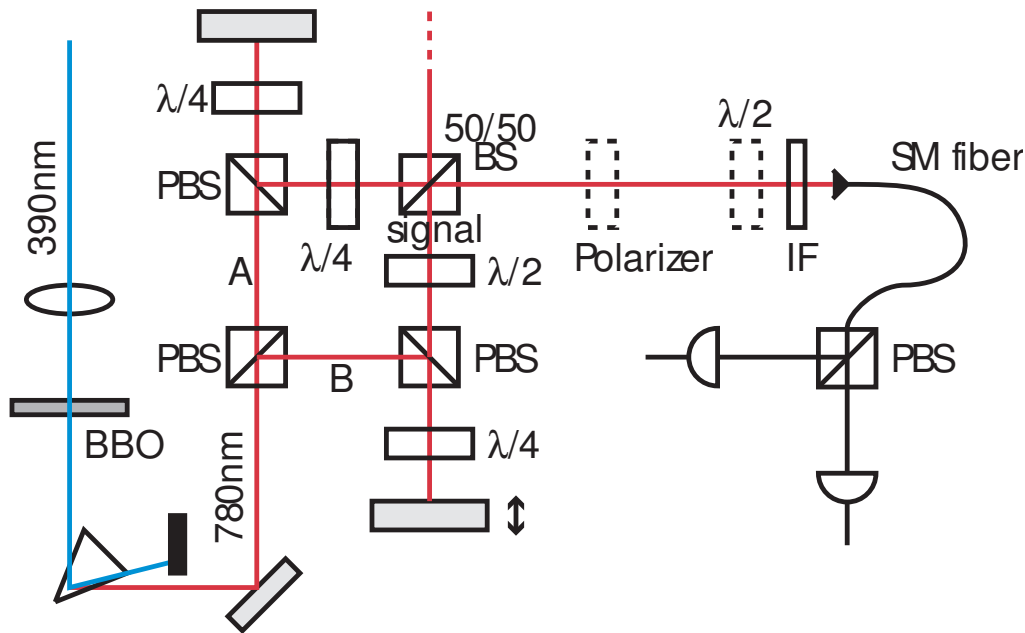


Figure 3.2: Schematic of the experimental setup. The downconverted photons are separated at the first PBS. The photon from arm A is circularly polarized when it is incident on the 50/50 BS. HOM interference occurs when the path lengths of arms A and B are matched, leading to cloning of the linearly polarized photon from arm B after post-selection.

nal polarization, are separated at a polarizing beam splitter. The signal photon (the linearly polarized photon) is rotated into its linear polarization state using a half wave plate. The cloning photon (the circularly polarized photon) is made circularly polarized by a quarter wave plate. They are then made to recombine at a 50/50 beam splitter.

The photons were generated by using a 390 nm laser (Toptica TA 100 DL series 780 nm source driving the Toptica series SG100 frequency doubling system) to pump a 2 mm BBO crystal. The downconverted photons centered at 780 nm were then separated out from the 390 nm pump using a UV grade fused-silica

---

**3.3. EXPERIMENTAL DEMONSTRATION**

prism. Interference filters of 10 nm bandwidth are used to increase the coherence length of the downconverted photons to approximately 60 microns, and to reduce background noise.

Owing to the symmetry of the 50/50 beam splitter, measurements were made in only one output port. The first experiment was to insert a horizontally polarized photon to be cloned. The two photon measurements are then horizontal-horizontal (H-H) or horizontal-vertical (H-V). As can be seen from the results in Fig. (3.3) we observe an enhancement in the H-H polarized pairs when the path lengths are matched without affecting the H-V pairs. The results were performed in two different non-orthogonal bases to confirm that the cloner works equally well in any linear basis. For any one basis, we ideally expect the measured H-H coincidences to be twice those of the H-V coincidences. However, long term laser instability affected count rates in between measurement runs. Even with this in mind, the qualitative information presented in the two measurements is critical. Using a theoretical gaussian fit for the H-H correlations the coherence length was estimated to be 75 microns, in good agreement with our initial expectations.

We now calculate the fidelity of the cloning from the peak and base values of the H-H coincidences. Examining the statistics at the peak of the H-H coincidences, we get

$$F = \frac{2 \times R_{H-H} + R_{H-V}}{2 \times R_{H-H} + 2 \times R_{H-V}}, \quad (3.6)$$

where  $R_{H-H}$  is the rate of H-H coincidences, and  $R_{H-V}$  is the rate of H-V coin-

### 3.3. EXPERIMENTAL DEMONSTRATION

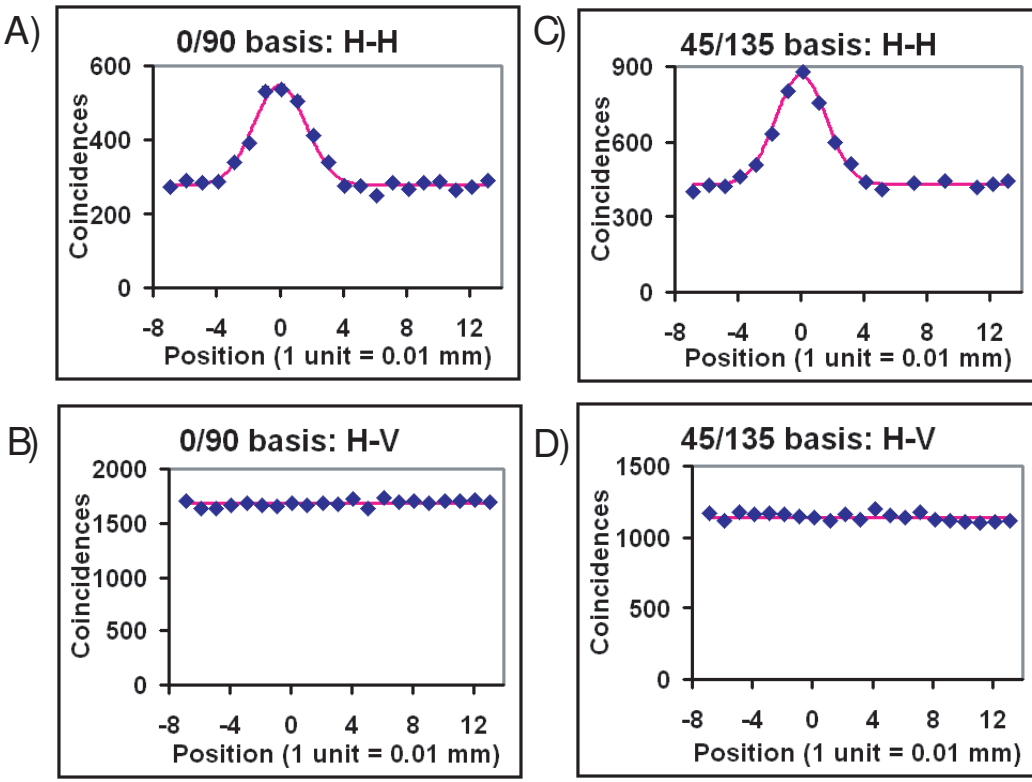


Figure 3.3: The figures show the results of measuring same port coincidences with respect to path length mismatch for the four possible polarization combinations. The *position* axes are only for scale, and have a systematic offset of  $\sim 0.08$  mm. Boson mode enhancement only occurs in A and C where both photons have the same polarizations, thus leading to the cloning effect.

cidences. Using this we get a fidelity of  $0 \cdot 829 \pm 0 \cdot 008$  for the 0/90 basis and  $0 \cdot 835 \pm 0 \cdot 006$  for the 45/135 basis, which is in good agreement with the 5/6 fidelity as predicted earlier in this paper. It should be noted that to obtain the fidelity in Eq. (3.6), the data was normalized by making the baselines equal. Owing to our inability to measure two identical photons (temporal, spatial, spectral and polarization), beam splitter cascading [83] was required. This leads to a lower

---

**3.4. DISCUSSION**

baseline for the H-H coincidences than the H-V coincidences. The baselines would have been the same with a photon number resolving detector.

## 3.4 Discussion

The HOM cloner represents a significant advance in cloning success rate. For example, in the demonstration of the UQCM via stimulated emission by Lamas-Linares *et. al.* [55] the cloning success rate was approximately  $10^{-5}$ . In the the UQCM experiment, two major problems limited the success rate. While the cloner we have reported here has a high cloning success rate, there are still technological issues of concern. Firstly, the collection and detection efficiency of the photons is still quite low ( $\approx 10\%$ ). This could be greatly improved with more efficient detectors and improved collection efficiency optics. One can envision a fiber based source of single photons on demand, which would dramatically improve the collection efficiency.

While it is unlikely that a HOM cloner will be a standard tool in the quantum key distribution eavesdropping, it does point out a potential weakness of only using two nonorthogonal bases for key distribution. As Bruss showed, three mutually unbiased bases provide additional security for which the HOM cloner is not symmetric [84]. Further, one can think of a myriad of ways to thwart any cloning machine as an eavesdropping tool such as creating spectral or temporal jitter to the signal photons.

### 3.5. CONCLUSION

Lastly, the fidelity of the HOM cloner is  $5/6=83.33\%$ , which is slightly smaller than the optimal predicted fidelity of a phase covariant cloner of 85.4%. For example, Fiurasek recently proposed an all-optical optimal cloner [72]. However, the experimental complexity is much greater and the maximum success probability of a cloning event is only 1/3. Thus, in our experiment fidelity is sacrificed at the expense of higher cloning success rate and experimental simplicity.

## 3.5 Conclusion

In this chapter we have demonstrated the first experimental ancilla-free phase-covariant quantum cloner by restricting the cloning to the linearly polarized photons (equator of the Bloch sphere). The experimental results of the HOM cloner agree well with theoretical predictions. Interestingly, the cloning device uses only linear optics and interference. All previous demonstrations have used seeded amplifiers (weak optical parametric amplifier [55] or a fiber amplifier [74]) to demonstrate the cloning effect.

In the next chapter we shall move away from quantum cloning and look at a new type of sum-variance entanglement measure to quantify two-qubit entanglement.

## Chapter 4

# Exploring the optimal sensitivity of sum-variance nonseparability criteria for spin-1/2 systems

In this chapter we report on experimental and theoretical studies on recently introduced entanglement measures which use a sum of spin-variances criteria for two spin-1/2 particles. Three inequalities are explored which exhibit useful concatenating properties. They are each shown to have greater sensitivities than a Bell measurement, while each requiring fewer measurements than a Bell measurement to obtain. The simplest inequality, requiring just four measurements, is shown to be efficient at testing for entanglement in downconversion sources which naturally exhibit maximally polarized noise. The most complex inequality, requiring just twelve measurements, is shown to have a sensitivity equal to that of the Peres separability criterion for

maximally polarized and Werner noise. This increased sensitivity implies optimality of the measure.

## 4.1 Introduction

Recently, there has been a strong interest in determining the degree of entanglement in a quantum system [5, 85–97]. Entanglement can be represented by a density matrix of a multi-particle system, which cannot be written as the tensor product of the individual density matrices of the particles. The implicit assumption of nonseparability is that the measurement of one particle has an unalterable effect on the measurement outcomes of the other particles to which it is entangled [3, 4, 6–10] even for space-like separated particles. Many techniques have been developed to determine the amount or degree of entanglement between quantum particles. Such techniques for spin-1/2 systems include Peres-Horodecki criterion [85, 86], entanglement witnesses [87, 88], Bell inequalities [6], CHSH inequalities [7], and entanglement visibility [10], to name a few.

Similar theoretical efforts have been put forward for continuous variables as well. Of particular interest are the works of Duan *et. al.* [89], Simon [90] and Mancini *et. al.* [91]. For example, Mancini *et. al.* derived a momentum-position variance product with a strict lower bound based on the separability of density matrices. Violation of the bound represented a sufficient condition for entanglement. Howell *et. al.* experimentally realized a violation of the momentum-position

## 4.1. INTRODUCTION

---

variance product by two orders of magnitude [5]. Similarly, Duan *et. al.* [89] introduced an inseparability criterion based on the sum of variances of a pair of EPR type operators. This inseparability criterion was shown to be a necessary and sufficient condition for entanglement for Gaussian states. Later, Julsgaard *et. al.* [92] showed that it was possible to use this sum-variance criterion for discrete states to demonstrate long-lived entanglement in collective spin ensembles. A formal treatment of the sum-variance inseparability criterion for discrete N-level systems was recently done by Hofmann and Takuechi [97], followed by a generalization of the derivation by Gühne [98].

In what follows we shall explore the bounds of the measurable entanglement range for the two-particle spin-1/2 sum-variance criteria for various types of noise. As will be seen, the sum-variance criteria allows for the derivation of three inequalities, each with different measurable entanglement ranges. We show that each of the three inequalities have greater sensitivities than a Bell measurement, with each requiring fewer measurements than a Bell measurement to obtain. Interestingly from a practical point of view, the inequalities also exhibit a naturally occurring concatenating hierarchy, which could make them very useful for experimental purposes. The least sensitive inequality requires only four measurements to obtain. To achieve a higher sensitivity, one needs only append four new measurements to the previous four, thus obtaining the second, more sensitive inequality. For even higher sensitivity, one can simply append a further four new measurements to the

---

**4.1. INTRODUCTION**

previous result to obtain the third inequality. The third inequality, which requires a total of only twelve measurements, is shown to possess optimum sensitivity for two-particle spin-1/2 systems with Werner and maximally polarized noise [85]. This is done by comparison of the measurable entanglement range of the inequality to that allowed by the Peres separability criterion [85]. It might be of interest to note that violation of these inequalities is a sign of non-separability, not necessarily non-locality. For convenience, all inequalities are written out in intuitive and experimentally tractable forms. The first inequality is seen to be a simple quadratic function of the visibilities in the 0/90 and 45/135 bases, which many have intuitively felt to be a good measure for entanglement. We show through this inequality that although visibility is sensitive to noise asymmetries, it is still a good signature for entanglement. It will be seen that by concatenating this first inequality with follow-up measurements, it is easy to formulate the more sensitive and robust inequalities which are not sensitive to noise asymmetries and are therefore appropriate for quantifying entanglement. All of these properties are explored theoretically as well as experimentally, showing thereby that this set of inequalities performs better than a Bell measurement. We believe these type of sum-variance measurements have exciting prospects as potentially standard tools for quantifying entanglement.

## 4.2 Sum-Variance Inequalities

The first sum-variance inequality is based on the conditional measurements of the variance of the  $\sigma_z$  and  $\sigma_x$  spin observable under two rotations of the state.

Consider the single particle variance function

$$(\Delta\sigma_z)^2 + (\Delta\sigma_x)^2 \geq 1 \quad (4.1)$$

Here,  $(\Delta\sigma_z)^2$  and  $(\Delta\sigma_x)^2$  are the variances of the pauli spin observables.

Now consider a two-particle system. One can envision that if two particles are separable (i.e., not entangled), then a measurement on particle 2 has no effect on the measurement of particle 1. This leads us to a conditional inequality given by

$$J_+ = (\Delta\sigma_{z2})^2|_{1z_+} + (\Delta\sigma_{x2})^2|_{1x_+} \quad (4.2)$$

where  $J_+$  is the sum of variances of particle 2 based on the conditional detection of particle 1,  $(\Delta\sigma_{z2})^2|_{1z_+}$  represents the variance of the  $\sigma_z$  operator for particle 2 based on the conditional detection of the particle 1 being in the + z-eigenstate and  $(\Delta\sigma_{x2})^2|_{1x_+}$  represents the variance of the  $\sigma_x$  operator for particle 2 based on the conditional detection of the particle 1 being in the + x-eigenstate. An analogous expression exists for  $J_-$ , where the sum of variances of particle 2 is measured based on the conditional detection of particle 1 being in the - x and z eigenstate. At first sight it seems as if  $J_+$  and  $J_-$  should be equivalent. However,

as is shown later on in the paper, the two expressions have different values for the case of asymmetric noise. It can be shown [97] that

$$J_+ \geq (\Delta\sigma_z)^2 + (\Delta\sigma_x)^2 \geq 1 \quad (4.3)$$

which means that for separable states, the  $J_+$  value will be greater than or equal to the single particle variance sum. It is straightforward to see that the same argument applies for  $J_-$  as well. This is the first inequality.

Without loss of generality, we will assume that the diagonal elements of the density matrix for particle 2 are  $|\alpha|^2$  and  $|\beta|^2$ . We also remind the reader that the Pauli matrix of the z-component of spin expanded in the z-eigenbasis is given by

$$\sigma_z = \begin{pmatrix} 1 & 0 \\ 0 & -1 \end{pmatrix} \quad (4.4)$$

which, using the definition of the variance, yields

$$(\Delta\sigma_{z2})^2|_{1z+} = \frac{|\alpha|^2 + |\beta|^2}{|\alpha|^2 + |\beta|^2} - \left( \frac{|\alpha|^2 - |\beta|^2}{|\alpha|^2 + |\beta|^2} \right)^2 \quad (4.5)$$

$$= 1 - (V_z|_+)^2 \quad (4.6)$$

where  $V_z|_+$  is the visibility in the z-basis, based on the conditional detection of the particle 1 being in the + z-eigenstate. Similarly, repeating these steps in the

x-eigenbasis and applying these results, we obtain a J-value

$$J_+ = 2 - (V_z|_+)^2 - (V_x|_+)^2. \quad (4.7)$$

which is greater than or equal to 1 for separable states. If, instead of using spin, we use the polarization states of light where the z-basis and x-basis are replaced by the 0/90 and 45/135 bases respectively, and +/- is replaced by H/V, then the following inequality for  $J_H$  is achieved

$$J_H = 2 - (V_{0/90}|_{H_0})^2 - (V_{45/135}|_{H_{45}})^2 \geq 1 \quad (4.8)$$

and similarly for  $J_V$ . Once again it must be kept in mind that although  $J_H$  and  $J_V$  look equivalent, they differ in value when asymmetric noise is present.

A violation of the inequality in Eq. (4.8) is then a sufficient condition for nonseparability. Computational simulations were run to test the ability of this inequality to measure entanglement for various choices of density matrices. The density matrices were formed using the method of Peres [85] by summing weighted density matrices representing the  $|\psi^-\rangle$  Bell singlet state and arbitrarily chosen noise  $\chi$

$$\rho = p. |\psi^-\rangle\langle\psi^-| + (1-p).\chi \quad (4.9)$$

where p is the weighting factor. It is generally accepted, as per the Peres Criterion [85], that for Werner noise ( $\chi = \mathbf{I}/4$ ; i.e. the Werner state [99]) entanglement

exists in the range  $1 \geq p > 1/3$ , whereas for *maximally polarized noise* entanglement exists in the range  $1 \geq p > 0$ . The Peres separability criterion states that for a  $2 \times 2$  state, the existence of any negative eigenvalue of a partially transposed density matrix is a necessary and sufficient condition for inseparability (i.e. entanglement) of the two states concerned. It is therefore this criterion which is used to obtain the above theoretical bounds. A Bell measurement is only sensitive enough to measure inseparability for  $p > 1/\sqrt{2}$  for Werner noise and  $p > \sqrt{2} - 1$  for maximally polarized noise, thus leaving a large unmeasurable range [85]. This range can be probed using the Peres separability criterion, however this requires a full quantum state tomography of the two-particle state which is significantly arduous. For example, James *et. al.* [100] showed experimentally that in addition to the sixteen measurements required for quantum state tomography of a pair of qubits, further data analysis and processing needed to be performed to ensure that the reconstructed density matrix was positive semidefinite; a requirement for physical states. Interestingly, the  $J_H$  measure in Eq. (4.8) is seen to have the same range as the Peres Criterion of  $p > 0$  for the maximally polarized state, while the range for Werner noise remained the same as the Bell measurement. For the case of Werner noise  $V_{0/90}|_{H/V} = V_{45/135}|_{H'/V'}$  and the minimum visibility for violating the bound is 0.71 as is commonly known. However, for maximally polarized noise it is possible to align the analyzers so that  $V_{0/90}|_{H/V} = 1$ , which means that a visibility of greater than 0.41 is required in the 45/135 basis to vio-

---

**4.2. SUM-VARIANCE INEQUALITIES**

late a Bell inequality. To violate  $J_{H/V}$ , however, requires only a non-zero visibility in the 45/135 basis, thus giving it a higher sensitivity. Thus we find that this inequality is as sensitive as the Peres criterion for maximally polarized noise, but equally sensitive to the Bell measure for Werner noise. Overall, therefore, it is more sensitive than a Bell measurement.

On the down side, however, it is also observed (as briefly mentioned in [97]) that the values of  $J_H$  and  $J_V$  differed from each other as asymmetries were introduced into the noise (e.g. lopsided noise). It is also seen that the measured values of  $J_{H/V}$  themselves varied as the measurement bases were simultaneously rotated. What this means experimentally is that for measuring entanglement produced from a downconversion source, one needs to be careful to align the measurement polarizers to the downconversion source as well as to each other. It also means that small noise asymmetries naturally arising in experiments will produce slightly different values for  $J_H$  and  $J_V$ . This indicates that while in general one needs to take care, the  $J_{H/V}$  measurements should be suitable for characterizing entanglement for balanced, polarized noise. Since this is generally the case for downconversion, it implies that using just four measurements one can obtain a quick test for the existence and magnitude of entanglement.

## 4.3 Concatenating Measurements

At this stage we would like to introduce the concatenation properties of this measurement. Using the values obtained for  $J_H$ , one can do a further four measurements for  $J_V$ . However, instead of obtaining two separate measurements, it is possible to combine the eight measurements into one single inequality which is insensitive to noise asymmetries as well as simultaneous rotations of the measurement bases; i.e. ideal for characterizing entanglement. This implies that it is sufficient to only align the measurement polarizers to each other without any regard for the source. It should be noted that by using polarizing beam splitters it is just as easy to perform eight measurements as it is to perform four. This concatenated variance for polarization states (as previously derived in [97]) is

$$L_2 = (\Delta[\sigma_1 + \sigma_2]_{0/90})^2 + (\Delta[\sigma_1 + \sigma_2]_{45/135})^2 \geq 2, \quad (4.10)$$

where  $\sigma_1$  and  $\sigma_2$  represent a polarization measurement on particle 1 and 2 respectively, and  $[\sigma_1 + \sigma_2]_{0/90}$  represents a coincidence measurement between the two particles in the 0/90 basis. It should be noted that the notation is slightly different from before since now we are not concerned with conditional measurements, just general coincidences. This inequality is therefore simply the sum of the variances of the coincident polarization measurements in the 0/90 and 45/135 bases. In an experimental situation, the following would be the equation for calculating the

---

**4.3. CONCATENATING MEASUREMENTS**

variance in the 0/90 basis

$$(\Delta[\sigma_1 + \sigma_2]_{0/90})^2 = 4 \frac{R_{HH}+R_{VV}}{R_{HH}+R_{VV}+R_{HV}+R_{VH}} - 4 \frac{(R_{HH}-R_{VV})^2}{(R_{HH}+R_{VV}+R_{HV}+R_{VH})^2}, \quad (4.11)$$

where  $R_{HH}$  is the measured rate of horizontal-horizontal coincidences in the 0/90 basis,  $R_{VV}$  is the measured rate of vertical-vertical coincidences in the 0/90 basis, and correspondingly for the other terms. The variance for the 45/135 basis is of exactly the same form, with  $R_{HH}$  now representing the measured rate of horizontal-horizontal coincidences in the 45/135 basis, and respectively for the other terms. This expression for the variance given in Eq. (4.11) is specific to the  $|\psi^-\rangle$  Bell state, with the general expression for variance given in Appendix C. Using the same simulations as above, it was seen that apart from being more robust, this new measure had an increased sensitivity of  $p > 1/2$  for Werner noise in addition to retaining the high sensitivity of  $p > 0$  for maximally polarized noise. Experimentally, this means that it is possible to get a robust measurement for entanglement with greater sensitivity than a Bell measure, but with eight measurements. To make this even more exciting, it is possible to measure the analogous variance of Eq. (4.11) in the circularly polarized basis, and to concatenate it to the previous inequality to give the following new inequality (as previously derived

---

**4.4. EXPERIMENTAL DEMONSTRATION**

in [97]) which has an even greater sensitivity

$$L_3 = (\Delta[\sigma_1 + \sigma_2]_{0/90})^2 + (\Delta[\sigma_1 + \sigma_2]_{45/135})^2 + (\Delta[\sigma_1 + \sigma_2]_{R/L})^2 \geq 4. \quad (4.12)$$

Here R/L implies the right and left circularly polarized basis. This measure has an increased sensitivity for Werner noise of  $p > 1/3$ , which is also the bound for the Peres separability criterion. Thus, with twelve measurements in three configurations, it is possible to measure the entire range of allowed entanglement in a spin-1/2 (or optically polarized) system, as compared to sixteen measurements in four configurations with lower sensitivity for a Bell measurement. This measurement therefore should be ideal for standardizing entanglement measures in spin-1/2 systems.

## 4.4 Experimental Demonstration

To demonstrate these various qualities of the entanglement measures mentioned above, an experiment is set up which allows us to produce  $|\psi^-\rangle$  entangled states with a large variety of weighted noise. Using the technique of Mitchell *et. al.* [101], entangled  $|\psi^-\rangle$  Bell states are produced using a Bell-state ‘filter’.

The experimental setup is shown in Fig. 4.1. A 30mW CW pump laser centered at 390 nm is focused onto a 2mm-thick type II BBO crystal using a 90 mm focal length lens (not shown). The resulting 780 nm downconverted photons are separated from the pump by using dichroic mirrors. The downconverted photon

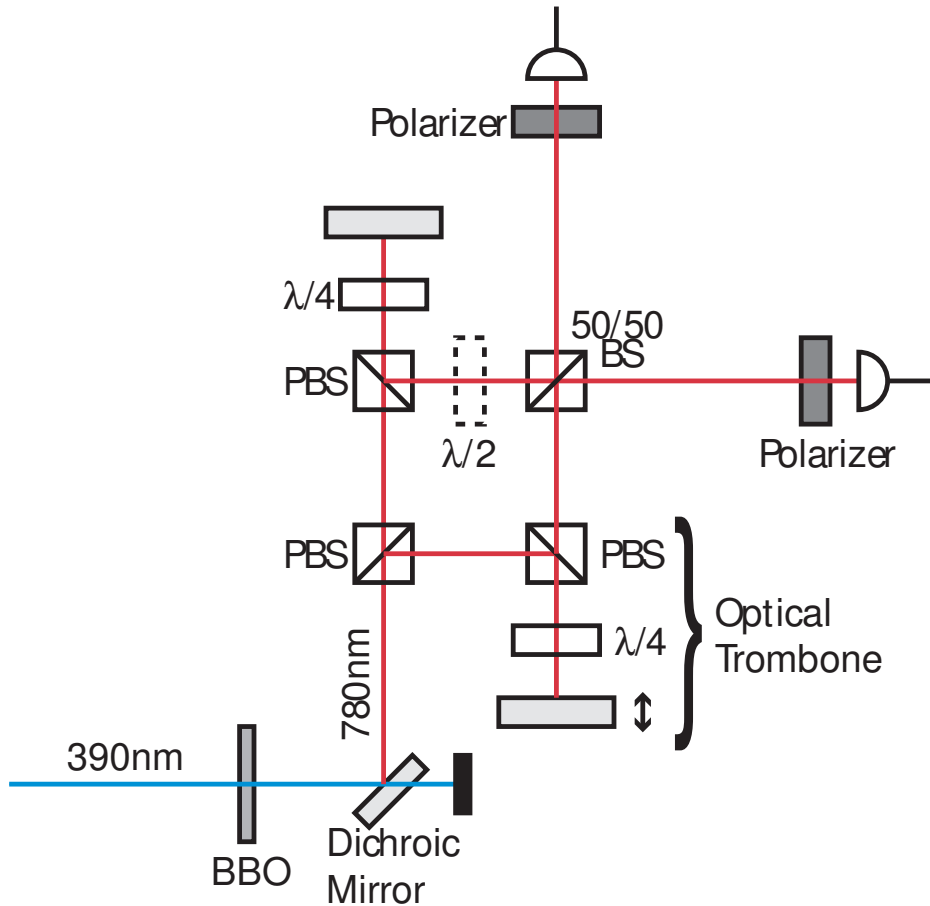


Figure 4.1: The Bell-state ‘filter’. An interferometer is set up to simulate entanglement via post-selection. The quality of the entanglement can be varied by tuning the path-mismatch between the two arms using an optical trombone.

pairs are then separated from each other at the first polarizing beam splitter. The two photons then traverse the two arms shown in Fig. 4.1 before being interfered at a 50/50 beam splitter. The two output ports of the beam splitter are coupled into single mode fiber for detection in avalanche photodiodes. The path mismatch between the two arms of the interferometer is tuned by using an optical trombone in one arm, along with a half waveplate to match the polarization states of the

#### 4.4. EXPERIMENTAL DEMONSTRATION

photons in both arms. In doing so, the HOM interference effect can be charted with respect to path mismatch, with the minimum of the dip corresponding to the best path matching. Using 10 nm interference filters, the width of the dip is measured to be  $\sim 70 \mu\text{m}$ .

The half waveplate is then rotated so that the polarization states of the two arms are orthogonal to each other. In this way, entanglement can be simulated by post-selecting different port output coincidences from the interferometer. The greater the path mismatch of the interferometer, the worse the simulated entanglement. At this point the relative ease of performing a measurement of  $J_{H/V}$  must be pointed out. For either one of the J's, only four measurements in only two configurations need to be performed, in contrast to sixteen measurements in four configurations for a corresponding Bell measurement. In addition to this, the direct use of visibility in this measurement has great intuitive appeal.

The measured entanglement  $J_H$  is plotted for various locations along the HOM dip in Fig. 4.2. As seen in the figure, measurements are performed at six different locations along visibility dip, with a Bell (CHSH [7]) measurement also performed for each of the three highest visibilities. Importantly, it can be seen from Fig. 4.2 that for a visibility of 0.32,  $J_H$  is measured to be  $0.957 \pm 0.0045$  ( $J_V$  is correspondingly  $0.912 \pm 0.0055$ ) in clear violation of the *lower* bound of 1, whereas a Bell measurement gives a corresponding value of  $1.937 \pm 0.013$  which clearly does not violate its *upper* bound of 2.  $L_2$  was also measured to be  $1.318 \pm 0.004$ , also in

clear violation of it's lower bound of 2. This represents an interesting example of the greater sensitivity available when using the J and L inequalities to measure entanglement with highly polarized noise. Using the above measurements, the density matrices of the noise and the entangled state are reconstructed and fed into the computer simulation. The explicit form of the noise was found to be:

$$\chi = \begin{pmatrix} 0.014 & 0 & 0 & 0 \\ 0 & 0.54 & 0 & 0 \\ 0 & 0 & 0.43 & 0 \\ 0 & 0 & 0 & 0.019 \end{pmatrix} \quad (4.13)$$

For alignment tolerances of  $\pm 2^\circ$ , the above results were reproduced almost exactly for a value of  $p \sim 0.37$  (as defined in Eq. (4.9)). The disparity in  $J_H$  and  $J_V$  is due to slight asymmetry in the noise, and is also reproduced in the simulation.

The next step is to produce Werner noise to demonstrate the higher sensitivity of the  $L_3$  inequality. This is achieved by increasing the level of the ambient room-light until a desired level of background coincidences is achieved. The polarized nature of the downconversion noise still remains, but is less pronounced. Thus, by varying the level of the ambient lights we are able to find a scenario in which all the entanglement measures fail to detect entanglement except for  $L_3$ . For this case the measurements obtained are shown in table 4.1. It is clear to see from these results that  $L_3$  has a much higher sensitivity than the Bell measurement. In

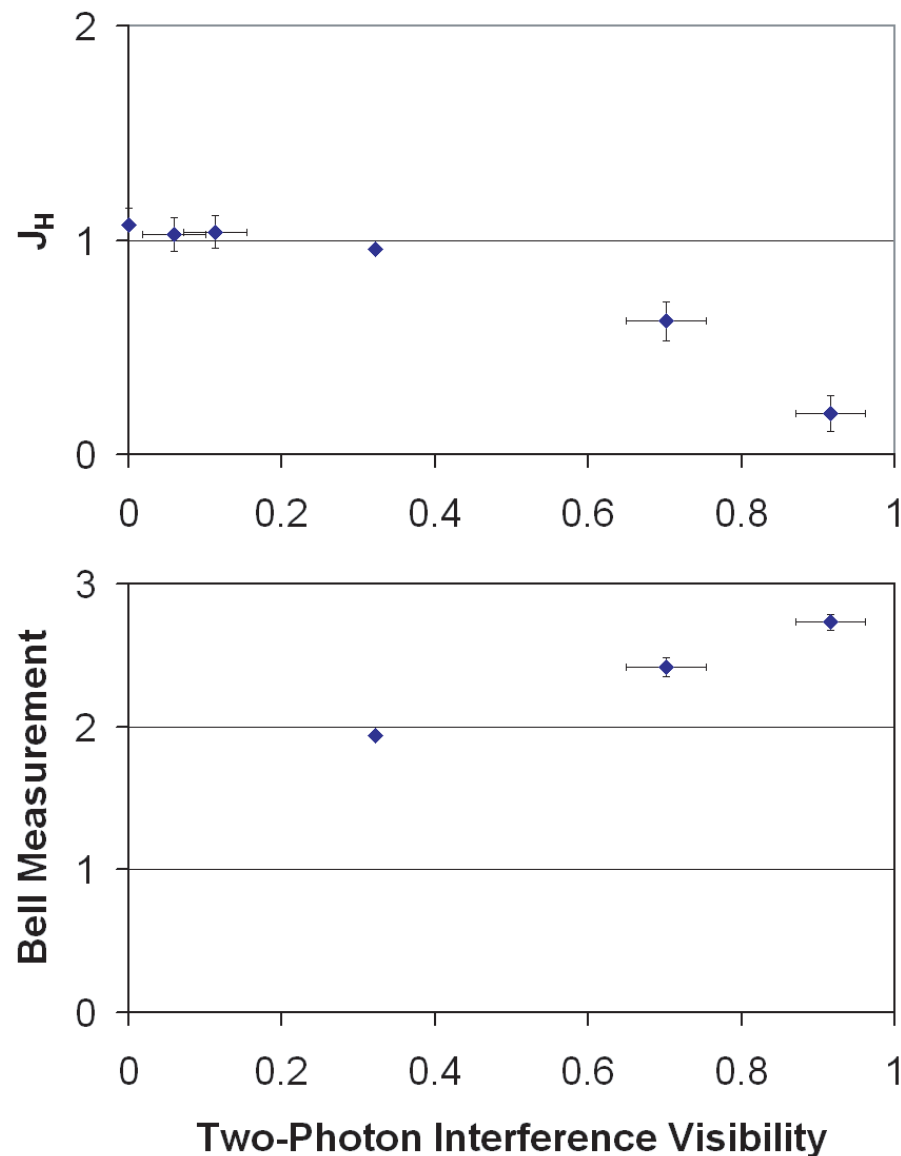


Figure 4.2: Entanglement is plotted for various two-photon interference visibilities. This is simply used as a convenient method of charting the entanglement, and is not intended to convey any deeper physical meaning. For a visibility of 0.32,  $J_H$  can be seen to violate its bound while the Bell measurement does not, thus demonstrating its higher sensitivity.

---

**4.4. EXPERIMENTAL DEMONSTRATION**


---

Inequality	Measured Value	Bound	Result
$J_H$	$1.55 \pm 0.05$	$> 1$	No Violation
$J_V$	$1.59 \pm 0.05$	$> 1$	No Violation
$L_2$	$2.207 \pm 0.059$	$> 2$	No Violation
$L_3$	$3.716 \pm 0.064$	$> 4$	Violation
$Bell$	$1.32 \pm 0.09$	$< 2$	No Violation

Table 4.1: The results of the various measurements for Werner-type noise. Only  $L_3$  is violated in this example, showing its higher sensitivity.

this particular case the surprising result should be noted that after  $L_2$  failed to measure entanglement, simply four extra measurements concatenated to  $L_2$  gives a higher sensitivity which is able to detect the entanglement. However, we would like to stress the fact that extra effort needed to be made to create Werner noise. This suggests that for downconversion sources where noise is naturally polarized, the  $L_2$  measure should be good enough by itself. That is to say that most of the time one can expect to characterize entanglement with only eight measurements. The density matrix for the entangled state and the noise term is reconstructed in the same way as was done above for the maximally polarized case. The explicit form of the noise was found to be:

$$\chi = \begin{pmatrix} 0.17 & 0 & 0 & 0 \\ 0 & 0.39 & 0 & 0 \\ 0 & 0 & 0.29 & 0 \\ 0 & 0 & 0 & 0.15 \end{pmatrix} \quad (4.14)$$

For alignment tolerances of  $\pm 2^\circ$  these results are reproduced almost exactly for a

value of  $p \sim 0.32$ . This value is slightly less than the lower bound of  $1/3$  for Werner noise because the density matrix of the noise term still had distinct polarization signatures as seen in Eq. (4.14), which allows for a smaller lower bound.

## 4.5 Summary and Conclusion

In summary, we have investigated an entanglement measure based on sum of spin-variances and have shown that it has an enormous advantage over a Bell measure. These types of spin-variance based measures were initially introduced by Hofmann and Takeuchi [97], where it was shown that variance sum arguments for characterizing entanglement in continuous variable systems could also be applied to discrete N-level systems. In this chapter we have explicitly investigated their increased sensitivities and experimental advantages. We suggest that these sum-variance inequalities could be very useful as standard entanglement measures for spin- $1/2$  systems. They are immediately intuitive, appealing to our knowledge of correlated conditional measurements in arbitrary bases as a signature of entanglement. They are concatenating, where higher sensitivities can be achieved simply by appending new measurements. Ultimately, we are able to measure the entire range of entanglement allowed by the Peres separability criterion for Werner and maximally polarized noise, which suggests that this is an optimum measurement of entanglement for bi-partite spin- $1/2$  entangled states. We believe that these sum-variance inequalities would be of immediate utility to experimentalists, being

very closely related to visibility measurements which are very popular. It provides a simpler and superior alternative to a Bell measurement, with the added incentive of being able to convert previous measurements of visibility into characterizable measurements of entanglement. Also of interest is whether the implied optimality of these inequalities extends to the multi-partite and higher N-level systems.

In the next chapter we shall explore the physical mechanism behind unambiguous state-discrimination of nonorthogonal, bipartite entangled-states. We demonstrate that the physical mechanism is analogous to that of entanglement reduction and restoration. We use the principle of sum-variance entanglement measures presented in this chapter to interpret the reduction and restoration of entanglement visibility as a demonstration of entanglement reduction and restoration respectively.

## Chapter 5

# Experimental Demonstration of Entanglement Reduction and Restoration for Three Party Secret Sharing

In this chapter we perform an experimental demonstration of the physical mechanism utilized in the Mimih and Hillery two-qubit, three-party secret sharing protocol [102]. We demonstrate that unambiguous state-discrimination of nonorthogonal, bipartite entangled states involves an analogous physical mechanism to that utilized in entanglement distillation of bipartite entangled states [103]. By local operations at distant locations, we reduce and restore entanglement in a bipartite qubit system. Using polarization-entangled two-photon states generated in the process of spontaneous parametric down-conversion we observe high contrast entanglement-visibility reduction from  $89.1 \pm 1.6\%$  to  $53.6 \pm 1.6\%$ , and reconstructed visibility

of  $93.5 \pm 4.9\%$ . This provides a clear demonstration of the physical mechanism required for this three-party secret sharing scheme. We also comment on the feasibility of practically implementing this three-party quantum key distribution scheme.

## 5.1 Introduction

Multi-party secret sharing is an important component of any cryptographic toolkit [104, 105]. Secret sharing provides a method for discouraging single-party abuse by sharing the responsibility of the knowledge of sensitive information among two or more known, relevant parties. This sharing of sensitive knowledge provides an extra level of security which is the common aim of all secret-sharing schemes. Recently there has been significant interest in realizing quantum secret sharing, i.e. secret sharing using quantum resources [102, 104–108]. Quantum secret sharing proves to be superior to classical and hybrid quantum-classical secret sharing since it not only guarantees uncompromised security of the quantum channel, but also requires a smaller amount of classical information to be transmitted once the key has been established[104].

A number of quantum secret sharing schemes have already been proposed which make use of three-or-more-particle Greenberger-Horne-Zeilinger (GHZ) states [104, 105, 108], two-particle pseudo-GHZ states [106], two-particle Bell states [105], two-particle unambiguous non-orthogonal state discrimination [102,

## 5.1. INTRODUCTION

---

[107], and single-particle sequential phase-delay [108]. The single-particle Schmid *et. al.* protocol [108] was experimentally implemented for six-party secret sharing, while a proof-of-principle experimental demonstration of the three-party pseudo-GHZ protocol was performed by Tittel *et. al.* [106].

In this chapter we demonstrate the physical mechanism that underlies unambiguous state discrimination of non-orthogonal entangled states that is the basis for the Mimih and Hillery secret sharing scheme [102]. The Mimih and Hillery scheme relies on the ability to unambiguously distinguish between two known, nonorthogonal entangled states, which requires the ability to reduce and then restore entanglement via local operations and classical communication. As will be seen, unambiguous state discrimination between two non-orthogonal, entangled states involves entanglement distillation of the states into orthogonal, entangled states which can then, by definition, be distinguished.

Unambiguous, nonorthogonal state-discrimination ensures that the presence of an eavesdropper is known, and also ensures that secret sharers in the three party scheme cannot gain error-free knowledge of the shared key by internal eavesdropping. Typically, the two states used to generate the binary alphabet (in the case of a bipartite qubit system) are made non-orthogonal by reducing the two-particle entanglement [102, 107]. We achieve this by selectively and coherently attenuating one of the polarizations of one of the photons of an entangled Bell  $|\Psi_{\pm}\rangle$  state. In doing so we observe a reduction in entanglement-visibility from  $89.1 \pm 1.6\%$

---

**5.2. THREE PARTY SECRET SHARING**

to  $53.6 \pm 1.6\%$ . In order to perform unambiguous state discrimination we must then restore the entanglement by selectively and coherently attenuating the same polarization of the other photon of the non-maximally entangled  $|\psi_{\pm}\rangle$  state, giving us a reconstructed visibility of  $93.5 \pm 4.9\%$ . This high visibility entanglement reconstruction demonstrates that the Mimih and Hillery method for unambiguous state discrimination can be feasibly implemented for practical purposes. It should be noted that environmental phase drifts on the order of  $\sim 100$  nm per half hour were observed which should be controllable with stabilization and regular recalibration for use in practical quantum key distribution (QKD).

Entanglement restoration or *distillation* has been previously demonstrated by Kwiat *et. al.* using Brewster's angle-selective polarization attenuation [103], however, for unambiguous state discrimination the Mimih and Hillery interferometer used in this current experiment possesses a number of distinct advantages, outlined below, that make it a preferred tool for the task of unambiguous state discrimination.

## 5.2 Three Party Secret Sharing

Let us begin by reminding the reader of the Mimih and Hillery protocol for three party secret sharing [102]. Using the Mimih and Hillery notation, let's say that Charlie wants to send a message to Alice and Bob. However, he does not want the message to be read by either Alice or Bob until they actively cooperate with

each other. In order to accomplish this Charlie creates a cryptographic key and selectively communicates information about the key to Alice and Bob, where Alice and Bob receive complementary information. Thus the individual information that Alice and Bob receive does not reveal the key, however the combined information, when shared, reveals the key. Charlie can then use the key to encrypt the message and send it to both Alice and Bob, where Alice and Bob will only be able to decrypt the message by cooperating with each other. This forms the basis of the three party secret sharing scheme.

As proposed by Mimih and Hillery [102], this can be accomplished with polarization-entangled biphoton states in the following way. Charlie creates the entangled state

$$|\psi_{\pm}\rangle = \alpha|HV\rangle \pm \beta|VH\rangle \quad (5.1)$$

in the traditional notation, where H/V denotes a photon with horizontal/vertical polarization respectively, and where  $|HV\rangle$  corresponds to a horizontally polarized photon sent to Alice and a vertically polarized photon sent to Bob, and so on. The state reduces to the  $|\Psi_{\pm}\rangle$  Bell state when  $\alpha = \beta = \frac{1}{\sqrt{2}}$ . Charlie randomly chooses whether to create the  $|\psi_+\rangle$  or the  $|\psi_-\rangle$  state. In terms of bit key generation, let us say that  $|\psi_+\rangle$  corresponds to a 0 and  $|\psi_-\rangle$  corresponds to a 1.

Let us first consider the simple case where Charlie creates maximally entangled Bell  $|\Psi_{\pm}\rangle$  states, i.e. when  $\alpha = \beta = \frac{1}{\sqrt{2}}$ . If Alice and Bob both measure the polarization of their photons in the 0/90 basis they will know that, whatever

polarization they measure, the other person will obtain the opposite polarization. However, they will obtain no information about whether the state sent by Charlie was the  $|\Psi_+\rangle$  or the  $|\Psi_-\rangle$  state, even if they cooperate. On the other hand, they would obtain this state-discrimination information if they were to both measure in the 45/135 basis. If Alice measures an H or V photon in the 45/135 basis and Bob also measures an H or V photon in the same basis (same polarization), then they know with certainty that Charlie sent the  $|\Psi_+\rangle$  state. Conversely, if Alice measures an H or V photon and Bob measures a V or H photon (opposite polarization), then they know with certainty that Charlie sent the  $|\Psi_-\rangle$  state. This is an example of optimal state discrimination between orthogonally prepared states, since for this case  $\langle \Psi_- | \Psi_+ \rangle = 0$  [109]. Thus, by cooperating, Alice and Bob could obtain the key that Charlie had sent. Unfortunately, due to the lossless state discrimination in this simple case, an eavesdropper (Eve) could easily measure the key and resend similarly prepared entangled states without detection (intercept-resend attack).

In order to avoid this eavesdropping vulnerability, Charlie must use non-maximally entangled states, i.e. non-orthogonal states for which  $\langle \psi_- | \psi_+ \rangle \neq 0$ . If Alice and Bob now perform polarization measurements in the 45/135 basis on non-maximally entangled photons then noise is obtained in the results, proportional to  $\langle \psi_- | \psi_+ \rangle$ , due to the non-orthogonality of the two states that Charlie is preparing. In order to obtain a high-fidelity key we must be able to unambiguously distinguish between these non-orthogonal states. Such unambiguous,

non-orthogonal state discrimination requires an unavoidable, detectable, non-zero probability of failure [107, 110, 111]. This failure reduces the rate of key generation, however, by careful monitoring of key generation rates, such failures should allow for the detection of an eavesdropper in a similar fashion to the B92 QKD protocol [102, 112–114]. Charlie can then be informed about which measurements succeeded and which failed, thus allowing accurate key generation. Further measures to prevent dishonesty in Alice and Bob are discussed in [102]. In this way three party secret sharing can be implemented using polarization-entangled bipartite states.

A simple optical implementation of unambiguous, non-orthogonal state discrimination is proposed by Mimih and Hillery [102]. The implementation involves the use of an interferometer on only one of the entangled photons (Alice’s photon for this discussion). The interferometer possesses two output ports, one for successful state discrimination and one for failure. The dominant polarization amplitudes of a photon which exits the ‘success’ port of the interferometer is coherently attenuated by exactly such an amount that, although acting on only one photon, the output biphoton state is a maximally entangled Bell state with unchanged phase. For example, for the case of the state in Eq. (5.1) where  $\alpha > \beta$  the interferometer coherently attenuates the horizontal polarization of Alice’s photon

---

**5.2. THREE PARTY SECRET SHARING**

by a factor of  $\frac{\alpha}{\beta}$  so that

$$\begin{aligned} \alpha|HV\rangle \pm \beta|VH\rangle &\rightarrow \frac{\beta}{\alpha} \times \alpha|HV\rangle \pm \beta|VH\rangle \\ &\propto |HV\rangle \pm |VH\rangle = |\Psi_{\pm}\rangle. \end{aligned} \quad (5.2)$$

This interferometer therefore performs entanglement distillation, similar to the method of Kwiat *et. al.* [103]. The polarization of Alice's photon that exits the 'success' port, along with Bob's photon, is then measured in the 45/135 basis as in the above mentioned case for Bell state discrimination. For such an event one key bit is generated as outlined in the above protocol. A measurement of a photon in the 'failure' port is reported to Charlie and Alice, whereupon that particular key bit is discarded. This is the process by which a high fidelity key can be generated.

Entanglement distillation has previously been demonstrated by Kwiat *et. al.* using Brewster-angle-oriented glass slabs, however, for the purpose of unambiguous state discrimination the Mimih and Hillery interferometer has a number of advantages which make it a preferred tool. The glass slabs in Ref. [103] have a finite loss in the horizontal polarization associated with selective attenuation of the vertical polarization, whereas the Mimih and Hillery interferometer coherently attenuates one polarization without affecting the transmission of the orthogonal polarization, hence improving the overall efficiency of the distillation process. The Mimih and Hillery interferometer allows for the easy and continuous manipulation of the magnitude of selective-polarization attenuation by the simple re-orientation

---

**5.3. EXPERIMENTAL SETUP**

of a half-waveplate, whereas the scheme in Ref. [103] requires the stacking of glass slabs which only provides discrete manipulation along with a re-optimization of the optical alignment that normally accompanies this process. Finally, the Mimih and Hillery interferometer possesses one natural ‘failure’ port irrespective of the magnitude of selective-polarization attenuation, whereas the scheme in Ref. [103] possesses as many ‘failure’ ports as glass slabs that are used. In all fairness, the scheme in Ref. [103] was intended for entanglement distillation and not for unambiguous state discrimination. Nevertheless, these advantages make the Mimih and Hillery interferometer a preferred tool for unambiguous state discrimination.

The purpose of this paper is to explore the entanglement reduction and restoration mechanism as outlined in the Mimih and Hillery protocol [102]. We therefore make use of a simpler Michelson-type interferometer where we observe only one output port, the success port. We demonstrate the effectiveness of such an interferometer in reducing and restoring polarization entanglement, and demonstrate the need for phase stabilization in such interferometers for practical QKD implementation.

### **5.3 Experimental Setup**

First we construct maximally entangled states  $|\Psi_{\pm}\rangle \propto |HV\rangle \pm |VH\rangle$  using the Mitchell *et. al.* Bell-state filter [101]. A  $\beta$ -barium-borate (BBO) crystal that is cut and aligned for degenerate type II collinear down-conversion is pumped by

---

**5.3. EXPERIMENTAL SETUP**

a 40 mW, 405 nm CW laser (Power Technology 405 nm IQ diode laser). The 810 nm orthogonally-polarized down-converted photons are then temporally and spatially aligned in a Hong-Ou-Mandel interferometer, where a half-wave plate is used to match the polarizations of the signal and idler photons. A 10 nm bandwidth filter centered at 810 nm needs to be used in one of the output ports of the HOM interferometer in order to see a high visibility HOM dip [115]. By then orienting the half wave-plate so that the polarization of the signal and idler photons are orthogonal we can generate the  $|\Psi_-\rangle$  Bell state. The  $|\Psi_+\rangle$  and  $|\Psi_-\rangle$  Bell states can then be selected by choosing the orientation of the quarter wave-plates immediately following the Hong-Ou-Mandel interferometer (see Fig. 5.1). This constitutes a Bell-state filter [101]. For the experiment only the  $|\Psi_-\rangle$  state was generated at the Bell-state filter, however, the results we obtained were observed to be independent of phase changes introduced at Charlie's P-filter (see below).

We send one of the output qubits to one of the recipient parties, Alice, and subject the other qubit to a selective polarization filter (P-filter) before sending it to Bob, the other recipient party. The selective polarization filter, detailed below, allows the horizontal and vertical polarizations in the 0/90 down-conversion basis of a given qubit to be coherently attenuated independent of one another so that,

$$|HV\rangle \pm |VH\rangle \rightarrow \alpha|HV\rangle \pm \beta e^{i\delta}|VH\rangle, \quad (5.3)$$

where  $\alpha, \beta, \delta \in \mathbb{R}$ , and  $\alpha^2 + \beta^2 = 1$ . Ideally  $\delta$  should equal zero however, as

### 5.3. EXPERIMENTAL SETUP

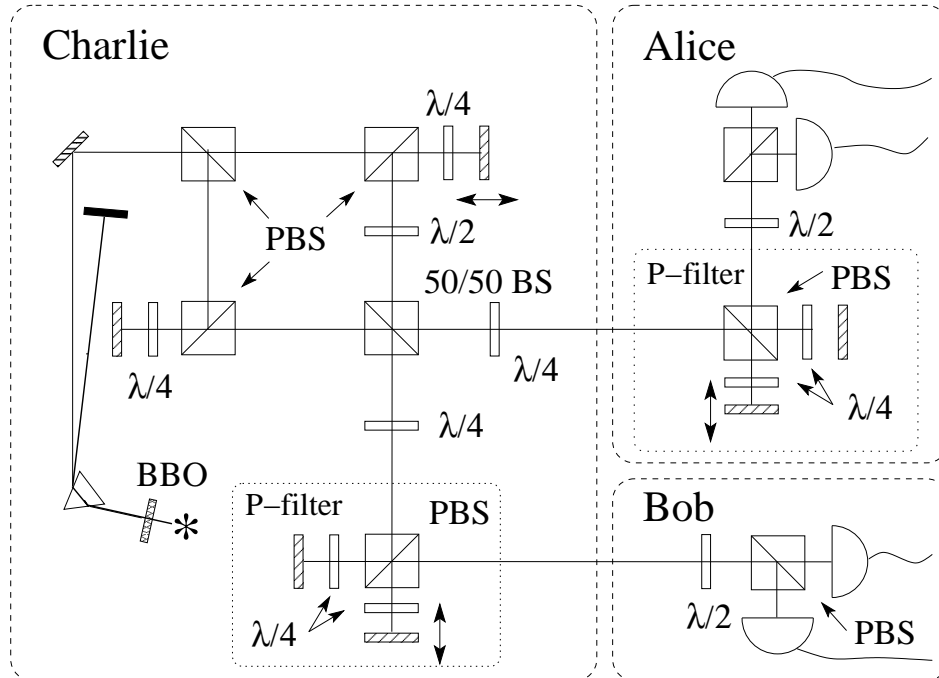


Figure 5.1: A 405 nm, 40 mW cw diode laser pumps a 2 mm thick BBO crystal that is cut and oriented for degenerate type-II collinear down conversion. Charlie's half wave-plate and the quarter wave-plates in the Hong-Ou-Mandel interferometer are used for alignment purposes only. The quarter wave-plates following the 50/50 beamsplitter determine whether Charlie will send an attenuated  $|\psi_+\rangle$  or  $|\psi_-\rangle$  state. For the experiment only the  $|\psi_-\rangle$  state was generated at the Bell-state filter, and only one detector each was used by Alice and Bob. The quarter wave-plates in Charlie's P-filter determine the attenuation of the qubit sent to Bob. Alice restores the entanglement by orientation of the quarter wave-plates in her P-filter.

---

**5.3. EXPERIMENTAL SETUP**

seen below, this is not always the case. While the P-filter reduces the overall transmission of qubits through the system it ensures that the states sent by the key generation party, Charlie, are not orthogonal. Attenuating the qubit sent to Bob as in Eq. (5.3) reduces its effective entanglement from  $J = 0$  to  $J = 1 - (2\alpha\beta)^2$  (in the sum-variance entanglement measure for bipartite, spin-1/2 systems [116, 117]), where  $J = 2 - (V_{0/90}|_H)^2 - (V_{45/135}|_H)^2$ ,  $V_{0/90}|_H$  is the visibility of Alice's photon based on the conditional detection of Bob's photon being in the horizontally polarized eigenstate, the entanglement in the J-measure is bounded by  $0 < J < 1$ , and  $J = 0$  represents the maximum entanglement. This constitutes Charlie's setup, where he produces a maximally entangled Bell state, then reduces the entanglement and sends one photon each of the entangled pair to Alice and Bob respectively.

The P-filter is constructed like a Michelson interferometer, where a polarizing beamsplitter replaces the 50/50 beamsplitter, and two quarter wave-plates are inserted in the arms of the interferometer. One of the interferometer mirrors is mounted on a 10 nm resolution linear stage in order to match the path lengths. The orientation of the wave-plates determine the relative amounts of horizontal and vertical attenuation, respectively, without affecting the coherence of the transmitted components. The transmission of a polarization component is given by  $\sin(2\theta)$  where  $\theta$  is the orientation of the optic axis in relation to the polarization of the filter arm.

### 5.3. EXPERIMENTAL SETUP

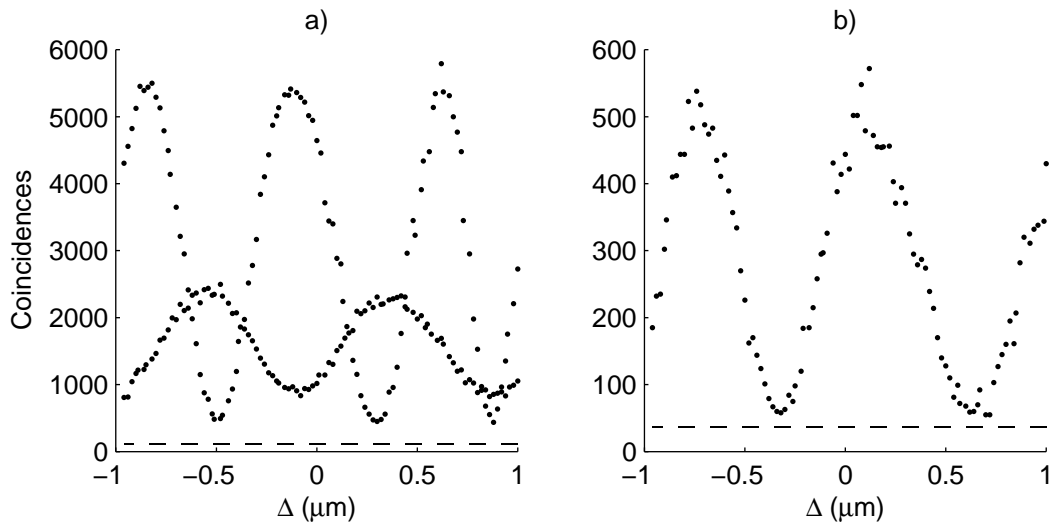


Figure 5.2: a) Maximally entangled coincidences (high visibility) and reduced entanglement coincidences (low visibility) per 20 second integration time vs.  $\Delta$ , the relative path delay in Alice's P-filter. b) Restored-entanglement, high-visibility coincidences per 20 second integration time vs.  $\Delta$ . The dashed line in both a) and b) indicates the background coincidences, 110, 56 and 37, respectively. As seen graphically, the high visibility entanglement can be reduced and then restored again. Different fringe periods are obtained for the three plots due to phase drifts in the P-filters (see text for details).

The two paths of the P-filter, although matched for optimal coherence to within a micron, introduce a phase delay  $\delta = 2\pi|\frac{\kappa}{\lambda} \bmod 1|$  into the entangled state (see Eq. 5.3), where  $\kappa$  is the exact path mismatch between the two arms (in nm) and  $\lambda = 810$  nm is the wavelength of the down-converted photons. Although inconvenient for QKD purposes, this phase delay can be used to easily plot the entanglement visibility of the relevant Bell states. The reduction of entanglement can therefore be seen by examining the rate of coincidences measured in a basis orthogonal to the horizontal/vertical down-conversion basis (i.e. the 45/135 basis), while changing the relative path delay in a P-filter held by Alice. A maximally entangled state will exhibit a visibility of 100%, whereas the non-maximally entangled state given in Eq. (5.3) will have a visibility less than 100% , when measured in a basis orthogonal to the horizontal/vertical basis [116]. The ability to quantify entanglement, given a certain visibility in the 0/90 basis, by measuring the visibility in the 45/135 basis is a result of the sum-variance entanglement measures in Chapter 4. Our down-conversion entangled source possesses a well-characterized, highly-polarized noise, where  $V_{0/90}|_H > 95\%$ , therefore entanglement should exist for a measured visibility of down to  $V_{0/90}|_H \sim 32\%$  in the 45/135 basis [116].

## **5.4 Entanglement Reduction and Revival**

Prior to any P-filter attenuation, the entangled state produced by Charlie possesses a visibility of  $89.1 \pm 1.6\%$  when measured in the diagonal/cross-diagonal

(45/135 degree) basis as seen in Fig. (5.2). This corresponds to an entanglement of  $J \sim 0.2$ . It should be noted that the measured visibility is qualitatively different from  $V_{45/135}|_H$ , however for simplicity we shall use them interchangeably due to the well-characterized nature of the noise. After Charlie reduced the entanglement by attenuating the horizontal polarization of Bob's qubit (by setting  $\theta_{Horizontal} \sim 40^\circ$  in Charlie's P-filter), we measure a visibility of  $53.6 \pm 1.6\%$ , corresponding to an entanglement of  $J \sim 0.8$ . This reduction of visibility evidences the loss of entanglement that is required in order for Charlie to create the two non-orthogonal entangled states  $|\psi_+\rangle$  and  $|\psi_-\rangle$  used in the Mimih and Hillery QKD scheme.

Alice, upon receiving her qubit from Charlie, may filter it with her own P-filter. In particular, if she attenuates her qubit so that

$$\begin{aligned} \alpha|HV\rangle \pm \beta e^{i\delta}|VH\rangle &\rightarrow \frac{\beta}{\alpha} \times \alpha|HV\rangle \pm \beta e^{i(\delta-\delta)}|VH\rangle \\ &\propto |HV\rangle \pm |VH\rangle, \end{aligned} \quad (5.4)$$

she can recover the maximally entangled state. While the coincidences will drop by an amount proportional to the attenuation, the visibility will return to 100%. By attenuating the same polarization in Alice's qubit by the same amount as before (by setting  $\theta_{Horizontal} \sim 40^\circ$  in Alice's P-filter) we restored the entanglement and measure a visibility of  $93.5 \pm 4.9\%$ , corresponding to an entanglement of  $J \sim 0.2$ . Although performed on the  $|\Psi_-\rangle$  state generated at the Bell-state

filter, this result is equally valid for the  $|\Psi_+\rangle$  state since the magnitude of the reduced and reconstructed entanglement visibility is observed to be independent of phase changes introduced in Charlie’s P-filter. This entanglement reduction and high-visibility restoration vividly demonstrates the physical mechanism required for unambiguous state discrimination that is central to most three party secret sharing schemes, particularly that of Mimih and Hillery [102].

In all visibility measurements the result is adjusted for background counts (see Fig. 5.2). It should be noted that the period of the three sinusoidal plots are slightly different in Fig. (5.2). This is because phase drifts were observed in the interferometer due to air currents and thermal drifts. These phase drifts were observed to be on the order of  $\sim \pm 100$  nm over the 33 minute interval of each measurement and should be easy to compensate for in a practical QKD system. It is worth pointing out that despite the aforementioned advantages of the Mimih and Hillery interferometer, the entanglement-distillation scheme in Ref. [103] is not susceptible to these phase-instabilities and might therefore be better suited for such QKD schemes, although with lower transmission efficiency.

## 5.5 Summary and Conclusion

In this chapter we have demonstrated one of the fundamental properties necessary for the Mimih and Hillery three-party secret sharing scheme [102], the ability to reduce and then restore entanglement for unambiguous state discrim-

ination via local operations and classical communication. We accomplish this using polarization-entangled photon pairs generated in the down-conversion process, using the optical realization proposed in [102] with some modifications. High contrast entanglement-visibility reduction and reconstruction was achieved, with an observed visibility reduction from  $89.1 \pm 1.6\%$  to  $53.6 \pm 1.6\%$ , and reconstructed visibility of  $93.5 \pm 4.9\%$ . A ten-fold reduction in coincidence rates accompanied the process of entanglement reduction and restoration, however this loss is an intrinsic property of this scheme. Phase drifts were also observed in the P-filters which can be overcome for practical QKD implementation. The entanglement-distillation scheme in Ref. [103] is not susceptible to such phase-instabilities and might therefore, with careful design, be better suited for this QKD application, albeit with lower efficiency. Additionally, one must keep in mind the well known difficulty of preserving polarization entanglement in optical fiber [118]. However, the high visibility of the reconstructed entanglement provides a good demonstration of the physical principles behind the proposed three party secret sharing schemes using this resource [102, 107]. In view of recent experimental demonstrations of the distribution of polarization-entanglement over large distances in free-space [119], this demonstration of unambiguous state discrimination via entanglement reduction/restoration along with the entanglement distillation demonstration of Kwiat *et. al.* [103] provides good incentive for practical free-space implementations of such three party secret sharing schemes.

This chapter concludes our discussion on discrete-variable entanglement. In this first part of the thesis we have discussed an optical implementation of an ancilla-free phase-covariant cloner, explored the sensitivity of sum-variance entanglement measures, and demonstrated the physical mechanism underlying unambiguous state-discrimination of nonorthogonal, bipartite entangled-states. The second part of this thesis will deal with continuous-variable entanglement, where we will explore the magnitude and applications of position-momentum and energy-time entanglement generated in the process of spontaneous parametric down-conversion.

## **Part II**

# **Continuous-Variable Regime**

# Chapter 6

## Pixel Entanglement: Experimental Realization of Optically Entangled $d = 3$ and $d = 6$ Qudits

In this chapter we demonstrate a simple experimental method for creating entangled qudits. Using transverse-momentum and position entanglement of photons emitted in spontaneous parametric down-conversion, we show entanglement between discrete regions of space, i.e. *pixels*. We map each photon onto as many as six pixels, where each pixel represents one level of our qudit state. The method is easily generalizable to create even higher dimensional, entangled states. Thus, the realization of quantum information processing in arbitrarily high dimensions is possible, allowing for greatly increased information capacity.

## 6.1 Introduction

Qubits, quantum mechanical two-level states, are the analog of classical bits. Just as most classical information processing relies on bits, qubits form the foundation of nearly all protocols in quantum information. Extending beyond two-level superposition states to  $d$ -dimensional qudit states has distinct advantages. By allowing each particle to carry  $d$  possible states instead of the usual two, the information flux increases. Recently, several quantum cryptographic protocols for qutrits and higher dimensional states were shown to increase security against eavesdropping attacks [120–122]. Furthermore, since entangled states [3] play a key role in many applications of quantum information including *quantum key distribution* [123], the secure sharing of information, *dense coding* [124], the encoding two classical bits onto a single photon of a bi-photon pair, and *teleporation* [125], the remote reconstruction of a quantum state, methods for creating entangled qudits are of particular interest.

Traditionally, spontaneous parametric down-conversion (SPDC) has offered a straightforward method for creating entangled photon pairs. To date, much of the work with optically entangled pairs concentrates on the polarization entanglement of photons created in SPDC [35]. In general though, type-II down-converted photon pairs are entangled in continuous variables as well, such as in transverse momentum and position [126–131], and which has proved useful in quantum imag-

## 6.1. INTRODUCTION

---

ing [132–134]. It was recently shown that position-momentum entangled photons created in SPDC violate separability criteria by two orders of magnitude [5].

In this chapter, we perform a proof-of-principle experiment that creates entangled qudits from the entangled transverse-momentum and position spaces of SPDC. The positions and transverse momenta of the entangled pairs are imaged into discrete regions of space forming our qudits. Thus, the system displays *pixel entanglement*. Alternative methods have been demonstrated for creating entangled qudits, but they suffer from complications when trying to generalize them to higher dimensions. For instance, angular momentum properties of light have been shown to create higher dimensional states [135, 136], but the diffraction efficiencies of computer-generated holograms limit the number of levels possible [137]. In addition, states with eleven levels have been realized using time binning [138]. This technique’s reliance on time-entanglement makes it challenging to implement in quantum information protocols. Further methods involving multiport beam-splitters have been proposed, but to the best of our knowledge they have not been experimentally realized [139]. Also multipair polarization-entangled photons were demonstrated to obey spin-1 statistics [83], but these states are produced with less efficiency than the bi-photons considered in our method. Additionally, our method is experimentally simple to realize and to generalize to high dimensions.

---

## 6.2. ENTANGLED PIXELS

### 6.2 Entangled Pixels

We used type-II phase-matching conditions for degenerate, nearly collinear SPDC.

Due to momentum conservation, the two down-converted photons, A and B (see Fig. 6.1), are anti-correlated in transverse momentum  $\mathbf{q}_{A,B}$ . In the limit of an infinite plane-wave pump field, the emitted photons are in a maximally entangled EPR output state, with delta function correlations in transverse momentum [133]. Thus, although each photon is emitted with a range of transverse momenta, measuring the momentum of one uniquely determines the momentum of the other. In practice, the pump beam is not an infinite plane wave, but rather a Gaussian beam with a finite waist. In this case, the correlations are no longer perfect. Instead, based on the approach in [128], the two-photon term of the output state is a superposition of Fock states  $|1_{\mathbf{q}_A}\rangle|1_{\mathbf{q}_B}\rangle$  given by

$$|\psi\rangle = N \int d^2\mathbf{q}_A \int d^2\mathbf{q}_B \tilde{E}(\mathbf{q}_A + \mathbf{q}_B) \frac{e^{i\Delta k_z L} - 1}{i\Delta k_z} |1_{\mathbf{q}_A}\rangle|1_{\mathbf{q}_B}\rangle,$$

with normalization constant  $N$ , longitudinal wavevector mismatch  $\Delta k_z = k_{p_z} - k_{A_z} - k_{B_z}$ , nonlinear crystal length  $L$ , and angular spectrum of the pump field  $\tilde{\mathbf{E}}(\mathbf{q})$ . The measurement of one photon's momentum determines the other's within a small region of uncertainty. This uncertainty or correlation area defines a limit to the system's resolution. The correlation length in momentum space  $\delta q_i \equiv \langle (\mathbf{q}_A + \mathbf{q}_B)_i^2 \rangle^{1/2}$  thus gives an estimate to the momentum pixel size in trans-

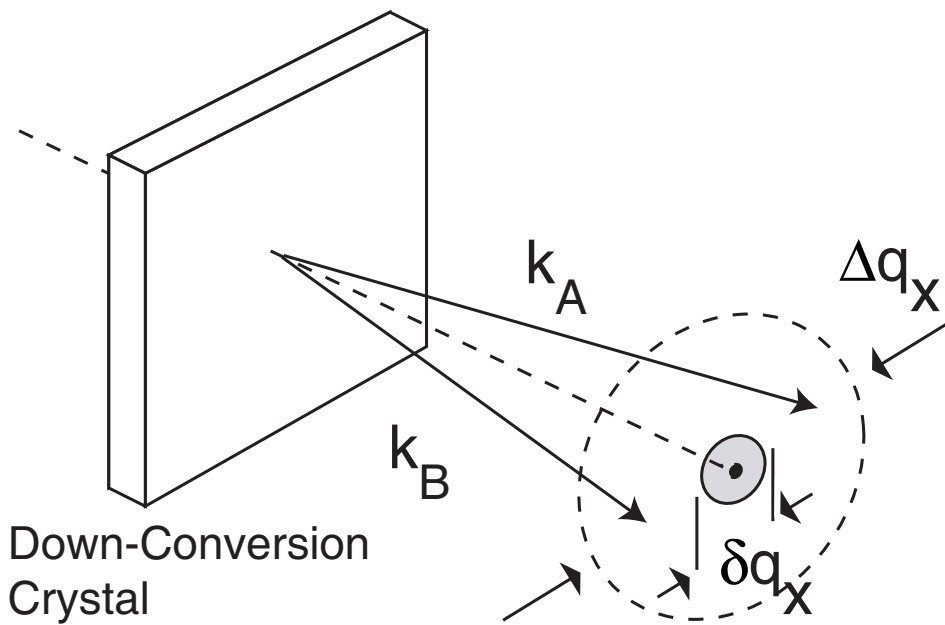


Figure 6.1: Visualization of pixels in the down-conversion process for the case of transverse-momentum entanglement. The photons are emitted with anti-correlated transverse momenta  $\mathbf{k}_{A\perp}$ ,  $\mathbf{k}_{B\perp}$  within a range  $\Delta q_x$ . The sum of the two momenta are uncertain over a range  $\delta q_x$  which is determined by the angular spread of the pump beam.

---

### 6.3. EXPERIMENTAL DEMONSTRATION

verse dimension  $i = x, y$ . In the focal plane of a lens, this length maps into real space through the relation  $\delta q_i^{(x)} = \delta q_i (\lambda f / 2\pi)$ . Entangled photons are strongly correlated in position as well. Thus, we can correspondingly define a correlation length in position as  $\delta x_i \equiv \langle (\mathbf{x}_A - \mathbf{x}_B)_i^2 \rangle^{1/2}$ , where the position representation of the state is simply a Fourier transform of the state in the momentum basis. We can discretize this two-photon state by considering each pixel, i.e. a discrete region of space, as a distinct quantum level. These regions, however, must be separated by a distance larger than the parameters  $\delta x, \delta q^{(x)}$  to ensure nearly perfectly correlated or anti-correlated fields when measuring photon coincidences in position or transverse momentum. Under these assumptions, we can describe the two-photon state as an entangled  $d$ -level qudit state.

## 6.3 Experimental Demonstration

We first considered the case of three entangled pixels for which  $d = 3$ . We performed an experiment that images either the position or the transverse momentum of the entangled photons emitted from the face of a 2-mm-thick  $\beta$ -barium borate (BBO) crystal onto a triangular optical fiber array of multimode fibers with core and cladding diameters of 62.5 and 125  $\mu\text{m}$  respectively (see Fig. 6.2). The coincidences of detection events involving the fibers in arms A and B were measured. The crystal was pumped by a 30 mW, cw beam at 390 nm with RMS intensity width of 0.17 mm. The orthogonally polarized entangled pair, emitted at 780

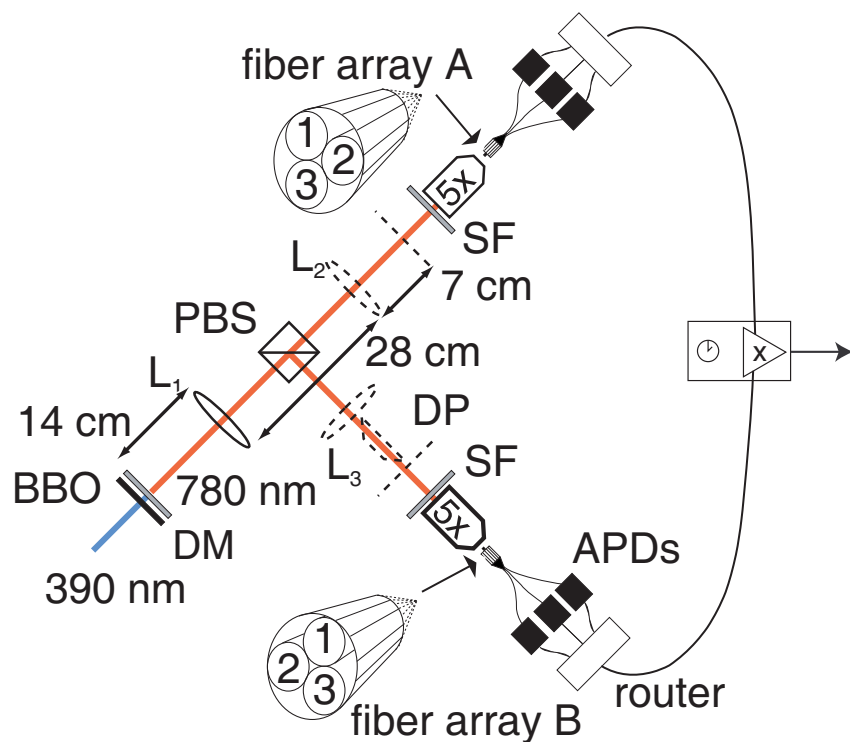


Figure 6.2: Experimental configuration used for measuring photon spatial and momentum correlations. Dichroic mirrors (DM) filter out the pump light. Lenses  $L_1$ ,  $L_2$ ,  $L_3$  have focal lengths of 100 mm, 50 mm and 50 mm respectively. The Dove prism (DP) inverts the image in momentum measurements. The distances indicated are the same in both arms.

---

**6.3. EXPERIMENTAL DEMONSTRATION**

nm, was separated using a polarizing beam splitter. To measure the position of an emitted photon, we use only lens  $L_1$ , which images the exit face of the BBO crystal onto the cleaved ends of the fibers. Lens  $L_1$  used in combination with lens  $L_{2,3}$  performed a measurement of the transverse momentum of the photon. Here, the Fourier transform properties of lenses were employed to map transverse momentum into positions in the back focal plane. A 10-nm-wide spectral filter placed before the imaging objectives limited the detection to photons of near degenerate frequency. Since the transverse momenta of the entangled pair are anti-correlated, a Dove prism was used to rotate the beam by  $180^\circ$ . The RMS intensity width of the field is 0.41 mm in the position detection plane and 0.48 mm and in the transverse-momentum detection plane. Thus, the fiber array fills the entire field in both planes, ensuring that we sample the photons equivalently for each measurement. The correlation lengths in real space, after accounting for system magnifications, were calculated to be  $\delta x = 50 \mu\text{m}$  and  $\delta q_x^{(x)} = 15 \mu\text{m}$ , both smaller than the fiber separation. Thus to reasonable approximation our state is an entangled qudit state.

We observed coincidences between the photons in each of the arms for each possible lens configuration. The results are shown in Fig. 6.3. We normalized all the graphs to the  $3_A 3_B$  peak in Fig. 6.3(a), corresponding to 475 coincidences/second, also taking into account the fiber transmission coefficients. When both arms were configured to measure in the same basis, three sharp coincidence peaks oc-

curred. The absence of any prominent off-diagonal peaks demonstrates that the two-photon state can be adequately described as a qutrit state. In the position basis, these peaks correspond to correlated pixels and in the transverse-momentum basis, they correspond to anti-correlated pixels. We note near perfect correlations exist both when imaging in the position and momentum spaces. The conditional uncertainty product is estimated to be  $\Delta x_{A|B}\Delta q_{A|B} \lesssim 0.13$  where we assume the distance between two neighboring pixels (separated by  $125\text{ }\mu\text{m}$ ) represents the  $1/e^2$  radius of the conditional distributions, justified by the high visibility observed. This uncertainty product is well below the classical limit of 0.5 demonstrating that the photon pairs are entangled in both position and momentum, a well-established property of SPDC [5, 130].

When the two arms are set to measure conjugate variables, i.e. one measuring position and one measuring momentum, we expect a uniform distribution of coincidences among all nine possible pixel combinations. As seen in Fig. 6.3(c) and (d), there is a nearly flat distribution of coincidences, indicating that the pixels are uncorrelated. This property is important for quantum cryptography, since a measurement in conjugate bases yields nine possible results, decreasing the odds of successfully eavesdropping in comparison to a qubit system.

We also investigated the scalability of the process by considering the case  $d = 6$ . We scanned a single fiber in the detector planes through six positions creating a pixel array and measured coincidences as before. The results are de-

## 6.3. EXPERIMENTAL DEMONSTRATION

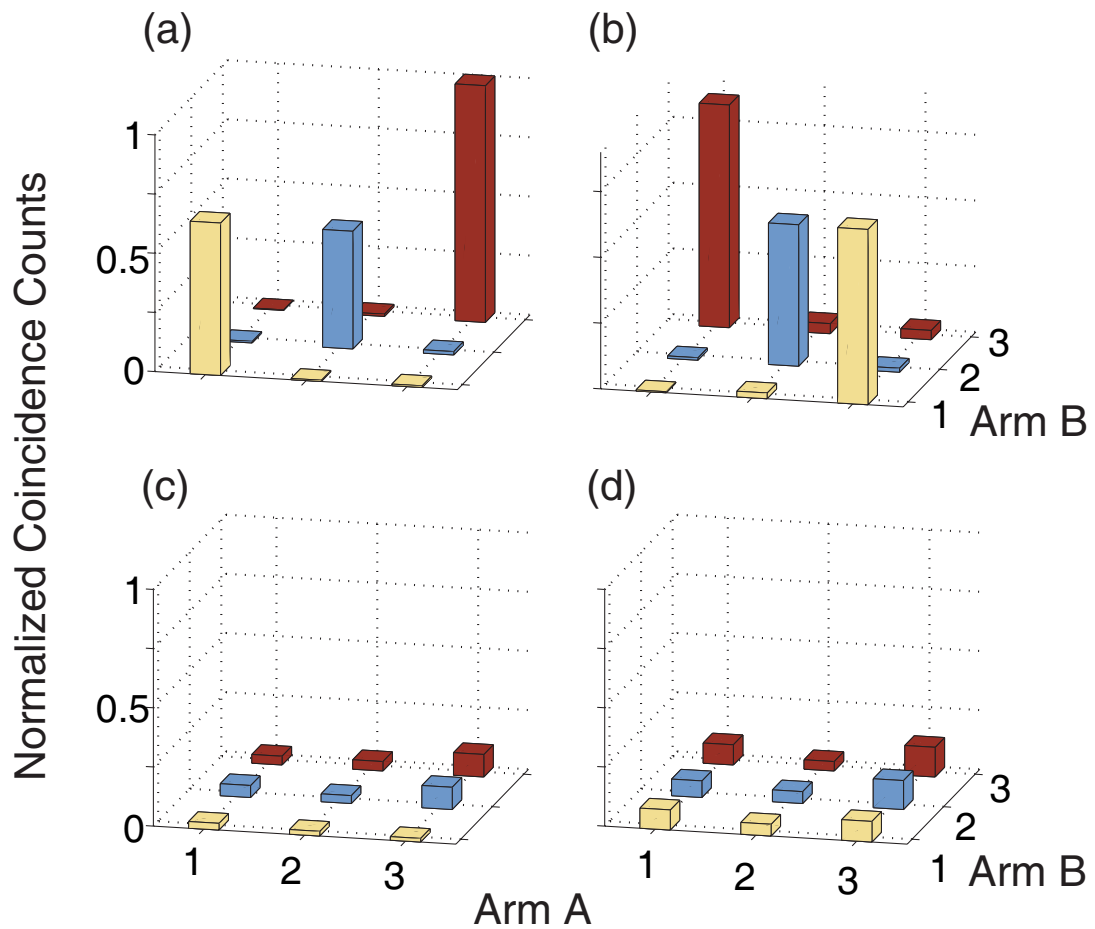


Figure 6.3: Normalized coincidence counts between photons in the two arms, when both arms measure (a) photon position (b) photon transverse momentum and when the arms measure (c), (d) conjugate variables.

---

**6.4. DISCUSSION**

picted in Fig. 6.4, normalized again to the highest peak. They show the behavior required for quantum information applications, namely highly correlated and anti-correlated pixels when measuring the photons' position and transverse momentum and an even distribution of correlations when measuring conjugate variables. Although, as a scanning system, this system does not realize the increased information flux advantage of qudit systems, it shows that this technique scales and can produce six-level qudit states.

## 6.4 Discussion

The question of how many realizable states are possible remains. Intuitively, the number of states should be the square of the ratio of the total field width to the correlation length, within an appropriate pixel-spacing factor to mitigate unwanted cross-pixel correlations. Alternatively, the Schmidt number is a measure of the effective dimension of the entangled state and can set an upper bound to the number of pixels. Recently, Eberly and Law estimated the Schmidt number for parametric-down conversion to be  $K \geq (\Delta q / 2\delta q)^2$  where  $(\Delta q)^2 = \langle q^2 \rangle$  is the RMS spread of the transverse wave-vector of the down-converted photon and  $\delta q$  is defined as before [140]. This agrees with the intuitive result in the transverse-momentum basis. In position space, we can define a similar bound  $N = (\Delta x / 2\delta x)^2$ . For our system we find  $N = 16$  which is significantly less than the calculated Schmidt number  $K \gtrsim 360$  since in general the Schmidt modes are

## 6.4. DISCUSSION

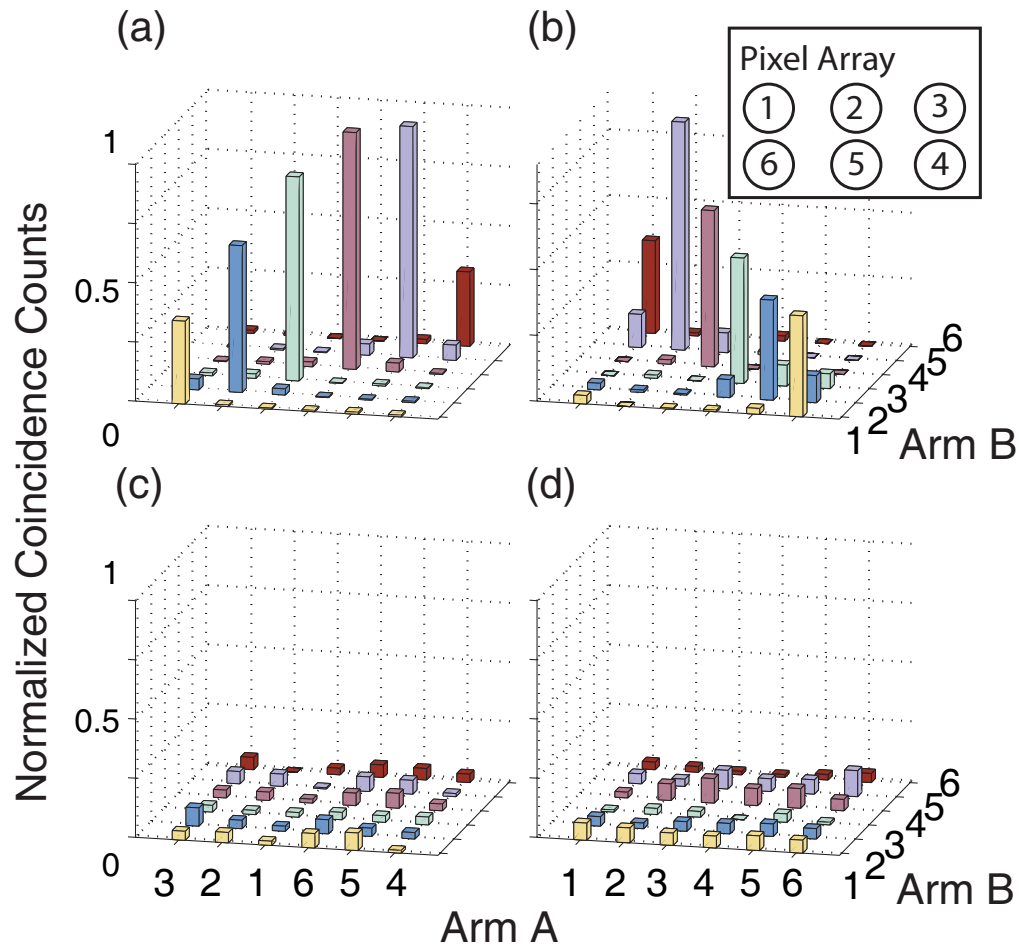


Figure 6.4: Normalized coincidence counts between two six-pixel arrays when both arms measure (a) photon position (b) transverse photon momentum and when the arms measure (c), (d) conjugate variables. The inset shows the pixel array configuration.

---

**6.4. DISCUSSION**

not well-localized in space. Hence, all  $K$  levels are not realizable as localized pixels in both the position and transverse-momentum bases. Even so,  $N$  is highly scalable since  $\Delta x$  depends only on the pump waist and  $\delta x$  depends only on the crystal length and phase-matching conditions.

Each of these  $N$  states, in position space for example, is conjugate to the entire transverse-momentum space and vice versa. Hence these can be considered qudits, but not in the usual sense. This property appears to be advantageous in quantum key distribution. In this case, one wants to effectively detect the presence of an eavesdropper while maximizing the number of highly correlated pixels. We consider an eavesdropper Eve intercepting a signal sent from Alice to Bob using a quantum cryptographic protocol. Eve's presence is typically revealed when Alice and Bob measure in the same basis and Eve measures in the conjugate basis. After Eve's measurement, Alice and Bob's photons will be uncorrelated and found anywhere in the detection plane. Thus, if a photon is detected, it will be randomly measured in one of the  $N$  states, increasing the bit error rate (BER) and resulting in a non-violation of the EPR bound. Additionally, due to the detection "dead" area, Eve will cause a drop in the overall key generation rate. For practical purposes, sufficient dead area is required to ensure high visibility correlations and low BER due to the finite correlation widths of the source. In practice, photons in this area would still be collected for security purposes, but would not contribute to key generation. Hence, these dead areas actually provide

an additional signature for the presence of eavesdropping. At present, we envision this system to be useful for cryptographic applications in free-space applications because the quality of entanglement strongly depends on the preservation of the wavefront, which cannot be done using current fiber technologies.

## 6.5 Summary and Conclusion

In summary, in this chapter we have experimentally demonstrated a simple method for producing entangled qudits using the two-photon output of type-II SPDC. We created qutrits using a three-pixel detector array and investigated six-level qudits. The method is easily extended to higher dimensional qudits. The number of levels possible is restricted ultimately only by the Schmidt number which can be engineered to be large [140]. Very high dimensional entangled states are therefore easily conceivable using the position and transverse-momentum entanglement of SPDC, though for applications in quantum cryptography it may be beneficial to use only a small fraction of these states. This method presents a simple, yet powerful, tool for investigating entangled qudit states for quantum information protocols.

In the next chapter we shall explore the magnitude of energy-time entanglement that is generated in the process of spontaneous parametric-downconversion. We utilize the framework of the Schmidt mode decomposition of continuous-variable entanglement [140], discussed in this chapter, to demonstrate that high

energy-time entanglement exists in the parametric down-conversion process that is commonly used in the laboratory.

## Chapter 7

# Experimental Demonstration of High Two-Photon Time-Energy Entanglement

In this chapter we report on the experimental demonstration of high energy-time entanglement in two-photon states created in the process of spontaneous parametric down-conversion. We show that the classical variance product, which we violate by three orders of magnitude, actually represents a lower bound estimate of the number of information eigenmodes  $K$ . Explicit measurements estimate  $K$  to be greater than 100, with theoretical estimates predicting a value of as high as  $1 \times 10^6$ . These results provide incentive for the practical feasibility of large bandwidth quantum information processing, particularly in cryptography over large distances.

## 7.1 Introduction

Many impressive advances have been made in the field of quantum key distribution (QKD) [44, 45], however in terms of practical bandwidths and communicable distances there is still a long way to go before this technology can be used effectively for the secure communication of streaming images or other such high bandwidth applications. Recently there has been interest in developing high-dimensional entangled states for use in QKD systems due to the higher information bandwidth which would become available [135, 141–144]. Analogous to the classical case, higher-dimensionality implies greater information content per particle, which for QKD implies larger alphabets for the same particle transmission rate, as well as possibly increasing the security tolerance to noise [34, 120]. Of course, for QKD these states would need to be easily transported over large distances, while at the same time preserving the entanglement. To this end photonic sources have been the medium of choice in most experimental proposals, being easily transportable over existing fiber optic networks. Additionally, the process of parametric down-conversion provides a ready source of photon pairs with a number of entangled quantum states to choose from. However, for most of these quantum states the entanglement either cannot be preserved over large distances in fiber, or the entanglement cannot be easily generalized to significantly higher dimensions [118, 120, 135].

In the previous chapter it was shown that by artificially discretizing the two-

---

**7.1. INTRODUCTION**

photon position-momentum entanglement created in down-conversion it is possible to generate D-dimensional entangled states, where D is an estimate of the number of exploitable information eigenmodes of the system [142]. Exciting though this prospect is, the entanglement cannot be preserved over large distances using current fiber optic technology. Similar to position and momentum, energy and time are conjugate variables which obey the single particle Heisenberg uncertainty relation  $(\Delta E)^2(\Delta t)^2 \geq \hbar^2/4$ , also known as the time-bandwidth product, where  $\Delta E$  and  $\Delta t$  are the measured single particle energy and time uncertainties respectively [1]. The joint uncertainties  $\Delta E_{12} = \Delta(E_1 + E_2)$  and  $\Delta t_{12} = \Delta(t_1 - t_2)$  of two entangled particles, on the other hand, can violate the classical separability bound [5, 91]

$$[\Delta E_{12}]^2[\Delta t_{12}]^2 \geq \hbar^2. \quad (7.1)$$

Such states are called energy-time entangled states. Some efforts have successfully used two-photon energy-time entanglement generated in the down-conversion process to perform quantum key distribution, and to generalize the scheme to higher dimensional states [141, 145]. Energy-time entanglement has already been demonstrated to be well preserved over large distances and currently seems to be the most promising of the available candidates [141, 145, 146]. By using the ideas proposed in the previous chapter with currently available energy-time entangled sources, in this chapter we show that it should be possible to generate D-dimensional entanglement with  $D > 100$  and possibly as high as  $D \sim 1 \times 10^6$ , where the estimates

are specific to our experimental parameters. In doing so, we also demonstrate an experimental violation of the classical variance product in Eq. (7.1) by 3 orders of magnitude, and show that this variance product actually represents a lower bound on the dimensionality of entanglement.

## 7.2 Experimental Setup

A schematic of the experiment is shown in Fig. (7.1). The energy-time entangled photons are created in the collinearly phasematched spontaneous parametric down-conversion process of a 2 mm long  $\beta$ -barium borate (BBO) crystal which is pumped by a 30 mW, cw, 390 nm laser beam. The down-converted signal and idler photons are separated from the pump by a dichroic mirror, and from each other via a polarizing beam splitter. They are then coupled into two single mode fibers. Each photon is then sent to two distinct arms of our setup (signal to arm A and idler to arm B in Fig. (7.1)), where it is manually routed to either one arm of a Franson interferometer [9, 147] or a monochromator. Using these two measurement devices we measure the two-photon coherence time and energy correlations respectively, and hence estimate the dimensionality of entanglement as well as the variance product. In the spirit of space-like separated detectors we use a Franson interferometer [9] even though the same information could be obtained using the Hong Ou Mandel interferometer [39].

## 7.2. EXPERIMENTAL SETUP

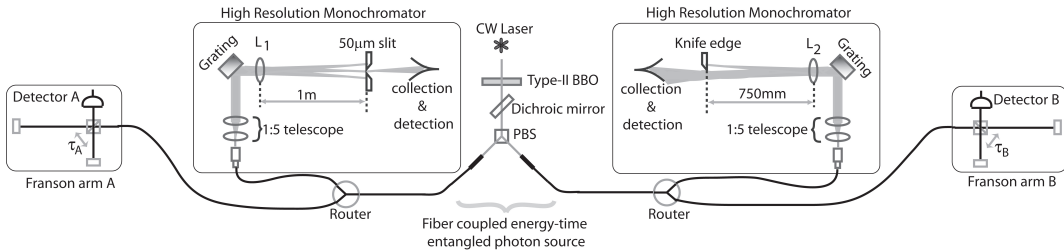


Figure 7.1: Schematic of the two-photon time-energy entangled source and analyzing devices. The Franson interferometer is used to measure the biphoton coherence time, while the monochromators are used to measure an upper bound of the two-photon spectral correlations. The beam diameter of the photons in the monochromators is increased to 3.85 mm using a 1:5 telescope, then diffracted off of a diffraction grating at an incidence angle of  $\sim 20^\circ$ .  $L_1$  and  $L_2$  are lenses of 1 m and 750 mm focal lengths respectively.  $\tau_A$  and  $\tau_B$  are the path mismatch in arms A and B of the Franson interferometer respectively.

### 7.2.1 Time Correlation

The Franson interferometer consists of two unbalanced Michelson interferometers, one in arm A and one in arm B. Each Michelson interferometer possesses a long and a short arm, with a time delay of  $\tau_A$  and  $\tau_B$  between the two arms in each Michelson respectively. The time delays are much longer than the single photon coherence length, ensuring that no single-photon interference occurs. Additionally, this allows us to post-select long-long and short-short coincidence events, as detailed later. The time delay  $\tau_A$  is varied by varying the length of the long arm in arm A with an automated linear stage. Let us consider the expected photo-coincidence rate  $P(\tau_A, \tau_B)$  which is detected at the output of the Franson interferometer as a function of the time delays  $\tau_A$  and  $\tau_B$  [148–150]:

$$P \propto \int \int |\langle 0 | a_A(t_A) a_B(t_B) | \Psi \rangle|^2 dt_A dt_B \quad (7.2)$$

---

**7.2. EXPERIMENTAL SETUP**

where  $|\Psi\rangle = \int \psi(t_s, t_i) e^{-i\frac{\omega_p}{2}(t_i+t_s)} a_s^\dagger(t_s) a_i^\dagger(t_i) |0\rangle dt_s dt_i$  is the biphoton wavefunction in the time domain, where  $\psi(t_s, t_i)$  is given by

$$\psi(t_s, t_i) = \Pi \left[ \frac{(t_s - t_i)}{(\pi/\Omega_f)} \right] e^{-2[\rho(t_s + t_i)]^2} \quad (7.3)$$

for a biphoton state generated in spontaneous parametric downconversion,  $\Pi[x]$  is a rectangular function such that  $\Pi[x] = 1$  if  $|x| < 1$  and  $\Pi[x] = 0$  otherwise,  $\Omega_f$  is half the zero-to-zero down-conversion bandwidth,  $\rho$  is the angular frequency spectrum width of the cw laser,  $a_s^\dagger$  and  $a_i^\dagger$  are the signal and idler creation operators, and  $a_A$  and  $a_B$  are the annihilation operators at the two detectors. In deriving Eq. (7.3) we have taken advantage of the fact that the cw pump has a much narrower spectrum than the phase-matching function, hence we have already assumed that the signal and idler frequencies are anti-correlated with respect to each other about  $\omega_p/2$ , where  $\omega_p$  is the central pump frequency [115, 149]. Consequently, the time at which the signal and idler are created in the non-linear crystal (birth-time) will be correlated to each other [149]. A derivation of the time-domain biphoton wavefunction is provided in Appendix A. For the Franson interferometer,  $a_A$  and  $a_B$  can be written in terms of the signal and idler annihilation operators:

$$a_A(t) = [a_s(t) + a_s(t + \tau_A)]/\sqrt{2} \quad (7.4)$$

$$a_B(t) = [a_i(t) + a_i(t + \tau_B)]/\sqrt{2} \quad (7.5)$$

---

**7.2. EXPERIMENTAL SETUP**

Using the creation and annihilation operator commutation relations  $[a_j(t_j), a_k^\dagger(t_k)] = \delta_{jk}\delta(t_j - t_k)$  and rejecting the long-short and short-long events through post-selection, Eq. (7.2) can be simplified to give:

$$P(\tau_A, \tau_B) = 2 + 2\cos\left[\frac{\omega_p}{2}(\tau_A + \tau_B)\right] \Lambda\left[\frac{\tau}{(\pi/\Omega_f)}\right] \quad (7.6)$$

where  $\Lambda[x]$  is a triangular function such that  $\Lambda[x] = 1 - |x|$  if  $|x| < 1$  and  $\Lambda[x] = 0$  otherwise, and  $\tau = \tau_A - \tau_B$ . A more general and detailed derivation of the output of the Franson interferometer is provided in Appendix B. The triangular function is a result of the convolution of two square functions in this interference effect. We thus expect an oscillating fringe pattern in the measured coincidences of the Franson interferometer with a period of  $4\pi/\omega_p$  and a triangular envelope of FWHM equal to the biphoton coherence time  $\pi/\Omega_f$  of the downconverted photons [149, 151]. The Franson interferometer therefore constitutes a nonlocal measure of the biphoton coherence time of our entangled source.

In the experiment a path mismatch of 90 cm ( $\tau_{A,B} \sim 3$  ns) was used for both Michelson interferometers, much larger than the single photon coherence length of  $\sim 60$   $\mu\text{m}$ . Additionally, the acceptance window of the coincidence circuit was set at 1 ns so that we only observe long-long or short-short coincidences. We are not interested in measuring the period of the fringes, but instead in measuring the envelope over which these fringes occur which represents the correlation width of the birth-time of the down-converted photons. By incrementally varying the

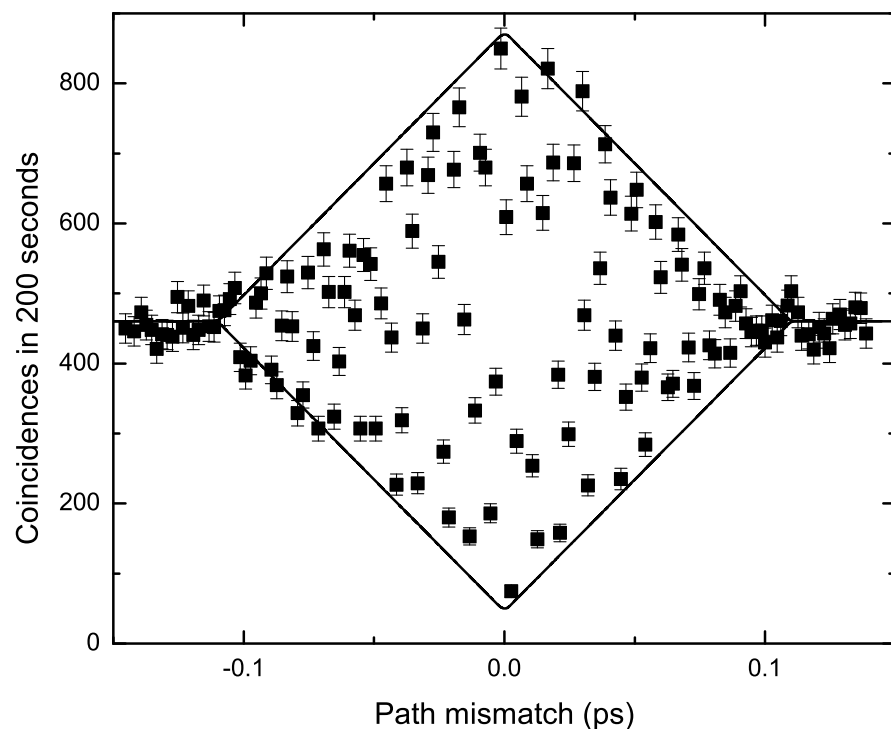


Figure 7.2: Data points depict the typical interference envelope which is observed in the coincidence rates of the Franson interferometer as a function of path mismatch. The solid line is the theoretical triangular envelope function which is calculated for a square biphoton wavefunction of coherence time  $\pi/\Omega_f = 100$  fs.

length of the long Michelson arm in arm A it is possible to chart out the envelope of the interference pattern as shown in Fig. (7.2). As can be seen, the results are in excellent agreement with the theoretical envelope predicted for a zero-to-zero phase-matching width of 20 nm, which gives a biphoton coherence time of  $\Delta t_{AB} = 100$  fs. The individual fringes of the interference have not been resolved since they are not central to the order-of-magnitude estimate of the envelope function. It should be noted that we measure a fringe visibility of 84% which indicates the presence of entanglement via a violation of Bell inequalities [145], however this violation gives no quantitative information on the dimensionality of the entanglement, which is the motivation of this paper.

### 7.2.2 Energy Correlation

Next, we measure the spectral coincidence width of the signal and idler photons by routing them to the monochromators. The monochromators are set up as shown in Fig. (7.1), with overall spectral resolutions of  $\sim 0.017$  nm (i.e. 8.4 GHz). By placing a  $50\ \mu\text{m}$  slit in the focal plane of the 1 m focal-length lens in arm A, we expect to create a ‘ghost image’ of the slit in the focal plane of the 750 mm focal-length lens in arm B [5, 152]. A smaller width was not chosen due to the low observed coincidence count rates. By performing a knife edge test in the focal plane of the 750 mm lens in arm B and observing coincidences we can thus measure the spectral correlations of the photons. The result of the knife edge test is shown

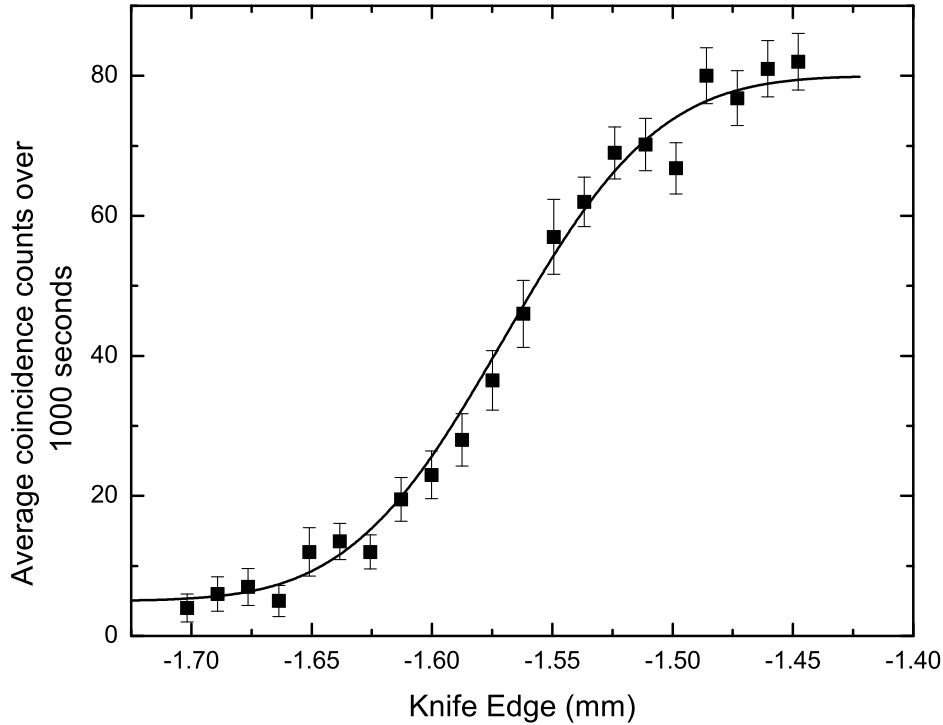


Figure 7.3: Using ghost imaging we estimate the two-photon spectral correlation width as 0.048 nm (details in text). The curve is a theoretical fit to the experimental data (squares).

in Fig. (7.3) where we measured a ghost slit width of 54  $\mu\text{m}$ , which corresponds to a conditional spectral correlation width of  $\Delta\lambda_A|_{\lambda_B} = 0.048 \text{ nm} (\sim 24 \text{ GHz})$  [5]. We would like to stress that this measurement is not optimized since it is near the limits of the resolution of the monochromators and only represents an upper bound. The true correlation width is expected to be much less, determined by the

bandwidth of the pump. We have thus measured the upper limit of the spectral correlations of the down-converted photons to be  $\Delta\lambda_A|_{\lambda_B} = 0.048$  nm.

### 7.2.3 Violation of EPR bound

Let us reiterate what we have obtained. We have measured the *joint* birth-time uncertainty (biphoton coherence time)  $\Delta t_{AB}$  of the entangled photons, which is relevant to the Mancini *et. al.* separability criterion [5, 91]. On the other hand we have measured the *conditional* spectral uncertainty  $\Delta E_A|_{E_B}$  which is relevant to the EPR criterion [5]. We do not expect the conditional uncertainties of time and energy to vary over the range of interest. Therefore, although conditional and joint uncertainties are qualitatively different, we shall assume in our case that their measured values can be used interchangeably to reasonable approximation. Using the energy and time correlation widths measured in the experiment, we can estimate the energy-time variance product to be  $(\Delta E_A|_{E_B})^2(\Delta t_A|_{t_B})^2 \sim [\Delta E_{AB}]^2[\Delta t_{AB}]^2 \sim 0.00022\hbar^2$ , which is a 3-order-of-magnitude violation of the EPR and the Mancini *et al.* separability criterion [5, 91]. Although an impressive result in itself, we would like to point out that the true violation could be much stronger; the energy correlation measurement is not optimized. Using the theoretical estimate of the spectral correlation width of  $\Delta\lambda_{si} \sim 5 \times 10^{-6}$  nm (calculated from a 2 MHz bandwidth servo-locked pump), we would expect an optimized measurement to give a violation of the order of eleven

orders of magnitude. It should be noted that these results follow through despite there being no time-operator in the framework of quantum mechanics. Although this is an interesting and perhaps surprising outcome, it is not a point of contention for our results and conclusions since they can just as easily be framed in terms of longitudinal position  $x_{\parallel} = ct$  and momentum  $p_{\parallel} = \hbar k_{\parallel} = E/c$ . By straightforward substitution we can obtain the familiar position-momentum uncertainty relation  $(\Delta x_{\parallel})^2(\Delta p_{\parallel})^2 \geq \hbar^2/4$  and separability bound  $[\Delta x_{\parallel 12}]^2[\Delta p_{\parallel 12}]^2 \geq \hbar^2$ . We have framed this work in terms of energy and time because of the common usage of this convention in the literature.

### 7.3 High Energy-Time Entanglement

Let us now consider the implications of these results when put into context of the previous chapter, and the work done in [140, 142] where it is shown that the dimensionality  $D$  of entanglement is equal to the Schmidt number  $K$  of the Schmidt mode decomposition of the two-photon wavefunction. For a wavefunction of the form  $\psi(t_+, t_-) = A(t_+)B(t_-)$ , as in Eq. (7.3) where  $t_{\pm} = t_s \pm t_i$ , the Schmidt number of the decomposition can in general be shown to be given by  $K \sim \frac{1}{2}(\delta t/\Delta t_{12} + \Delta t_{12}/\delta t)$ , where  $\delta t$  and  $\Delta t_{12}$  are widths associated with the gaussian-like functions  $A(t_+)$  and  $B(t_-)$  respectively [140]. Similarly, the Schmidt decomposition can be performed in the conjugate basis  $\tilde{\psi}(E_+, E_-) = \tilde{A}(E_+)\tilde{B}(E_-)$ , giving  $\tilde{K} \sim \frac{1}{2}(\delta E/\Delta E_{12} + \Delta E_{12}/\delta E)$ , where  $\delta E$  and  $\Delta E_{12}$  are widths associ-

ated with the gaussian-like functions  $\tilde{B}(E_-)$  and  $\tilde{A}(E_+)$  respectively. In general, because  $E$  and  $t$  are conjugate variables, it can be shown that  $\delta E \Delta t_{12} \geq \hbar/2$  and  $\delta t \Delta E_{12} \geq \hbar/2$ . This is simply a statement of the fact that we cannot use correlation measurements to gain more information about a single particle than what is allowed by the Heisenberg uncertainty product. Using this, the Schmidt number becomes  $K, \tilde{K} \geq \frac{1}{4}(\hbar/\Delta t_{12}\Delta E_{12})$ , where the equality holds for when A and B are gaussian functions. This is a noteworthy statement that the variance product in Eq. (7.1), i.e. the EPR product, is actually an estimate of the lower bound of the dimensionality of the entanglement. For our case, the variance product measured above predicts that the dimensionality of entanglement is  $D \gtrsim 16$ . However, since our functions are not both gaussian, we use the measured values of the spectral widths  $\delta\lambda_{dc} \sim 10$  nm and  $\Delta\lambda_A|_{\lambda_B} = 0.048$  nm to obtain the more accurate estimate of  $D \sim 100$ . This is smaller than the estimate of  $D \sim 3 \times 10^6$  obtained using the temporal widths  $\Delta t_{AB} \sim 100$  fs and  $\delta t \sim 300$  ns (from the 100 m pump coherence length), and therefore implies that the measured number of exploitable information eigenmodes in our source is of the order of  $D \sim 100$  [142]. We would like to point out that this estimate is still low considering that we are limited by the resolution of the monochromators. Using another technique we have measured over 1000 exploitable eigenmodes, as discussed in the following chapter. The theoretical estimate of the two-photon correlation width (2 MHz) predicts that the number of eigenmodes could in reality be as high as

$D \sim 1 \times 10^6$ . Of course, measurements with much higher spectral resolution are required to verify this. Nevertheless, this represents a very large potential information bandwidth for quantum information applications. Especially in the realm of quantum cryptography, where evidence strongly suggests that energy-time entanglement is well preserved over very large distances in fiber [146, 153], these results present an exciting prospect for immediate applicability. High dimensional cryptographic schemes have already been proposed and experimentally realized [141, 154], however this work represents the first insight into the orders of magnitude of improvement which this source might be able to provide.

## 7.4 Discussion

Considerable practical challenges still remain to be overcome before this large information bandwidth can be exploited. For example, a simplistic discrete-pixel QKD system with  $D \sim 10^5$ , as envisaged in the previous chapter [142], would require single photon detectors of sub-picosecond timing resolution (compared with contemporary cutting-edge  $\sim 10$  ps resolution), and monochromators of  $\sim 10^{-4}$  nm spectral resolution with meters long optics and  $\sim 500$  nm detectors of nanosecond resolution which span an uninterrupted array of  $\sim 5\text{cm}$  (compared with contemporary  $\sim 50$   $\mu\text{m}$  ccds with microlens arrays). A more sophisticated method for exploiting this entanglement is discussed in the next chapter, where a large-alphabet QKD protocol that utilizes continuous-variable time-energy entan-

---

**7.4. DISCUSSION**

lement is demonstrated. We believe the protocol represents a significant breakthrough in the drive to establish practical large-bandwidth quantum information communication and processing, however the exploitable dimensionality of entanglement is still limited by the non-ideal resolution of time-resolved detection and electronics.

# Chapter 8

## Demonstration of Secure, Large-Alphabet QKD Using Continuous Variable Energy-Time Entangled Bipartite States

In this chapter we present a protocol for large alphabet quantum key distribution using energy-time entangled biphotons that are generated in the process of spontaneous parametric down-conversion using a cw pump. Binned, high-resolution timing measurements are used to generate a large alphabet key of up to 1278 characters, while the security of the quantum channel is determined from the measured visibility of Franson interference fringes. The protocol is easily generalizable to even larger alphabets, requires as few as only two detectors for arbitrary alphabet sizes, and utilizes energy-time entanglement which is robust to transmission over large distances in fiber.

## 8.1 Introduction

Quantum key distribution (QKD) has continued to progress toward the goal of practical and provably secure key distribution operating at high bandwidths and over large distances [44, 45]. Achieving high bandwidths over large distances remains a challenge to researchers, and it is for this reason that recent studies have focused on the possibility of increasing the information content of each transmitted quantum state by using states with higher dimensionality [43, 135, 141–143, 155], i.e. qudits instead of qubits. Higher dimensional quantum states also have the attractive properties of an increased sensitivity to eavesdropping and a decreased sensitivity to noise [34, 156].

Higher dimensional states for QKD have been investigated previously. In Chapter 6 we demonstrated artifical discretization of entangled transverse position-momentum quantum states with  $d = 6$  qudits [142]. Artifical discretization of entangled transverse position-momentum quantum states with  $d = 37$  qudits [155] has now also been demonstrated in the laboratory. However, such spatially encoded states are not well suited to QKD over large distances owing to the difficulties of preserving the phase fronts in free space and the inability to transport the states in single mode fiber. Hyper-entangled states of polarization, spatial mode, and energy-time has also been achieved with  $d = 36$  [43]. Lastly, time-bin entangled states having  $d = 3$  have been implemented in a QKD scheme

operable over large distances. Unfortunately, time-bin entangled states are not easily generalized to larger dimensions [141].

In the previous chapter we demonstrated that time-energy entangled photons can have very large information content per biphoton [157]. In this chapter we show experimentally that the continuously entangled time-energy system can be discretized in such a way to achieve very large alphabets, and we demonstrate an alphabet of up to 1278 characters. Further, this scheme is fiber-based and requires as few as 2 detectors for alphabets of arbitrary size.

## 8.2 Motivation

Consider the unnormalized biphoton state

$$|\Psi\rangle \propto \int \int dt_1 dt_2 A(t_1, t_2) B(t_1, t_2) e^{-i\frac{\omega_p}{2}(t_1+t_2)} \hat{a}_1^\dagger(t_1) \hat{a}_2^\dagger(t_2) |0\rangle, \quad (8.1)$$

where  $\omega_p$  is the down-conversion pump frequency and  $a_i^\dagger(t_i)$  is the photon creation operator in mode  $i$  at time  $t_i$ . After passing through spectral filters, a Gaussian correlation function  $A(t_1, t_2) = e^{-\frac{(t_1-t_2)^2}{4\tau^2}}$  provides a good approximation for the biphoton temporal correlation function, where the correlation time  $\tau$  is on the order of  $\sim 100$  fs, as determined by the phasematching conditions of the non-linear crystal. The biphoton temporal correlation function  $A(t_1, t_2)$  can be understood as the correlation between the time at which the two photons exit the non-linear crystal. Also,  $B(t_1, t_2) = e^{-\frac{(t_1+t_2)^2}{16\tau^2}}$  represents the biphoton envelope function,

## 8.2. MOTIVATION

---

where the biphoton envelope  $T$  is given by the coherence time of the pump photon of frequency  $\omega_p$  that was destroyed in the creation of the entangled biphoton. The biphoton coherence time is on the order of  $\sim 500$  ns corresponding to the inverse laser linewidth. For mathematical simplicity it is straightforward to show that for  $T \gg \tau$

$$A(t_1, t_2)B(t_1, t_2) \simeq e^{-\frac{(t_1-t_2)^2}{4\tau^2}} e^{-\frac{t_1^2}{4T^2}}. \quad (8.2)$$

As shown in the previous chapter,  $|\Psi\rangle$  is highly entangled and can be used to send enormous amounts of information per photon pair [157]. The Schmidt number, or number of information eigenmodes, of Eq. (8.1) is given by  $K \sim T/\tau$  [140].

Suppose that a party, Alice, sends another party, Bob, one photon of the entangled time-energy biphoton state discussed above, and keeps the other photon under her control. Suppose now that an eavesdropper, Eve, makes a positive operator value measurement (POVM) on the arrival time of the photon sent to Bob [158, 159]. We model Eve's measurement as a projective filter function,

$$\hat{M}_e = \int dt f(t, T_E) a_e^\dagger(t) |0\rangle \langle 0| a_e(t), \quad (8.3)$$

where  $f(t, T_E)$  is a general filter function and  $T_E$  is related to the resolution of Eve's POVM. Computation of the resulting state for a gaussian filter function  $f(t, T_E) = e^{-\frac{t^2}{4T_E^2}}$  gives,

$$|\Psi_M\rangle \propto e^{-\frac{(t_1-t_2)^2}{4\tau^2}} e^{-\frac{t_1^2}{4} \left( \frac{1}{T^2} + \frac{1}{T_E^2} \right)} \hat{a}_1^\dagger(t_1) \hat{a}_2^\dagger(t_2) |0\rangle, \quad (8.4)$$

---

**8.2. MOTIVATION**

which represents the biphoton wavefunction after Eve's POVM. For  $T_E \ll T$  we get  $(\frac{1}{T^2} + \frac{1}{T_E^2}) \sim \frac{1}{T_E^2}$ , which gives us  $K \sim T_E/\tau$ . This implies that Eve's POVM results in a decrease in the Schmidt number; eavesdropping has decreased the number of information eigenmodes.

It has been shown that the visibility of the interference pattern in a Franson interferometer [9] can be used as a Bell-type entanglement measure for energy-time entanglement [146, 153]. We find that the visibility of the Franson fringe pattern, along with the known path mismatch, also provides specific information about the biphoton envelope width  $T$  (or equivalently  $T_E$  after Eve's POVM). If Alice and Bob send the biphoton state in Eq. (8.4) through a Franson interferometer, the post-selected coincidence rate will be given by

$$\begin{aligned} R_M &\propto \int dt_a dt_b |\langle 0 | (\hat{a}_1(t_a + \Delta t + \delta t) \hat{a}_2(t_b + \Delta t) + \hat{a}_1(t_a) \hat{a}_2(t_b)) | \Psi_M \rangle|^2 \\ &\cong 1 + \cos[\frac{\omega_p}{2}(2\Delta t + \delta t)] e^{-\frac{\delta t^2}{8\tau^2}} e^{-\frac{\Delta t^2}{8T_E^2}}, \end{aligned} \quad (8.5)$$

where  $a_{1,2}(t)$  is the destruction operator for Alice's and Bob's detectors respectively,  $\Delta t$  is the path mismatch in Bob's arm of the Franson interferometer, and  $\delta t$  is the difference in path mismatches between Alice's and Bob's arms of the Franson interferometer. One can see that a strong drop in franson fringe visibility is observed when  $T_E \lesssim \Delta t$ . Therefore we can detect the presence of Eve's POVM by observing a reduction in the visibility of the fringes obtained in Alice's and Bob's Franson interferometer, as predicted by the exponential function in Eq. (8.5). It

should be noted that a larger path mismatch  $\Delta t$  allows for a more sensitive test against Eve's POVM.

### 8.3 Energy-Time Entanglement Protocol

The energy-time entanglement QKD protocol we present here is accomplished in 6 steps. 1) Alice sends Bob one photon of an energy-time entangled biphoton and keeps one for herself. 2) Alice and Bob randomly and independently measure arrival times of their incoming photon either directly with low-jitter (FWHM  $\sim 50$  ps,  $1/e^2$  width  $\sim 350$  ps) detectors (timing detector) or after sending their photon through an unbalanced Michelson interferometer acting as one-half of a Franson interferometer (see Fig. (8.1)). These timing measurements of Alice and Bob are accurately synchronized to each other by using a shared, public, synchronization pulse signal. This sync signal has a period of 64 ns between consecutive pulses in our experiment, where each pulse is measured, counted and recorded. During the entirety of the QKD process Alice privately scans one arm of her unbalanced interferometer between two, neighboring, Franson interference maximum and minimum locations (predetermined during initial calibration). 3) After all the photons have been detected, Bob publicly sends Alice the exact arrival times of the photons that were detected in the output of his Michelson interferometer. Alice uses this information, along with her own Franson timing measurements and respective interferometer scan locations, to determine the visibility of the Franson

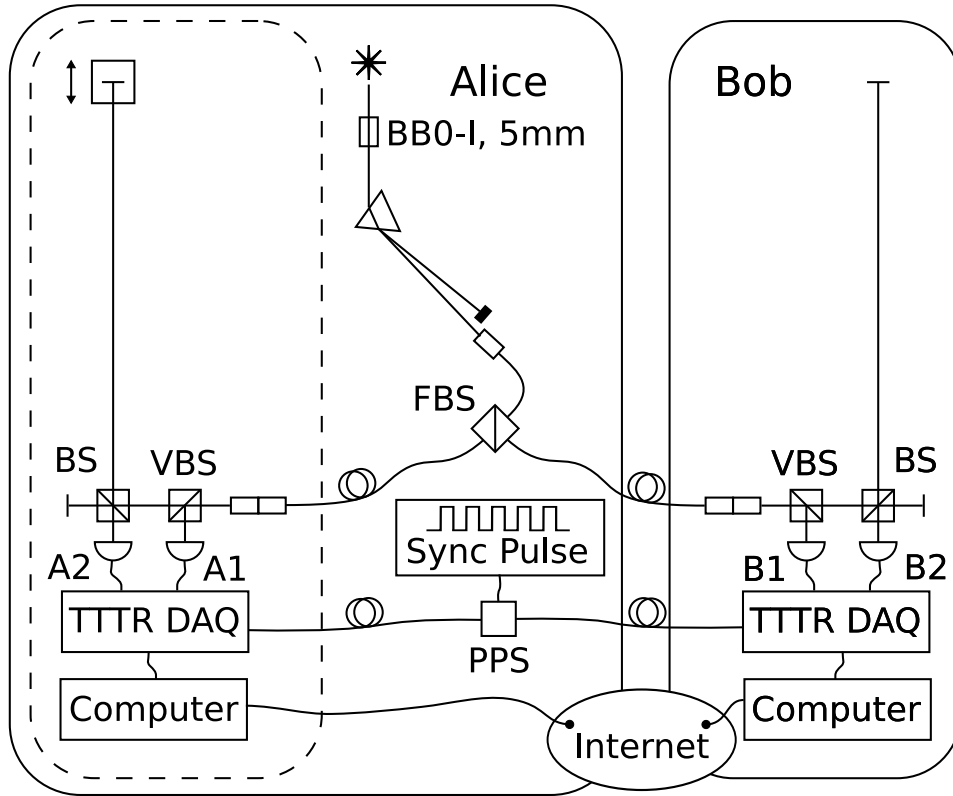


Figure 8.1: Experimental Setup. BS, FBS, VBS, and PPS, refer to a 50:50 beamsplitter, a fiber 50:50 beamsplitter, a variable beamsplitter made with a half wave plate and a polarizing beam splitter, and a passive power splitter, respectively.

fringes. 4) Using the measured visibility, Alice determines the security of the system and communicates the status of security to Bob. If the system is measured to be secure then Alice and Bob can proceed with the QKD protocol. 5) Alice and Bob privately bin their remaining (non-Franson) timing measurements, where each bin corresponds to a character of the QKD alphabet (see Fig. (8.3)). Details of the binning procedure are explained below. For our experiment the bin size is varied between  $\sim 200 - 500$  ps (limited by the  $1/e^2$  detector electronics jitter of

---

**8.4. EXPERIMENTAL DEMONSTRATION**

$t_c \sim 350$  ps), where a tradeoff between alphabet size and key fidelity is explored.

The first bin of the alphabet begins with each sync pulse, and the alphabet extends over the period of the sync signal (64 ns for our experiment). 6) Alice and Bob publicly publish the relevant sync periods in which they measure the arrival of non-Franson photons, however they keep the precise binning information from step (5) private. Alice and Bob discard the non-Franson photon arrival events that do not occur in the same sync periods, and keep the rest. Alice and Bob are thus left with identical photon events, where both photons of a downconversion pair are measured in the same time bin by Alice and Bob. The unpublished, precise arrival times for the accepted photon detection events thus give Alice and Bob a common, secret, and secure key.

## **8.4 Experimental Demonstration**

An outline of the experiment is shown in Fig. (8.1). Alice uses a 50 mW, 390 nm, cw laser having a bandwidth of 2 MHz to pump 5 mm of BBO-I cut for collinear, degenerate downconversion. The downconverted photons are coupled into a singlemode, 50:50, fiber beamsplitter, where one photon is sent to Alice and the other to Bob. The instances where both photons travel to either Alice or Bob can presently be ignored. Using a variable beamsplitter, Alice and Bob randomly and independently send their photons either to a high resolution timing detector (A1/B1; MPD PMD) or an unbalanced Michelson interferometer. The output of

the unbalanced Michelson interferometer is sent to a correlation detector (A2/B2; PerkinElmer SPAD). Signals from the detectors (A1/B1/A2/B2) are routed to two high-resolution data acquisition devices (DAQ; PicoQuant PicoHarp), one DAQ for A1 and A2, and the other DAQ for B1 and B2. The two DAQs are synchronized to each other via a clock signal that is generated by Alice. The clock signal has a period of  $T_{sync} = 64$  ns. Alice' and Bob's unbalanced Michelson interferometers both have a path mismatch of  $\tau \simeq 10$  ns. Alice's unbalanced Michelson interferometer has an automated 20 nm resolution translation stage in the long arm that she scans as part of the key generation protocol outlined above.

Ideally, for the duration of the QKD process, Alice need only randomly measure the maximum and minimum of the Franson fringes at predetermined locations of her automated stage. The maximum and minimum of the fringes determine the visibility of the fringe pattern that is used to determine the security of the quantum channel. However, due to phase drifts, for the duration of the experiment Alice's stage is scanned from  $c\Delta\tau = 0$  to  $c\Delta\tau = 600$  nm  $\cong 3\frac{\lambda_p}{2}$  in 20 nm steps with 2 s integral periods. After taking data for a nominal duration of 60 s, Bob sends Alice his Franson event arrival times. Alice uses Bob's Franson event arrival times along with her own Franson event arrival times to obtain a measured visibility  $V = 95 \pm 5\%$  of the Franson interferometer. The large error in measured visibility is due to phase instabilities (we require 10 nm stability over 3 m path lengths), which we are currently working on improving. The measured visibility

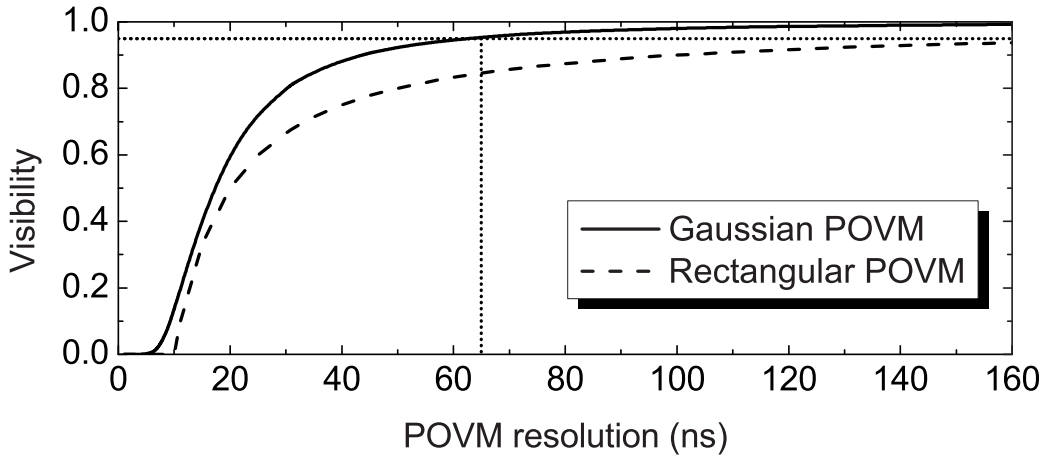


Figure 8.2: Franson fringe visibility versus Eve’s POVM resolution. The solid curve represents a gaussian POVM, while the dashed curve represents a rectangular-form POVM. A measured visibility of 95% corresponds to a POVM resolution of  $\gtrsim 65$  ns, demonstrating nominal security (details in text).

is used to estimate the resolution of Eve’s POVM in the intercept-resend-type attack discussed previously. It is assumed that Eve performs a POVM on every photon-pair. A theoretical plot of franson fringe visibility versus Eve’s POVM resolution is shown in Fig. (8.2). A gaussian POVM and a rectangular-form POVM are analysed, where the resolution corresponds to four standard deviations for a gaussian POVM (corresponding to 99.99% of the distribution) and the FWHM for the rectangular-form POVM. As seen in Fig. (8.2), a measured visibility of  $\sim 95\%$  corresponds to a POVM resolution of  $\gtrsim 65$  ns. As discussed below, the largest alphabet obtained in our experiment spans a period of 64 ns. Hence Eve does not gain any detailed information about the key, demonstrating nominal security of the quantum channel (a more rigorous security analysis is required for

unconditional security, and is currently being performed at the time of the writing of this thesis). Alice communicates to Bob that the quantum channel is secure and they proceed with the protocol.

Alice and Bob then bin the arrival times of their timing photons. Since the arrival times of each photon is measured with respect to the clock cycle immediately preceding it, the first level of binning is accomplished by Alice and Bob publicly communicating the respective clock cycle, denoted  $n_a$  for Alice's clock cycle and  $n_b$  for Bob's, during which each photon detection event occurred. Coarse-grained coincidence events are those for which  $n_a = n_b$ . The simplest form of binning in order to obtain a  $D$ -dimensional alphabet involves dividing each 64 ns sync period into  $D$ , equally sized bins. Each bin has an equal chance of containing a photon event since a cw-pump is used in the experiment. Using a bin size of 192 ps gives us an alphabet of  $D = \frac{64 \text{ ns}}{192 \text{ ps}} \sim 332$  characters. However, the detector electronics jitter has a  $1/e^2$  width of 350 ps that results in a very high quantum dit error rate (QDER), due to one photon registering in the  $d$ 'th bin with Alice while the other photon registers in the  $d \pm 1$ 'th bin with Bob.

In order to reduce the QDER, a process of indexing and redundancy is performed on the bins. Each of the 332 bins are relabeled so that all odd bins are given an index of  $i = 1$ , while all even bins are given an index of  $i = 2$ . Additionally, starting from the first bin, every two consecutive bins now represent the same character of an alphabet. This is defined as indexing with index-parameter

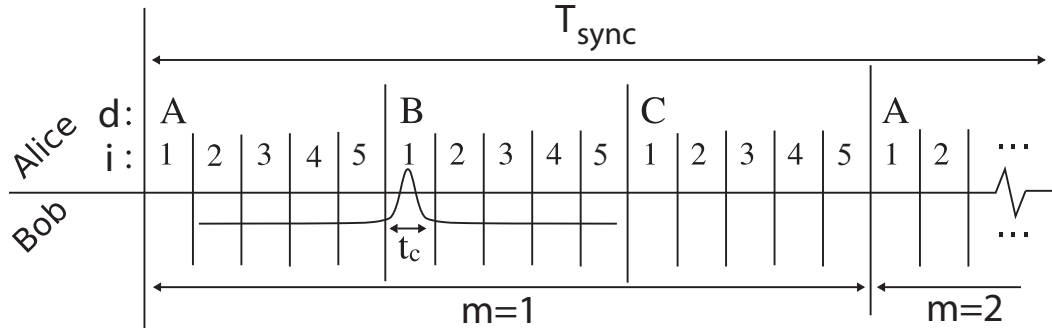


Figure 8.3: An example of the binning procedure as outlined in the text. In this example we have used  $I = 5$ ,  $M = 2$  and  $D = 3$ .

$I = 2$ . Alice and Bob publicly announce the index  $i$  of their binned photons (but keep the character private). Alice and Bob keep those coarse-grained correlation events that also have the same index, and discard the rest. This indexing process reduces the alphabet to 166 characters, but also reduces the QDER to  $\sim 50\%$ . Higher order indexing can similarly be performed. For example, for  $I = 5$ , the 332 bins are consecutively indexed from 1 to 5, with every five consecutive bins representing the same character, thus reducing the alphabet size by a factor of 5 (see Fig. (8.3)) and the QDER to  $\sim 25\%$ . This process significantly reduces the QDER due to the jitter in the detector electronics, however a sizeable QDER remains due to erroneous coincidences that are caused by low collection and detection efficiency, ambient room light, fluorescence in the optics, and dark counts in the detectors.

The QDER due to these accidental coincidences can be further reduced by reducing the coarse-grained coincidence window of 64 ns. This is done by dividing

the sync period (64 ns) into  $M$ , separate periods, denoted  $n_a^m$  and  $n_b^{m'}$  for Alice and Bob respectively. Alice and Bob publicly announce the sync-division,  $m$ , during which a photon is measured, and keep only those coarse-grained coincidences for which  $n_a^m = n_b^{m'}$ . This reduces the QDER due to accidental coincidences, but also reduces the alphabet size  $D = 332$  by a factor  $M$ . For example, for  $M = 2$ , the alphabet size is reduced to 166 characters (assuming  $I = 1$ ). It should be noted that the security of the system, determined by the Franson fringe visibility, is independent of the QDER.

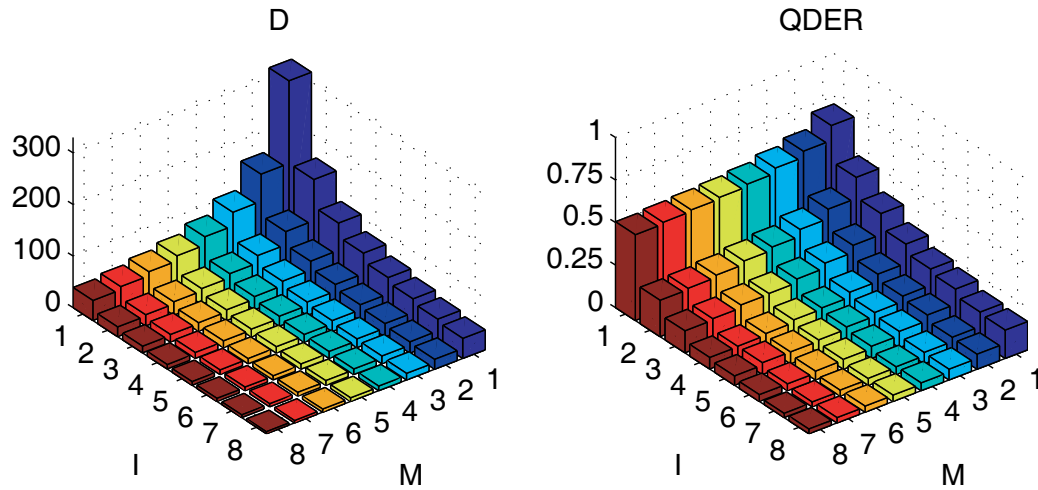


Figure 8.4: Experimental key generation for a bin size of 192 ps. The size of the alphabet,  $D$ , and the corresponding QDER can be varied by varying the index-parameter,  $I$ , and sync-division-parameter,  $M$ . An alphabet of over 150 characters was observed, with an associated QDER of  $\sim 50\%$ .

A plot of the key alphabet size and corresponding experimentally obtained QDER for various parameters of  $I$  and  $M$  is shown in Fig. (8.4). For the case of  $I = 2$  and  $M = 1$ , an alphabet of  $\sim 150$  characters is obtained, however with

a QDER of  $\sim 50\%$ . As can be seen, the QDER can be significantly reduced by increasing the values of  $I$  and  $M$ , however with an associated reduction in the alphabet size. For  $M \geq 2$  and  $I \geq 7$ , a QDER of less than 10% can be obtained while maintaining an alphabet size of  $\sim 30$  characters. These results were obtained for an estimated eavesdropping POVM resolution of  $\gtrsim 65$  ns, larger than the 64 ns period of the largest alphabet, thus demonstrating nominal security.

Next, the binning is repeated for a number of bin sizes ranging from 348 ps to 30672 ps, corresponding to a range of alphabets ranging from 1278 characters to 2 characters per photon. For ease of cryptographic implementation, each character is converted into its binary equivalent. The number of bits used to represent a character depends on the alphabet size obtained for any one bin size. For each bin size, the I and M parameters are optimized in order to maximize the bit transmission rates within bit error rate (BER) bounds of 10% and 15% respectively. The results of this optimization process are shown in Fig. (8.5). As seen in Fig. (8.5), in the case for both error bounds a distinct improvement in transmission rates is observed by utilizing higher bits per photon. A peak advantage is observed for a bin size of 480 ps, corresponding to  $\sim 5$  bits per photon.

Next, we demonstrate cryptographic encryption and decryption of a 175 KB, BMP image using the optimal key obtained for an error bound of 10%. This key corresponds to a bin size of 480 ps, with  $I = 4$  and  $M = 1$ . The encryption and decryption results are shown in Fig. (8.6). The image is converted to binary

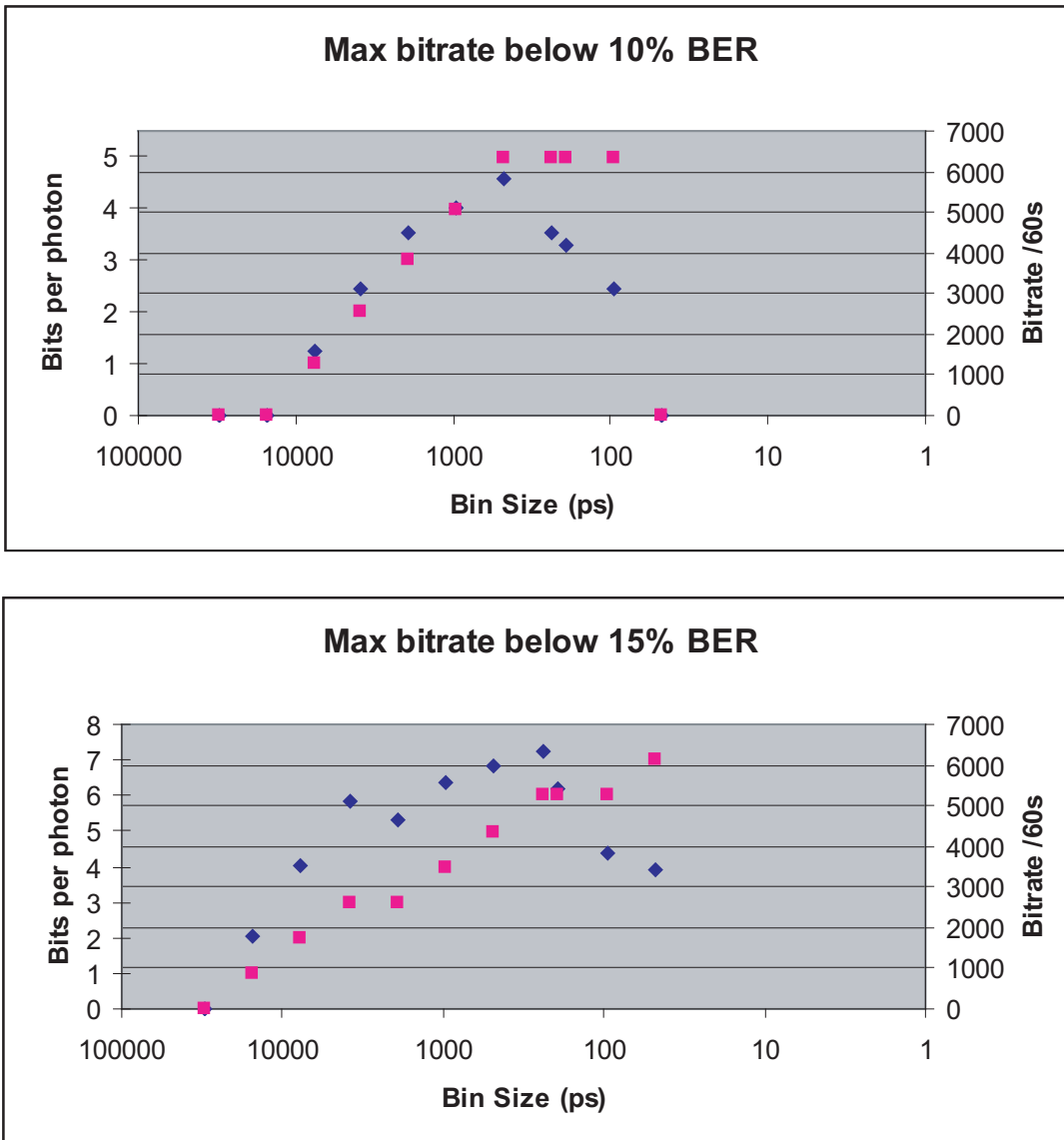


Figure 8.5: A range of bin sizes were used for the binning procedure. Blue diamonds represent the total transmitted bits of 60 seconds, while pink squares represent the information content per photon (bits per photon). The I and M parameters of each bin size were optimized in order to obtain maximum bit transmission rates within bit error bounds of 10% and 15% respectively. The number of bits per photon after the optimization for any one bin size is also shown in the figure. As seen, in both cases a distinct improvement in transmission rates is observed by utilizing higher bits per photon, with a peak advantage occurring for a bin size of 480 ps.

format, and encrypted using the key held by Alice. To demonstrate the strength of encryption, the encrypted image, as observed by the eavesdropper Eve, is shown in Fig. (8.6). As seen, Eve obtains almost no information about the initial image. It should be noted that, in contrast to the ideal one time pad, the key has been recycled 223 times since the image size (175 KB) is much larger than the key size ( $\sim 1$  KB). Hence the process is not perfectly secure, however it effectively demonstrates the utility of the QKD system. Finally, the image is decoded using Bob's key. As seen in Fig. (8.6), the original image is reconstructed with some noise. The noise originates from the  $\sim 10\%$  bit error rate of the key. If the key is considered to be a transmission channel then the BER of transmission can be reduced using efficient error correction codes on the image [160].

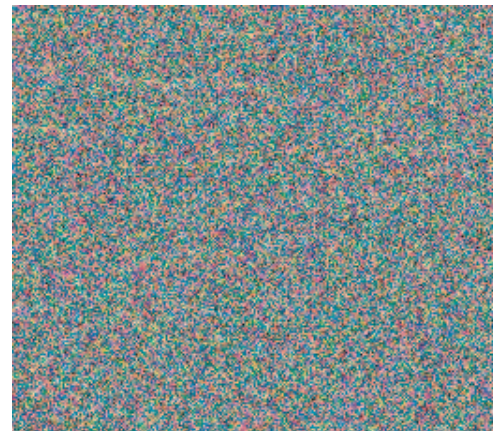
## 8.5 Summary and Discussion

We have presented a protocol for large-alphabet QKD using energy-time entangled photons generated by a cw pump, as motivated in the previous chapter [157]. In this QKD protocol, one conjugate basis is used exclusively for key generation while the other conjugate basis is used exclusively for measuring the security of the quantum channel. Thus, the security of the generated key is independent of the QDER in the key generation process, however, the QDER does reduce the fraction of the key that can be used for cryptography due to classical error correction and privacy amplification constraints that are not discussed here. We

Original BMP Image



Encrypted Image



Decrypted Image

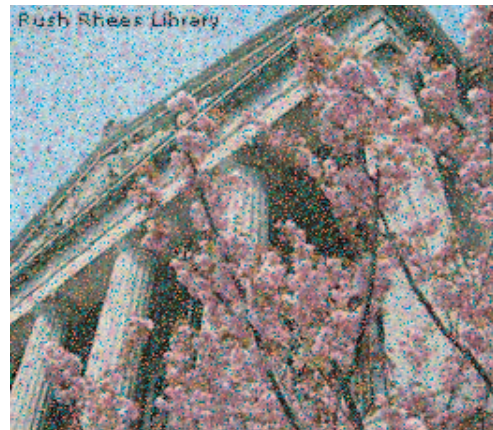


Figure 8.6: A BMP image was encrypted and decrypted using the optimal key for a 10% BER bound. As seen, information is effectively encrypted using Alice's generated key, hence providing security against eavesdropping. The image is successfully reconstructed with some noise after decryption using Bob's key. The source of the noise is the BER of the key, that can be reduced using error correction codes.

have experimentally demonstrated nominally-secure QKD with an alphabet of up to 1278 characters, corresponding to  $\sim 10.32$  bits of information per photon. Cryptographic encryption and decryption was demonstrated for a bmp image using a generated key of  $/sim5$  bits per photon, with a key bit error rate of just under 10%. Even larger alphabets can be obtained by using larger sync pulses or higher resolution timing detectors. The QDER can be significantly reduced by reducing losses and noise in the system. Energy-time entanglement has previously been demonstrated to be well preserved over large distances in fiber [146, 153], which makes the application of this protocol an exciting prospect for practical QKD.

This chapter concludes our discussion on continuous-variable entanglement. In this second part of the thesis we demonstrated that transverse-position and -momentum entanglement generated in the process of parametric down-conversion can be used to generate entangled qudits with  $d = 3$  and  $d = 6$ , with promising application for free-space QKD. We also demonstrated that energy-time entanglement generated in the process of parametric down-conversion possesses a large Schmidt number. We then demonstrated a novel method for performing large-alphabet QKD utilizing energy-time entanglement that is generated in the process of parametric down-conversion.

# Chapter 9

## Conclusions

In this dissertation we have explored some of the entangled parameters of the two-photon state generated in the process of spontaneous parametric down-conversion.

The work is divided into discrete-variable and continuous-variable regimes.

In the discrete-variable regime we first explored a practical implementation of phase-covariant cloning. Polarization-correlated photon pairs generated in the down-conversion process were used to demonstrate phase-covariant cloning in a Hong-Ou-Mandel interferometer with a measured fidelity of  $0 \cdot 829 \pm 0 \cdot 008$  in the 0/90 basis and  $0 \cdot 835 \pm 0 \cdot 006$  in the 45/135 basis, which is in good agreement with the theoretical prediction of 5/6 fidelity. The practical simplicity of the cloner lends itself to use within linear optics quantum computing. We also explored the sensitivity of sum-variance entanglement measures. These measures demonstrate useful concatenation properties, where greater sensitivity is achieved by simply performing additional measurements. The ultimate concatenated form was also

shown to possess the maximum sensitivity allowed by the Peres separability criterion, while requiring 12 measurements to obtain. Thus, the ultimate concatenated form of the sum-variance entanglement measure was shown to possess greater sensitivity than a Bell measurement while requiring fewer measurements than a Bell measurement to obtain. These properties suggest the use of the sum-variance measure as a standardized measure for two-particle entangled qubits. Finally, we explored the physical mechanism behind unambiguous state-discrimination of non-orthogonal entangled qubits. It was shown that the physical mechanism behind this type of unambiguous state-discrimination is analogous to the physical mechanism of entanglement reduction and restoration. The phenomenon of entanglement reduction and restoration was experimentally demonstrated using an optical implementation that was similar to the one suggested by Mimih and Hillery [102]. Mimih and Hillery proposed a 3-party secret sharing protocol that is based upon this type of unambiguous state-discrimination. Therefore, this experimental demonstration of entanglement reduction and restoration suggests the possibility of practically implementing the 3-party secret sharing scheme proposed by Mimih and Hillery.

In the continuous variable regime we explored the magnitude of entanglement for position-momentum and time-energy entanglement, and demonstrated proof-of-principle quantum key distribution protocols for both types of entanglement. We estimate that, for our experimental parameters, the position-momentum en-

tanglement of the two-photon state generated in the process of down-conversion possesses  $\sim 16$  exploitable information eigenmodes. By artificially discretizing this position-momentum entanglement, we demonstrated a proof-of-principle method for generating optically-entangled qudits, experimentally demonstrating  $d = 3$  and  $d = 6$  qudits. The method is easily generalizable to even higher dimensional qudits. These qudits could find useful application in free-space quantum key distribution. Next, we experimentally demonstrated that, for our experimental parameters, time-energy entanglement in down-conversion possess  $\gtrsim 100$  exploitable information eigenmodes, with a theoretical estimate of  $\sim 1 \times 10^6$  information eigenmodes. We then demonstrated a novel quantum key distribution protocol that is able to significantly exploit these information eigenmodes using currently available technology. Using high-resolution timing detectors with a Franson interferometer we demonstrate fiber-based, large-alphabet quantum key distribution with alphabets as large as 1278 characters, corresponding to  $\sim 10.32$  bits per photon pair. We also demonstrated encryption and decryption of a bmp image using a generated key of  $/sim 5$  bits per photon, with a key bit error rate of just under 10%. Time-energy entanglement has already been shown to be well preserved over large distances using current fiber technology, which makes the application of this protocol an exciting prospect for practical QKD.

# Bibliography

- [1] A. Messiah, *Quantum Mechanics* (Dover Publications, Inc., Mineola NY, ADDRESS, 1999).
- [2] E. Schrödinger, Naturwissenschaften **23**, 807 (1935).
- [3] A. Einstein, B. Podolsky, and N. Rosen, Phys. Rev. **47**, 777 (1935).
- [4] D. Bohm, *Quantum Theory* (Prentice-Hall, Englewood Cliff, NJ, ADDRESS, 1951), pp. 614–619.
- [5] J. C. Howell, R. S. Bennink, S. J. Bentley, and R. W. Boyd, Phys. Rev. Lett. **92**, 210403 (2004).
- [6] J. S. Bell, *Physics* (Long Island City, N.Y., ADDRESS, 1965), Vol. 1, p. 195.
- [7] J. F. Clauser, M. A. Horne, A. Shimony, and R. A. Holt, Phys. Rev. Lett. **23**, 880 (1969).
- [8] A. Aspect, P. Grangier, and G. Roger, Phys. Rev. Lett. **47**, 460 (1981).
- [9] J. D. Franson, Phys. Rev. Lett. **62**, 2205 (1989).
- [10] P. G. Kwiat, W. A. Vareka, C. K. Hong, H. Nathel, and R. Y. Chiao, Phys. Rev. A **41**, 2910(R) (1990).
- [11] C. Jönsson, Z. Phys. **161**, 454 (1961).
- [12] G. F. M. P. G. Merli and G. Pozzi, Am. J. Phys. **44**, 306 (1976).
- [13] A. Tonomura, J. Endo, T. Matsuda, T. Kawasaki, and H. Ezawa, Am. J. Phys. **57**, 117 (1989).
- [14] A. Zeilinger, R. Gähler, C. G. Shull, W. Treimer, and W. Mampe, Rev. Mod. Phys. **60**, 1067 (1988).
- [15] O. Carnal and J. Mlynek, Phys. Rev. Lett. **66**, 2689 (1991).

- [16] E. J. S. Fonseca, C. H. Monken, S. Padua, and G. A. Barbosa, Phys. Rev. A **59**, 1608 (1999).
- [17] Z. Y. Ou, S. F. Pereira, H. J. Kimble, and K. C. Peng, Phys. Rev. Lett. **68**, 3663 (1992).
- [18] M. D. Reid and P. D. Drummond, Phys. Rev. Lett. **60**, 2731 (1988).
- [19] S. Lloyd, Phys. Rev. Lett. **71**, 943 (1993).
- [20] P. Benioff, J. Stat. Phys. **22**, 563 (1980).
- [21] P. Benioff, Phys. Rev. Lett. **48**, 1581 (1982).
- [22] P. Benioff, J. Stat. Phys. **29**, 515 (1982).
- [23] P. Benioff, Ann. N.Y. Acad. Sci. **480**, 475 (1986).
- [24] D. Deutsch, Proc. R. Soc. London A **400**, 97 (1985).
- [25] D. Deutsch, Proc. R. Soc. London A **425**, 73 (1989).
- [26] R. P. Feynman, Opt. News **11**, 11 (1985).
- [27] R. P. Feynman, Found. Phys. **16**, 507 (1986).
- [28] R. P. Feynman, Int. J. Theor. Phys. **21**, 467 (1982).
- [29] C. H. Bennett, IBM J. Des. Rev. **17**, 525 (1973).
- [30] C. H. Bennett, Int. J. Theor. Phys. **21**, 905 (1982).
- [31] C. Bennett and G. Brassard, Proceedings of IEEE International Conference on Computers, Systems and Signal Processing, Bangalore, India (IEEE, New York) 175 (1984).
- [32] C. Bennett, Phys. Rev. Lett. **68**, 3121 (1982).
- [33] D. Bruß and C. Macchiavello, Phys. Rev. Lett. **88**, 127901 (2002).
- [34] N. J. Cerf, M. Bourennane, A. Karlsson, and N. Gisin, Phys. Rev. Lett. **88**, 127902 (2002).
- [35] N. Gisin, G. Ribordy, W. Tittel, and H. Zbinden, Rev. Mod. Phys. **74**, 145 (2002).
- [36] P. W. Shor, Proc. 35th Annual Symp. Foundation of Computer Science. Los Alamitos, CA: IEEE Computer Society 124 (1994).

- [37] D. Deutsch and R. Jozsa, Proc. R. Soc. London A **439**, 553 (1992).
- [38] L. K. Grover, Proceedings, 28th Annual ACM Symposium on the Theory of Computing 212 (1996).
- [39] C. K. Hong, Z. Y. Ou, and L. Mandel, Phys. Rev. Lett. **59**, 2044 (1987).
- [40] D. C. Burnham and D. L. Weinberg, Phys. Rev. Lett. **25**, 84 (1970).
- [41] R. Ghosh and L. Mandel, Phys. Rev. Lett. **59**, 1903 (1987).
- [42] Z. Y. Ou and L. Mandel, Phys. Rev. Lett. **61**, 54 (1988).
- [43] J. T. Barreiro, N. K. Langford, N. A. Peters, and P. G. Kwiat, Phys. Rev. Lett. **95**, 260501 (2005).
- [44] D. Stucki, N. Gisin, O. Guinnard, G. Ribordy, and H. Zbinden, New Journal of Physics **4**, 41 (2002).
- [45] X. Li, P. L. Voss, J. E. Sharping, and P. Kumar, Phys. Rev. Lett. **94**, 053601 (2005).
- [46] P. G. Kwiat, A. M. Steinberg, R. Y. Chiao, P. H. Eberhard, and M. D. Petroff, Phys. Rev. A **48**, 867(R) (1993).
- [47] J. Kim, S. Takeuchi, Y. Yamamoto, and H. H. Hogue, App. Phys. Lett. **74**, 902 (1999).
- [48] S. Takeuchi, J. Kim, Y. Yamamoto, and H. H. Hogue, App. Phys. Lett. **74**, 1063 (1999).
- [49] D. F. V. James and P. G. Kwiat, Phys. Rev. Lett. **89**, 183601 (2002).
- [50] H. Gao, M. Rosenberry, J. Wang, and H. Batelaan, J. Phys. B: At. Mol. Opt. Phys. **38**, 1857 (2005).
- [51] L. P. A. Maia1, B. Baseia1, A. T. Avelar, and J. M. C. Malbouisson, J. Opt. B: Quantum Semiclass. Opt. **6**, 351 (2004).
- [52] D. L. Moehring, M. J. Madsen, B. B. Blinov, and C. Monroe, Phys. Rev. Lett. **93**, 090410 (2004).
- [53] M. Saffman and T. G. Walker, Phys. Rev. A **72**, 042302 (2005).
- [54] C. Simon, G. Weihs, and A. Zeilinger, Phys. Rev. Lett. **84**, 2993 (1999).
- [55] A. Lamas-Linares, C. Simon, J. C. Howell, and D. Bouwmeester, Science **296**, 712 (2002).

- [56] I. Ali-Khan and J. Howell, Phys. Rev. A **70**, 010303(R) (2004).
- [57] N. Herbert, Found. Phys. **12**, 1171 (1982).
- [58] W. Wootters and W. Zurek, Nature **299**, 802 (1982).
- [59] L. Mandel, Nature **304**, 188 (1983).
- [60] V. Bužek and M. Hillery, Phys. Rev. A **54**, 1844 (1996).
- [61] N. Gisin and S. Massar, Phys. Rev. Lett. **79**, 2153 (1997).
- [62] N. J. Cerf, A. Ipe, and X. Rottenberg, Phys. Rev. Lett. **85**, 1754 (2000).
- [63] S. L. Braunstein, N. J. Cerf, S. Iblisdir, P. van Loock, and S. Massar, Phys. Rev. Lett. **86**, 4938 (2001).
- [64] D. Bruß, A. Ekert, and C. Macchiavello, Phys. Rev. Lett. **81**, 2598 (1998).
- [65] N. Gisin, Phys. Lett. A **242**, 1 (1998).
- [66] E. F. Galvao and L. Hardy, Phys. Rev. A **62**, 022301 (2000).
- [67] H. Barnum, C. M. Caves, C. A. Fuchs, R. Jozsa, and B. Schumacher, Phys. Rev. Lett. **76**, 2818 (1996).
- [68] B. Schumacher, Phys. Rev. A **51**, 2738 (1995).
- [69] D. Bruß, D. P. DiVincenzo, A. Ekert, C. A. Fuchs, C. Macchiavello, and J. A. Smolin, Phys. Rev. A **57**, 2368 (1998).
- [70] D. Bruß, M. Cinchetti, G. M. D'Ariano, and C. Macchiavello, Phys. Rev. A **62**, 012302 (2000).
- [71] V. Karimipour and A. T. Rezakhani, Phys. Rev. A **66**, 052111 (2002).
- [72] J. Fiurasek, Phys. Rev. A **67**, 052314 (2003).
- [73] F. D. Martini, V. Mussi, and F. Bovino, Opt. Commun. **179**, 581 (2000).
- [74] S. Fasel, N. Gisin, G. Ribordy, V. Scarani, and H. Zbinden, Phys. Rev. Lett. **89**, 107901 (2002).
- [75] R. Werner, Phys. Rev. A **58**, 1827 (1998).
- [76] D. Bruss, D. P. DiVincenzo, A. Ekert, C. A. Fuchs, C. Macchiavello, and J. A. Smolin, Phys. Rev. A **57**, 2368 (1998).
- [77] L.-M. Duan and G.-C. Guo, Phys. Rev. Lett. **80**, 4999 (1998).

- [78] H. Fan, K. Matsumoto, X.-B. Wang, and M. Wadati, Phys. Rev. A **65**, 012304 (2002).
- [79] G. M. D'Ariano and C. Macchiavello, Phys. Rev. A **67**, 042306 (2003).
- [80] D. Bouwmeester, J.-W. Pan, K. Mattle, M. Eibl, H. Weinfurter, and A. Zeilinger, Nature **390**, 575 (1997).
- [81] K. Mattle, H. Weinfurter, P. G. Kwiat, and A. Zeilinger, Phys. Rev. Lett. **76**, 4656 (1996).
- [82] I. Ali-Khan and J. Howell, Quant. Inf. and Comp. **4**, 114 (2004).
- [83] J. Howell, A. Lamas-Linares, and D. Bouwmeester, Phys. Rev. Lett. **88**, 030401 (2002).
- [84] D. Bruss, Phys. Rev. Lett. **81**, 3018 (1998).
- [85] A. Peres, Phys. Rev. Lett. **77**, 1413 (1996).
- [86] R. Horodecki and M. Horodecki, Phys. Rev. A **54**, 1838 (1996).
- [87] M. Lewenstein, B. Kraus, J. I. Cirac, and P. Horodecki, Phys. Rev. A **62**, 052310 (2000).
- [88] M. Barbieri, F. DeMartini, G. DiNepi, P. Mataloni, G. M. D'Ariano, and C. Macchiavello, Phys. Rev. Lett. **91**, 227901 (2003).
- [89] L. M. Duan, G. Giedke, J. I. Cirac, and P. Zoller, Phys. Rev. Lett. **84**, 2722 (2000).
- [90] R. Simon, Phys. Rev. Lett. **84**, 2726 (2000).
- [91] S. Mancini, V. Giovannetti, D. Vitali, and P. Tombesi, Phys. Rev. Lett. **88**, 120401 (2002).
- [92] B. Julsgaard, A. Kozhekin, and E. S. Polzik, Nature **413**, 400 (2001).
- [93] C. Silberhorn, P. K. Lam, O. Weiss, F. Konig, N. Korolkova, and G. Leuchs, Phys. Rev. Lett. **86**, 4267 (2001).
- [94] W. P. Bowen, N. Treps, R. Schnabel, and P. Lam, Phys. Rev. Lett. **89**, 253601 (2002).
- [95] W. P. Bowen, R. Schnabel, P. K. Lam, and T. C. Ralph, Phys. Rev. Lett. **90**, 043601 (2003).

- [96] N. Korolkova, G. Leuchs, R. Loudon, T. C. Ralph, and C. Silberhorn, Phys. Rev. A **65**, 052306 (2002).
- [97] H. Hofmann and S. Takeuchi, Phys. Rev. A **68**, 032103 (2003).
- [98] O. Guhne, Phys. Rev. Lett. **92**, 117903 (2004).
- [99] R. Werner, Phys. Rev. A **40**, 4277 (1989).
- [100] D. F. V. James, P. G. Kwiat, W. J. Munro, and A. G. White, Phys. Rev. A **64**, 052312 (2001).
- [101] M. W. Mitchell, C. W. Ellenor, S. Schneider, and A. M. Steinberg, Phys. Rev. Lett. **91**, 120402 (2003).
- [102] J. Mimih and M. Hillery, Phys. Rev. A **71**, 012329 (2005).
- [103] P. G. Kwiat, S. Barraza-Lopez, A. Stefanov, and N. Gisin, Nature **409**, 1014 (2001).
- [104] M. Hillery, V. Buzek, and A. Berthiaume, Phys. Rev. A **59**, 1829 (1999).
- [105] A. Karlsson, M. Koashi, and N. Imoto, Phys. Rev. A **59**, 162 (1999).
- [106] W. Tittel, H. Zbinden, and N. Gisin, Phys. Rev. A **63**, 042301 (2001).
- [107] M. Hillery and J. Mimih, Phys. Rev. A **67**, 042304 (2003).
- [108] C. Schmid, P. Trojek, M. Bourennane, C. Kurtsiefer, M. Zukowski, and H. Weinfurter, Phys. Rev. Lett. **95**, 230505 (2005).
- [109] J. Walgate, A. Short, L. Hardy, and V. Vedral, Phys. Rev. Lett. **85**, 4972 (2000).
- [110] S. Virmani, M. F. Sacchi, M. B. Plenio, and D. Markham, Phys. Lett. A **288**, 62 (2005).
- [111] Y. Chen and D. Yang, Phys. Rev. A **65**, 22320 (2002).
- [112] C. H. Bennett, Phys. Rev. Lett. **68**, 3121 (1992).
- [113] Z. Quan and T. Chaojing, Phys. Rev. A **65**, 062301 (2002).
- [114] K. Tamaki, M. Koashi, and N. Imoto, Phys. Rev. Lett. **90**, 167904 (2003).
- [115] W. P. Grice and I. A. Walmsley, Phys. Rev. A **56**, 1627 (1997).
- [116] I. Ali-Khan and J. C. Howell, Phys. Rev. A **70**, 062320 (2004).

- [117] H. F. Hofmann and S. Takeuchi, Phys. Rev. A **68**, 032103 (2003).
- [118] T. Jennewein, C. Simon, G. Weihs, H. Weinfurter, and A. Zeilinger, Phys. Rev. Lett. **84**, 4729 (2000).
- [119] M. Aspelmeyer *et al.*, Science **301**, 621 (2003).
- [120] H. Bechmann-Pasquinucci and W. Tittel, Phys. Rev. A **61**, 062308 (2000).
- [121] C. Macchiavello and D. Bruss, J. Mod. Opt. **50**, 1025 (2003).
- [122] T. Durt, N. J. Cerf, N. Gisin, and M. Zukowski, Phys. Rev. A **67**, 012311 (2003).
- [123] A. K. Ekert, Phys. Rev. Lett. **67**, 661 (1991).
- [124] C. H. Bennett and S. J. Wiesner, Phys. Rev. Lett. **69**, 2881 (1992).
- [125] C. H. Bennett, G. Brassard, C. Crépeau, R. Jozsa, A. Peres, and W. K. Wootters, Phys. Rev. Lett. **70**, 1895 (1993).
- [126] D. N. Klyshko, Sov. Phys. JETP **56**, 753 (1981).
- [127] A. Joobeur, B. E. A. Saleh, T. S. Larchuk, and M. C. Teich, Phys. Rev. A **53**, 4360 (1996).
- [128] C. H. Monken, P. H. Souto Ribeiro, and S. Pádua, Phys. Rev. A **57**, 3123 (1998).
- [129] C. K. Hong and L. Mandel, Phys. Rev. A **31**, 2409 (1985).
- [130] A. Gatti, E. Brambilla, and L. A. Lugiato, Phys. Rev. Lett. **90**, 133603 (2003).
- [131] E. Brambilla, A. Gatti, M. Bache, and L. A. Lugiato, Phys. Rev. A **69**, 023802 (2004).
- [132] D. V. Strekalov, A. V. Sergienko, D. N. Klyshko, and Y. H. Shih, Phys. Rev. Lett. **74**, 3600 (1995).
- [133] T. B. Pittman, Y. H. Shih, D. B. Strekalov, and A. V. Sergienko, Phys. Rev. A **52**, 3429(R) (1995).
- [134] R. S. Bennink, S. J. Bentley, R. W. Boyd, and J. C. Howell, Phys. Rev. Lett. **92**, 033601 (2004).
- [135] A. Mair, A. Vaziri, G. Weihs, and A. Zeilinger, Nature **412**, 313 (2001).

- [136] A. Vaziri, J. W. Pan, T. Jennewein, G. Weihs, and A. Zeilinger, Phys. Rev. Lett. **91**, 227902 (2003).
- [137] X. F. Ren, G. P. Guo, B. Yu, J. Li, and G. C. Guo, J. Opt. B: Quantum Semiclass. Opt. **6**, 243 (2004).
- [138] H. de Riedmatten, I. Marcikic, H. Zbinden, and N. Gisin, Quantum Inf. Comput. **2**, 425 (2002).
- [139] M. Żukowski, A. Zeilinger, and M. A. Horne, Phys. Rev. A **55**, 2564 (1997).
- [140] C. K. Law and J. H. Eberly, Phys. Rev. Lett. **92**, 127903 (2004).
- [141] H. de Riedmatten, I. Marcikic, V. Scarani, W. Tittel, H. Zbinden, and N. Gisin, Phys. Rev. A **69**, 050304(R) (2004).
- [142] M. N. O'Sullivan-Hale, I. Ali-Khan, R. W. Boyd, and J. C. Howell, Phys. Rev. Lett. **94**, 220501 (2005).
- [143] L. Neves, G. Lima, J. G. Aguirre Gómez, C. H. Monken, C. Saavedra, and S. Pádua, Phys. Rev. Lett. **94**, 100501 (2005).
- [144] M. P. Almeida, S. P. Walborn, and P. H. S. Ribeiro, Phys. Rev. A **72**, 022313 (2005).
- [145] W. Tittel, J. Brendel, H. Zbinden, and N. Gisin, Phys. Rev. Lett. **84**, 4737 (2000).
- [146] W. Tittel, J. Brendel, H. Zbinden, and N. Gisin, Phys. Rev. Lett. **81**, 3563 (1998).
- [147] P. G. Kwiat, A. M. Steinberg, and R. Y. Chiao, Phys. Rev. A **47**, 2472(R) (1993).
- [148] J. Rarity and P. Tapster, Phys. Rev. A **45**, 2052 (1992).
- [149] V. Giovannetti, L. Maccone, J. H. Shapiro, and N. C. Wong, Phys. Rev. A **66**, 043813 (2002).
- [150] O. Kuzucu, M. Fiorentino, M. A. Albota, N. C. Wong, and F. X. Kärtner, Phys. Rev. Lett. **94**, 083601 (2005).
- [151] T. B. Pittman, D. V. Strekalov, A. Migdall, M. H. Rubin, A. V. Sergienko, and Y. H. Shih, Phys. Rev. Lett. **77**, 1917 (1996).
- [152] M. Bellini, F. Marin, S. Viciani, A. Zavatta, and F. Arecchi, Phys. Rev. Lett. **90**, 043602 (2003).

- [153] I. Marcikic, H. de Riedmatten, W. Tittel, H. Zbinden, M. Legre, and N. Gisin, Phys. Rev. Lett. **93**, 180502 (2004).
- [154] R. T. Thew, A. Acin, H. Zbinden, and N. Gisin, Phys. Rev. Lett. **93**, 10503 (2004).
- [155] S. P. Walborn, D. S. Lemelle, M. P. Almeida, and P. H. S. Ribeiro, Phys. Rev. Lett. **96**, 090501 (2006).
- [156] G. M. Nikolopoulos, K. S. Rande, and G. Alber, Phys. Rev. A **73**, 32325 (2006).
- [157] I. Ali-Khan and J. C. Howell, Phys. Rev. A **73**, 031801(R) (2006).
- [158] G. J. Pryde, J. L. O'Brien, A. G. White, T. C. Ralph, and H. M. Wiseman, Phys. Rev. Lett. **94**, 220405 (2005).
- [159] T. C. Ralph, S. D. Bartlett, J. L. O'Brien, , G. J. Pryde, and H. M. Wiseman, Phys. Rev. A **73**, 012113 (2006).
- [160] D. J. Mackay, *Information Theory, Inference, and Learning Algorithms* (Cambridge University Press, The Edinburgh Building, Cambridge CB2 2RU, UK, ADDRESS, 2003, reprinted 2005).
- [161] S. Samuelsson and G. Bjork, Phys. Rev. A **73**, 012319 (2006).

## Appendix A

# Derivation of the time-domain biphoton wavefunction

In this Appendix I provide a derivation of the biphoton wavefunction in the time domain. This wavefunction is used in Chapters 7 and 8. It should be noted that the wavefunction can just as easily be expressed in terms of longitudinal-position and momentum variables. Energy and time is used due to its prevalence in the literature.

### A.1 The biphoton wavefunction

Following the method of Grice and Walmsley [115], the wavefunction of down-conversion is given by:

$$|\psi\rangle = \frac{2\pi A}{i\hbar} \int d\omega_o \int d\omega_e \beta(\omega_o + \omega_e) \Phi(\omega_o, \omega_e) |\omega_o\rangle_o |\omega_e\rangle_e, \quad (\text{A.1})$$

where  $|\omega_i\rangle_j$  is a one-photon Fock state in mode  $j$  with frequency  $\omega_i$ , where  $i = o, e$  are the ordinary and extraordinary polarizations of down-conversion,  $L$  is the length of the crystal,  $A$  is a constant which has subsumed all other constants,  $\beta(\omega_e + \omega_o)$  is the bandwidth of the pump, and where

$$\Phi(\omega_o, \omega_e) = \frac{\sin\{[k_o(\omega_o) + k_e(\omega_e) - k_p(\omega_o + \omega_e)]L/2\}}{[k_o(\omega_o) + k_e(\omega_e) - k_p(\omega_o + \omega_e)]L/2} \quad (\text{A.2})$$

is determined by the phase-matching conditions of the crystal. It should be kept in mind that we are dealing with birefringent crystals and type-II down-conversion, therefore in general  $k_o(\omega) \neq k_e(\omega)$ . Since this is a weak interaction, we have ignored higher order terms and concentrate only on the biphoton.

Let us try to simplify the expression in Eq. (A.2) by the following steps. First, if we use a Taylor expansion about the central frequencies of the  $k$ 's we obtain

$$k_p(\omega) = k_{p0} + (\omega - 2\bar{\omega})k'_p + \dots \quad (\text{A.3})$$

$$k_j(\omega) = k_{j0} + (\omega - \bar{\omega})k'_j + \dots \quad (\text{A.4})$$

where  $j = o, e$ ,  $k_{p0} = k_p(2\bar{\omega})$ ,  $k_{j0} = k_j(\bar{\omega})$ ,  $k'_p = \frac{\partial k_p(\omega)}{\partial \omega}|_{\omega=2\bar{\omega}}$  and  $k'_j = \frac{\partial k_j(\omega)}{\partial \omega}|_{\omega=\bar{\omega}}$ .

Here  $2\bar{\omega}$  is the central pump frequency. Keeping only the first two terms of the expansion gives

$$k_o(\omega_o) + k_e(\omega_e) - k_p(\omega_o + \omega_e) \cong \nu_o(k'_o - k'_p) + \nu_e(k'_e - k'_p), \quad (\text{A.5})$$

where  $\nu_j = \omega_j - \bar{\omega}$  are the difference frequencies. Perfect phase matching at the center frequencies gives  $k_{o0} + k_{e0} - k_{p0} = 0$ . Using Eq. (A.5), the phase-matching function in Eq. (A.2) becomes

$$\Phi(\bar{\omega} + \nu_o, \bar{\omega} + \nu_e) = \frac{\sin\{[\nu_o(k'_o - k'_p) + \nu_e(k'_e - k'_p)]L/2\}}{[\nu_o(k'_o - k'_p) + \nu_e(k'_e - k'_p)]L/2} \quad (\text{A.6})$$

## A.2 The time domain

To obtain the wavefunction in the time domain let us first re-express the wavefunction in Eq. (A.1) as

$$\begin{aligned} |\psi\rangle \sim & \frac{2\pi A}{i\hbar} \int d\nu_1 \int d\nu_2 \Phi(\nu_1 - \nu_2) \beta(\nu_1 + \nu_2) \\ & \times |\bar{\omega} + \nu_1\rangle_o |\bar{\omega} + \nu_2\rangle_e, \end{aligned} \quad (\text{A.7})$$

where we have re-expressed  $e, o$  as 1, 2, and have used the knowledge of strong energy correlations (i.e.  $\nu_1 = -\nu_2$ ) to express the phase-matching function as  $\Phi(\nu_1, \nu_2) = \Phi(\nu_1 - \nu_2)$ . This approximation is valid due to the very narrow

$\sim 2$  MHz bandwidth of the pump laser. More explicitly:

$$\begin{aligned}
 \Phi(\nu_1, \nu_2) &= \Phi(\gamma_1\nu_1 + \gamma_2\nu_2) \\
 &\simeq \Phi(\gamma_1\nu_1 - \gamma_2\nu_1) \\
 &= \Phi(\nu_1[\gamma_1 - \gamma_2]) \\
 &= \Phi(\nu_1\gamma) \\
 &\simeq \Phi([\nu_1 - \nu_2]\gamma/2)
 \end{aligned} \tag{A.8}$$

Let us now express each of the frequency components in Eq. (A.7) as their respective Fourier transforms in the time domain

$$\begin{aligned}
 |\psi\rangle \sim & \frac{2\pi A}{i\hbar} \int d\nu_1 \int d\nu_2 \int dt_3 \tilde{\Phi}(t_3) e^{-i(\nu_1 - \nu_2)t_3} \\
 & \times \int dt_4 \tilde{\beta}(t_4) e^{-i(\nu_1 + \nu_2)t_4} \int dt_1 e^{-i(\bar{\omega} + \nu_1)t_1} \\
 & \times \int dt_2 e^{-i(\bar{\omega} + \nu_2)t_2} |t_1\rangle_o |t_2\rangle_e,
 \end{aligned} \tag{A.9}$$

which can be rewritten as

$$\begin{aligned}
 |\psi\rangle \sim & \frac{2\pi A}{i\hbar} \int dt_3 \int dt_4 \int dt_1 \int dt_2 \tilde{\Phi}(t_3) \tilde{\beta}(t_4) \\
 & \times e^{-i\bar{\omega}(t_1 + t_2)} \int d\nu_1 e^{-i\nu_1(t_3 + t_4 + t_1)} \\
 & \times \int d\nu_2 e^{-i\nu_2(-t_3 + t_4 + t_2)} |t_1\rangle_o |t_2\rangle_e.
 \end{aligned} \tag{A.10}$$

Integrating over  $\nu_1$  and  $\nu_2$  we obtain two delta functions which can be rewritten

as

$$\delta(t_3 + t_4 + t_1)\delta(-t_3 + t_4 + t_2) = \delta(2t_3 - t_2 + t_1)\delta(-2t_4 + t_2 + t_1) \quad (\text{A.11})$$

Substituting Eq. (A.11) into Eq. (A.10) and integrating over  $t_3$  and  $t_4$  thus gives

$$\begin{aligned} |\psi\rangle \sim & \frac{2\pi A}{i\hbar} \int dt_1 \int dt_2 \tilde{\Phi}([t_1 - t_2]/2) \tilde{\beta}([t_1 + t_2]/2) \\ & \times e^{-i\bar{\omega}(t_1+t_2)} |t_1\rangle_o |t_2\rangle_e, \end{aligned}$$

It should be kept in mind that the integrals of  $t$  are taken from  $+\infty$  to  $-\infty$ , therefore this is a function of what we expect to observe long after the interaction of the pump pulse with the crystal.

# Appendix B

## The Franson interferometer

In this Appendix I provide a derivation of the coincidence rate that is expected to be measured at the output of a Franson interferometer.

### B.1 Entangled biphotons

The Franson interferometer consists of two unbalanced Michelson interferometers, one in arm A and one in arm B. Each Michelson interferometer possesses a long and a short arm, with a time delay of  $\tau_A$  and  $\tau_B$  between the two arms in each Michelson respectively. Provided the time delays are much longer than the single photon coherence length, they ensure that no single-photon interference occurs. Additionally, it allows us to post-select long-long and short-short coincidence events, as detailed later. The time delay  $\tau_A$  between the arms of the Michelson interferometer in arm A is varied by varying length of the long arm with an automated linear stage. Let us consider the expected photo-coincidence rate  $P(\tau_A, \tau_B)$  which is detected at the output of the Franson interferometer as a

function of the time delays  $\tau_A$  and  $\tau_B$  [149, 150]:

$$P \propto \int \int |\langle 0 | a_A(t_A) a_B(t_B) | \Psi \rangle|^2 dt_A dt_B \quad (\text{B.1})$$

where  $|\Psi\rangle = \int \psi(t_s, t_i) a_s^\dagger(t_s) a_i^\dagger(t_i) |0\rangle dt_s dt_i$  is the biphoton wavefunction in the time domain. For the Franson interferometer,  $a_A$  and  $a_B$  can be written in terms of the signal and idler annihilation operators:

$$a_A(t) = [a_s(t) + a_s(t + \tau_A)]/\sqrt{2} \quad (\text{B.2})$$

$$a_B(t) = [a_i(t) + a_i(t + \tau_B)]/\sqrt{2} \quad (\text{B.3})$$

Let's plug the expressions above into Eq. (B.1)

$$\begin{aligned} P \propto & \int dt_A dt_B |\langle 0 | [a_1(t_A) + a_1(t_A + \tau_A)] \\ & \times [a_2(t_B) + a_2(t_B + \tau_B)] \int dt_1 dt_2 \tilde{\Phi}([t_1 - t_2]/2) \\ & \times \tilde{\beta}([t_1 + t_2]/2) e^{-i\bar{\omega}(t_1+t_2)} a_1^\dagger(t_1) a_2^\dagger(t_2) |0\rangle|^2 \end{aligned} \quad (\text{B.4})$$

Using the creation and annihilation operator commutation relations  $[a_j(t_j), a_k^\dagger(t_k)] = \delta_{jk}\delta(t_j - t_k)$  (via the inner product) this becomes:

$$\begin{aligned} P \propto & \int dt_A dt_B \left| \int dt_1 dt_2 [\delta(t_A - t_1) + \delta(t_A + \tau_A - t_1)] \right. \\ & \times [\delta(t_B - t_2) + \delta(t_B + \tau_B - t_2)] \tilde{\Phi}([t_1 - t_2]/2) \\ & \times \tilde{\beta}([t_1 + t_2]/2) e^{-i\bar{\omega}(t_1+t_2)} \left. \right|^2 \end{aligned} \quad (\text{B.5})$$

We then integrate out the delta functions. We shall shortly express  $t_B = t_A + \tau$  (i.e. given that we measure a photon in detector A, what do we measure in detector B over some range  $\tau$ ?). Technically, as far as what is seen experimentally,  $\tau$  should be integrated over the detector response time (or coincidence window of the electronics  $\sim 1$  ns). We know that  $\tau_A$  and  $\tau_B > 1$  ns, and that  $\tau_A - \tau_B \ll 1$  ns. Therefore, if we ignore all coincidence terms which differ by  $\tau_A$  or  $\tau_B$  we obtain

$$\begin{aligned}
P \propto & \int dt_A dt_B \\
& \{\tilde{\Phi}([t_A - t_B]/2) \tilde{\beta}([t_A + t_B]/2) e^{i(t_A + t_B)\bar{\omega}} \\
& + \tilde{\Phi}([t_A + \tau_A - t_B - \tau_B]/2) \\
& \times \tilde{\beta}([t_A + \tau_A + t_B + \tau_B]/2) e^{i(t_A + \tau_A + t_B + \tau_B)\bar{\omega}}\} \\
\times & \{\tilde{\Phi}^*([t_A - t_B]/2) \tilde{\beta}^*([t_A + t_B]/2) e^{-i(t_A + t_B)\bar{\omega}} \\
& + \tilde{\Phi}^*([t_A + \tau_A - t_B - \tau_B]/2) \\
& \times \tilde{\beta}^*([t_A + \tau_A + t_B + \tau_B]/2) e^{-i(t_A + \tau_A + t_B + \tau_B)\bar{\omega}}\} \\
\end{aligned} \tag{B.6}$$

Let us now re-express this equation by making the substitution  $t_B = t_A + \tau$ . Additionally, since we have removed the coincidence terms in Eq. (B.6) which do not occur within the coincidence window of the electronics, we can extend the integral of  $\tau$  over all time. An alternative method would be to include in the

integral a function that represents the coincidence-window of the electronics.

$$\begin{aligned}
 P \propto & \int dt_A \int d\tau |\tilde{\Phi}(-\tau)/2|^2 |\tilde{\beta}(2t_A + \tau)/2|^2 \\
 & + |\tilde{\Phi}(-\tau + \tau_A - \tau_B)/2|^2 \times |\tilde{\beta}(2t_A + \tau + \tau_A + \tau_B)/2|^2 \\
 & + \tilde{\Phi}(-\tau)/2 \tilde{\Phi}^*(-\tau + \tau_A - \tau_B)/2 \\
 & \quad \times \tilde{\beta}(2t_A + \tau)/2 \tilde{\beta}^*(2t_A + \tau + \tau_A + \tau_B)/2 e^{-i(\tau_A + \tau_B)\bar{\omega}} \\
 & + \tilde{\Phi}^*(-\tau)/2 \tilde{\Phi}(-\tau + \tau_A - \tau_B)/2 \\
 & \quad \times \tilde{\beta}^*(2t_A + \tau)/2 \tilde{\beta}(2t_A + \tau + \tau_A + \tau_B)/2 e^{i(\tau_A + \tau_B)\bar{\omega}}
 \end{aligned} \tag{B.7}$$

Keeping in mind that  $\Phi$  and  $\beta$  are both real functions, we can write the expression as:

$$\begin{aligned}
 P \propto & \int dt_A \int d\tau (\tilde{\Phi}(-\tau)/2)^2 (\tilde{\beta}(2t_A + \tau)/2)^2 \\
 & + (\tilde{\Phi}(-\tau + \tau_A - \tau_B)/2)^2 \times (\tilde{\beta}(2t_A + \tau + \tau_A + \tau_B)/2)^2 \\
 & + \tilde{\Phi}(-\tau)/2 \tilde{\Phi}(-\tau + \tau_A - \tau_B)/2 \\
 & \quad \times \tilde{\beta}(2t_A + \tau)/2 \tilde{\beta}(2t_A + \tau + \tau_A + \tau_B)/2 \\
 & \quad \times (e^{-i(\tau_A + \tau_B)\bar{\omega}} + e^{i(\tau_A + \tau_B)\bar{\omega}})
 \end{aligned} \tag{B.8}$$

Now, it must be kept in mind that  $\beta$  (width  $\sim 300$  ns) is a much broader function than  $\Phi$  (width  $\sim 100$  fs) since we are dealing with a cw pump. Also,  $\Phi[x]$  tends

to be non-zero only around  $x \sim 0$ . Therefore we can simplify  $\beta[t_A, \tau] \rightarrow \beta[t_A]$  and take the  $\beta$  functions outside the  $\tau$  integral. Now, since  $t_A$  is integrated from  $-\infty$  to  $+\infty$ , we have that  $\int dt_A \tilde{\beta}[t_A]^2 = \int dt_A \tilde{\beta}[t_A + T]^2$ , for all  $T$ . Hence, after normalizing, we are left with:

$$\begin{aligned} P \propto & 1 + (\cos[(\tau_A + \tau_B)\bar{\omega}]) \frac{\int d\tau \tilde{\Phi}([\tau]/2) \tilde{\Phi}([\tau + \tau_A - \tau_B]/2)}{\int d\tau (\tilde{\Phi}([\tau]/2))^2} \\ & \times \frac{\int dt_A \tilde{\beta}[t_A] \tilde{\beta}[t_A + (\tau_A + \tau_B)/2]}{\int dt_A (\tilde{\beta}[t_A])^2} \end{aligned} \quad (\text{B.9})$$

The first convolution is a function of  $\tau_A - \tau_B$ , the difference in the Michelson path mismatches in arm A and B of the Franson interferometer, and represents the interference envelope obtained upon scanning one of the Franson arms. The second convolution is a function of  $\frac{\tau_A + \tau_B}{2}$ , the average Michelson path mismatch between arm A and B of the Franson interferometer, and represents the maximum visibility obtainable for a particular average Michelson path mismatch in the Franson interferometer. The convolutions also express ‘which-way’ information that can be obtained from a Franson interferometer of the respective path mismatch parameters. In Chapter 7 we made the approximation that  $\frac{\tau_A + \tau_B}{2}$  is much smaller than the width of  $\tilde{\beta}[t]$ , hence the second convolution  $\mapsto 1$ .

## B.2 Classically correlated photons

Let us examine what we expect to see at the output a Franson interferometer if classically correlated photons are used. In order to not see interference in the singles rates,  $\tau_{A/B}$  must be larger than the single photon coherence time  $\delta t_{sp}$ . Preferably  $\tau_{A/B} \gtrsim 10 \times \delta t_{sp}$ . Now, we have the coherence time given by the pump  $\Delta t$  which is related to the energy correlations by  $\Delta t \delta E \sim \hbar/2$ . Similarly, the energy spectrum of down-conversion  $\Delta E$  is related to the arrival-time correlations by  $\Delta E \delta t \sim \hbar/2$ . In order for the wavefunction to be entangled we must have  $\delta E \delta t < \hbar/2$ . Suppose we have monochromators with resolution  $\delta E'$ . We must ensure that  $\delta t < \hbar/(2\delta E')$ . Let  $\delta t_{sp} = \delta t$ . We can perform the Franson and measure the envelope width to estimate  $\delta t$ . However, what if the source is not entangled, but instead consists of classically correlated particles with  $\delta E'' = \delta E$ , of single photon widths  $\delta t''_{sp} = \sqrt{2}\hbar/(2\delta E'')$  such that their correlation arrival-time widths are  $\delta t'' = \sqrt{2}\delta t''_{sp} = \hbar/\delta E''$  (from classical arguments; this is the crux of the Mancini *et. al.* bound [91]). I.e. Eve sends an incoherent mixture of photon pairs:

$$\begin{aligned}
 |\Psi\rangle\langle\Psi| &= \int dE e^{-\frac{(E)^2}{2\Delta E^2}} \left| \int dE_1 dE_2 \right. \\
 &\quad \left. e^{-\frac{(E_1-E)^2}{2(\delta E''/\sqrt{2})^2}} e^{-\frac{(E_2-E)^2}{2(\delta E''/\sqrt{2})^2}} |E_1; E_2\rangle \right|^2
 \end{aligned} \tag{B.10}$$

I.e.  $|\Psi\rangle\langle\Psi| = \int dE f(E)|\Phi\rangle_E\langle\Phi|_E$ . Taking  $E \rightarrow \omega$  and expressing the internal integrals as their Fourier relations, we get

$$\begin{aligned} |\Phi\rangle_{\bar{\omega}} &= \int d\omega_1 d\omega_2 \\ &\quad \int dt_1 e^{-2(t_1\delta\omega/\sqrt{2})^2} e^{-i(\omega_1 - \bar{\omega})t_1} \\ &\quad \int dt_2 e^{-2(t_2\delta\omega/\sqrt{2})^2} e^{-i(\omega_2 - \bar{\omega})t_2} \\ &\quad \int dt_3 e^{-i\omega_1 t_3} \int dt_4 e^{-i\omega_2 t_4} |t_3; t_4\rangle \end{aligned} \tag{B.11}$$

After integrating out the  $\omega$ s and respective  $t$ s we are left with

$$\begin{aligned} |\Phi\rangle_{\bar{\omega}} &= \int dt_1 dt_2 \\ &\quad e^{-2(t_1\delta\omega/\sqrt{2})^2} e^{-2(t_2\delta\omega/\sqrt{2})^2} \\ &\quad e^{-i\bar{\omega}(t_1+t_2)} |t_1; t_2\rangle \end{aligned} \tag{B.12}$$

Let's now consider the coincidence rate at the output of the Franson interferometer:

$$\begin{aligned} P &\propto \int \int |\langle 0 | a_A(t_A) a_B(t_B) | \Psi \rangle|^2 dt_A dt_B \\ &= \int d\bar{\omega} e^{-\frac{(\bar{\omega})^2}{2\Delta\omega^2}} \int \int |\langle 0 | a_A(t_A) a_B(t_B) | \Phi \rangle_{\omega}|^2 dt_A dt_B \end{aligned} \tag{B.13}$$

Substituting Eq. (B.12) into Eq. (B.13) gives us

$$\begin{aligned}
 P \propto & \int d\bar{\omega} e^{-\frac{(\bar{\omega})^2}{2\Delta\omega^2}} \int \int dt_A dt_B \\
 & |(e^{-2(t_a\delta\omega/\sqrt{2})^2} e^{-i\bar{\omega}t_a} + e^{-2((t_a+\tau_a)\delta\omega/\sqrt{2})^2} e^{-i\bar{\omega}(t_a+\tau_a)}) \\
 & (e^{-2(t_b\delta\omega/\sqrt{2})^2} e^{-i\bar{\omega}t_b} + e^{-2((t_b+\tau_b)\delta\omega/\sqrt{2})^2} e^{-i\bar{\omega}(t_b+\tau_b)})|^2
 \end{aligned} \tag{B.14}$$

which gives us:

$$\begin{aligned}
 P \propto & \int d\bar{\omega} e^{-\frac{(\bar{\omega})^2}{2\Delta\omega^2}} \int \int dt_A dt_B \\
 & (e^{-4(t_a\delta\omega/\sqrt{2})^2} + e^{-4((t_a+\tau_a)\delta\omega/\sqrt{2})^2} \\
 & + 2 \cos(\bar{\omega}\tau_a) e^{-2((t_a+\tau_a)\delta\omega/\sqrt{2})^2} e^{-2(t_a\delta\omega/\sqrt{2})^2}) \\
 & \times (a \mapsto b)
 \end{aligned} \tag{B.15}$$

Now, keep in mind that  $t_A$  and  $t_B$  are integrated over the response time of the detectors, which are less than the Franson path mismatches  $\tau_A$  and  $\tau_B$  (in order to differentiate long-long, long-short etc. coincidence events). Therefore, in the limit that  $\frac{\sqrt{2}}{2\delta\omega} \ll \tau_{a/b}$  the exponential terms  $e^{-2((t_a/b+\tau_a/b)\delta\omega/\sqrt{2})^2} \rightarrow 0$ , and no interference pattern is observed, either in the singles or in the coincidences. On the other hand, if  $\sqrt{2}/2\delta\omega \gtrsim \tau_{a/b}$ , then interference will be observed in both the singles and the coincidences. There is no regime in which interference fringes will

be observed in the coincidences but not in the singles. It is also interesting to

note that

$$e^{\frac{-t_1^2}{2\sigma^2}} e^{\frac{-t_2^2}{2\sigma^2}} = e^{\frac{-(t_1+t_2)^2}{4\sigma^2}} e^{\frac{-(t_1-t_2)^2}{4\sigma^2}} \quad (\text{B.16})$$

i.e. this is the limiting case for weak entangled states. In this case  $\delta t = \sqrt{2}\sigma$

(width of  $\langle [t_1 - t_2]^2 \rangle$ ) and  $\Delta t = \hbar/2\delta E = \sqrt{2}\sigma/2$  (width of  $\langle [(t_1 + t_2)/2]^2 \rangle$ )

therefore  $\delta t \delta E = \hbar$ , i.e. the classical case.

## Appendix C

# General expression for the $L_2$ and $L_3$ sum-variance inequalities

In this appendix we provide the more general form of the variance used for the sum-variance inequalities  $L_2$  and  $L_3$ . The form of the variance given in Eq. (4.11) of Chapter 4 is specific to the  $|\psi^-\rangle$  Bell state since its density matrix is invariant to rotations. The general form of the variance is given by

$$(\Delta[\sigma_1 + \sigma_2]_{0/90})^2 = \min[\Delta(HH, VV), \Delta(HV, VH)], \quad (\text{C.1})$$

where  $\min[x, y]$  equals the minimum value of the two functions x and y,

$$\Delta(HH, VV) = 4 \frac{R_{HH}+R_{VV}}{R_{HH}+R_{VV}+R_{HV}+R_{VH}} - 4 \frac{(R_{HH}-R_{VV})^2}{(R_{HH}+R_{VV}+R_{HV}+R_{VH})^2}, \quad (\text{C.2})$$

and

$$\Delta(HV, VH) = 4 \frac{R_{HV}+R_{VH}}{R_{HH}+R_{VV}+R_{HV}+R_{VH}} - 4 \frac{(R_{HV}-R_{VH})^2}{(R_{HH}+R_{VV}+R_{HV}+R_{VH})^2}. \quad (\text{C.3})$$

This is the more general form of the variance, as pointed out by Samuelsson and Bjork [161]. This more general form of the variance takes away from the flow of the chapter, and so has been included in this appendix for completeness.

# 10. Explanation of entanglement

**Abstract:** Quantum entanglement is independent of space and time. The World's biggest quantum entanglement experiment just proved Einstein wrong.

**Keywords:** Space, time, non-locality



*To arrive at the edge of the world's knowledge, seek out the most complex and sophisticated minds, put them in a room together, and have them ask each other the questions they are asking themselves.*

<https://www.edge.org/response-detail/26790>

Printed On Wed June 20th 2018

## 2016 : WHAT DO YOU CONSIDER THE MOST INTERESTING RECENT [SCIENTIFIC] NEWS? WHAT MAKES IT IMPORTANT?

[In the News \[ 21 \]](#)

|

[Contributors \[ 199 \]](#) | [View All Responses \[ 199 \]](#)



[Anton Zeilinger](#)

*Physicist, University of Vienna; Scientific Director, Institute of Quantum Optics and Quantum Information; President, Austrian Academy of Sciences; Author, Dance of the Photons: From Einstein to Quantum Teleportation*

Quantum Entanglement Is Independent Of Space And Time

The notion of quantum entanglement, famously called “spooky action at a distance” by Einstein emerges more and more as having deep implications for our understanding of the World. Recent experiments have perfectly verified the fact that quantum correlations between two entangled particles are stronger than any classical, local pre-quantum worldview allows. So, since quantum physics predicts these measurement results for at least eighty years, what’s the deal?

The point is that the predictions of quantum mechanics are independent of the relative arrangement in space and time of the individual measurements. Fully independent of their distance, independent of which is earlier or later etc. One has perfect correlations between all of an entangled system even as these correlations cannot be explained by properties carried by the system before measurement. So quantum mechanics transgresses space and time in a very deep sense. We would be well advised to reconsider the foundations of space and time in a conceptual way.

To be specific, consider an entangled ensemble of systems. This could be two photons, or any number of photons, electrons, atoms, and even of larger systems like atomic clouds at low temperature, or superconducting circuits. We now do measurements individually on those systems. The important point is that, for a maximally entangled state, quantum physics predicts random results for the individual entangled property.

To be specific, for photons this could be the polarization. That is, for a maximally entangled state of two or more entangled photons, the polarization observed in the experiment could be anything, horizontal, vertical, any direction linear, right-handed circular, left-handed circular, any elliptical state, again, for the individual photon. Thus, if we do a measurement we observe a random polarization. And this for each individual photon of

the entangled ensemble. But a maximally entangle state predicts perfect correlations= between the polarizations of all photons making the entangled state up.

To me, the most important message is that the correlations between particles like photons,= electrons, or atoms, or larger systems like superconducting circuits are independent of= which of the systems are measured first and how large the spatial distance between them= is.

At first sight, this might not be surprising. After all, if I measure the heights of peaks of= the mountains around me, it also does not matter in which sequence I do the= measurements and whether I measure the more distant ones first or the ones closer to each other. The same is true for measurements on entangled quantum systems. However, the= important point is that the first measurement on any system entangled with others instantly= changes the common quantum state describing all, the subsequent measurement on the= next does that again and so on. Until, in the end, all measurement results on all systems= entangled with each other, are perfectly correlated.

Moreover, as recent experiments finally prove, we now know definitely that all this cannot= be explained by any communication limited by Einstein's cosmic speed limit—the speed= of light. Also, one might think that there is a difference if two measurements are done= such that one if after the other in way that a signal could tell the second one what to do= as a consequence of the first earlier measurements. Or whether they are arranged at such a= distance and done sufficiently simultaneously such that no signal is fast enough.

Thus, it appears that on the level of measurements of properties of members of an= entangled ensemble, quantum physics is oblivious to space and time.

It appears that an understanding is possible via the notion of information. Information seen= as the possibility of obtaining knowledge. Then quantum entanglement describes a= situation where information exists about possible correlations between possible future= results of possible future measurements without any information existing for the individual= measurements. The latter explains quantum randomness, the first quantum entanglement.= And both have significant consequences for our customary notions of causality.

It remains to be seen what the consequences are for our notions of space and time, or= space-time for that matter. Space-time itself cannot be above or beyond such= considerations. I suggest we need a new deep analysis of space-time, a conceptual analysis= maybe analogous to the one done by the Viennese physicist-philosopher Ernst Mach who= kicked Newton's absolute space and absolute time form their throne. The hope is that in= the end we will have new physics analogous to Einstein's new physics in the two theories= of relativity.

Science & Technology (</subjects/science-technology/topics/>)

# The World's Biggest Quantum Entanglement Experiment Just Proved Einstein Wrong

---

*Our editors delve into Curiosity's top stories every day on a podcast that's shorter than your commute. Click here (<https://omny.fm/shows/curiosity-podcast/playlists/podcast/embed>) to listen and learn — in just a few minutes!*

You know you've made an impact on the world when people are still testing your ideas six decades after your death. Einstein was no fan of the concept known as quantum entanglement (<https://curiosity.com/topics/quantum-entanglement-connects-particles-across-any-distance-curiosity/>) and believed that any explanation for it had to involve some other variables we just don't know about yet. Well, Einstein wasn't right about everything (<https://curiosity.com/topics/one-of-einstiens-greatest-regrets-has-turned-out-to-be-useful-after-all-curiosity/>) — and the biggest experiment of quantum entanglement yet adds his objection to that list.



0

## Made You Look

For the very, very small particles described by quantum mechanics, there is no definitive state of being. Quantum particles exist as a swarm of probabilities, basically existing in several states at once — say, spinning clockwise and counterclockwise — until they're measured, when they seem to "choose" a state and stick with it. A particle that makes this "choice" is said to have collapsed, as if all of its various potential states have fallen away to reveal the one state it settled on. Even weirder, it's possible for two particles to become "entangled," meaning they will retain a sort of causal relationship with each other, no matter their distance in time

(<https://curiosity.com/topics/entangled-quantum-particles-can-communicate-through-time-curiosity/>) and space. If you measure one particle and it spins clockwise, for example, then its entangled companion would instantly collapse into a counterclockwise spin, even if it's on the other side of the universe. That either means that one communicated with the other in an instant, or the state of each particle only popped into existence once one was measured.

We know what you're thinking. For one thing, this whole idea is ridiculous: things are what they are regardless of whether you're looking at them. For another, nothing can go faster than light, so how can two particles communicate across the universe in an instant?

Einstein thought the same thing (<https://www.technologyreview.com/s/427174/einsteins-spooky-action-at-a-distance-paradox-older-than-thought/>), derisively calling the idea "spooky action at a distance." Those in Einstein's camp are in favor of a concept called "local realism." "Locality" says that no signal can travel faster than light, and "realism" says that particles have definite states even before you measure them.

If, in fact, two particles "communicate" through a vast distance, then according to local realism, something else must be going on. Maybe the measurement tools are somehow in on it, or maybe the universe places some limits on the particles' possible states that we just don't know about yet. MIT's Andrew Friedman told Quanta (<https://www.quantamagazine.org/physicists-are-closing-the-bell-test-loophole-20170207/>) that it's as if the universe is a restaurant with 10 dishes on the menu. "You think you can order any of the 10, but then they tell you, 'We're out of chicken,' and it turns out only five of the things are really on the menu. You still have the freedom to choose from the remaining five, but you were overcounting your degrees of freedom."

This idea that there might be less freedom of measurement than we think there is called the "freedom-of-choice" loophole. This loophole poses a challenge, because even seemingly total randomness can't close it: use a random number generator to decide which properties to measure, and there's still the chance that the entangled particles have influenced the random number generator. That's why in November of

2016, a global experiment used a method that can't be influenced by puny quantum particles: free will. Specifically, the free will of a bunch of gamers.

## Saved by the Bell

---

The experiment, dubbed the BIG Bell Test (<https://www.sciencedaily.com/releases/2018/05/180509135409.htm>), was modeled on a classic experiment designed by physicist John Stewart Bell. In the traditional version of the experiment, pairs of entangled particles are generated, separated, and sent to different locations, where various properties of those particles are measured. (Like we mentioned before, researchers will typically use random-number generators to decide which property to measure at any given time.) If the measurements match, then that's evidence for quantum entanglement and against local realism.

The BIG Bell test happened with the help of 100,000 people around the world, who used an online video game to contribute their own random sequences of zeros and ones to 12 labs on five continents, including in Brisbane, Australia; Shanghai, China; Vienna, Austria; Rome, Italy; Munich, Germany; Zurich, Switzerland; Nice, France; Barcelona, Spain; Buenos Aires, Argentina; Concepción, Chile; and Boulder, Colorado. In many different individual experiments, those labs used the numbers, or "bits," to set the angles of polarizers and other tools to determine how the entangled particles would be measured.

The results, published in May 2018 (<https://www.nature.com/articles/s41586-018-0085-3>) in the journal Nature, are robust: "The

observed correlations strongly contradict local realism," the authors write. Sorry, Einstein. You'll always have relativity.